

Organozinc Reagents: Structural Tailoring for Synthetic Applications

Matthew D. McCall

A thesis submitted to the Department of Pure and Applied Chemistry, University of Strathclyde, in part
fulfilment of the requirements for the degree of Doctor of Philosophy.

January 2012

This thesis is the result of the author's original research. It has been composed by the author and has not been previously submitted for examination which has led to the award of a degree.

The copyright of this thesis belongs to the author under the terms of the United Kingdom Copyright Acts as qualified by University of Strathclyde Regulation 3.50. Due acknowledgement must always be made of the use of any material contained in, or derived from, this thesis.

Acknowledgements

Firstly, I would like to thank my supervisor Dr Eva Hevia for everything she has done for me over the last few years. I have really enjoyed working with her on some fantastic projects, and couldn't have asked for a better PhD supervisor. I'm extremely grateful for all the work she has put in to help me during the last few years, and to get so many of these results published. I particularly want to thank her for all the help in proof reading this thesis, which I think has caused her more stress than it has me.

Special thanks also go to all the members of the Hevia group - Zoe, Sharon, Vicki and Thomas. Particularly to Zoe, who has had to put up with working next to me in the lab for the last few years (maybe she'll start keeping the glove box a bit tidier now that I'm gone!), and Sharon for helping me out many times while I was writing up and putting up with my driving on our road trip to Oxford. It's been great to work with such nice people every day, and they have both given me a lot of laughs during the last few years. Although they'll pretend not to, I'm sure they will miss me. I would also like to mention two of my project students, Jonathan Chua and Lorraine Nuttall, for their important contributions to the magnesium-zincate work.

I am extremely thankful for all of the help and advice I have received from Professor Robert Mulvey and Dr Charlie O'Hara, their input and suggestions have been greatly appreciated. Equally important has been everyone else in the lab who I have had the chance to work with over the last three and a half years, who have all contributed to this thesis in some way. Special mentions have to go to Pablo, my second favourite Spaniard, for all his help in the lab and some hilarious but un-repeatable stories, to Stuart for in-depth discussions on the important things in life (TV and football), although some of his jokes need some work, and also the "fun gang" (Jan, Ross and Stuart) for occasionally letting me join them for a few drinks on a Friday night. These acknowledgments wouldn't be complete without mentioning the important contribution of Ross, the ridiculous things he said every day provided a welcome distraction from chemistry. Finally to Ben, for constantly getting terrible songs stuck in my head all day, and being the only person in the lab who loves the Borders more than I do.

The thing I'll remember most from this PhD is all the fantastic people I have had the chance to work with, and all the great memories of trips to Rothesay, the conference in Hawaii, the

Retro Bar in Manchester, being part of the worst football team ever to play in the University of Strathclyde 5-a-side league, and being pushed to the limits of diabetes by eating more cake than I realised existed.

I would also like to take this opportunity to thank the following people; Dr Alan Kennedy, Dr Jan Klett, Dr Pablo Garcia-Álvarez, Dr Luca Russo and Prof. William Clegg (X-ray crystallography), Dr Dave Armstrong (DFT calculations), Dr John Parkinson and Craig Irving (NMR spectroscopy), Dr Pamela Alan (atomic absorption analysis), Pat Keating (GC/MS) and Denise Gilmour (Elemental analysis). I cannot thank them enough for giving up their time to help me, and I can only apologise to the X-ray crystallographers who have had to deal with numerous samples of my nemesis $[(\text{THF})_4\text{MgCl}_2]$ that I have sent their way.

A huge thank you to my Mum and Dad for all their guidance and support over the last 26 years. Even though they have no idea exactly what it is that I do, they still make the effort to appear interested in it (although I doubt they'll ever read past this page).

Finally, and most importantly I want to say thank you to my girlfriend Kirsty, who even after all this time still manages to put up with me. Her support over the last few years has been so important, and I definitely couldn't have done this without her. She's the one who has to put up with me when things aren't going so well, and always manages to get me smiling again. She has also been very understanding of me turning our kitchen into a make-shift office for the last few months. I promise we'll go back to Hawaii sometime soon!

Abstract

Building on recent advances in zincate chemistry, but going beyond the state-of-the-art, this project sought to advance the understanding of the mechanisms involved in alkali metal-mediated zincation (AMMZn), as well as design a new type of mixed-metal reagent, magnesium-zinc hybrids, focussing on their applications in nucleophilic additions to ketones and direct zinc-iodine exchange reactions.

Unveiling two new applications of the alkali metal TMP-zincates [(THF)Li(TMP)Zn^tBu₂] (**1**) and [(TMEDA)Na(TMP)Zn^tBu₂] (**3**), reaction with trimethyl(phenoxy)silane (**12**) allowed the isolation of the first intermediates of direct lateral zincation (D/Zn) of an aromatic substrate, while the reaction of **3** with benzoylferrocene (**17**) has shown that two competing pathways are available: (i) remote 1,6-nucleophilic addition of a *tert*-butyl group to the phenyl ring of **17** and (ii) simultaneous α -deprotonation of the substituted cyclopentadienyl ring and 1,2-addition of a *tert*-butyl anion to the carbonyl group of the ketone.

Shedding new light on the mechanism by which these alkali metal TMP-zincates react, the proposed intermediate species of the two-step mechanism (previously proposed by theoretical studies) [(THF)₂Li(*o*-C₆H₄OMe)ZnMe₂] (**26**) and [(THF)₃Li(*o*-C₆H₄OMe)Zn^tBu₂] (**29**) were prepared. Reactivity studies of **26** and **29** with TMP(H) provided the first tangible experimental evidence that the AMMZn of anisole by **1** proceeds via a two-step mechanism, which is greatly influenced by both the nature of the alkyl groups of the zincate (Me vs. ^tBu) and the polarity of the solvent in which the reaction is performed (hexane/benzene vs. THF).

In addition, investigations into the seemingly simple stoichiometric salt metathesis reactions of Grignard reagents with ZnCl₂ led to the isolation of a series of magnesium-zinc hybrid species [(THF)Mg(μ -Cl)₂Zn(^tBu)(Cl)] (**34**) and [(THF)Mg(μ -Cl)₃ZnR]₂] (R = ^tBu (**36**), ⁿBu (**37**), Et (**38**), *o*-C₆H₄OMe (**39**)), formed via metathetical co-complexation. Altering the stoichiometry of these reactions (from 1:1 to 3:1) to mimic the conditions employed in ZnCl₂ catalysed reactions of Grignard reagents led to the formation of the alkyl-rich Mg-Zn hybrids [{"Mg₂Cl₃(THF)₆"}⁺{Zn^tBu₃}⁻] (**40**) and [{"Mg₂Cl₃(THF)₆"}⁺{Zn₂Et₅}⁻] (**41**).

Probing the possible applications of these Mg-Zn hybrid species in various key synthetic methodologies revealed that **41** can be employed both stoichiometrically, and catalytically in

the presence of an excess of EtMgCl, to perform the chemoselective alkylation of ketones. In contrast, the analogous 1st generation Mg-Zn hybrid **38** displayed diminished reactivity even towards activated ketones, although the addition of LiCl resulted in improved reactivity, hinting at the existence of trimetallic Li-Mg-Zn hybrid species in solution. Furthermore, **40** can readily undergo direct Zn-I exchange reactions with a wide range of functionalised aryl iodide substrates, demonstrating high atom economy, with the subsequent aryl-zincate species proving to be valuable precursors for Pd-catalysed Negishi cross-coupling reactions.

Publications

1. “Assessing the Reactivity of Sodium Zincate [(TMEDA)Na(TMP)Zn^tBu₂] Towards Benzoylferrocene: Deprotonative Metalation vs Alkylation Reactions”; E. Hevia, A. R. Kennedy and **M. D. McCall**, *Dalton Trans.*, **2012**, 41, 98.
2. “Expanding Mg-Zn hybrid chemistry: Inorganic salt effects in addition reactions of organozinc reagents to trifluoromethyl acetophenone and implications for a synergistic lithium-magnesium-zinc activation”; D. R. Armstrong, W. Clegg, P. García-Alvarez, A. R. Kennedy, **M. D. McCall**, L. Russo and E. Hevia, *Chem. Eur. J.*, **2011**, 17, 8333.
3. “Shedding New Light on ZnCl₂-Mediated Addition Reactions of Grignard Reagents to Ketones: Structural Authentication of Key Intermediates and Diffusion-Ordered NMR Studies”; D. R. Armstrong, W. Clegg, P. García-Alvarez, **M. D. McCall**, L. Nuttall, A. R. Kennedy, L. Russo and E. Hevia, *Chem. Eur. J.*, **2011**, 17, 4470.
4. “Hidden Complexity of Stoichiometric and Catalytic Metathesis Reactions: Synthesis and Structural Elucidation of Mg-Zn hybrids”; J. Z. Chua, P. García-Álvarez, E. Hevia, A. R. Kennedy and **M. D. McCall**, *Proc. Natl. Acad. Sci. USA*, **2010**, 107, 5294.
5. “New Insights into Addition Reactions of Dialkylzinc Reagents to Trifluoromethyl Ketones: Structural Authentication of a β -hydride Elimination Product Containing a Tetranuclear Zinc Chain”; E. Hevia, A. R. Kennedy, J. Klett, Z. Livingstone and **M. D. McCall**, *Dalton Trans.*, **2010**, 39, 520.
6. “Donor-dictated Interlocking Co-complexation Reactions of LiNHDipp with Dimethylzinc: Synthesis and Structures of New Methyl(amido)zincates”; W. Clegg, D. V. Graham, E. Herd, E. Hevia, A. R. Kennedy, **M. D. McCall** and L. Russo, *Inorg. Chem.*, **2009**, 48, 5320.

7. “*Direct Lateral Metallation using Alkali-Metal Mediated Zincation (AMMZn): SiC-H vs Si-O Bond Cleavage*”; E. Hevia, A. R. Kennedy, J. Klett and **M. D. McCall**, *Chem. Commun.*, **2009**, 3240.
8. “*Closer Insight into the Reactivity of TMP-dialkyl Zincates in Directed ortho-Zincation of Anisole: Experimental Evidence of Amido Basicity and Structural Elucidation of Key Reaction Intermediates*”; W. Clegg, B. Conway, E. Hevia, **M. D. McCall**, L. Russo and R. E. Mulvey, *J. Am. Chem. Soc.*, **2009**, 131, 2375.

Conference Oral Presentations

1. “*Exposing the Hidden Complexity of Metathesis Reactions: Applications of Mg-Zn Hybrids*”; International Congress of the Pacificchem Societies, Hawaii, USA, December 2010.
2. “*Organozinc Reagents: Structural Tailoring for Mixed-Metal Applications*”; University of Strathclyde Postgraduate Awards lecture, October 2010.
3. “*New Insights into Direct Zincation of Aromatic Molecules*”; Universities of Scotland Inorganic Conference, Heriot-Watt University, Edinburgh, September 2009.
4. “*New Insights into Direct Zincation of Aromatic Molecules*”; University of Strathclyde, Inorganic Section Research Day, June 2009.
5. “*New Insights into Direct Zincation of Aromatic Molecules*”; 4th WestChem Research Day, University of Glasgow, June 2009.

Conference Poster Presentations

1. “*Expanding Magnesium-Zinc Hybrid Chemistry*”; Universities of Scotland Inorganic Conference, Glasgow University, July 2011.
2. “*Exposing the Hidden Complexity of Stoichiometric and Catalytic Metathesis Reactions: Elucidation and Applications of Mg-Zn Hybrids*”; Universities of Scotland Inorganic Conference, Durham University, July 2010.
3. “*Hidden Complexity of Salt Metathesis Reaction*”; RSC Dalton Division Meeting on Main Group Chemistry, University of Manchester, September 2009. Awarded 1st prize in poster competition.
4. “*Hidden Complexity of Salt Metathesis Reaction*”; 42nd IUPAC Congress, Scottish Exhibition and Conference Centre, Glasgow, July 2009.
5. “*Unveiling the Reactivity of TMP-dialkyl Zincates in Directed ortho-Zincation of Anisole*”; Universities of Scotland Inorganic Conference, University of Strathclyde, Glasgow, September 2008.

Table of Common Abbreviations

acac	Acetylacetonate
AMMZn	Alkali metal mediated zincation
CCDB	Cambridge crystallographic database
CDDE	Cyclododecene
CIP	Contacted ion-pair
COSY	^1H - ^1H correlated spectroscopy
Cp	Cyclopentadiene anion (C_5H_5^-)
Cp'	Substituted cyclopentadiene ring of benzoylferrocene
CSI-MS	Cold-spray ionization - mass spectroscopy
DA	Diisopropylamide
DFT	Density functional theory
DIZn	Direct lateral zincation
DMG	Direct metallating group
DoL	Directed <i>ortho</i> lithiation
DoM	Directed <i>ortho</i> metallation
DOSY	Diffusion ordered NMR spectroscopy
dppf	1,1'-bis(diphenylphosphino)ferrocene
ee	Enantiomeric excess (%)
ESI-MS	Electrospray ionization - mass spectroscopy
FAAS	Flame atomic absorption spectroscopy
GC-FID	Gas chromatography - flame ionization detector
HSQC	Heteronuclear single quantum correlation spectroscopy
LDA	Lithium diisopropylamide
(-)-MIB	(2 <i>S</i>)-3- <i>exo</i> -(Morpholino)isoborneol
MOM ethers	Methoxymethyl ethers
MVK	Methyl vinyl ketone
NMR	Nuclear magnetic resonance
ODE	1-octadiene
PGSE	Pulsed gradient spin echo
PhN	Phenylnaphthalene
PMDETA	<i>N,N,N',N'',N'''</i> -pentamethyldiethylenetriamine

SSIP	Solvent separated ion-pair
TEEDA	<i>N,N,N',N'</i> -tetraethylethylenediamine
TEMPO	(2,2,6,6-Tetramethylpiperidin-1-yl)oxyl
THF	Tetrahydrofuran
THP	Tetrahydropyran
TMEDA	<i>N,N,N',N'</i> -tetramethylethylenediamine
TMP	2,2,6,6-tetramethylpiperidide
TMP(H)	2,2,6,6-tetramethylpiperidine
TMS	Trimethylsilyl or tetramethylsilane
TPhN	1,2,3,4-tetraphenylnaphthalene
TS [‡]	Transition state

Table of Contents

Acknowledgements	I
Abstract	III
Publications	V
Oral Presentations	VI
Poster Presentations	VII
Table of Common Abbreviations	VIII
Table of Contents	X
Table of Compounds	XIV

Chapter 1: Introduction to organozinc chemistry and recent advances in alkali metal zincates

1.1	Organozinc reagents	1
1.2	Alkali metal zincates	4
1.2.1	Preparation of alkali metal zincates	6
1.2.2	Applications of alkali metal zincates in 1,4-conjugate addition and 1,2-addition	7
1.2.3	Applications of alkali metal zincates in metal-halogen exchange	9
1.3	Alkali metal TMP-zincates in directed <i>ortho</i> metallation (DoM)	15
1.3.1	Directed <i>ortho</i> metallation (DoM)	15
1.3.2	Recent developments in alkali metal TMP-zincates	16
1.3.3	Zinc modified turbo-Hauser bases	29

Chapter 2: Unveiling new reactivity patterns in AMMZn

2.1	Direct lateral metallation using alkali metal-mediated zincation (AMMZn): SiC-H vs. Si-O bond cleavage	32
2.1.1	Investigating the reactivity of trimethyl(phenoxy)silane (12) with 1 and 3	34
2.1.2	Investigating the regioselectivity of the DIZn of 12 by 1	42
2.1.3	Applications of DIZn to other silyl-substituted substrates	46
2.1.4	Conclusions	48
2.2	Assessing the reactivity of sodium TMP-zincate (3) towards benzoylferrocene: deprotonative metallation vs. alkylation reactions	49
2.2.1	Investigating the reactivity of benzoylferrocene (17) with sodium TMP-zincate (3)	52
2.2.2	Electrophilic quenching studies	57
2.2.3	Further investigation into the two-fold activation of Zn ^t Bu ₂ in 3	61
2.2.4	Conclusions	63

2.3	Summary	64
<u>Chapter 3: Closer insight into the mechanisms of AMMZn of anisole by TMP-dialkyl zincates</u>		65
3.1	Theoretical studies on DoM of anisole using lithium TMP-zincates	66
3.2	Theoretical studies on metallation of benzene using sodium TMP-zincates	69
3.3	New insight into the reactivity of lithium TMP-zincates in DoM of anisole	72
3.3.1	Co-complexation of [(THF) ₂ Li ₄ (<i>o</i> -C ₆ H ₄ OMe) ₄] (25) with ZnMe ₂	74
3.3.2	Co-complexation of [(THF) ₂ Li ₄ (<i>o</i> -C ₆ H ₄ OMe) ₄] (25) with Zn ^t Bu ₂	78
3.3.3	Investigating the reactivity of [(THF) ₂ Li(<i>o</i> -C ₆ H ₄ OMe)ZnMe ₂] (26) with TMP(H)	83
3.3.4	Investigating the reactivity of [(THF) ₃ Li(<i>o</i> -C ₆ H ₄ OMe)Zn ^t Bu ₂] (29) with TMP(H)	87
3.3.5	Disproportionation process of 26 and 29 to [(THF) ₂ Li ₂ Zn(<i>o</i> -C ₆ H ₄ OMe) ₄] (27)	97
3.4	Conclusions	101
<u>Chapter 4: Investigating metathesis reactions of Grignard reagents with ZnCl₂</u>		104
4.1	Investigating the salt metathesis reaction of ^t BuMgCl and ZnCl ₂	108
4.2	Further studies on the metathesis reaction Grignard reagents with ZnCl ₂	115
4.3	Applications of ZnCl ₂ catalysed reactions of Grignard reagents	123
4.4	Investigating the salt metathesis reaction of ^t BuMgCl with substoichiometric amounts of ZnCl ₂	128
4.5	Investigating the salt metathesis reaction of EtMgCl with substoichiometric amounts of ZnCl ₂	134
4.6	Conclusions	146
<u>Chapter 5: Expanding Mg-Zn hybrid chemistry: nucleophilic alkylation reactions of ketones</u>		148
5.1	Investigating the reactivity of [{Mg ₂ Cl ₃ (THF) ₆ } ⁺ {Zn ₂ Et ₅ } ⁻] (41) in stoichiometric alkylation reactions of benzophenone	149
5.2	Investigating the catalytic activity of [{Mg ₂ Cl ₃ (THF) ₆ } ⁺ {Zn ₂ Et ₅ } ⁻] (41) in alkylation reactions of benzophenone by EtMgCl	157
5.3	Insight into the constitution of the reduction products	160
5.4	Assessing the reactivity of 1 st generation magnesium-zinc hybrid reagents in nucleophilic addition reactions: salt effects	163
5.5	Conclusions	169
<u>Chapter 6: Applying magnesium-zinc hybrid chemistry to direct Zn-I exchange and Pd-catalysed Negishi cross-coupling reactions</u>		171
6.1	Investigating the reactivity of [{Mg ₂ Cl ₃ (THF) ₆ } ⁺ {Zn ^t Bu ₃ } ⁻] (40) in Zn-I exchange and Pd-catalysed Negishi cross-coupling Reactions	172
6.2	Expanding the scope of Zn-I exchange and Negishi cross-coupling reactions of	

	[{Mg ₂ Cl ₃ (THF) ₆ } ⁺ {Zn ^t Bu ₃ }] (40) to 2-Iodotoluene and 3-Iodotoluene	178
6.3	Investigating Zn-I Exchange and Negishi cross-coupling reactions of 40 with iodoanisole substrates	180
6.4	Investigating Zn-I exchange and Negishi Cross-coupling reactions of 40 with iodobenzonitrile substrates	184
6.5	Conclusions	196
 <u>Chapter 7: General experimental techniques & procedures</u>		 198
7.1	General experimental techniques	198
7.1.1	Schlenk techniques	198
7.1.2	Glove box	199
7.1.3	Solvent purification	200
7.1.4	Standardisation of organometallic reagents	200
7.1.5	Analytical procedures	201
7.2	Synthesis of common starting materials	201
7.2.1	Synthesis of Zn ^t Bu ₂	201
7.2.2	Synthesis of BuNa	201
7.2.3	Synthesis of [(THF)Li(TMP)Zn ^t Bu ₂] (1)	202
7.2.4	Synthesis of [(TMEDA)Na(TMP)Zn ^t Bu ₂] (3)	202
7.3	Synthesis of Products	202
7.3.1	Synthesis of [(THF)Li(TMP){PhOSi(CH ₃) ₂ CH ₂ }Zn ^t Bu] (13)	202
7.3.2	Synthesis of [(TMEDA)Na(TMP){PhOSi(CH ₃) ₂ CH ₂ }Zn ^t Bu] (14)	203
7.3.3	Synthesis of [(PhOSiMe ₃)Li(TMP){PhOSi(CH ₃) ₂ CH ₂ }Zn ^t Bu] (16)	203
7.3.4	Synthesis of [(TMEDA)Na(μ-TMP)Zn{OC(^t Bu)(η ⁵ -C ₅ H ₃)Fe(η ⁵ -C ₅ H ₅)}] (18)	204
7.3.5	Synthesis of [PhC(OH)(^t Bu)(η ⁵ -C ₅ H ₃ I)Fe(η ⁵ -C ₅ H ₅)] (19) and [4- ^t Bu-C ₆ H ₄ C(=O)(η ⁵ -C ₅ H ₄)Fe(η ⁵ -C ₅ H ₅)] (21)	205
7.3.6	Synthesis of [C ₆ H ₅ C(OH) ^t Bu(η ⁵ -C ₅ H ₃ D)Fe(η ⁵ -C ₅ H ₅)] (23) and [^t Bu-C ₆ H ₄ CO(η ⁵ -C ₅ H ₄)Fe(η ⁵ -C ₅ H ₅)] (21)	206
7.3.7	Synthesis of [C ₆ H ₅ C(OH) ^t Bu(η ⁵ -C ₅ H ₄)Fe(η ⁵ -C ₅ H ₅)] (24) and [^t Bu-C ₆ H ₄ CO(η ⁵ -C ₅ H ₄)Fe(η ⁵ -C ₅ H ₅)] (21)	207
7.3.8	Synthesis of [Li ₄ (<i>o</i> -C ₆ H ₄ OMe) ₄ (THF) ₂] (25)	207
7.3.9	[(THF) ₂ Li(<i>o</i> -C ₆ H ₄ OMe)ZnMe ₂] (26)	208
7.3.10	Synthesis of [(THF) ₂ Li ₂ Zn(<i>o</i> -C ₆ H ₄ OMe) ₄] (27)	209
7.3.11	Synthesis of [(TMEDA)Li(<i>o</i> -C ₆ H ₄ OMe)ZnMe ₂] (28)	209
7.3.12	Synthesis of [(THF) ₃ Li(<i>o</i> -C ₆ H ₄ OMe)Zn ^t Bu ₂] (29)	210
7.3.13	[(PMDETA)Li(<i>o</i> -C ₆ H ₄ OMe)Zn ^t Bu ₂] (30)	210
7.3.14	Synthesis of [(THF)Li(TMP)ZnMe ₂] (32)	211
7.3.15	Synthesis of [(THF) ₄ Mg(μ-Cl) ₂ Zn(^t Bu)(Cl)] (34)	211

7.3.16	Synthesis of [$\{(THF)_2Mg(\mu-Cl)_3ZnR\}_2$] (36-39)	212
7.3.17	Synthesis of [$\{Mg_2Cl_3(THF)_6\}^+\{Zn^tBu_3\}^-$] (40)	213
7.3.18	Synthesis of [$\{Mg_2Cl_3(THF)_6\}^+\{Zn_2Et_5\}^-$] (41)	214
7.3.19	Synthesis of [$\{Mg_3(OEt)_2Br_3(THF)_6\}^+\{Zn_2Et_5\}^-$] (42)	215
7.3.20	Synthesis of [$\{Mg_2Cl_3(THF)_6\}^+\{Mg_2(OC(Et)Ph)_2Cl_3(THF)\}^-$] (44)	215
7.3.21	Synthesis of [$\{(THF)_5Mg_3Cl_4\{OC(H)Ph(CF_3)\}_2\}$] (50)	216
7.3.22	General procedure for alkylation studies of 2,2,2-trifluoroacetophenone (47)	216
7.3.23	Synthesis of [$\{Mg_2Cl_3(THF)_6\}^+\{Zn(p-C_6H_4Me)_3\}^-$] (52)	217
7.3.24	Cross-coupling reaction of 52 with iodobenzene	217
7.3.25	General procedure for monitoring Zn-I exchange reactions of 40 with functionalised aryl iodide substrates in d_8 -THF	218
7.3.26	General procedure for Zn-I exchange reactions of 40 with functionalised aryl iodide substrates followed by Negishi cross-coupling with iodobenzene	218
	(a) 4-methylbiphenyl (53)	219
	(b) 3-methylbiphenyl (56)	219
	(c) 2-methylbiphenyl (57)	220
	(d) 2-methoxybiphenyl (61)	220
	(e) 3-methoxybiphenyl (62)	221
	(f) 4-methoxybiphenyl (63)	221
	(g) 2-cyanobiphenyl (70)	221
	(h) 3-cyanobiphenyl (71)	222
	(i) 4-cyanobiphenyl (72)	222
7.3.27	Synthesis of [$\{Mg(THF)_6\}^{2+}\{Zn(o-C_6H_4OMe)_3\}_2^-$] (64)	222
7.3.28	Synthesis of [$(THF)_4MgCl\{N\equiv C-C_6H_4\}ZnI(C_6H_4CN)(THF)$] (68)	223

Chapter 8: Overview, conclusions and outlook 224

Bibliography 230

CD-ROM: Appendices (X-ray crystallographic data, DOSY studies, DFT studies and publications)

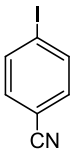
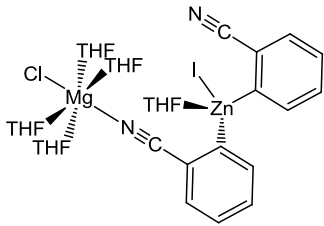
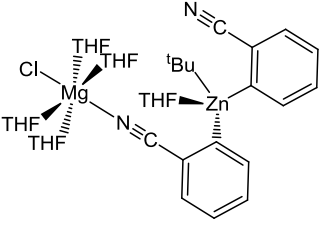
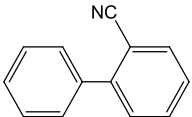
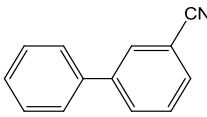
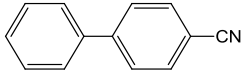
Table of Compounds

Number	Compound	Number	Compound
1		2	
3		4	
5		6	
7		8	
9		10	
11		12	
13		14	

Number	Compound	Number	Compound
15		16	
17		18	
19		20	
21		22	
23		24	
25		26	
27		28	

Number	Compound	Number	Compound
29		30	
31		32	
33		34	
35		36	
37		38	
39		40	
41		42	
43		44	

Number	Compound	Number	Compound
45		46	
47		48	
49		50	
51		52	
53		54	
55		56	
57		58	
59		60	
61		62	
63		64	
65		66	

Number	Compound	Number	Compound
67		68	
69		70	
71		72	

Chapter 1: Introduction to organozinc chemistry and recent advances in alkali metal zincates

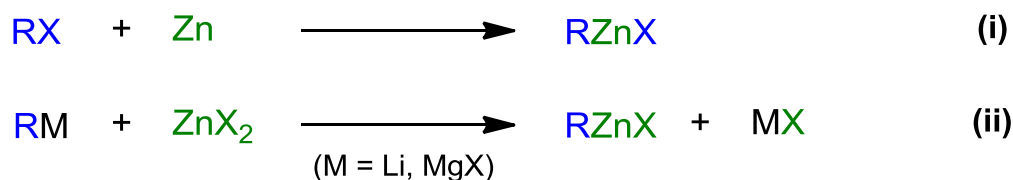
1.1 Organozinc reagents

The discovery of the first organozinc reagent in 1849 by Frankland, who formed ZnEt_2 by heating ethyl iodide with zinc powder,^[1] was a breakthrough which for many authors heralded the birth of modern organometallic chemistry. Although initially these organozinc reagents captured the attention of synthetic chemists, they became somewhat neglected with the emergence of Grignard and organolithium reagents in the early part of the 20th century.^[2] However, recently we have seen the re-emergence of organozinc reagents as key organometallic reagents in organic and organometallic chemistry, used in a number of key synthetic methodologies.

Although it is present in the transition metal series, zinc has few common properties with the other transition metals. This is due to the very stable valence electron configuration of zinc ($[\text{Ar}] 4s^2 3d^{10}$), with the filled d-shell resulting in zinc chemistry being dominated by the $4s^2$ valence electrons, sharing many reactivity features with magnesium ($[\text{Ne}] 3s^2$).^[3] However, despite their similar chemical properties and size (atomic radii $\text{Mg} = 160 \text{ pm}$; $\text{Zn} = 133 \text{ pm}$)^[4] they have some important differences. Zinc is more electronegative than magnesium, and as a result organozinc reagents exhibit stronger, more covalent C-M bonds which makes them less reactive than organomagnesium reagents, but also more selective.^[3]

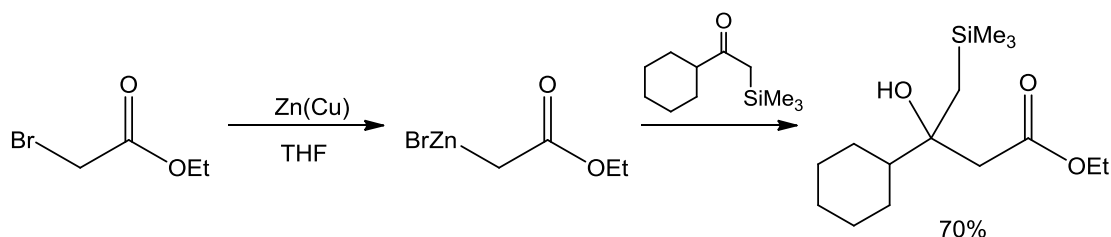
Neutral organozinc reagents exist in two main formulations; organozinc halides (RZnX) and diorganozinc reagents (ZnR_2). Historically, they have been primarily used in organic synthesis as soft nucleophiles for performing addition reactions, such as the Reformatsky reaction.^[5] Unlike more polar organometallic species such as organolithium and organomagnesium compounds, organozinc reagents are significantly less reactive due to the covalent nature and low kinetic reactivity of Zn-C bonds.^[6] However, this lower reactivity accounts for the greatest advantage of organozinc reagents, which is their greater selectivity and functional group tolerance.^[2]

Another important advantage of organozinc reagents is their relatively straightforward preparation. Starting first with organozinc halides (RZnX), there are two common methods for their preparation; (i) direct insertion of zinc metal into an organic halide (R-X), and (ii) metathesis reaction of a zinc halide (ZnX₂) with a more polar organometallic reagent, typically an organolithium (RLi) or a Grignard reagent (RMgX) (**Scheme 1.1**).^[7]



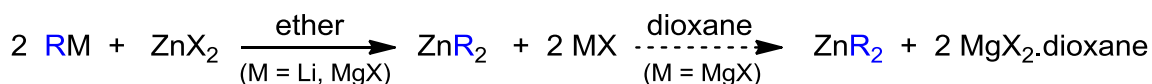
Scheme 1.1: Synthesis of organozinc halides (RZnX) by (i) direct Zn insertion and (ii) metathesis reaction.

When using the direct insertion approach the zinc has to first be activated due to the general low reactivity of zinc metal caused by surface oxide formation. This can be done by preparing a Zn/Cu couple (treatment of zinc dust with HCl then CuSO_{4(aq)}, followed by washing/drying),^[8] using Rieke zinc (reduction of ZnX₂ in dry THF by lithium, sodium or potassium naphthalenide),^[9] or by treatment of zinc dust with catalytic amounts of 1,2-dibromoethane and chlorotrimethylsilane.^[10] More recently, Knochel has also shown that zinc insertion into organic halides can be induced by the addition of stoichiometric amounts of LiCl.^[11] Although the metathesis approach can be used to prepare organozinc halides, the need for reactive organometallic reagents (RLi, RMgX) in the synthesis greatly limits the formation of functionalised organozinc reagents due to unwanted side-reactions of the starting materials, and as a result zinc insertion is a more favourable approach.^[7] Organozinc halides prepared via these methods have been most commonly used in Reformatsky reactions, which dating back to 1887 is one of the oldest applications of organozinc halide reagents in synthesis.^[2] Typically this reaction involves the insertion of Zn into the C-X bond of an α-halocarbonyl compound to form a zinc enolate, which can then be subsequently reacted with an electrophile. The most common electrophiles are aldehydes and ketones to form β-hydroxyketones (**Scheme 1.2**). The main advantage of this reaction is that the low basicity of the zinc enolates prevents any unwanted side reactions and so can be reacted with highly enolizable carbonyl compounds.^[5, 12]



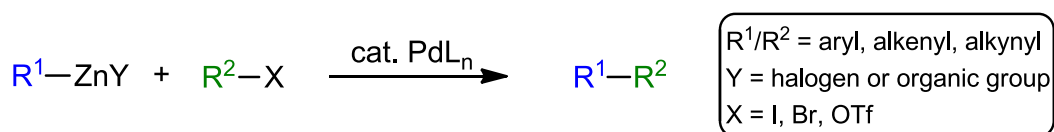
Scheme 1.2: Reformatsky reaction.^[13]

Turning to diorganozinc species, simple dialkylzinc reagents are most commonly prepared by a metathesis reaction between ZnX_2 and two equivalents of RLi or RMgX (**Scheme 1.3**). The organozinc reagent can then be purified by distillation/sublimation, or removal of the inorganic salt by-products by filtration, whereby dioxane can be added to induce the precipitation of magnesium salts.^[14]



Scheme 1.3: Synthesis of diorganozinc reagents (ZnR_2) by metathesis reaction.

A final important advantage of organozinc reagents, which has seen their use in synthetic chemistry flourish in the last 30 years, is that they can readily undergo transmetalation with transition metal complexes such as palladium and nickel, allowing the generally sluggish reactivity of organozinc reagents to be circumvented. As a result, organozinc reagent have become essential reagents in transition metal catalysed carbon-carbon bond forming reactions, in particular in Negishi cross coupling,^[15] whereby an unsaturated organozinc reagent can be coupled to an unsaturated organic electrophile in the presence of a palladium (or nickel catalyst) (**Scheme 1.4**).^[16] Recently, this methodology has even been successfully applied to the $\text{C}(\text{sp}^3)\text{-C}(\text{sp}^2)$ cross-coupling of alkylzinc species with various unsaturated organic halides.^[17] Further examples of reactions which can be performed by organozinc reagents in the presence of a Ni or Pd catalysts include acylations, conjugate addition to α,β -unsaturated ketones and 1,2-addition to carbonyls.^[16]



Scheme 1.4: General scheme for palladium catalysed Negishi cross-coupling reaction.^[16]

1.2 Alkali metal zincates

Group I organometallic compounds such organolithium and lithium amide reagents (LiR , LiNR_2) have been the cornerstone of organometallic chemistry for many years. The high polarity of the Li-C (or Li-N) bonds make these species highly reactive, and ideal reagents for performing deprotonative metallation, metal-halogen exchange and carbometallation reactions, displaying levels of reactivity unequalled by any other homometallic reagents.^[18] However, this high level of reactivity comes at a cost, and organolithium reagents have a number of disadvantages such as their lack of functional group tolerance, incompatibility with both chlorinated and ethereal solvents, they often require cryogenic temperatures, and are incompatible with important synthetic methods to generate new C-C bonds such as palladium catalysed cross-coupling reactions. By combining organolithium and organozinc reagents to form alkali metal zincates, the high reactivity of organolithium reagents can be combined with the great functional group tolerance and solvent compatibility of organozinc reagents, simultaneously overcoming the poor selectivity of organolithium reagents and low kinetic reactivity of the organozinc reagents. The result is the formation of new mixed-metal reagents that display chemical properties which cannot be replicated by either of their relevant homometallic reagents.

Dating back to 1858, alkali metal zincates constitute the oldest known class of heterobimetallic (ate) compound, first prepared by Wanklyn who reacted sodium metal with diethyl zinc to form “ NaZnEt_3 ”.^[19] In 1948 Hurd reported the successful synthesis of the lithium tetra(alkyl)zincate $[\text{Li}_2\text{ZnMe}_4]$,^[20] the structure of which was reported in 1968 by Weiss.^[21] The term ‘ate’ itself was coined by Wittig in 1951, to describe the new lithium tris(aryl)zincate $[\text{LiZnPh}_3]$.^[22] Despite this pioneering work in the area of alkali metal zincates, the use of these compounds in synthetic chemistry remained dormant for some time, and only recently have they emerged as a highly versatile type of organometallic reagent which can participate in numerous fundamental organic transformations such as deprotonative metallation,^[3, 23] metal-halogen exchange^[24] and nucleophilic addition.^[25]

Primarily, there are two major formulations for this type of mixed-metal reagent; $\text{M}^{\text{I}}\text{ZnR}_3$ and $\text{M}^{\text{I}}_2\text{ZnR}_4$, which are usually referred to as triorganozincates and “high order” tetraorganozincates respectively. These compounds can exhibit; (i) a solvent separated ion-pair (SSIP) structure, where the alkali metal forms the cationic part of the molecule, solvated

by donor solvent or a Lewis base, and the zinc bonds to the anionic ligands to form the counterion, or alternatively (ii) a contacted ion-pair (CIP) structure, giving rise to a molecular structure where both metals are connected through one or more of the anionic ligands.^[26]

The conformation adopted by the zincate is dependent on a number of factors, including the solvent employed, presence of a Lewis base and the anionic ligands bonded to zinc, as has been demonstrated in a recent study of the triorganozincate LiZnMe_3 . In the presence of the tridentate amide donor, N,N,N',N'',N''' -pentamethyldiethylenetriamine (PMDETA), the zincate adopts the CIP structure $[(\text{PMDETA})\text{LiZnMe}_3]$ (**Figure 1.1(a)**), whereas in the presence of the analogous ethereal donor, diglyme, a SSIP species is formed $[\text{Li}(\text{diglyme})_2]^+[\text{ZnMe}_3]^-$ (**Figure 1.1(b)**).^[27]

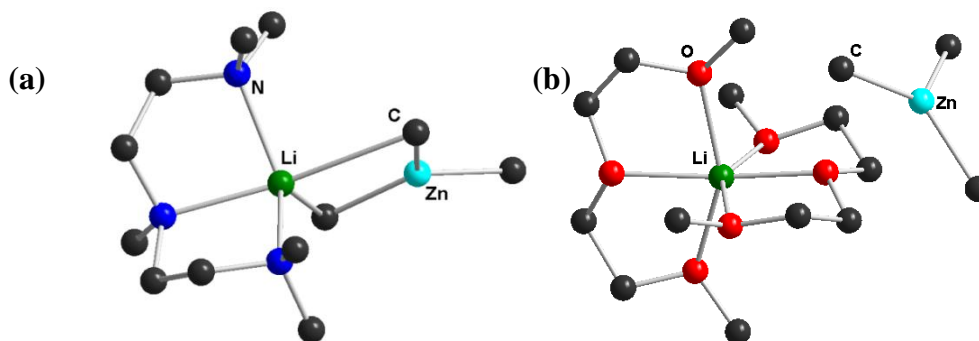


Figure 1.1: Crystal structures of (a) CIP triorganozincate $[(\text{PMDETA})\text{LiZnMe}_3]$ and (b) SSIP triorganozincate $[\text{Li}(\text{diglyme})_2]^+[\text{ZnMe}_3]^-$. Hydrogen atoms have been omitted for clarity.

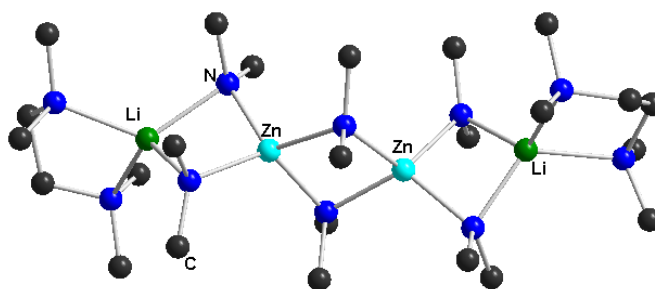


Figure 1.1(c): Crystal structure of triorganozincate $[\{(\text{TMEDA})\text{LiZn}(\text{NMe}_2)_3\}_2]$. Hydrogen atoms have been omitted for clarity.

In both of these compounds the zinc centre is three co-ordinate, adopting a trigonal (sp^2 like) conformation. However, triorganozincates are not solely confined to such bonding modes, as shown by the homoleptic tris-amido zincate “ $(\text{TMEDA})\text{LiZn}(\text{NMe}_2)_3$ ” (TMEDA= N,N,N',N' tetramethylethylenediamine) which exists as dimeric $[\{(\text{TMEDA})\text{LiZn}(\text{NMe}_2)_3\}_2]$ (**Figure 1.1(c)**).^[26b] Thus, although this compound is a triorganozincate, each of the zinc centres is

four co-ordinate, adopting a distorted tetrahedral (sp^3 like) geometry. In this regard the geometry of Zn in $\{[(\text{TMEDA})\text{LiZn}(\text{NMe}_2)_3]_2\}$ is more related to tetraorganozincates, where usually the zinc will also adopt a tetrahedral geometry, examples of which include the homoleptic zincate $[(\text{TMEDA})_2\text{Li}_2\text{ZnMe}_4]$ and heteroleptic $[(\text{TMEDA})_2\text{Li}_2\text{Zn}(\text{NMe}_2)_3\text{Me}]$ (**Figure 1.2**).^[26b]

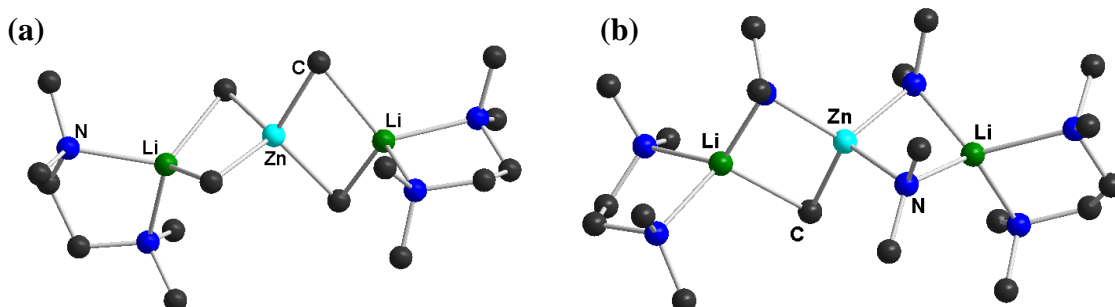
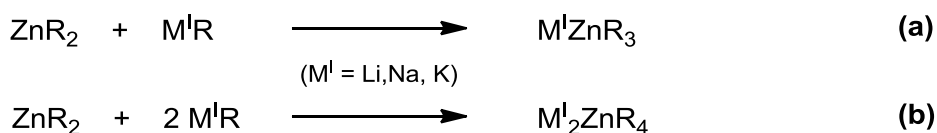


Figure 1.2: Crystal structures of tetraorganozincates (a) $[(\text{TMEDA})_2\text{Li}_2\text{ZnMe}_4]$ and (b) $[(\text{TMEDA})_2\text{Li}_2\text{Zn}(\text{NMe}_2)_3\text{Me}]$. Hydrogen atoms have been omitted for clarity.

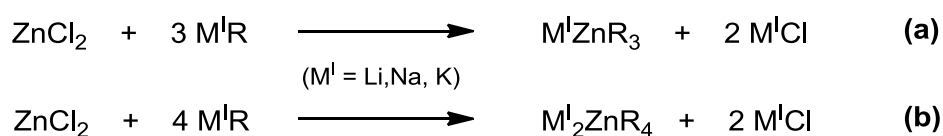
1.2.1 Preparation of alkali metal zincates

Two common methods for the preparation of alkali metal zincates are; (i) co-complexation of an organozinc reagent (ZnR_2) with an organolithium reagent (LiR) (or other organo-alkali metal species such as organosodium (NaR) and organopotassium (KR) reagents), and (ii) metathesis reaction of zinc salts, most commonly ZnCl_2 , with a group I organometallic reagent. Starting with the co-complexation approach, the formation of a triorganozincate or tetraorganozincate can be determined simply by adjusting the stoichiometry of the reagents. Thus, for a triorganozincate a ratio of ZnR_2 to M^IR of 1:1 is required, and for a tetraorganozincate a ratio of 1:2 (**Scheme 1.5**),^[28] although in some cases the formation of one of these types of zincates is more energetically favoured than the other, giving rise to disproportionation reactions.^[24d, 26b, 29] This protocol can be easily adapted for the preparation of heteroleptic zincates of the form $\text{M}^I\text{Zn}(\text{R}')\text{R}_2$ by reacting a diorganozinc reagent (ZnR_2) with a group one organometallic reagent possessing a different organic fragment ($\text{M}^I\text{R}'$).



Scheme 1.5: Synthesis via a co-complexation approach of (a) a triorganozincate and (b) a tetraorganozincate.

Turning to the metathesis approach, which involves the reaction of ZnCl_2 with a more polar organometallic reagent, the formation of triorganozincates and tetraorganozincates can again be controlled by the ratio of monometallic reagents employed (**Scheme 1.6**).^[28] Heteroleptic zincates can also be prepared through this method, by the successive reaction of different organometallic reagents ($\text{M}^{\text{I}}\text{R}$ and $\text{M}^{\text{I}}\text{R}'$) with ZnCl_2 .^[30] One of the main drawbacks to this approach is the formation of two equivalents of alkali metal chloride ($\text{M}^{\text{I}}\text{Cl}$), which in some cases can greatly affect the reactivity of the newly generated mixed-metal species, as will be discussed later (**Chapters 1.3.2** and **Chapters 4-6**). In addition, this metathetical approach requires the use of ethereal solvents (usually THF or diethyl ether) to solubilise the inorganic salt, which can lead to side-reactions of the polar organometallic reagent with the solvent.

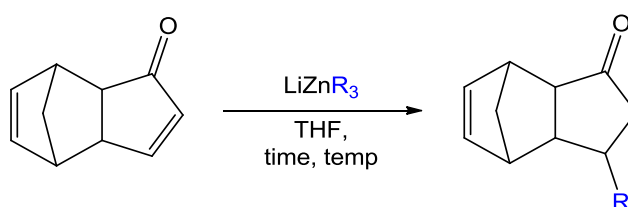


Scheme 1.6: Synthesis via metathesis reaction of **(a)** triorganozincates and **(b)** tetraorganozincates.

1.2.2 Applications of alkali metal zincates in 1,4-conjugate addition and 1,2-addition

The most common applications of homometallic reagents such as organolithium and Grignard reagents in synthetic chemistry have been in both nucleophilic 1,2-addition and 1,4-conjugate addition, metal halogen exchange and deprotonative metallation.^[18, 31] Thus, early studies into the reactivity of alkali metal zincates focussed on these cornerstone synthetic methodologies.

One of the earliest reported synthetic reactions involving triorganozincates was in 1977 by Isobe and co-workers, who described the use of “trialkyl lithiumzinc” compounds, LiZnR_3 , as new reagents for performing selective conjugate addition to α,β -unsaturated carbonyl compounds. The generality of this reaction was shown by performing the conjugate addition of a range of different lithium triorganozincates to dicyclopentadien-1-one (**Scheme 1.7**), with the reactions yielding none of corresponding 1,2-adducts.^[32] Since this initial report, numerous examples have followed on the use of lithium triorganozincates for performing conjugate addition reactions,^[30a, 33] and sparked a steady growth in the use of these bimetallic reagents in synthetic organic chemistry.^[28]

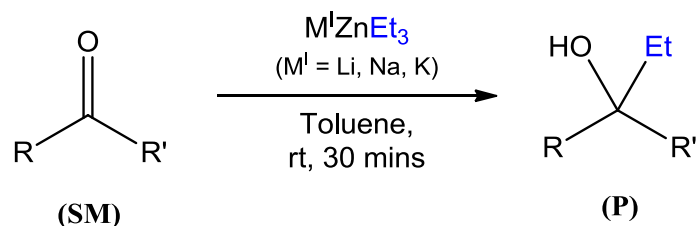


R	Time (mins)	Temp. (°C)	Yield (%)
Me	30	0	92
ⁿ Bu	30	-78 to 0	92
^s Bu	60	-78	66
^t Bu	60	-78	58
Ph	180	-78	15
1-butynyl	180	-78	0

Scheme 1.7: 1,4-conjugate addition of LiZnR_3 to dicyclopentadien-1-one.

Not solely restricted to lithium, alkali metal zincates of the form $\text{M}^{\text{I}}\text{ZnEt}_3$ ($\text{M}^{\text{I}} = \text{Li, Na, K}$) have proved to be excellent reagents for selective nucleophilic 1,2-addition to a series of aldehydes and ketones at ambient temperature (**Scheme 1.8**).^[34] Substrates which successfully underwent nucleophilic addition included benzaldehyde, acetaldehyde and benzophenone, although the α,β -unsaturated substrate, 2-cyclohexenone, gave only the 1,4-adduct for all three zincates. Possible side reactions include reduction (through β -hydride elimination) and aldol dimerization when the substrate possesses α -hydrogens. Although such side reactions are commonly seen when using organolithium reagents, in the case of $\text{M}^{\text{I}}\text{ZnEt}_3$ these by-products were seen only in trace amounts, although reaction of hexan-2-one with NaZnEt_3 and KZnEt_3 gave significant amounts of the aldol product (23% and 28% respectively). In all cases, reaction of homometallic ZnEt_2 with the substrate led almost entirely to recovery of the starting material (**Scheme 1.8**). It has also been shown that heteroleptic alkali metal zincates of the form $\text{M}^{\text{I}}\text{ZnMe}_2\text{H}$ ($\text{M}^{\text{I}} = \text{Li, Na}$), prepared by co-complexation of ZnMe_2 and $\text{M}^{\text{I}}\text{H}$, could selectively perform a 1,2-addition of the hydride ligand to a broad range of different aldehydes and ketones yielding the corresponding alcohols. The reduction of these substrates proceeded without any nucleophilic addition of the alkyl ligand, demonstrating the chemoselectivity of these mixed-metal species and highlighting their potential as effective reducing agents. Adding to the scope of this reaction, the same protocol could be applied to

perform the selective reduction of esters, amides, epoxides and lactones, and the reaction could also be performed using catalytic amounts of ZnMe_2 (20 mol%).^[25]



R	R'	LiZnEt ₃		NaZnEt ₃		KZnEt ₃		ZnEt ₂	
		SM (%)	P (%)	SM (%)	P (%)	SM (%)	P (%)	SM (%)	P (%)
Ph	H	0	97	0	97	0	87	98	0
CH ₃ (CH ₂) ₅	H	0	95	4	90	3	85	98	0
Ph	CH ₃	0	98	27	71	62	36	99	0
Ph	Ph	0	99	0	97	0	99	100	0
CH ₃	CH ₂ CH ₂ CH(CH ₃) ₂	3	94	38	37	38	31	98	0

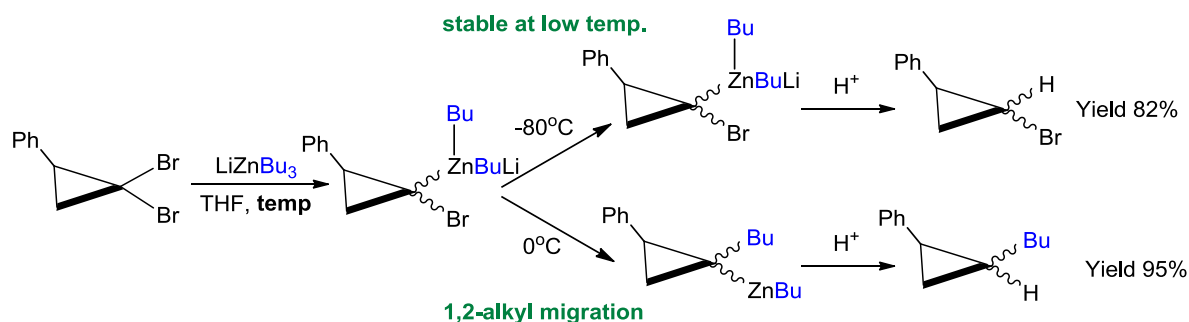
Scheme 1.8: Nucleophilic 1,2-addition of $\text{M}^{\text{I}}\text{ZnEt}_3$ to aldehydes, ketones and enones.

1.2.3 Applications of alkali metal zincates in metal-halogen exchange

Metal-halogen exchange is one of the most common applications of organolithium reagents in synthetic chemistry, with these highly polar organometallic reagents showing high levels of reactivity towards aryl-, heteroaryl-, vinyl- and alkyl-halides.^[35] However, to prevent any unwanted deprotonation of the substrate, or side-reactions with sensitive functional groups present, the reactions have to be performed at sub-ambient temperatures. In addition, an excess of the organolithium reagent (RLi) is usually required to prevent reaction of the new lithiated species with the by-product of the reaction R-X.^[36]

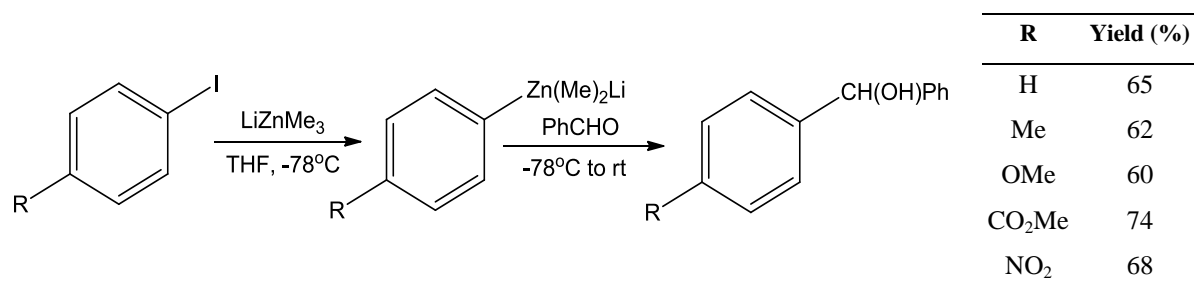
Early reports of the use of zincates in metal-halogen exchange reactions came from Harada and Oku, who showed the ability of triorganozincates to successfully perform zinc-bromine and zinc-chlorine exchange reactions with 1,1-dibromocyclopropane and 1,1-dihaloalkenes (**Scheme 1.9**).^[37] The zincate carbenoid intermediates could then undergo subsequent 1,2-alkyl migration with loss of a second halogen atom to form cyclopropylzinc and alkenylzinc

species respectively, which could in turn be quenched with a suitable electrophile. Furthermore, the authors found that this 1,2-alkyl migration could be inhibited if the reaction was performed at -80°C , at which point the zincate carbenoid species remained stable and could be quenched with the relevant electrophile (**Scheme 1.9**).

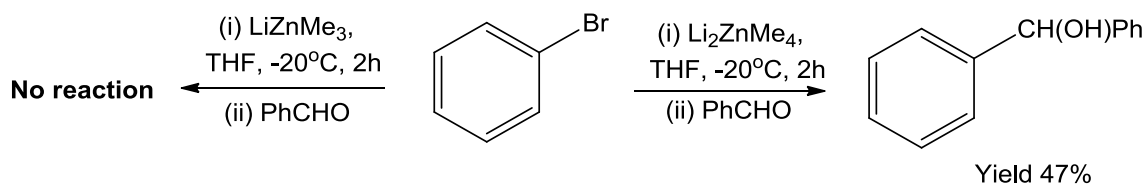


Scheme 1.9: Zinc-halogen exchange reactions of 1,1-dibromocyclopropane with LiZnBu_3 followed by electrophilic quenching with H^+ at variable temperatures.

Moving onto aromatic substrates, in 1994 Kondo and co-workers successfully reported the efficient metal-halogen exchange reactions of a variety of aryl iodides using the lithium trimethylzincate, LiZnMe_3 . The resulting aryldimethyl zincates could then be reacted with benzaldehyde to give the corresponding benzhydrol product in yields of 60-74% (**Scheme 1.10(a)**).^[38] This reagent failed to promote direct zinc-bromine exchange when bromobenzene was reacted with LiZnMe_3 under the same conditions. However, when the tetraorganozincate Li_2ZnMe_4 was employed, followed by electrophilic interception with benzaldehyde, the resulting secondary alcohol could be obtained in a yield of 47% (**Scheme 1.10(b)**).^[24b] This greater reactivity of the tetraalkylzincate over the trialkylzincate was rationalised by the authors in terms of the greater anionic character of the alkylzinc centre (ZnMe_4^{2-} vs. ZnMe_3^-).

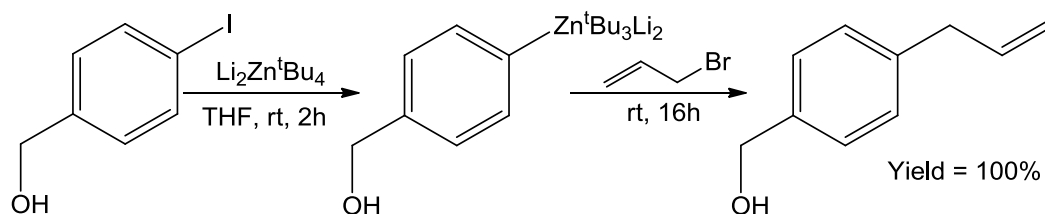


Scheme 1.10(a): Zn-I exchange reaction of Ar-I with LiZnMe_3 , followed by reaction with benzaldehyde.



Scheme 1.10(b): Zn-Br exchange reaction of bromobenzene with LiZnMe_3 and Li_2ZnMe_4 , followed by reaction with benzaldehyde.

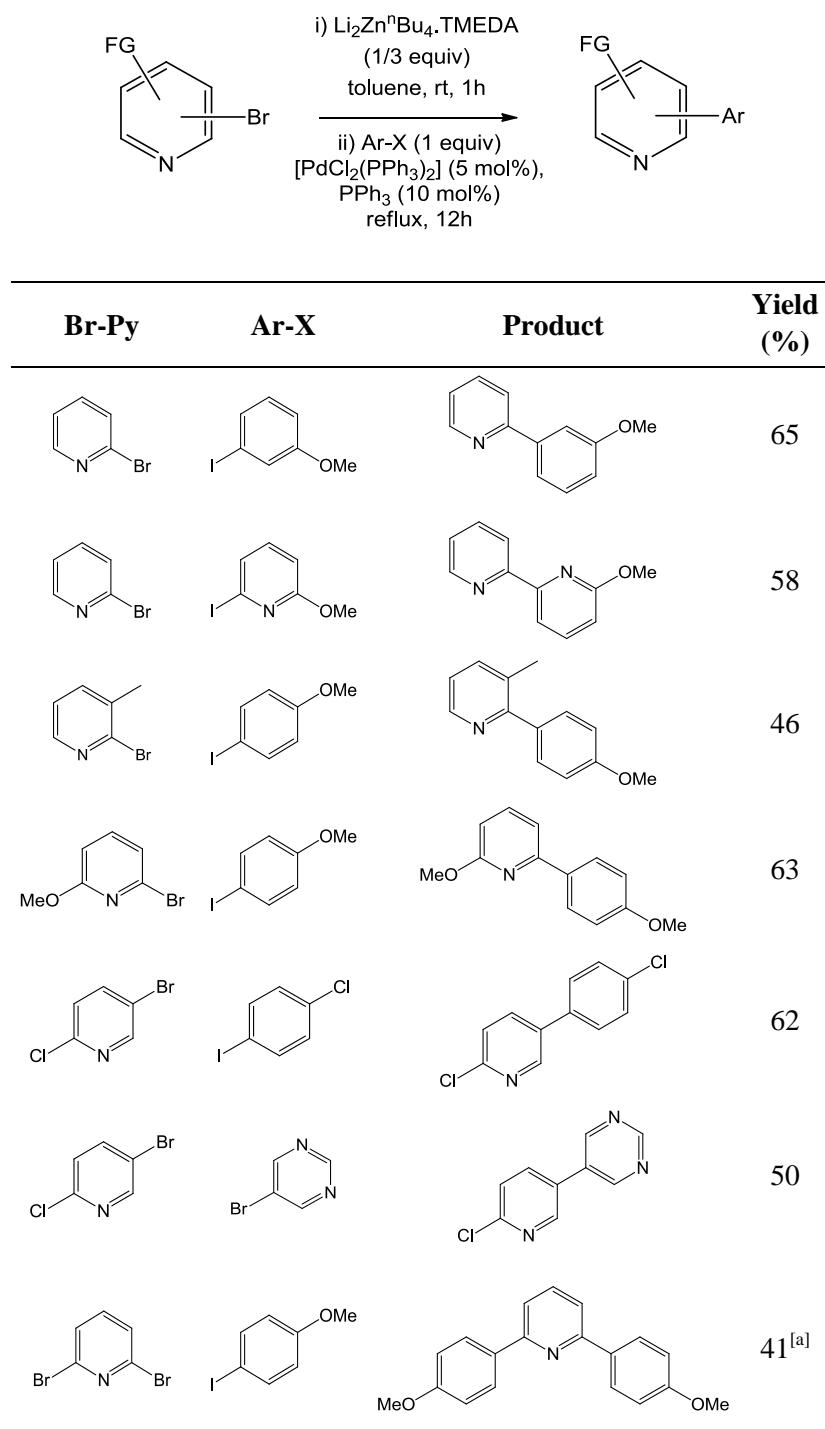
More recently the great versatility displayed by the high order lithium *tert*-butylzincate ($\text{Li}_2\text{Zn}^t\text{Bu}_4$) in metal-halogen exchange reactions has been shown.^[24c, 24d] This reagent proved highly effective in both Zn-I and Zn-Br exchange reactions of aromatic halides which possessed sensitive functional groups such as esters and amides in almost quantitative yields. Even more interestingly this mixed-metal reagent selectively promotes the relevant metal-halogen exchange products when reacted with aryl iodides possessing unprotected acidic protons (including amide NH and phenolic OH protons), which after quenching with allyl bromide gave the desired product in almost quantitative yields (**Scheme 1.11**). However, in Zn-Br exchange reactions elevated temperatures were required (60°C) and in the case of *p*-bromobenzylalcohol this resulted in deprotonation of the alcohol instead of the expected metal-halogen exchange, and subsequent C-C bond formation when the intermediate was reacted with the organic electrophile did not take place.



Scheme 1.11: Reaction of $\text{Li}_2\text{Zn}^t\text{Bu}_4$ with 4-iodobenzyl alcohol followed by quenching with allyl bromide.

Electrospray ionisation mass spectroscopy (ESI-MS) and NMR studies of LiZn^tBu_4 suggest that in solution the constitution of this high order zincate is retained, even in a strongly donating solvent such as THF, with no indication of an equilibrium between the mixed-metal species and its monometallic components taking place.^[24d] In contrast, similar studies of the trialkylzincate LiZn^tBu_3 showed that the monoanionic Zn^tBu_3^- fragment of this species is not retained in solution, instead disproportionating to Zn^tBu_2 and $\text{Li}_2\text{Zn}^t\text{Bu}_4$. Analysis of the gas-phase properties of these two compounds by DFT studies was in agreement with these

spectroscopic results, showing that the disproportionation of LiZn^tBu_3 to $\text{Li}_2\text{Zn}^t\text{Bu}_4$ and Zn^tBu_2 is thermodynamically favoured ($\Delta E_{\text{rel}} = -6.9 \text{ kcal mol}^{-1}$).^[24d, 29] Previously it has been reported that LiZn^tBu_3 is able to carry out Zn-I exchange reactions with functionalised aromatic iodides.^[39] However, these results would suggest that the active species involved in this process is actually the more stable lithium tetra-*tert*-butylzincate.

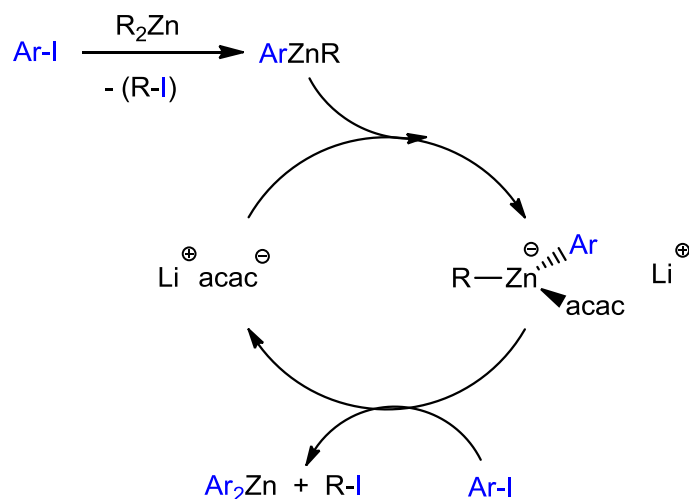


Scheme 1.12: Zn-Br exchange of bromopyridines with $\text{Li}_2\text{Zn}^n\text{Bu}_4\cdot\text{TMEDA}$ followed by Negishi cross-coupling. ^[a] one equivalent of $\text{Li}_2\text{Zn}^n\text{Bu}_4\cdot\text{TMEDA}$ employed.

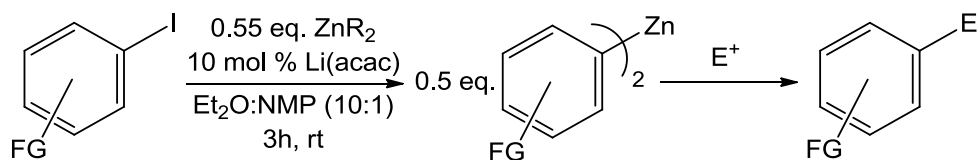
The application of the related zincate, $\text{Li}_2\text{Zn}^n\text{Bu}_4\cdot\text{TMEDA}$, in the zinc-halogen exchange of bromopyridine has also been recently reported (**Scheme 1.12**). Interestingly in this case it was shown that not only could the zincate successfully perform the Zn-Br exchange reaction of 2- and 3-bromopyridines, but that it could also react substoichiometrically (1/3 equivalent) allowing one molecule of the zincate to simultaneously metallate three molecules of the substrate.^[40] This polybasic behaviour of lithium zincates has previously been reported in both deprotonative metallation^[41] and metal-halogen exchange^[42], but this is the first example where it has been described for a homoleptic zincate. Unfortunately all four alkyl groups of the zincate could not be activated towards Zn-Br exchange, which was believed to be due to low solubility of the proposed tripyridyl zincate species formed $[\text{Li}_2\text{Zn}(\text{py})_3]^n\text{Bu}$. Having optimised the reaction conditions, a series of bromopyridine substrates were successfully metallated and then subjected to Negishi cross-coupling to form the final products in yields ranging from 41-65% (**Scheme 1.12**).

Previously, it has been reported that the neutral dialkylzinc reagents Zn^iPr_2 and ZnEt_2 show no reactivity in terms of metal-halogen exchange reactions with aryl iodides in THF or Et_2O solutions. However, when the solvent was changed to a 1:10 mixture of Et_2O and *N*-methylpyrrolidinone (which is a highly polar solvent) the metal-halogen exchange reaction occurred, forming ArZnR . In an attempt to induce the activation of the second alkyl group on the zinc, $\text{Li}(\text{acac})$ was employed as an additive to form a putative heteroleptic lithium zincate species “[Li^+ [(acac) $\text{ZnAr}(\text{R})$]]”. Undergoing a second metal-halogen exchange reaction led to the formation of ZnAr_2 along with regeneration of the $\text{Li}(\text{acac})$ (**Scheme 1.13(a)**). As a result, the lithium additive could be employed catalytically (10 mol%), successfully activating Zn^iPr_2 towards two-fold metal-halogen exchange with a series of aryl iodide substrates (**Scheme 1.13(b)**).^[42] Thus, we see another example of lithium-zincates not only providing high levels of reactivity, selectivity and functional group tolerance, but also high atom economy, where in this case two alkyl “arms” of the zincate can promote metal-halogen exchange under catalytic conditions.

Although proving to be extremely successful in 1,4-conjugate addition, 1,2-addition and metal halogen exchange, lithium alkylzincates, such as those described above, have proved to be sluggish to react with aromatic molecules to promote direct Zn-H exchange reactions (deprotonative metallations).



Scheme 1.13(a): Proposed catalytic cycle for the reaction of ZnR_2 and $\text{Li}(\text{acac})$ with Ar-I .



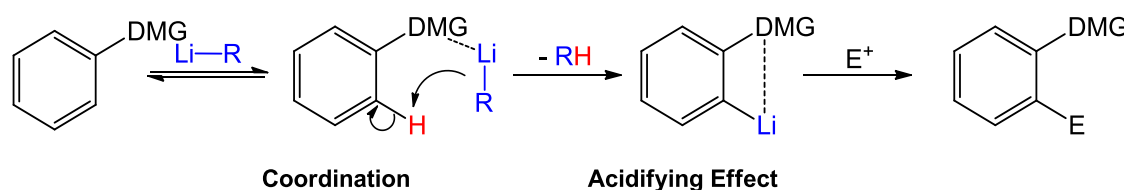
Ar-I	E	Yield (%)	Ar-I	E	Yield (%)
	PhCO-	82		MeCO-	87
	4-NO ₂ -C ₆ H ₄ -	71		4-CO ₂ Me-C ₆ H ₄ -	81
	4-F-C ₆ H ₄ -	83		4-CO ₂ Me-C ₆ H ₄ -	52
	Me ₃ Sn-	66		CH ₂ =CH-CH ₂ -	84
	4-CO ₂ Me-C ₆ H ₄ -	86		cyclohexyl-CO-	75
	2-NO ₂ -C ₆ H ₄ -	84		CH ₂ =CH-CH ₂ -	77
	4-Cl-C ₅ H ₃ N-CO-	77		4-CO ₂ Me-C ₆ H ₄ -	60

Scheme 1.13(b): Metal-halogen exchange of Ar-I with ZnR_2 and $\text{Li}(\text{acac})$ and subsequent electrophilic quenching.

1.3 Alkali metal TMP-zincates in directed *ortho* metallation (DoM)

1.3.1 Directed *ortho* metallation (DoM)

The process of directed *ortho* metallation (DoM) involves the selective metallation of an aromatic proton *ortho* to a specific functional group, often referred to as a direct metallating group (DMG) (**Scheme 1.14**). This process has arguably now overtaken the more classical approach of electrophilic aromatic substitution as the most useful tool to regioselectively functionalise an aromatic ring.^[43]



Scheme 1.14: A simplified reaction mechanism for DoM.

DoM is primarily favoured by two factors; (i) the DMG provides the organometallic reagent with a coordination point (usually a basic heteroatom), which directs the reactivity adjacent to the functional group (*ortho*), and thus fixes the regioselectivity of the reaction (ii) usually the DMG is an electron withdrawing substituent, and therefore it can acidify nearby protons (via inductive effect), and as a result those protons *ortho* to the DMG will be metallated more readily than those which are at *meta* or *para* positions.^[43]

In a comprehensive review of directed *ortho* lithiation (DoL) carried out in 1990 by Snieckus,^[44] a number of DMG were divided into different categories based on their ability to facilitate *ortho* lithiation (**Table 1.1**). In general, the stronger DMG contain a basic heteroatom and are strongly electron withdrawing (e.g. tertiary amines and carbamates), whereas the less powerful DMG tend to be weaker Lewis bases, acidifying nearby protons by the presence of an electronegative atom (via the inductive effect), and usually contain only a nitrogen or oxygen atom (e.g. ethers and amines), or a halide. One of the main drawbacks of the strong DMG is that the metallation reactions have to be carried out at low temperatures to avoid possible side reactions, as they all contain an electrophilic carbonyl group or an equivalent group (e.g. sulfone, sulfoxide).

Decreasing ability to facilitate DoM

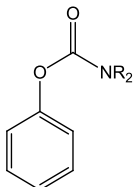
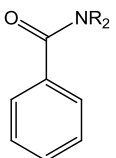
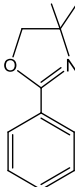
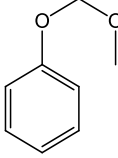
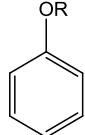
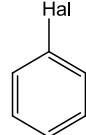
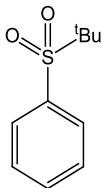
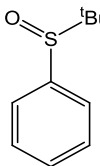
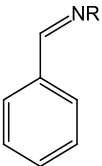
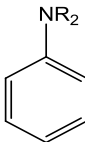
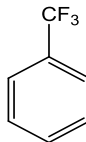
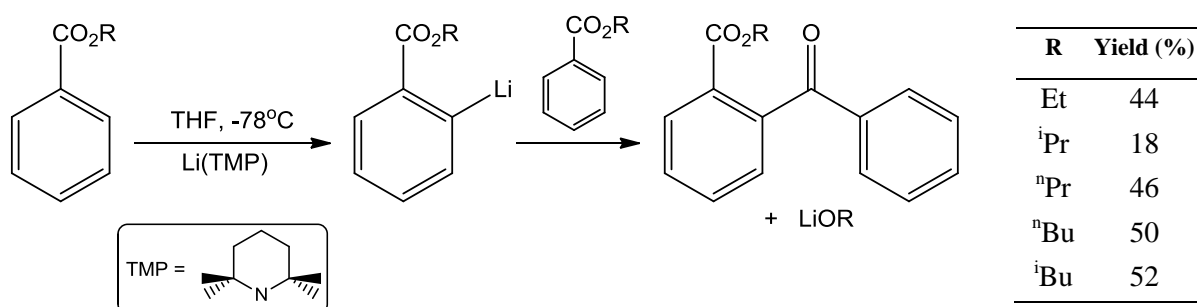
Strong -78°C		Moderate -50°C -20°C		Weak 0°C >0°C	
					
Carbamates	3 ^y Amides	Oxazolines	MOM ethers	Ethers	Halides
					
Sulfones	Sulfoxides	Imines		Amines	Trifluoromethyl

Table 1.1: Table of functionalised aromatic substrates showing their relative ability to facilitate DoM and general reaction temperature required for lithiation using ⁿBuLi in THF.

1.3.2 Recent developments in alkali metal TMP-zincates

One of the most widely used metallating reagents in organic synthesis is the secondary amide lithium 2,2,6,6-tetramethylpiperidide (Li(TMP)). The steric hindrance afforded by the bulky, cyclic amide, coupled with its strong basicity ($pK_a = 37$),^[45] makes it an excellent reagent for performing deprotonation reactions with a wide range of organic molecules.

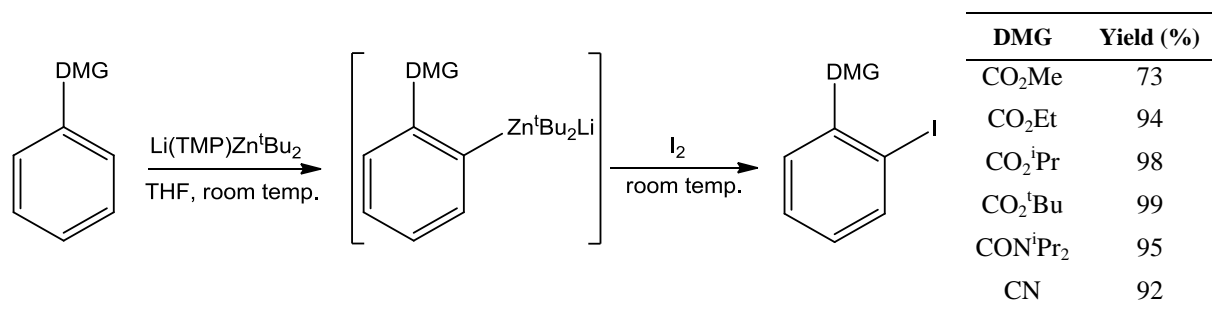


Scheme 1.15: Directed *ortho* lithiation of arylcarboxylic esters followed by condensation reaction of lithiated intermediate with unreacted starting material.

In some cases the relevant organolithium intermediate resulting from the deprotonation (lithiation) can undergo side reactions (even at low temperatures) with the starting materials.

For example, Upton and Beak have shown that when Li(TMP) is employed to metallate arylcarboxylic esters (e.g. ethyl, methyl, propyl and butyl benzoate) the *ortho*-metallated intermediate underwent unwanted condensation reactions with a molecule of the starting material to give the corresponding *ortho*-benzoylbenzoates in low to moderate yields (**Scheme 1.15**).^[46]

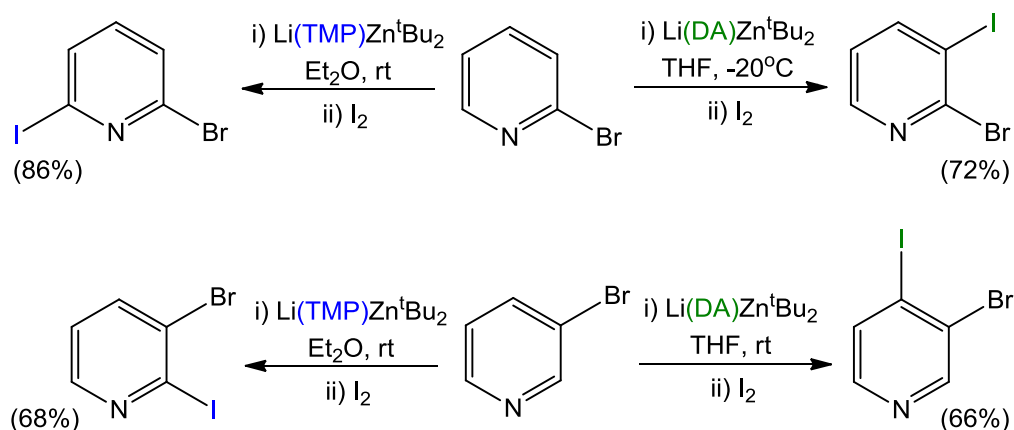
Previous reactivity studies of alkali metal zincates had focussed mainly on homoleptic species, either tri(alkyl)- or tetra(alkyl)-zincates. However, in 1999 Kondo and co-workers developed a heteroleptic lithium dialkyl-amidozincate, [Li(TMP)Zn^tBu₂], which was prepared by combining di-*tert*-butylzinc with a solution of lithium-TMP in THF.^[47] This proved to be both a highly efficient and regioselective reagent for performing the *ortho*-metallation of a variety of functionalised aromatics at room temperature, with the resulting arylzincates being intercepted using I₂ as an electrophile to afford the corresponding *ortho*-iodinated species in yields of 73-99% (**Scheme 1.16**). In the case of ethylbenzoate, the *ortho*-zincated species could also be subjected to Negishi cross-coupling with either iodobenzene or 3-iodopyridine in the presence of [Pd(PPh₃)₄] to give the relevant asymmetric bis(aryl) products in yields of 58% and 43% respectively.



Scheme 1.16: *Ortho* metallation of functionalised aromatics using [Li(TMP)Zn^tBu₂] followed by electrophilic quenching with I₂.

Furthermore, this lithium TMP-zincate proved to be equally efficient for the selective metallation of ethyl-3-thiophenecarboxylate at the 2-position and ethyl-2-furancarboxylate at the 3-position, and more interestingly still was the successful α -metallation of electron deficient heteroaromatic substrates such as pyridine and isoquinoline.^[47] Analysis of the metallated intermediates from this reaction by ¹³C{¹H} NMR spectroscopy suggested these reactions were in fact zincations, with the zincate acting as an amido base and TMP(H) formed as the by-product.

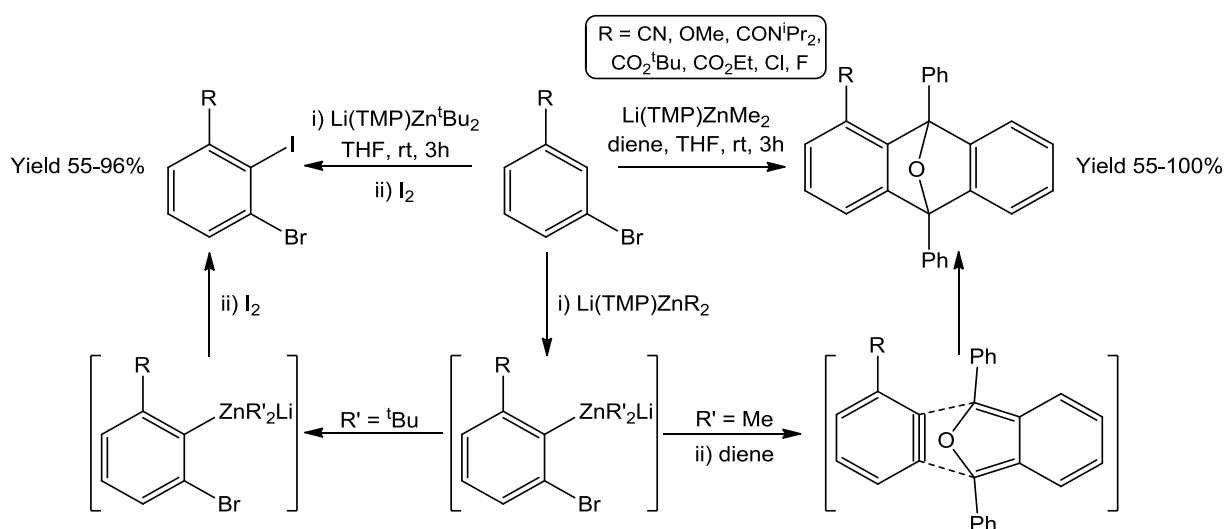
Two further publications by the same group highlighted the complexity of the reactivity of these lithium amido-zincates. For example, studies on the metallation of bromopyridines revealed that the regioselectivities can be tuned by modifying the amide group in the mixed-metal reagent. Thus, when the reaction of the lithium TMP-zincate $[\text{Li}(\text{TMP})\text{Zn}^t\text{Bu}_2]$ with 2-bromopyridine was performed in Et_2O at room temperature and quenched with I_2 , 2-bromo-6-iodopyridine was obtained in an 86% yield, with metallation occurring almost exclusively at the 6-position (**Scheme 1.17**). However, when the same substrate was reacted with the closely related lithium dialkylamido-zincate $[\text{Li}(\text{DA})\text{Zn}^t\text{Bu}_2]$ (DA = diisopropylamide) in THF, metallation occurred at the 3-position, yielding 2-bromo-3-iodopyridine in a 72% yield. Similarly, when the same reaction was performed on 3-bromopyridine, metallation with the lithium TMP-zincate occurred favourably at the 2-position, but with the lithium DA-zincate selectivity switched to the 4-position (**Scheme 1.17**).^[48]



Scheme 1.17: Metallation of 2/3-bromopyridine using $[\text{Li}(\text{TMP})\text{Zn}^t\text{Bu}_2]$ or $[\text{Li}(\text{DA})\text{Zn}^t\text{Bu}_2]$ followed by electrophilic quenching with I_2 .

Turning to the influence of the alkyl groups on the reactivity of the lithium TMP-zincates, in a similar study the authors compared the reactivity of $[\text{Li}(\text{TMP})\text{Zn}^t\text{Bu}_2]$ and the related methyl derivative $[\text{Li}(\text{TMP})\text{ZnMe}_2]$ with bromobenzene substrates bearing substituents at the 3-position. For both mixed-metal reagents selective metallation at the 2-position, between bromine and the functional group, was observed. However, the stabilities of the resulting arylzincate intermediates differed substantially. The *tert*-butyl containing intermediate remained stable at room temperature, and could easily be quenched with I_2 to give the desired tri-substituted aromatic product in yields ranging from 55-96% (**Scheme 1.18**). However,

under the same reaction conditions the methyl containing intermediates proved to be far less stable, readily undergoing elimination to form benzyne, which could be trapped with the diene 1,3-diphenylisobenzofuran to yield the resulting Diels-Alder adduct in yields of 55-100% (**Scheme 1.18**).^[49] Collectively, these studies highlight the important role which solvent and the different components of the mixed-metal reagent can have on tuning their reactivity, as well as their effects on the overall stabilities of the newly generated arylzincate intermediates. Despite these pioneering studies by Kondo and Uchiyama, the available information regarding the mechanisms involved in these reactions was scarce, with no tangible proof of the identity of the organometallic species involved in these processes.



Scheme 1.18: Reaction of 3-substituted bromobenzene using $[\text{Li(TMP)ZnR}_2]$ ($\text{R} = ^t\text{Bu}$ or Me) and quenching with I_2 or 1,3-diphenylisobenzofuran.

Shedding new light on this matter, in 2006 Mulvey and co-workers successfully isolated $[\text{Li(TMP)Zn}^t\text{Bu}_2]$, and were able to determine its molecular structure by X-ray crystallography, revealing that this zincate exists as the CIP species $[(\text{THF})\text{Li(TMP)Zn}^t\text{Bu}_2]$ (**1**) (**Figure 1.3(a)**).^[50] The lithium and zinc atoms are connected by a bridging TMP ligand and by one of the *tert*-butyl groups, which binds strongly to zinc through the quaternary carbon (forming a short σ -bond) and through one of the methyl groups to lithium giving rise to a secondary (electrostatic) interaction, resulting in the presence of a five-membered $\{\text{LiNZnCC}\}$ ring at the core of the structure. The lithium is also bound to the monodentate donor ligand, THF, with the coordination of the zinc completed by a terminal *tert*-butyl group.

As well as successfully elucidating the molecular structure of **1**, the authors also investigated its reactivity towards the aromatic ether anisole, a classical substrate in DoM chemistry.^[45, 51] Pioneering work in this area, carried out in 1939 by Gilman, involved the *ortho* metallation of a variety of organic substrates by ⁿBuLi, including anisole.^[52] Recent years have seen a number of studies into the lithiation of anisole in an attempt to determine the mechanism for DoM. These have included NMR spectroscopy,^[53] kinetic isotope effects^[54] and rate studies.^[55] An example of the practical application of the DoM of anisole is the synthesis of the antibiotic Methicillin (**Scheme 1.19**), which involves the lithiation of 1,3-dimethoxybenzene, followed by reaction with carbon dioxide.^[56] Thus, when the reaction of **1** with one molar equivalent of anisole was performed the arylzincate intermediate [(THF)Li(TMP)(*o*-C₆H₄OMe)Zn^tBu] (**2**) was isolated, the structure of which was determined by X-ray crystallography (**Figure 1.3(b)**).^[41]

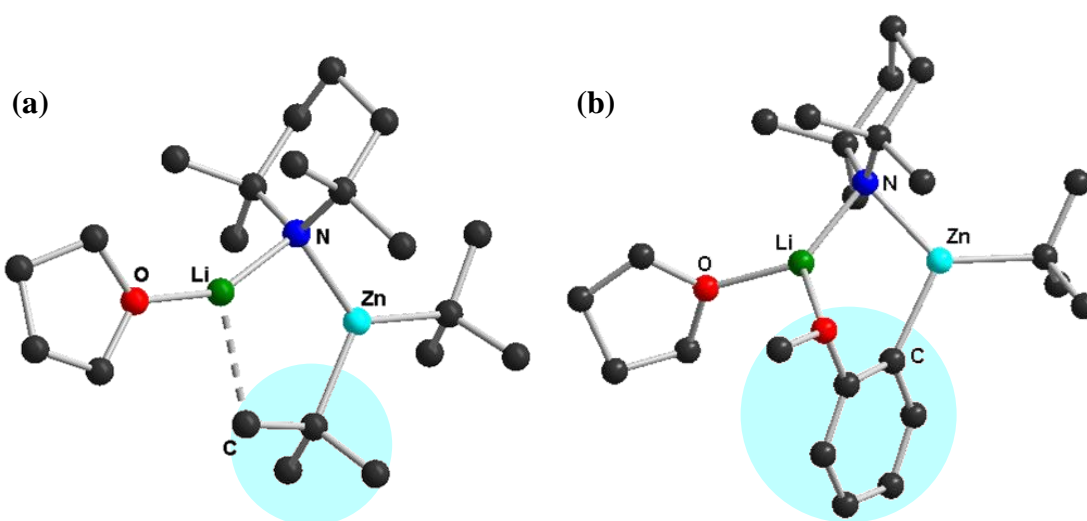
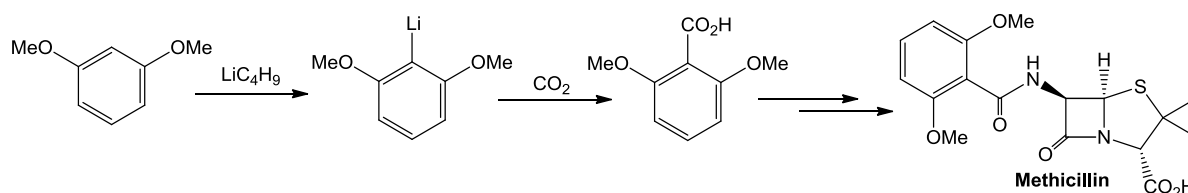
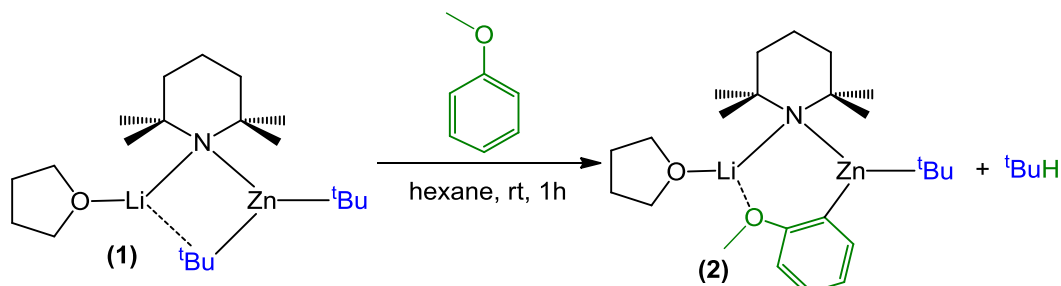


Figure 1.3: Molecular structure of (a) [(THF)Li(TMP)Zn^tBu₂] (**1**) and (b) [(THF)Li(TMP)(*o*-C₆H₄OMe)Zn^tBu] (**2**). Hydrogen atoms have been omitted for clarity.

The molecular structure of **2** displays a number of similar features to that of **1**, with the lithium and zinc metal centres again connected by a bridging TMP ligand, a terminal THF on lithium and a terminal *tert*-butyl group on zinc. The main difference is the presence of a molecule of *ortho*-metallated anisole, which bonds to zinc via the metallated carbon of the

aromatic ring, and to lithium through the oxygen atom of the methoxy group. The formation of this Zn-C_{ortho} bond confirms that this reaction is in fact a direct zincation, as proposed by Kondo and Uchiyama in their initial studies. However, the structural elucidation of **2** also shows that the deprotonation of anisole by **1** has occurred with loss of one of the *tert*-butyl ligands, generating isobutane, and retention of the bridging TMP ligand, which is consistent with the zincate acting as an alkyl base (**Scheme 1.20**). This alkyl basicity indicates a different reaction mechanism compared to that which had previously been proposed for this zincate (where a preference for amido basicity was suggested). This apparent discrepancy was initially explained by the different solvent employed in the metallation reactions, non-polar hexane versus strongly coordinating THF (used by Kondo and Uchiyama in their studies).^[47]



Scheme 1.20: Reaction of [(THF)Li(TMP)Zn^tBu₂] (**1**) with anisole to form [(THF)Li(TMP)(*o*-C₆H₄OMe)Zn^tBu] (**2**).

In 2005, Mulvey reported a study on the related sodium zincate [(TMEDA)Na(TMP)Zn^tBu₂] (**3**) (**Figure 1.4(a)**).^[57] This mixed-metal reagent is almost isostructural to **1**, with the sodium centre now co-ordinated to a molecule of the chelating diamine TMEDA. This bimetallic base **3** can deprotonate benzene, the simplest aromatic molecule where the protons are not activated by any functional group (p*K*_a = 44.7),^[58] at room temperature to afford [(TMEDA)Na(TMP)(C₆H₅)Zn^tBu] (**4**) (**Figure 1.4(b)**). This deprotonation reaction was also found to be a zincation, with zinc occupying the position on the benzene ring previously occupied by a proton, demonstrating that this reaction is a genuine example of direct zincation. Considering that both of the parent homometallic reagents (NaTMP and ^tBu₂Zn) show no reactivity towards benzene,^[57] this reaction can be described as an alkali metal-mediated zincation (AMMZn) (**Scheme 1.21**).^[3, 23]

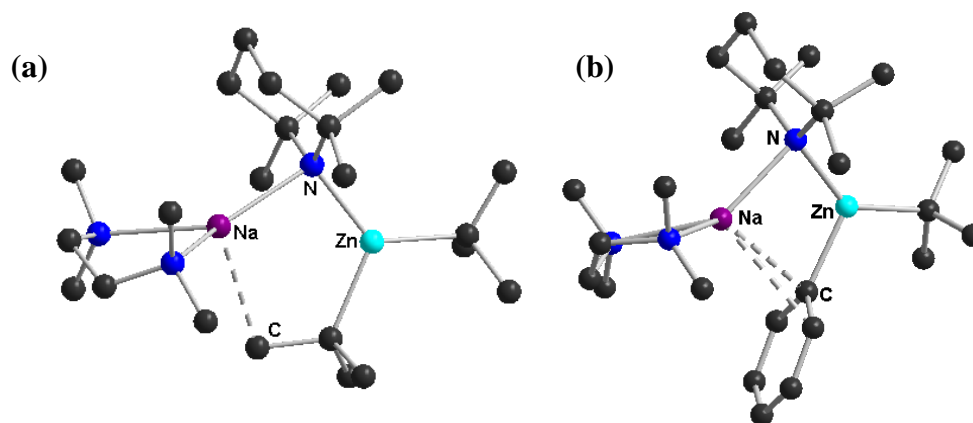
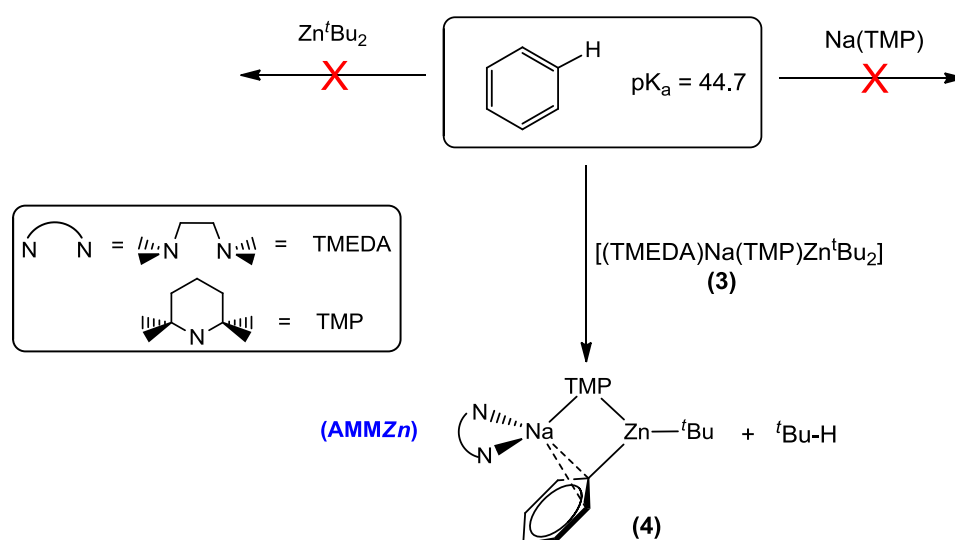
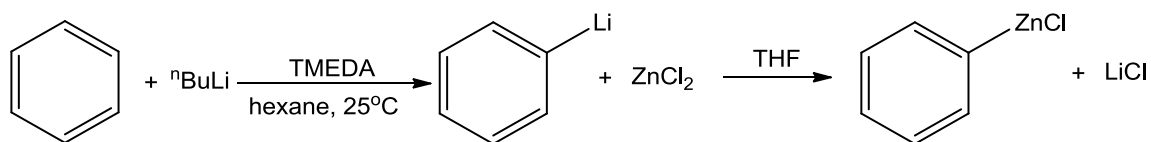


Figure 1.4: Molecular structure of (a) [(TMEDA)Na(TMP)Zn^tBu₂] (**3**) and (b) [(TMEDA)Na(TMP)(C₆H₅)Zn^tBu] (**4**). Hydrogen atoms have been omitted for clarity.



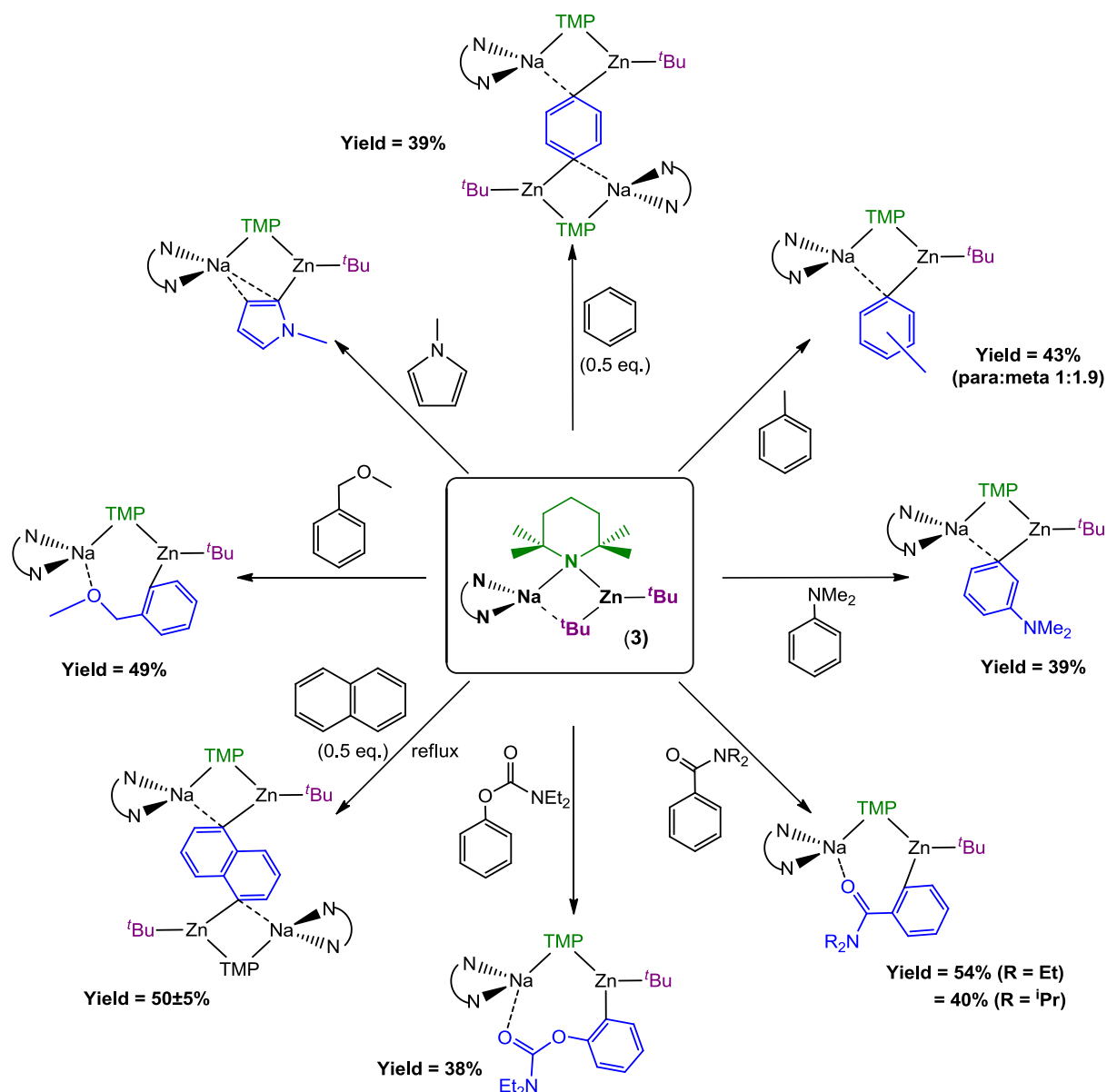
Scheme 1.21: AMMZn of benzene with [(TMEDA)Na(TMP)Zn^tBu₂] (**3**) to afford [(TMEDA)Na(TMP)(C₆H₅)Zn^tBu] (**4**).

Reactions of this type, where zinc is the active metal which performs the deprotonation, but requires the presence of the alkali metal for the reaction to occur, represent a useful atom economical methodology for performing zincations. In contrast, the more conventional indirect route requires the deprotonation of the substrate with a more polar group I organometallic reagent such as ⁿBuLi (activated by a Lewis base such as TMEDA),^[59] followed by a metathesis reaction with ZnCl₂ to form the relevant organozincate intermediate (**Scheme 1.22**).^[60] Thus, the phrase AMMZn has been coined to describe the special synergic reactivity which exists when zinc and an alkali metal are combined in the same molecular framework, whereby surprising reactivity and/or selectivity is achieved which cannot be replicated by either of the substituent homometallic reagents.



Scheme 1.22: Indirect method for the formation of zincated benzene.

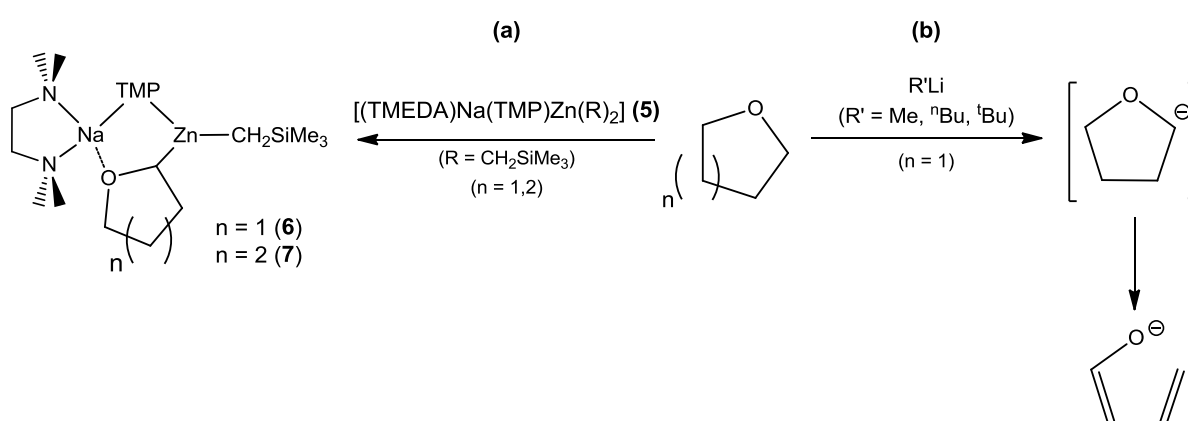
Since it was first reported in 2006 sodium TMP-dialkyl zincate [(TMEDA)Na(TMP)Zn^tBu₂] (**3**) has proved to be an extremely versatile reagent for performing the direct zincation of a wide range of aromatic substrates, the metallated intermediates of which have been structurally characterised (**Scheme 1.23**).



Scheme 1.23: Reaction of [(TMEDA)Na(TMP)Zn^tBu₂] (**3**) with various aromatic substrates. Yields given are isolated crystalline yields.

The substrates which have been successfully metallated include benzene,^[57, 61] toluene,^[62] anilines,^[63] benzonitriles,^[64] benzamides,^[65] carbamates,^[65b] naphthalene,^[66] aromatic ethers,^[67] and *N*-heterocyclic aromatic compounds.^[68] Worthy of mention for the unusual selectivity observed are the *meta*-metallation of aniline, and the mixed *meta/para*-metallation (ratio ~1:2) of toluene, as well as the dimetallation of both benzene and naphthalene. Furthermore, the metallation of substrates containing sensitive functional groups such as nitriles, carbamates and amides could be performed at room temperature, whereas classical homometallic organolithium reagents would require significantly lower temperatures to carry out such metallations. It should also be noted that in all the examples shown in **Scheme 1.23** the metallated intermediates still possess a bridging TMP ligand between the two metal centres, which would be consistent with the zincate acting as an alkyl base (with loss of a *tert*-butyl ligand as isobutane).

Furthermore, as recently showcased in *Science*,^[69] the trimethylsilylmethyl (Me_3SiCH_2) variant of **3**, $[(\text{TMEDA})\text{Na}(\text{TMP})\text{Zn}(\text{CH}_2\text{SiMe}_3)_2]$ (**5**), is able to promote the selective α -zincation of the cyclic ethers THF and THP without observing the expected ether cleavage, which commonly occurs in α -metallated cyclic ethers formed during reaction with monomeric organolithium reagents (**Scheme 1.24**).^[70] The authors rationalise the trapping of these highly unstable anions in terms of the synergic co-ordination of the bimetallic fragment, with Zn bonding to the metallated carbon and sodium to the oxygen of the ether, providing a synergic sedation of the α -metallated ethers (**Figure 1.5**).



Scheme 1.24: Reaction of (a) $[(\text{TMEDA})\text{Na}(\text{TMP})\text{Zn}(\text{CH}_2\text{SiMe}_3)_2]$ (**5**) with THF and THP to form **6** and **7**, and (b) THF with $\text{R}'\text{Li}$ showing resulting ether cleavage.

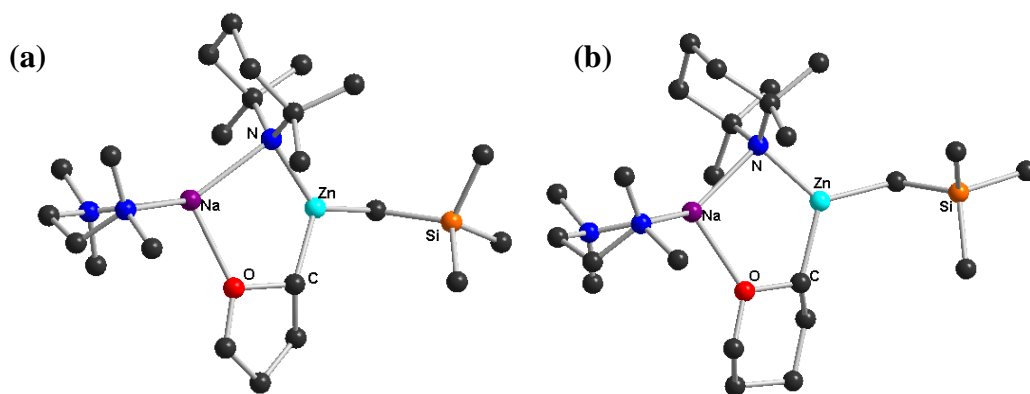
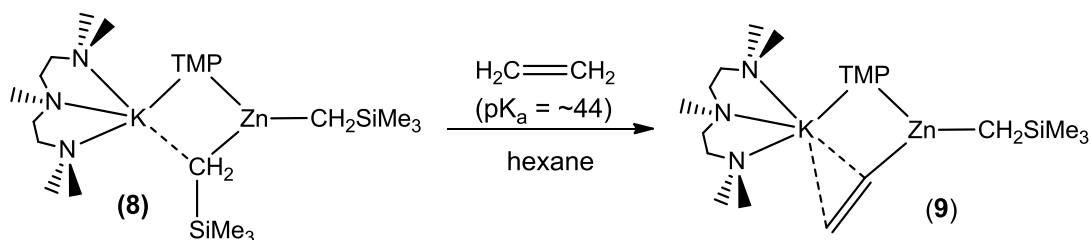


Figure 1.5: Molecular structure of (a) [(TMEDA)Na(TMP)(C₄H₇O)Zn(CH₂SiMe₃)] (**6**) and (b) [(TMEDA)Na(TMP)(C₅H₉O)Zn(CH₂SiMe₃)] (**7**). Hydrogen atoms omitted for clarity.

In addition, the analogous potassium compound [(PMDETA)K(TMP)Zn(CH₂SiMe₃)₂] (**8**) possessed significantly increased reactivity, achieving the selective metallation of ethene, a substrate which is reported to possess an estimated pK_a of ~ 44 (**Scheme 1.25**).^[71] Not only does this potassium TMP-zincate overcome the weak acidity of the protons of ethene, it also demonstrates the ability to trap a highly unstable anionic fragment (CH₂=CH⁻), inhibiting the expected polymerisation of this anion, which was believed to be as a result of the π -interactions between K and CH₂=CH⁻ (**Figure 1.6**).^[69]



Scheme 1.25: Reaction of [(PMDETA)K(TMP)Zn(CH₂SiMe₃)₂] (**8**) with ethene to form [(PMDETA)K(TMP)Zn(CH=CH₂)(CH₂SiMe₃)] (**9**).

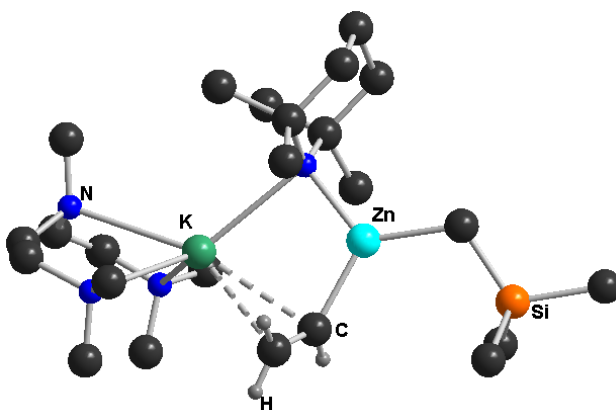
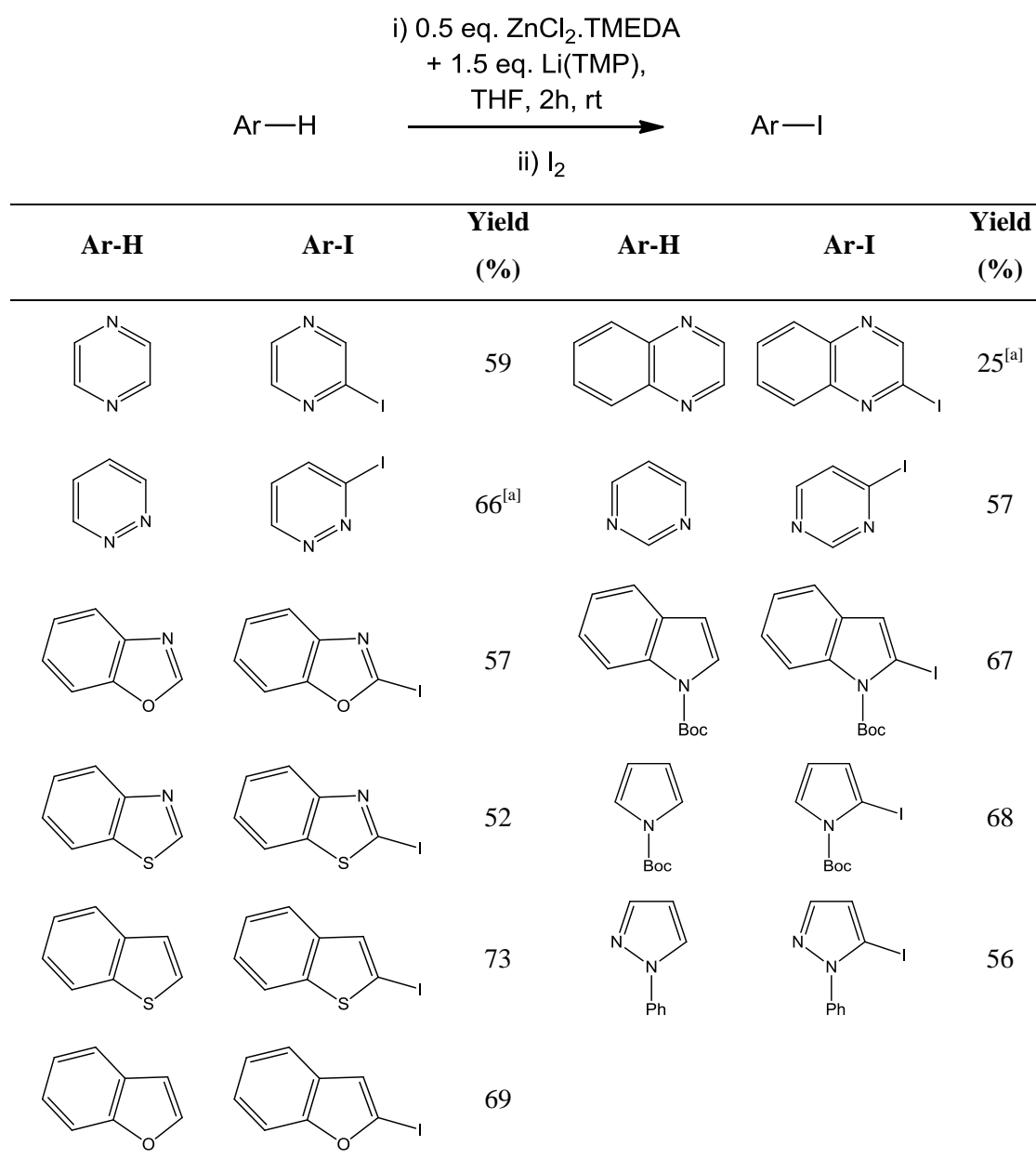


Figure 1.6: Molecular structure of [(PMDETA)K(TMP)(CH=CH₂)Zn(CH₂SiMe₃)] (**9**). Hydrogen atoms (except those of CH=CH₂) have been omitted for clarity.

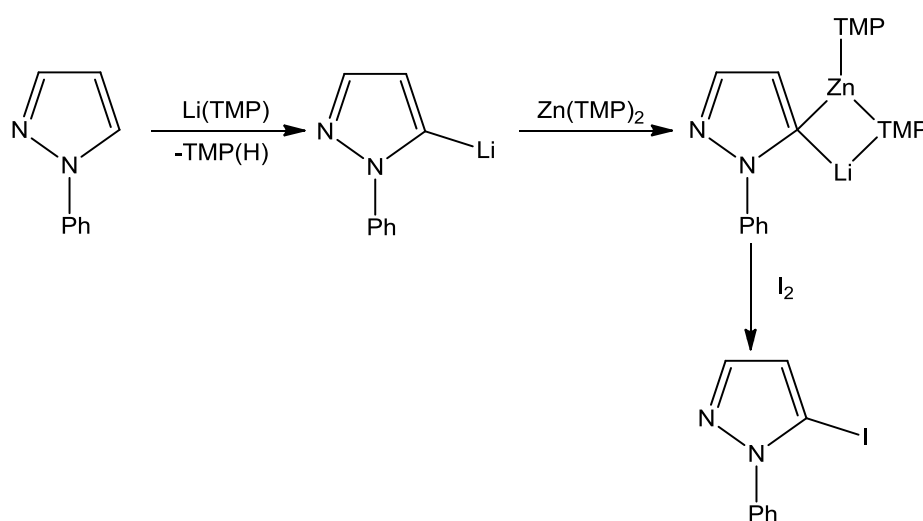
Another important mixed-metal combination which has shown numerous applications in AMMZn is the homoleptic lithium zincate “LiZn(TMP)₃”, reported for the first time in 2007 by Mongin. This base can deprotonate a number of diazine species such as pyrazine, quinoxaline, pyridazine and pyrimidine,^[72] and a wide range heterocyclic species including benzoxazole, benzothiazole, benzo[*b*]thiophene, benzo[*b*]furan, *N*-Boc indole, *N*-Boc pyrrole and *N*-phenylpyrazole,^[73] in yields ranging from 25-73% after electrophilic quenching with I₂ (Scheme 1.26).



Scheme 1.26: Reaction of Li(TMP).Zn(TMP)₂ with diazines and aromatic heterocycles followed by electrophilic quenching with I₂. ^[a] Reaction performed at reflux.

Investigation into the effect of changing the amide component of the zincate to diisopropylamide or piperidide, or preparing mixed amido zincates from these amides showed that the homoleptic TMP-zincate was the most efficient for performing deprotonative metallation reactions. Furthermore, replacing one TMP ligand with an alkyl group (ⁿBu, ^sBu, ^tBu or Me₃SiCH₂) led to a slight decrease in reactivity compared to that observed for “Li(TMP)₃Zn”.^[74]

The homoleptic lithium TMP-zincate used in these reactions is prepared by reacting [ZnCl₂(TMEDA)] with three equivalents of Li(TMP), generating the active zincate *in situ*. Although the authors describe this reaction mixture as “LiZn(TMP)₃” they acknowledge in their report the complex nature of the organometallic species present in solution (as determined by ¹³C{¹H} NMR spectroscopy). This spectroscopic analysis suggests that the major species present in solution are Li(TMP) and Zn(TMP)₂.^[72] Furthermore, DFT studies indicate that the relevant homometallic components Li(TMP) and Zn(TMP)₂ are energetically more favourable (-3.8 kcal mol⁻¹) than the expected lithium tris-amidozincate LiZn(TMP)₃.^[73b] The unfavoured co-complexation of Li(TMP) and Zn(TMP)₂ in solution appears to be due to the fact that mixed-metal species would be highly sterically hindered due to the presence of three molecules of the bulky amide TMP around the zinc centre. Thus, for these reactions the base is described as a 1:1 *in situ* mixture of Li(TMP) and Zn(TMP)₂, and the mechanism by which it reacts is believed to be first via metallation of the substrate by Li(TMP) to generate an aryl lithium intermediate which can then undergo subsequent reaction with Zn(TMP)₂ to generate a more stable zincated species (**Scheme 1.27**).^[73b, 74]



Scheme 1.27: Proposed reaction of Li(TMP) with *N*-phenylpyrazole followed by reaction with Zn(TMP)₂ to generate the final arylzincate intermediate.

A recent multinuclear (^1H and ^7Li) DOSY study of the *in situ* mixture of $\text{Li}(\text{TMP})$ and $\text{Zn}(\text{TMP})_2$ (prepared by the metathesis reaction of $\text{Li}(\text{TMP})$ with $\text{ZnCl}_2 \cdot \text{TMEDA}$ in a ratio of 3:1) has shown an even more complex scenario to exist, due to the presence of TMEDA, and two equivalents of LiCl , formed as a co-product of the metathesis reaction. Diffusion-ordered NMR spectroscopy (DOSY) is a pseudo two-dimensional NMR technique where one dimension shows chemical shift data and the second dimension relates to the diffusion properties of the species in solution. Thus, DOSY can be used to identify the individual components of mixtures in solution by their diffusion coefficients (D), and has been described as “chromatography by NMR”.^[75]

A DOSY study of the *in situ* mixture of $[\text{Li}(\text{TMP}) \cdot \text{Zn}(\text{TMP})_2 \cdot \text{TMEDA} \cdot 2\text{LiCl}]$ was performed in d_8 -THF (**Figure 1.7**), confirming first of all that there is no interaction between $\text{Li}(\text{TMP})$ and $\text{Zn}(\text{TMP})_2$ in solution, as previously proposed. Furthermore, the study also shows an interaction in solution between $\text{Li}(\text{TMP})$ and the two equivalents of LiCl , hinting at the presence of a $[\text{Li}(\text{TMP}) \cdot 2\text{LiCl}]$ complex with some degree of solvation by THF, and a weak interaction with TMEDA.^[76] Therefore, these results support Mongin’s reactivity studies, which proposed that this mixture initially performs a lithiation of the aromatic substrate, followed by transmetalation with $\text{Zn}(\text{TMP})_2$. However, they also show that the active species in solution is in fact a complex of $\text{Li}(\text{TMP})$ and LiCl , highlighting the important role of inorganic salts in the reactivity of organometallic bases.

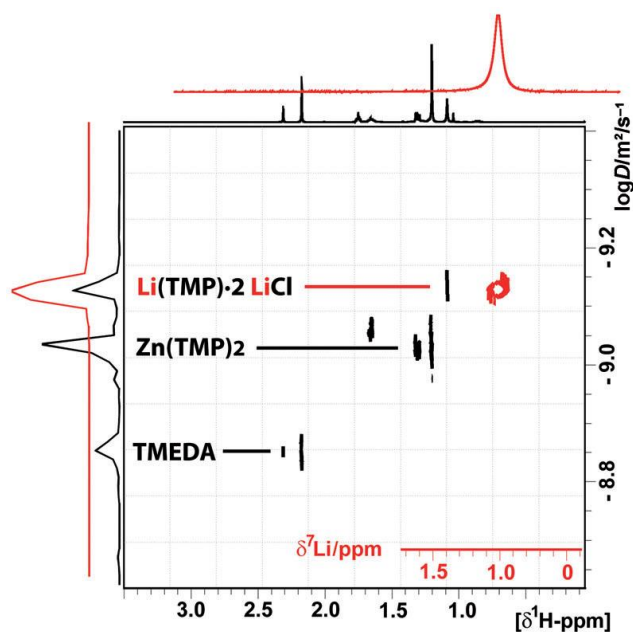
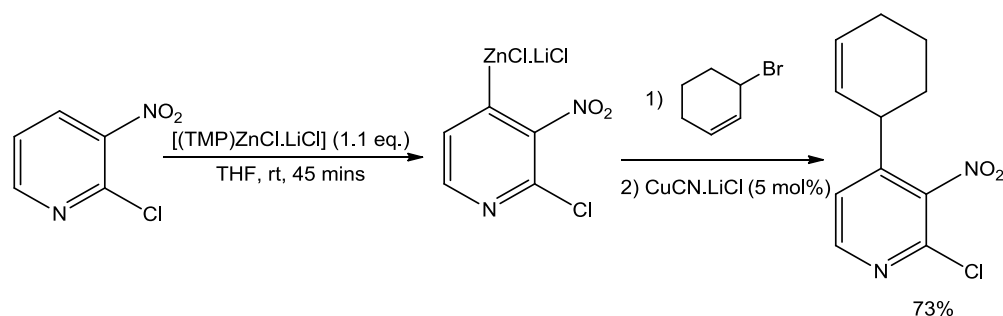


Figure 1.7: ^1H (black) and ^7Li (red) DOSY spectra for the *in situ* mixture of $[\text{Li}(\text{TMP}) \cdot \text{Zn}(\text{TMP})_2 \cdot 2\text{LiCl} \cdot \text{TMEDA}]$ in d_8 -THF.^[76]

1.3.3 Zinc modified turbo-Hauser bases

The area of AMMZn is not confined solely to the use of zincates possessing only alkyl and/or amido ligands. In the last ten years Knochel and co-workers have developed the halogen containing lithium-magnesiato turbo-Hauser bases ($R_2NMgCl \cdot LiCl$) as a new class of bimetallic reagent for performing deprotonative metallation reactions.^[77] The analogous zinc turbo-Hauser bases ($R_2NZnCl \cdot LiCl$) have been shown to be highly selective bases for the direct zincation of many aromatic and heteroaromatic compounds.^[78] Most impressively was $[(TMP)ZnCl \cdot LiCl]$, which could be used to successfully metallate aromatic species possessing highly sensitive functional groups such as fluoro, nitro, ester and aldehyde functionalities, which after quenching with a wide range of electrophiles yielded the desired products in yields ranging from 67-92%. This new $[(TMP)ZnCl \cdot LiCl]$ base was also compatible with highly sensitive heterocycles including pyridazines, pyrimidines, pyrazines, furans, thiophenes and purines (**Scheme 1.28**). Impressively, all of these reactions were performed at room temperature, without any unwanted side reactions, a feat which could not be mirrored by any of the corresponding lithium-magnesiato turbo bases such as $[(TMP)MgCl \cdot LiCl]$.



Scheme 1.28: Deprotonation of 2-chloro-3-nitropyridine with $[(TMP)ZnCl \cdot LiCl]$ and subsequent quenching via Negishi cross-coupling.

Recent advances in this area have revealed that for less sensitive organic substrates the trimetallic combination of $[Zn(TMP)_2 \cdot 2LiCl \cdot 2MgCl_2]$ shows an enhanced metallating power than bimetallic $[(TMP)ZnCl \cdot LiCl]$. Thus, these turbo mixtures have been used to selectively metallate a myriad of aromatic and heteroaromatic substrates, with numerous examples reported to date.^[79] Notwithstanding, since three different metals (Li, Mg and Zn) are present in the reaction mixture we can no longer regard these species as simple alkali metal zincates, but instead as more complex trimetallic Li/Mg/Zn amide bases. Recent solid-state (X-ray crystallography)^[80] studies have established that the turbo-Hauser bases $[(TMP)MgCl \cdot LiCl]$ and $[(DA)MgCl \cdot LiCl]$ exists as the contacted ion-pair species $[(TMP)MgCl_2Li(THF)_3]$ (**10**)

and $[\{(DA)MgCl_2Li(THF)_2\}_2]$ (**11**) in the solid state, with the alkali metal connected to the magnesium centre via two bridging chlorine atoms (**Figure 1.8**). Subsequent solution studies using DOSY NMR spectroscopy have inferred that their behaviour in solution is far more complex, with the solid state structures not being retained in solution, and the two metals most likely existing as solvent separate ion pairs.^[80b] Furthermore, these inherent differences in structure, both in the solid-state and in solution, of **10** and **11** go some way towards explaining the different reactivity characteristics observed for these two turbo-Hauser bases. Thus, whereas reaction of **10** with ethyl-3-chlorobenzoate leads to selective metallation at the 2-position, reaction of **11** with the same substrate under identical conditions results only in nucleophilic addition/elimination.^[80]

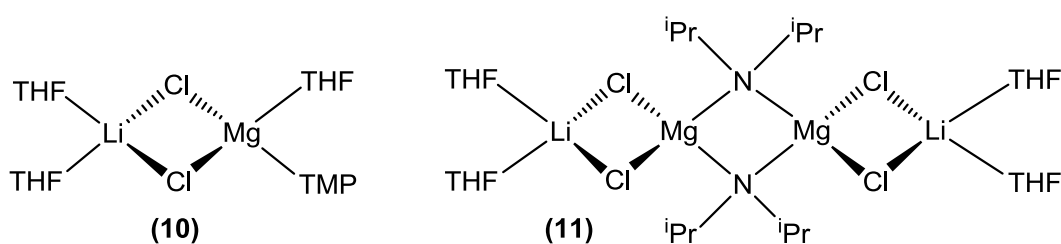


Figure 1.8: Molecular structures of turbo-Hauser bases $[(TMP)MgCl_2Li(THF)_3]$ (**10**) and $[(DA)MgCl_2Li(THF)_2]_2$ (**11**).

Despite these studies, to date there is very little known about the exact nature of the trimetallic Li/Mg/Zn amide bases, either in the solid state or in solution. However, given that the presence of all three metals is required for the reactions to proceed it would suggest that some form of interaction does exist between the three different metals.^[79c]

Alkali metal zincates have emerged as a useful class of organometallic reagents, showing enhanced levels of reactivity in a wide range of fundamental reactions such as nucleophilic addition, metal-halogen exchange and deprotonative metallation. The area of alkali metal-mediated zincation (AMMZn) is one of growing interest to both organic and organometallic chemists, allowing access to new levels of reactivity and selectivity, which in some cases are not available for homometallic reagents. However, there is still much about these mixed-metal bases which remains unknown, including the exact mechanism of how they operate, and the origins of the unique synergic behaviour of these reagents.

Building on these initial breakthroughs the first part of this thesis (**Chapters 2 and 3**) will focus on advancing the understanding of AMMZn, shedding new light on the “*modus operandi*” of these bimetallic reagents, which can help to tune their reactivity. On the other hand, the second part (**Chapters 4-6**) will thesis our findings on the development of a new type of mixed-metal reagent, magnesium-zinc hybrids, using salt metathesis reactions as a vehicle for their preparation, as well as exploring their applications in two fundamental types of organic transformations, namely nucleophilic addition to ketones and metal-halogen exchange reactions.

Thus, this thesis is divided into eight main chapters; **Chapter 1** provides a brief introduction on recent advances in organozinc chemistry, placing special emphasis on those involving alkali metal zincates. **Chapters 2 and 3** explore the reactivity of lithium and sodium TMP-zincates in deprotonation reactions; the former unveiling new reactivity trends of these bimetallic reagents, while the latter focuses on the mechanism of AMMZn. In **Chapter 4** a series of new bimetallic Mg-Zn hybrids will be unveiled, prepared through the salt metathesis reaction of Grignard reagents with ZnCl₂. **Chapters 5 and 6** will focus on the synthetic applications of these Mg-Zn hybrid reagents in nucleophilic alkylation of ketones and metal-halogen exchange reactions respectively. Finally, **Chapter 7** will describe the synthesis and characterisation of the new compounds reported herein, and **Chapter 8** will provide an overview of the results reported within this thesis along with some conclusions and further work.

In addition, an electronic appendix containing crystallographic data of the compounds whose structure have been determined by X-ray crystallography, and details of DOSY experiments and DFT calculations is provided in the form of a CD-ROM.

Chapter 2: Unveiling new reactivity patterns in AMMZn

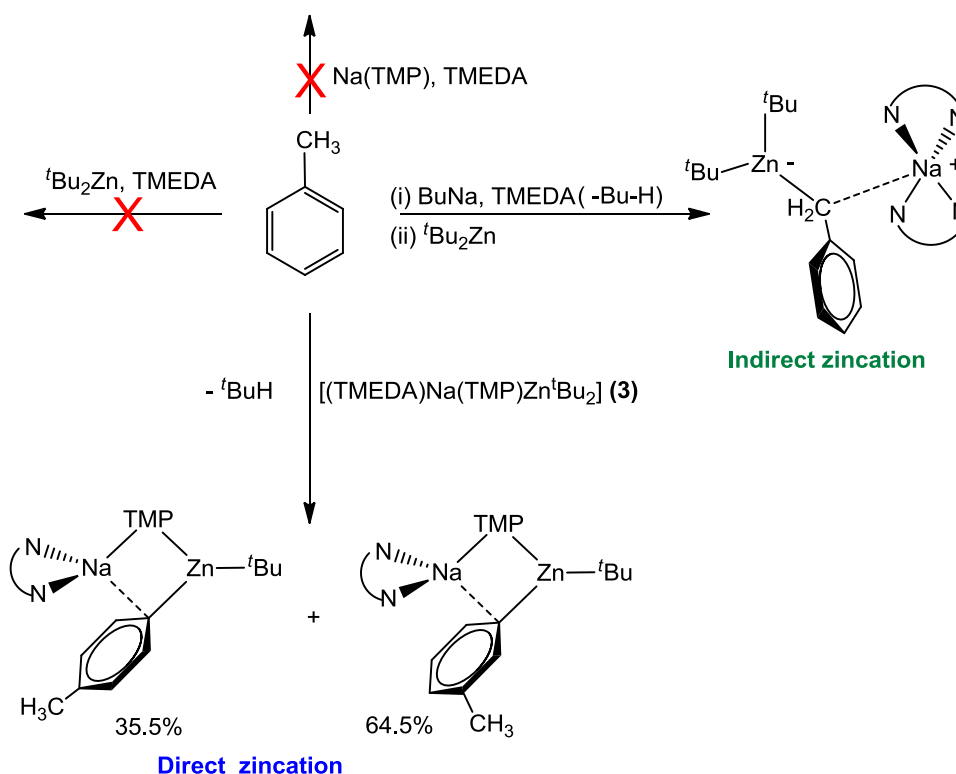
The lithium TMP-zincate [(THF)Li(TMP)Zn^tBu₂] (**1**) and sodium TMP-zincate [(TMEDA)Na(TMP)Zn^tBu₂] (**3**) have both been shown to be highly chemo- and regioselective bases for the metallation of a variety of aromatic substrates under mild conditions, including unactivated substrates such as benzene and naphthalene,^[57, 61, 66] and those containing highly sensitive functional groups such as carbamates,^[65b] nitriles^[47, 64] and amides^[47, 65] (see **Chapter 1**). In the following chapter the reactivity of these two bimetallic bases towards new aromatic substrates will be investigated, revealing some interesting new selectivities and applications of these zincates.

2.1 Direct lateral metallation using alkali metal-mediated zincation (AMMZn): SiC-H vs. Si-O bond cleavage

Previous studies investigating the reactivity of **3** with toluene showed that the aromatic molecule is deprotonated exclusively on the ring, although a mixture of the *meta*- and *para*-metallated products was obtained in a ratio of 1.9:1.^[62] The most surprising feature of this reaction was that the methyl group, which is the most thermodynamically preferred position for metallations when monometallic reagents such as ^tBuLi are employed,^[81] remained intact. The ratio of products is very close to the 2:1 ratio of *meta* and *para* protons present in toluene, which would suggest that metallation at these two positions is equally favoured.

This reaction is another genuine example of AMMZn, as neither of the homometallic reagents (Na(TMP) or Zn^tBu₂) shows any reactivity towards toluene (**Scheme 2.1**). In contrast, indirect lateral zincation at the methyl group could be achieved by treating toluene first with BuNa to give benzyl sodium, and subsequent reaction with Zn^tBu₂ and two equivalents of TMEDA to afford the new mixed metal product [(TMEDA)₂Na]⁺[(CH₂Ph)Zn^tBu₂]⁻, resulting from a co-complexation reaction. DFT calculations for the reaction of **3** with toluene revealed a thermodynamic preference for *meta* and *para* metallation over *ortho* or methyl, and can be rationalised at least in part by the favourable Na-C_{tolyl} π -interactions present in the *meta* and *para*-metallated products (**Scheme 2.1**), interactions which would be much weaker (almost non-existent) if metallation had occurred at the lateral methyl group. Furthermore, this reactivity pattern shows a reversal in the order of stabilities which is seen when conventional

homometallic reagents are employed (where lateral metallation is favoured over metallation on the ring).



Thus, to date all examples of AMMZn of aromatic substrates using alkali metal TMP-zincates have resulted in metallation occurring exclusively at aromatic (sp^2) carbons, with no examples of direct lateral zincation (DIzn) at an sp^3 carbon atom. With this in mind, we investigated the reactivity of the lithium TMP-zincate **1** and sodium TMP-zincate **3** with the aromatic substrate, trimethyl(phenoxy)silane (**12**). This aromatic molecule was chosen for a number of reasons (**Figure 2.1**), the first of which is that its trimethylsilyl (TMS) group is a highly sterically demanding substituent, and in fact **12** could be viewed as a bulky analogue of anisole. As a result it is possible that reaction of **12** with the mixed-metal bases **1** and **3** will direct metallation towards the *meta* or *para* positions of the ring. In addition, this substrate may also react in the same fashion as anisole, affording *ortho* metallation due to the directing effect of the OR group ($R = \text{SiMe}_3$), or alternatively the PhO group could provide an activating effect to the SiMe_3 group, favouring deprotonation of one of the methyl groups to form an α -metallated silane (α -carbanion). Finally, it is important to mention that TMS groups are commonly employed in organic synthesis as protecting groups for alcohol functionalities, so **12** can essentially be envisaged as a protected phenol molecule. Such

protecting groups are usually removed by nucleophilic displacement under acidic or basic conditions,^[82] and as a result it is possible that reaction of **12** with an alkali metal TMP-zincate may simply lead to nucleophilic substitution at the silicon, with the cleavage of the Si-O bond. Therefore, despite the simplicity of this substrate, **12** provides five possible sites for reaction with the TMP-zincates **1** and **3**; *ortho*, *meta*, *para* or lateral metallation, and Si-O bond cleavage (nucleophilic substitution) (**Figure 2.1**).

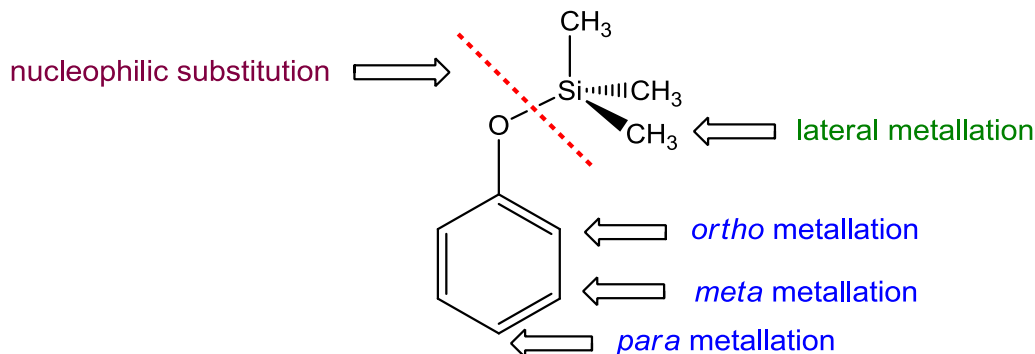


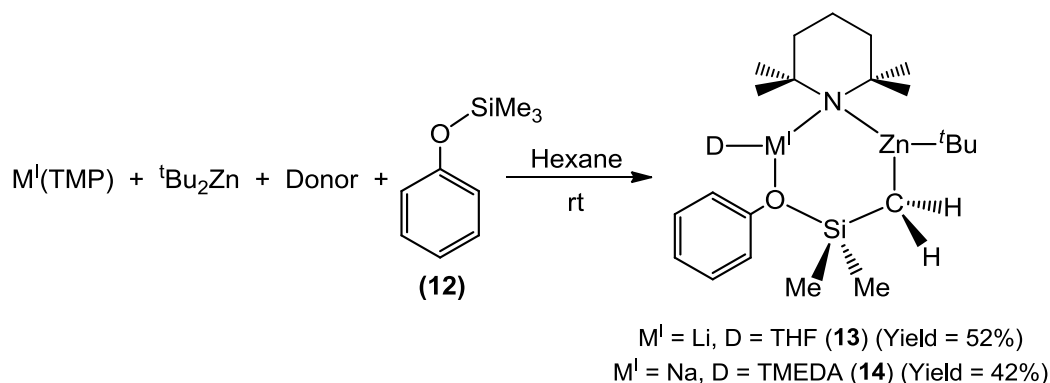
Figure 2.1: Possible reaction sites of **12**.

2.1.1 Investigating the reactivity of trimethyl(phenoxy)silane (**12**) with **1** and **3**

Zincates **1** and **3** were prepared *in situ* by combining the relevant alkali metal amide and ^tBu₂Zn in the presence of one molar equivalent of donor (**1**; Li(TMP) and THF, **3**; Na(TMP) and TMEDA) in hexane. To the resulting solution was added **12**, and the reaction mixtures stirred for one hour at room temperature (**Scheme 2.2**), affording a pale yellow solution. Cooling the solutions overnight (-30°C) allowed the isolation of colourless crystals of [(THF)Li(TMP){PhOSi(CH₃)₂CH₂}Zn^tBu] (**13**) and [(TMEDA)Na(TMP){PhOSi(CH₃)₂CH₂}Zn^tBu] (**14**) in isolated yields of 52% and 42% respectively. **13** and **14** were characterised by NMR spectroscopy, and their molecular structures determined by X-ray crystallography.

The successful lateral zincation of **12** was confirmed by determining the structure of [(THF)Li(TMP){PhOSi(CH₃)₂CH₂}Zn^tBu] (**13**) (**Figure 2.2(a)**) using X-ray crystallography. The structure can be described as a CIP, with the lithium and zinc connected by two bridging ligands. Firstly, the monodentate TMP ligand bridges the two metals directly through its nitrogen atom, while the second bridging ligand is the metallated trimethyl(phenoxy)silane, which bridges the two metals in an ambidentate fashion. The zinc bonds directly to the metallated methyl carbon, forming a short (strong) sigma bond (Zn-C14, 2.0769(15) Å),

confirming that the α -metallation of **12** is in fact an α -zincation. The metallated silane fragment also binds to lithium through a dative Li-O bond (Li-O1, 1.974(3) Å).



Scheme 2.2: Reaction of alkali metal zincates (**1** and **3**) with **12** to form $[(\text{D})M^I(\text{TMP})\{\text{PhOSi}(\text{CH}_3)_2\text{CH}_2\}\text{Zn}^t\text{Bu}]$ ($M^I = \text{Li}, \text{D} = \text{THF}$, **13**; $M^I = \text{Na}, \text{D} = \text{TMEDA}$, **14**).

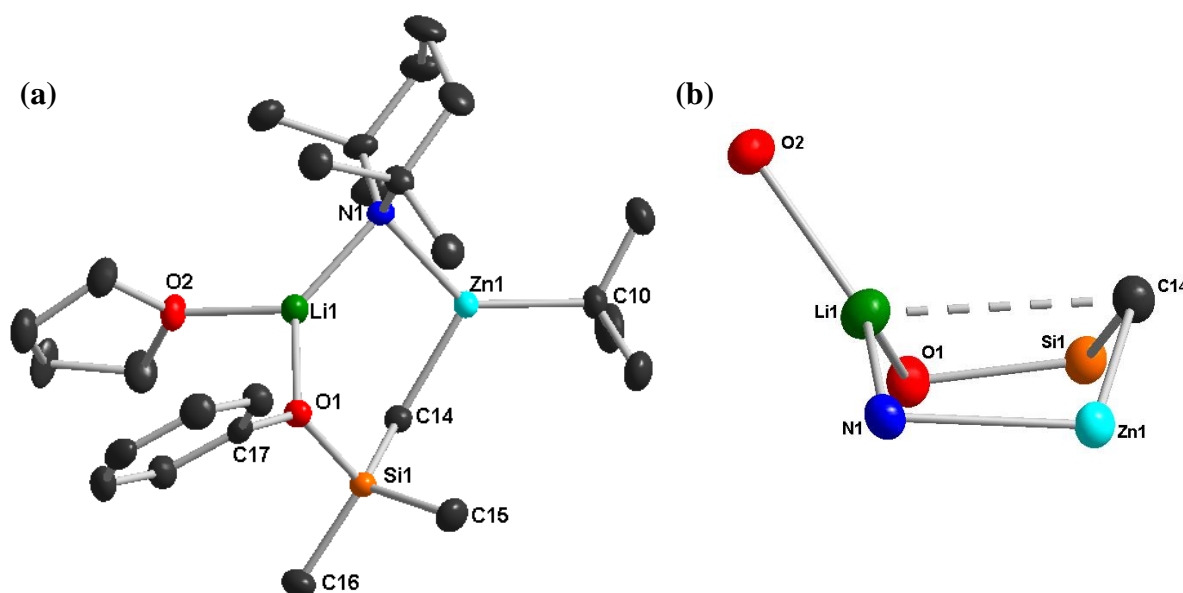


Figure 2.2(a): Molecular structure of $[(\text{THF})\text{Li}(\text{TMP})\{\text{PhOSi}(\text{CH}_3)_2\text{CH}_2\}\text{Zn}^t\text{Bu}]$ (**13**), with 50% probability ellipsoids. Hydrogen atoms and minor disorder component of THF have been omitted for clarity. **(b)** Inorganic core of **13** highlighting the pseudo boat conformation of the $\{\text{LiZnCSiO}\}$ ring and secondary Li-C interaction. Selected bond distances (Å) and bond angles ($^\circ$): Zn-C14 2.0769(15), Zn-C10 2.0296(14), Zn-N 2.0315(12), Li-C14 2.568(3), Li-O1 1.974(3), Li-N 2.000(3), Li-O2 1.937(3), Si-O1 1.7028(11), Si-C14 1.8181(15), Si-C15 1.8540(16), Si-C16 1.8635(16); C14-Zn-C10 118.71(6), C14-Zn-N 108.24(5), C10-Zn-N 133.04(6), O1-Li-O2 98.42(11), O1-Li-N 128.71(14), O2-Li-N 130.45(15).

This non-symmetrical coordination of the metallated substrate gives rise to a unique heteroatomic six-element {LiN₂ZnCSiO} ring at the core of the structure (**Figure 2.2(b)**). This ring adopts a pseudo boat conformation, where the N, Zn, Si and O lie almost co-planar (torsion angle 4.84(2)°), with Li and C forming the boat vertices. This boat conformation is most likely stabilised by a weak secondary electrostatic interaction between the electropositive lithium and the metallated carbon, which bears a partial negative charge (Li-C14, 2.568(3) Å). This Li-C bond is relatively long (weak) compared to the Li-C bonds of other similar compounds such as [(TMEDA)LiCH₂SiMe₃]₂, [(sparteine)LiCH₂SiMe₃]₂ and [(PMDETA)LiCH₂SiMe₃] (average Li-C bond length 2.265, 2.404 and 2.113 Å respectively),^[83] but appears to be sufficient to favour the boat conformation displayed in **13**. The zinc coordination is completed by a terminal *tert*-butyl group (Zn-C10, 2.0296(14) Å) and lithium is solvated by a molecule of THF (Li-O2, 1.937(3) Å), which results in **13** retaining the same {(THF)Li(TMP)Zn^tBu} backbone to that exhibited in **1**, showing that the zincate has again acted as an overall alkyl base, liberating isobutane as the co-product of the reaction.

The molecular structure of **14** was also determined by X-ray crystallography [(TMEDA)Na(TMP){PhOSi(CH₃)₂CH₂}Zn^tBu] (**Figure 2.3(a)**), displaying a similar CIP motif to that of **13**, with the only major difference being the alkali metal and donor ligand present (Na and TMEDA). The two metals are again connected by a bridging TMP ligand and an ambidentate α -zincated trimethyl(phenoxy)silane ligand, giving rise to a heteroatomic {NaNZnCSiO} six-membered ring which also adopts a pseudo-boat conformation (**Figure 2.3(b)**).

The difference in alkali metal from **13** to **14** (lithium to sodium) has very little effect on the zinc bond lengths and angles. Thus, in **14** zinc adopts a distorted trigonal planar geometry (sum of angles around Zn = 360°) displaying similar Zn-^tBu (Zn-C10, 2.041(4) Å), Zn-CH₂ (Zn-C14, 2.083(4) Å) and Zn-N (2.021(3) Å) bond lengths to those observed for **13** (2.0296(14), 2.0769(15) and 2.0315(12) Å respectively). However, the Na-N1 (2.430(3) Å) and Na-O1 (2.385(4) Å) bond lengths in **14** are much larger than the corresponding Li-N1 and Li-O1 bond lengths in **13** (2.000(3) and 1.974(3) Å respectively), due to the sodium atom being larger in size than the lithium, as well as the different coordination number exhibited by each metal (Na = 4, Li = 3). A further consequence of the larger Na atom in **14** is that the secondary electrostatic Na-C14 interaction (2.971(4) Å) is much longer than the Li-C14

interaction in **13** (2.568(3) Å). This Na-C distance is also longer than that found in the laterally metallated toluene species [(PMDETA)NaCH₂(Ph)]_∞, reported in 1991 by Weiss (Na-C 2.752(6) Å),^[84] showing that this secondary interaction in **14** must be relatively weak.

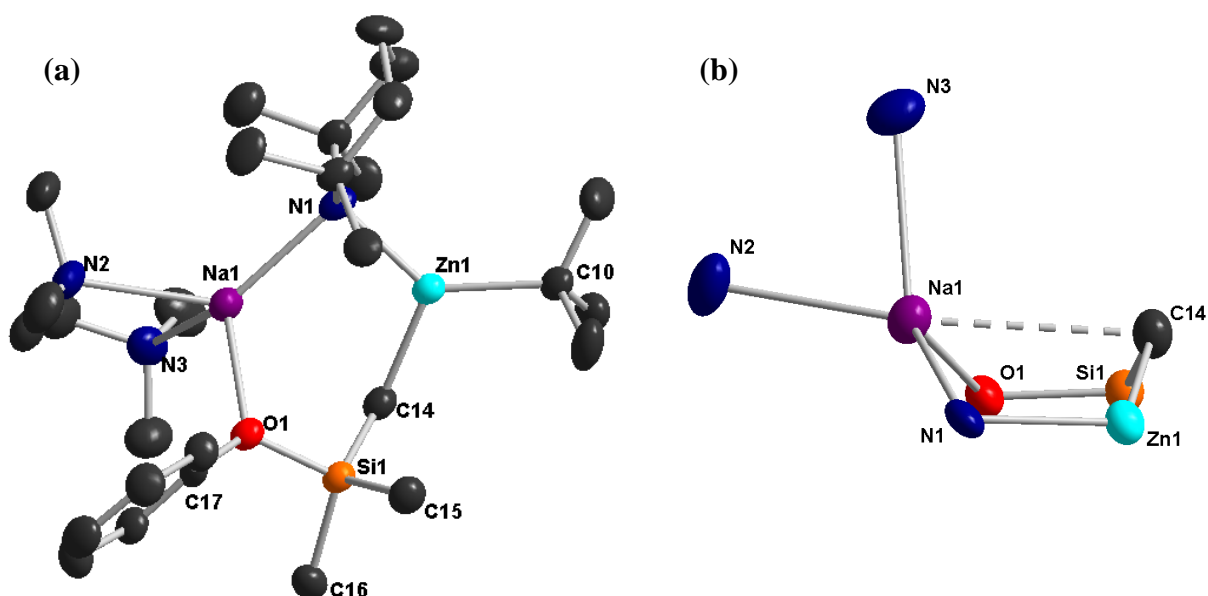


Figure 2.3(a): Molecular structure of [(TMEDA)Na(TMP){PhOSi(CH₃)₂CH₂}Zn^tBu] (**14**) with 50% probability ellipsoids. Hydrogen atoms and minor disordered component of TMEDA have been omitted for clarity. **(b)** Inorganic core of **14** highlighting the pseudo boat conformation of the {NaNZnCSiO} ring and the secondary Na-C interaction. *Selected bond distances (Å) and bond angles (°):* Zn-C14 2.083(4), Zn-C10 2.041(4), Zn-N1 2.021(3), Na-C14 2.971(4), Na-O 2.385(4), Na-N1 2.430(3), Na-N2 2.577(4), Na-N3 2.571(5), Si-O1 1.701(3), Si-C14 1.778(5), Si-C15 1.842(5), Si-C16 1.865(4); C14-Zn-C10 115.23(16), C14-Zn-N1 112.01(14), C10-Zn-N1 132.74(14), O-Na-N1 112.94(15), O-Na-N2 100.50(14), O-Na-N3 103.96(13), N1-Na-N2 125.43(13), N1-Na-N3 131.75(19), N2-Na-N3 73.87(16).

The ¹H NMR spectrum of **13** in d₆-benzene (**Figure 2.4**) was consistent with the molecular structure [(THF)Li(TMP){PhOSi(CH₃)₂CH₂}Zn^tBu], displaying a triplet at δ 7.04 ppm and a multiplet at δ 6.84 ppm (resulting from an overlapping triplet and doublet) for the aromatic protons of the phenoxy group, which appeared at similar chemical shift to those of **12** (triplet and multiplet at δ 7.10 and 6.87 ppm) (**Table 2.1**). The presence of two singlets at δ 1.19 and 1.38 ppm for the α-methyl protons of TMP was indicative of the amide bridging between the two metal centres, caused by the stereochemical inflexibility of this bridging ligand,^[41] and confirmed that the Li-TMP-Zn backbone found in the molecular structure of **13** is retained in

solution. The most indicative resonances were those of the two singlets at δ 0.29 and -0.59 ppm corresponding to the CH_3 and CH_2 groups bound to silicon in a ratio of 6:2 respectively. The CH_3 groups appear at a similar resonance to those of **12** (δ 0.15 ppm), while the CH_2 group is shifted remarkably upfield, as a result of the α -deprotonation of the methyl group. This chemical shift is almost identical to that observed for ZnMe_2 (δ -0.52 ppm), but markedly different from that of MeLi (δ -1.42 ppm), confirming that the Zn-CH_2 bond of **13** is retained in solution. The ^7Li NMR spectrum confirmed the presence of only one species, with a singlet at δ 1.07 ppm.

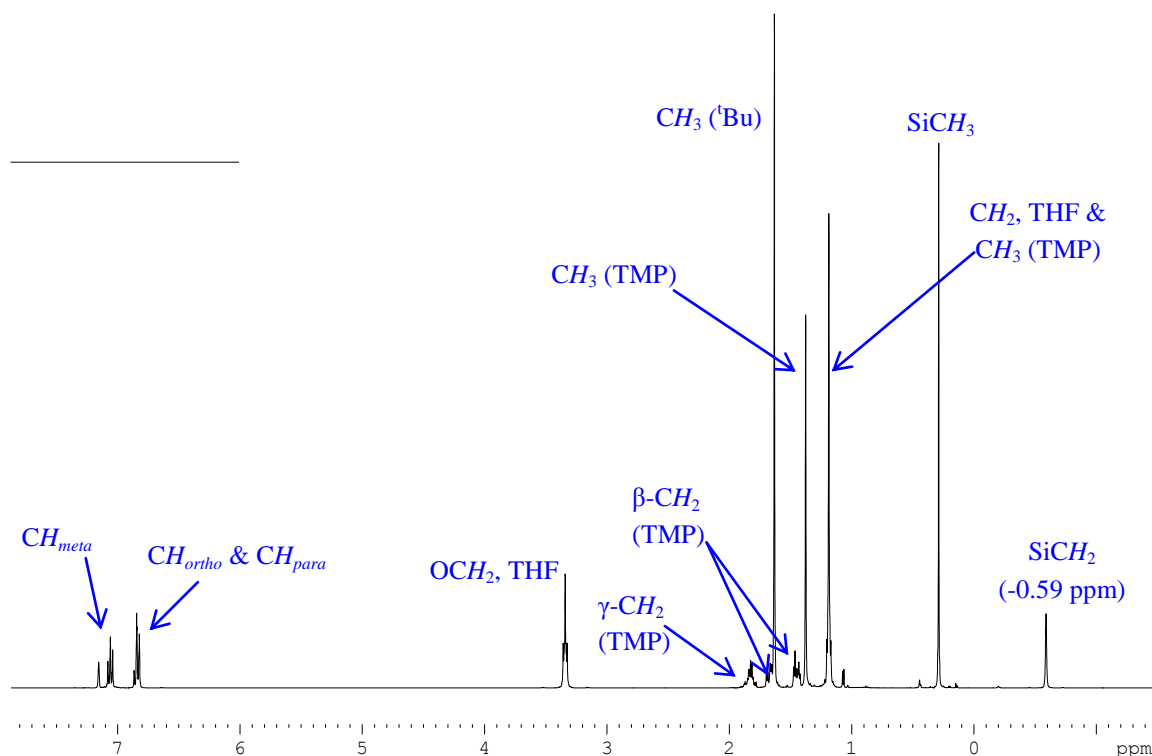


Figure 2.4: ^1H NMR spectrum of **13** in d_6 -benzene.

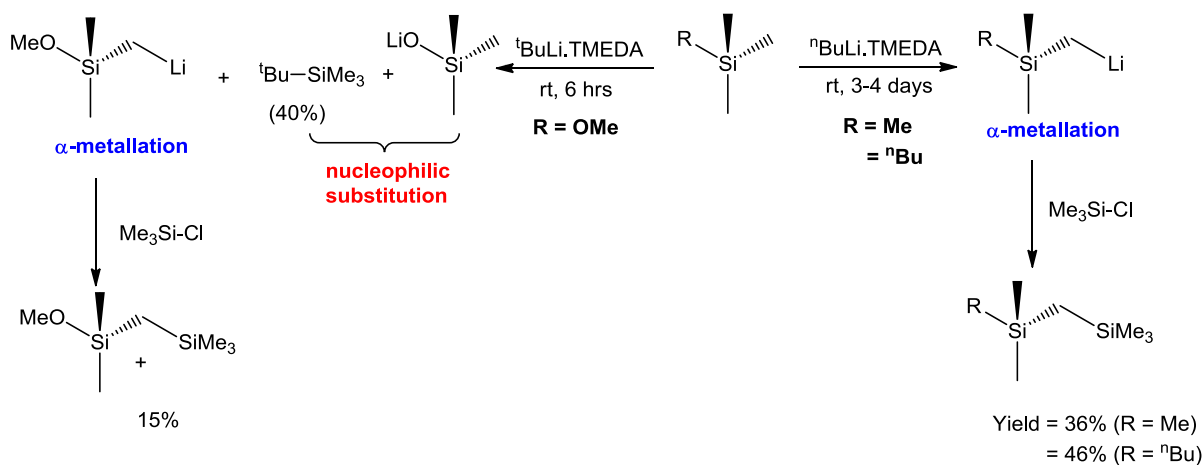
Comparison of the ^1H NMR spectra of **13** and **14** show them to be very similar (**Table 2.1**), with the main differences being for the resonance of the Si-CH_2 group and the α -methyl groups of TMP, which show a slight upfield shift in **14**, most likely due to the presence of the more electropositive sodium atom, compared to the lithium atom in **13**. The $^{13}\text{C}\{^1\text{H}\}$ NMR spectra of **13** and **14** were also very similar, with the most informative resonance being that of the SiCH_2 group, appearing at δ -3.9 ppm in **13** and δ -3.3 ppm in **14**. As was seen in the ^1H NMR spectra, this is shifted significantly upfield compared to that of the non-metallated SiCH_3 groups in **12** (δ 0.1 ppm) and the SiCH_3 groups of **13** and **14** (δ 2.6 and 2.7 ppm respectively).

	$\delta(\text{ppm})$	${}^t\text{Bu}$	SiCH_3	SiCH_2	Ar-H	TMP ($\alpha\text{-Me}$)
$[(\text{THF})\text{Li}(\text{TMP})\{\text{PhOSi}(\text{CH}_3)_2\text{CH}_2\}\text{Zn}{}^t\text{Bu}]$ (13)	1.63	0.29	-0.59	7.04, 6.84	1.38, 1.19	
$[(\text{TMEDA})\text{Na}(\text{TMP})\{\text{PhOSi}(\text{CH}_3)_2\text{CH}_2\}\text{Zn}{}^t\text{Bu}]$ (14)	1.70	0.31	-0.73	7.07, 6.90, 6.85	1.50, 1.16	
${}^t\text{Bu}_2\text{Zn}$	1.02	-	-	-	-	
PhO-SiMe_3 (12)	-	0.15	-	7.10, 6.87	-	

Table 2.1: Comparison of selected resonances of the ${}^1\text{H}$ NMR spectra of **12**, **13**, **14** and ${}^t\text{Bu}_2\text{Zn}$ in d_6 -benzene.

Although **13** and **14** were only isolated in crystalline yields of 52% and 42% respectively, analysis of the filtrate revealed these were the major species present in solution. Furthermore, when the reaction of isolated crystals of $[(\text{THF})\text{Li}(\text{TMP})\text{Zn}{}^t\text{Bu}_2]$ (**1**) with an equimolar amount **12** was performed in d_6 -benzene and monitored by ${}^1\text{H}$ NMR spectroscopy conversion of **12** to the α -metallated species **13** proceeded in a yield of 92% after one hour, showing that this reaction is almost quantitative.

Due to the low acidity of silyl methyl protons only a small number of examples for preparing α -metallated silanes by direct metal-hydrogen exchange have been reported to date. This problem was highlighted by Peterson in 1967, where the metallation of tetramethylsilane with a 1:1 mixture of ${}^n\text{BuLi}$ and TMEDA required reaction times of three days, and afforded the α -lithiated silane in a yield of only 36% (**Scheme 2.3**).^[85] West and co-workers have shown that when the reaction was performed with methoxytrimethylsilane using ${}^t\text{BuLi}$ and TMEDA, the presence of the alkoxide substituent on the silicon made the substrate more susceptible to α -metallation, reducing the reaction time to 6 hours. However, the competing nucleophilic attack by the *tert*-butyl group at the silicon was also observed, with subsequent quenching with TMS-Cl resulting in the expected product from α -metallation being isolated in a yield of only 15%, and one of the products from nucleophilic substitution, ${}^t\text{Bu-SiMe}_3$, being isolated in a 40% yield. Even more interestingly, when the reaction of ethoxytrimethylsilane with ${}^t\text{BuLi}/\text{TMEDA}$ was carried out, quenching with TMS-Cl gave the expected product of α -metallation in a much improved yield of 50%.^[86] In this latter example it was believed that the more bulky EtO (compared to MeO) group inhibited the nucleophilic cleavage of the Si-O bond.

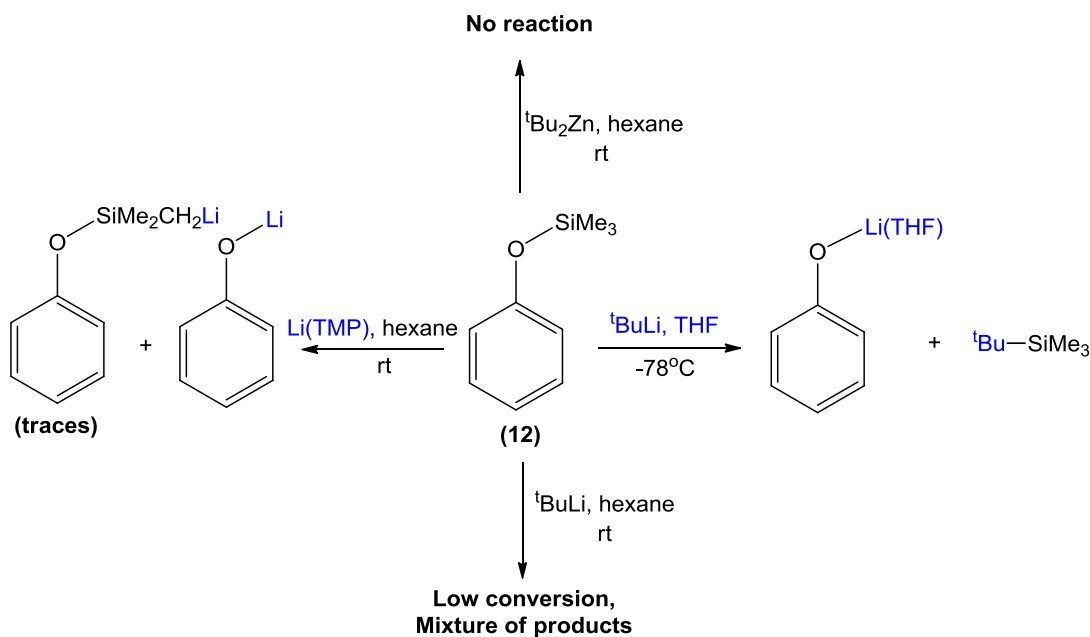


Scheme 2.3: Comparison of reactivity of $^n\text{BuLi.TMEDA}$ towards Me_4Si and Me_3SiOMe .

More recently, Thomas has shown that the α -lithiation of methoxytrimethylsilane and methoxymethyltrimethylsilane using $^t\text{BuLi}$ proceeds in high yields when carried out in non-polar solvents (e.g. pentane, cyclopentane) and in the absence of any Lewis base, with almost no substitution at silicon taking place.^[87] However, when this same methodology was applied to the phenyl substituted alkoxy silane, diphenylmethylethoxysilane [$\text{EtOSiPh}_2\text{Me}$], both the α -lithiated product and the substitution products ($\text{EtO-Li} + ^t\text{Bu-SiPh}_2\text{Et}$) were obtained, suggesting that substitution at silicon was a competitive reaction pathway for this substrate.^[88] Thus, to date attempts to apply direct α -metallation to phenyl silanes has proved unsuccessful, which makes the DIZn of **12** by alkali metal zincates **1** and **3** a result of great interest.

As the direct α -metallation of **12** has not previously been investigated, it was necessary to compare the results obtained using hetero-bimetallic base **1** with the reactivities exhibited by more conventional homometallic reagents. Thus, the reactions of **12** with; (i) $^t\text{BuLi/THF}$, (ii) $^t\text{BuLi}$, (iii) Li(TMP) and (iv) Zn^tBu_2 were investigated (**Scheme 2.4**). As previously mentioned, TMS groups are commonly used as protecting groups for alcohols, and can be cleaved by nucleophilic displacement under acidic or basic conditions. Hence, when **12** is treated with $^t\text{BuLi}$ in THF at -78°C then the sole products obtained were those resulting from nucleophilic substitution at the silicon, $[(\text{THF})\text{Li-OPh}]$ and $^t\text{Bu-SiMe}_3$. Previously it has been suggested that although the presence of a Lewis base such as THF can increase the rate of α -metallation of silanes by activating the organolithium reagent, it can also lead to the organolithium reagent favouring substitution at the silicon.^[87] In this case reaction of **12** with $^t\text{BuLi}$ in THF results only in nucleophilic substitution with no α -metallation of the substrate

observed. This is most likely due to the great leaving ability of the PhO group, resulting in a preference for cleavage of the Si-O bond over the C-H bond of the methyl group.



Scheme 2.4: Comparison of the reactivity of $t\text{BuLi}$, Li(TMP) and $t\text{Bu}_2\text{Zn}$ with **12**.

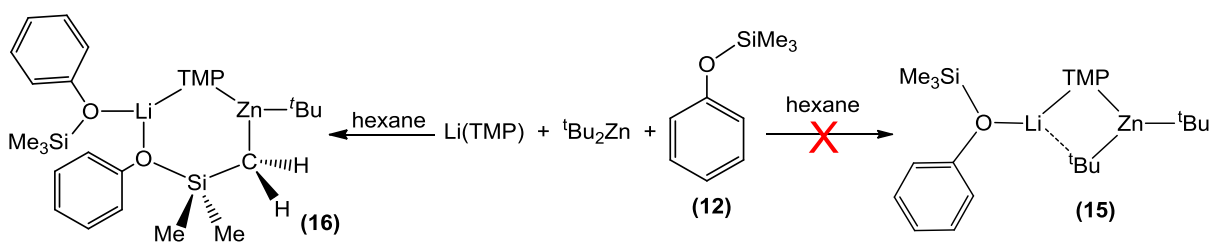
Thomas and co-workers have reported that α -metallation can be favoured over nucleophilic substitution when the reactions are carried out in the absence of donor solvents, or using more sterically hindered alkyl lithium reagents.^[87-88] However, reaction of **12** with $t\text{BuLi}$ in hexane proceeded sluggishly, with only ~33% of the substrate having reacted after 24 hours at room temperature. The reaction produced a white powder, only soluble in d_8 -THF, which when analysed by ^1H and ^7Li NMR spectroscopy revealed a complex mixture of products, with no resonances at negative chemical shifts, which would be indicative of α -metallation. When Li(TMP) was employed a similar complex mixture of products was observed, including the substitution products Li-OPh and TMP-SiMe_3 , as well as traces of the α -lithiated product. Unsurprisingly, the significantly less polar organometallic reagent $t\text{Bu}_2\text{Zn}$ showed no reactivity towards **12** (**Scheme 2.4**).

Thus, the selective α -metallation of **12** by **1** constitutes a new addition to the existing catalogue of examples of AMMZn, whereby the reactivity of the zincate towards **12** cannot be replicated by either of the homometallic species (Li(TMP) and Zn^tBu_2), and also represents the first reported example of a direct lateral zincation (DlZn). Furthermore, taking into consideration the results observed for the reactions of **12** with conventional group 1

organometallic reagents, the synthesis of α -zincated trimethyl(phenoxy)silanes through an indirect route, involving the initial deprotonation of **12** by a more reactive organolithium reagent (e.g. Li(TMP), ^tBuLi) followed by a metathesis reaction with ZnCl₂ is not viable. This illustrates the vast scope of AMMZn as a powerful synthetic tool, achieving the regioselective α -metallation of **12** that is otherwise inaccessible when conventional monometallic reagents are employed.

2.1.2 Investigating the regioselectivity of the DiZn of **12** by **1**

In order to gain more understanding of the α -metallation of **12** by **1**, the reaction of Li(TMP) and Zn^tBu₂ with **12** in the absence of any other donor ligand was performed, in an attempt to isolate the pre-metallation complex [(PhOSiMe₃)Li(TMP)Zn^tBu₂] (**15**), where **12** is coordinated to the lithium centre prior to deprotonation (**Scheme 2.5**).



Scheme 2.5: Synthesis of [(PhOSiMe₃)Li(TMP){PhOSi(CH₃)₂CH₂}Zn^tBu] (**16**), along with the proposed formation of the pre-metallation complex **15**.

Thus, to a solution of Li(TMP) and ^tBu₂Zn was added one equivalent of **12**, and the solution stirred at room temperature for 30 minutes. Storage of the solution at low temperatures (-30°C) for several days, yielded a batch of colourless crystals of [(PhOSiMe₃)Li(TMP){PhOSi(CH₃)₂CH₂}Zn^tBu] (**16**) in an isolated yield of 16% (**Scheme 2.5**), which were analysed by X-ray crystallography and multinuclear (¹H, ⁷Li and ¹³C{¹H}) NMR spectroscopy. The molecular structure of **16** was confirmed by X-ray crystallographic analysis (**Figure 2.5(a)**), which revealed the product to be the mixed-metal compound [(PhOSiMe₃)Li(TMP){PhOSi(CH₃)₂CH₂}Zn^tBu]. The structure is very similar to that of **13**, with the two metals connected through a bridging TMP ligand and an ambidentate α -zincated trimethyl(phenoxy)silane ligand, resulting in the formation of a six-membered {LiZnCSiO} ring stabilised by a secondary Li-C11 interaction (**Figure 2.5(b)**).

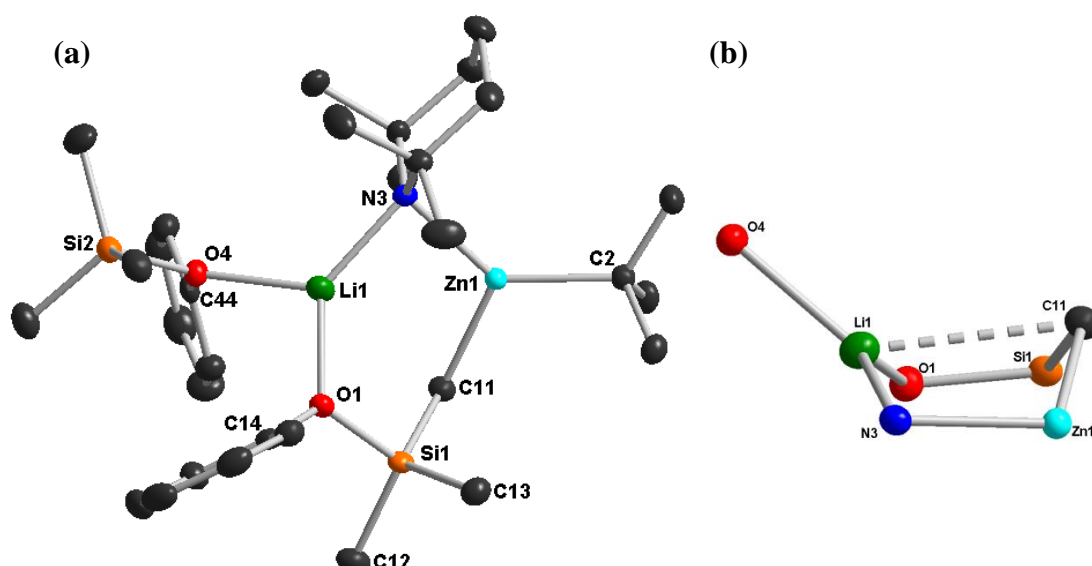


Figure 2.5(a): Molecular structure of $[(\text{PhOSiMe}_3)\text{Li}(\text{TMP})\{\text{PhOSi}(\text{CH}_3)_2\text{CH}_2\}\text{Zn}^t\text{Bu}]$ (**16**) with 50% probability ellipsoids. Hydrogen atoms have been omitted for clarity. **(b)** Inorganic core of **16** highlighting the pseudo boat conformation of the $\{\text{LiNZnCSiO}\}$ ring and the secondary Li-C interaction. *Selected bond distances (\AA) and bond angles ($^\circ$):* Zn-C11 2.0738(15), Zn-C2 2.0421(15), Zn-N 2.0422(12), Li-C11 2.776(3), Li-O1 2.025(3), Li-N 2.021(3), Li-O4 2.075(3), Si1-O1 1.7132(11), Si1-C11 1.8117(16), Si1-C12 1.8621(16), Si1-C13 1.8625(16), Si2-O4 1.7018(11), Si2-C41 1.8525(18), Si2-C42 1.8537(17), Si2-C43 1.8461(17); C11-Zn-C2 114.20(6), C11-Zn-N 109.91(6), C2-Zn-N 135.80(5), O1-Li-O4 102.39(12), O1-Li-N 123.81(14), O4-Li-N 132.73(15).

Zinc bonds directly to the metallated methyl group, where the Zn-C bond length (Zn-C11, 2.0738(15) \AA) is almost identical to that found for **13** (2.0769(15) \AA). Both of the metals adopt distorted trigonal planar geometries (sum of angles around Zn = 360° , Li = 358.8°), with the major difference being that whereas in **13** the coordination sphere of lithium was completed by a terminal molecule of THF (Li-O2, 1.937(3) \AA), in **16** it is a molecule of **12** which completes the coordination of lithium, forming a dative bond from the oxygen which is slightly longer (Li-O4, 2.075(3) \AA) due to the greater steric bulk around the oxygen. This also leads to a slight elongation of the secondary Li-C interaction in **16** (Li-C11, 2.776(3) \AA) compared to that of **13** (2.568(3) \AA), which, prevents the lithium from approaching more closely to the carbanionic centre.

Comparison of the ^1H NMR spectrum of **16** in d_6 -benzene solution (**Figure 2.6**) with that of **13** also shows them to be very similar (**Table 2.2**). The resonances which are of most interest

are two singlets at δ 0.22 and -0.68 for the SiCH_3 and SiCH_2 protons of the molecule of α -metallated silane, in addition to another singlet at δ 0.15 ppm corresponding to a second set of SiCH_3 protons, in a ratio of $\text{SiCH}_2:\text{SiCH}_3:\text{SiCH}_3$ of 2:6:9, consistent with the presence of one molecule of α -metallated substrate along with a second molecule where all three of the methyl groups remain intact.

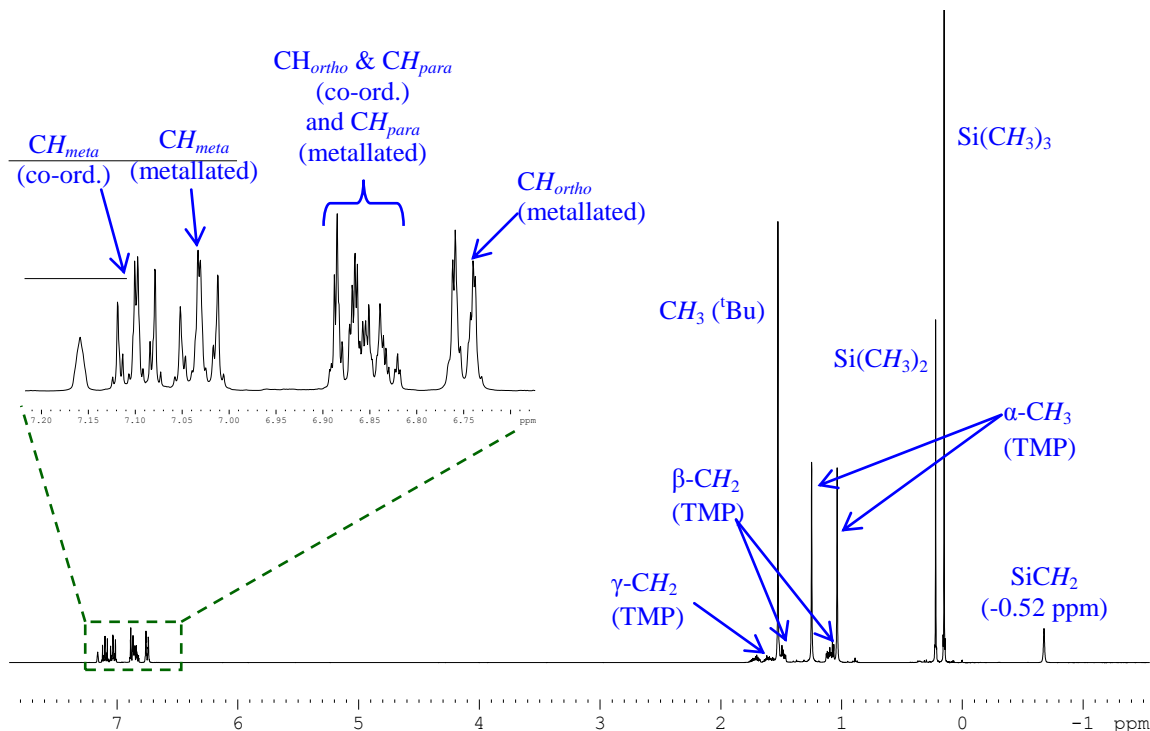


Figure 2.6: ^1H NMR spectrum of **16** in d_6 -benzene.

This was mirrored by the aromatic region, which indicated the presence of two different phenyl groups, as shown by two different sets of aromatic protons, two triplets and a doublet at δ 7.04, 6.85 and 6.74 ppm for the α -metallated molecule of the substrate, and a triplet and an overlapping triplet and doublet at δ 7.10 and 6.87 ppm for the molecule of coordinated substrate, in a ratio of approximately 1:1. Comparison of the ^1H NMR resonances of the coordinating molecule of trimethyl(phenoxy)silane in **16** (δ 0.15, 6.84, 7.10 ppm) with those of **12** (δ 0.15, 6.87, 7.10 ppm) show them to be almost identical.

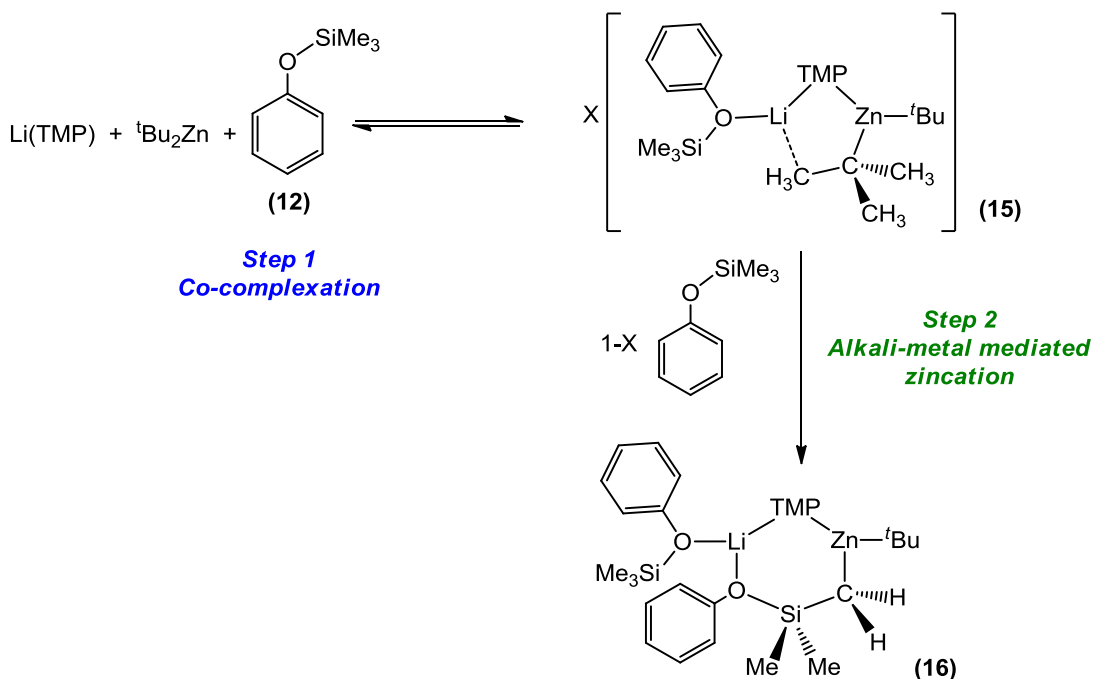
	$\delta(\text{ppm})$	^tBu	SiCH_3	SiCH_2	Ar-H	TMP (α -Me)
$[(\text{PhOSiMe}_3)\text{Li}(\text{TMP})\{\text{PhOSi}(\text{CH}_3)_2\text{CH}_2\}\text{Zn}^t\text{Bu}]$ (16)	1.53	0.22, 0.15	-0.68		7.04, 6.85, 6.74 7.10, 6.87	1.04, 1.25
$[(\text{THF})\text{Li}(\text{TMP})\{\text{PhO-Si}(\text{CH}_3)_2\text{CH}_2\}\text{Zn}^t\text{Bu}]$ (13)	1.63	0.29	-0.59		7.04, 6.84	1.19, 1.38
PhO-SiMe_3 (12)	-	0.15	-		7.10, 6.87	-

Table 2.2: Selected ^1H NMR data (ppm) for **12**, **13** and **16** in d_6 -benzene.

The $^{13}\text{C}\{^1\text{H}\}$ NMR spectrum of **16** also confirms the presence of two different molecules of phenoxysilane, one set of aromatics resonances for the α -metallated molecule of **12** (δ 153.7, 130.2, 123.5 and 119.9 ppm) and one set of resonances for the coordinated molecule of **12** (δ 155.7, 129.8, 121.8 and 120.4 ppm). The ^7Li NMR of **16** showed a single resonance at δ 1.89 ppm, which was different from that of **13** (δ 1.07 ppm) and consistent with a different environment for the lithium centre.

In order to prepare **16** via a rational route, the reaction of Li(TMP) and $^t\text{Bu}_2\text{Zn}$ was repeated with two molar equivalents of the silane **12**, affording a batch of colourless crystals which when characterised by multinuclear NMR (^1H , ^7Li and $^{13}\text{C}\{^1\text{H}\}$) spectroscopy displayed identical spectra to those reported for $[(\text{PhOSiMe}_3)\text{Li}(\text{TMP})\{\text{PhOSi}(\text{CH}_3)_2\text{CH}_2\}\text{Zn}^t\text{Bu}]$ (**16**), in an improved yield of 37% (compared to 16% when one equivalent of **12** was employed). Analysis of the filtrate indicated traces of the product were present, but the major species was Li(TMP), indicating that the reaction had not gone to completion (*vide infra*).

The fact that **16** is obtained even when only one equivalent of **12** is employed suggests that metallation of the substrate must occur at a faster rate than coordination to lithium to form the putative pre-metallation complex $[(\text{PhOSiMe}_3)\text{Li}(\text{TMP})\text{Zn}^t\text{Bu}_2]$ (**15**). So, once **15** is formed it must react rapidly with another molecule of non-coordinated **12**, metallating the substrate and giving the final product **16** (**Scheme 2.6**). Previous work on the α -lithiation of methoxytrimethylsilane by Thomas and co-workers had suggested that at low temperatures (-78°C) a pre-metallation complex of the substrate and $^t\text{BuLi}$ was formed $[\text{}^t\text{BuLi}\cdot 2\text{MeOSiMe}_3]_2$, which could be characterised spectroscopically (^7Li and $^{13}\text{C}\{^1\text{H}\}$ NMR),^[88] and was found to be in equilibrium with the starting materials ($(^t\text{BuLi})_4$ and MeOSiMe_3). With this in mind, the reaction of Li(TMP) and $^t\text{Bu}_2\text{Zn}$ with one equivalent of **12** was carried out at -78°C in an attempt to detect the pre-metallation complex **15**. After 30 minutes a white precipitate was formed, which was isolated and identified as Li(TMP) by ^1H and ^7Li NMR. The volatiles were removed from filtrate *in vacuo*, and analysis by ^1H and ^7Li NMR also revealed the presence of only Li(TMP) (both **12** and $^t\text{Bu}_2\text{Zn}$ are volatile, and can be easily removed *in vacuo*), which suggested firstly that no deprotonation of the substrate had occurred, and that at low temperatures precipitation of Li(TMP) must drive the proposed equilibrium in **Scheme 2.6** towards the monometallic compounds.



Scheme 2.6: Proposed mechanism for the formation of **16**.

These results suggest that in hexane solutions the pre-metallation complex **15** lies in equilibrium with the starting materials ($\text{Li}(\text{TMP})$, ${}^t\text{Bu}_2\text{Zn}$ and **12**), and once formed, **15** rapidly reacts to metallate a second non-coordinated molecule of **12** to give the final product **16**, driving the equilibrium between the starting material and **15** towards the formation of the mixed-metal species. At low temperatures (-78°C) the solubility of $\text{Li}(\text{TMP})$ decreases and it precipitates from solution, driving the equilibrium towards the starting materials, which results in no metallation or complexation of **12** being observed (**Scheme 2.6**).

2.1.3 Applications of $\text{DI}Z\text{n}$ to other silyl-substituted substrates

To extend the concept of $\text{DI}Z\text{n}$, two silyl-substituted aromatic molecules similar to **12** were investigated, trimethyl(phenyl)silane and N,N -bis(trimethylsilyl)aniline (**Figure 2.7**). Trimethyl(phenyl)silane is very similar to **12**, with the exception that instead of a phenoxide group bonding to the silicon it is a phenyl group, whereas N,N -bis(trimethylsilyl)aniline can be viewed as the amido analogue of **12**, so instead of an OSiMe_3 functional group there is a $\text{N}(\text{SiMe}_3)_2$ group.

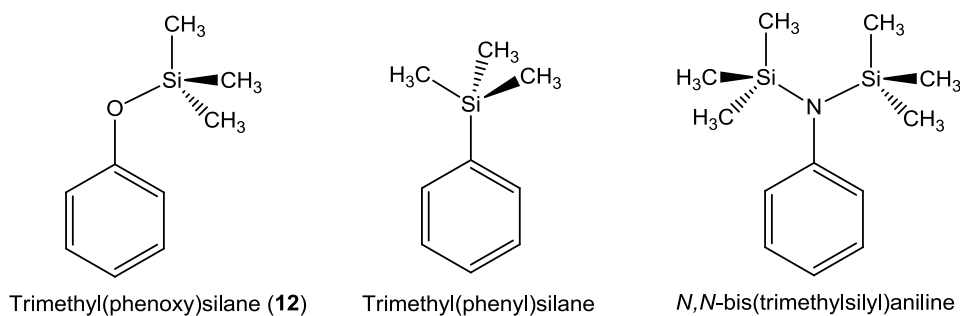


Figure 2.7: Comparison of the substrates **12**, trimethyl(phenyl)silane and *N,N*-bis(trimethylsilyl)aniline.

After reacting each of these substrates with the lithium TMP-zincate **1** analysis of the reaction mixtures by ^1H NMR spectroscopy indicated that no metallation had occurred, even after leaving the reactions to stir for 4 days at room temperature or refluxing the solutions for 4 hours. Reaction of *N,N*-bis(trimethylsilyl)aniline with the sodium TMP-zincate **3** also showed no metallation after 4 days at room temperature or 4 hours under reflux when analysed by ^1H NMR. However, when **3** was reacted with the unactivated trimethyl(phenyl)silane, analysis of the reaction mixture after 4 hours at room temperature by ^1H NMR revealed traces of metallated substrate (<5% conversion) along with unreacted zincate (the unreacted substrate is volatile and can therefore be removed *in vacuo*). If the reaction was refluxed for 6 hours, analysis by ^1H NMR spectroscopy showed only a slight increase in the yield (~5-10%), with the main species present still the unreacted base **3**. Analysis of the crude reaction mixture indicated a mixture of products which included the substrate metallated at the *meta* position, as shown by the presence of a singlet, two doublets and a triplet, and a second product appeared to be that of the *para* metallated species, due to the presence of two doublets. Analysis of the aliphatic region showed no signals at negative ppm, suggesting that no α -metallation of the SiCH_3 groups had occurred. As mentioned previously, a similar mixture of *meta* and *para* metallated products has been found for the reaction of **3** with toluene, but in this case metallation is quantitative at room temperature.^[62]

Thus, these results show that zincates **1** and **3** show almost no reactivity towards trimethyl(phenyl)silane and *N,N*-bis(trimethylsilyl)aniline. The lack of reactivity towards trimethyl(phenyl)silane can be rationalised by considering that in general the reactivity of tetra(alkyl)silanes towards organometallic bases is known to be very poor, due to the lack of acidity of the protons, and the stability of Si-C bonds.^[87] Therefore, trimethyl(phenyl)silane

will be much less activated towards metallation than the corresponding phenoxysilane **12**. The presence of a nitrogen heteroatom in *N,N*-bis(trimethylsilyl)aniline should enhance the acidity of the methyl protons compared to those of trimethyl(phenyl)silane, but since nitrogen is less electronegative than oxygen, these protons will be less acidic than those in **12**. Furthermore, the N(SiMe₃)₂ group is much more sterically demanding than the OSiMe₃ of **12**, which is likely to have an effect on the ability of the substrate to coordinate to the zincate, and therefore prevent any metallation.

Despite the negative results when attempting to metallate trimethyl(phenyl)silane and *N,N*-bis(trimethylsilyl)aniline there are still further substrates which could be investigated, including trimethylalkoxysilanes (RO-SiMe₃), and other related phenyl silanes such as PhO-SiEt₃ or EtO-SiPh₂Me, the latter of which Thomas has previously unsuccessfully tried to metallate using ^tBuLi.^[87] In addition, it would also be interesting to investigate the reactivity of **13** and **14** with a range of electrophiles such as MeI, I₂ or PhCHO.

2.1.4 Conclusions

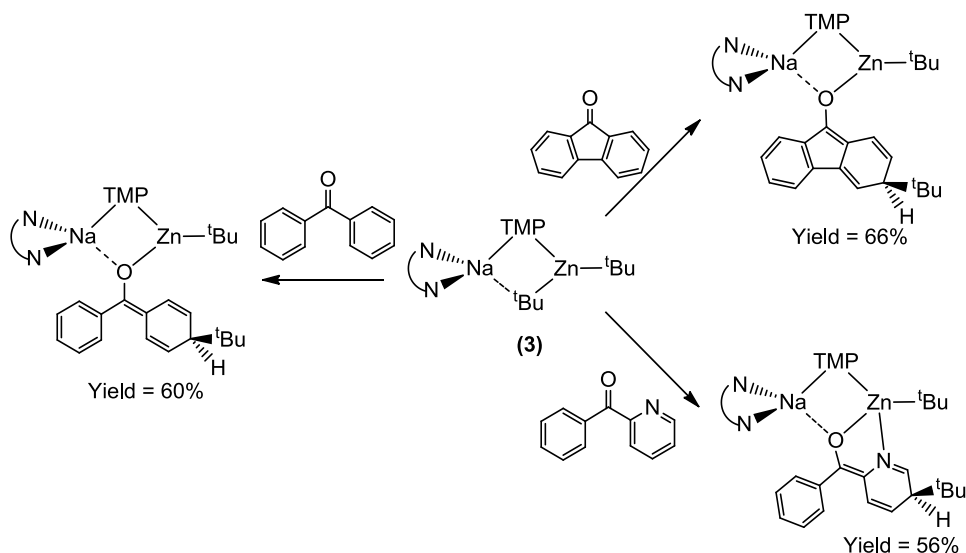
The reactions of the lithium TMP-zincate [(THF)Li(TMP)Zn^tBu₂] (**1**) and the sodium TMP-zincate [(TMEDA)Na(TMP)Zn^tBu₂] (**3**) with trimethyl(phenoxy)silane (**12**) have provided the first examples of quantitative α-zincation of a phenoxysilane, forming the alkali metal zincates [(THF)Li(TMP){PhOSi(CH₃)₂CH₂}Zn^tBu] (**13**) and [(TMEDA)Na(TMP){PhOSi(CH₃)₂CH₂}Zn^tBu] (**14**), with no competitive nucleophilic substitution at the silicon having taken place even though the reactions are performed at ambient temperatures. Moreover, these reactions provide the first ever examples of direct lateral zincation (DI Zn) of an aromatic substrate, demonstrating a new application of alkali metal zincates in synthetic chemistry.

In addition, the reaction of Li(TMP) and ^tBu₂Zn with **12** has been investigated, suggesting that a mixed-metal reagent of similar structure to **1**, where **12** is coordinated to the lithium instead of THF to give [(PhOSiMe₃)Li(TMP)Zn^tBu₂] (**15**) must first be formed, which reacts rapidly with a second molecule of **12** to give the metallated intermediate [(PhOSiMe₃)Li(TMP){PhOSi(CH₃)₂CH₂}Zn^tBu] (**16**), which has been isolated and fully characterised.

Compounds **13**, **14** and **16** have been structurally characterised by X-ray crystallography, revealing that each of these compounds contains a novel heteroatomic six-element $\{M^I\text{OSiCZnN}\}$ ring, which adopts a pseudo boat conformation, stabilised by an additional secondary interaction between the alkali metal and the metallated carbon.

2.2 Assessing the reactivity of sodium TMP-zincate (**3**) towards benzoylferrocene: deprotonative metallation vs. alkylation reactions

So far alkali metal TMP-zincates **1** and **3** have only been discussed within the context of metallation reactions. However, the reactivity of this species is not solely restricted to deprotonative metallation. The previously reported reaction of **3** with the aromatic ketone, benzophenone, resulted in the unexpected nucleophilic addition of a *tert*-butyl group at the *para* position of one of the aromatic rings to yield the *tert*-butylated 1,6-adduct $[(\text{TMEDA})\text{Na}(\text{TMP})\{\mu\text{-OC}(\text{Ph})(4\text{-}^t\text{Bu-C}_6\text{H}_5)\}\text{Zn}^t\text{Bu}]$ in an isolated crystalline yield of 60%.^[89] Furthermore, subsequent studies have shown that this remote 1,6-addition can also be extended to fluorenone and 2-benzoylpyridine, with the expected products isolated in yields of 66% and 56% respectively (**Scheme 2.7**),^[90] showing a new application of **3** as a reagent capable of performing remote alkylations to aromatic ketones.



Scheme 2.7: Reaction of $[(\text{TMEDA})\text{Na}(\text{TMP})\text{Zn}^t\text{Bu}_2]$ (**3**) with benzophenone, fluorenone and 2-benzoylpyridine.

Applications of bimetallic combinations in the deprotonation of metallocenes have also been reported. Previous studies into the metallation of ferrocene have shown that reaction of the

lithium TMP-zincate $[(\text{TMEDA})\text{Li}(\text{TMP})\text{Zn}^n\text{Bu}_2]$ with either one or two equivalents of ferrocene yielded the neutral bis(ferrocenyl) zinc compound $[(\text{TMEDA})\text{Zn}(\text{Fc})_2]$ and the solvent separated tris(ferrocenyl)zincate $[\text{Li}(\text{THF})_4]^+[\text{Zn}(\text{Fc})_3]^-$ respectively (**Figure 2.8(a)**).^[91] Furthermore, ferrocene can be tetra-metallated using the alkali metal magnesiate “ $\text{NaMg}(\text{N}^i\text{Pr}_2)_3$ ” to form the inverse-crown species $[\text{Fe}(\eta^5\text{-C}_5\text{H}_3)_2\text{Na}_4\text{Mg}_4(\text{N}^i\text{Pr}_2)_8]$ (**Figure 2.8(b)**).^[92]

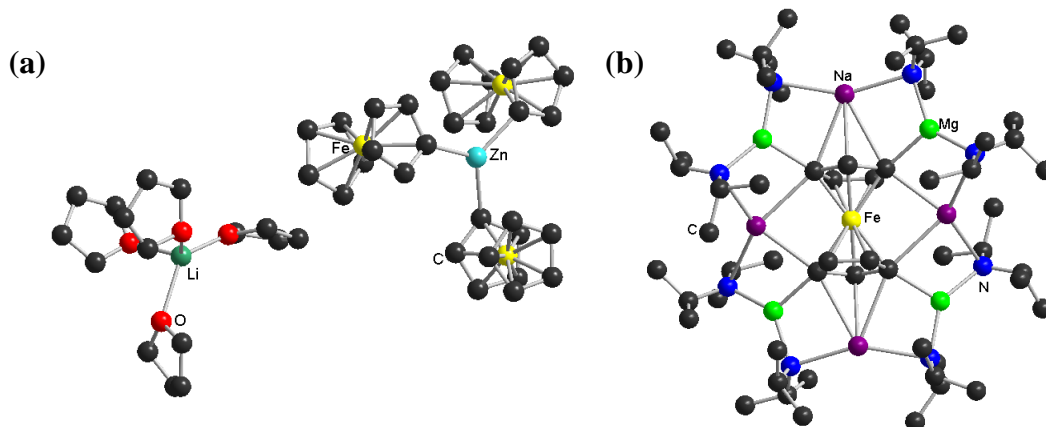
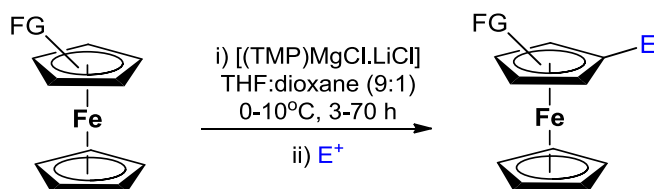


Figure 2.8: Molecular structures of metallated ferrocenyl species (a) $[\text{Li}(\text{THF})_4]^+[\text{Zn}(\text{Fc})_3]^-$ and (b) $[\text{Fe}(\eta^5\text{-C}_5\text{H}_3)_2\text{Na}_4\text{Mg}_4(\text{N}^i\text{Pr}_2)_8]$. Hydrogen atoms have been omitted for clarity.

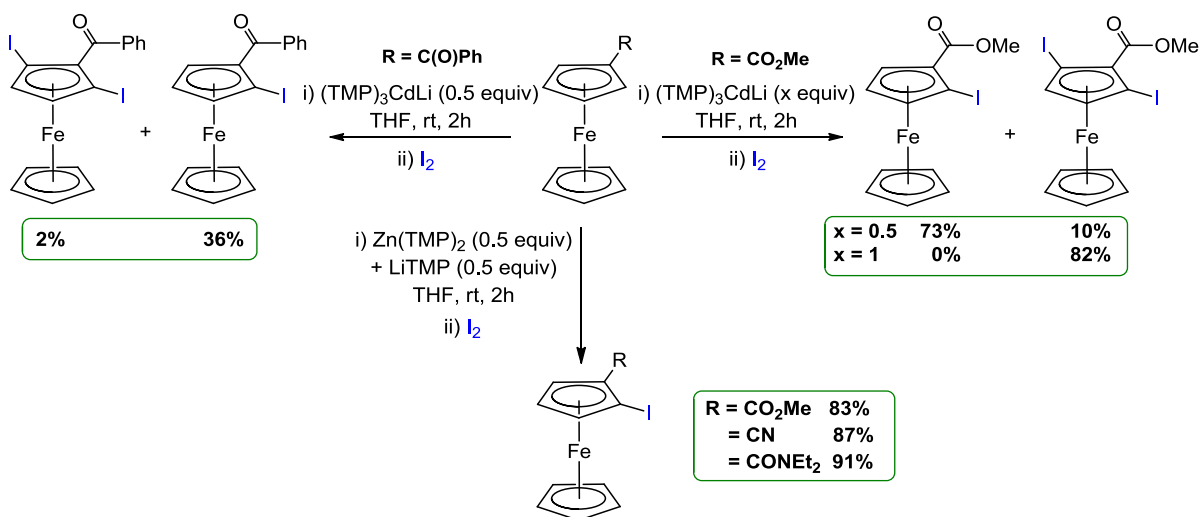
Turning to functionalised ferrocene substrates, it has been shown that the turbo-Hauser base $[(\text{TMP})\text{MgCl}.\text{LiCl}]$ can selectively deprotonate a wide range of substituted ferrocenyl substrates containing ester, nitrile and carboxylic acid groups, which after electrophilic quenching yielded the expected di-substituted ferrocenes in good yields (**Scheme 2.8**).^[93] These species could further undergo consecutive metallation and quenching to yield tri- and tetra-substituted ferrocenyl products.

It has also been reported that using the lithium-cadmiate base $(\text{TMP})_3\text{CdLi}$, mono- and di-metallation of ester substituted ferrocenes can be achieved by controlling the stoichiometry of the base used from 0.5 to 1 equivalents respectively (**Scheme 2.9**).^[94] Furthermore, this protocol could be extended to some chiral ferrocene esters, to give diastereoselective deprotonation, with subsequent iodination yielding the final product in good diastereomeric excess.^[95] However, with weakly activated substrates such as benzoylferrocene a mixture mono- and diiodo-products was obtained in relatively low yields (36% and 2% respectively). Turning to the lithium zincate combination of $\text{Li}(\text{TMP})$ and $\text{Zn}(\text{TMP})_2$ (1:1), the selective mono-iodination of ferrocenecarboxylate, cyanoferrocene and *N,N*-dimethylferrocenecarboxamide could be achieved in excellent yields (**Scheme 2.9**).^[94]



FG	E ⁺	Product	Yield (%)	FG	E ⁺	Product	Yield (%)
CO ₂ Et	I ₂		60	CO ₂ ^t Bu	^t BuCHO		82
	PhCOCl		70		PhCOCl		80
	ClCO ₂ Et		67		Boc ₂ O		78
CO ₂ H			76	CN	^t BuCHO		62

Scheme 2.8: Reaction of [(TMP)MgCl.LiCl] with functionalised ferrocenyl substrates followed by electrophilic quenching.



Scheme 2.9: Reaction of (TMP)₃CdLi and Li(TMP)/Zn(TMP)₂ with functionalised ferrocenyl substrates followed by electrophilic quenching with iodine.

Herein, we extend our studies on the reactivity of sodium zincate **3** to their application in metallocene functionalisation, using benzoylferrocene (**17**) as a case study. This substrate was of interest as it combines relatively acidic protons of the Cp rings (therefore susceptible towards C-H deprotonation) with an electrophilic benzoyl fragment (which can undergo 1,2- or 1,6-addition reactions) (**Figure 2.9**).

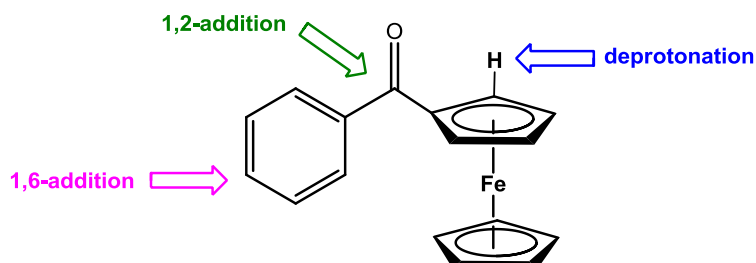
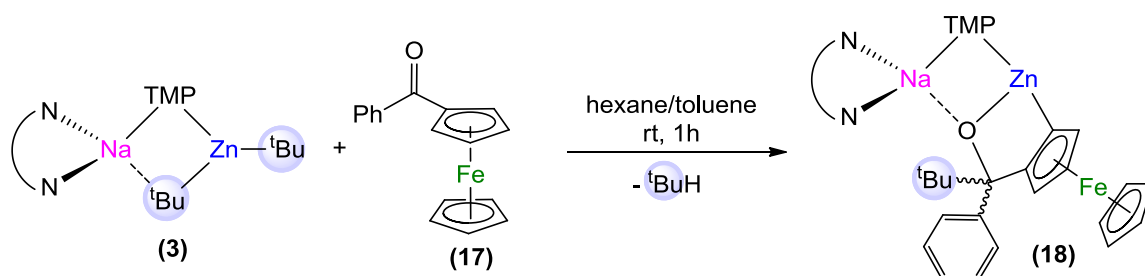


Figure 2.9: Possible sites of reactivity on benzoylferrocene (**17**) from reaction with $[(\text{TMEDA})\text{Na}(\text{TMP})\text{Zn}^t\text{Bu}_2]$ (**3**).

2.2.1 Investigating the reactivity of benzoylferrocene (**17**) with sodium TMP-zincate (**3**)

A hexane solution of **3** was prepared by combining the constituent homometallic reagents, Na(TMP) and Zn^tBu_2 , along with the bidentate ligand TMEDA in hexane, to which was added one molar equivalent of **17** giving a deep red suspension which was stirred at room temperature for 1 hour. Removal of hexane *in vacuo* and addition of toluene gave a deep red solution, which after storing in the freezer (-30°C) a batch of orange crystals of $[(\text{TMEDA})\text{Na}(\mu\text{-TMP})\text{Zn}\{\text{OC}(\text{Ph})(^t\text{Bu})(\eta^5\text{-C}_5\text{H}_3)\text{Fe}(\eta^5\text{-C}_5\text{H}_5)\}]$ (**18**), as determined by ^1H and $^{13}\text{C}\{^1\text{H}\}$ NMR spectroscopy and X-ray crystallography, were deposited in an isolated yield of 12% (**Scheme 2.10**).



Scheme 2.10: Reaction of $[(\text{TMEDA})\text{Na}(\text{TMP})\text{Zn}^t\text{Bu}_2]$ (**3**) with **17** to form $[(\text{TMEDA})\text{Na}(\mu\text{-TMP})\text{Zn}\{\text{OC}(\text{Ph})(^t\text{Bu})(\eta^5\text{-C}_5\text{H}_3)\text{Fe}(\eta^5\text{-C}_5\text{H}_5)\}]$ (**18**).

The molecular structure of [(TMEDA)Na(μ -TMP)Zn{OC(Ph)(^tBu)(η^5 -C₅H₃)Fe(η^5 -C₅H₅)}] (**18**) was determined by X-ray crystallography (**Figure 2.10**), revealing that an unprecedented two-fold activation of the *tert*-butyl groups in **3** had taken place. Thus, the substrate had been simultaneously deprotonated at the α -carbon of the functionalised Cp ring (Cp'), and undergone nucleophilic 1,2-addition of the second *tert*-butyl ligand across the carbonyl group of the ketone.

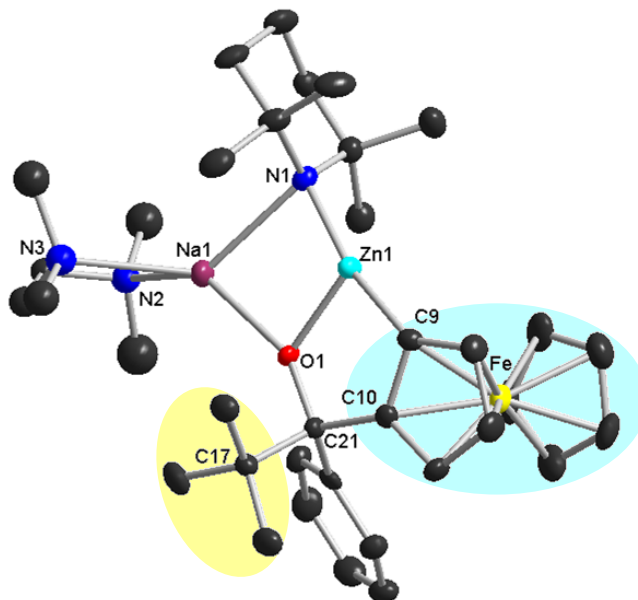


Figure 2.10: Molecular structure of [(TMEDA)Na(μ -TMP)Zn{OC(Ph)(^tBu)(η^5 -C₅H₃)Fe(η^5 -C₅H₅)}] (**18**) with 50% probability ellipsoids. Hydrogen atoms and minor disordered component of TMEDA have been omitted for clarity. *Selected bond lengths (Å) and angles (°):* Zn(1)-N(1) 1.926(2), Zn(1)-C(9) 1.930(3), Zn(1)-O(1) 1.9827(17), Na(1)-O(1) 2.229(2), Na(1)-N(1) 2.527(2), O(1)-C(21) 1.415(3), N(1)-Zn(1)-C(9) 166.66(11), N(1)-Zn(1)-O(1) 104.30(8), C(9)-Zn(1)-O(1) 89.03(10), O(1)-Na(1)-N(1) 80.66(7), Zn(1)-O(1)-Na(1) 90.26(7), N(1)-Zn(1)-Na(1)-O(1) 166.83(11).

The CIP structure of **18** retains the “(TMEDA)-Na-(μ -TMP)-Zn” backbone of the bimetallic base (**3**), a feature which is commonly found in metallated intermediates from reactions involving this zincate (see **Chapter 1.3**). In addition to the amido ligand, the two metals are bridged by the oxygen atom of a tertiary alkoxide, formed by the nucleophilic addition of one of the *tert*-butyl groups of **3** across the carbonyl of the ketone to form a tetrahedral (sp³) carbon atom (average angle around C21, 109.4°). The C-O bond length in **18** (C21-O1, 1.415(3) Å) is longer than that of the carbonyl bond length in **17** (C=O, 1.225 and 1.203 Å),^[96] providing further evidence of the successful nucleophilic addition to the ketone. A

consequence of this addition reaction is that it leads to the formation of a chiral centre (C21), although the product obtained is a racemic mixture.

Another common characteristic of the molecular structures of AMMZn intermediates from reactions of **3** is the presence of a terminal *tert*-butyl ligand on the zinc. This is not the case in **18** as the second *tert*-butyl group has been replaced by the Cp' ring which has been deprotonated at the α -position to form a Zn-C_{Cp} sigma bond (Zn1-C9 1.930(3) Å), confirming that the metallation is a direct zincation. This bond is of similar length to the Zn-C_{Cp} bonds of the related zincated ferrocenyl compounds [*C,N*-[Fe(η^5 -C₅H₃-CH₂NMe₂)(η^5 -C₅H₅)]₂Zn] (1.948(2) and 1.945(2) Å),^[97] and [(TMEDA)Zn{(η^5 -C₅H₄)Fe(η^5 -C₅H₅)₂}] (1.9814(11) Å).^[91]

The two-fold reaction of **3** with the substrate leads to the formation of a dianionic ferrocenyl fragment {OC(Ph)(^tBu)(η^5 -C₅H₃)Fe(η^5 -C₅H₅)}²⁻ which binds to the zinc centre in a bidentate fashion, through the oxygen atom of the alkoxide group (which bridges between the two metal centres) and the zincated carbon of the Cp' ring. As a consequence of this rigid bidentate bonding the zinc centre adopts a highly distorted trigonal planar geometry, where the two bonding atoms of the ligand form an acute C9-Zn-O1 bond of 89.03(10)^o which consequently results in a markedly obtuse N1-Zn-C9 angle (166.66(11)^o). Furthermore, the bonding of the metallated fragment gives rise to a five-membered {Zn-O-C(21)-C(10)-C(9)} ring. This ring is fused through C9 and C10 to the Cp' ring, lying almost co-planar (maximum deviation from the mean plane = 0.072 Å for Zn), and through Zn and O to a slightly more distorted four-membered {Zn-O-Na-N1} ring (N-Na-O-Zn torsion angle, 8.49(7)^o).

Thus, the molecular structure of **18** reveals a unique two-fold activation of the ^tBu₂Zn in **3**, where one of the *tert*-butyl groups has selectively α -deprotonated the substituted ferrocenyl ring, whilst the second *tert*-butyl group successfully undergoes a 1,2-addition across the carbonyl group of the substrate. Previously, it has been shown that by reacting the lithium TMP-zincate (**1**) with two equivalents of anisole both *tert*-butyl ligands can be activated towards deprotonation, selectively *ortho* metallating both molecules of the substrate to give [(THF)Li(μ -TMP)Zn(*o*-C₆H₄OMe)₂].^[41] However, **18** constitutes not only the first example where both *tert*-butyl ligands react simultaneously with the same substrate molecule, but also the first example where the *tert*-butyl groups exhibit different forms of reactivity (deprotonation and 1,2-addition).

The ^1H and $^{13}\text{C}\{^1\text{H}\}$ NMR spectra of **18** were recorded in d_6 -benzene solution. The most indicative resonances in the ^1H NMR spectrum (**Figure 2.11**) were three broad singlets at δ 4.70, 4.63 and 4.33 ppm in a ratio of 1:1:1, for the three C-H bonds on the metallated Cp' ring, which differ significantly from the two multiplets present on the Cp' ring of the substrate (δ 4.14 and 4.84 ppm). When the ^1H NMR spectrum is recorded at a higher temperature (343K) these three singlets give a more defined splitting pattern of doublet, triplet and doublet, as would be expected for this substitution pattern. There is also a singlet at δ 1.07 ppm for the *tert*-butyl group which has added across the carbonyl group of the ketone, which differs significantly from previous metallated intermediates involving **3**, where the *tert*-butyl ligand remains terminally bound to zinc (usually found between δ 1.46-1.66 ppm).^[57, 61-63, 65] Furthermore, the TMP ligand which bridges between the two metals in **18** must remain in the same orientation in solution, as shown by the presence of two singlets at δ 1.44 and 1.52 ppm for the inequivalent α -methyl groups of TMP.

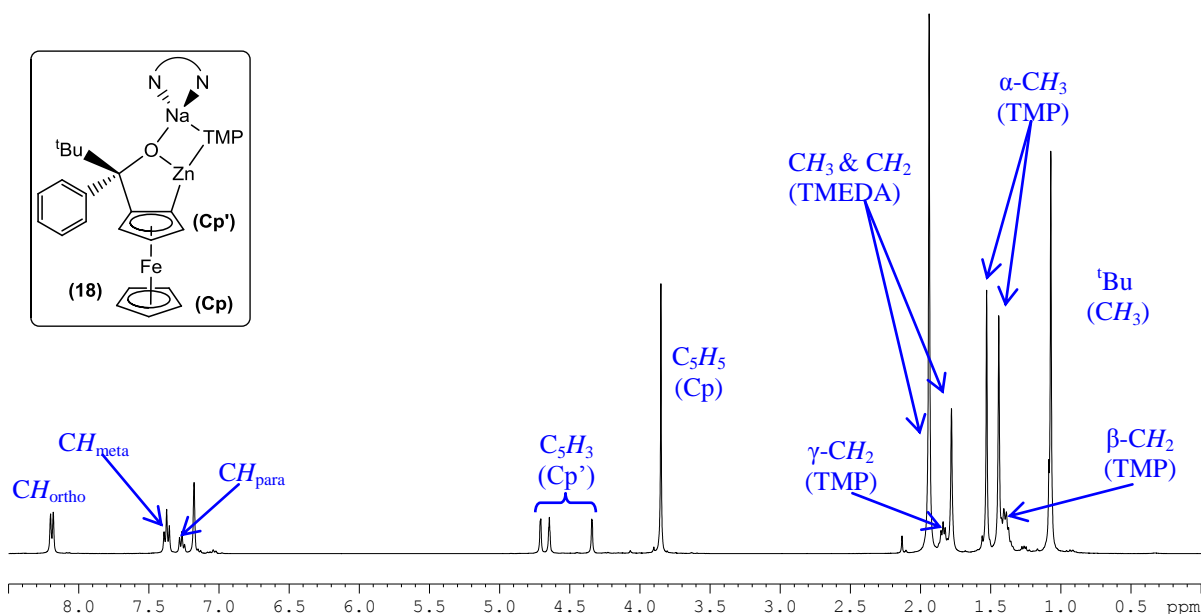
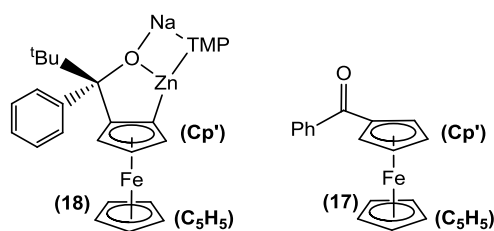


Figure 2.11: ^1H NMR spectrum of **18** in d_6 -benzene.

Further confirmation of the nucleophilic addition of a *tert*-butyl group across the carbonyl group of the substrate was provided by the $^{13}\text{C}\{^1\text{H}\}$ NMR spectrum of **18** in d_6 -benzene, which showed the C-O resonance has moved upfield to δ 81.3 ppm, compared to the C=O group of the substrate which is found at δ 197.4 ppm. Further changes are observed for the zincated Cp' ring, which now has five separate resonances (δ 111.8, 75.3, 73.0, 70.8 and 70.0 ppm) compared to the three resonances of the unreacted substrate (δ 79.2, 72.3 and 71.8

ppm), with the most dramatic effect seen for the zincated carbon, which experiences a large downfield shift from 72.3 ppm in the substrate to 111.8 ppm in **18** (Table 2.3).

Given the low crystalline yield (16%) obtained from the reaction, the filtrate solution was also analysed by ^1H and $^{13}\text{C}\{^1\text{H}\}$ NMR spectroscopy to determine the overall conversion of **17** to **18**. Surprisingly, the spectra showed only traces of **18** to be present, and no unreacted substrate **17**. However, there were a series of broad resonances (δ 6.7-7.5, 5.4-6.0, 4.8-3.7, 3.0-3.6 ppm) which could not be easily assigned, but were shown to couple to one another through COSY NMR. The presence of these resonances along with the lack of unreacted **17** suggested that the major product of this reaction must be something other than the isolated crystalline species **18**. Numerous attempts to isolate and characterise this unknown species were unsuccessful. Therefore, in an attempt to shed some light on the overall outcome of the reaction between **3** and **17** and determine the constitution of this unknown species, electrophilic interception of the organometallic intermediates was performed.

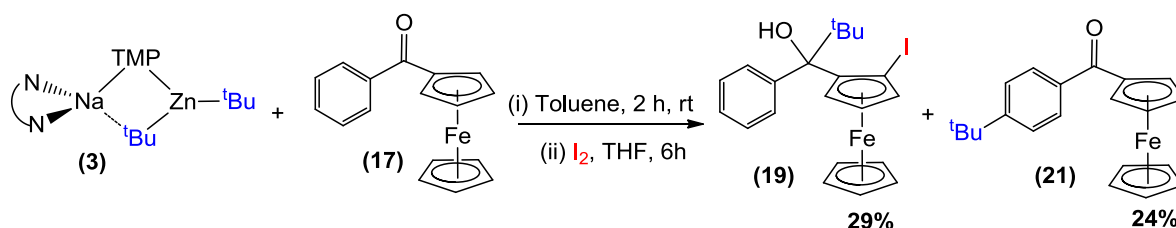


δ (ppm)	^1H (17)	^1H (18)	$^{13}\text{C}\{^1\text{H}\}$ (18)	$^{13}\text{C}\{^1\text{H}\}$ (17)
Ph (C_{ipso})	-	-	154.5	140.5
Ph(CH_{ortho})	7.94	8.19	128.7	131.3
Ph(CH_{meta})	7.12	7.36	126.0	128.5
Ph(CH_{para})	7.18	7.26	124.9	128.3
C-O	-	-	81.3	197.3
Cp'(CH)	4.84, 4.13	4.70, 4.63, 4.33	73.0, 70.8, 70.0	72.3, 71.8
Cp'(C-CO)	-	-	75.3	79.2
Cp' (C-Zn)	-	-	111.8	-
C_5H_5	3.91	3.84	68.0	70.3
TMEDA	-	1.94 (NCH ₃), 1.78 (NCH ₂)	57.5, 46.6	-
TMP	-	1.79 (γ -H), 1.39 (β -H)	53.0 (C_α), 41.2 (C_β), 19.8 (C_γ)	-
α -Me (TMP)	-	1.52, 1.44	36.8, 36.1	-
t Bu	-	1.07	40.5 (CH ₃), 28.2 (C)	-

Table 2.3: ^1H and $^{13}\text{C}\{^1\text{H}\}$ NMR resonances of [(TMEDA)Na(μ -TMP)Zn{OC(Ph)(t Bu)(η^5 - C_5H_3)Fe(η^5 - C_5H_5)}] (**18**) and benzoylferrocene (**17**) in d_6 -benzene solutions.

2.2.2 Electrophilic quenching studies

Initially, electrophilic quenching of the reaction was performed with I_2 , an electrophile which has previously been used for the successful isolation of metallated functionalised-ferrocenyl species, where the metallating agents used were the turbo-Hauser base $[(TMP)MgCl.LiCl]$,^[93] the lithium-cadmiate $[(TMP)_3CdLi]$,^[94-95] and the lithium-zinc mixture $Li(TMP).Zn(TMP)_2$.^[94] Thus, benzoylferrocene (**17**) was treated with one molar equivalent of **3** in toluene at room temperature for 2 hours, followed by subsequent reaction with a THF-solution of iodine. After aqueous work-up, and purification by chromatography the expected ferrocenyl product $[PhC(OH)(^tBu)(\eta^5-C_5H_3I)Fe(\eta^5-C_5H_5)]$ (**19**) and the *tert*-butylated 1,6-adduct $[4-^tBu-C_6H_4C(=O)(\eta^5-C_5H_4)Fe(\eta^5-C_5H_5)]$ (**21**) were obtained in isolated yields of 29% and 24% respectively (**Scheme 2.11**). The constitution of **19** and **21** were determined by X-ray crystallography (**Figures 2.12** and **2.13** respectively), as well as 1H and $^{13}C\{^1H\}$ NMR spectroscopy, elemental analysis and GC-MS (see **Chapter 7.3.5** for details).



Scheme 2.11: Electrophilic quenching of the reaction of **3** and **17** with I_2 to yield $[PhC(OH)(^tBu)(\eta^5-C_5H_3I)Fe(\eta^5-C_5H_5)]$ (**19**) and $[4-^tBu-C_6H_4C(=O)(\eta^5-C_5H_4)Fe(\eta^5-C_5H_5)]$ (**21**).

Disubstituted-ferrocenyl species **19** is the expected product from I_2 interception of the organometallic intermediate **18**, where the position previously occupied by Zn on the Cp' ring of **18** is now occupied by an iodine atom and the alkoxide group has been hydrolysed to form a tertiary alcohol. X-ray crystallographic analysis revealed that a mixture of **19** and the di-iodinated analogue $[PhC(OH)(^tBu)(\eta^5-C_5H_3I)Fe(\eta^5-C_5H_4I)]$ (**20**) in a respective ratio 95:5 was found in the crystal lattice. The formation of **20** could be attributed to a double zincation of benzoylferrocene by **3**. However, when the same reaction was quenched with D_2O (vide infra) there is no indication of the presence of a related doubly deuterated species. Furthermore, given the yield of **20** is extremely small it seems more plausible that the formation of this di-iodinated species is as a result of a side reaction of iodine (used in excess) with the mono-iodinated species **19**. Similar selectivity problems when using I_2 as a

quenching agent for organometallic intermediates which lead to polysubstituted products has previously been reported in the literature.^[98]

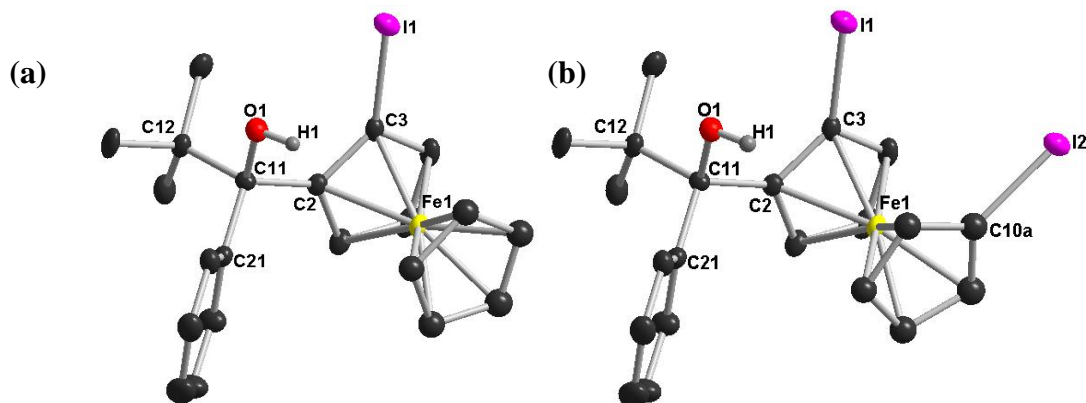


Figure 2.12: Molecular structures of (a) $[\text{PhC}(\text{OH})(t\text{Bu})(\eta^5\text{-C}_5\text{H}_3\text{I})\text{Fe}(\eta^5\text{-C}_5\text{H}_5)]$ (**19**) and (b) $[\text{PhC}(\text{OH})(t\text{Bu})(\eta^5\text{-C}_5\text{H}_3\text{I})\text{Fe}(\eta^5\text{-C}_5\text{H}_4\text{I})]$ (**20**) (present as a mixture in the crystalline lattice in a ratio of 95:5) with 50% probability ellipsoids. Hydrogen atoms (apart from -OH group) have been omitted for clarity. *Selected bond lengths (Å) and angles (°):* $C(11)\text{-}O(1)$ 1.436(5), $C(11)\text{-}C(2)$ 1.535(5), $C(11)\text{-}C(21)$ 1.549(5), $C(11)\text{-}C(12)$ 1.574(6), $I(1)\text{-}C(3)$ 2.099(4), $C(10A)\text{-}I(2)$ 2.084(9), $O(1)\text{-}C(11)\text{-}C(2)$ 107.9(3), $O(1)\text{-}C(11)\text{-}C(21)$ 108.4(3), $C(2)\text{-}C(11)\text{-}C(21)$ 113.0(3), $O(1)\text{-}C(11)\text{-}C(12)$ 104.2(3), $C(21)\text{-}C(11)\text{-}C(12)$ 111.3(3), $C(2)\text{-}C(11)\text{-}C(12)$ 111.5(3), $C(1)\text{-}C(2)\text{-}C(3)\text{-}I(1)$ 176.5(3), $C(7A)\text{-}C(6A)\text{-}C(10A)\text{-}I(2)$ 174(7).

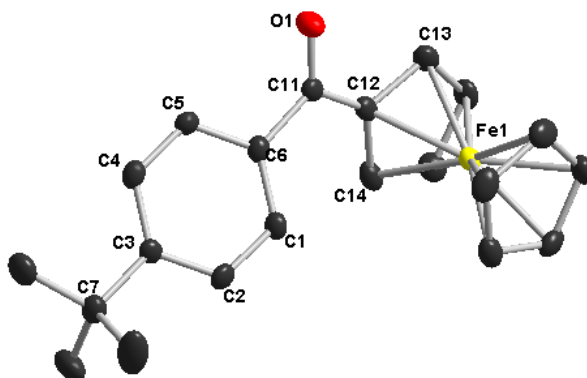
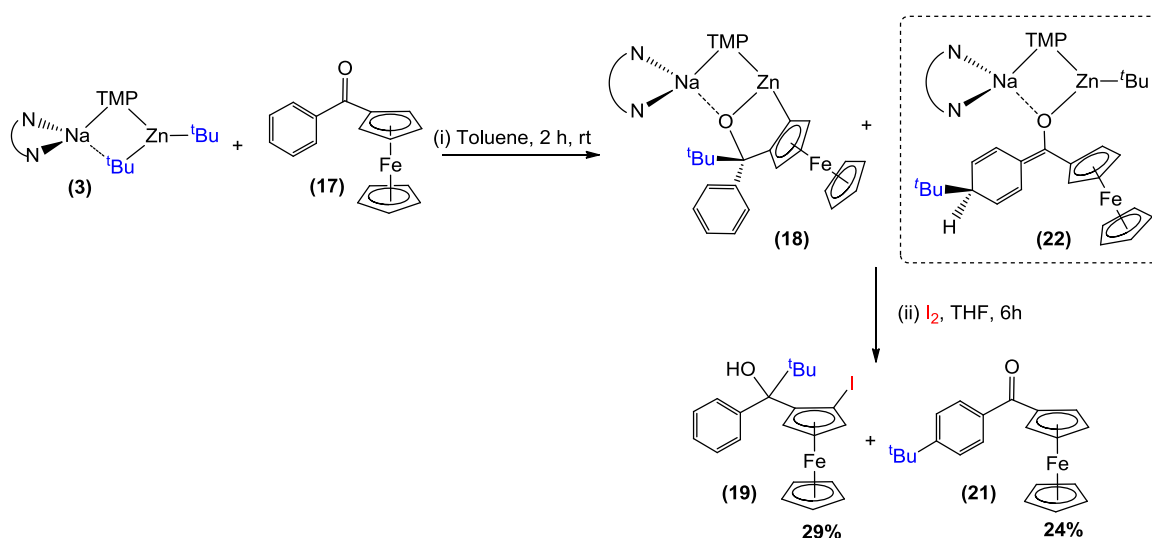


Figure 2.13: Molecular structures of $[4\text{-}t\text{Bu}\text{-C}_6\text{H}_4\text{C}(=\text{O})(\eta^5\text{-C}_5\text{H}_4)\text{Fe}(\eta^5\text{-C}_5\text{H}_5)]$ (**21**) with 50% probability ellipsoids. Hydrogen atoms have been omitted for clarity. *Selected bond lengths (Å) and angles (°):* $O(1)\text{-}C(11)$ 1.226(4), $C(3)\text{-}C(7)$ 1.540(5), $C(11)\text{-}C(12)$ 1.482(5), $C(6)\text{-}C(11)$ 1.504(5), $C(4)\text{-}C(3)\text{-}C(2)$ 117.9(3), $C(4)\text{-}C(3)\text{-}C(7)$ 122.7(3), $C(2)\text{-}C(3)\text{-}C(7)$ 119.4(3), $C(1)\text{-}C(6)\text{-}C(5)$ 119.2(3), $C(1)\text{-}C(6)\text{-}C(11)$ 124.4(3), $C(5)\text{-}C(6)\text{-}C(11)$ 116.3(3), $O(1)\text{-}C(11)\text{-}C(12)$ 119.3(3), $O(1)\text{-}C(11)\text{-}C(6)$ 120.6(3), $C(12)\text{-}C(11)\text{-}C(6)$ 120.0(3), $C(7)\text{-}C(3)\text{-}C(4)\text{-}C(5)$ 178.7(3), $C(2)\text{-}C(1)\text{-}C(6)\text{-}C(11)$ 178.1(3).

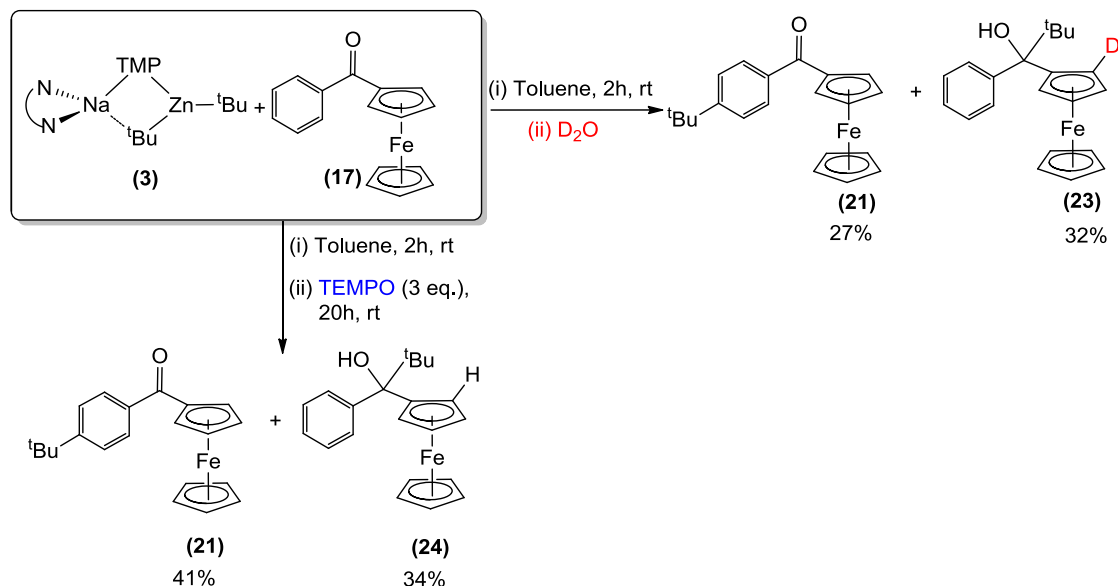
Interestingly, unlike in the previous reactions between **3** and aromatic ketones where only 1,6-addition was reported, the reaction of **3** and **17** after electrophilic quenching yields both the α -metallation/1,2-addition and the 1,6-addition products, **19** and **21**. The isolation of $[\text{4-}^t\text{Bu-C}_6\text{H}_4\text{C(=O)}(\eta^5\text{-C}_5\text{H}_4)\text{Fe}(\eta^5\text{-C}_5\text{H}_5)]$ (**21**), formed by the nucleophilic 1,6-addition of a *tert*-butyl group to **17**, confirms that the reaction between **3** and **17** prior to electrophilic quenching must yield two different organometallic intermediates. Based on the isolation of this 1,6-adduct and the previously isolated organometallic intermediates of nucleophilic 1,6-addition of aromatic ketones by **3**,^[89-90] a possible organometallic intermediate of constitution $[(\text{TMEDA})\text{Na}(\text{TMP})\{\mu\text{-OC(4-}^t\text{Bu-C}_6\text{H}_5\text{)(Fc)}\}\text{Zn}^t\text{Bu}]$ (**22**), formed by *tert*-butylation of **17** at the *para*-position, could be the precursor to the final isolated product **21** (Scheme 2.12). This intermediate may also account for the series of broad resonances observed in the ¹H NMR spectrum of the filtrate solution of the reaction. Following electrophilic quenching and aqueous work-up **22** would be expected to yield a conjugated enol species, which would then undergo spontaneous aerobic oxidation, with loss of H₂, to form the final product **21**.^[99]



Scheme 2.12: Proposed intermediate species (**18** and **22**) from the reaction of **3** and **17**, which after electrophilic quenching with I₂ and aqueous work-up yield **19** and **21**.

The isolation of **19** and **21** (isolated yields of 29% and 24% respectively) as the only major products from this reaction after electrophilic quenching with I₂ confirms that organometallic species **18** and **22** are the two intermediates formed from the initial reaction between **3** and **17**. Surprisingly, a large amount of unreacted benzoylferrocene was recovered after purification of the crude reaction mixture which, coupled with the relatively modest yields obtained for **19** and **21**, is somewhat surprising considering that ¹H NMR analysis of the reaction prior to the I₂ quenching step showed no unreacted benzoylferrocene present in solution. Intrigued by

these results we decided to investigate the quenching of this reaction with other electrophiles. Initially D₂O was employed in order to determine the overall formation of α -metallation/1,2-addition species, which led to the isolation of [C₆H₅C(OH)^tBu(η^5 -C₅H₃D)Fe(η^5 -C₅H₅)] (**23**) in a marginally improved yield of 32%. Under these quenching conditions [4-^tBu-C₆H₄C(=O)(η^5 -C₅H₄)Fe(η^5 -C₅H₅)] (**21**) was also obtained in a slightly higher yield of 27% (**Scheme 2.13**), along with the recovery of the unreacted substrate **17** in a 25% yield.



Scheme 2.13: Electrophilic quenching of the reaction between **3** and **17** with D₂O and oxidative work-up with TEMPO.

Previous studies on the ring alkylation of benzophenone with ^tBuLi have revealed that aqueous workups can lead to the decomposition of the 1,6-addition intermediate to regenerate benzophenone, but if a strong oxidising agent such as SOCl₂ is used it is possible to minimise this degradation route and significantly increase the yield of *tert*-butylbenzophenone.^[99a, 100] As a similar decomposition process could be taking place in the 1,6-alkylation of benzoylferrocene by **3**, SOCl₂ was employed in an attempt to isolate the 1,6-adduct in a higher yield, but this an oxidative work-up still lead to a large amount of unreacted substrate being recovered. However, turning to the radical oxidant TEMPO [(2,2,6,6-tetramethylpiperidin-1-yl)oxyl]^[101] followed by aqueous work-up, [4-^tBu-C₆H₄C(=O)(η^5 -C₅H₄)Fe(η^5 -C₅H₅)] (**21**) could be isolated in a yield of 41%, along with the 1,2-adduct [C₆H₅C(OH)^tBu(η^5 -C₅H₄)Fe(η^5 -C₅H₅)] (**24**) in a 34% yield (**Scheme 2.13**). In this case only 7% of unreacted substrate was recovered, which suggests that although this is the most

successful oxidative work-up discovered to date, the total conversion of **17** to the 1,6-addition product **21** could potentially be even greater than 41%.

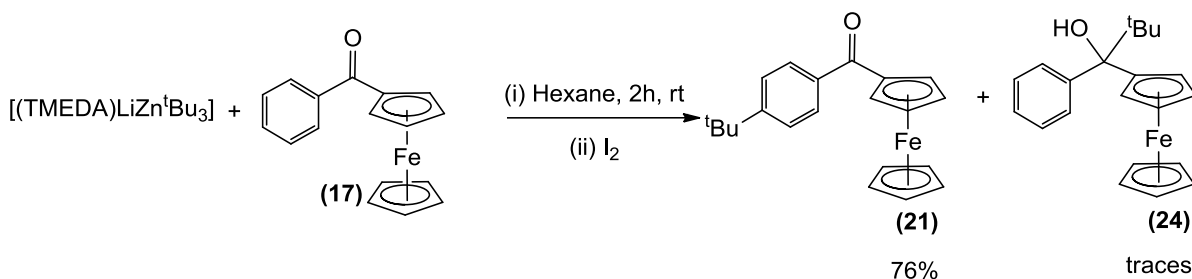
The results of these quenching reactions provide a very useful insight into the reaction of **3** with **17**. The isolation of the **21** confirms that the second major species formed prior to electrophilic quenching is the 1,6-adduct [(TMEDA)Na(TMP){ μ -OC(4-^tBu-C₆H₅)(Fc)}Zn^tBu] (**22**). Thus, although isolation and characterisation of the organometallic intermediates yields only the 1,2-addition/deprotonation species [(TMEDA)Na(μ -TMP)Zn{OC(Ph)(^tBu)(η^5 -C₅H₃)Fe(η^5 -C₅H₅)}] (**18**), this is not the major product of the reaction. Different electrophilic quenches (I₂, D₂O, TEMPO/H₂O) allow the expected product of α -metallation/1,2-addition [C₆H₅C(OH)^tBu(η^5 -C₅H₃X)Fe(η^5 -C₅H₅)] (X = I, **19**; D, **23**; H, **24**) to be isolated in yields ranging from only 29-34%, which would suggest that during the reaction with **3** only around one third of the benzoylferrocene undergoes simultaneous deprotonation and 1,2-addition. Thus, it would appear that the reaction in fact favours a nucleophilic 1,6-addition, as has been previously reported for related aromatic ketones, with the major species obtained when a suitable oxidative work-up is employed being [4-^tBu-C₆H₄C(=O)(η^5 -C₅H₄)Fe(η^5 -C₅H₅)] (**21**) in a 41% yield. This yield may be even higher, as some unreacted benzoylferrocene is still recovered from the reaction, which is most likely formed by decomposition of the organometallic 1,6-adduct during aqueous work-up, as NMR analysis of the reaction prior to quenching shows there to be no unreacted substrate present.

2.2.3 Further investigation into the two-fold activation of Zn^tBu₂ in **3**

Returning our attention to the surprising two-fold activation of Zn^tBu₂ in **3** towards benzoylferrocene (**17**) we decided to investigate this unusual dual reactivity more closely. From the electrophilic quenches of the reaction discussed above we found that there were no isolated products obtained from the reaction whereby only 1,2-addition or metallation of the Cp' ring had occurred. Furthermore, when the reaction is performed at lower temperatures, although the yields of the products decrease, 1,2-addition or α -metallation cannot be obtained selectively. This would suggest that the initial metallation of the Cp' ring by **3** must bring the second *tert*-butyl into close proximity to the carbonyl group, and therefore induce simultaneous 1,2-addition. To confirm this, the reaction of **17** with the heteroleptic zincate [(TMEDA)LiZn^tBu₃], prepared by co-complexation of ^tBuLi and Zn^tBu₂ in the presence of TMEDA, was investigated. Previously it has been shown that heteroleptic trialkylzincates are

poor bases in terms of metallating activity, but they exhibit an enhanced reactivity in nucleophilic addition^[32-33] and metal-halogen exchange.^[24b-d, 38] Thus, the reaction of [(TMEDA)LiZn^tBu₃] with **17** will inhibit metallation of the Cp' ring of the substrate and therefore prevent the subsequent 1,2-addition.

To a suspension of [(TMEDA)LiZn^tBu₃] was added one equivalent of **17**, and the reaction stirred at room temperature for 1 hour. Unfortunately it was not possible to obtain suitable crystalline material from the reaction for X-ray crystallographic analysis, and NMR spectroscopy was inconclusive as to the reactivity of this zincate towards **17**, due to the broadness of the resonances observed. Therefore, the reaction was quenched with I₂, and [4-^tBu-C₆H₄C(=O)(η⁵-C₅H₄)Fe(η⁵-C₅H₅)] (**21**) was obtained in an isolated yield of 76% (**Scheme 2.14**), as confirmed by ¹H and ¹³C{¹H} NMR spectroscopy. Furthermore, the reaction yielded only trace amount of the expected product from 1,2-addition [C₆H₅C(OH)^tBu(η⁵-C₅H₄)Fe(η⁵-C₅H₅)] (**24**), and the expected product from α-metallation/1,2-addition [C₆H₅C(OH)^tBu(η⁵-C₅H₃I)Fe(η⁵-C₅H₅)] (**19**) could not be detected at all. Highlighting the important role of lithium in these bimetallic reagents the reaction of **17** with Zn^tBu₂ was also performed, showing that the homometallic species displayed no reactivity (metallation or addition) towards the substrate.



Scheme 2.14: Reaction of [(TMEDA)LiZn^tBu₃] with **17**, followed by electrophilic quenching with I₂ to form **21**.

This series of reactions demonstrates the great difference in reactivity of dialkylamido zincates such as [(TMEDA)Na(TMP)Zn^tBu₂] (**3**) and heteroleptic trialkylzincates such as [(TMEDA)LiZn^tBu₃], whereby the presence of the amido group in **3** promotes some metallation of the Cp' ring, inducing simultaneous 1,2-addition to the carbonyl group, most likely driven by the proximity of the electrophilic C=O group of the ketone and the *tert*-butyl group still bound to zinc. However, this reactivity only accounts for around one third of the substrate, with the remainder reacting via 1,6-addition. Using [(TMEDA)LiZn^tBu₃] it is not

possible to perform deprotonative metallation reactions due to kinetic stability of the Zn-C bonds (compared to the Zn-N bond in **3**). Therefore a significant decrease in 1,2-addition to **17** occurs (only trace amounts), and the zincate performs selective 1,6-addition to benzoylferrocene. Furthermore, we see in this case that oxidation of the organometallic 1,6-adduct with I₂ occurs without substantial decomposition of the intermediate back to starting material. This contrasts significantly with the reaction of **3** and **17**, where the radical oxidant TEMPO was required to successfully prepare the final 1,6-addition product **21**.

2.2.4 Conclusions

From these results it has been determined that sodium zincate **3** can react with benzoylferrocene (**17**) via two distinct reaction pathways; (i) direct α -zincation of the functionalised Cp ring (Cp') of the substrate, with loss of one *tert*-butyl group from the zincate, followed by simultaneous 1,2-addition of the second *tert*-butyl group of **3** across the C=O group of the substrate, and (ii) nucleophilic 1,6-addition of one *tert*-butyl group of **3** to the aromatic ring of the substrate (see **Scheme 2.12**).

Isolation and characterisation of the organometallic intermediates from the reaction of **3** and **17** yielded [(TMEDA)Na(μ -TMP)Zn{OC(Ph)(^tBu)(η^5 -C₅H₃)Fe(η^5 -C₅H₅)}] (**18**), formed as a result of the unprecedented two-fold activation of Zn^tBu₂, where not only is each of the *tert*-butyl groups of **3** activated towards the same substrate, but they each react in a different way (deprotonation and nucleophilic addition). However, NMR spectroscopic analysis of the organometallic intermediates formed during the reaction suggested that this dual α -metallation/1,2-addition product **18** was not the major species. Subsequent electrophilic quenches with I₂, D₂O and H₂O, yielded the expected products [C₆H₅C(OH)^tBu(η^5 -C₅H₃X)Fe(η^5 -C₅H₅)] (X = I, **19**; D, **23**; H, **24**) (see **Scheme 2.12** and **2.13**) in yields of 29-34%, which established that only around one third of the α -metallation/1,2-addition product was formed. A second organic product was also isolated [4-^tBu-C₆H₄C(=O)(η^5 -C₅H₄)Fe(η^5 -C₅H₅)] (**21**), which after finding a suitable oxidative work-up could be obtained in an isolated yield of 41% (see **Scheme 2.13**). Based on these results, and previous work involving nucleophilic 1,6-addition of other aromatic ketones with **3**,^[89-90] it can be concluded that the major organometallic species formed during the reaction of **3** and **17** is [(TMEDA)Na(TMP){ μ -OC(4-^tBu-C₆H₅)(Fc)}Zn^tBu] (**22**) formed via nucleophilic 1,6-

addition of the substrate. Therefore, although **3** can react with **17** via two separate pathways, it is the remote 1,6-addition process which is the favoured route.

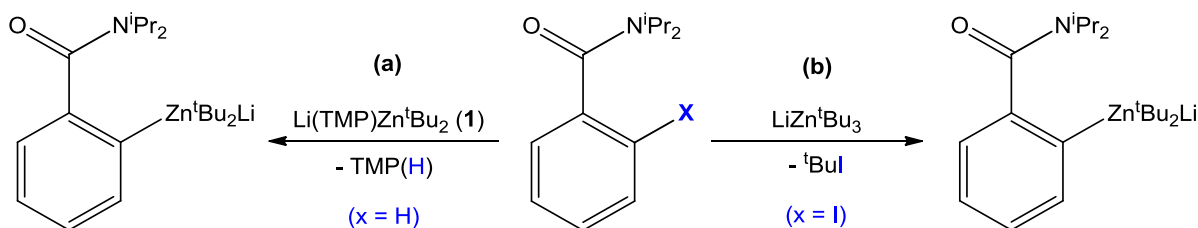
2.3 Summary

In the course of this chapter two new applications of the alkali metal TMP-zincates [(THF)Li(TMP)Zn^tBu₂] (**1**) and [(TMEDA)Na(TMP)Zn^tBu₂] (**3**) have been reported, displaying new reactivity patterns for these mixed-metal reagents. Both of these zincates have demonstrated the ability to perform the first ever examples of direct lateral zincation (DI Zn), where reaction with the aromatic substrate trimethyl(phenoxy)silane (**12**) at ambient temperatures, yielded the first phenyl containing α -metallated silane species [(THF)Li(TMP){PhOSi(CH₃)₂CH₂}Zn^tBu] (**13**) and [(TMEDA)Na(TMP){PhOSi(CH₃)₂CH₂}Zn^tBu] (**14**). This high level of reactivity and selectivity towards this aromatic substrate cannot be replicated by the constituent homometallic species, where a lack of reactivity is seen for Zn^tBu₂ and organolithium reagents suffer from competing nucleophilic substitution at the O-Si bond even at reduced temperatures, showcasing the advantages of this mixed-metal approach.

Turning to the functionalised metallocene, benzoylferrocene (**17**), it has been shown that reaction with the sodium zincate (**3**) leads to the isolation of the organometallic intermediate [(TMEDA)Na(μ -TMP)Zn{OC(Ph)(^tBu)(η^5 -C₅H₃)Fe(η^5 -C₅H₅)}] (**18**). This species is formed through the unprecedented two-fold activation of Zn^tBu₂ in **3** where one of the *tert*-butyl groups has performed the α -metallation of the functionalised Cp' ring, bringing the second *tert*-butyl group into position to perform a simultaneous nucleophilic 1,2-addition to the carbonyl group of the substrate. However, subsequent electrophilic quenching (with I₂, D₂O and H₂O) of this organometallic intermediate gave the expected products in yields ranging from only 29-34%. Under suitable oxidative work-up (with TEMPO) the major product of the reaction [4-^tBu-C₆H₄C(=O)(η^5 -C₅H₄)Fe(η^5 -C₅H₅)] (**21**) formed via a nucleophilic 1,6-addition was isolated in a 41% yield. Using the heteroleptic trialkylzincate [(TMEDA)LiZn^tBu₃], the absence of an amido ligand allows the selectivity of this reaction to be tuned towards solely the 1,6-addition product, highlighting the important role of the TMP ligand in the mixed metal bases **1** and **3** to promote metallation, and further emphasising the complexity of reactions involving alkali metal zincates.

Chapter 3: Closer insight into the mechanisms of AMMZn of anisole by TMP-dialkyl zincates

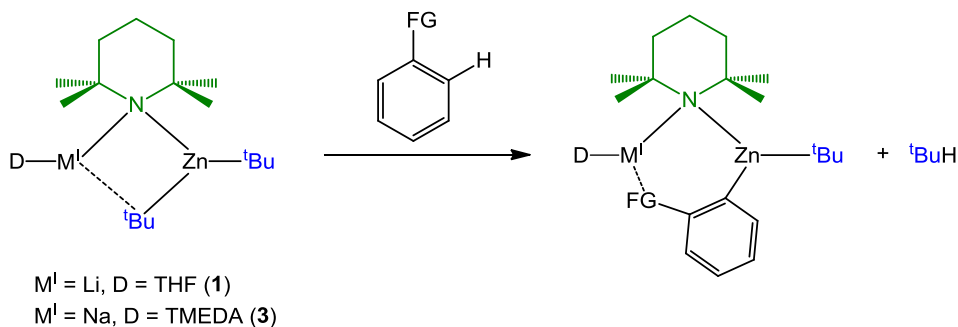
Taking into account the heteroleptic nature of alkali metal TMP-zincates such as $[(\text{THF})\text{Li}(\text{TMP})\text{Zn}^t\text{Bu}_2]$ (**1**) and $[(\text{TMEDA})\text{Na}(\text{TMP})\text{Zn}^t\text{Bu}_2]$ (**3**), different mechanistic hypotheses for their unique reactivity have been proposed in the literature. The mixture of *tert*-butyl and TMP ligands within the zincate means that theoretically the zincate could either be acting as an alkyl base or as an amido base.^[57] When the use of lithium TMP-zincate **1** as a reagent for performing DoM was first reported in 1999 it was proposed that it had reacted as an amido base, with the TMP ligand providing the source of basicity, generating an aryl zincate intermediate $[(\text{Ar})\text{Zn}^t\text{Bu}_2\text{Li}]$ and $\text{TMP}(\text{H})$. Although there was no tangible structural evidence to support this proposal, $^{13}\text{C}\{^1\text{H}\}$ NMR analysis of the metallated intermediates from the reaction between *N,N*-diisopropylbenzamide and **1** (**Scheme 3.1(a)**), and 2-iodo-*N,N*-diisopropylbenzamide with the heteroleptic zincate $[\text{LiZn}^t\text{Bu}_3]$ (**Scheme 3.1(b)**), indicated that the same arylzincate intermediates were formed, which would point towards zincate (**1**) retaining both of its *tert*-butyl groups following deprotonation of the aromatic substrate.^[47]



Scheme 3.1: Comparison of the metallated intermediates proposed on the basis of $^{13}\text{C}\{^1\text{H}\}$ NMR data for (a) the deprotonative metallation of *N,N*-diisopropylbenzamide with **1**, and (b) the Zn-I exchange reaction of 2-iodo-*N,N*-diisopropylbenzamide and LiZn^tBu_3 .

Since these initial findings, numerous metallated intermediates from the deprotonation of aromatic substrates by **1** and **3** have been isolated and structurally characterised (see **Chapters 1** and **2**), and in almost every example reported to date these species have retained the same $\text{M}^1\text{-TMP-Zn}$ backbone as is observed in the molecular structure of the bases (**Scheme 3.2**). However, it must be taken into consideration that although these structural and reactivity studies provide evidence of the constitution of the starting materials and final

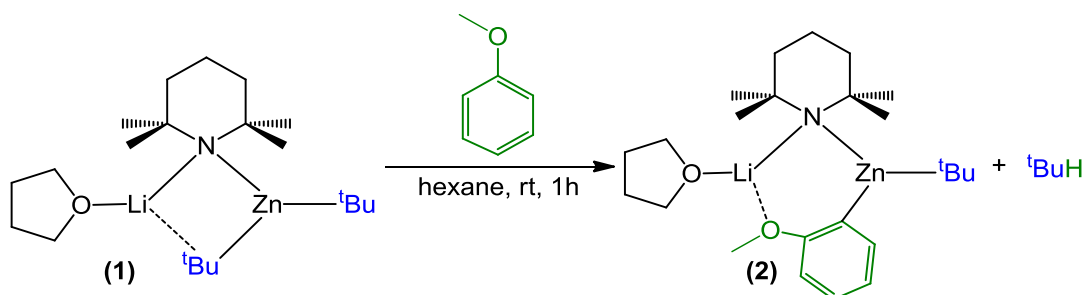
metallated products, any possible organometallic intermediates involved in these reactions could remain invisible to these studies. Thus, these apparently divergent proposals have led to further debate over the mechanism of deprotonative metallations of aromatic substrates using alkali metal TMP-zincates, involving both theoretical and experimental studies.



Scheme 3.2: General scheme for the deprotonative metallation of aromatic substrates by alkali metal zincates **1** and **3**.

3.1 Theoretical studies on DoM of anisole using lithium TMP-zincates

As mentioned in **Chapter 1** the metallated intermediate from the reaction between **1** and anisole was successfully isolated and characterised by Mulvey and co-workers in 2006, revealing the formation of the CIP species $[(\text{THF})\text{Li}(\text{TMP})(o\text{-C}_6\text{H}_4\text{OMe})\text{Zn}^t\text{Bu}]$ (**2**) which retained the Li-TMP-Zn backbone of the mixed-metal base **1**, suggesting that the zincate had behaved as an overall alkyl base, with the generation of isobutane (^tBuH) (**Scheme 3.3**).^[41] Contrasting with previous studies,^[47] these results pointed towards a preferred alkyl basicity for this bimetallic system. Initially the apparent difference in the reactivity of **1** was attributed to the different solvent employed in the reactions, with a polar solvent such as THF favouring amido basicity, and a non-polar solvent such as hexane favouring alkyl basicity.^[41]



Scheme 3.3: Reaction of $[(\text{THF})\text{Li}(\text{TMP})\text{Zn}^t\text{Bu}_2]$ (**1**) with anisole to form $[(\text{THF})\text{Li}(\text{TMP})(o\text{-C}_6\text{H}_4\text{OMe})\text{Zn}^t\text{Bu}]$ (**2**).

In the same year that the molecular structure of **2** was reported, Uchiyama and co-workers published a theoretical study of the different reaction pathways of lithium TMP-zincate [(THF)Li(TMP)Zn^tBu₂] (**1**) with anisole.^[102] For these DFT calculations simplified structural models of the lithium zincate were used, with [(Me₂O)Li(NMe₂)ZnMe₂] employed as the a model for [(THF)Li(TMP)Zn^tBu₂] (**1**), where the ^tBu groups and THF were replaced by Me and Me₂O respectively, and NMe₂ was used instead of TMP (**Figure 3.1**). Although the authors justify these simplifications on the basis of the computational cost of their study, they must be taken into account when comparing the structures of the transition states involved in the study since they significantly minimize the steric interactions of these bimetallic systems.

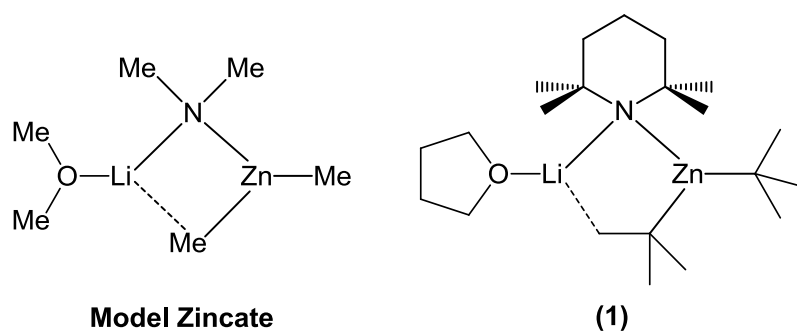
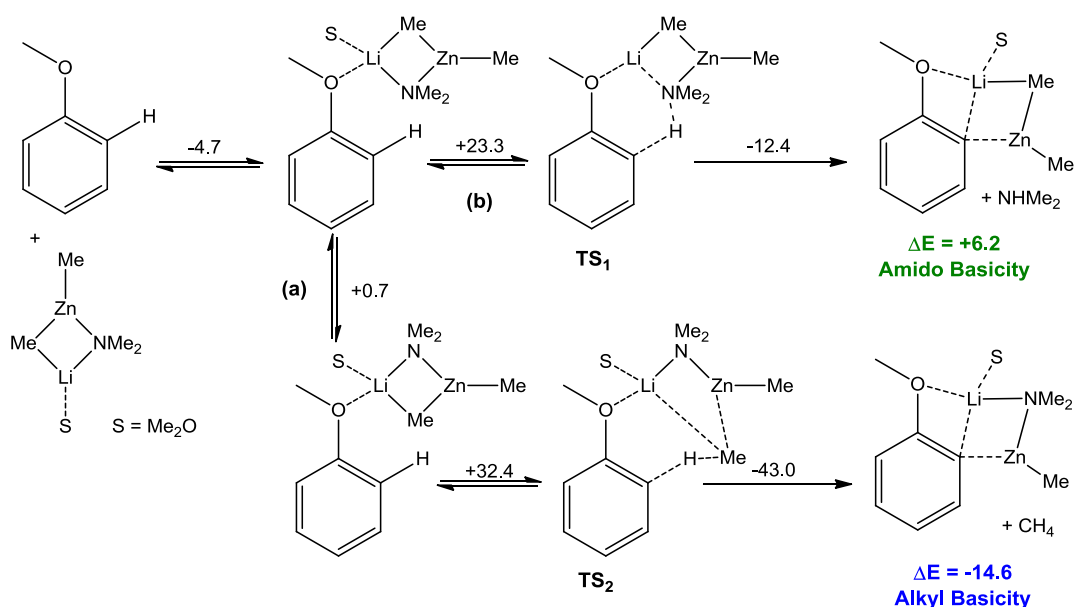


Figure 3.1: Comparison of model zincate, used for the DFT calculations, with zincate **1**.

In these theoretical studies, the activation energies of the proposed transition states were calculated for two possible pathways; where the model zincate acted as an alkyl base (**Scheme 3.4(a)**), and where it acted as an amido base (**Scheme 3.4(b)**). As can be seen from these results there is a thermodynamic preference for the bimetallic reagent to act as an alkyl base, with the reaction being overall exothermic ($\Delta E = -14.6 \text{ kcal mol}^{-1}$) compared to an endothermic reaction when the zincate acts as an amido base ($\Delta E = +6.2 \text{ kcal mol}^{-1}$). However, for the alkyl basicity pathway the most likely transition state had an overall activation energy (ΔE_a) of $+28.4 \text{ kcal mol}^{-1}$, which was significantly higher than that calculated when the zincate acts as an amido base ($\Delta E_a = +18.6 \text{ kcal mol}^{-1}$) (**Figure 3.2**). This would suggest that although there is a thermodynamic preference for alkyl basicity, the alternative pathway where the zincate acts as an amido base is kinetically favoured. Thus, these theoretical studies seemed to disagree with the experimental findings reported Mulvey.^[41]



Scheme 3.4: Proposed reaction pathways for the DoM of anisole with $[(\text{Me}_2\text{O})\text{Li}(\text{NMe}_2)\text{ZnMe}_2]$ where the zincate acts (a) as an alkyl base, and (b) as an amido base (energy values shown are in kcal mol^{-1}).

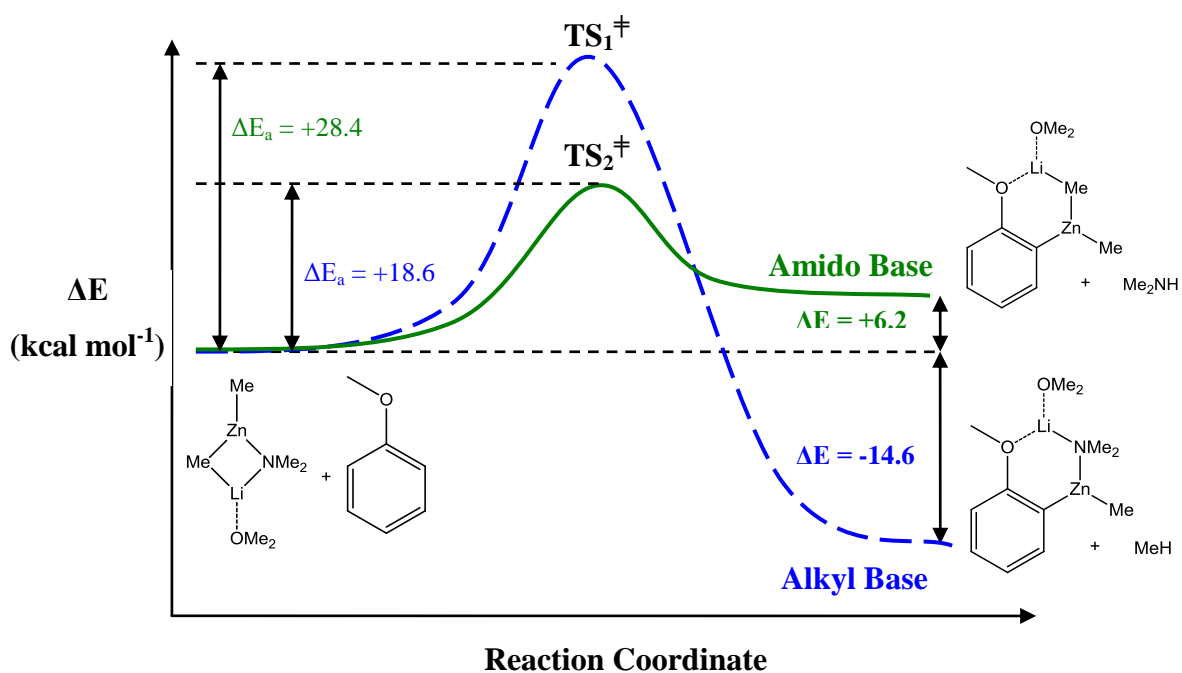
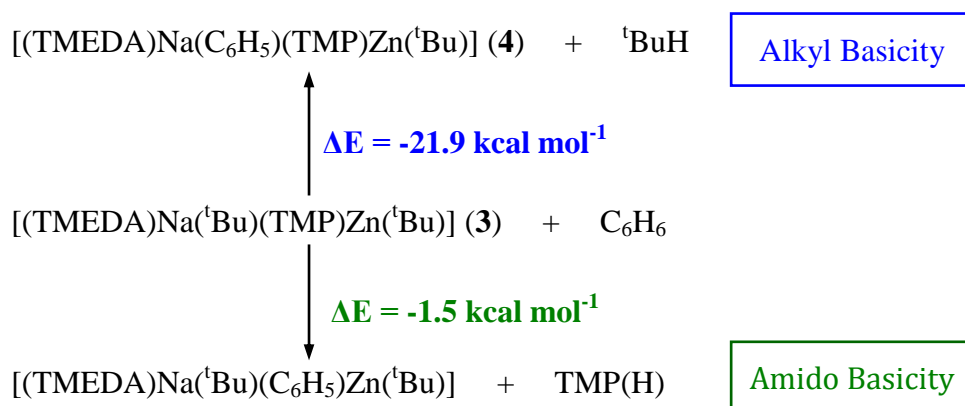


Figure 3.2: Energy profile for the reaction of $[(\text{Me}_2\text{O})\text{Li}(\text{NMe}_2)\text{ZnMe}_2]$ with anisole.

3.2 Theoretical studies on metallation of benzene using sodium TMP-zincates

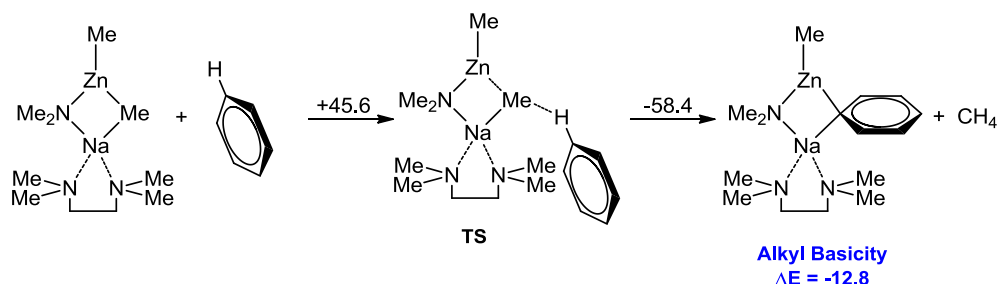
Turning to sodium TMP-zincate [(TMEDA)Na(TMP)Zn^tBu₂] (**3**), as was shown in **Chapter 1** this base can react with benzene to yield the metallated intermediate [(TMEDA)Na(TMP)(C₆H₅)Zn^tBu] (**4**), showing an overall alkyl basicity for **3**. The thermodynamic preference for this alkyl behaviour was supported by DFT calculations which showed when the zincate acts as an alkyl base the process is exothermic by -21.9 kcal mol⁻¹, and if it acts as an amido base the process would also be exothermic, but only by -1.5 kcal mol⁻¹ (**Scheme 3.5**).^[57]



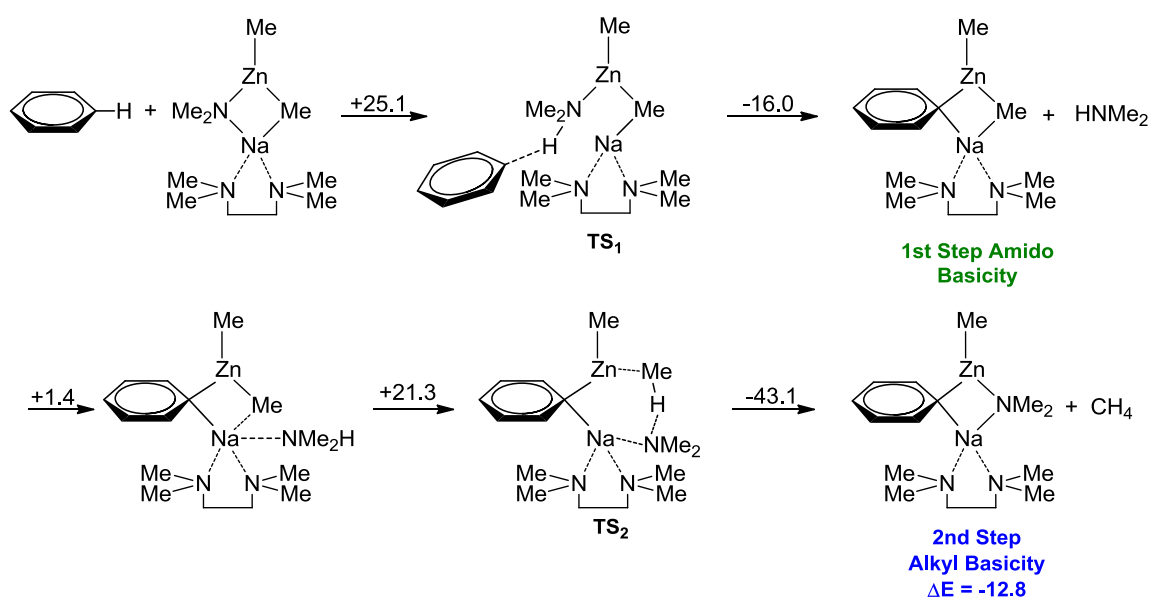
Scheme 3.5: Results of DFT calculations for the reaction of [(TMEDA)Na(TMP)Zn^tBu₂] with benzene.

A more comprehensive theoretical study was reported by Uchiyama on the same reaction where a simplified structural model of the zincate **3** was employed, [(TMEDA)Na(NMe₂)ZnMe₂].^[103] Similar to the calculation performed for the AMMZn of anisole, the activation energies of the proposed transition states were calculated for two possible reaction pathways; (i) where the model zincate acted as an alkyl base (**Scheme 3.6(a)**), and (ii) where it acted as an amido base (**Scheme 3.6(b)**). In this case the authors also observed a kinetic preference for amido basicity over alkyl basicity ($\Delta E_a = +25.1$ kcal mol⁻¹ vs. $\Delta E_a = +45.6$ kcal mol⁻¹). In order to account for the overall alkyl basicity shown by experimental studies, the authors proposed a two-step mechanism where the zincate first acted as an amido base towards benzene, forming Me₂NH and [(TMEDA)Na(C₆H₅)ZnMe₂]. The zincate could then act as an alkyl base, with one of the remaining methyl groups reacting with the previously formed amine (Me₂NH) to generate methane (MeH) and

$[(\text{TMEDA})\text{Na}(\text{NMe}_2)(\text{C}_6\text{H}_5)\text{ZnMe}]$, which is similar to the isolated intermediates previously structurally characterised (**Scheme 3.6(b)**).



Scheme 3.6(a): Proposed mechanisms for the reaction of $[(\text{TMEDA})\text{Na}(\text{NMe}_2)\text{ZnMe}_2]$ with benzene, with zincate acting as an alkyl base (energy changes shown in kcal mol^{-1}).



Scheme 3.6(b): Proposed two-step mechanism for the reaction of $[(\text{TMEDA})\text{Na}(\text{NMe}_2)\text{ZnMe}_2]$ with benzene, showing initial amido basicity, followed by alkyl basicity (energy changes shown in kcal mol^{-1}).

In the case of the one step reaction, with the zincate acting as an alkyl base, the reaction proceeded through a single transition state with an activation energy of $+44.8 \text{ kcal mol}^{-1}$, and the overall process being exothermic ($\Delta E = -12.8 \text{ kcal mol}^{-1}$). In the two-step mechanism, the reaction proceeded through two transition states, each of which had a lower activation energy ($\Delta E_a = +25.1$ and $+21.3 \text{ kcal mol}^{-1}$) than that of the one step alkyl basicity reaction ($\Delta E_a = +45.6 \text{ kcal mol}^{-1}$), and involved the formation of the intermediate dialkylzincate species $[(\text{TMEDA})\text{Na}(\text{C}_6\text{H}_5)\text{ZnMe}_2]$ (**Figure 3.3**). The lower activation energies of this process, compared to the one step mechanism, would suggest that it was kinetically more favourable

for the zincate to act initially as an amido base, and then act as an alkyl base to form the final metallated product [(TMEDA)Na(TMP)(C₆H₅)ZnMe] and methane (CH₄).

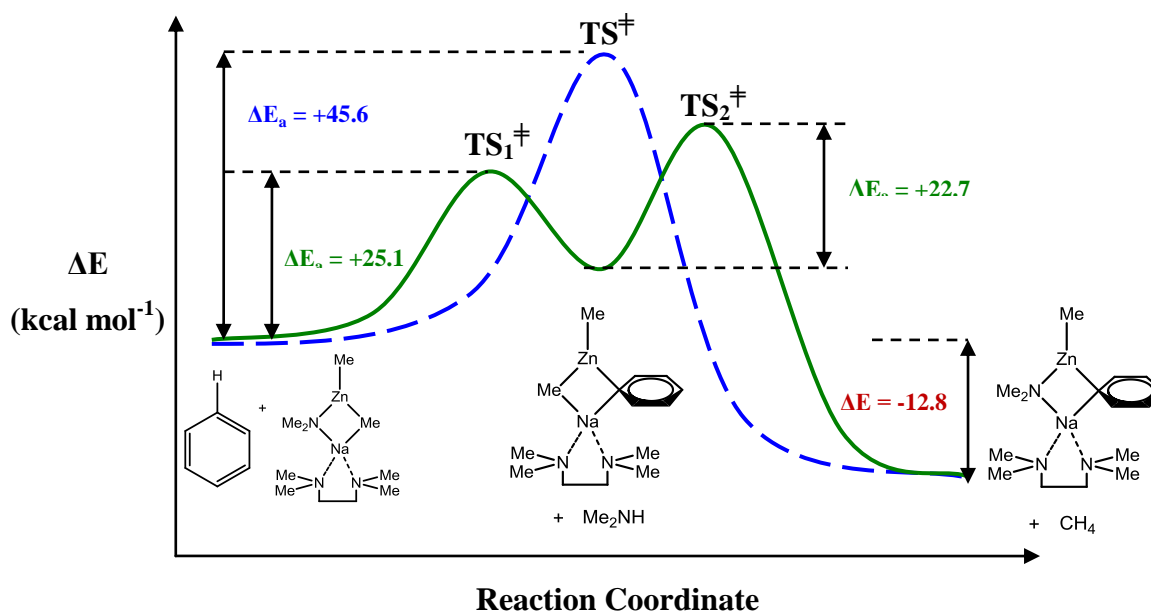


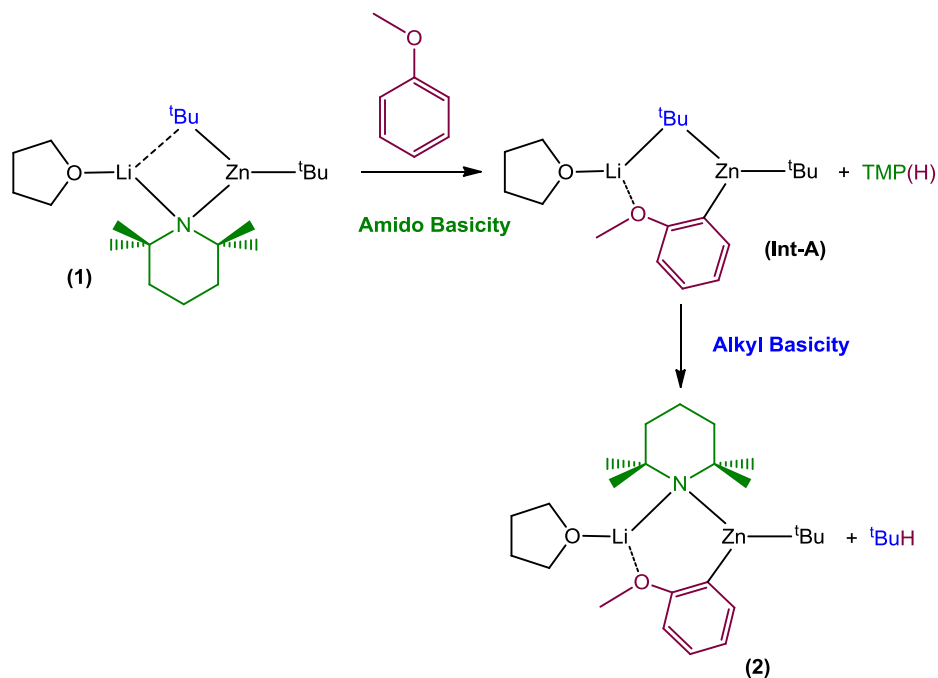
Figure 3.3: Energy profile for the reaction of [(TMEDA)Na(NMe₂)ZnMe₂] with benzene showing one-step (alkyl basicity) mechanism (Blue), and two-step (amido then alkyl basicity) mechanism (Green).

Similar DFT studies has also been carried out to model the reactions of [(THF)Li(TMP)Zn^tBu₂] (**1**) with *N,N*-diisopropylbenzamide,^[104] methyl benzoate^[105] and benzonitrile,^[105] showing a similar kinetic preference for the zincate to react via a two-step mechanism, acting first as an amido base then as an alkyl base. A simplified model of the zincate was again used for these calculations [(Me₂O)Li(NMe₂)ZnMe₂], and in the reaction with *N,N*-diisopropylbenzamide the substrate was modelled as *N,N*-dimethylbenzamide.

However, it must be stressed that although these theoretical studies strongly support the existence of a two-step mechanism for these bimetallic bases, there is no tangible experimental evidence to confirm this.^[102] Furthermore, as mentioned above, the simplified models adopted by the authors for the real bimetallic systems can greatly underestimate the influence that steric factors may have in these reactions. For example, it has recently been reported that mixed alkyl-amido zincates, prepared by combining Li(NMe₂) and ZnMe₂ in THF, show no metallating ability towards aromatic substrates such as anisole, benzonitrile, and *N,N*-diisopropylbenzamide.^[26b]

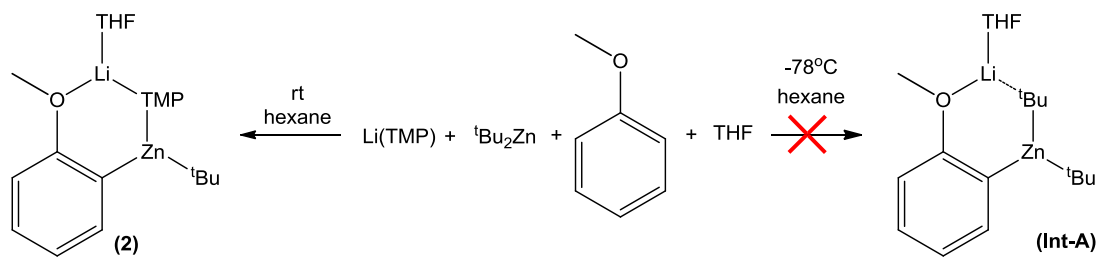
3.3 New insight into the reactivity of lithium TMP-zincates in DoM of anisole

In order to shed some light on the mechanisms of AMMZn and to provide new experimental insights into the “modus operandi” of these bimetallic bases, the deprotonation of anisole, a classical substrate in monometallic DoM,^[52] with the lithium zincate **1** was investigated. As previously mentioned, the final product of this reaction is **2**, which has been previously characterised by Mulvey and co-workers (Scheme 3.7).^[41] If the reaction of **1** with anisole follows the two-step mechanism suggested by Uchiyama’s theoretical studies, then it must proceed via an intermediate species [(THF)Li(*o*-C₆H₄OMe)Zn^tBu₂] (**Int-A**), where TMP has been replaced in **1** by a molecule of *ortho*-metallated anisole (Scheme 3.7).



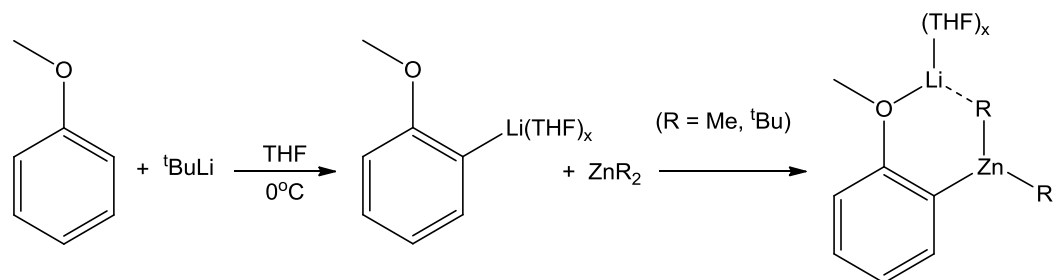
Scheme 3.7: Proposed two-step mechanism for the reaction of **1** with anisole.

Attempts to isolate or even detect the formation of [(THF)Li(*o*-C₆H₄OMe)Zn^tBu₂] (**Int-A**) were unsuccessful. Thus, when the reaction of **1** with anisole was performed at room temperature only the final metallated species [(THF)Li(TMP)(*o*-C₆H₄OMe)Zn^tBu] (**2**) was obtained, whereas if the temperature of the reaction was reduced to -78°C the starting materials, **1** and anisole, were recovered (Scheme 3.8). These results suggest that if the reaction does proceed through a two-step mechanism and **Int-A** is formed, then the second step where this intermediate zincate species reacts with concomitant TMP(H) must proceed rapidly in solution to form **2**.



Scheme 3.8: Synthetic approach to the synthesis of [(THF)Li(*o*-C₆H₄OMe)Zn^{*t*}Bu₂] (**Int-A**).

Given these results, an alternative indirect approach to synthesise this putative intermediate **Int-A** was attempted, with the objective of studying its reactivity towards the amine TMP(H) in order to assess if the second step of the two-step mechanism was plausible. To prepare this intermediate an indirect co-complexation approach was used, where anisole was initially *ortho*-lithiated using ^{*t*}BuLi in THF at 0°C, followed by addition of a dialkylzinc reagent (ZnR₂) (**Scheme 3.9**). In the course of these studies two different ZnR₂ reagents were investigated, Zn^{*t*}Bu₂ and ZnMe₂. The former is the dialkylzinc species present in **1**, and so preparation of the proposed intermediate containing *tert*-butyl ligands will provide a direct comparison for the two-step mechanism through which alkali metal TMP-zincates such as **1** are believed to react. On the other hand, although ZnMe₂ is not present in **1**, use of this dialkylzinc species does mirror the simplified structural models used for **1** in previous DFT studies,^[103-104] and therefore synthesis of this proposed dimethyl intermediate provides a useful insight into the species involved in these theoretical studies. Furthermore, it has been shown that variation of the alkyl groups can have a dramatic effect on the structure and the reactivity of zincates,^[49] and synthesis of these two different intermediate species will be of use for investigating the reaction mechanism of different dialkyl TMP-zincates.



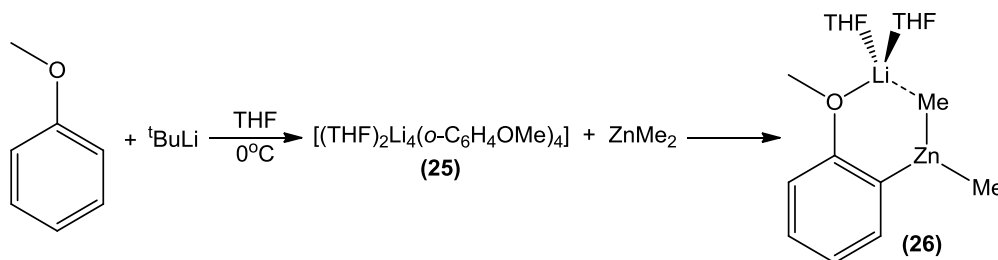
Scheme 3.9: Synergic co-complexation approach for the synthesis of the proposed reaction intermediate.

Following standard experimental procedures anisole can be selectively *ortho*-lithiated using ^{*t*}BuLi in THF at 0°C, and colourless crystals of tetrameric THF solvate [(THF)₂Li₄(*o*-

$\text{C}_6\text{H}_4\text{OMe}_4$] (**25**) could be obtained by addition of hexane, which were characterised by ^1H , ^7Li and $^{13}\text{C}\{^1\text{H}\}$ NMR spectroscopy and X-ray crystallography (see **Chapter 7.3.8 – Experimental Procedures** for details).

3.3.1 Co-complexation of $[(\text{THF})_2\text{Li}_4(o\text{-C}_6\text{H}_4\text{OMe})_4]$ (**25**) with ZnMe_2

Firstly, the co-complexation of **25** with the commercially available ZnMe_2 was studied. Thus, it was found that combining equimolar amounts of both homometallic reagents in THF afforded the novel bimetallic species $[(\text{THF})_2\text{Li}(o\text{-C}_6\text{H}_4\text{OMe})\text{ZnMe}_2]$ (**26**) as a colourless oil (**Scheme 3.10**), which was characterised by ^1H , ^7Li and $^{13}\text{C}\{^1\text{H}\}$ NMR spectroscopy.



Scheme 3.10: Co-complexation reaction of (**25**) with ZnMe_2 to form $[(\text{THF})_2\text{Li}(o\text{-C}_6\text{H}_4\text{OMe})\text{ZnMe}_2]$ (**26**).

The ^1H NMR spectrum of **26** in d_6 -benzene solution (**Figure 3.4**) showed four multiplets at δ 8.26, 7.24, 7.17 and 6.78 ppm for the aromatic protons, consistent with the formation of a molecule of *ortho*-metallated anisole, and a singlet at δ 3.44 ppm for the methoxy group. There was a further singlet at δ -0.17 ppm which was indicative of a methyl group bonded to zinc, and two multiplets at δ 1.21 and 3.24 ppm corresponding to the THF protons. Analysis of the integration revealed a ratio of anisole:THF:Me of 1:2:2, which is consistent with **26** being of composition $[(\text{THF})_2\text{Li}(o\text{-C}_6\text{H}_4\text{OMe})\text{ZnMe}_2]$. While the resonances for the aromatic protons and the methoxy group showed a small shift compared to those of **25** (**Table 3.1**), the singlet at δ -0.17 ppm for the Zn-Me protons showed a significant downfield shift compared to that of free ZnMe_2 (δ -0.52 ppm), which confirmed that co-complexation had occurred.

The ^7Li NMR spectrum possessed a single resonance at δ 0.72 ppm, appearing markedly upfield in comparison to that of **25** (δ 3.28 ppm), suggesting a significant change in environment of the Li atom. The most noticeable difference between the $^{13}\text{C}\{^1\text{H}\}$ NMR spectra of **26** and **25** is the chemical shifts for the metallated *ortho*-carbon, which appears at

δ 154.8 ppm in **26** (compared to δ 159.2 ppm in **25**), and the methyl groups attached to zinc, which appear at δ -8.6 ppm.

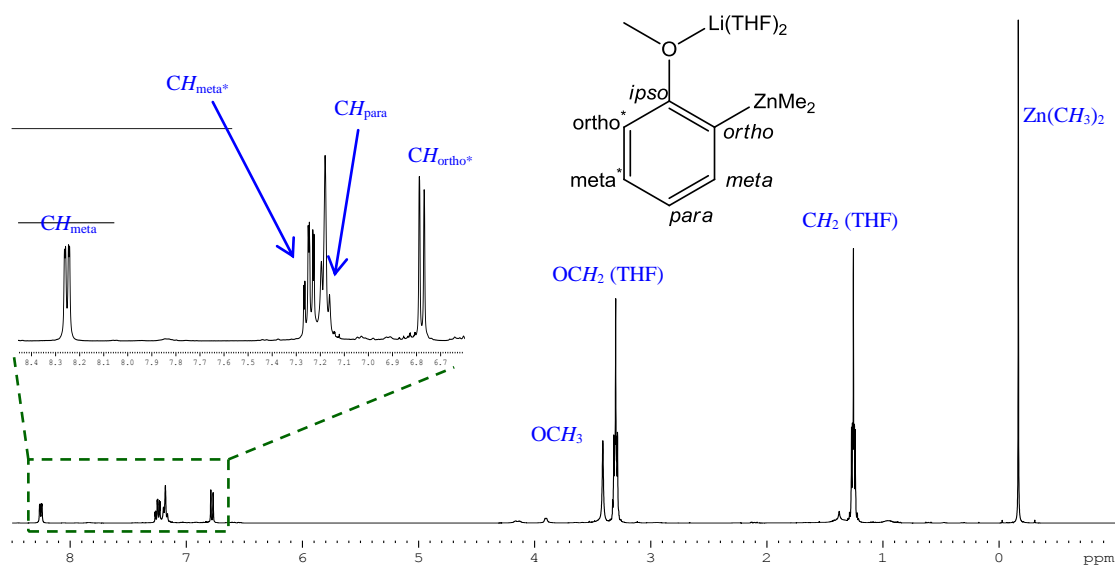


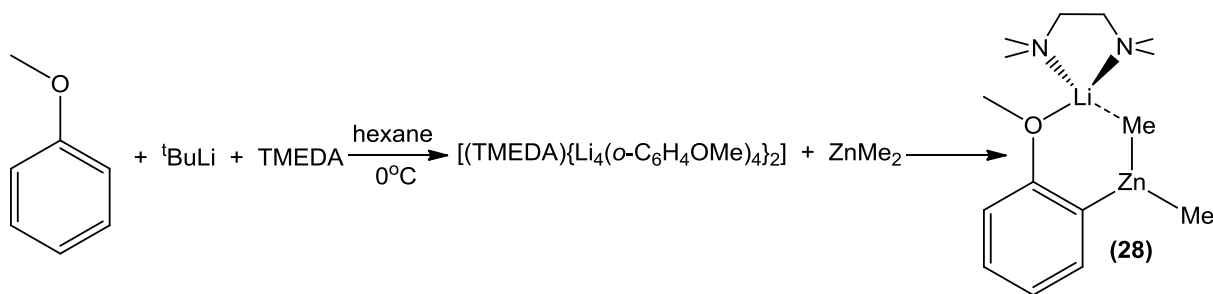
Figure 3.4: ^1H NMR spectrum of **26** in d_6 -benzene solution.

$\delta(^1\text{H})$	Me	OMe	Ar-H	THF/ TMEDA	^7Li
$[(\text{THF})_2\text{Li}(o\text{-C}_6\text{H}_4\text{OMe})\text{ZnMe}_2]$ (26)	-0.17	3.44	8.26, 7.24, 7.17, 6.78	1.21, 3.24	0.72
$[(\text{THF})_2\text{Li}_4(o\text{-C}_6\text{H}_4\text{OMe})_4]$ (25)	-	3.41	8.18, 7.39, 7.26, 6.78	1.17, 3.10	3.28
ZnMe ₂	-0.52	-	-	-	-
C ₆ H ₅ OMe	-	3.31	7.12, 6.81, 6.84	-	-
$[(\text{TMEDA})\text{Li}(o\text{-C}_6\text{H}_4\text{OMe})\text{ZnMe}_2]$ (28)	-0.14	3.42	8.27, 7.23, 7.19, 6.77	1.65, 1.62	0.67

Table 3.1: Comparison of ^1H and ^7Li NMR chemical shifts (ppm) of **26**, **25**, ZnMe₂, anisole and **28** in d_6 -benzene solution.

Attempts to grow crystals of **26** from neat THF or toluene were unsuccessful due to the high solubility of this compound in these solvents, even at lower temperatures (-30°C). Use of a less polar solvent such as hexane gave a white solid, which could be re-dissolved by addition of toluene, and after leaving at room temperature overnight deposited colourless crystals of the tetraorganozincate $[(\text{THF})_2\text{Li}_2(o\text{-C}_6\text{H}_4\text{OMe})_4\text{Zn}]$ (**27**) (average isolated yield = 9%), whose formation can be attributed to a disproportionation process as a result of the large change in polarity of the organic solvent (see **Chapter 3.5** for further discussion of **27**).

Thus, despite numerous attempts to prepare **26** as a crystalline solid using different solvent systems and conditions, only tetraorganozincate **27** could be isolated. In a deliberate attempt to form a crystalline derivative of **26**, THF was replaced with the bidentate ligand TMEDA, which can coordinate in a chelating fashion, providing additional stabilisation to the proposed organometallic intermediate, and prevent its disproportionation to **27**. Using a similar approach to that described above anisole was *ortho*-lithiated by ^tBuLi at 0°C, this time using hexane as the bulk solvent in the presence of one molar equivalent of TMEDA, followed by the addition of ZnMe₂ (**Scheme 3.11**). The resulting solution was left at room temperature overnight, affording a crop of colourless crystals of [(TMEDA)Li(*o*-C₆H₄OMe)ZnMe₂] (**28**) (Isolated yield = 62%), which were analysed by X-ray crystallography and ¹H, ⁷Li and ¹³C{¹H} NMR spectroscopy. The ¹H NMR spectrum of **28** in d₆-benzene solution proved to be almost identical to that of the THF analogue **26**, showing marginal variations for the chemical shifts of the aryl and methyl groups (**Table 3.1**), and two singlets at δ 1.65 and 1.62 ppm corresponding to the CH₃ and CH₂ groups respectively of the TMEDA ligand.



Scheme 3.11: Synthesis of [(TMEDA)Li(*o*-C₆H₄OMe)ZnMe₂] (**28**).

The mixed-metal constitution of **28** was confirmed by an X-ray crystallographic study (**Figure 3.5(a)**), demonstrating that co-complexation of ZnMe₂ with [(TMEDA){Li₄(*o*-C₆H₄OMe)₄}₂]^[106] had taken place. The *ortho* carbon of the metallated anisole fragment, which was initially bound to lithium is now bonded to zinc, forming a strong σ-bond (Zn-C3 2.016(3) Å). The two metal centres are connected through both a bridging methyl group (Zn-C1 2.048(3), Li-C1 2.290(4) Å) and an ambidentate *ortho*-metallated anisole fragment, where lithium forms a dative bond to the oxygen (Li-O 1.960(4) Å), and zinc binds covalently to the *ortho*-carbon of the anisole group, giving rise to a CIP structure which is completed by a terminal methyl group on the zinc, and the bidentate TMEDA ligand, which chelates the lithium centre.

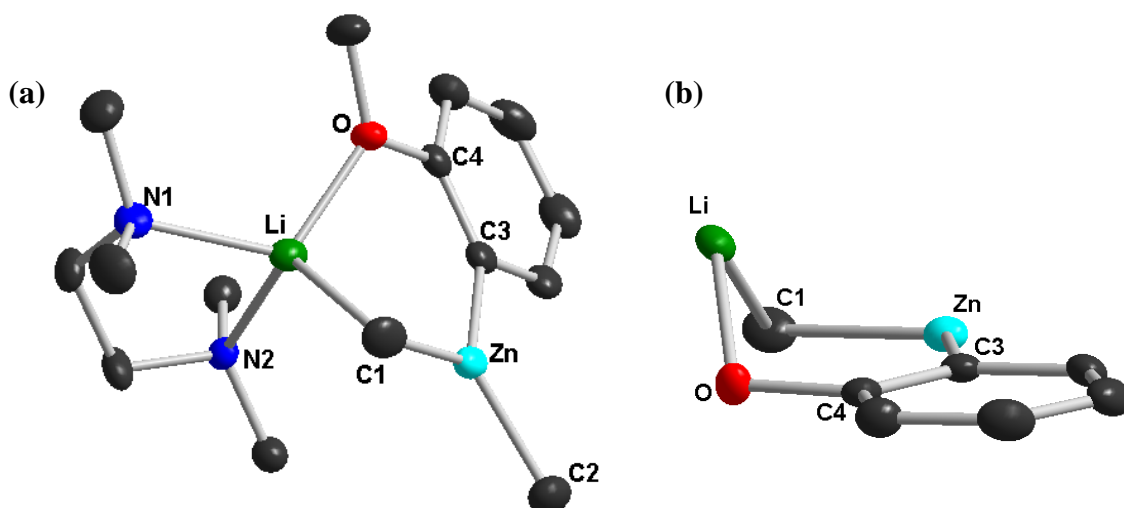


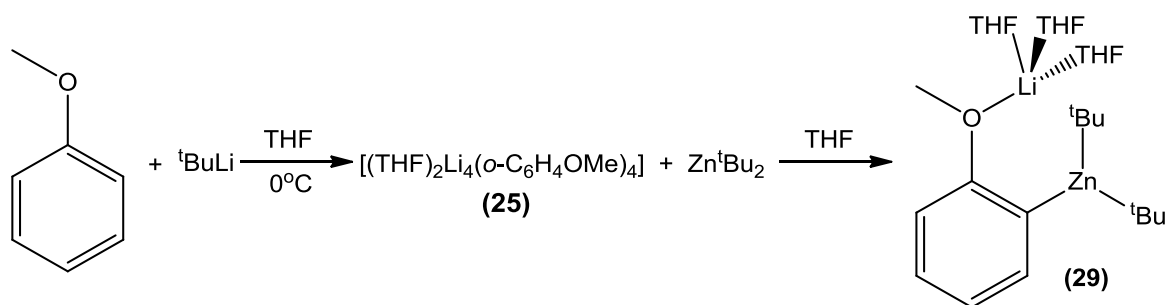
Figure 3.5(a): Molecular structure of [(TMEDA)Li(*o*-C₆H₄OMe)ZnMe₂] (**28**) with 40% probability ellipsoids. Hydrogen atoms have been omitted for clarity. **(b)** Central six-membered {LiOCCZnC} ring of **28** fused to the aromatic ring of anisole, with 30% probability ellipsoids. *Selected bond distances (Å) and bond angles (°):* Zn-C1 2.048(3), Zn-C2 2.045(2), Zn-C3 2.016(3), Li-C1 2.290(4), Li-N1 2.144(4), Li-N2 2.108(4), Li-O 1.960(4); C1-Zn-C3 122.71(10), C2-Zn-C3 116.20(11), C1-Zn-C2 121.09(10), C1-Li-N1 113.90(18), C1-Li-N2 114.34(18), C1-Li-O 107.24(17), N1-Li-N2 86.96(14), N1-Li-O 115.07(19), N2-Li-O 118.55(19).

The bonding in **28** results in a closed structure comprising of a central six-membered {LiOCCZnC} ring, which is fused to the aromatic ring of anisole through the *ipso* and metallated *ortho* carbon atoms, which can be envisaged as a hetero-naphthalenyl fragment (**Figure 3.5(b)**). Thus, Zn, O and C1 lie almost co-planar with the aromatic ring (maximum deviation from mean plane 0.031 Å for O), whereas the lithium centre adopts an almost perpendicular disposition, as evidenced by the angle of 76.7° between the Li-O-C1 and C1-Zn-C3-C4-O planes. The *ortho*-metallated anisole fragment in **28** bonds in a similar fashion to that displayed in [(THF)Li(TMP)(*o*-C₆H₄OMe)Zn^tBu] (**2**), with similar bond distances for the dative Li-O bonds (1.960(4) Å in **28** compared to 1.985(3) Å in **2**) and the Zn-C_{ortho} bonds (2.045(2) Å in **28** compared to 2.0937(16) Å in **2**). The bridging methyl group in **28** forms not only a strong, short bond to zinc (Zn-C1, 2.0483(3) Å), but also a short-medium contact to lithium (Li-C1, 2.290(4) Å). This Li-C bond in **28** is significantly shorter than that of the analogous lithium dimethylzincate compound [(TMEDA)Li(TMP)ZnMe₂] (Li-C bond length 2.603(5) Å),^[107] and is more comparable with those found in the methyl lithium tetramer [(THF)LiMe₄] (average Li-C bond length 2.240 Å),^[108] suggesting that this bridging methyl

group in **28** may possess a substantial amount of lithium character. However, in d_6 -benzene solution at room temperature this Li-C contact must be broken, as the ^1H NMR spectrum shows the two methyl groups to be equivalent, and the chemical shift (δ -0.14 ppm) suggests the methyl groups possess more zinc character than lithium character when compared to the resonances of the methyl groups in each of these homometallic reagents ($\text{ZnMe}_2 = \delta$ -0.52 ppm, $\text{MeLi} = \delta$ -1.42 ppm).

3.3.2 Co-complexation of $[(\text{THF})_2\text{Li}_4(o\text{-C}_6\text{H}_4\text{OMe})_4]$ (**25**) with Zn^tBu_2

After the successful synthesis and characterisation of the monoaryl-dimethylzincates **26** and **28**, we next endeavoured to prepare a di-*tert*-butyl derivative. Thus, a THF solution of *ortho*-lithiated anisole was reacted with $^t\text{Bu}_2\text{Zn}$ to form the corresponding monoaryl-di-*tert*-butylzincate $[(\text{THF})_3\text{Li}(o\text{-C}_6\text{H}_4\text{OMe})\text{Zn}^t\text{Bu}_2]$ (**29**) via synergic co-complexation (**Scheme 3.12**).



Scheme 3.12: Synthesis of $[(\text{THF})_3\text{Li}(o\text{-C}_6\text{H}_4\text{OMe})\text{Zn}^t\text{Bu}_2]$ (**29**) via synergic co-complexation.

The ^1H NMR spectrum of the crude reaction mixture in d_6 -benzene solution (**Figure 3.6**) was consistent with the formation of the mixed-metal compound $[(\text{THF})_3\text{Li}(o\text{-C}_6\text{H}_4\text{OMe})\text{Zn}^t\text{Bu}_2]$ (**29**). Analysis of the aromatic resonances showed significant change in the chemical shifts compared to those found in the ^1H NMR spectrum of **25** (**Table 3.2**), the most notable of which was the resonance of the *meta* proton, which appears at δ 8.18 ppm in **25**, where the proton is adjacent to the Li-C bond, but in **29** it has moved further up-field to δ 7.26 ppm. This is also significantly different when compared to that of the analogous dimethylzinc species (**26**), which has a chemical shift of δ 8.15 ppm for its *meta* proton (**Table 3.2**).

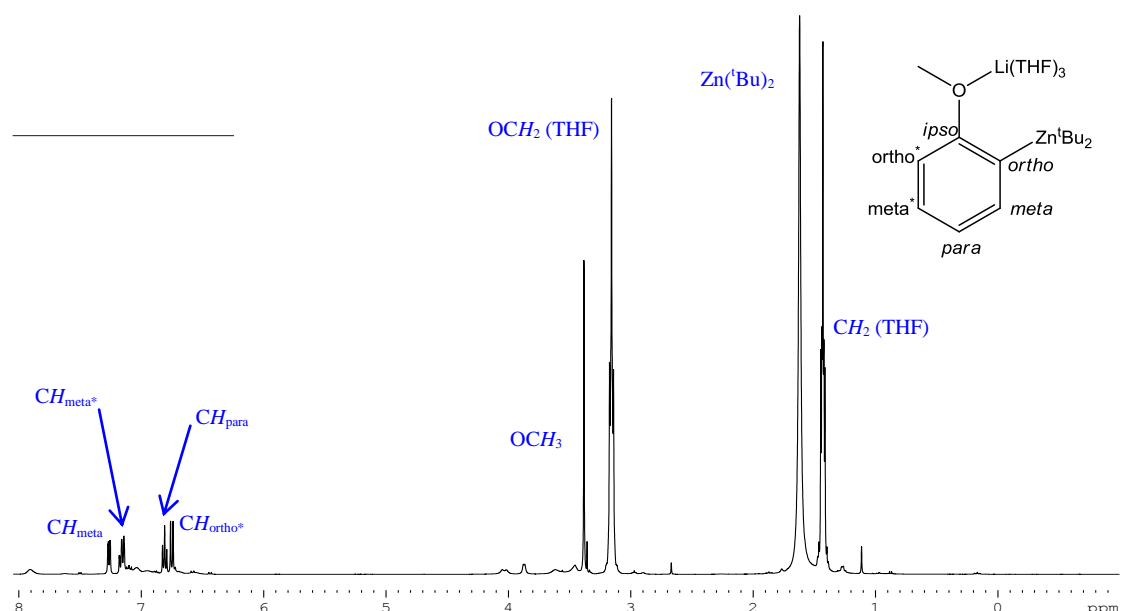


Figure 3.6: ^1H NMR spectrum of **29** in d_6 -benzene solution.

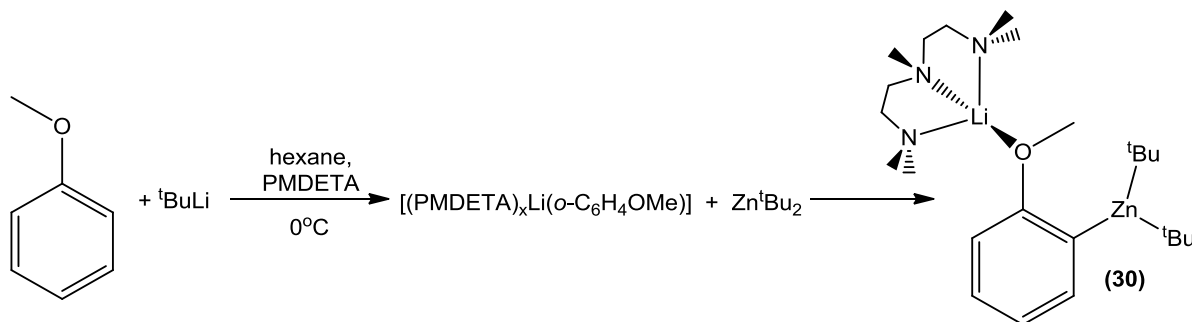
	$\delta(^1\text{H})$	^tBu	OMe	Ar-H	THF/ PMDETA	^7Li
$[(\text{THF})_3\text{Li}(o\text{-C}_6\text{H}_4\text{OMe})\text{Zn}^t\text{Bu}_2]$ (29)	1.58	3.43	7.26, 7.14, 6.80, 6.74	1.38, 3.13	-0.28	
$[(\text{PMDETA})\text{Li}(o\text{-C}_6\text{H}_4\text{OMe})\text{Zn}^t\text{Bu}_2]$ (30)	1.75	3.83	8.18, 7.19, 7.06, 6.21	1.81, 1.65, 1.63	-0.15	
$^t\text{Bu}_2\text{Zn}$	1.02	-	-	-	-	
$[(\text{THF})_2\text{Li}_4(o\text{-C}_6\text{H}_4\text{OMe})_4]$ (25)	-	3.41	8.18, 7.39, 7.26, 6.78	1.17, 3.10	3.28	
$[(\text{THF})_2\text{Li}(o\text{-C}_6\text{H}_4\text{OMe})\text{ZnMe}_2]$ (26)	-0.17	3.44	8.26, 7.24, 7.17, 6.78	1.21, 3.24	0.72	
$[(\text{THF})\text{Li}(\text{TMP})(o\text{-C}_6\text{H}_4\text{OMe})\text{Zn}^t\text{Bu}]$ (2)	1.61	3.31	7.94, 7.22, 7.16, 6.56	1.17, 3.00	0.87	

Table 3.2: Selected ^1H and ^7Li NMR chemical shifts (ppm) of **29**, **30**, $^t\text{Bu}_2\text{Zn}$, **25**, **26** and **2**^[41] in d_6 -benzene.

A large singlet at δ 1.58 ppm can be assigned to the methyl protons of the ^tBu groups, which is shifted downfield compared to that found for free $^t\text{Bu}_2\text{Zn}$ (δ 1.02 ppm), but appears at a similar chemical shift to that observed for the ^tBu group of the related mixed metal compound $[(\text{THF})\text{Li}(\text{TMP})(o\text{-C}_6\text{H}_4\text{OMe})\text{Zn}^t\text{Bu}]$ (**2**) (δ 1.61 ppm) (Table 3.2).^[41] Further confirmation that co-complexation has taken place is gained from the ^7Li NMR spectrum, which displays a single resonance at δ -0.28 ppm, which is shifted considerably downfield when compared to that of **25** (δ 3.28 ppm), suggesting a substantial difference in the coordination environment of

the Li atom. The presence of coordinated THF is indicated by two multiplets at δ 1.38 and 3.13 ppm, which are very different to those of free THF in the same deuterated solvent (δ 1.88 and 3.74 ppm). Analysis of the integration of these resonances reveals a ratio of metallated anisole:THF: ^tBu of 1:3:2, which would suggest a species of composition $[(\text{THF})_3\text{Li}(o\text{-C}_6\text{H}_4\text{OMe})\text{Zn}^t\text{Bu}_2]$ (**29**).

As previously observed for **26**, attempts to obtain **29** in crystalline form proved to be unsuccessful due to the high solubility of this compound in neat THF or toluene, and the addition of hexane giving the disproportionation product $[(\text{THF})_2\text{Li}_2(o\text{-C}_6\text{H}_4\text{OMe})_4\text{Zn}]$ (**27**) (see **Chapter 3.5** for further discussion of **27**). After the success of employing the bidentate ligand TMEDA to isolate the analogous dimethylzincate $[(\text{TMEDA})\text{Li}(o\text{-C}_6\text{H}_5\text{OMe})\text{ZnMe}_2]$ (**28**), the same approach was used for **29**. Taking into account that **29** appears to contain three molecules of THF, the tridentate amine PMDETA was employed in an attempt to stabilise the intermediate and prevent disproportionation to the tetraorganozincate **27**. Thus, anisole was first *ortho*-lithiated by $^t\text{BuLi}$ at 0°C in hexane in the presence of one molar equivalent of PMDETA, and to the resulting suspension was added Zn^tBu_2 . After removing the volatiles *in vacuo* the resulting residue was dissolved in warm toluene and left to slowly cool to room temperature, affording a crop of cubic crystals $[(\text{PMDETA})\text{Li}(o\text{-C}_6\text{H}_4\text{OMe})\text{Zn}^t\text{Bu}_2]$ (**30**) (Isolated yield = 34%) (**Scheme 3.13**), which were analysed by ^1H , ^7Li and $^{13}\text{C}\{^1\text{H}\}$ NMR spectroscopy and X-ray crystallography.



Scheme 3.13: Synthesis of $[(\text{PMDETA})\text{Li}(o\text{-C}_6\text{H}_4\text{OMe})\text{Zn}^t\text{Bu}_2]$ (**30**).

As can be observed in **Table 3.2**, multinuclear NMR analysis confirmed the successful co-complexation of $^t\text{Bu}_2\text{Zn}$ with $[(\text{PMDETA})_x\text{Li}(o\text{-C}_6\text{H}_4\text{OMe})]$, with the most indicative resonance being the protons of the *tert*-butyl groups, appearing at δ 1.75 ppm (compared to unco-complexed Zn^tBu_2 δ 1.02 ppm). The differences between the ^1H NMR spectra of **29** and **30** (**Table 3.2**) are most likely caused by the stronger coordinating ability of the chelating

PMDETA compared to monodentate THF, which may result in the THF molecules coordinated to the Li centre in **29** being partially labile in solution, whereas in **30** this is unlikely to occur with the tridentate PMDETA ligand.

Analysis of the crystalline material of **30** by X-ray crystallographic studies revealed the molecular structure of the CIP lithium zincate [(PMDETA)Li(*o*-C₆H₄OMe)Zn^tBu₂] (**Figure 3.7**), evidence that the co-complexation of Zn^tBu₂ with lithiated anisole had taken place. As in the dimethylzincate derivative [(TMEDA)Li(*o*-C₆H₄OMe)ZnMe₂] (**28**), the *ortho*-carbon of the metallated anisole fragment is bonded to zinc, forming a strong σ -bond (Zn-C9 2.050(3) Å) and lithium bonds to the oxygen of anisole, resulting in a molecule of *ortho*-metallated anisole which bridges the two metal centres in an ambidentate fashion. Zinc completes its coordination sphere by bonding to the two terminal *tert*-butyl groups in a trigonal planar geometry (sum of the angles around Zn 358.2°), whereas lithium exhibits a distorted tetrahedral geometry (average angle around Li 108.2°), bonded to the oxygen of anisole and the three nitrogen atoms of PMDETA.

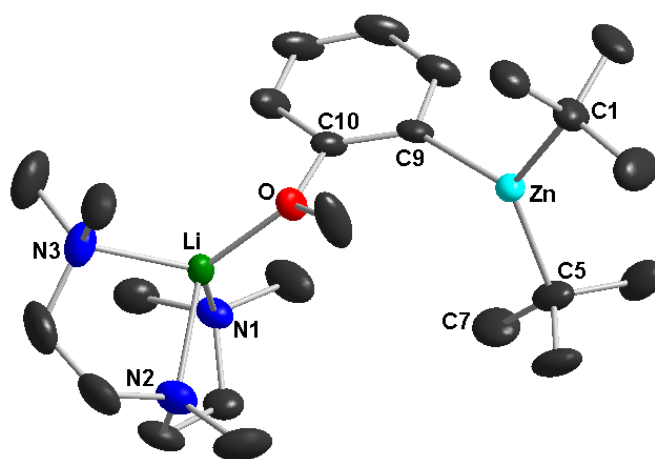


Figure 3.7: Molecular structure of [(PMDETA)Li(*o*-C₆H₄OMe)Zn^tBu₂] (**30**) with 30% probability ellipsoids. Hydrogen atoms have been omitted for clarity. *Selected bond distances* (Å) *and bond angles* (°): Zn-C1 2.044(9), Zn-C5 1.975(8), Zn-C9 2.050(3), Li-O 1.929(4), Li-N1 2.118(6), Li-N2 2.129(6), Li-N3 2.086(7), Li-C7 4.869(12); C1-Zn-C5 124.2(5), C1-Zn-C9 117.2(3), C5-Zn-C9 116.8(3), O-Li-N1 117.8(2), O-Li-N2 123.3(2), O-Li-N3 116.2(2), N1-Li-N2 86.8(2), N1-Li-N3 119.2(2), N2-Li-N3 85.9(2).

Importantly, where **28** had a closed structure, with the two metals also linked by one of the methyl groups, **30** exhibits a much more open structural motif, having the *ortho*-metallated anisole fragment as the only ligand bridging between the Li and Zn centres. Thus, there is no

secondary interaction between the lithium and any of the methyl groups of the *tert*-butyl ligands of **30** (shortest Li-CH₃ bond distance 4.869(12) Å for Li-C7), contrasting with the previously reported molecular structure of the mixed-metal base [(THF)Li(TMP)Zn^tBu₂] (**1**) (shortest Li-CH₃ bond distance 2.4090(3) Å),^[50] where Li and Zn are connected by both a TMP and one of the ^tBu ligands. A similar open structural motif to **30** has been reported for the related lithium aluminate [(THF)₃Li{O(=C)NⁱPr₂(C₆H₄)}Al(^tBu)₃], resulting from the direct *ortho*-alumination of *N,N*-diisopropylbenzamide by the mixed-metal base [(THF)₃Li(TMP)Al^tBu₃] (**Figure 3.8**).^[109] Encouragingly, this compound has a contacted ion-pair structure containing a lithium atom coordinated to three molecules of THF and to the oxygen of the aromatic substrate, providing a similar motif to that which would be expected for [(THF)₃Li(*o*-C₆H₄OMe)Zn^tBu₂] (**29**).

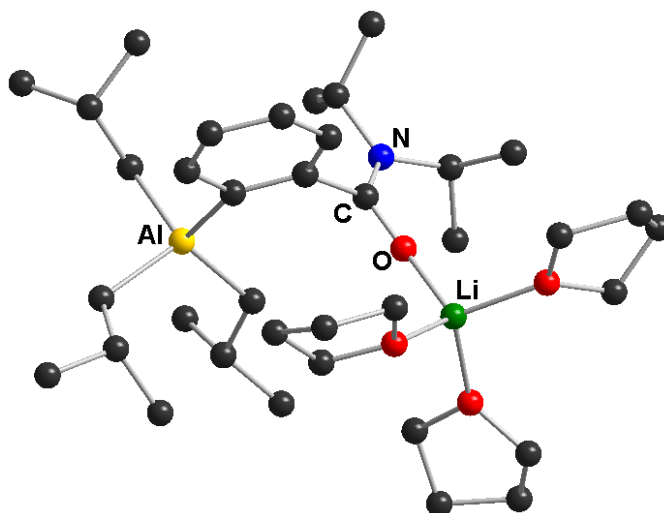
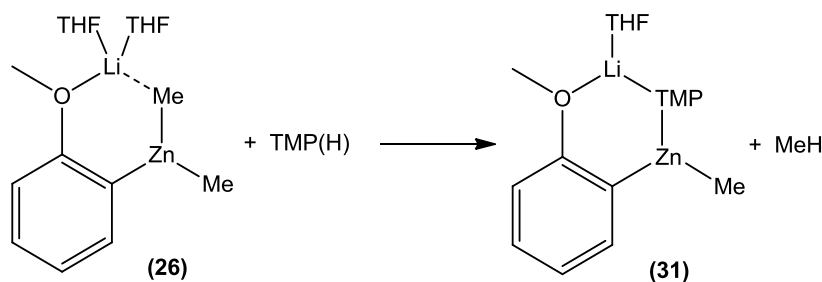


Figure 3.8: Molecular structure of the [(THF)₃Li{O(=C)NⁱPr₂(C₆H₄)}Al(^tBu)₃]. Hydrogen atoms have been omitted for clarity.

Having characterised both the dimethyl and di-*tert*-butyl intermediates it has been shown that they possess remarkably different structural motifs, with [(THF)₂Li(*o*-C₆H₄OMe)ZnMe₂] (**26**) adopting a closed structure compared to the open structure of [(THF)₃Li(*o*-C₆H₄OMe)Zn^tBu₂] (**29**). The next step in these studies was to investigate the reactivity of these bimetallic species with TMP(H) in order to mimic the second step of the mechanism for AMMZn proposed by Uchiyama in his theoretical studies, as well as assessing the effect that the different alkyl groups (Me vs. ^tBu) may have on the reactivity of this family of alkali metal zincates.

3.3.3 Investigating the reactivity of [(THF)₂Li(*o*-C₆H₄OMe)ZnMe₂] (**26**) with TMP(H)

Based on the data provided by theoretical studies, the reaction of lithium dialkyl-amidozincates [(THF)Li(TMP)ZnR₂] with anisole would be expected to afford an intermediate of similar structure to [(THF)₂Li(*o*-C₆H₄OMe)ZnMe₂] (**26**), which in turn reacts with concomitant TMP(H) to afford the final product of AMMZn [(THF)Li(TMP)(*o*-C₆H₄OMe)ZnMe] (**31**) and methane. Thus, in order to replicate experimentally the proposed second step of this theoretical study, the reactivity of **26** with equimolar amounts of TMP(H) was investigated (**Scheme 3.14**).



Scheme 3.14: Proposed 2nd step for AMMZn of anisole: reaction of [(THF)₂Li(*o*-C₆H₄OMe)ZnMe₂] (**26**) with TMP(H).

In general, it is well known that the reactivity of mixed-metal reagents is greatly influenced by the donor ability of the solvent employed,^[73a] so these reactivity studies have been carried out in both d₆-benzene and the more polar solvent d₈-THF. An advantage of carrying out such reactions in deuterated solvents is that they can be monitored directly by NMR spectroscopy, which means that any volatile reagents or by-products formed can be detected, and therefore a more complete picture of the reaction can be observed.

The reactivity of **26** with TMP(H) was first investigated in deuterated benzene, with the synthesis of **26** carried out as described in **Chapter 3.3.1**, followed by removal of the solvent and volatiles *in vacuo*. The product was then dissolved in d₆-benzene, and its purity confirmed by ¹H and ⁷Li NMR spectroscopy (**Figure 3.9(a)**). One equivalent of TMP(H) was then added to the NMR tube, and the reaction mixture analysed by ¹H NMR spectroscopy after 2 hours (**Figure 3.9(b)** and **(c)**). Analysis of the aliphatic region (**Figure 3.9(c)**) indicated that TMP(H) had been successfully metallated by the presence of two characteristic singlets at δ 1.23 and 1.50 ppm, corresponding to the α-methyl groups of TMP. The inequivalence of these methyl groups is indicative of a fixed stereochemically rigid Li-TMP-Zn backbone in the

product. However, a second set of resonances was also present at δ 1.12 and 1.44 ppm, which would indicate the presence of a second species possessing a Li-TMP-Zn backbone, along with some unreacted TMP(H) as indicated by a singlet at δ 1.06 ppm, corresponding to the α -methyl groups. Thus, it would appear that the reaction of TMP(H) with **26** has yielded two different products. This was confirmed by analysis of the aromatic region (**Figure 3.9(b)**), which showed four multiplets at δ 7.96, 7.16, 7.10 and 6.53 ppm, which were consistent with the presence of *ortho*-metallated anisole, but shifted slightly compared to those of **26** (8.26, 7.24, 7.17 and 6.78 ppm). However, these resonances were only a minor product, the major species present was indicated by three resonances at δ 7.11, 6.84 and 6.79 ppm (a triplet, triplet and doublet respectively), and a singlet at δ 3.36 ppm, which were consistent with those of free anisole in the same deuterated solvent.

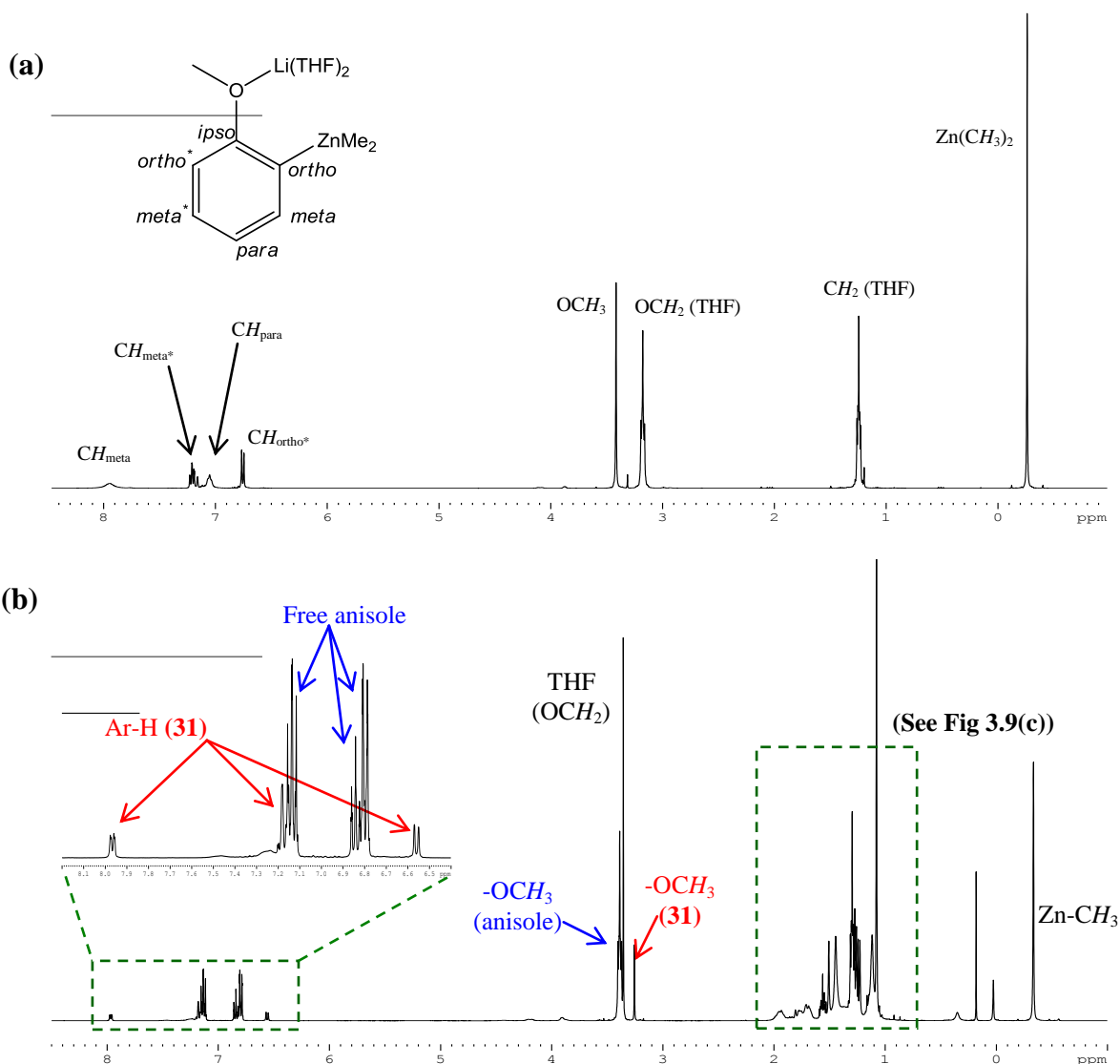


Figure 3.9: Reaction of **26** with TMP(H) in d₆-benzene, monitored by ¹H NMR. (a) before addition of TMP(H) and (b) 2 hours after addition one equivalent of TMP(H).

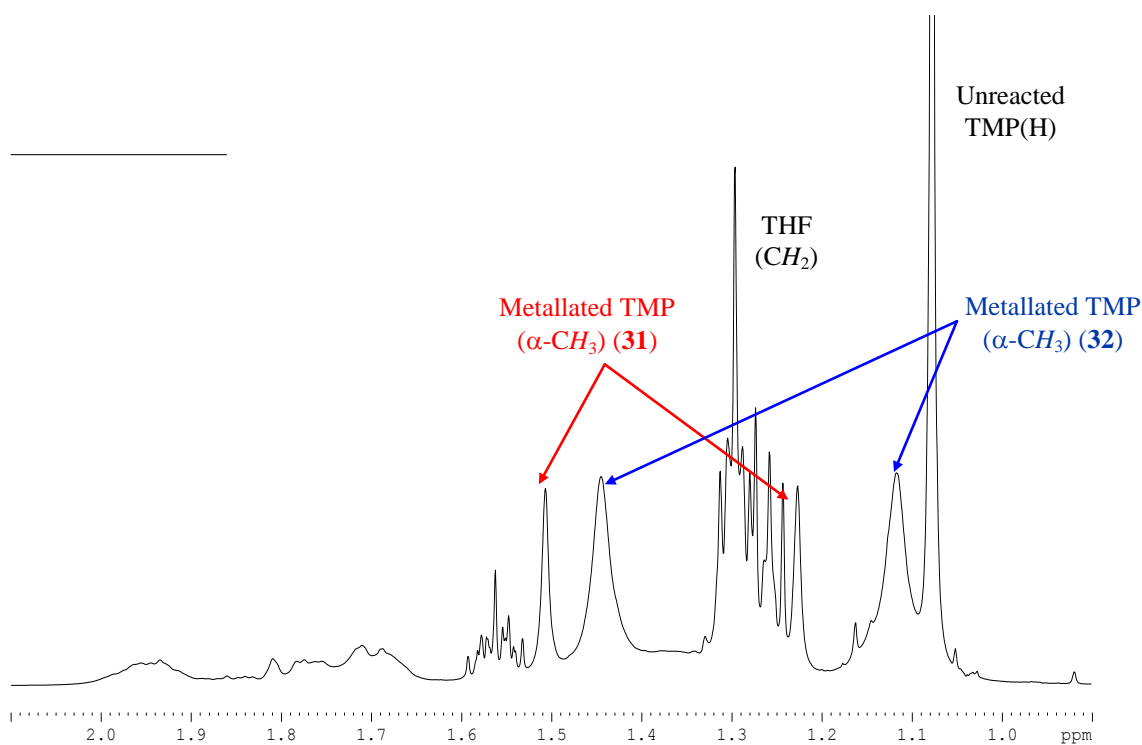
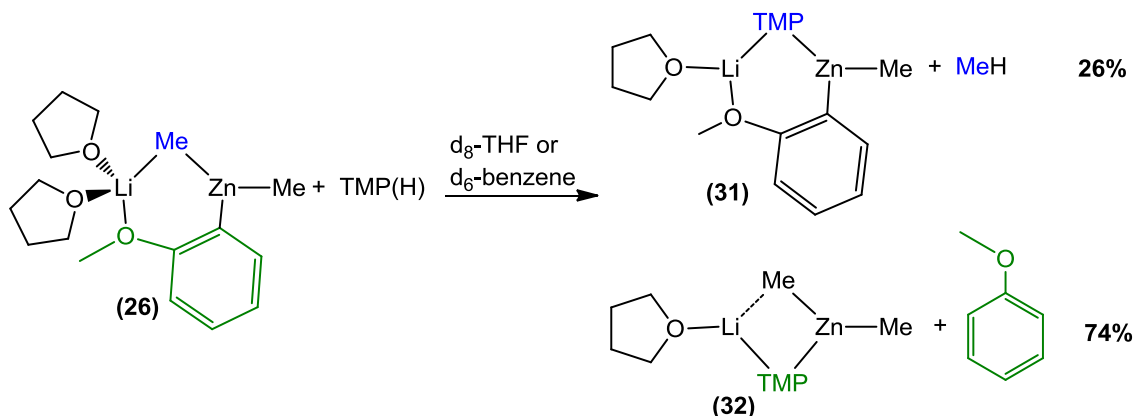


Figure 3.9(c): Aliphatic region of the ^1H NMR spectrum of the reaction between **26** and TMP(H) in d_6 -benzene after 2 hours.

This data would suggest that although TMP(H) has reacted with **26**, the expected product $[(\text{THF})_2\text{Li}(\text{TMP})(o\text{-C}_6\text{H}_4\text{OMe})\text{ZnMe}]$ (**31**), formed by reaction of TMP(H) with one of the methyl groups of **26**, is only the minor species present. The major product in the aromatic region is anisole, implying that **26** has reacted with TMP(H) in a completely different manner to that suggested by Uchiyama, and instead of the TMP(H) replacing one of the methyl ligands it has instead displaced the *ortho*-metallated anisole of **26**, affording the lithium dimethyl-TMP zincate $[(\text{THF})\text{Li}(\text{TMP})(\text{Me})\text{ZnMe}]$ (**32**) and free anisole (**Scheme 3.15**). The formation of **31** and **32** is consistent with the presence of two sets of α -methyl resonances for two different Li-TMP-Zn fragments observed in the aliphatic region (δ 1.23 and 1.50 ppm, δ 1.12 and 1.44 ppm). Analysis of the integration of the aromatic resonances reveals a ratio of *ortho*-metallated anisole to free anisole of $\sim 1:3$.

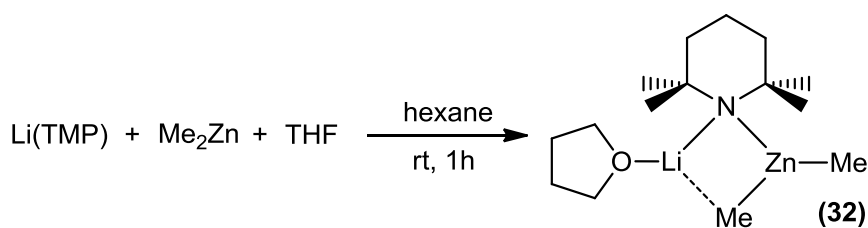
Furthermore, this reaction showed no dependence on the nature of the solvent employed, with the same results observed when the reaction was carried out in the more polar d_8 -THF, giving an almost identical ratio of products. It should also be noted that reaction of the TMEDA analogue, $[(\text{TMEDA})\text{Li}(o\text{-C}_6\text{H}_4\text{OMe})\text{ZnMe}_2]$ (**28**), with one equivalent of TMP(H) in

deuterated benzene gave the same result as was seen for **26**, with [(TMEDA)Li(TMP)ZnMe₂] and free anisole being the main products formed.



Scheme 3.15: Reaction of **26** with TMP(H) to form **31** and methane, and **32** and free anisole.

The unexpected formation of [(THF)Li(TMP)(Me)ZnMe] (**32**) from the reaction of **26** with TMP(H) was confirmed by preparing this dialkyl-TMP-zincate via a rational co-complexation approach, by reacting equimolar amounts of LiTMP, Me₂Zn and THF in hexane (**Scheme 3.16**). After stirring at room temperature for 1 hour the solvent was removed *in vacuo*, affording a colourless oil which was analysed by ¹H NMR spectroscopy, showing almost identical resonances to those seen in the reaction of **26** and TMP(H) in d₆-benzene, the most indicative of which were those of the α-methyl groups of the bridging TMP ligand at δ 1.10 and 1.45 ppm (compared to δ 1.12 and 1.44 ppm in the reaction between **26** and TMP(H) - **Figure 3.9(c)**).

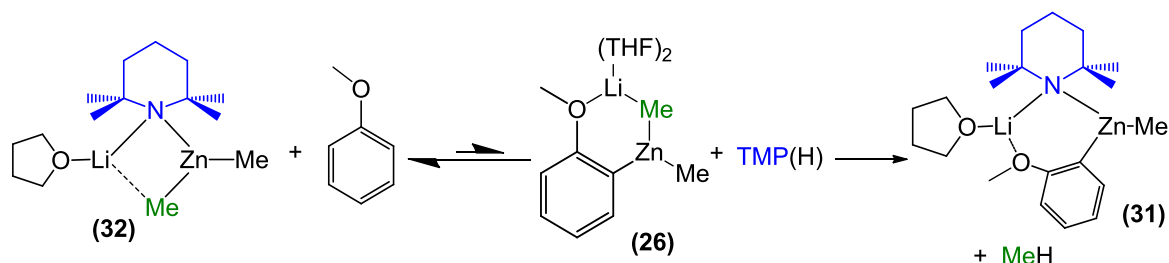


Scheme 3.16: Rational synthesis of **32**.

These results fill an important gap in the understanding of the reactivity of dialkyl-TMP zincates [(THF)Li(TMP)ZnR₂]. In theory, if they behaved as amido bases it might be expected that the alkyl groups would play only a spectating role in the reactivity of these zincates, and that both **1** (R= ^tBu) and **32** (R= Me) would exhibit similar reactivities. However, whereas [(THF)Li(TMP)Zn^tBu₂] (**1**) *ortho*-deprotonates anisole at room

temperature in hexane in an almost quantitative yield after 2 hours,^[41] the methyl analogue [(THF)Li(TMP)ZnMe₂] (**32**) showed very low reactivity, with only 20% of the aromatic substrate being metallated after 48 hours at room temperature. These differences in reactivity between **1** and **32** could be attributed to a one-step reaction, where the zincate acts solely as an alkyl base, and the lower basicity of methyl ligands compared to *tert*-butyl ligands accounting for the different levels of deprotonation. However, taking into account the results observed for the reaction of **26** with one equivalent of TMP(H) (where the yield of metallated anisole is 26%), this study provides an alternative explanation for the poor reactivity exhibited by **32**.

Thus, if [(THF)Li(TMP)ZnMe₂] (**32**) did behave initially as an amido base, it would first metallate anisole forming the proposed intermediate species **26** and TMP(H). However, due to the lower basicity of the methyl ligands (in comparison with *tert*-butyl ligands), TMP(H) is able to react with the molecule of metallated anisole more rapidly than it does with the methyl ligands of **26**. Therefore, a reversal of the first step of the reaction, where TMP(H) displaces anisole to regenerate **32** and free anisole could compete with the formation of the final metallated species **31** and methane (**Scheme 3.17**). The net result of which is that the metallation of anisole by **32** occurs in very low yields (only 20%).



Scheme 3.17: Summary of the reactivity of [(THF)Li(TMP)ZnMe₂] (**32**) with anisole.

3.3.4 Investigating the reactivity of [(THF)₃Li(*o*-C₆H₄OMe)Zn^tBu₂] (**29**) with TMP(H)

Building on these results, attention next turned to investigating the reactivity of [(THF)₃Li(*o*-C₆H₄OMe)Zn^tBu₂] (**29**) towards TMP(H). These reactivity studies were also carried out in both *d*₆-benzene and *d*₈-THF, to give an insight into the role of solvent in these metallation reactions. Compound **29** was prepared *in situ*, then dissolved in *d*₆-benzene, and a ¹H NMR spectrum was recorded which confirmed the purity of the bimetallic compound (**Figure 3.10(a)**).

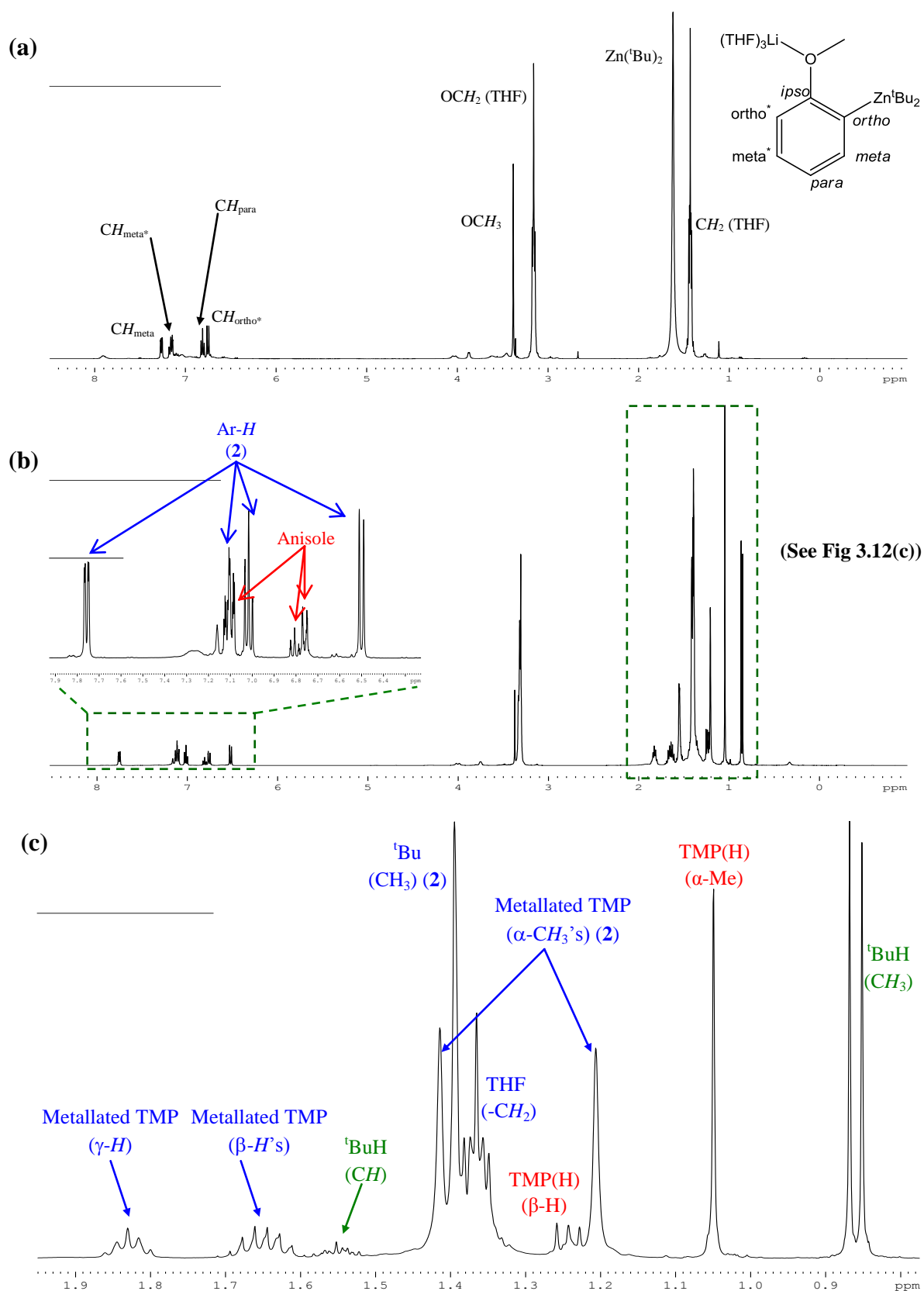
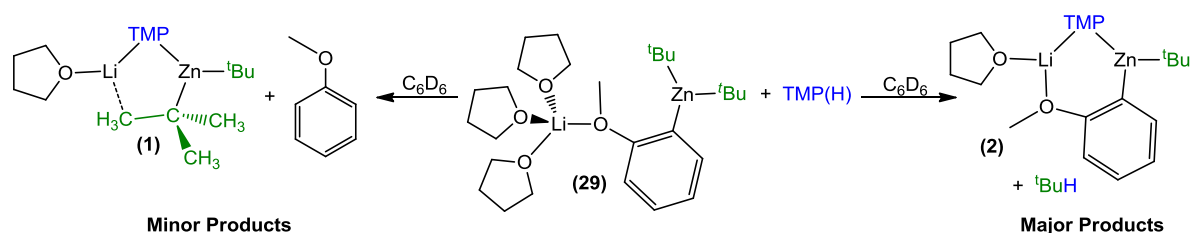


Figure 3.10: Reaction of **29** with TMP(H) in d_6 -benzene, monitored by ^1H NMR (a) before addition of TMP(H), (b) 2 hours after addition of TMP(H), and (c) Expanded aliphatic region 2 hours after addition of TMP(H).

To the NMR tube was added one equivalent of TMP(H), and the reaction mixture analysed after 2 hours (**Figure 3.10(b)**). In this case, analysis of the aliphatic region revealed the presence of only one set of α -methyl resonances for metallated TMP, with two distinct singlets at δ 1.21 and δ 1.40 ppm consistent with a bridging TMP ligand, along with a further peak at δ 1.04 ppm corresponding to the α -methyl groups from some remaining unreacted TMP(H) (**Figure 3.10(c)**).

Analysis of the aromatic region again showed the presence of two different sets of aromatic resonances. A set of four multiplets (δ 7.76, 7.11, 7.02 and 6.50 ppm) indicated the presence of a molecule of *ortho*-metallated anisole, which were different to those of observed for **29** (δ 7.26, 7.14, 6.80, 6.74 ppm), but consistent with those found for the product of direct AMMZn of anisole by the lithium TMP-zincate (**1**), [(THF)Li(TMP)(*o*-C₆H₄OMe)Zn^tBu] (**2**) (δ 7.94, 7.22, 7.16, 6.56 ppm).^[41] In addition, there were three resonances at δ 7.11, 6.84 and 6.79 ppm indicating the presence of free anisole, which was the minor product of this reaction, with integration of the aromatic resonances indicating a ratio of approximately 4:1 between the product [(THF)Li(TMP)(*o*-C₆H₄OMe)Zn^tBu] (**2**) and free anisole. Thus, the expected reaction of **29** with TMP(H) to form **2** is favoured over the reaction of TMP(H) with the metallated anisole ligand to regenerate **1** and anisole (**Scheme 3.18**), showing a contrasting reactivity pattern to that which was observed for the dimethyl derivative **26**. Further confirmation that the reaction of **29** and TMP(H) had proceeded to form **2** is the presence of a distinct doublet at δ 0.87 ppm and a multiplet at δ 1.56 ppm (**Figure 3.10(c)**), which can be assigned to the CH₃ and CH groups respectively of isobutane (^tBuH), the expected by-product of this reaction (**Scheme 3.18**).



Scheme 3.18: Reaction of **29** with TMP(H), forming **2** and isobutane preferentially, over **1** and anisole.

Since **2** is the product obtained from direct zincation of anisole by [(THF)Li(TMP)Zn^tBu₂] (**1**), these results constitute the first experimental evidence to support the two-step

mechanism, previously suggested by Uchiyama's theoretical studies. Thus, zincate (**1**) first acts as an amido base, metallating anisole to yield **29** and liberating TMP(H), which can in turn react in a second step to afford the final metallated species [(THF)Li(TMP)(*o*-C₆H₄OMe)Zn^tBu] (**2**) and release isobutane. The reaction shows overall alkyl basicity, although kinetically it is the TMP ligand which has removed the proton from the aromatic molecule.

These studies also highlight the important role that the alkyl groups play in the reactivity of dialkyl TMP-zincates [(THF)Li(TMP)ZnR₂]. The increase in the basicity of the R group in **29** (^tBu) compared to **26** (Me) allows the TMP(H) to be deprotonated preferentially by the alkyl group, to give the final metallated product **2**, while the alternative reaction, where TMP replaces the molecule of *ortho*-metallated anisole to regenerate zincate **1** and anisole is only a minor pathway in this reaction. In contrast when the reaction between the dimethyl intermediate **26** and TMP(H) is performed in the same solvent, the TMP(H) reacts preferentially with the metallated anisole ligand, regenerating [(THF)Li(TMP)ZnMe₂] (**32**) and releasing anisole.

In order to evaluate the effect of the donor solvent in these experiments the reaction of **29** with TMP(H) was studied in deuterated THF. Thus, compound **29** was prepared *in situ*, followed by removal of the solvent and volatiles *in vacuo*. The product was then dissolved in d₈-THF, and analysed by ¹H, ¹³C{¹H} and ⁷Li NMR spectroscopy. Surprisingly, the ¹H NMR spectrum of **29** (**Figure 3.11**) was found to be much more complicated in a d₈-THF solution than in a d₆-benzene solution. The *tert*-butyl peak still appeared as a singlet, in this case at δ 0.94 ppm compared with δ 1.58 ppm in d₆-benzene, but the aromatic region showed two different sets of resonances for the *ortho*-metallated anisole fragment. One set (at δ 7.50, 6.85, 6.71 and 6.59 ppm) was much broader than the other (at δ 7.31, 6.68, 6.53 and 6.43 ppm), and confirmation that these resonances corresponded to two different species was provided by COSY NMR. The spectrum also showed two different singlets for two distinct methoxy groups at δ 3.69 and 3.66 ppm.

It should also be noted that the ¹H spectrum of **29** in d₈-THF showed a small amount of free anisole (**Figure 3.11**). However, this was most likely caused by some partial hydrolysis of **29** by the solvent. Although the d₈-THF is freeze-dried over molecular sieves to remove any

traces of water or oxygen, it is very difficult to ensure that this solvent is perfectly dried due to its high polarity. However, a sample of **29** dissolved in d_8 -THF was monitored by ^1H NMR over 4 days, and apart from the initial traces of free anisole no further hydrolysis (or decomposition) of **29** was observed.

* = metallated anisole (I) * = metallated anisole (II) * = free anisole

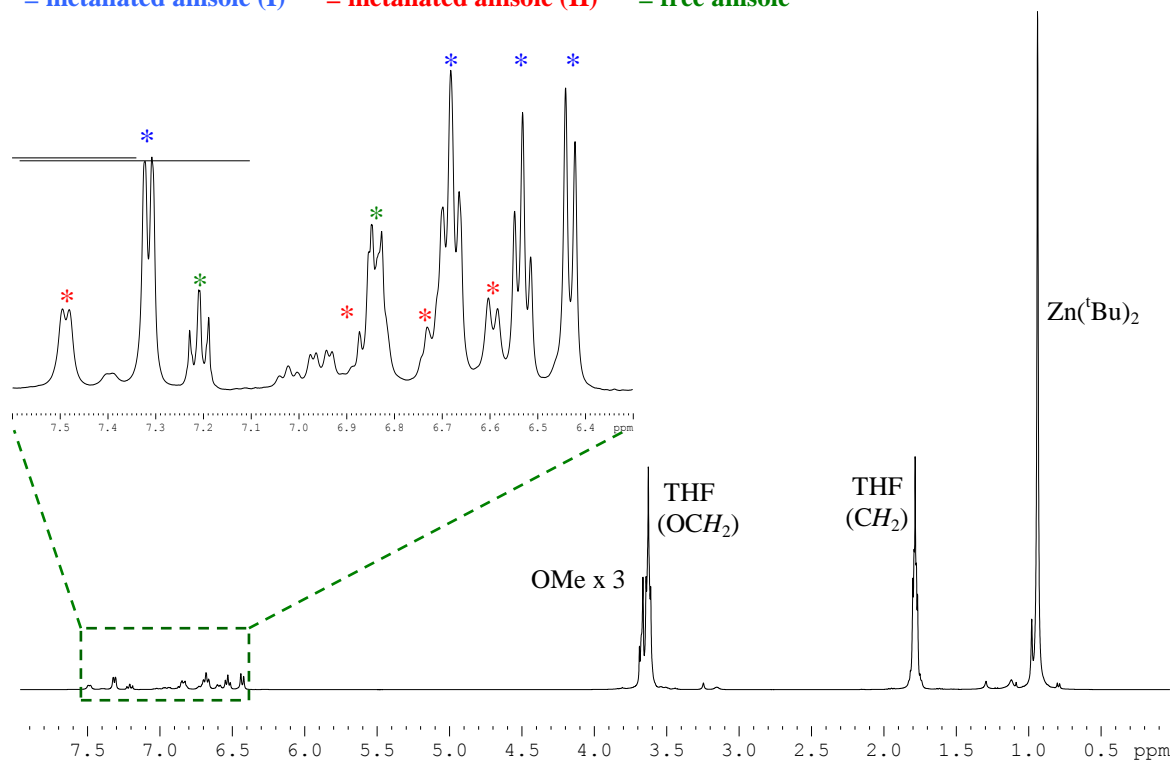
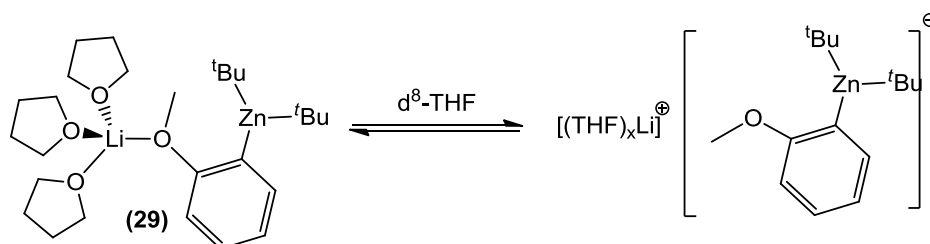


Figure 3.11: Crude ^1H NMR spectrum of **29** in d_8 -THF.

In order to rule out the possibility that these additional resonances observed in the aromatic region were caused by an impurity, the *in situ* preparation of **29** was repeated and an aliquot of the solution analysed by ^1H NMR in d_6 -benzene solution. The spectrum showed the same ^1H NMR spectrum as previously discussed for **29** in this deuterated solvent with a single set of resonances (four multiplets) for the metallated anisole fragment. A second aliquot was analysed in d_8 -THF solution, which again showed the aforementioned two sets of resonances in the aromatic region.

A possible explanation for the complex ^1H NMR spectrum of **29** in d_8 -THF solution could be that in a strong donor solvent such as THF this species exists in equilibrium between its CIP structure $[(\text{THF})_3\text{Li}(o\text{-C}_6\text{H}_4\text{OMe})\text{Zn}^t\text{Bu}_2]$, and a SSIP species $[\{\text{Li}(\text{THF})_x\}^+\{\text{Zn}(o\text{-C}_6\text{H}_4\text{OMe})^t\text{Bu}_2\}^-]$ (**Scheme 3.19**). This would account for the presence of two different sets of

metallated anisole resonances, as in the solvent-separated structure anisole bonds only to the zinc, but in the contacted ion pair structure it is also coordinated to the lithium, so it can be expected that different chemical shifts would be observed for these metallated anisole fragments. This equilibrium is also consistent with the presence of a single resonance for the *tert*-butyl groups (δ 0.94 ppm), which suggests that the alkyl ligands remain in a similar environment, bound terminally to zinc, in both of the equilibrium species.



Scheme 3.19: Proposed equilibrium of **29** in d_8 -THF solution.

Having confirmed the purity of **29** in d_8 -THF solution (**Figure 3.11**), one equivalent of TMP(H) was added to the NMR tube, and the reaction mixture analysed by ^1H and ^7Li NMR spectroscopy after two hours. The ^1H NMR spectrum (**Figure 3.12(a)**) indicated there were two different types of metallated TMP by the presence of two sets of inequivalent α -methyl resonances at δ 1.21 and 0.92 ppm, and δ 1.06 and 0.97 ppm (**Figure 3.12(b)**), confirming that the TMP(H) had reacted with **29** to form two different products. (N.B. In **Figure 3.12(b)** the α -methyl resonances at δ 1.06 and 0.92 ppm cannot be seen clearly as they overlap with the ^tBu and TMP(H) peaks respectively). Analysis of the aromatic region again showed the presence of two sets of *ortho*-metallated anisole resonances, which were observed at slightly different chemical shifts to those of **29** (**Figure 3.13(a)** and **(b)**). As seen for **29** one set of peaks (at δ 7.35, 6.65, 6.52 and 6.44 ppm) were much broader than the other set (at δ 7.48, 7.07, 6.86 and 6.74 ppm). In addition to the two sets of resonances for metallated anisole, a substantial amount of free anisole was also present, with a triplet at δ 7.21 and a multiplet at δ 6.84 ppm.

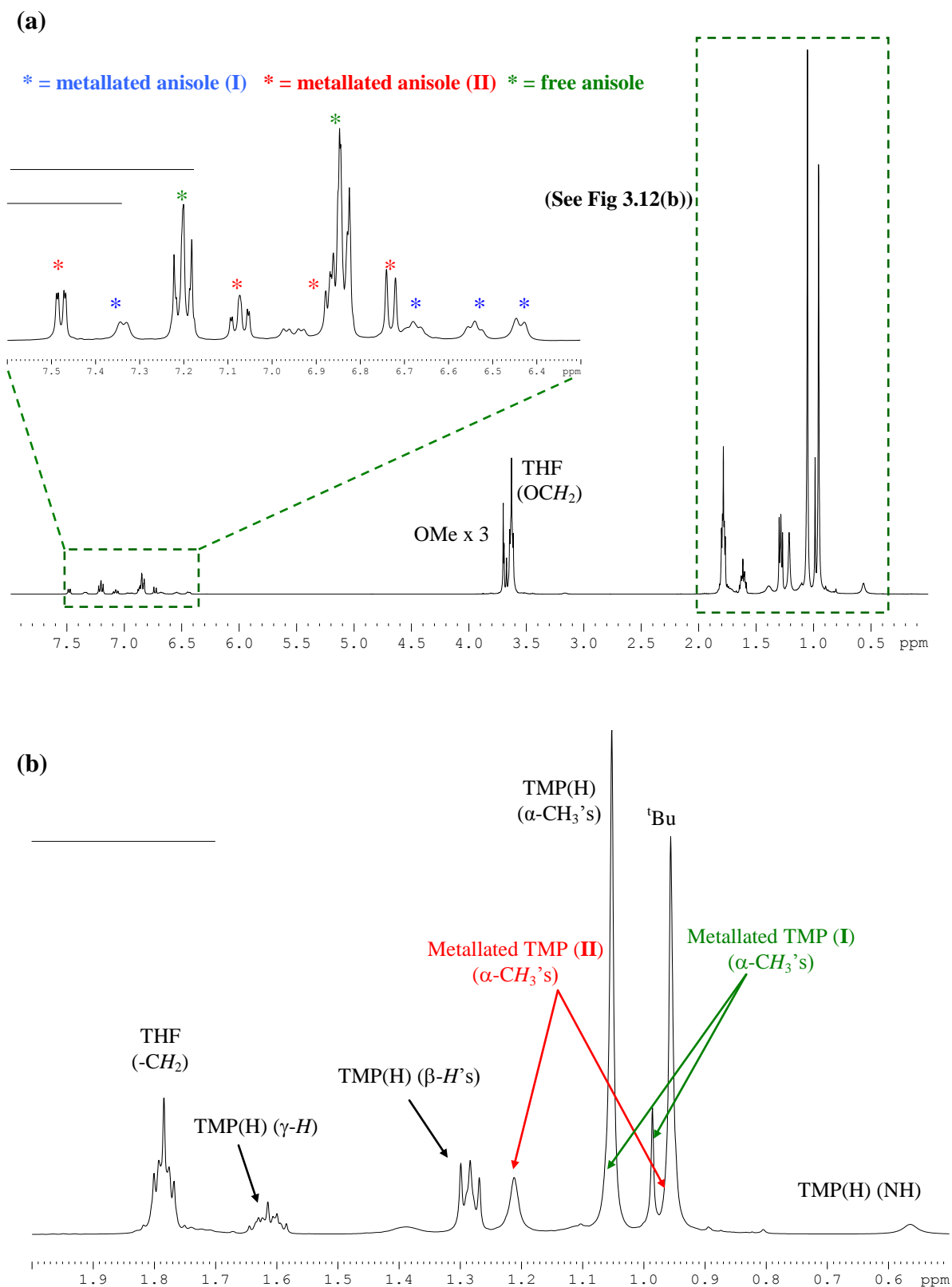


Figure 3.12: Reaction of **29** and TMP(H) in d_8 -THF monitored by ^1H NMR (a) after 2 hours, and (b) expanded aliphatic region of the ^1H NMR spectrum after 2 hours.

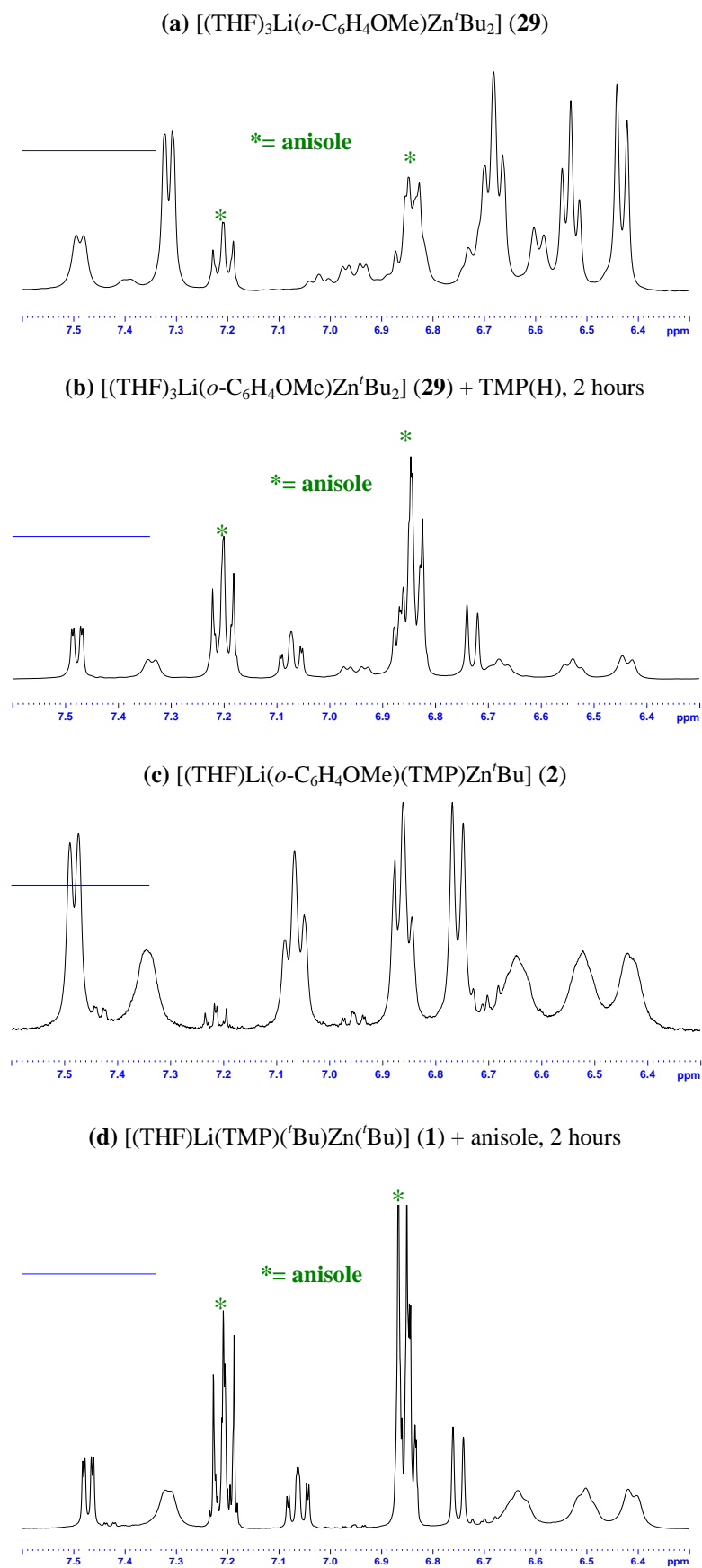
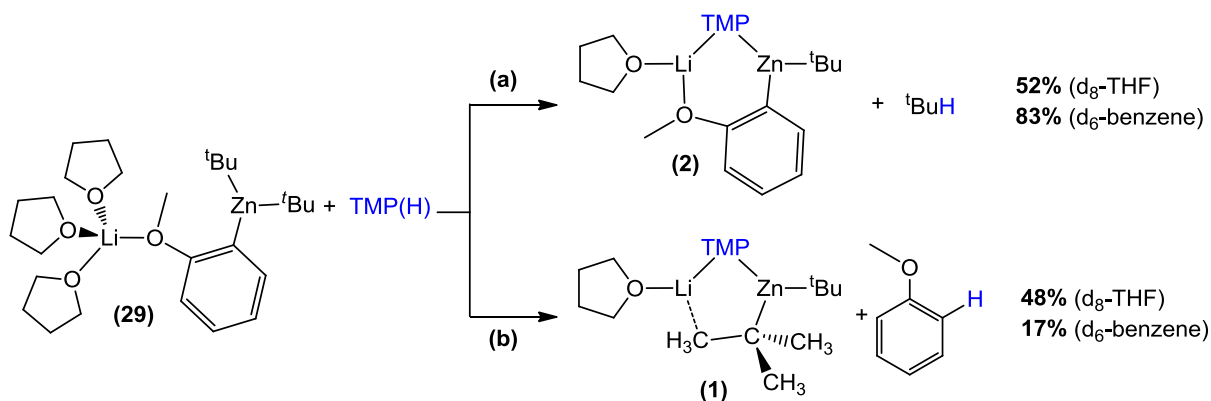


Figure 3.13: Aromatic region of the ^1H NMR spectra in d_8 -THF of (a) **29** (b) **29** + TMP(H) after 2 hours, (c) **2** and (d) **1** + anisole after 2 hours.

In order to confirm that TMP(H) had reacted with **29** to form the expected product [(THF)Li(TMP)(*o*-C₆H₄OMe)Zn^tBu] (**2**), some isolated crystals of **2** were dissolved in d₈-THF and analysed by ¹H NMR spectroscopy. Interestingly, as was observed for **29**, the ¹H NMR spectra of **2** in d₈-THF solutions displayed two different species in the aromatic region, with four sharp resonances (δ 7.48, 7.07, 7.86 and 6.75 ppm) and four broad resonances (δ 7.35, 6.66, 6.52 and 6.43 ppm). However, if the same crystalline material is analysed in d₆-benzene solution, only one set of aromatic resonances are observed (δ 7.94, 7.22, 7.16, 6.56 ppm).^[41] This again hints at the existence of an equilibrium in polar solvents such as THF, where **2** can exist as a CIP species [(THF)Li(TMP)(*o*-C₆H₄OMe)Zn^tBu] and as a SSIP species [$\{\text{Li}(\text{THF})_x\}^+ \{\text{Zn}(\text{TMP})(\textit{o}\text{-C}_6\text{H}_4\text{OMe})^t\text{Bu}\}^-$], similar to the equilibrium which existed for **29** in THF solutions (**Scheme 3.19**). Comparison of ¹H NMR spectrum of **2** in d₈-THF with that of reaction between **29** and TMP(H), and in particular the aromatic region (**Figure 3.13(b)** and **(c)**) shows good correlation, confirming that **2** is one of the species formed during the reaction of **29** with TMP(H), where TMP had replaced one of the ^tBu groups of **29** to form **2** and isobutane (^tBuH) (**Scheme 3.20(a)**). In this case, unlike when d₆-benzene is used as the solvent, the formation of ^tBuH could not be detected, most likely due to the low solubility of this non-polar gas in a polar solvent such as THF.

In addition to the aromatic resonances corresponding to the formation of **2**, the ¹H NMR spectrum from the reaction of **29** and TMP(H) after 2 hours (**Figure 3.12(a)**) also showed the presence of free anisole (δ 7.21 and 6.84 ppm), in a much more significant ratio to that observed in the initial spectrum of **29** (**Figure 3.11**). As mentioned above, a study of **29** in d₈-THF solution over 4 days had shown that no further hydrolysis had occurred after the initial addition of the solvent. Therefore, the increase in the moiety of free anisole in this spectrum must have been a result of TMP(H) reacting with **29** via the alternate pathway (with the molecule of metallated anisole) to give free anisole and lithium zincate (**1**) (**Scheme 3.20(b)**). Thus, the reaction between **29** and TMP(H) can again proceed via two separate pathways, either reacting with one of the *tert*-butyl ligands (to form **2** and isobutane) or with the *ortho*-metallated anisole ligand (to form **1** and anisole) (**Scheme 3.20**). Although this same dual reactivity was observed when the reaction was performed in d₆-benzene, the ratio of metallated anisole to free anisole observed in this non-polar solvent was ~4:1, compared to a ratio of ~1:1 when the reaction is performed in the highly polar solvent d₈-THF.



Scheme 3.20: Reaction of **29** and TMP(H) in d_8 -THF/ d_6 -benzene to form (a) [(THF)Li(TMP)(*o*-C₆H₄OMe)Zn^tBu] (**2**) and isobutane and (b) [(THF)Li(TMP)Zn^tBu₂] (**1**) and anisole.

These results also have implications for the metallation of anisole by [(THF)Li(TMP)Zn^tBu₂] (**1**), whereby if the reaction does proceed via the proposed two step mechanism then the overall yield would be lower when carried out in a polar solvent such as THF than it would in a non-polar solvent such as benzene or hexane. To investigate this possibility, isolated crystals of **1** were reacted with anisole in d_8 -THF, with the reaction monitored by ¹H NMR spectroscopy. After 2 hours at room temperature, the metallation of anisole to form **2** had proceeded in a yield of only 62% (as determined by comparison of the integration of free anisole to metallated anisole - **Figure 3.13(d)**). However, when the reaction is performed in hexane under the same conditions the metallation of anisole proceeds in an almost quantitative yield. Previous reports from Kondo and Uchiyama which probed the metallating ability of **1** in bulk THF employed two equivalents of the zincate to deprotonate several aromatic substrates in high yields.^[47] Thus, when the reaction of **1** with anisole was repeated in d_8 -THF using two equivalents of the zincate **1**, the metallated product **2** was obtained in an improved yield of 88%.

Collectively these studies on the reactivity of **29** with TMP(H) in both d_6 -benzene and d_8 -THF provide tangible experimental evidence that the metallation of aromatic substrates by lithium TMP-zincates can proceed via a two step mechanism, as previously predicted by DFT studies.^[102-105] However, as well as the reacting with TMP(H) to generate the final metallated species **2**, the intermediate species **29** can also react via a second pathway, where TMP(H) can displace the metallated anisole ligand to regenerate the zincate **1** and anisole. This unexpected reaction of **29** with TMP(H) occurs to a much greater extent in THF (48%) than it does in a

non-polar solvent such as benzene (17%) (**Scheme 3.20**). As a result, when the AMMZn of anisole by **1** is performed in THF solutions, two equivalents of the zincate are required to achieve a high yield of metallation (88%), whereas in hexane a similar yield can be obtained by employing only one equivalent of the zincate.

3.3.5 Disproportionation process of **26** and **29** to $[(\text{THF})_2\text{Li}_2\text{Zn}(o\text{-C}_6\text{H}_4\text{OMe})_4]$ (**27**)

As previously mentioned, when $[(\text{THF})_2\text{Li}(o\text{-C}_6\text{H}_4\text{OMe})\text{ZnMe}_2]$ (**26**) and $[(\text{THF})_3\text{Li}(o\text{-C}_6\text{H}_4\text{OMe})\text{Zn}^t\text{Bu}_2]$ (**29**) are placed in hexane a white precipitate is formed almost instantaneously, which could then be recrystallised from a hexane/toluene solution yielding the tetraorganozincate $[(\text{THF})_2\text{Li}_2\text{Zn}(o\text{-C}_6\text{H}_4\text{OMe})_4]$ (**27**) in an average crystalline yield of 9%. Full characterisation of **27** was carried out using ^1H , ^7Li and $^{13}\text{C}\{^1\text{H}\}$ NMR spectroscopy and X-ray crystallography. Analysis of the crystalline material by X-ray crystallography revealed the structure to be the homoleptic lithium tetra-aryl-zincate $[(\text{THF})_2\text{Li}_2(o\text{-C}_6\text{H}_4\text{OMe})_4\text{Zn}]$ (**27**) (**Figure 3.14**). Exhibiting a CIP structure, **27** consists of four molecules of *ortho*-metallated anisole, each bonded directly to zinc, whereas each lithium atom bonds to two of these *ortho*-metallated anisole anions through the oxygen of the methoxy group, and to one molecule of THF.

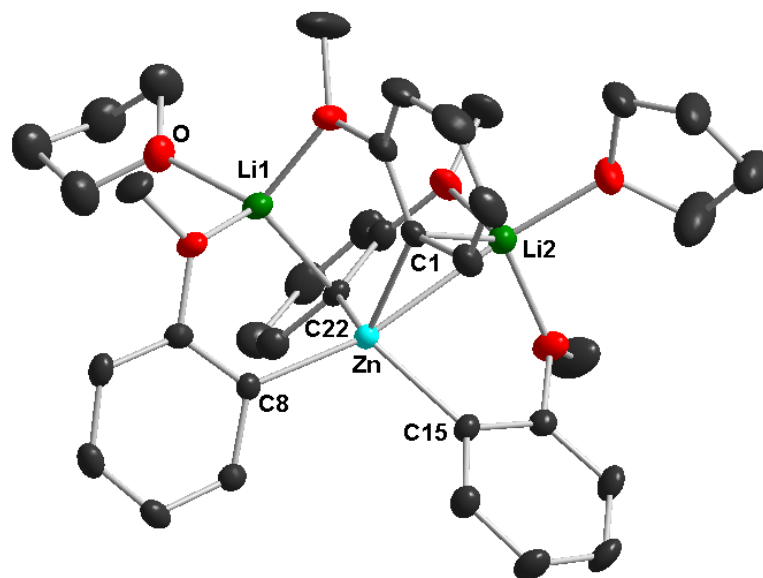


Figure 3.14: Molecular structure of **27** with 40% probability ellipsoids. Hydrogen atoms have been omitted for clarity. Selected bond distances (\AA) and bond angles ($^\circ$): Zn-C1 2.150(3), Zn-C8 2.075(3), Zn-C15 2.072(3), Zn-C22 2.148(3), Li1-C22 2.373(6), Li2-C1 2.308(6); C22-Zn-C15 111.65(10), C22-Zn-C8 103.12(11), C22-Zn-C1 113.34(10), C15-Zn-C8 112.96(11), C15-Zn-C1 103.12(10), C8-Zn-C1 113.01(10), Li2-Zn-Li1 91.10(15).

Comparison of the Zn-C bond lengths shows two longer (2.148(3) and 2.150(3) Å) and two shorter contacts (2.072(3) and 2.075(3) Å). This can be explained by the fact that in the crystal structure of **27** each of the lithium atoms forms an additional π -interaction with the *ortho* carbon of one of the molecules of metallated anisole (Li2-C1 and Li1-C22), to give two different bonding environments for the $\{o\text{-C}_6\text{H}_4\text{OMe}\}^-$ ligand. For those *ortho*-deprotonated anisole fragments which form these additional Li- π contacts the Zn-C bond is slightly elongated (Zn-C1 2.148(3), Zn-C4 2.150(3)) when compared to the Zn-C bonds where the *ortho* carbon of the $\{o\text{-C}_6\text{H}_4\text{OMe}\}^-$ group is bonded solely to zinc (Zn-C2 2.072(3), Zn-C3 2.075(3) Å). Regarding the Li-C bond distances, the values found for the Li1-C22 and Li2-C1 interactions (2.373(6) and 2.308(6) Å respectively) fall within the range of the Li-C bond distances found in lithiated anisole $[(\text{THF})_2\text{Li}_4(o\text{-C}_6\text{H}_4\text{OMe})_4]$ (**25**) (2.14(11)-2.49(13) Å) (see **Chapter 7.3.8 – Experimental Procedures** for details).

The additional π -interactions between Li and the anisole ring have further consequences for the crystal structure of **27**. Most tetraorganozincates (LiZnR_4) adopt linear conformations, where the Li1-Zn-Li2 vector is close to 180° . However, in the case of **27** these Li- C_{ortho} contacts distort the structure from its linear arrangement, resulting in **27** possessing a much more acute Li1-Zn-Li2 vector of $91.10(15)^\circ$. A search of the Cambridge Crystallographic Database (CCDB) for zincates of similar chemical formula to **27** revealed a range of Li-Zn-Li vectors (**Table 3.3** and **Figure 3.15**), the majority of which tend towards linearity, with three of the examples approaching almost perfect linearity ($172.06\text{-}177.83^\circ$). The smallest Li-Zn-Li vector found was 121.91° for $[(\text{Et}_2\text{O})_2\text{Li}_2(\mu_2\text{-}^t\text{BuN})_2\text{BPh})_2\text{Zn}]$,^[110] which is still significantly larger than that of **27**.

Compound	Li-Zn-Li Vector ($^\circ$)
$[(\text{THF})_2\text{Li}_2\text{Zn}(o\text{-C}_6\text{H}_4\text{OMe})_4]$ (27)	91.10
$[(\text{Et}_2\text{O})_2\text{Li}_2(\mu_2\text{-}^t\text{BuN})_2\text{BPh})_2\text{Zn}]$ ^[110]	121.91
$[(\text{TMEDA})_2\text{Li}_2(\mu_2\text{-}(\text{CH}_2)_4)_2\text{Zn}]$ ^[111]	172.06
$[\text{Li}_2(\mu_2\text{-C}_6\text{H}_4\text{CH}_2\text{NMe}_2)_4\text{Zn}]$ ^[112]	177.83
$[(\text{TMEDA})_2\text{Li}_2(\mu_2\text{-CH}_2\text{Si}(\text{CH}_3)_2\text{CH}_2)_2\text{Zn}]$ ^[113]	136.32
$[(\text{TMEDA})_2\text{Li}_2(\mu_3\text{-C}_5\text{H}_{10})_2\text{Zn}]$ ^[114]	173.58
$[(\text{TMEDA})_2\text{Li}_2\text{Zn}(\text{C}\equiv\text{C-Ph})_4]$ ^[115]	146.70

Table 3.3: Comparison of Li-Zn-Li vectors ($^\circ$) in selected tetraorganozincates.

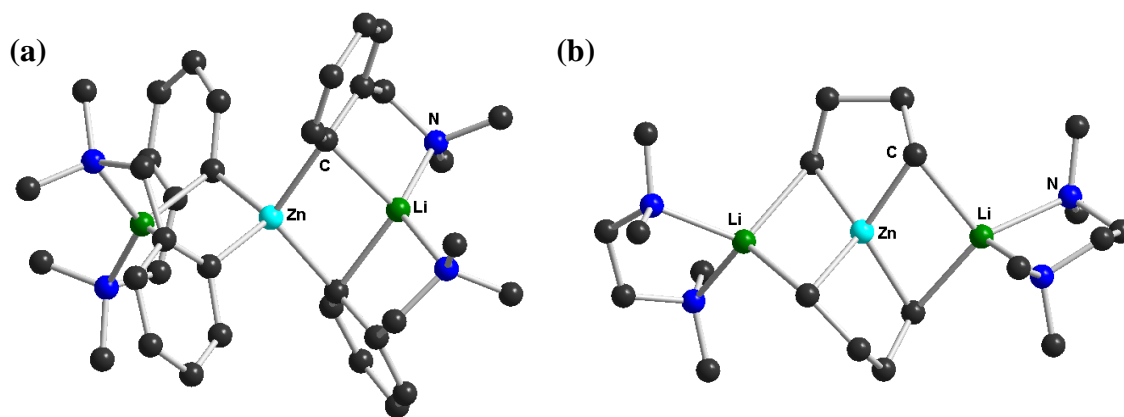
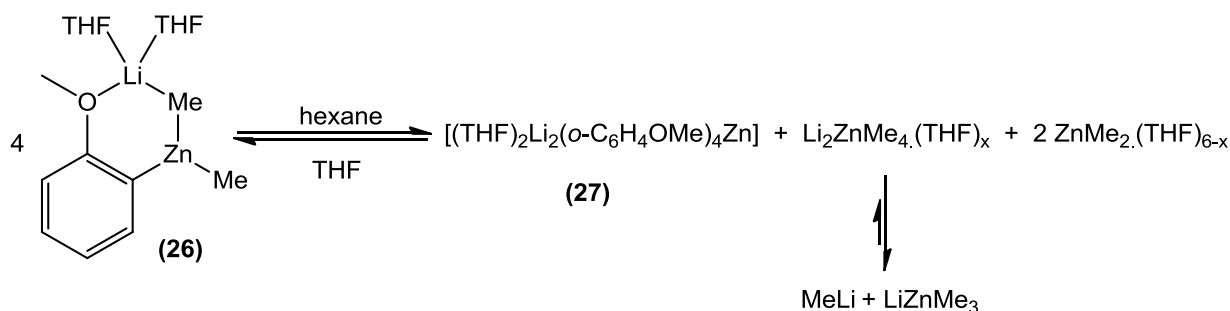


Figure 3.15: Molecular structure of (a) $[(\text{TMEDA})_2\text{Li}_2(\mu_2\text{-(CH}_2)_4)_2\text{Zn}]^{[111]}$ and (b) $[\text{Li}_2(\mu_2\text{-C}_6\text{H}_4\text{CH}_2\text{NMe}_2)_4\text{Zn}]^{[112]}$ displaying Li-Zn-Li bond angles of 177.83 and 172.06° respectively.

Despite the two different coordination modes of the metallated anisole ligand in the molecular structure, analysis of crystals of **27** in d_6 -benzene by ^1H and ^7Li NMR spectroscopy revealed all four molecules to be equivalent. Thus, the ^1H NMR spectrum displayed a single set of four multiplets at δ 8.35, 7.20, 7.10 and 6.73 ppm and a singlet at δ 3.24 ppm corresponding to the four aromatic protons and the methoxy group of *ortho*-metallated anisole respectively. This may be as a result of two factors; (i) in solution the π -interactions between Li and anisole are not retained, making the four equivalent molecules of *ortho*-metallated anisole equivalent, or (ii) a dynamic process is taking place where the two different types of $\{\text{o-C}_6\text{H}_4\text{OMe}\}^-$ fragments present in the molecular structure of **27** are rapidly exchanging. In addition, two multiplets at δ 1.23 and 3.16 ppm for the THF molecules were observed, and integration indicated a ratio of metallated anisole to THF of 2:1, as predicted by the molecular structure of **27**. The presence of lithium in the molecule was confirmed by the ^7Li NMR spectrum which showed a singlet at δ 0.96 ppm.

Turning to the possible reactions involved in the formation of **27**, NMR analysis of the filtrate solution revealed traces of **27** were present along with a large singlet at δ -0.28 ppm, which can be assigned to methyl groups bonded to zinc (see later), and two multiplets at δ 1.23 and 3.23 ppm for coordinated THF. Given that **27** precipitates readily from hexane solutions of $[(\text{THF})_2\text{Li}(\text{o-C}_6\text{H}_4\text{OMe})(\text{Me})\text{Zn}(\text{Me})]$ (**26**), this suggests that a disproportionation process must be taking place (**Scheme 3.21**) to afford **27** and “ $\text{Li}_2\text{Zn}_3\text{Me}_8$ ”. The latter will probably exist in solution as a mixture of the tetraorganozincate (Li_2ZnMe_4) and dimethylzinc (ZnMe_2). However, it is known that in solution, Li_2ZnMe_4 lies in equilibrium with LiZnMe_3 and MeLi , with the equilibrium lying far to the side of the triorganozincate.^[116]



Scheme 3.21: Possible reaction scheme for the disproportionation of **26**.

As a result, the filtrate is likely to contain a number of organometallic species in equilibrium, including MeLi, ZnMe₂, LiZnMe₃ and Li₂ZnMe₄, which would be consistent with the resonances observed at δ -0.28 ppm, which along with two multiplets at δ 1.23 and 3.23 ppm would indicate these organometallic species are solvated by THF. The chemical shift observed for the methyl groups is further upfield than those found for methyl lithium (-1.42 ppm) and in the same region as the chemical shifts of the other likely species present in solution (ZnMe₂, LiZnMe₃ and Li₂ZnMe₄) (**Table 3.4**). The presence of only one resonance for the methyl groups in the ¹H NMR spectrum must be the result of a rapid exchange process between the different organometallic species present in solution. Interestingly this dismutation process appears to be reversible, and when hexane is added to a solution of **26** in THF, compound **27** precipitates as a white solid. However if at this stage the solvent is removed under vacuum and the resulting residue is dissolved in THF solution, analysis of the solution by ¹H and ⁷Li NMR spectroscopy reveals that only compound **27** is present (**Scheme 3.21**). Furthermore, the low yields obtained for **27** (average isolated crystalline yield 9%) can be explained by its formation through the disproportionation process outlined in **Scheme 3.21**, where the maximum possible yield of **27** is only 25%.

Compound	δ_{Me} (ppm)
LiMe	-1.42
ZnMe ₂	-0.52
LiZnMe ₃	-0.41
Li ₂ ZnMe ₄	-0.45
Filtrate of 27	-0.29

Table 3.4: Comparison of ¹H NMR resonance's of the filtrate of **27** with a variety of methyl lithium and methyl zinc species in d₆-benzene.

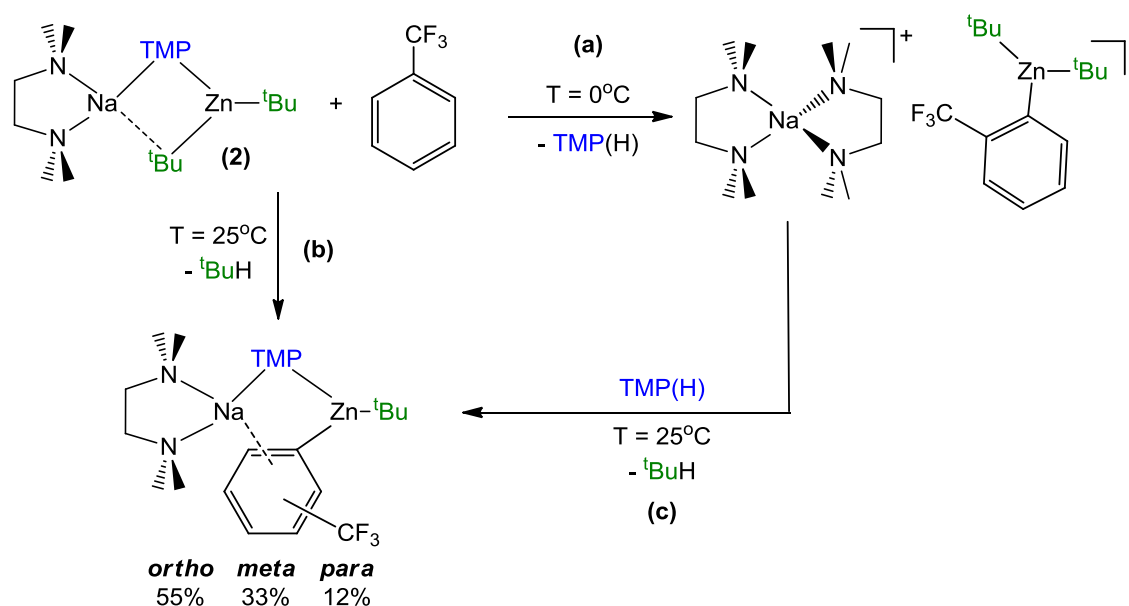
3.4 Conclusions

The new dialkyl(aryl) lithium zincates [(THF)₂Li(*o*-C₆H₄OMe)ZnMe₂] (**26**) and [(THF)₃Li(*o*-C₆H₄OMe)Zn^tBu₂] (**29**) have been prepared using a co-complexation approach by reacting lithiated anisole [Li₄(*o*-C₆H₄OMe)₄(THF)₂] (**25**) with the relevant dialkylzinc compound, and characterised in solution by NMR spectroscopy. Compounds **26** and **29** are stable in THF solutions but in a less polar solvent such as hexane they disproportionate to form the tetraorganozincate [(THF)₂Li₂Zn(*o*-C₆H₄OMe)₄] (**27**) whose structure has been determined by X-ray crystallography. The molecular structures of the TMEDA solvate of **26** and the PMDETA solvate of **29** have also been characterised by X-ray crystallography, showing different structural motifs. In [(TMEDA)Li(*o*-C₆H₄OMe)ZnMe₂] (**28**) the two metals are connected through the metallated anisole molecule which binds in an ambidentate fashion (through the *ortho* carbon to zinc and the oxygen to lithium) and also through one of the methyl groups, forming a six-membered ring. On the other hand, [(PMDETA)Li(*o*-C₆H₄OMe)Zn^tBu₂] (**30**) displays an open structure where anisole connects the two metals (in the same ambidentate fashion as **28**) but the *tert*-butyl groups are solely bonded to zinc.

Following the successful preparation of compounds **26** and **29**, their reactivity with TMP(H) was investigated, in an attempt to replicate the second step of the two-step mechanism previously predicted by theoretical studies.^[102-105] The results of these studies provided the first experimental evidence that lithium zincate [(THF)Li(TMP)Zn^tBu₂] (**1**) operates via a two-step mechanism for the AMMZn of anisole. Thus, anisole is first *ortho*-metallated by the TMP ligand of **1** to yield the intermediate [(THF)₃Li(*o*-C₆H₄OMe)Zn^tBu₂] (**29**) along with TMP(H), which could then react in a second step giving rise to the final metallated species [(THF)Li(*o*-C₆H₄OMe)(TMP)Zn^tBu] (**2**) and isobutane. However, the intermediate species can also react via a second pathway, where TMP(H) instead protonates the metallated anisole ligand to regenerate zincate **1** and anisole. It appears that the role of solvent in these reactions is particularly important, as in non-polar benzene or hexane, the competing reversal of the first step of the reaction only occurs to a small extent, but in a polar solvent such as THF the two possible reactions of the intermediate species **29** with TMP(H) occur in a ratio of ~1:1.

These reactivity studies also highlighted the importance of the alkyl groups in tuning the reactivity of lithium dialkyl-TMP zincates [(THF)Li(TMP)ZnR₂]. It could be expected that as

it is the amido ligand which carries out the initial metallation of the aromatic substrate then the alkyl ligands must play only a spectating role in these reactions. However, these results have revealed that the alkyl ligands play an important part in the final outcome of the metallation, by reacting with the TMP(H) released in the first step of the reaction to form the final metallated product. Thus, when methyl ligands are present, the reaction favours the regeneration of the starting zincate and anisole in both polar and non-polar solvents. However, more basic *tert*-butyl groups favour the formation of the final product of AMMZn [(THF)Li(TMP)(*o*-C₆H₄OMe)Zn^tBu] (**2**) and isobutane.



Scheme 3.22: Reaction of **2** with trifluoromethyl benzene at (a) 0°C to form the kinetic product $[\{(TMEDA)_2Na\}^+\{Zn(o-C_6H_4CF_3)^tBu_2\}^-]$, (b) 25°C to form the thermodynamic product $[(TMEDA)Na(TMP(o/m/p-C_6H_4CF_3)Zn^tBu)]$ and (c) reaction of the kinetic product with TMP(H) to form $[(TMEDA)Na(TMP(o/m/p-C_6H_4CF_3)Zn^tBu)]$.

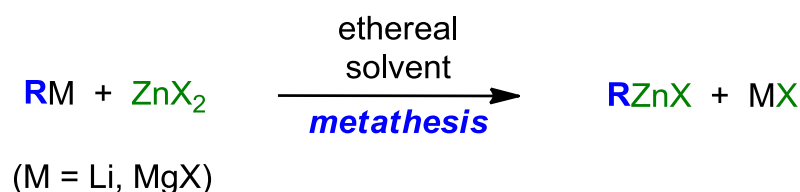
Lending support to these results, a recent study into the reaction of trifluoromethyl benzene with the sodium TMP-zincate **3** at 0°C allowed the isolation of a genuine kinetic intermediate of the AMMZn reaction, solvent separated zincate $[\{(TMEDA)_2Na\}^+\{Zn(o-C_6H_4CF_3)^tBu_2\}^-]$ (**Scheme 3.22**).^[117] Contrastingly, if the reaction is performed at room temperature a different type of product is obtained, where both metals (Na and Zn) are connected by a bridging TMP ligand and molecule of trifluoromethyl benzene, present in a mixture of *ortho*-, *meta*- and *para*-metallated regioisomers (ratio 55:33:12 respectively). Furthermore, the kinetic product could be reacted with TMP(H) to yield a mixture of the *ortho*-, *meta*- and *para*-metallated

organometallic species [(TMEDA)Na(TMP(*o/m/p*-C₆H₄CF₃))Zn^tBu], along with free trifluoromethyl benzene (**Scheme 3.22**). These results not only provide further evidence of the two-step mechanism, but they also show for the first time that the second step of the reaction can tune the overall regioselectivity of the reaction. Furthermore, the regeneration of the starting materials of the reaction, trifluoromethyl benzene and **3**, is also observed on addition of TMP(H), showing that the competitive reaction pathway where TMP(H) reacts with the metallated aromatic substrate instead of a ^tBu group, also occurs in this reaction (**Scheme 3.22**).

Chapter 4: Investigating metathesis reactions of Grignard reagents with ZnCl₂: Introducing Magnesium-Zinc Hybrids

Organomagnesium compounds such as Grignard and dialkylmagnesium reagents (RMgX, MgR₂) are, along with organolithium reagents (RLi), the most commonly used polar organometallic reagents in synthesis. Their easy preparation, relative stability and high reactivity make them excellent reagents for participating in several organic transformations such as nucleophilic addition to carbonyl compounds, C=C bonds, imines and nitriles,^[118] as well as transition-metal catalysed cross-coupling reactions.^[118b] Their high reactivity can be attributed to the presence of relatively polar Mg-C bonds,^[119] which can also be an important drawback, resulting in low functional group tolerance.^[120]

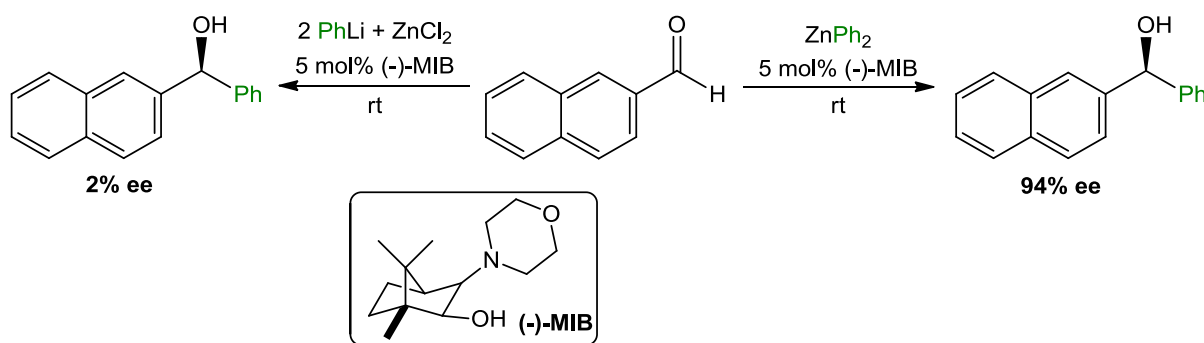
In contrast, organozinc reagents exhibit an enhanced functional group tolerance but significantly lower kinetic reactivity. As mentioned in **Chapter 1**, one of the most common methods for preparing organozinc reagents, together with the oxidative insertion of zinc into C-X bonds,^[14] is salt metathesis reactions of ZnCl₂ with more polar organometallic reagents (typically organolithium, RLi, or Grignard reagents, RMgX), which are usually performed in an ethereal solvent (e.g. THF, Et₂O) (**Scheme 4.1**).^[121] These reactions are favoured by the formation of ionic salts (e.g. MgCl₂ or LiCl) with high lattice energies.^[11d, 14]



Scheme 4.1: Metathesis approach for the preparation of organozinc reagents.

Usually, the relevant organozinc reagent is prepared *in situ*, followed by addition of the desired organic substrate, without isolation or purification of the organometallic compound. More often than not the formation of inorganic salts (MgCl₂ or LiCl) as the co-product of these reactions, and their possible effects on the reactivity of the newly generated organozinc reagent is not studied or even considered. However, a series of recent studies have shown that far from being mere spectators, these inorganic salts can greatly influence, and in some ways also dictate, the reactivity of the newly generated organozinc reagent.

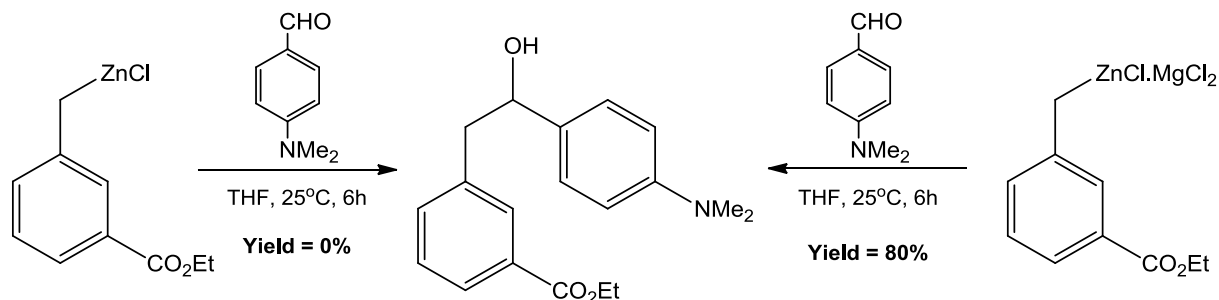
For example, Walsh has shown that the asymmetric arylation of naphthaldehyde by ZnPh₂ in the presence of catalytic amounts of a chiral amino alcohol ligand ((2*S*)-3-*exo*-(Morpholino)isoborneol, (-)-MIB) proceeds in a 94% ee, when commercial sources of the bis(aryl)zinc reagent are employed. However, if ZnPh₂ is prepared *in situ* by the salt metathesis reaction of ZnCl₂ with two equivalents of PhLi, then the reaction leads to the isolation of the racemic alcohol (only 2% ee) (**Scheme 4.2**).^[122] These low enantioselectivities have been attributed to the presence of LiCl (a by-product of the metathesis reaction) in the reaction mixture which promotes the background addition reaction of ZnPh₂ to the aldehyde faster than the catalytic asymmetric addition. However, the addition of the chelating diamine (*N,N,N',N'*-tetraethylethylenediamine – TEEDA) inhibits the effect of LiCl by sequestering the inorganic salt, and thus, a wide range of bis(aryl)zinc reagents prepared via salt metathesis reaction could be employed in the catalytic asymmetric arylation of a series of aldehydes in yields of 78-99% and 80-92% ee.^[122]



Scheme 4.2: Catalytic asymmetric arylation of naphthaldehyde by ZnPh₂ – commercial ZnPh₂ vs. ZnPh₂ prepared *in situ* via salt metathesis.

In contrast with these results, Knochel has reported that the presence of inorganic salts can also be advantageous, enhancing the reactivity of organozinc reagents. For example, addition of MgCl₂ to both organozinc halides and diorganozinc reagents can significantly improve their nucleophilicity, facilitating the selective addition reaction to a wide range of functionalised aldehydes and ketones, and even to CO₂.^[123] A representative example of which is the nucleophilic addition of (3-ethoxycarbonyl)benzylzinc chloride to 4-dimethylaminobenzaldehyde, which showed no reactivity at room temperature. However, the addition of one molar equivalent of MgCl₂ to the reaction mixture lead to the isolation of the expected secondary alcohol in an 80% yield (**Scheme 4.3**). Furthermore, Ellman has shown that the scope of this enhanced reactivity can be extended to the asymmetric synthesis of

amines by reaction of benzyl zinc reagents with *N-tert*-butanesulfinyl aldimines in the presence of sensitive functional groups such as nitriles, with excellent diastereomeric ratios.^[124]



Scheme 4.3: Reaction of (3-ethoxycarbonyl)benzylzinc chloride with 4-dimethylaminobenzaldehyde, demonstrating enhanced reactivity in the presence of $MgCl_2$.

The authors rationalised this enhanced reactivity of the organozinc reagents in the presence of $MgCl_2$ by assuming that the reactions proceeded through a six membered transition state (**Figure 4.1**), whereby the more Lewis acidic $MgCl_2$ (compared to $RZnCl$) coordinates to the carbonyl group of the substrate, providing greater activation of the substrate towards nucleophilic addition.^[123]

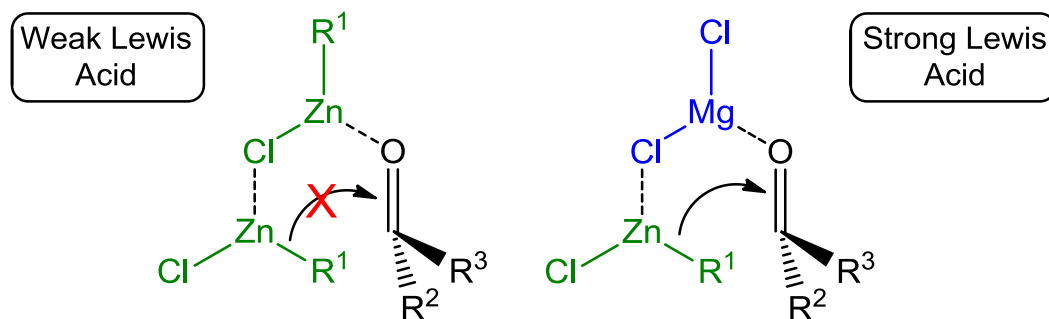
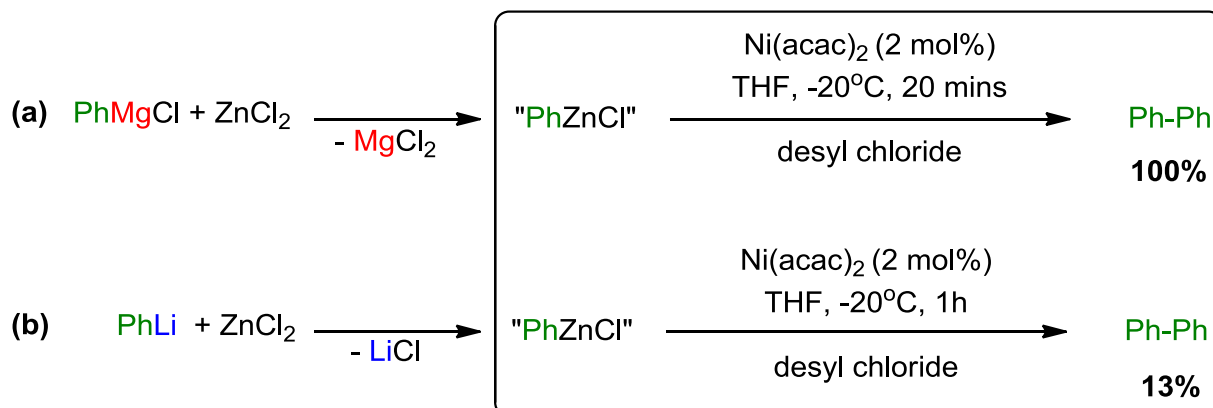


Figure 4.1: Proposed transition states for the nucleophilic addition of $RZnCl$ to aldehydes and ketones in the presence and absence of $MgCl_2$.

Adding a new level of complexity to the role of inorganic salts when present with organozinc reagents, recent reports have shown that the organometallic source employed to perform the salt metathesis reaction can also have a dramatic effect on the reactivity of the organozinc reagent. Thus, Lei and Marder have reported that the nickel catalysed oxidative homocoupling reaction of $PhZnCl$ proceeds in a quantitative yield after 4 minutes at $-20^\circ C$, when the organozinc reagent is prepared from $PhMgCl$ and $ZnCl_2$. However, if $PhLi$ is employed as the organometallic reagent, then under the same reaction conditions only 13% conversion to the

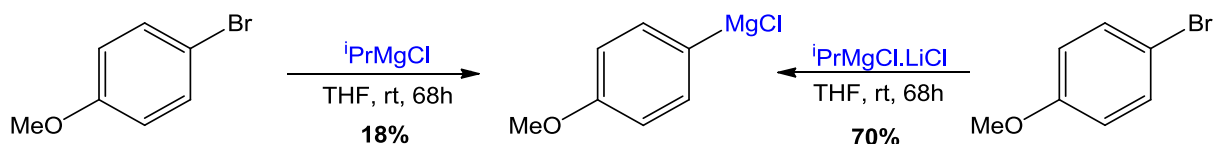
desired product is observed (**Scheme 4.4**).^[125] The authors suggest that this remarkable difference in reactivity is primarily due to the different roles played by the relevant inorganic salt formed concomitantly in the metathesis reaction.



Scheme 4.4: Ni-catalysed oxidative homocoupling of PhZnCl, prepared via *in situ* salt metathesis of (a) PhMgCl and ZnCl₂ and (b) PhLi and ZnCl₂.

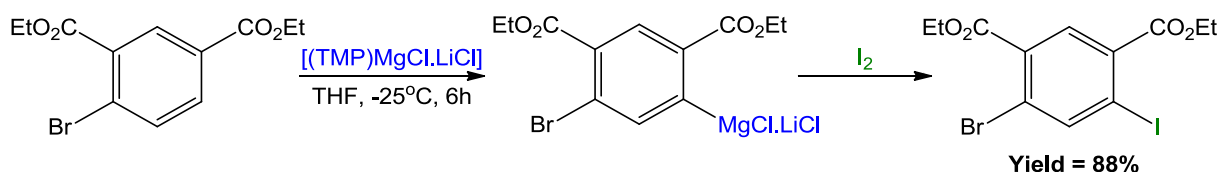
Kinetic studies revealed that whereas the transmetalation of PhZnCl with the Ni catalyst occurred rapidly when prepared from PhMgCl, with reductive elimination the rate determining step, when the organozinc halide was prepared from PhLi transmetalation became rate-limiting. Furthermore, if MgCl₂ was added to the PhLi/ZnCl₂ system, the reaction rate increased, becoming comparable with that of the PhMgCl/ZnCl₂ system. These results suggest that MgCl₂ may in fact be interacting closely with PhZnCl, accelerating the transmetalation step and allowing the oxidative homocoupling reaction to proceed rapidly.

The important influence that inorganic salts exert on the performance of organometallic reagents is not solely confined to organozinc reagents. Previously, Knochel has reported that the addition of LiCl to ⁱPrMgCl can significantly increase the rate of Mg-Br exchange, whereby reaction of 4-bromoanisole with ⁱPrMgCl leads to only an 18% conversion, compared to a 70% conversion when one equivalent of LiCl is added (**Scheme 4.5**).



Scheme 4.5: Comparison of the reactivity of ⁱPrMgCl and ⁱPrMgCl.LiCl in the Mg-Br exchange of 4-bromoanisole.

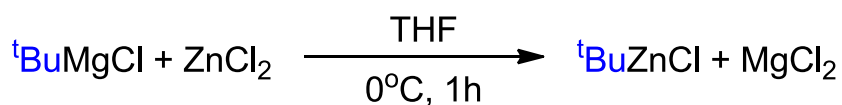
Subsequently, this Turbo Grignard reagent, ^tPrMgCl.LiCl, proved to be an extremely effective reagent for performing metal-halogen exchange reactions with a wide range of functionalised haloaromatic molecules.^[126] Furthermore, as previously mentioned in **Chapter 1.3.3**, the analogous Turbo Hauser bases [(R₂N)MgCl.LiCl] are capable of effectively performing the selective deprotonation of aromatics bearing sensitive functional groups (**Scheme 4.6**).^[77] Thus, these “turbo” mixtures display enhanced levels of reactivity and functional group tolerance compared to the corresponding homometallic organomagnesium reagents.^[80b, 127]



Scheme 4.6: Direct magnesiation of 2,4-bis(ethoxycarbonyl)bromobenzene with [(TMP)MgCl.LiCl], followed by electrophilic quenching with I₂.

4.1 Investigating the salt metathesis reaction of ^tBuMgCl and ZnCl₂

Building on these important precedents, and aiming to shed new light on the role played by inorganic salts on the reactivity and constitution of organozinc reagents, studies initially focussed on the simple metathesis reaction of equimolar amounts of ^tBuMgCl and ZnCl₂ (performed in THF at 0°C), from which the monometallic reagents ^tBuZnCl and MgCl₂ were expected to be obtained (**Scheme 4.7**).



Scheme 4.7: Expected salt metathesis reaction of ^tBuMgCl and ZnCl₂.

When ^tBuMgCl (1 M solution in THF) was added dropwise to a THF solution of ZnCl₂ a white precipitate was formed before the addition was complete, which was initially attributed to the formation of MgCl₂ (later discovered to be the magnesium halozincate species $[\{\text{Mg}(\text{THF})_6\}^{2+}\{\text{Zn}_2\text{Cl}_6\}^{2-}]$ (**33**) (vide infra)). After stirring the resulting suspension for one hour at 0°C the precipitate was removed by filtration, and hexane was added to the filtrate which was left at -30°C for 48 hours, affording a crop of colourless crystals of [(THF)₄Mg(μ-

$\text{Cl})_2\text{Zn}(\text{}^t\text{Bu})(\text{Cl})$] (**34**) (isolated in yields ranging from 5-10%), which were analysed by ^1H and $^{13}\text{C}\{^1\text{H}\}$ NMR spectroscopy and X-ray crystallography.

The bimetallic constitution of **34** was confirmed by X-ray crystallographic analysis (**Figure 4.2**). Exhibiting an unprecedented structure in the bimetallic chemistry of zinc, to the best of our knowledge, $[(\text{THF})_4\text{Mg}(\mu\text{-Cl})_2\text{Zn}(\text{}^t\text{Bu})(\text{Cl})]$ (**34**) constitutes the first example of a magnesium zincate which possesses a CIP structure. As a result, **34** can be envisaged as a magnesium-zinc hybrid reagent, where both metals (Mg and Zn) can communicate to each other through the two bridging chlorine ligands (Cl2 and Cl3), giving rise to a planar $[\text{MgClZnCl}]$ four-membered ring (sum of angles = 360°).

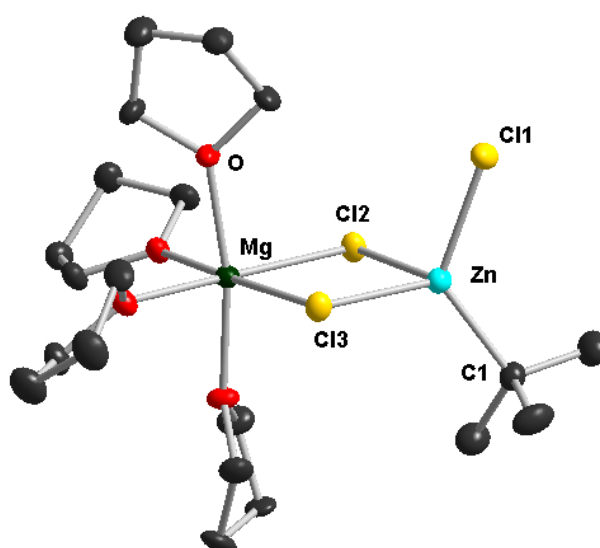
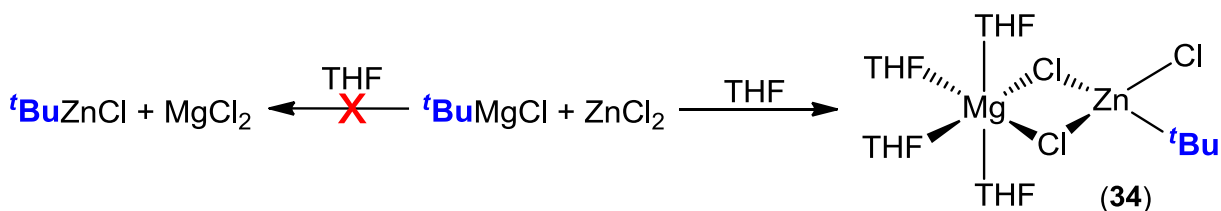


Figure 4.2: Molecular structure of $[(\text{THF})_4\text{Mg}(\mu\text{-Cl})_2\text{Zn}(\text{}^t\text{Bu})(\text{Cl})]$ (**34**) with 50% probability ellipsoids. Hydrogen atoms and minor THF disorder components have been omitted for clarity. Selected bond distances (\AA) and bond angles ($^\circ$): Zn-C1 2.000(3), Zn-Cl1 2.2788(7), Zn-Cl2 2.4107(7), Zn-Cl3 2.4226(7), Mg-Cl2 2.4774(10), Mg-Cl3 2.4972(10); C1-Zn-Cl1 123.46(8), C1-Zn-Cl2 114.56(8), Cl1-Zn-Cl2 103.24(3), C1-Zn-Cl3 115.51(8), Cl1-Zn-Cl3 104.78(3), Cl2-Zn-Cl3 89.51(2), Cl2-Mg-Cl3 86.33(3), Zn-Cl2-Mg 92.45(3), Zn-Cl3-Mg 91.68(3).

Zinc adopts a distorted tetrahedral geometry (average angle around $\text{Zn} = 108.5^\circ$), completing its coordination sphere by bonding to a terminal chlorine atom and forming a strong sigma bond with the quaternary carbon of the ${}^t\text{Bu}$ ligand (2.000(3) \AA), which was originally bound to magnesium in the Grignard reagent. This Zn-C bond is comparable to those found in the

related *tert*-butyl containing organozinc compounds, such as monomeric ^tBu₂Zn (1.977(4) Å)^[128] and [(TMEDA)Zn^tBu₂] (2.0592(19) and 2.0536(18) Å).^[129] As expected, the terminal Zn-Cl bond (Zn-Cl11 = 2.2788(7) Å) is significantly shorter than those observed for the bridging Zn-Cl bonds (2.4107(7) and 2.4226(7) Å), which lie marginally closer to the zinc centre than they do to the magnesium (2.4774(10) and 2.4972(10) Å), as a result of the slightly larger size of magnesium, as well as its higher coordination number, adopting a distorted octahedral geometry by bonding to four molecules of THF.



Compound **34** can be described as a metathetical intermediate of the reaction between ^tBuMgCl and ZnCl₂, where the alkyl group has transferred from Mg to Zn to form ^tBuZnCl, and the inorganic salt co-product, MgCl₂, has been trapped within the molecular framework of the zincate (**Scheme 4.8**). Interestingly, at the same time that we published this study, Lei and Marder reported their investigations on the synthesis of PhZnCl and its applications in nickel catalysed homocoupling processes. They found that the reaction of PhMgBr with ZnCl₂ led to the isolation of the related compound [(THF)₄Mg(μ-Cl)₂Zn(Ph)(X)] (X = Cl/Br) (**35**) (**Figure 4.3**),^[125] which suggests that the formation of these new Mg-Zn hybrids may be more common than initially thought.

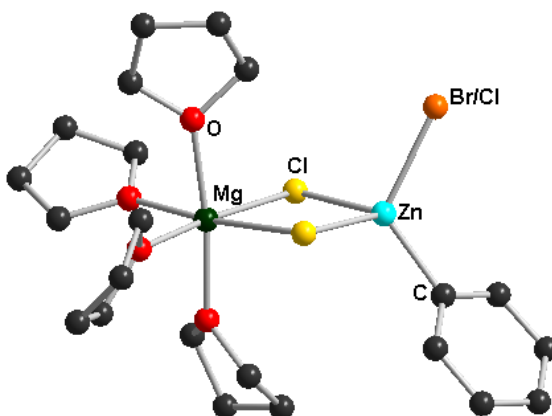


Figure 4.3: Molecular structure of [(THF)₄Mg(μ-Cl)₂ZnPhX] (X = Br/Cl, 56:44) (**35**).

Hydrogen atoms have been omitted for clarity.

The heteroleptic halide/alkyl composition of **34**, which can be described as an adduct of ${}^t\text{BuZnCl}$ and MgCl_2 , allows its direct comparison with Knochel's "turbo" Hauser bases ($\text{R}_2\text{NMgCl}\cdot\text{LiCl}$), with the structure of the TMP analogue $[(\text{THF})_2\text{Li}(\mu\text{-Cl})_2\text{Mg}(\text{TMP})(\text{THF})]$ (**10**) having been recently unveiled.^[80a] **10** exhibits a similar CIP structural motif to that of **34**, where both metals (magnesium and lithium) are connected by two chlorine bridges and the remaining anionic ligand (TMP) bonds terminally to magnesium. Both metals display tetrahedral geometries, with magnesium bonding to an additional molecule of THF whereas lithium completes its coordination sphere with two molecules of THF (**Figure 4.4**). The major difference between the molecular structure of **10** and that of **34** is that the greater electronegativity of zinc (compared to magnesium) leads to a reversal in the role of the magnesium centre, which acts as the Lewis acid in **34**, being solvated by the THF molecules, whereas in **10** it adopts the role of zinc, binding to the anionic ligands.

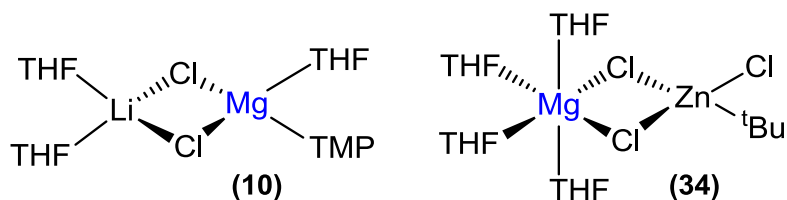


Figure 4.4 Comparison of the molecular structures of the turbo Hauser base $[(\text{THF})_2\text{Li}(\mu\text{-Cl})_2\text{Mg}(\text{TMP})(\text{THF})]$ (**10**), and Mg-Zn hybrid **34**.

It is well known that the constitution of Grignard reagents (RMgX) in solution can be extremely complex, and is dependent on several factors such as temperature, concentration, solvent (THF, Et_2O) and the nature of the R and X groups present.^[119] Therefore, in many cases it is difficult to establish a direct comparison between their structures in the solid and in solution.^[130] In contrast, the ${}^1\text{H}$ NMR spectrum of **34** in d_8 -THF solution appears to be much more simple, displaying a single resonance at δ 0.99 ppm corresponding to the methyl protons of a *tert*-butyl group and two multiplets at δ 1.77 and 3.63 ppm for THF. The integration of these signals indicated a ratio of ${}^t\text{Bu}:\text{THF}$ of 1:4, which is consistent with the crystal structure obtained. The most diagnostic signals in the ${}^{13}\text{C}\{{}^1\text{H}\}$ NMR spectrum were two resonances at δ 33.6 and 21.9 ppm for the methyl and quaternary carbon of the *tert*-butyl group respectively, which appear at similar chemical shifts to those found for ${}^t\text{BuZnCl}$ (δ 33.8 and 21.5 ppm) in the same solvent, but differ significantly from those of ${}^t\text{BuMgCl}$ (δ 35.8 and 15.6 ppm) and ${}^t\text{Bu}_2\text{Mg}$ (δ 35.9 and 15.8 ppm) (**Table 4.1**), which suggests that the *tert*-butyl group of **34** retains most of its "zinc" character in solution.

$\delta(\text{ppm})$	^1H (CH_3 ^tBu)	$^{13}\text{C}\{^1\text{H}\}$ (CH_3 ^tBu)	$^{13}\text{C}\{^1\text{H}\}$ ($\text{C}(\text{CH}_3)_3$ ^tBu)
$[(\text{THF})_4\text{Mg}(\mu\text{-Cl})_2\text{Zn}(^t\text{Bu})(\text{Cl})]$ (34)	0.99	33.6	21.9
$^t\text{Bu}_2\text{Zn}$	0.97	33.0	25.4
$^t\text{BuZnCl}$	0.95	33.8	21.6
$^t\text{Bu}_2\text{Mg}$	0.86	36.0	15.8
$^t\text{BuMgCl}$	0.85	35.8	15.6

Table 4.1: ^1H and $^{13}\text{C}\{^1\text{H}\}$ NMR shifts (ppm) of the *tert*-butyl groups of **34** and related organozinc and organomagnesium compounds in d_8 -THF.

It is noteworthy that cold spray ionisation mass spectroscopy (CSI-MS) studies by Imamoto and Yamaguchi into the constitution of Grignard reagents have revealed that the major species present for MeMgCl in THF solution is binuclear $[\text{MeMg}_2\text{Cl}_3(\text{THF})_x]$ ($x = 4-6$).^[130] This species can be envisaged as a homometallic analogue of **34**, combining MeMgCl and MgCl_2 within the same molecular structure.

Given that the yield of $[(\text{THF})_4\text{Mg}(\mu\text{-Cl})_2\text{Zn}(^t\text{Bu})(\text{Cl})]$ (**34**) proved to be very low (isolated yield 5-10%) using the metathetical approach described above, attention next turned to the composition of the white solid which was formed when $^t\text{BuMgCl}$ was initially added to ZnCl_2 . The solid was shown to be highly insoluble in a variety of organic solvents, including THF, toluene and diethyl ether, even after reflux or sonication. This ruled out the possibility that this species was either ZnCl_2 or MgCl_2 , as both are soluble in THF. Due to its low solubility this unknown product could not be analysed by NMR spectroscopy, although atomic absorption spectrometry (FAAS) revealed that this precipitate contained both magnesium and zinc (**Table 4.2**). Furthermore, when $^t\text{BuMgCl}$ was added to a static solution of ZnCl_2 in THF and left to stand at room temperature overnight a small batch of colourless crystals $[\{\text{Mg}(\text{THF})_6\}^{2+}\{\text{Zn}_2\text{Cl}_6\}^{2-}]$ (**33**) were obtained, which were analysed by X-ray crystallography.

The molecular structure of **33** was shown to be the SSIP mixed magnesium-zinc chloride species $[\{\text{Mg}(\text{THF})_6\}^{2+}\{\text{Zn}_2\text{Cl}_6\}^{2-}]$ (**Figure 4.5**), comprising of an octahedral magnesium dication solvated by six molecules of THF, and a dianionic fragment containing two zinc and six chlorine atoms. The two zinc centres are connected by two bridging chlorine atoms, with two further terminal chlorines atoms on each of the metal centres, which adopt a distorted

tetrahedral geometry (average angle around Zn = 109.1°). A search of the CCDB revealed that there were thirty-one previously reported structures which contained the same {Zn₂Cl₆}²⁻ anion as **33**, but this fragment has never been reported within the context of a magnesium-zincate species.

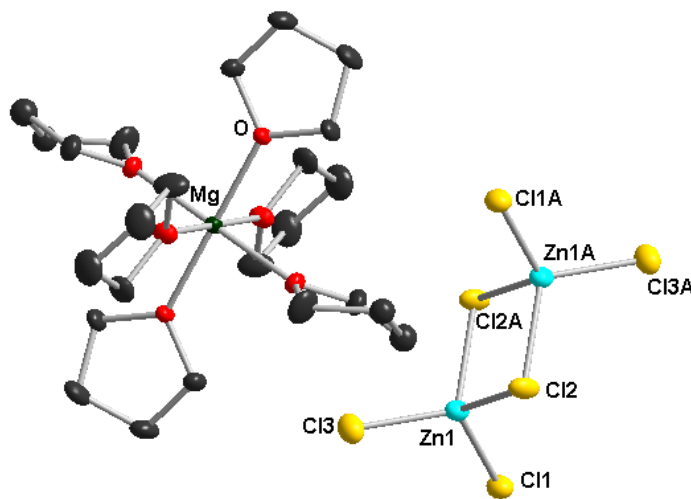
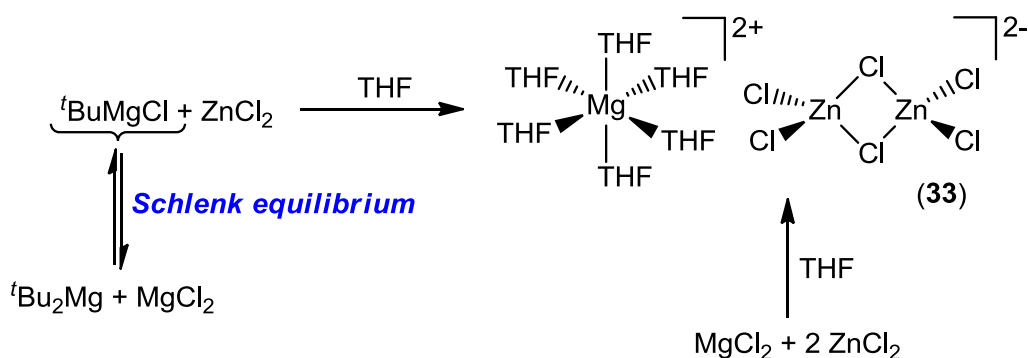


Figure 4.5: Molecular structure of [$\{\text{Mg}(\text{THF})_6\}^{2+}\{\text{Zn}_2\text{Cl}_6\}^{2-}$] (**33**) with 50% probability ellipsoids. Hydrogen atoms and minor THF disorder components have been omitted for clarity. *Selected bond distances (Å) and bond angles (°):* Zn-Cl1 2.2098(7), Zn-Cl3 2.2077(7), Zn-Cl2 2.3650(6), Zn-Cl2a 2.3511(5); Cl1-Zn1-Cl2 109.85(3), Cl1-Zn1-Cl2a 114.79(2), Cl1-Zn1-Cl3 115.46(2), Cl2-Zn1-Cl3 112.91(3), Cl2-Zn1-Cl2a 92.36(2), Cl3-Zn1-Cl2a 109.29(3).

The formation of **33** can be rationalised by a co-complexation reaction of ZnCl₂ with MgCl₂, where the MgCl₂ must be present in solution due to the Schlenk equilibrium which affects ^tBuMgCl (**Scheme 4.9**). Thus, in THF solution ^tBuMgCl will be in equilibrium with ^tBu₂Mg and MgCl₂, allowing the latter to react with ZnCl₂ to give **33**, the formation of which must be greatly favoured by its low solubility in THF solution. This hypothesis was supported by reacting one equivalent of MgCl₂ with two equivalents of ZnCl₂ in THF solution, which led to the formation of **33** in an isolated yield of 80-85%. The results of the atomic absorption analysis for the solid obtained from this reaction (3.87% Mg, 15.95% Zn) showed good correlation to the theoretical data for **33** (3.03% Mg, 16.34% Zn) (**Table 4.2**). The data was also more satisfactory than that obtained for **33** synthesised from the reaction of ^tBuMgCl and ZnCl₂, which suggests that in the latter approach another magnesium containing species may also be present in the isolated solid.



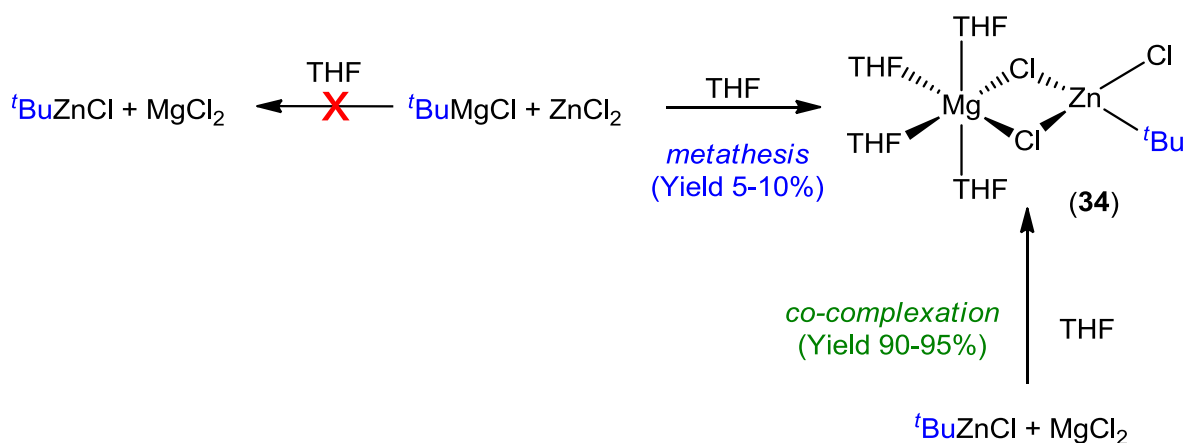
Scheme 4.9: Reaction of ^tBuMgCl (or MgCl₂) with ZnCl₂ and to form **33**.

The formation of **33** from the reaction of ^tBuMgCl and ZnCl₂ will not only have a dramatic effect on the Schlenk equilibrium, pushing it towards the formation of MgCl₂ and ^tBu₂Mg, but it will also greatly reduce the amount of ZnCl₂ available for the metathesis reaction. In fact, from the yield of **33** obtained when ^tBuMgCl is reacted with ZnCl₂ it can be estimated that approximately 50-60% of the ZnCl₂ present in the reaction mixture is consumed in the formation of this magnesium halozincate, thus explaining the very low yields obtained for the formation of **34**.

Synthesis of [$\{\text{Mg}(\text{THF})_6\}^{2+}\{\text{Zn}_2\text{Cl}_6\}^{2-}$] (33)	Mg (%)	Zn (%)
^t BuMgCl + ZnCl ₂	5.27	13.14
MgCl ₂ + 2 ZnCl ₂	3.87	15.95
Theoretical Mg % and Zn % in 33	3.03	16.34

Table 4.2: Atomic Absorption data for [$\{\text{Mg}(\text{THF})_6\}^{2+}\{\text{Zn}_2\text{Cl}_6\}^{2-}$] (**33**) prepared by the reaction of (i) ^tBuMgCl + ZnCl₂, and (ii) MgCl₂ + 2 ZnCl₂.

Thus, the formation of **34** via a co-complexation approach between ^tBuZnCl and MgCl₂ was investigated (**Scheme 4.10**). It was found that by carrying out this reaction the isolated yield of **34** could be greatly improved (90-95%) compared to the metathesis approach (5-10%). For this co-complexation approach it appears that the magnesium halozincate [$\{\text{Mg}(\text{THF})_6\}^{2+}\{\text{Zn}_2\text{Cl}_6\}^{2-}$] (**33**) is not formed, probably due to the lower extent which the Schlenk equilibrium affects RZnX compounds in comparison with Grignard reagents, minimizing the amount of ZnCl₂ available.

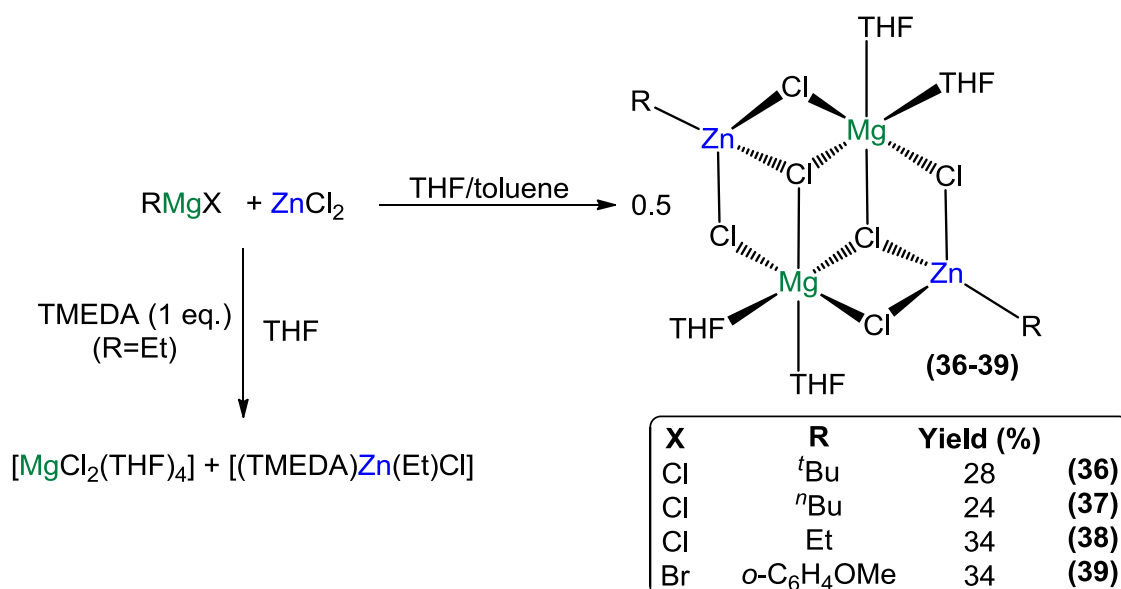


Scheme 4.10: Formation of **34** via salt metathesis and co-complexation approaches.

4.2 Further studies on the metathesis reaction Grignard reagents with ZnCl₂

Following on from these initial results, studies of salt metathesis reactions were extended to other Grignard reagents, as well as investigating the effect of altering the solvent employed. Thus, the metathesis reaction of ZnCl₂ with a series of different Grignard reagents (*t*BuMgCl, *n*BuMgCl, EtMgCl and *o*-MeO-C₆H₄MgBr) was initially carried out in THF. In all cases the almost immediate precipitation of a white solid was observed, which was removed by filtration, and addition of toluene to the remaining filtrates led to the isolation of the new magnesium-zinc hybrid species [$\{(\text{THF})_2\text{Mg}(\mu\text{-Cl})_3\text{ZnR}\}_2$] (R = *t*Bu, **36**; *n*Bu, **37**; Et, **38**; *o*-C₆H₄OMe, **39**) in isolated yields ranging from 24-34% (**Scheme 4.11**), which were characterised by X-ray crystallography and NMR spectroscopy.

As previously observed in the synthesis of **34**, the low-moderate yields of these bimetallic species can be attributed to the formation of magnesium halozincate [$\{[\text{Mg}(\text{THF})_6]^{2+}[\text{Zn}_2\text{Cl}_6]^{2-}\}$] (**33**), resulting from the competing co-complexation reaction of ZnCl₂ with MgCl₂. Interestingly the reaction of arylmagnesium bromide (*o*-C₆H₄OMe)MgBr with ZnCl₂ results in the formation of the magnesium chloro-arylzincate [$\{(\text{THF})_2\text{Mg}(\mu\text{-Cl})_3\text{Zn}(\textit{o}\text{-C}_6\text{H}_4\text{OMe})\}_2$] (**39**). The absence of bromine in this product suggests that in this case instead of the precipitation of **33** a related mixed halide magnesium-zincate [$\{[\text{Mg}(\text{THF})_6]^+[\text{Zn}_2\text{Br}_x\text{Cl}_{6-x}]^{2-}\}$] containing both bromine and chlorine ligands must be formed.



Scheme 4.11: Metathesis reaction of RMgX with ZnCl₂ to form Mg-Zn hybrids **36-39**, and reaction of EtMgCl with ZnCl₂ in the presence of TMEDA.

When the initial metathesis reactions were performed using poorly coordinating toluene as the bulk solvent instead of THF, the formation of **33** was still observed, and magnesium-zinc hybrids **36-39** were obtained in similar yields to those obtained when the reactions were performed in THF, followed by the addition of toluene. In contrast, if the reaction of EtMgCl with ZnCl₂ was performed in THF in the presence of the chelating diamine TMEDA (ZnCl₂.TMEDA was used instead of ZnCl₂), the formation of **33** is precluded, affording a solution from which a batch of colourless crystals were isolated. When analysed by X-ray crystallography and NMR spectroscopy these were revealed to be a mixture of the two expected monometallic products of the reaction, TMEDA-solvated ethylzinc chloride [(TMEDA)Zn(Et)Cl]^[131] and THF-solvated magnesium chloride [MgCl₂(THF)₄]^[132] (**Scheme 4.11**). These results reveal that the presence of TMEDA inhibits not only the formation of the magnesium halozincate species **33**, but also the magnesium-zinc hybrid [{"(THF)₂Mg(μ-Cl)₃ZnEt"}₂] (**39**), illustrating the important effect that coordinating solvents may exert on these metathesis reactions.

The mixed-metal composition of the magnesium-zinc hybrids **36-39** was established by X-ray crystallographic studies (**Figure 4.6** and **Chapter 7.3.16 – Experimental Procedures**). These compounds display the same structural motif, with the only variation of note being the difference in the organic fragment bound terminally to zinc (^tBu, ⁿBu, Et and *o*-C₆H₄OMe).

The extent of these similarities can be observed by comparison of the principal bond lengths and angles of their structures which revealed very little variation (**Table 4.3**), including the relevant Zn-C bond lengths which range from 1.944(8) to 1.984(3) Å.

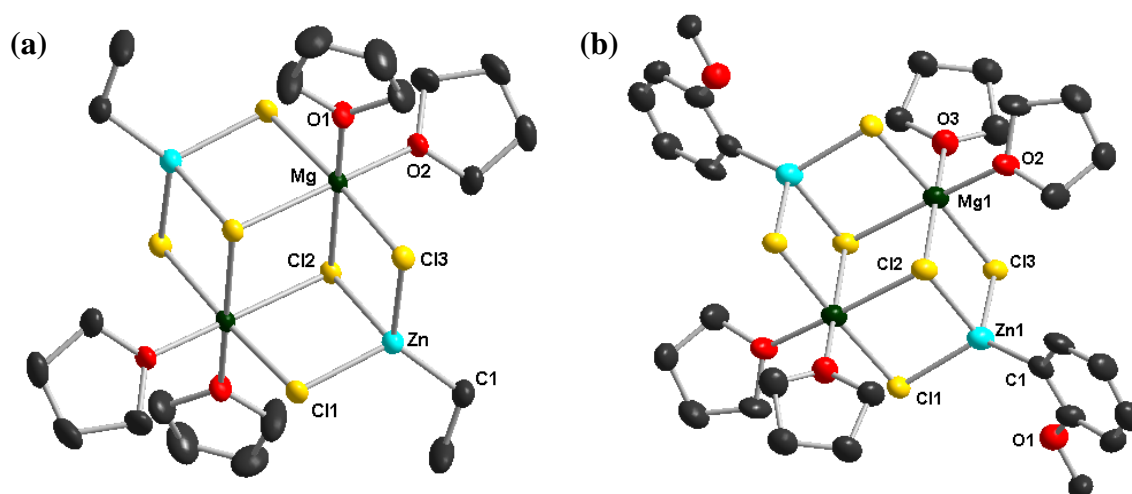


Figure 4.6: Molecular structure of (a) $[\{(\text{THF})_2\text{Mg}(\mu\text{-Cl})_3\text{ZnEt}\}_2]$ (**38**) with 40% probability ellipsoids and (b) $[\{(\text{THF})_2\text{Mg}(\mu\text{-Cl})_3\text{Zn}(o\text{-C}_6\text{H}_4\text{OMe})\}_2]$ (**39**) with 50% probability ellipsoids. Hydrogen atoms and minor THF disorder components are omitted for clarity. For selected bond distances (Å) and angles ($^\circ$) see **Table 4.3**.

Compound	36	37	38	39
R	^t Bu	ⁿ Bu	Et	<i>o</i> -C ₆ H ₄ OMe
Zn-C	1.982(3), 1.984(3)	1.964(2)	1.967(3)	1.944(8)
Zn-Cl	2.3410(5)-2.4512(7)	2.3422(5)-2.4760(5)	2.3265(6)-2.5085(7)	2.347(2)-2.504(2)
Av. Zn-Cl	2.3751	2.3879	2.3934	2.400
Mg-Cl	2.4577(8)-2.5829(7)	2.4809(7)-2.5718(7)	2.4780(10)-2.5761(9)	2.512(3)-2.563(3)
Av. Mg-Cl	2.5369	2.5257	2.5271	2.530
C-Zn-Cl	120.40(9)-122.09(8)	120.90(8)-122.96(7)	117.76(9)-125.87(8)	107.0(2)-126.7(2)
Av. C-Zn-Cl	121.15	121.98	121.26	119.10
Cl-Zn-Cl	91.541(17)-103.20(3)	90.349(16)-101.301(19)	89.75(2)-103.38(2)	91.90(7)-104.31(7)
Av. Cl-Zn-Cl	95.443	94.233	94.71	96.05

Table 4.3. Selected bond distances (Å) and angles ($^\circ$) of Mg-Zn hybrids **36-39** $[\{(\text{THF})_2\text{Mg}(\mu\text{-Cl})_3\text{ZnR}\}_2]$.

The CIP structures **36-39** display a dimeric motif, comprising of two crystallographically equivalent $\{(\text{THF})_2\text{MgCl}_3\text{ZnR}\}$ units. Each magnesium-zinc pair and both magnesium atoms

are connected by two bridging chlorines, giving rise to a face-fused double heterocubane structures with two opposite vertices removed. Alternatively, these structures can be described as inverse crown species, a term previously coined by Mulvey *et al* to describe bimetallic ring systems which comprise of an outer cationic ring which hosts an anionic fragment in the core.^[133] Thus, **36-39** can be envisaged as a $[\{ZnClMgCl\}_2]$ cationic eight-membered rings hosting two chloride anion guests, with the R groups bound terminally to the distorted tetrahedral zinc atoms and each magnesium centre completing its octahedral coordination sphere by bonding to two molecules of THF.

As was observed for $[(THF)_4Mg(\mu-Cl)_2Zn(tBu)(Cl)]$ (**34**), compounds **36-39** are formed by the co-complexation of the two expected homometallic products of the metathesis reaction, $MgCl_2$ and $RZnCl$, where the inorganic magnesium salt is trapped within the molecular framework of a zincate species. However, in this case, instead of the monomeric arrangement observed for **34**, compounds **36-39** adopt dimeric structures, most likely due to the use of toluene as the bulk solvent, which limits the availability of THF and favours the formation of a dimeric species. Although unprecedented in magnesium-zinc chemistry, compounds **36-39** are closely related to the homometallic molecular structures observed for Grignard reagents $[\{RMg_2Cl_3(THF)_3\}_2]$ (R= Et, Me, tBu , CH_2Ph),^[130, 134] which are adducts of $RMgCl$ and $MgCl_2$, and the recently reported mixed magnesium-manganese complex $[\{(THF)_2Mg(\mu-Cl)_2Mn(CH_2Ph)Cl\}_2]$,^[135] which is formed as a side product from the metathesis reaction of dibenzylmagnesium with $MnCl_2$ (**Figure 4.7**).

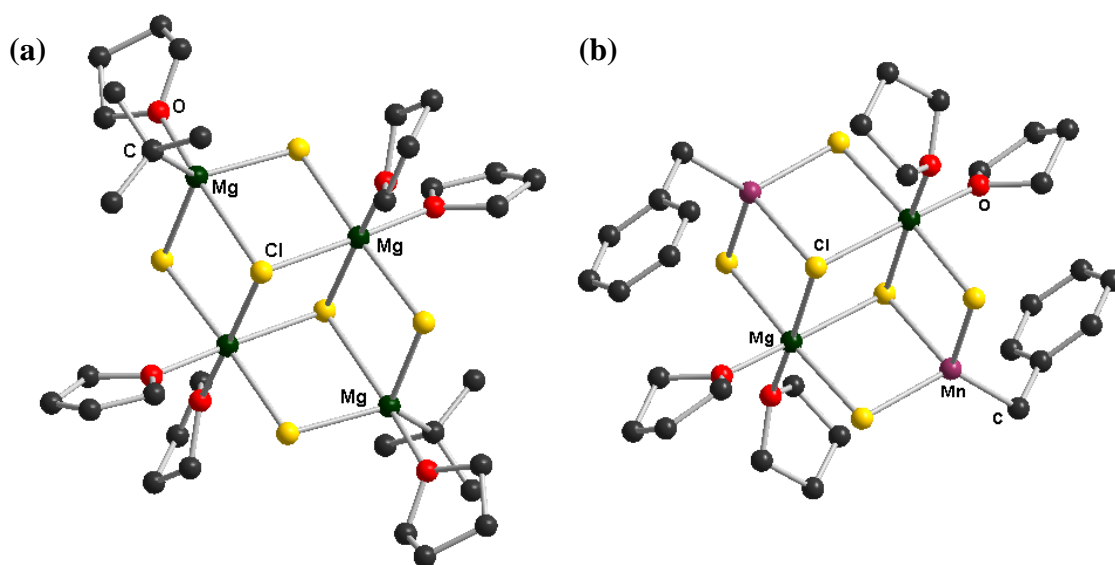


Figure 4.7: Comparison of the molecular structures of (a) $[\{(THF)_3Mg_2(\mu-Cl)_3tBu\}]$ ^[130] and (b) $[\{(THF)_2Mg(\mu-Cl)_3Mn(CH_2Ph)_2\}]$.^[135] Hydrogen atoms have been omitted for clarity.

Compounds **36-39** [$\{(THF)_2Mg(\mu-Cl)_3ZnR\}_2$] were also characterised by ¹H and ¹³C{¹H} NMR spectroscopy in d₈-THF solution. The spectra of the four species displayed two resonances for free THF (which would be displaced by the large excess of d₈-THF), along with a single set of resonances for the relevant R group (**Table 4.4** and **Chapter 7.3.16 – Experimental Procedures**). Analysis of the integration of these resonances revealed the ratio of R:THF was approximately 2:3 in each case. This is slightly lower than would be expected from the crystal structures (R:THF = 2:4), but can be explained by the loss of some of the THF when the compounds are dried *in vacuo*. The spectra also showed varying amounts of free toluene, which was present in the crystal structure as solvent of crystallisation.

The chemical shifts displayed in the ¹H and ¹³C{¹H} NMR spectra for the R groups present in **36-39** differ significantly from those found for the relevant Grignard reagent precursors (see **Table 4.4** for comparison), exhibiting values closer to those observed for related monometallic organozinc species. Thus, for example the ¹H NMR spectrum of the ethyl-zincate **38** displayed a quartet at 0.06 ppm corresponding to the CH₂ group of the Et fragment, which is similar to that observed for the same group in [(TMEDA)ZnEt₂] (δ -0.15 ppm) and ZnEt₂ (δ 0.04 ppm) but shifted significantly downfield compared to that in EtMgCl (-0.84 ppm).

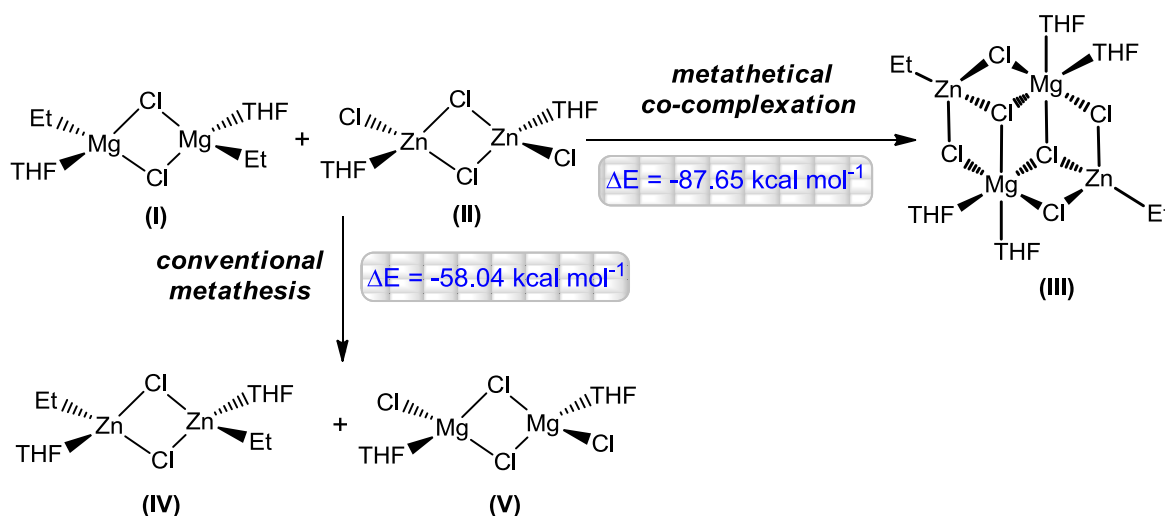
Compound	δ(¹ H) (ppm)	δ(¹³ C{ ¹ H}) (ppm)
$\{(THF)_2Mg(\mu-Cl)_3Zn^iBu\}_2$ (36)	1.01 (Zn-C(CH ₃) ₃)	22.0 (Zn-C), 33.7 (CH ₃)
ⁱ BuMgCl	0.84 (Mg-C(CH ₃) ₃)	15.6 (Mg-C), 35.8 (CH ₃)
$\{(THF)_2Mg(\mu-Cl)_3Zn^nBu\}_2$ (37)	0.14 (Zn-CH ₂)	10.1 (Zn-CH ₂)
ⁿ BuMgCl	-0.71 (Mg-CH ₂)	7.8 (Mg-CH ₂),
$\{(THF)_2Mg(\mu-Cl)_3ZnEt\}_2$ (38)	0.06 (Zn-CH ₂)	1.0 (Zn-CH ₂)
EtMgCl	-0.84 (Mg-CH ₂)	-2.4 (Mg-CH ₂)
$\{(THF)_2Mg(\mu-Cl)_3Zn(o-C_6H_4OMe)\}_2$ (39)	6.65, 6.73, 7.01, 7.39 (ArH)	142.4 (Zn-C _{ipso})
<i>o</i> -MeO-C ₆ H ₄ MgBr	6.53, 6.68, 6.89, 7.47 (ArH)	158.4 (Mg-C _{ipso})

Table 4.4: Selected chemical shifts (ppm) of the ¹H and ¹³C{¹H} NMR spectra of compounds **36-39** and commercial sources of ⁱBuMgCl, ⁿBuMgCl, EtMgCl and *o*-OMe-C₆H₄MgBr in d₈-THF solutions.

Similarly, the ¹³C{¹H} NMR spectrum of **38** displayed a resonance for the CH₂ group at 1.0 ppm, compared to 1.7 ppm for that in [(TMEDA)ZnEt₂] and -2.4 ppm for that in EtMgCl,

reflecting that the Et group in **38** retains its “zinc-character” in solution. The same trend is observed for the *tert*-butyl-zincate **36**, with the ¹³C{¹H} NMR resonances of the *tert*-butyl ligand (δ 21.4 and 33.5 ppm for the quaternary and methyl carbons respectively) differing significantly to those of the corresponding Grignard reagent (^tBuMgCl, 15.6, 35.8 ppm), and lying closer to those of ^tBuZnCl (21.0, 33.2 ppm) (**Table 4.4**).

To gain a greater understanding of the energetics involved in the formation of these bimetallic hybrids, a theoretical study on the reaction of EtMgCl and ZnCl₂ was also carried out, to determine if the formation of [(THF)₂Mg(μ-Cl)₃ZnEt]₂ (**38**) was energetically favoured (For full details of DFT calculations see **Appendix**). Firstly, the energies of the reaction of the homometallic reagents, EtMgCl and ZnCl₂, was investigated, with the reagents modelled as THF-solvated dimers [(THF)EtMgCl]₂ (**I**) and [(THF)ZnCl₂]₂ (**II**) (**Scheme 4.12**). Interestingly, the formation of the CIP magnesium-zinc hybrid [(THF)₂Mg(μ-Cl)₃ZnEt]₂ (**III**), obtained via metathetical co-complexation, is thermodynamically more favoured (by 29.61 kcal mol⁻¹) than the expected homometallic products from the classical salt-metathesis reaction, [(THF)EtZnCl]₂ (**IV**) and [(THF)MgCl₂]₂ (**V**) (**Scheme 4.12**).



Scheme 4.12: DFT study of the energies of the reaction between the model homometallic reagents [(THF)EtMgCl]₂ (**I**) and [(THF)ZnCl₂]₂ (**II**).

The geometrical optimisation of **III** was performed by sequential addition of THF molecules to the solvent-free magnesium zinc hybrid [(MgCl₃ZnEt)₂] (**VI**). Surprisingly, for this unsolvated species a conformation where the four metals adopt a linear Zn-Mg-Mg-Zn arrangement with two chlorine atoms bridging between each pair of metal-centres [(ClMg(μ-

$(Cl)_2Zn(Et)\}_2$ (**VIB**) was found to be $11.36 \text{ kcal mol}^{-1}$ more stable than the cyclic isomer **VIA** (**Figure 4.8**).

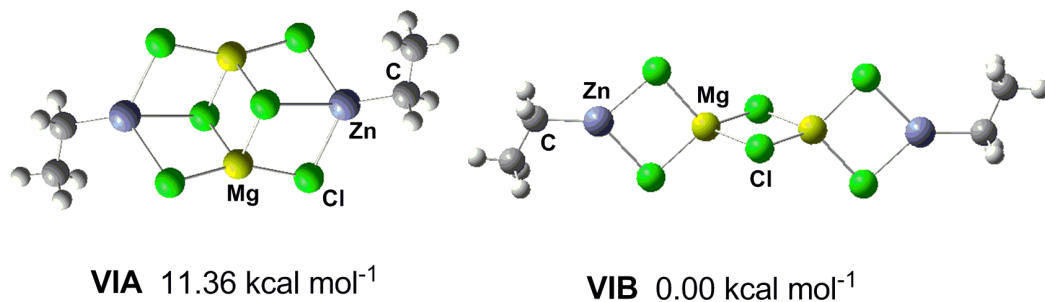


Figure 4.8: Structural models and relative energies of solvent free Mg-Zn hybrid $[MgCl_3ZnEt]_2$ in its cyclic conformation **VIA** and its linear conformation **VIB**.

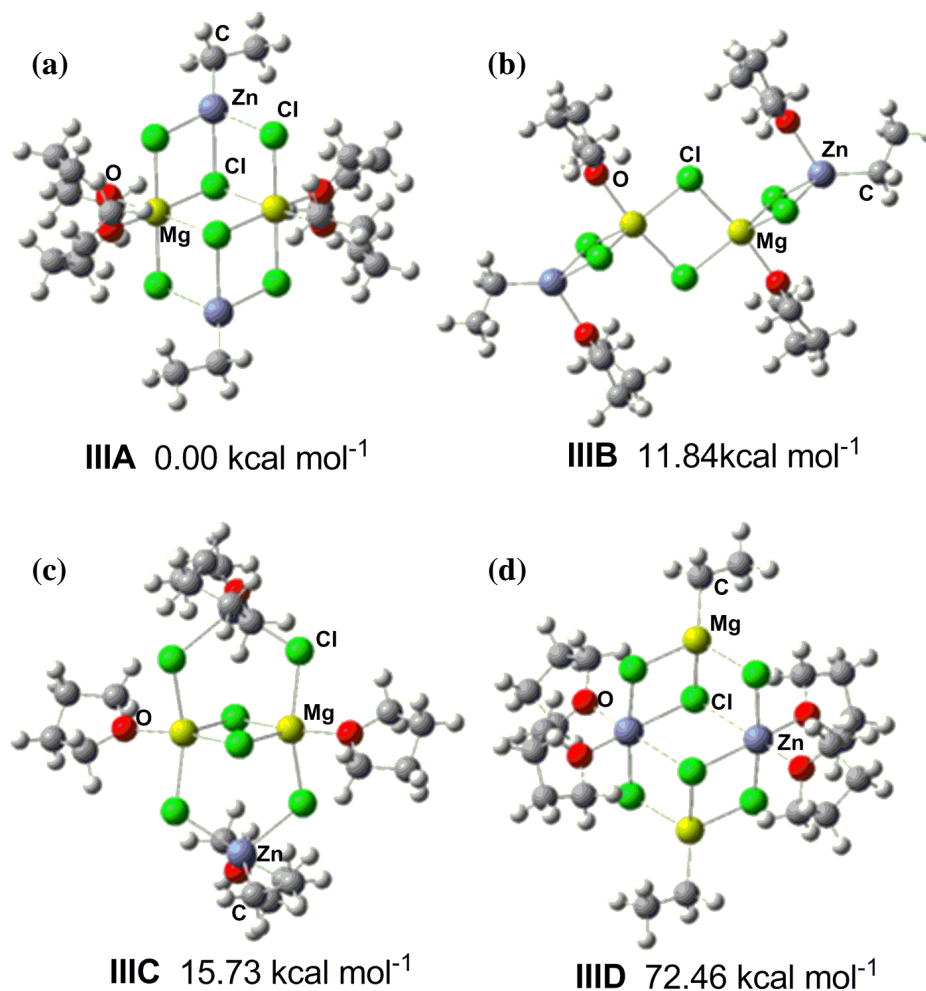


Figure 4.9: Structural models and relative energies of THF-solvated Mg-Zn hybrids $[(THF)_4Mg_2(\mu-Cl)_6Zn_2R_2]$ **IIIA-D**.

However, on addition of four molecules of THF (as found in the X-ray structure of **38**), the relative energies of these two theoretical models is reversed, and the cyclic species **III**A, where each Mg centre is solvated by two molecules of THF (**Figure 4.9(a)**), is 11.84 kcal mol⁻¹ more stable than the chain conformation **III**B, where each metal centre (Mg and Zn) is solvated by one molecule of THF (**Figure 4.9(b)**). Furthermore, **III**A was found to be 15.73 kcal mol⁻¹ more stable than the analogous cyclic species where each Mg and Zn centre is coordinated to one molecule of THF **III**C (**Figure 4.9(c)**), and 72.46 kcal mol⁻¹ more stable than **III**D (**Figure 4.9(d)**), the species resulting from the direct co-complexation of the two monometallic reagents present prior to the metathesis reaction ($[\{(THF)EtMgCl\}_2]$ (**I**) and $[\{(THF)ZnCl_2\}_2]$ (**II**)). The energy gap between **III**A and **III**D is even more remarkable considering that both species are almost isostructural, with Mg and Zn having swapped positions and the ethyl group remaining bonded to Mg in **III**D, which shows that the metathesis reaction of EtMgCl and ZnCl₂ is largely thermodynamically driven, even without the formation of the highly ionic MgCl₂ lattice.

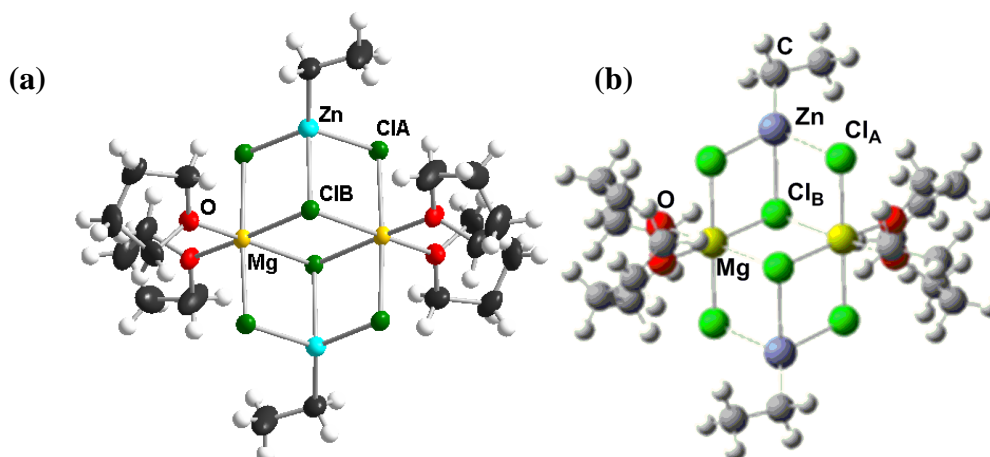


Figure 4.10: Comparison of the molecular structure of (a) $[\{(THF)_2Mg(\mu-Cl)_3ZnEt\}_2]$ (**38**) and (b) the computed minimum energy theoretical structure of $[\{(THF)_2Mg(\mu-Cl)_3ZnEt\}_2]$ (**III**A).

Thus, the energy minimum observed for the theoretical model **III**A is in good agreement with the molecular structure of the isolated crystalline product obtained from the reaction of EtMgCl with ZnCl₂ $[\{(THF)_2Mg(\mu-Cl)_3ZnEt\}_2]$ (**38**), as determined by X-ray crystallographic analysis (**Figure 4.10**), and further supported by the comparable bond lengths of these two species (**Table 4.5**). Collectively these experimental and theoretical studies suggest that the formation of Mg-Zn hybrids as the products of metathesis reactions are more common than

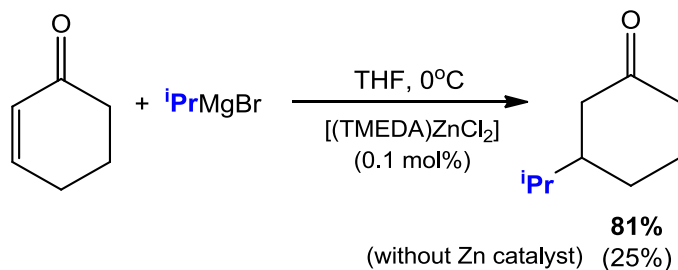
originally thought. Furthermore, these findings pose the intriguing question that perhaps some of the reactivities previously attributed to organozinc reagents prepared via this well-established methodology actually belong to mixed magnesium zincate species.

Bond distance (Å)	38	III A
Zn-C	1.967	1.969
Zn-Cl _A	2.3452, 2.3265	2.412, 2.432
Zn-Cl _B	2.509	2.738
Mg-Cl _A	2.4780, 2.512	2.511, 2.496
Mg-Cl _B	2.5632, 2.5761	2.570, 2.563
Mg-O	2.0589, 2.0559	2.119, 2.117

Table 4.5: Comparison of the calculated bond distances (Å) for the computed minimum energy theoretical structure of **III** (**III A**) with those of [$\{(THF)_2Mg(\mu-Cl)_3ZnEt\}_2$] (**38**).

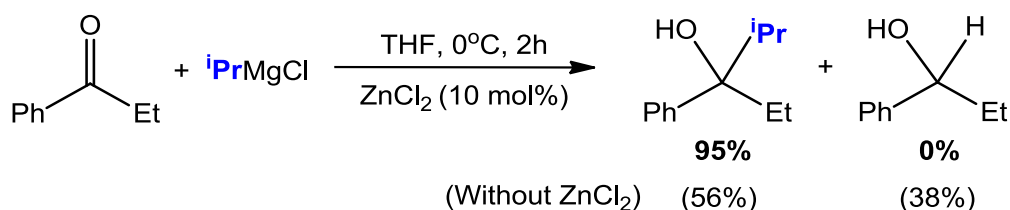
4.3 Applications of ZnCl₂ catalysed reactions of Grignard reagents

Related to these stoichiometric metathesis reactions, a number of studies have shown that the addition of catalytic amounts of ZnCl₂ can greatly enhance both the reactivity and selectivity of Grignard reagents in a variety of synthetic methodologies. The first reported use of catalytic ZnCl₂ to improve the reactivity of Grignard reagents was by Feringa in 1989, where the addition of catalytic amounts of [(TMEDA)ZnCl₂] increased the selectivity for 1,4-addition over 1,2-addition (ratio of 3:1 without catalyst vs. 6:1 with catalyst) in the reaction of a variety of Grignard reagents with α,β -unsaturated ketones as well as significantly improving the overall isolated yield of the desired product (**Scheme 4.13**).^[136]

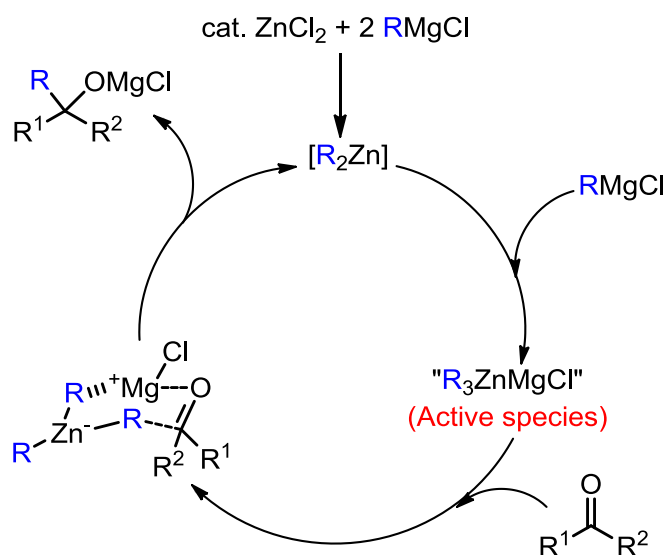


Scheme 4.13: 1,4-conjugate addition of $iPrMgCl$ to cyclohexenone, showing the effects of adding catalytic amounts of ZnCl₂.

More recently, Ishihara reported that catalytic ZnCl₂ can greatly improve the selectivity of the alkylation of ketones by Grignard reagents.^[137] The nucleophilic addition of ketones to give the desired alcohols is often hindered by the formation of unwanted reduction products, formed as a result of β-hydride elimination. However, the addition of ZnCl₂ (10 mol%) was found to significantly reduce, and in some cases inhibit, the formation of these unwanted side-products (**Scheme 4.14**).



Scheme 4.14: Reaction of ⁱPrMgCl with propiophenone, showing the effects of adding catalytic amounts of ZnCl₂.



Scheme 4.15: Proposed catalytic cycle for the ZnCl₂ catalysed nucleophilic addition of RMgCl to ketones, showing likely R₃ZnMgCl active species.

This methodology proved to be successful for a variety of Grignard reagents (RMgCl, R = Me, Et, ⁱPr, etc.) and organic substrates (including functionalised ketones and imines), allowing their chemoselective alkylation in excellent yields. In the report, the authors also proposed a possible catalytic cycle for these reactions (**Scheme 4.15**), where catalytic ZnCl₂ first reacts with two equivalents of RMgCl to form a dialkylzinc species (ZnR₂), which can in turn react with a third equivalent of RMgCl to form a putative magnesium trialkylzincate

species “ $R_3ZnMgCl$ ”. It is this species which is proposed as the active species for the reaction, forming a six-membered chair conformation transition state with the ketone, activating it towards nucleophilic addition by one of the alkyl groups to form the relevant magnesium tertiary alkoxide. This regenerates the dialkylzinc reagent, which can then react with another molecule of $RMgCl$ to regenerate the trialkylzincate active species.

Magnesium trialkylzincates of this type have also been proposed as the active species in 1,4-conjugate addition reactions. Following the successful 1,4-addition of α,β -unsaturated ketones with lithium triorganozincates (prepared from $[(TMEDA)ZnCl_2]$ and RLi in a ratio of 1:3) reported by Isobe and co-workers (see **Chapter 1.2.2**),^[32] Kjonaas revealed that related magnesium triorganozincates can be prepared by reacting $[(TMEDA)ZnCl_2]$ with three equivalents of the relevant Grignard reagent. Both the tri-butyl- and tri-isopropylzincates proved to be highly selective reagents for performing 1,4-addition to 2-cyclohexenone, methyl vinyl ketone (MVK) and 2-cyclopentenone in yield ranging from 50-96%.^[138] The author also reported that altering the ratio of Grignard reagent and $[(TMEDA)ZnCl_2]$ to 1:1, 2:1 or 4:1 lead to significantly lower yields of the desired product. However, they remained cautious in their characterisation of the active species, stating that their experiments “offer no real evidence for the existence of a magnesium triorganozincate”,^[138] and use the formula “ R_3ZnMgX ” only to denote the stoichiometry of the reagents involved.

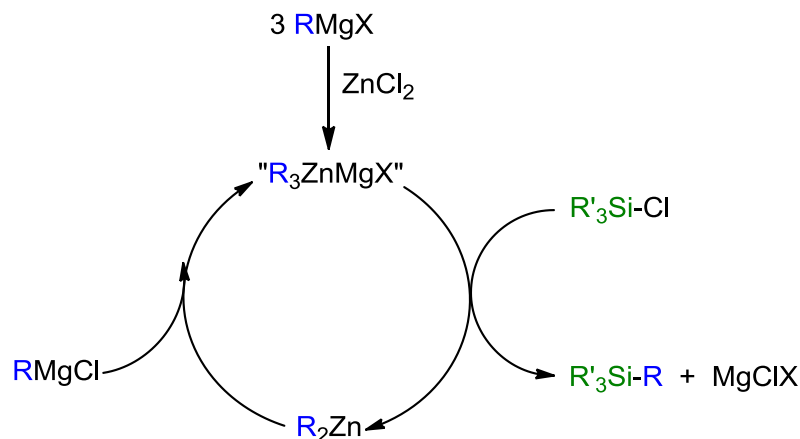
Similarly, in 2009 a magnesium triorganozincate was proposed as the active species for the nucleophilic substitution reactions of chlorosilanes by Grignard reagents reported by Oshima and Yorimitsu. They found that the addition of catalytic amounts of $[(TMEDA)ZnCl_2]$ could substantially improve the yields of nucleophilic substitution reactions of aryl-, vinyl- and benzyl-Grignard reagents ($RMgX$) with chlorosilanes (R'_3SiCl) (**Scheme 4.16**).^[139] In order to investigate the active species present in these reactions, the reactivity of $[(TMEDA)ZnCl_2]$ with varying amounts of *para*-tolylmagnesium bromide (1-3 equivalents) towards chlorodimethylphenylsilane ($PhMe_2SiCl$) was examined. The authors found that when $[(TMEDA)ZnCl_2]$ and the Grignard reagent were combined in a ratio of 1:1 and 1:2 no reactivity towards the silane was observed. However, when the ratio was increased to 1:3 the expected arylsilane product was obtained in a 72% yield, suggesting that the active species in this reaction must be a tris(aryl)zincate of the form “ R_3ZnMgX ” (where $R = (p-MeC_6H_4)$). Following a similar catalytic cycle to that proposed for Ishihara’s alkylation reactions, this magnesium triorganozincate can react with the chlorosilane (R'_3Si-Cl) to form the desired

product R₃Si-R and XMgCl, along with ZnR₂ which can then react with another equivalent of the Grignard to regenerate the active triorganozincate species (**Scheme 4.17**).

$$\text{RMgX} + \text{R}'_3\text{Si-Cl} \xrightarrow[\text{1,4-dioxane, time, 20}^\circ\text{C}]{\text{[(TMEDA)ZnCl}_2\text{] (1 mol\%)}} \text{R-SiR}'_3$$

RMgX	SiR' ₃	t (h)	Yield (%)
<i>o</i> -MeC ₆ H ₄ MgBr	PhMe ₂ Si	5	92
<i>p</i> -MeOC ₆ H ₄ MgBr	PhMe ₂ Si	1	87
<i>m</i> -CF ₃ C ₆ H ₄ MgBr	PhMe ₂ Si	3	99
PhMgBr	(ClCH ₂)Me ₂ Si	1	74
<i>p</i> -MeC ₆ H ₄ MgBr	PhMe ₂ Si	15	89
<i>p</i> -MeC ₆ H ₄ MgBr	<i>p</i> -CNC ₆ H ₄ SiMe ₂	1	75
CH ₂ =CMeMgBr	PhMe ₂ Si	3	84
PhCH ₂ MgCl	^t BuMe ₂ Si	7	70
CH ₂ =CHCHMgCl	ⁱ Pr ₃ Si	12	91
BuMgBr	ⁱ Pr ₃ Si	1	trace

Scheme 4.16: Zinc catalysed nucleophilic substitution of chlorosilanes with Grignard reagents.

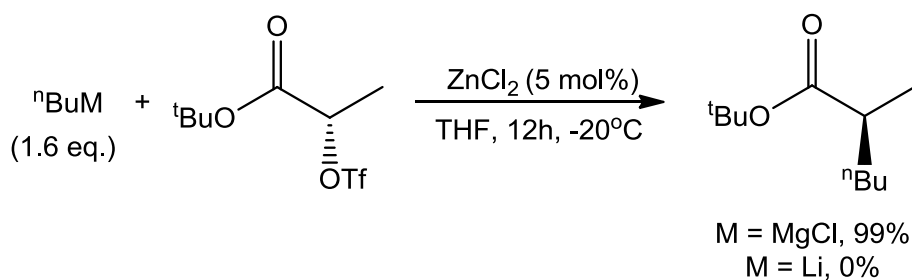


Scheme 4.17: Proposed catalytic cycle for the ZnCl₂ catalysed nucleophilic substitution of a Grignard reagent with a chlorosilane substrate.

Despite magnesium triorganozincates ("R₃ZnMgX") having been proposed as the active species in many reactions, the isolation and characterisation (in the solid state or in solution)

of such species within this context has not been explored. The lack of tangible experimental proof that these mixed-metal species are involved in these important organic transformations is somewhat surprising. Furthermore, a search of the CCDB revealed that only a handful of structurally defined magnesium zincates have been reported (none of which are obtained via salt metathesis reactions),^[140] which contrasts with the relatively abundant number of structures known for alkali metal magnesiates and zincates.^[3, 23b]

The important role of Mg/Zn mixtures in catalytic studies has also been demonstrated by Breit within the context of ZnCl₂ catalysed enantiospecific sp³-sp³ cross-coupling reactions of α-hydroxy ester triflates with Grignard reagents.^[141] Thus, although the reaction proceeded in an almost quantitative yield when ⁿBuMgCl was employed, when performed under otherwise identical conditions with the alkyl lithium reagent (ⁿBuLi) no coupling was observed (**Scheme 4.18**), showing that the presence of the magnesium counterion is essential for this reaction to proceed, and highlighting the fact that magnesium trialkylzincates can display a different level of reactivity to that of lithium trialkylzincates. Under optimised conditions, reaction of this ester triflate could be performed with a range of different Grignard reagents (RMgCl, R = Et, ⁱPr, ⁱBu, etc.) in yields of 90-99% and >99% ee. In addition, this methodology could also be applied to other commercially available α-hydroxy ester triflates, showing similarly impressive yields and ee. A proposed catalytic cycle for these reactions mirrored those of Ishihara and Oshima, suggesting the presence of a magnesium triorganozincate (R₃ZnMgCl) as the active species.^[142]



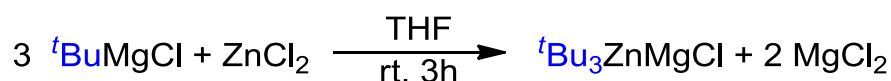
Scheme 4.18: ZnCl₂ catalysed sp³-sp³ cross-coupling reactions of α-hydroxy ester triflates with ⁿBuMgCl and ⁿBuLi.

Thus, the use of catalytic ZnCl₂ to enhance the performance of Grignard reagents in a variety of different synthetic methodologies is a rapidly growing area of organic chemistry. Mixed magnesium-zinc species of the form “R₃ZnMgX”, formed from the metathesis reaction of the relevant Grignard reagent with ZnCl₂, have been generally accepted as the likely active

species in these reactions. However, their presence has only been proposed, and as mentioned above no definitive spectroscopic or structural proof of their formation has been provided. Therefore, in an attempt to provide some new insights into the constitution of these mixed-metal species, the salt metathesis reactions of Grignard reagents with ZnCl₂ were further investigated, employing a sub-stoichiometric amount of ZnCl₂ (Grignard reagent : ZnCl₂ of 3:1) in order to mimic the catalytic conditions of the aforementioned reactions.

4.4 Investigating the salt metathesis reaction of ^tBuMgCl with substoichiometric amounts of ZnCl₂

Following a similar approach to that described for the synthesis of [(THF)₄Mg(μ-Cl)₂Zn(^tBu)(Cl)] (**34**), investigation of the sub-stoichiometric metathesis reaction between ^tBuMgCl and ZnCl₂ in a ratio of 3:1 was initially studied (**Scheme 4.19**).



Scheme 4.19: Proposed metathesis reaction of ^tBuMgCl and ZnCl₂ using a 3:1 excess of Grignard reagent.

Thus, following standard experimental protocol reported in the literature, one equivalent of ZnCl₂ was added to a THF solution of ^tBuMgCl (three equivalents). Interestingly, these reagents combined to give a colourless solution, contrasting with the stoichiometric reaction which yielded a large amount of the insoluble magnesium halozincate [$\{\text{Mg}(\text{THF})_6\}^{2+}\{\text{Zn}_2\text{Cl}_6\}^{2-}$] (**33**). After stirring at room temperature for 3 hours the solution was cooled to -30°C overnight, affording a crop of large hexagonal crystals of [(THF)₄MgCl₂]^[132] which were removed by filtration. Addition of hexane to the remaining filtrate and cooling to -30°C afforded a batch of colourless cubic crystals of the magnesium trialkylzincate [$\{\text{Mg}_2\text{Cl}_3(\text{THF})_6\}^+\{\text{Zn}^t\text{Bu}_3\}^-$] (**40**) (isolated yield = 11%), which were analysed by NMR spectroscopy and X-ray crystallographic analysis. The isolated yield of **40** could be greatly increased (average isolated yield 67%) by performing a co-complexation reaction between ^tBu₂Zn, ^tBuMgCl and MgCl₂, and could also be prepared by the metathesis reaction of ^tBu₂Mg with ZnCl₂ in a ratio of 1.5:1 (isolated yield 29%). Furthermore, NMR analysis of the respective filtrate solutions indicated that **40** is the major species present.

The molecular structure of **40** was found to be the SSIP magnesium-zincate $[\{\text{Mg}_2\text{Cl}_3(\text{THF})_6\}^+\{\text{Zn}^t\text{Bu}_3\}^-]$ (**Figure 4.11**). The cationic fragment comprises of two magnesium centres, bridged by three chlorine atoms, with each of the magnesium atoms bonding to three molecules of THF, giving rise to a distorted octahedral geometry. The anionic fragment is made up of a zinc centre bonded to three *tert*-butyl groups, with the zinc adopting a trigonal planar geometry (average angle around Zn = 119.5°). The Zn-C bonds of **40** (2.068(5), 2.073(4) and 2.081(4) Å) are marginally longer than those found in $[(\text{THF})_4\text{Mg}(\mu\text{-Cl})_2\text{Zn}(^t\text{Bu})(\text{Cl})]$ (**34**) (2.000(3) Å) and $[\{(\text{THF})_2\text{Mg}(\mu\text{-Cl})_3\text{Zn}^t\text{Bu}\}_2]$ (**36**) (1.982(3) and 1.984(3) Å), probably as a consequence of the increased steric hindrance around the zinc centre in **40**. As far as we can ascertain, **40** constitutes the first example of a magnesium trialkylzincate prepared via a metathesis approach to be structurally characterised. However, both the cationic and anionic fragments have previously been found separately in other organometallic species. Thus, Imamoto has reported that the binuclear $\{\text{Mg}_2\text{Cl}_3(\text{THF})_6\}^+$ cation is commonly found in the solid state structures of Grignard reagents,^[130] whilst the tri-*tert*-butylzinc anion has been reported in a number of alkali metal zincate structures, such as $[\{(\text{TMEDA})_2\text{Na}(\text{NC}^t\text{Bu})_2\}^+\{\text{Zn}^t\text{Bu}_3\}^-]$ and $[\{\text{Li}_8\text{H}(\mu_4\text{-C}_7\text{N}_3\text{H}_{12})_6\}^+\{\text{Zn}^t\text{Bu}_3\}^-]$.^[64, 143]

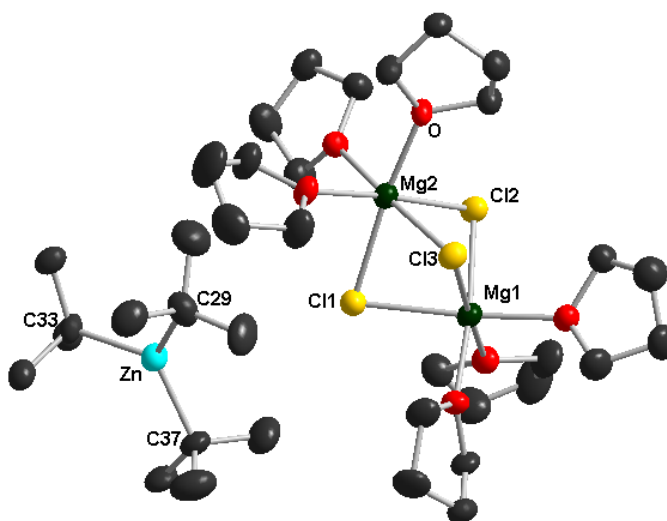
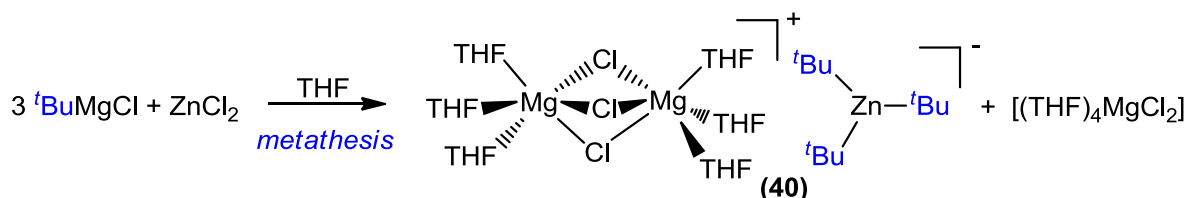


Figure 4.11: Molecular structure of $[\{\text{Mg}_2\text{Cl}_3(\text{THF})_6\}^+\{\text{Zn}^t\text{Bu}_3\}^-]$ (**40**) with 40% probability ellipsoids. Hydrogen atoms and minor THF disorder components have been omitted for clarity. Selected bond distances (Å) and bond angles (°): Zn-C1 2.068(5), Zn-C2 2.073(4), Zn-C3 2.081(4), Mg1-Cl1 2.4998(17), Mg1-Cl2 2.4979(16), Mg1-Cl3 2.5084(17), Mg2-Cl1 2.4953(17), Mg2-Cl2 2.4871(15), Mg2-Cl3 2.5117(18); Cl1-Zn(1)-C2 117.14(19), Cl1-Zn(1)-C3 120.8(2), C2-Zn(1)-C3 120.50(18), Cl2-Mg1-Cl1 83.65(5), Cl2-Mg1-Cl3 86.43(5), Cl1-Mg1-Cl3 84.70(5), Cl2-Mg2-Cl1 83.97(5), Cl2-Mg2-Cl3 86.605, Cl1-Mg2-Cl3 84.73(5).

Despite its SSIP structure, **40** shares some similarities with **34** and **36**, as in both cases the *tert*-butyl group of the Grignard reagent is transferred from magnesium to the more electronegative zinc. Furthermore, MgCl_2 (the co-product of the metathesis reaction) has been incorporated into the constitution of the Mg-Zn hybrid. In the case of **40**, only one equivalent of MgCl_2 is added to form the dinuclear cation $\{\text{Mg}_2\text{Cl}_3(\text{THF})_6\}^+$, whereas the remaining equivalent is isolated as $[(\text{THF})_4\text{MgCl}_2]$ (Scheme 4.20).^[132]



Scheme 4.20: Formation of **40** via metathesis approach.

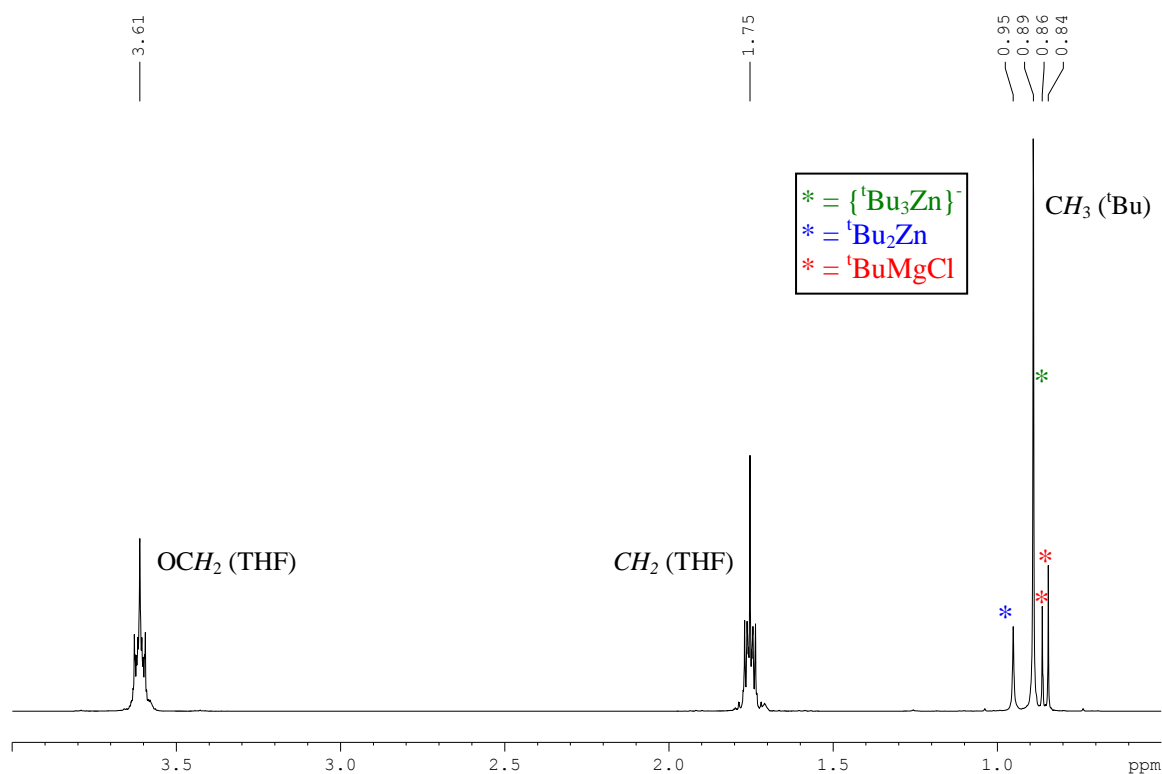


Figure 4.12: ^1H NMR spectrum of **40** in d_8 -THF solution.

Turning to the constitution of **40** in solution, the ^1H NMR spectrum in d_8 -THF solution (Figure 4.12) appears to be much more complex than that observed for **34** (which displayed only one resonance for the ^tBu group), showing four different resonances in the region of the *tert*-butyl groups (major resonance at δ 0.89 ppm, along with three smaller resonances at δ 0.95, 0.86 and 0.84 ppm) which suggests the presence of several organometallic species in

solution. The combined integration of the four singlets in the ^1H NMR spectrum, compared to those of the THF resonances (at δ 3.61 and 1.75 ppm), show a ratio of $^t\text{Bu}:\text{THF}$ of 1:2, which is the same as is seen in the crystal structure of **40**. As shown in **Figure 4.13** the presence of four different *tert*-butyl groups is also observed in the $^{13}\text{C}\{^1\text{H}\}$ NMR spectrum, showing four sets of signals for the methyl groups (major resonance at δ 36.4 ppm, and three smaller resonances at δ 35.6, 34.9 and 32.8 ppm) and quaternary carbons (major resonance at δ 23.9 ppm, and three smaller resonances at δ 24.9, 15.5 and 14.9 ppm).

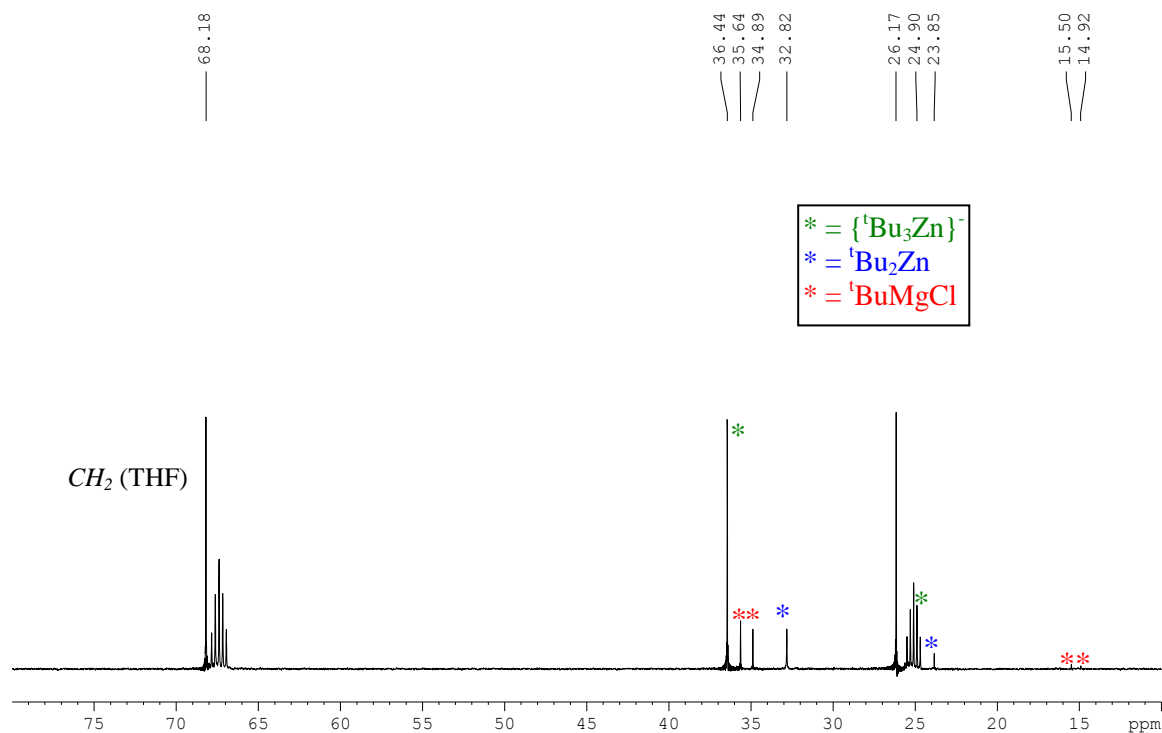
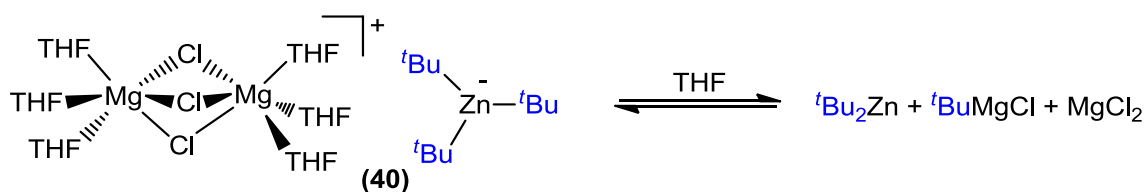


Figure 4.13: $^{13}\text{C}\{^1\text{H}\}$ NMR spectrum of **40** in d_8 -THF solution.

A plausible explanation for this mixture of species could be that in solution **40** is in equilibrium with its monometallic components ($^t\text{Bu}_2\text{Zn}$ and $^t\text{BuMgCl}$) (**Scheme 4.21**). Thus, a comparison of the different resonances observed for **40** with those of the relevant homometallic species ($^t\text{Bu}_2\text{Zn}$, $^t\text{BuZnCl}$, $^t\text{Bu}_2\text{Mg}$ and $^t\text{BuMgCl}$ – **Table 4.6**) shows that the major product in solution (^1H δ 0.89 ppm, $^{13}\text{C}\{^1\text{H}\}$ δ 36.4 and 23.9 ppm) does not correlate with any of the homometallic species, and so is most likely the parent anion of **40** $\{\text{Zn}^t\text{Bu}_3\}^-$. One of the minor species (^1H δ 0.959 ppm, $^{13}\text{C}\{^1\text{H}\}$ δ 32.8 and 24.9 ppm) can be attributed to $^t\text{Bu}_2\text{Zn}$ (^1H δ 0.97 ppm, $^{13}\text{C}\{^1\text{H}\}$ δ 33.0 and 25.4 ppm), while the remaining two species (^1H δ 0.86 and 0.84 ppm, $^{13}\text{C}\{^1\text{H}\}$ δ 35.6, 34.9, 15.5 and 14.9 ppm) are consistent with a compound containing *tert*-butyl groups bonded to magnesium, most likely $^t\text{BuMgCl}$ and $^t\text{Bu}_2\text{Mg}$, which will both be present in THF solutions of $^t\text{BuMgCl}$ due to the Schlenk equilibrium.



Scheme 4.21: Proposed equilibrium of **40** in THF solutions.

Compound	$\delta^1\text{H}$ (CH_3 ^tBu)	$\delta^{13}\text{C}$ (CH_3 ^tBu)	$\delta^{13}\text{C}$ ($\text{C}(\text{CH}_3)_3$ ^tBu)
$[\{\text{Mg}_2\text{Cl}_3(\text{THF})_6\}^+\{\text{Zn}^t\text{Bu}_3\}^-]$ (40)	0.89 (0.95, 0.86, 0.84)	36.4 (35.6, 34.9, 32.8)	23.9 (24.9, 15.5, 14.9)
$^t\text{Bu}_2\text{Zn}$	0.97	33.0	25.4
$^t\text{BuZnCl}$	0.95	33.8	21.6
$^t\text{Bu}_2\text{Mg}$	0.86	36.0	15.8
$^t\text{BuMgCl}$	0.85, 0.86	35.8, 35.0	15.6, 14.9

Table 4.6: ^1H and $^{13}\text{C}\{^1\text{H}\}$ NMR resonances (ppm) for **40** and a variety of homometallic reagents in d_8 -THF. (minor species in parenthesis).

To further investigate the possibility of this equilibrium, concentration and variable temperature studies were carried out. Thus, it was found that at higher concentration (0.22 M) (low dilution) the ^1H NMR spectrum shows only traces of the resonances which correspond to the homometallic species, with a singlet at δ 0.90 ppm showing the $\{^t\text{Bu}_3\text{Zn}\}^-$ anion to be the major species (**Figure 4.14(a)**). Analysis of the integration showed a ratio of $\{^t\text{Bu}_3\text{Zn}\}^-$: $^t\text{Bu}_2\text{Zn}$: $^t\text{BuMgCl}$ of 8:1:1. In contrast, at lower concentration (0.07 M) (high dilution) the ^1H NMR spectrum shows an almost equal mixture of species, with integration showing a ratio of $\{^t\text{Bu}_3\text{Zn}\}^-$: $^t\text{Bu}_2\text{Zn}$: $^t\text{BuMgCl}$ of 3:4:4. (**Figure 4.14(b)**). This behaviour is consistent with the hypothesis that **40** is in equilibrium with its homometallic components, as it would be expected that in a dilute sample disproportionation of **40** into $^t\text{BuMgCl}$ and $^t\text{Bu}_2\text{Zn}$ would be favoured, whilst in a concentrated sample the equilibrium would be shifted towards **40**. The equilibrium between **40** and its homometallic components is also sensitive to changes in temperature. Thus, at elevated temperatures (65°C) (**Figure 4.14(c)**) the resonance at δ 0.90 ppm for the $\{^t\text{Bu}_3\text{Zn}\}^-$ species (which is the major species at 25°C – **Figure 4.14(a)**) disappears almost completely, leaving the homometallic species as the major compounds present in solution, which also supports the proposed equilibrium (see **Scheme 4.21**).

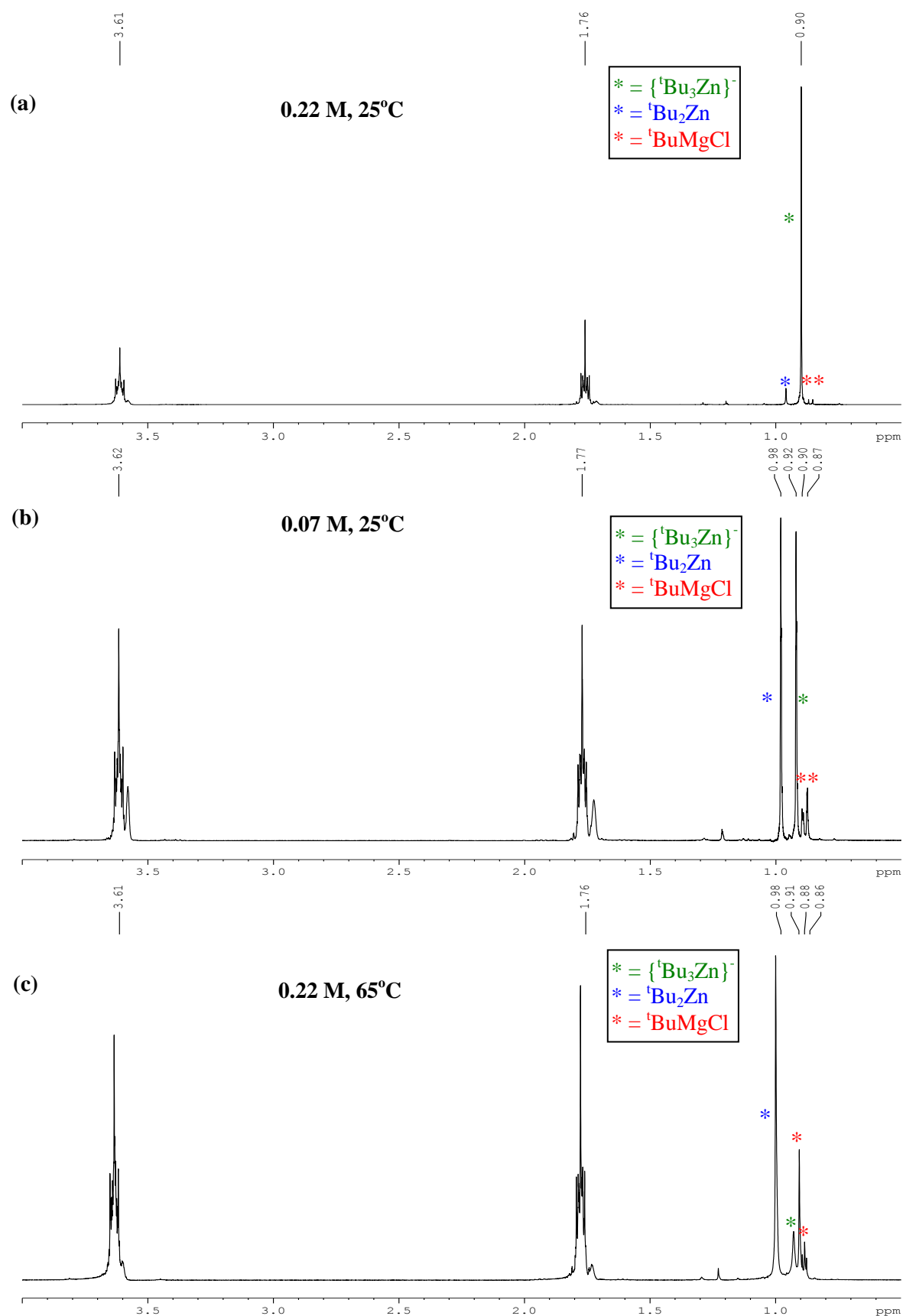


Figure 4.14: ^1H NMR spectrum of **40** in d_8 -THF at (a) high concentration (0.22 M) at 25°C, (b) low concentration (0.07 M) at 25°C and (c) high concentration (0.22 M) at 65°C.

Further evidence for this equilibrium was provided by carrying out controlled addition experiments. A sample of **40** was dissolved in d₈-THF and analysed by ¹H NMR spectroscopy, to which was then added one equivalent of ^tBu₂Zn and the sample analysed again by ¹H NMR spectroscopy. In addition to an increase in ^tBu₂Zn resonance (δ 0.99 ppm), the spectra also showed an increase in the relative intensity of the {^tBu₃Zn}⁻ resonance compared to those of ^tBuMgCl. The experiment was then repeated, but with the addition of ^tBuMgCl to **40**, which resulted in an increase in ^tBuMgCl resonances, along with an increase in the relative intensity of the {^tBu₃Zn}⁻ resonance compared to that of ^tBu₂Zn. These results are consistent with the equilibrium depicted in **Scheme 4.21**, where addition of each of the homometallic species will shift the equilibrium towards the formation of the {Zn^tBu₃}⁻ anion.

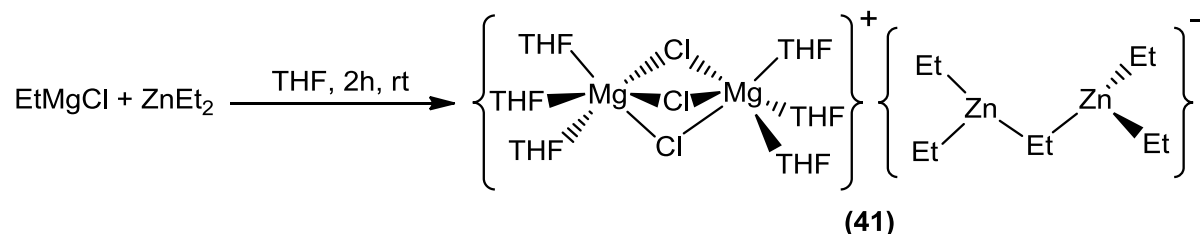
4.5 Investigating the salt metathesis reaction of EtMgCl with substoichiometric amounts of ZnCl₂

In order to investigate the effect of changing the alkyl ligand present, the synthesis of an ethyl magnesium-zinc species, analogous to that of [{Mg₂Cl₃(THF)₆}⁺{Zn^tBu₃}⁻] (**40**), was investigated. Thus, following the same procedure as was employed in the synthesis of **40**, EtMgCl was reacted with ZnCl₂ in a ratio of 3:1 in THF solution. Initially, the reaction yielded a colourless solution, which on leaving to stir for a few minutes formed a precipitate, which could be re-dissolved by gentle heating or the addition of more solvent. Cooling of the reaction mixture yielded colourless crystals, which when analysed by NMR spectroscopy and X-ray crystallography were confirmed as [(THF)₄MgCl₂].^[132]

Despite numerous attempts to isolate a mixed magnesium-zinc species from the filtrate solutions, only crystals of magnesium chloride could be detected by X-ray crystallographic analysis. However, when the crude reaction mixture was analysed by ¹H NMR spectroscopy, in addition to an excess of THF (δ 3.64 and 1.76 ppm) which coordinates to MgCl₂, there were two resonances, a triplet and quartet at δ 1.10 and -0.20 ppm, which were consistent with the CH₃ and CH₂ protons of an ethyl group respectively. Comparison of these resonances with those of EtMgCl (triplet and quartet at δ 1.13 and -0.80 ppm respectively) displayed a significant downfield shift of the CH₂ group, suggesting that EtMgCl was no longer present in the reaction mixture. Furthermore, the ethyl resonances of this unknown species were very

similar to those of [(TMEDA)ZnEt₂] (δ 1.19 and -0.15 ppm) and ZnEt₂ (δ 1.12 and 0.04 ppm), which suggested the transfer of the ethyl group from the Grignard reagent to zinc.

Given that the magnesium tri-*tert*-butylzincate **40** could also be prepared by a co-complexation approach, EtMgCl was reacted with one equivalent of ZnEt₂ in THF solution, and after addition of hexane the resulting solution could be cooled, yielding a crop of colourless crystals of [$\{\text{Mg}_2\text{Cl}_3(\text{THF})_6\}^+\{\text{Zn}_2\text{Et}_5\}^-$] (**41**) in an isolated crystalline yield of 21% which were analysed by NMR spectroscopy and X-ray crystallography. The molecular structure of **41** contained the same $\{\text{Mg}_2\text{Cl}_3(\text{THF})_6\}^+$ cation as was observed in **40**, but instead of the expected trialkylzincate anion, X-ray crystallographic analysis suggested that **41** contained the unusual “zinc rich” anion $\{\text{Zn}_2\text{Et}_5\}^-$ (**Scheme 4.22**). Unfortunately, due to a high degree of static and/or dynamic disorder around the ethyl groups and zinc centres of the anionic fragment, the presence of this $\{\text{Zn}_2\text{Et}_5\}^-$ anion could not be unequivocally confirmed.



Scheme 4.22: Proposed molecular structure of **41**, prepared by reaction of ZnEt₂ and EtMgCl.

Employing a different Grignard reagent, the reaction between EtMgBr and ZnEt₂ could be performed under otherwise identical conditions, from which a less disordered magnesium-zincate [$\{\text{Mg}_3\text{Br}_3(\text{OEt})_2(\text{THF})_6\}^+\{\text{Zn}_2\text{Et}_5\}^-$] (**42**) could be obtained in an isolated yield of 24%, which contains the same $\{\text{Zn}_2\text{Et}_5\}^-$ anion as was proposed for **41** (**Figure 4.15**). Although this compound is still too disordered for a detailed discussion of the bond lengths and angles, the connectivity of the anion is definite, comprising of two distorted trigonal planar zinc centres, each bonded to two terminal Et groups and one further Et ligand which bridges between the two metal centres. The $\{\text{Mg}_3\text{Br}_3(\text{OEt})_2(\text{THF})_6\}^+$ cation contains a six-membered ring comprising of alternating Mg-Br atoms, with each Mg centre solvated by two molecules of THF. The cation also contains two EtO⁻ ligands, each bridging between the three metal centres, the presence of which is probably due to partial oxygen contamination of the Grignard reagent (repeated attempts to prepare **42** without the presence of EtO⁻ ligands proved unsuccessful). Although this cationic fragment has not been previously reported, the related heterobimetallic species [$\{\text{Mg}_3\text{Br}_4(\text{OEt})(\text{Et}_2\text{O})_6\}^+\{\text{MR}_4\}^-$] ($\{\text{MR}_4\}^- = \{\text{Ph}_2\text{InBr}_2\}^-$,

$\{\text{Me}_2\text{Ga}(\text{adamantyl})_2\}^-$ and $\{\text{Me}_2\text{Al}(\text{adamantyl})_2\}^-$,^[144] where Mg is solvated by Et_2O instead of THF, and the three metal centres are bridged by one Br^- and one EtO^- ligand, have been reported as the products of metathesis reactions between metal halides and Grignard reagents, although in these cases the EtO^- group may come from ether cleavage of Et_2O .

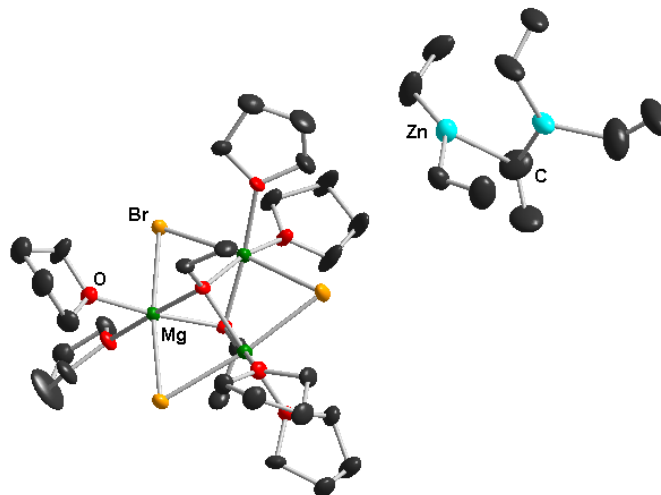


Figure 4.15: Molecular structure of $[\{\text{Mg}_3\text{Br}_3(\text{OEt})_2(\text{THF})_6\}^+\{\text{Zn}_2\text{Et}_5\}^-]$ (**42**) with 40% probability ellipsoids. Hydrogen atoms, disorder component of $\{\text{Zn}_2\text{Et}_5\}^-$ anion and minor THF disorder components have been omitted for clarity. Due to disorder present in the molecular structure bond lengths and angles are not discussed herein.

A related sodium penta(organo)-dizincate $[\{\text{Na}(\text{THF})_6\}^+\{\text{Zn}_2\text{Cp}_5\}^-]$ has been reported by Carmona, prepared by reacting NaCp with ZnCl_2 in a ratio of 5:2.^[145] Interestingly, when this stoichiometry was altered to 3:1 the sodium triorganozincate $[(\text{THF})_2\text{NaZnCp}_3]$ was obtained. In contrast, when the reaction of ZnEt_2 with EtMgCl is performed in a stoichiometry of 1:1 or 2:1 (matching that of the product) only $[\{\text{Mg}_2\text{Cl}_3(\text{THF})_6\}^+\{\text{Zn}_2\text{Et}_5\}^-]$ (**41**) is obtained in an isolated yield of 21% and 45% respectively. Furthermore, returning to the *tert*-butyl magnesium-zincate $[\{\text{Mg}_2\text{Cl}_3(\text{THF})_6\}^+\{\text{Zn}^t\text{Bu}_3\}^-]$ (**40**), when the reaction of $^t\text{BuMgCl}$ and ZnCl_2 was performed in a ratio of 5:2 or $^t\text{BuMgCl}$ with Zn^tBu_2 in a ratio of 1:2 only the trialkylzincate **40** was obtained, suggesting that in the case of **40** and **41**, the steric demands of the alkyl group employed (^tBu and Et) determine the final conformation of the zincate anion, and not the stoichiometry of the reagents employed.

Having prepared a pure sample of $[\{\text{Mg}_2\text{Cl}_3(\text{THF})_6\}^+\{\text{Zn}_2\text{Et}_5\}^-]$ (**41**) through the co-complexation of ZnEt_2 and EtMgCl the constitution of this species in solution was then studied. Thus, the ^1H NMR spectrum of **41** in d_8 -THF solution showed a single set of

resonances for the ethyl groups, with a triplet at δ 1.09 ppm for the CH₃ group and a quartet at δ -0.21 ppm for the CH₂ group, along with two multiplets at 3.64 and 1.76 ppm for THF. The resonances of the ethyl group were almost identical to those observed for the crude reaction mixture from the metathesis reaction between three equivalents of EtMgCl and ZnCl₂ (δ 1.10 and -0.20 ppm), which is consistent with the formation of the same magnesium-zincate from these two different synthetic approaches. As mentioned above the resonances of the ethyl groups of **41** are similar to those of [(TMEDA)ZnEt₂] (δ 1.19 and -0.15 ppm) but shifted downfield compared to those of EtMgCl (δ 1.13 and -0.80 ppm) (**Table 4.7**), emphasising the zinc character of these groups in solution. The ¹³C{¹H} NMR spectrum of **41** displayed only two resonances at δ 0.8 and 13.6 ppm, corresponding to the CH₂ and CH₃ carbons of the ethyl group respectively, which also confirm the retention of the zinc character in solution when compared to the equivalent chemical shifts of [(TMEDA)ZnEt₂] and EtMgCl (**Table 4.7**).

Compound	δ ¹ H (CH ₂)	δ ¹ H (CH ₃)	δ ¹³ C{ ¹ H} (CH ₂)	δ ¹³ C{ ¹ H} (CH ₃)
[{Mg ₂ Cl ₃ (THF) ₆ } ⁺ {Zn ₂ Et ₅ } ⁻] (41)	-0.21	1.09	0.8	13.6
[(TMEDA)ZnEt ₂]	-0.15	1.19	1.7	14.6
EtMgCl	-0.80	1.13	-2.4	14.0

Table 4.7: ¹H and ¹³C{¹H} NMR data (ppm) for the ethyl groups of **41**, [(TMEDA)ZnEt₂] and EtMgCl in d₈-THF.

Interestingly, whereas [{Mg₂Cl₃(THF)₆}⁺{Zn^tBu₃}⁻] (**40**) displayed a complex equilibrium in solution between the mixed metal species and the homometallic components, Zn^tBu₂ and ^tBuMgCl (vide supra), both the ¹H and ¹³C{¹H} NMR spectra of **41** indicate the presence of only one ethyl species. However, if the molecular structure was retained in solution the presence of two different ethyl resonances for **41** would be expected, one for the four terminal ligands and a further resonance for the bridging Et ligand. To try and clarify the constitution of the {Zn₂Et₅}⁻ anion in solution, a variable temperature study (from 25°C to -78°C) of a d₈-THF solution (0.125 M) of **41** was performed (**Figure 4.16**). The biggest change observed on reducing the temperature from 25°C was for the CH₂ resonance, which shifted slightly upfield from δ -0.21 ppm to -0.25 ppm between 25°C and -43°C, combined with a marked broadening of the sharp quartet observed at 25°C to a broad singlet at -43°C. This slight upfield shift of the resonances continued between -43°C and -78°C to δ -0.28 ppm, along with the re-emergence of a sharp quartet below -58°C (**Figure 4.16**). This data suggests the existence of a

dynamic equilibrium in solution, where one species is favoured at ambient temperatures, but at lower temperatures the equilibrium shifts, and a different species is formed. One possible explanation for this would be a situation whereby the $\{\text{Zn}_2\text{Et}_5\}^-$ anionic fragment of **41** is present at lower temperatures, but at room temperature this species can break to form $\{\text{ZnEt}_3\}^-$ and ZnEt_2 (Scheme 4.23).

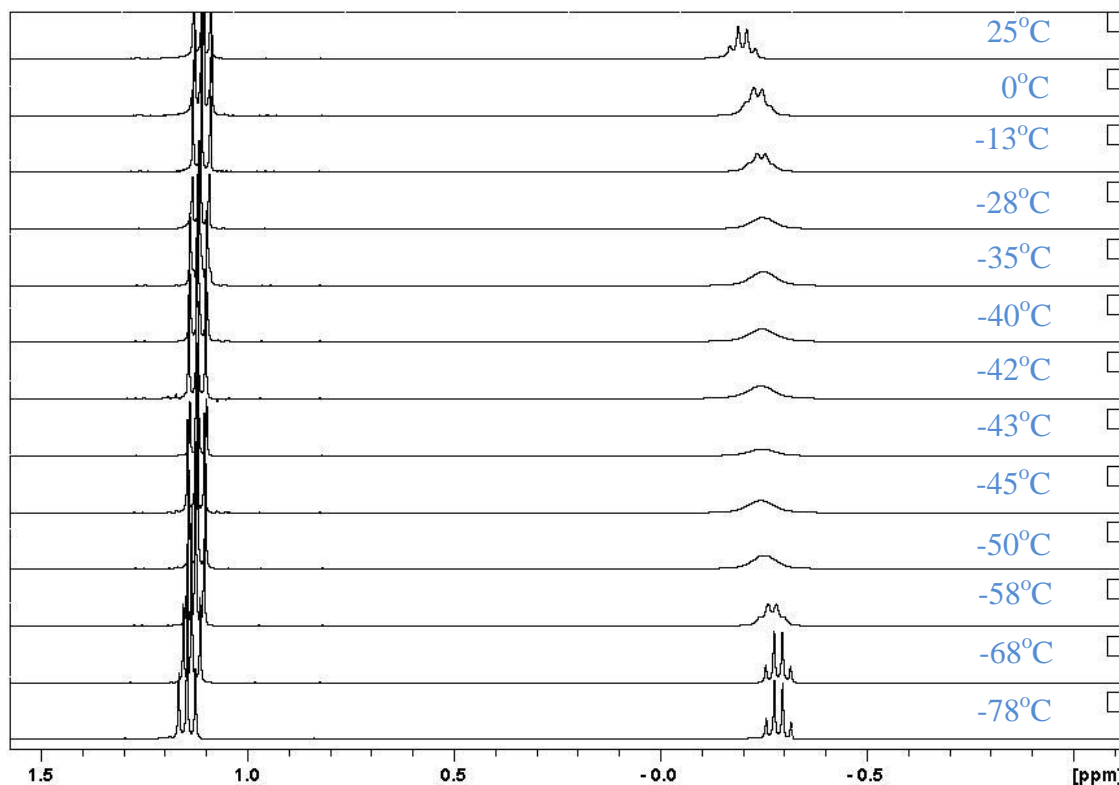
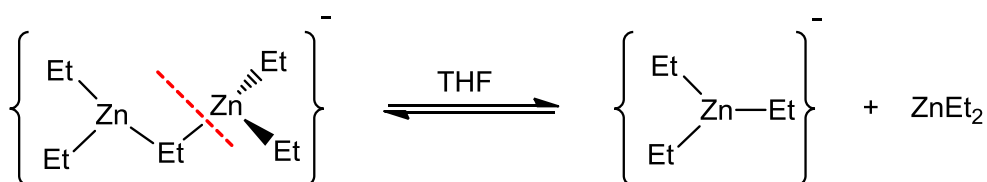


Figure 4.16: Variable temperature study of the CH_2 resonance of **41** in d_8 -THF solution (0.125 M) from 25°C to -78°C .



Scheme 4.23: Proposed equilibrium in solution between $\{\text{Zn}_2\text{Et}_5\}^-$ and $\text{ZnEt}_2/\{\text{ZnEt}_3\}^-$.

In order to further explore this proposed equilibrium, a series of experiments were performed where to a d_8 -THF solution of **41** (0.125 mmol, 0.25 M) was added half an equivalent of a ferrocene internal standard (0.062 mmol). Analysis of this sample by ^1H NMR spectroscopy displayed a quartet at δ -0.29 ppm for the $\text{Zn}-\text{CH}_2$ protons and a triplet at δ 1.13 ppm for the CH_3 protons. Integration of these resonances relative to that of the singlet for the Cp rings of

the ferrocene internal standard (integrated to 5H) revealed that the CH_2 quartet accounted for 10 protons and the CH_3 triplet for 15 protons (**Figure 4.17(a)**). This solution was then placed under vacuum for 1 hour, and the resulting orange residue re-dissolved in d_8 -THF solution and analyzed again by ^1H NMR spectroscopy, showing a significant upfield shift of the Zn-CH_2 quartet from δ -0.25 to -0.73 ppm (**Figure 4.17(b)**). Furthermore, the relative integration of the CH_2 and CH_3 groups with respect to the internal standard showed that the integration of these resonances had dropped to 6.2 and 9.2 protons respectively, which suggested the loss of two ethyl groups from the original $\{\text{Zn}_2\text{Et}_5\}^-$ anionic fragment.

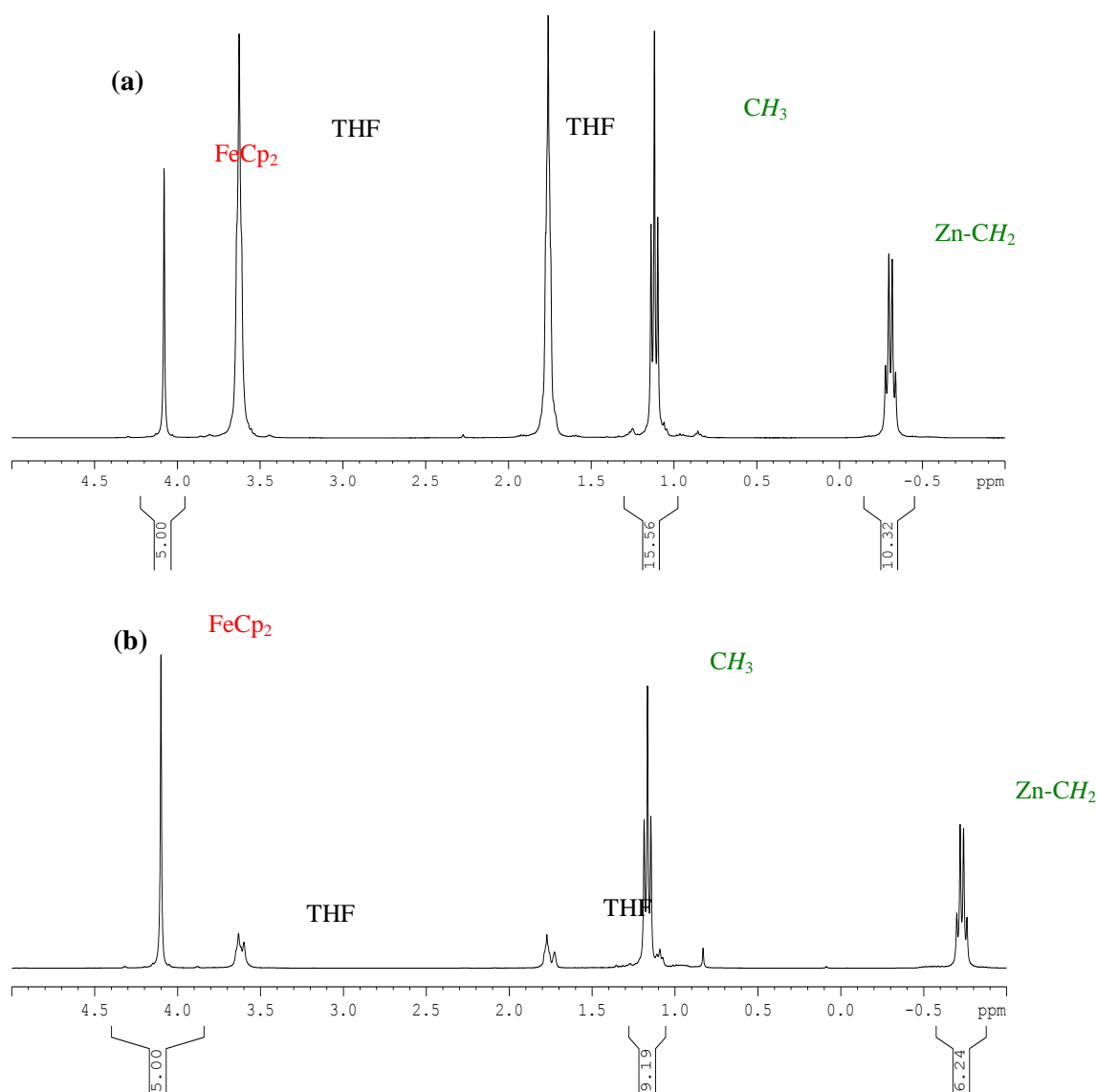


Figure 4.17. ^1H NMR spectra of (a) a mixture of $[\{(\text{THF})_6\text{Mg}_2\text{Cl}_3\}^+\{\text{Zn}_2\text{Et}_5\}^-]$ (**41**) and ferrocene (used as an internal standard) in a 2:1 ratio in d_8 -THF at room temperature and (b) after the sample was left under vacuum for 1 hour, then re-dissolved in d_8 -THF.

The significant decrease in the integration of the ethyl resonances can be explained by taking into account the high volatility of ZnEt_2 , which is readily removed *in vacuo*, even in the presence of a coordinating solvent such as THF. Thus, if in THF solution $\{\text{Zn}_2\text{Et}_5\}^-$ does break up into smaller species such as $\{\text{ZnEt}_3\}^-$ and ZnEt_2 , then when placed under vacuum the dialkylzinc species will be removed, leaving only $\{\text{ZnEt}_3\}^-$. Therefore, these results confirm the existence of ZnEt_2 in THF solutions of **41**, which can be readily removed *in vacuo*. Furthermore, the significant upfield shift of the CH_2 resonance from δ -0.25 to -0.73 ppm suggests that a more carbanionic Zn-Et species has been formed, which is consistent with the conversion of a $\{\text{Zn}_2\text{Et}_5\}^-$ anion into a $\{\text{ZnEt}_3\}^-$ anion. In order to further assess the constitution of **41** in solution, a sample of the crystalline material was also studied by ^1H DOSY.

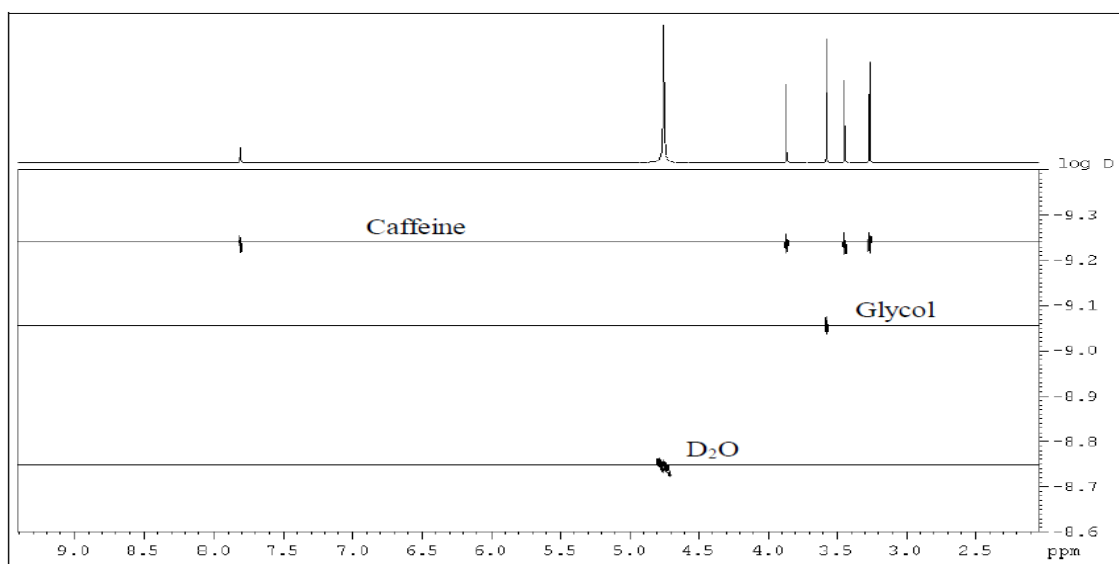


Figure 4.18: Example of a ^1H DOSY spectrum of a mixture of ethyleneglycol and caffeine in D_2O .^[146]

As briefly mentioned in **Chapter 1.3.2**, DOSY is an NMR technique which can be used to identify the individual components of mixtures in solution. In this pseudo two-dimensional technique, one dimension represents normal chemical shift data (e.g. ^1H , ^7Li , $^{13}\text{C}\{^1\text{H}\}$ NMR spectrum), while in the second dimension species are resolved by their diffusion properties (diffusion coefficient D), where D is inversely proportional to the size of the molecule.^[75] The measurement of D is performed using a technique called pulsed gradient spin-echo (PGSE), which was first reported almost 50 years ago,^[147] but was only incorporated into the two-dimensional technique in 1992,^[148] which is now referred to as DOSY. A simple example to demonstrate the effect of this technique is the ^1H DOSY of a mixture of caffeine and

ethyleneglycol in D_2O (**Figure 4.18**).^[146] Thus, the smallest component of the mixture, D_2O , has the largest D value and will appear lower down on the y-axis ($\log D$). Resolution of the two larger components, glycol and caffeine, is also observed, with the larger molecule, caffeine, possessing a smaller D value than that of glycol or D_2O .

Recent DOSY studies have revealed that the addition of simple hydrocarbon molecules as internal standards can be used to determine the aggregation state of organometallic species. Thus, Williard and co-workers have demonstrated that in the presence of internal standards DOSY can be used to determine the formula weight (FW) of a number of organolithium compounds, by correlation of their diffusion coefficients with the diffusion coefficients and FW of the internal standards.^[149] For example, analysis of THF-solvated lithium diisopropylamide (LDA) by $^{13}C\{^1H\}$ DOSY in d_8 -toluene solution in the presence of internal standards (benzene, ethylbenzene, 1-octadecene (ODE) and *cis*-/*trans*-cyclododecene (CDDE)) revealed that the lithium amide possesses a smaller D value than the internal standards present. Correlation of $\log D$ vs. $\log FW$ allowed an approximate FW of the lithium amide species to be estimated, which revealed that in solution it probably exists as the dimeric species $[(THF)Li(DA)]_2$ (**Figure 4.19**).^[149b]

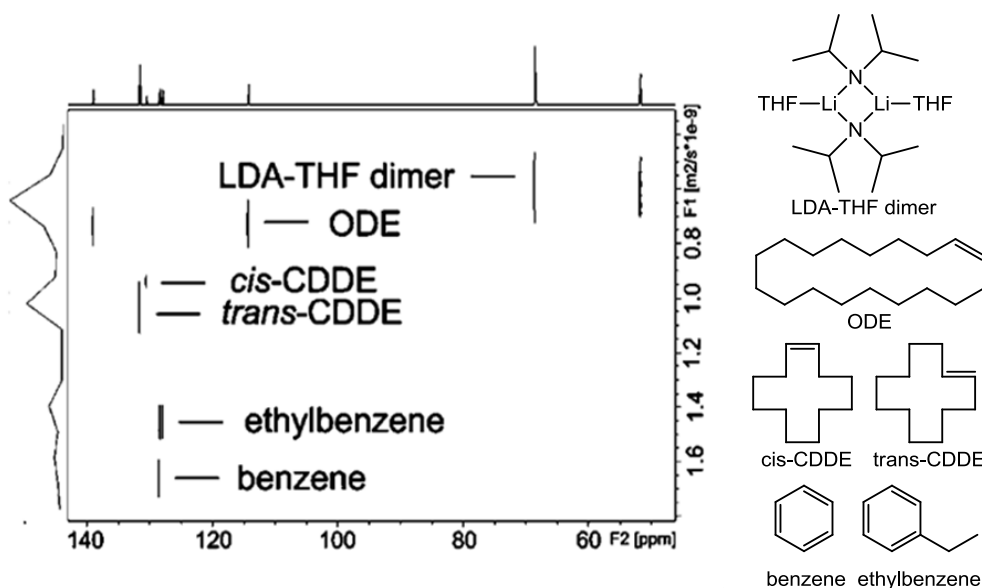


Figure 4.19: $^{13}C\{^1H\}$ DOSY of $[(THF)Li(DA)]_2$ in d_8 -toluene solution in the presence of internal standards.^[75, 149b]

As mentioned in **Chapter 1**, following a similar procedure Mulvey and co-workers have elucidated the complex solution behaviour of the turbo Hauser bases $[(TMP)MgCl_2Li(THF)_3]$ (**10**) and $[(DA)MgCl_2Li(THF)_2]_2$ (**11**),^[80b] and more recently have demonstrated that the *in*

situ mixture of [Li(TMP).Zn(TMP)₂.TMEDA.2LiCl], prepared by metathesis reaction of Li(TMP) with ZnCl₂.TMEDA (in a ratio of 3:1), contains a THF solvated [Li(TMP).2LiCl] complex and Zn(TMP)₂, as two distinct species.^[76] Furthermore, DOSY studies have also been used to demonstrate that the lithium triorganozincate [(PMDETA)LiZnMe₃] retains its CIP structure in d₈-toluene solutions, whereas the SSIP triorganozincate [(diglyme)₂Li]⁺{ZnMe₃}⁻ displays no interaction between lithium centre and the {ZnMe₃}⁻ anion in solution.^[27]

Thus, DOSY is emerging as an extremely powerful tool for advancing the understanding of the complex constitution of organometallic species in solution. Following a similar procedure to that reported by Mulvey and co-workers, **41** was analysed by diffusion-ordered NMR spectroscopy (DOSY) in d₈-THF solution in the presence of internal standards (TPhN: 1,2,3,4-tetraphenylnaphthalene; PhN: phenylnaphthalene; and TMS: tetramethylsilane), in an attempt to provide further confirmation of the identity of the species present in solution.

Analysis of **41** by variable temperature ¹H NMR spectroscopy had revealed a distinct change in the resonance of the Zn-CH₂ group between 25°C and -43°C, with the sharp quartet which appeared at ambient temperature collapsing down to a broad singlet at -43°C, consistent with a change in the constitution of the “Zn-Et” species present in solution. To provide a clear picture of these two different situations, DOSY studies of **41** in d₈-THF solution (0.125 M) were performed at both 25°C (**Figure 4.20(a)**) and at -40°C (**Figure 4.20(b)**). At both temperatures the CH₂ and CH₃ resonances of the Zn-Et species show a single cross peak with the same diffusion coefficient (*D*). However, the value of *D* at 25°C [*D*(Zn-Et, 25°C) = 1.24(3) × 10⁻⁹ m² s⁻¹] is significantly larger than that obtained at -40°C [*D*(Zn-Et, 40°C) = 2.69(1) × 10⁻¹⁰ m² s⁻¹]. Thus, when the *D* of the “Zn-Et” species is compared to that of the internal standards, it appears at a similar value to that of PhN at 25°C [1.18(2) × 10⁻⁹ m² s⁻¹] (**Figure 4.20(a)**), but lies somewhere between PhN [3.3(1) × 10⁻¹⁰ m² s⁻¹] and TPhN [1.79(1) × 10⁻¹⁰ m² s⁻¹] at -40°C (**Figure 4.20(b)**). As *D* is inversely proportional to the size of the molecule, these results suggest that as the temperature decreases there must be an important change in the constitution of **41** in solution, with a larger “Zn-Et” species present at -40°C compared to that at 25°C.

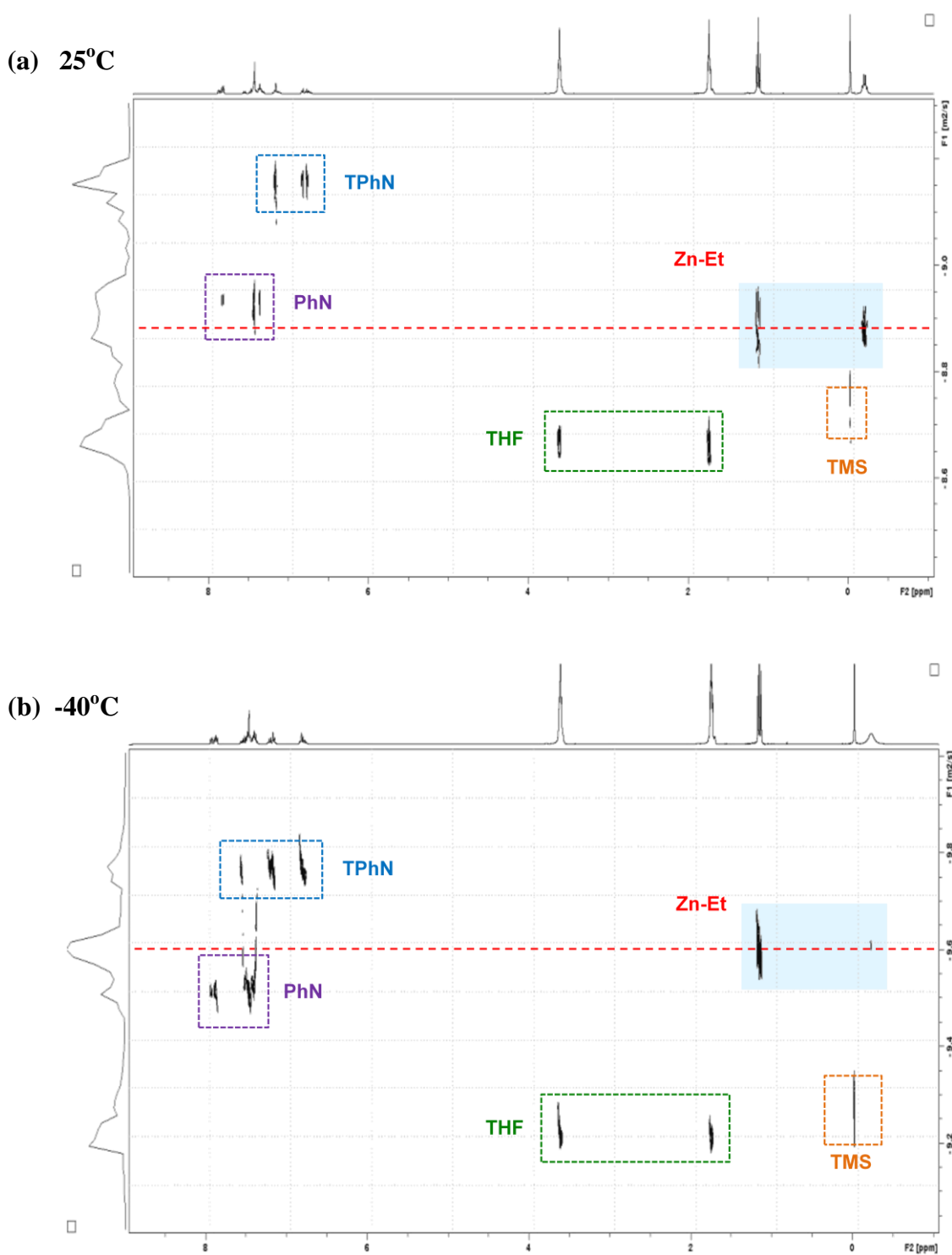


Figure 4.20: ^1H DOSY experiment of a d_8 -THF solution of **41** in the presence of three internal standards (TPhN, PhN and TMS) at (a) 25°C [$D(\text{Zn-Et}) = 1.24(3) \times 10^{-9} \text{ m}^2 \text{ s}^{-1}$] and (b) at -40°C [$D(\text{Zn-Et}) = 2.69(1) \times 10^{-10} \text{ m}^2 \text{ s}^{-1}$].

In the previously mentioned DOSY studies,^[75, 149] correlation of $\log D$ with $\log \text{FW}$ of the unknown species and the internal standards allowed the FW of the organometallic species to be determined, which relied on the assumption that the approximate size of a species is

proportional to its FW. However, an added complication when studying zinc organometallic species is that zinc has a much larger FW compared to its size than lithium, and as a result the approximation that FW is proportional to size may not hold for zinc containing species. To investigate this further, the 1H DOSY of $[(TMEDA)ZnEt_2]$, the molecular structure of which is known to be monomeric,^[131] was performed in the presence of internal standards (TPhN, PhN, TMS). The values obtained for D were correlated against FW ($\log D$ vs. $\log FW$), and against molar volume (V) (V determined by DFT optimised geometries – see **Appendix**) ($\log D$ vs. $\log V$). The results revealed that the FW determined by DOSY for $[(TMEDA)ZnEt_2]$ (187 g mol^{-1}) had an error of -22% compared to the actual FW ($239.72 \text{ g mol}^{-1}$), but the volume determined by DOSY for $[(TMEDA)ZnEt_2]$ ($173 \text{ cm}^3 \text{ mol}^{-1}$) had an error of only -9% compared to volume determined by DFT ($189.30 \text{ cm}^3 \text{ mol}^{-1}$). Therefore, the results suggest that a $\log D$ vs. $\log V$ correlation seems to be more accurate than $\log D$ vs. $\log FW$ for organozinc species, and data extracted from the diffusion properties of **41** would be treated in this way.

Thus, the presence of internal standards (TPhN, PhN and TMS) of known volume in the DOSY studies of **41** allowed the calibration curve of $\log D$ vs. $\log V$ to be prepared for the DOSY spectra at each of the two different temperatures (see **Appendix** for full DOSY data). By applying the D value obtained for the “Zn-Et” species at each temperature into these calibration curves an approximate value of the size of these unknown species could be determined, and could therefore be used to estimate the constitution of the species present in d_8 -THF solutions of **41**. Thus, at 25°C the volume obtained for the “Zn-Et” species is $160 \text{ cm}^3 \text{ mol}^{-1}$, compared to $226 \text{ cm}^3 \text{ mol}^{-1}$ at -40°C . The DFT optimized molar volume obtained for the $\{Zn_2Et_5\}^-$ (see Appendix for details of DFT optimized geometries) indicates that the volume of the penta(ethyl)-dizinc anion present in **41** is $232 \text{ cm}^3 \text{ mol}^{-1}$. Therefore, the data obtained by 1H DOSY studies indicates that at -40°C the $\{Zn_2Et_5\}^-$ anion is the major species present, with an error of only 3% between the molar volume of $\{Zn_2Et_5\}^-$ ($232 \text{ cm}^3 \text{ mol}^{-1}$, determined by DFT optimization) and that obtained for the unknown “Zn-Et” species by DOSY at -40°C ($226 \text{ cm}^3 \text{ mol}^{-1}$) (**Figure 4.21**).

However, analysis of the DOSY data at room temperature reveals that the parent anion of **41** $\{Zn_2Et_5\}^-$ is not the major species present, as in this case there is an error of 31% between the DFT optimized molar volume (V) of the anion ($232 \text{ cm}^3 \text{ mol}^{-1}$) and the volume obtained from the 1H DOSY ($160 \text{ cm}^3 \text{ mol}^{-1}$) (**Figure 4.21**). Therefore, at room temperature, the “Zn-Et”

species present must be significantly smaller than the parent anion of **41** $\{\text{Zn}_2\text{Et}_5\}^-$. The volumes of some smaller aggregates which could be present in solution were calculated by DFT optimization (see **Appendix**), and the error of these species with respect to the volume obtained by DOSY studies determined (**Figure 4.21**).

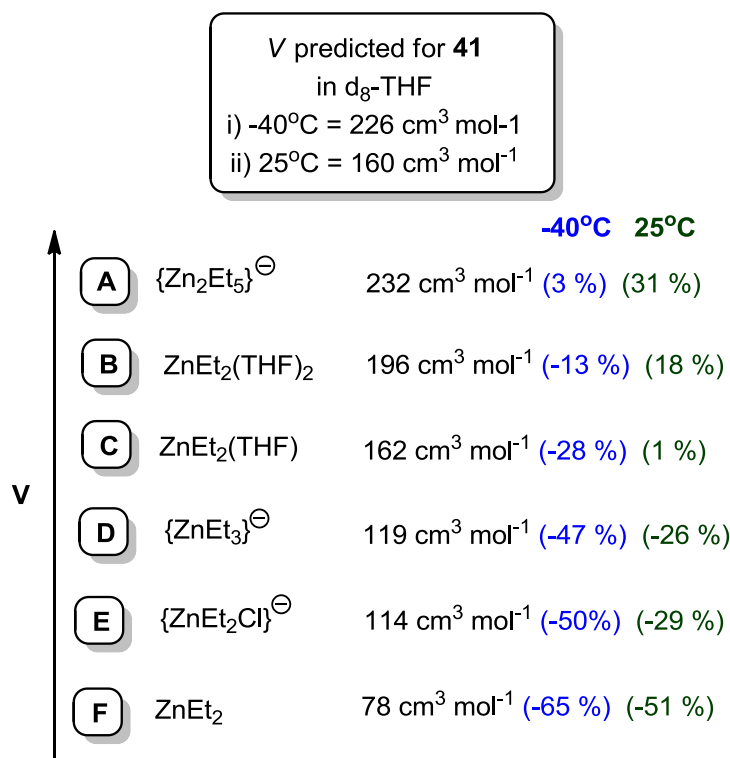
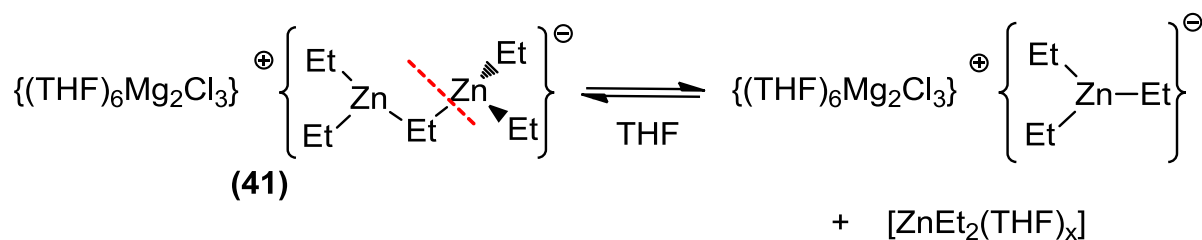


Figure 4.21: Possible species of the parent anion $\{\text{Zn}_2\text{Et}_5\}^-$ present for **41** in d_8 -THF solution with errors (in parentheses) with respect to the estimated volume (V) predicted by ^1H DOSY studies at -40°C (blue) and 25°C (green).

Thus, the data suggests that smaller aggregates such as $\{\text{ZnEt}_3\}^-$ and ZnEt_2 are the most likely species present at this temperature. DOSY studies are unable to differentiate between species of similar size, and so the volume determined will be an average of the species present, a situation made even more complex by differing grades of THF solvation, and by the presence of MgCl_2 in solution which could also interact with the zinc centres (vide infra – **Chapter 5**). Although DOSY cannot be used to determine the absolute constitution of the species present in solution at room temperature, it can establish that the parent anion of **41** $\{\text{Zn}_2\text{Et}_5\}^-$ is unlikely to be the major species present under these conditions (25°C , 0.125 M). One possible explanation for this would be the existence of an equilibrium of $\{\text{Zn}_2\text{Et}_5\}^-$ with a triethylzincate $\{\text{ZnEt}_3\}^-$ and $[(\text{THF})_x\text{ZnEt}_2]$ ($x = 0-2$) (**Scheme 4.24**), which is consistent with the results obtained from the NMR solution studies of **41** in the presence of a ferrocene internal standard mentioned previously.



Scheme 4.24: Possible temperature dependant equilibrium of **41** in d₈-THF solution.

4.6 Conclusions

Initial studies into the seemingly simple stoichiometric metathesis reaction between ^tBuMgCl and ZnCl₂ have provided a number of interesting results. The reaction, which would be expected to form the homometallic species ^tBuZnCl and MgCl₂, in fact yielded the new mixed-metal magnesium zincate [(THF)₄Mg(μ-Cl)₂Zn(^tBu)(Cl)] (**34**), formed by co-complexation of the two expected products of the reaction. This reaction also resulted in the formation of a second product, the solvent separated mixed magnesium-zinc chloride species [[Mg(THF)₆]²⁺{Zn₂Cl₆}²⁻] (**33**), which is formed by the reaction of ZnCl₂ and MgCl₂ (present in solution due to the Schlenk equilibrium), diminishing the amount of ZnCl₂ present in solution to react with ^tBuMgCl, resulting in the low yields obtained for **34**.

Altering the bulk solvent employed in these metathesis reactions from THF to toluene the analogous dimeric species [{(THF)₂Mg(μ-Cl)₃Zn(R)}₂] (R = ^tBu, **36**; ⁿBu, **37**; Et, **38**; *o*-C₆H₄OMe, **39**) can be obtained by reacting ZnCl₂ with a number of different Grignard reagents (^tBuMgCl, ⁿBuMgCl, EtMgCl and (*o*-C₆H₄OMe)MgBr), although formation of the insoluble magnesium halozincate species still occurs under these conditions. Subsequent DFT studies have also revealed that the formation of these Mg-Zn hybrid species is thermodynamically favoured over the formation the relevant homometallic species (RZnCl and MgCl₂), which suggests that the presence of these hybrid species in organic transformations which involve the synthesis of organozinc reagents *in situ* may be much more common than initially thought.

When the metathesis reaction of ^tBuMgCl with ZnCl₂ is performed under substoichiometric conditions (^tBuMgCl:ZnCl₂ 3:1) the new magnesium-zinc alkyl-rich hybrid [[Mg₂Cl₃(THF)₆]⁺{Zn^tBu₃}⁻] (**40**) is formed. The isolation of this species provides important structural insights for these types of compounds, which have previously been proposed as the

active species in organic reactions involving Grignard reagents with catalytic amounts of ZnCl₂. Analysis of d₈-THF solutions of this compound by ¹H and ¹³C{¹H} NMR spectroscopy revealed that it exists in a temperature and concentration dependant equilibrium with its constituent homometallic components, ^tBuMgCl and Zn^tBu₂, illustrating the complex behaviour that these species can display in solution.

Turning to the analogous metathesis reaction between EtMgCl and ZnCl₂, the unexpected “zinc rich” magnesium-zinc hybrid species [$\{\text{Mg}_2\text{Cl}_3(\text{THF})_6\}^+ \{\text{Zn}_2\text{Et}_5\}^-$] (**41**) was obtained along with [(THF)₄MgCl₂]. Using a similar co-complexation approach to that employed in the synthesis of **40**, pure crystalline material of **41** could be obtained. NMR studies, including ¹H DOSY experiments, have revealed the intricate constitution of **41** in solution, which appears to exist in a temperature dependant equilibrium with the related triethylzincate species $\{\text{ZnEt}_3\}^-$ and neutral $[\text{ZnEt}_2(\text{THF})_x]$ (x = 0-2).

Thus, this systematic study of the metathesis reactions of ZnCl₂ with variable amounts of Grignard reagent offers a closer insight into the mixed-metal species involved in this fundamental synthetic methodology. Collectively, these results highlight that the constitution of the organometallic species involved can be an extremely complicated subject.

Chapter 5: Expanding magnesium-zinc hybrid chemistry: **nucleophilic alkylation reactions of ketones**

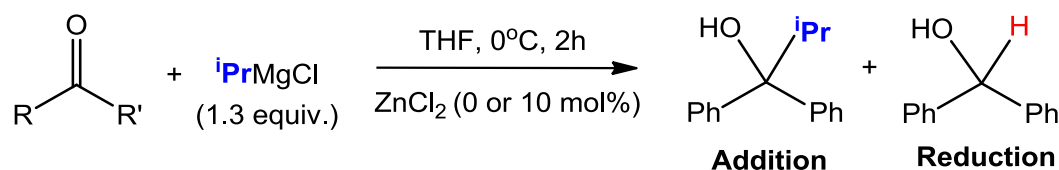
Amongst the different synthetic tools available for forming new C-C bonds, the addition of polar organometallic reagents to carbonyl compounds constitutes one of the most important methodologies in organic chemistry.^[150] Combining strong nucleophilic power with ready availability and ease of preparation,^[31] Grignard reagents (RMgX) have emerged as the reagent of choice for performing these reactions.^[118b] Notwithstanding, on many occasions the desired addition products are obtained along with the formation of unwanted reduction and/or enolization products, as a result of competing β -hydride elimination and α -deprotonation reactions respectively.^[118a] To overcome this drawback, several synthetic strategies have been developed to enhance the nucleophilicity of Grignard reagents as well as activating the carbonyl group of the substrate. For example, previous reports have shown that the addition of stoichiometric (or excess) amounts of inorganic salts such as CeCl₃,^[151] LiCl,^[152] FeCl₂^[153] or LnCl₃.2LiCl (Ln = La, Ce, Nd)^[154] can enhance the selectivity and functional group tolerance of Grignard reagents, minimizing the formation of unwanted side-products.

On the other hand, due to their softer nucleophilic character organozinc reagents (ZnR₂) display much greater levels of selectivity in the nucleophilic addition of carbonyl compounds. However, on many occasions the presence of a chelating ligand,^[155] or transition-metal catalysts^[156] is required to promote the alkylation reactions, due to low kinetic reactivity of the Zn-C bonds.

As mentioned in **Chapter 4**, Ishihara and co-workers have shown that catalytic amounts of ZnCl₂ can be employed to significantly improve the selectivity of Grignard reagents in nucleophilic addition reactions of ketones, suppressing, and in some cases completely inhibiting, the formation of the reduction products, allowing the relevant tertiary alcohols to be obtained in excellent yields (**Scheme 5.1**).^[137] Closely related to this work, Knochel has recently reported that the addition of MgCl₂ to organozinc reagents can greatly accelerate their addition to aldehydes, ketones and CO₂.^[123]

Despite these excellent organic studies, which suggest the participation of mixed Mg-Zn compounds in addition reactions, to date these proposed intermediates have not been detected

or characterised (either in solution or in the solid-state). Building on the results reported in **Chapter 4**, this chapter will investigate the alkylating ability of the magnesium-zinc hybrids species $[\{\text{Mg}_2\text{Cl}_3(\text{THF})_6\}^+\{\text{Zn}^t\text{Bu}_3\}^-]$ (**40**) and $[\{\text{Mg}_2\text{Cl}_3(\text{THF})_6\}^+\{\text{Zn}_2\text{Et}_5\}^-]$ (**41**), as well as halide-rich $[\{(\text{THF})_2\text{Mg}(\mu\text{-Cl})_2\text{ZnEt}\}_2]$ (**38**) (all of which are obtained via salt metathesis reactions of the relevant Grignard reagent with varying amounts of ZnCl_2), in order to assess if these compounds could be the true active species involved in these chemoselective organic transformations.



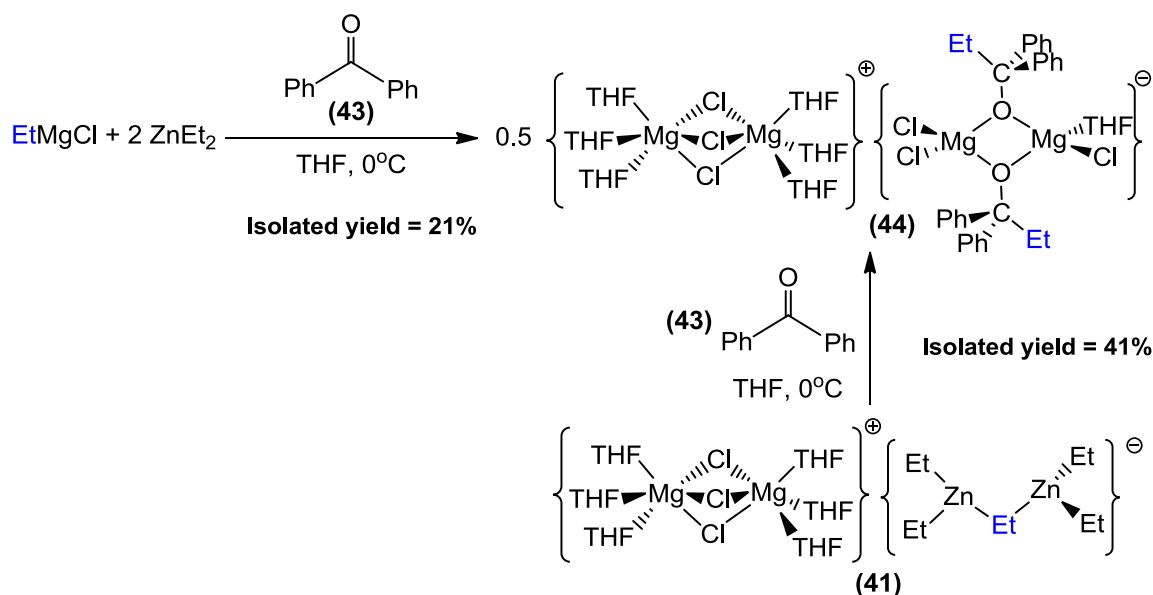
Ketone	with ZnCl_2		without ZnCl_2	
	Addition (%)	Reduction (%)	Addition (%)	Reduction (%)
PhC(O)Me	85	0	31	11
PhC(O)Et	95	0	56	38
PhC(O) ⁱ Pr	87	12	38	59
PhC(O)CF ₃	78 ^[a]	20	23	73
α-naphthyl-C(O)Me	76	0	33	12
β-naphthyl-C(O)Me	76	0	35	12
2-thienyl-C(O)Me	91	0	40	0
4-pyridyl-C(O)Me	80	7	73	11
2-adamantanone	52 ^[a]	27	16	78

Scheme 5.1: Alkylation of ketones by ⁱPrMgCl in the presence and absence of catalytic amounts of ZnCl_2 . ^[a] 30 mol% ZnCl_2 employed.^[137]

5.1 Investigating the reactivity of $[\{\text{Mg}_2\text{Cl}_3(\text{THF})_6\}^+\{\text{Zn}_2\text{Et}_5\}^-]$ (**41**) in stoichiometric alkylation reactions of benzophenone

In order to investigate if Mg-Zn hybrids **40** and **41** can be the active species in the chemoselective alkylation of ketones by Grignard reagents in the presence of ZnCl_2 , their

reactivity towards benzophenone was studied. However, it was found that the *tert*-butyl derivative **40** fails to react with the ketone, probably due to the steric bulk of the alkyl groups in this compound (which also precludes the reduction product). Turning to the less sterically demanding ethyl derivative **41**, a THF solution of **41** (prepared *in situ* via co-complexation of ZnEt_2 and EtMgCl in a ratio of 2:1) was cooled to 0°C , to which was added one molar equivalent of **43** and the reaction mixture stirred for 1 hour. Addition of hexane, and cooling of the solution overnight in the freezer afforded a crop of colourless crystals of $[\{\text{Mg}_2\text{Cl}_3(\text{THF})_6\}^+\{\text{Mg}_2(\text{OC}(\text{Et})\text{Ph}_2)_2\text{Cl}_3(\text{THF})\}^-]$ (**44**) in an isolated yield of 21%, which could be improved to 41% by reacting isolated crystals of **41** with **43** under otherwise identical conditions (**Scheme 5.2**). Furthermore, *in situ* monitoring of the reaction between **41** and **43** by NMR spectroscopy indicated that the alkylation of benzophenone to form **44** proceeded in a yield of 89% (*vide infra*).



Scheme 5.2: Alkylation of benzophenone by **41** to form $[\{\text{(THF)}_6\text{Mg}_2\text{Cl}_3\}^+\{\text{Mg}_2(\text{OC}(\text{Et})\text{Ph}_2)_2\text{Cl}_3(\text{THF})\}^-]$ (**44**).

The successful addition of an ethyl group from **41** to benzophenone was confirmed by the molecular structure of **44** (determined by X-ray crystallography), which surprisingly revealed the formation of the homometallic magnesium-magnesiato compound $[\{\text{Mg}_2\text{Cl}_3(\text{THF})_6\}^+\{\text{Mg}_2(\text{OC}(\text{Et})\text{Ph}_2)_2\text{Cl}_3(\text{THF})\}^-]$ (**Figure 5.1**). Exhibiting a SSIP structure, **44** contains the same dinuclear magnesium cation $\{\text{Mg}_2\text{Cl}_3(\text{THF})_6\}^+$ as previously reported in the magnesium-zinc hybrid species **40** and **41**. However, the anionic part of this molecule is very unusual, comprising of two $\{\text{OC}(\text{Et})\text{Ph}_2\}^-$ alkoxide fragments, resulting from the

nucleophilic addition of one of the ethyl groups of **41** across the carbonyl group of the ketone, to form a tetrahedral (sp^3) carbon atom (average angle around C1 = 109.5° and C16 = 109.5°). Consistent with the formation of a C-O single bond, an elongation of the C-O bond distances in **44** (C1–O1 1.424(3), C16–O2 1.431(3) Å) compared to that of the ketone **43** (C=O 1.214–1.223 Å)^[157] is observed. These two newly formed alkoxide ligands bridge between two magnesium centres (Mg1 and Mg2) to form a central four membered {Mg–O–Mg–O} ring (sum of internal angles = 359.5°), with the two magnesium centres exhibiting different chemical environments. Thus, whereas Mg2 is bonded to two terminal Cl atoms, Mg1 only coordinates to one Cl, completing its tetrahedral coordination by bonding to a molecule of THF, giving rise to an extremely rare non-symmetrical magnesium alkoxide dimeric arrangement, contrasting with the numerous examples of symmetrical dimeric magnesium alkoxide species which have previously been reported.^[158] In addition, the fact that the resulting $\{\text{OC}(\text{Et})\text{Ph}_2\}^-$ alkoxide fragment forms part of an anion rather than a neutral magnesium compound can be an advantage to its further functionalisation, as in general, magnesiate display enhanced nucleophilicity than the corresponding neutral species.

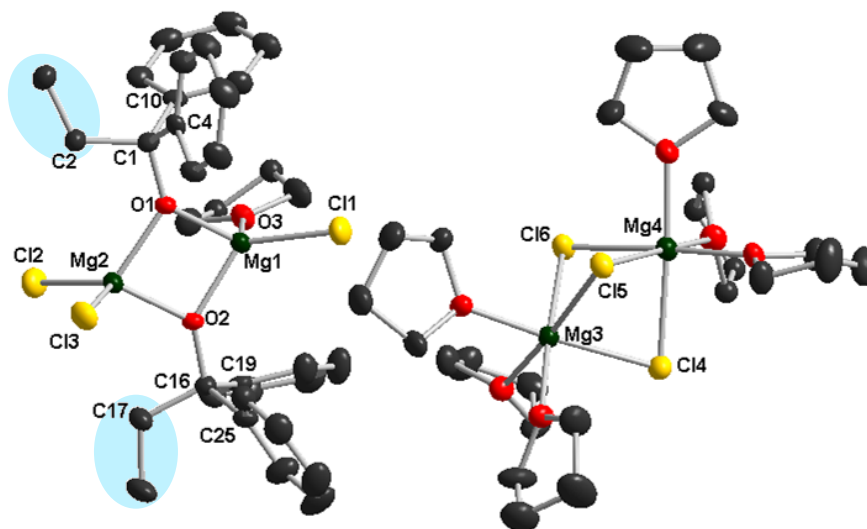


Figure 5.1: Molecular structure of $[\{\text{Mg}_2\text{Cl}_3(\text{THF})_6\}^+ \{\text{Mg}_2(\text{OC}(\text{Et})\text{Ph}_2)_2\text{Cl}_3(\text{THF})\}^-]$ (**44**) with 50% probability ellipsoids. Hydrogen atoms have been omitted for clarity. *Selected bond distances (Å) and bond angles ($^\circ$) of the anion* : Mg1–Cl1 2.2732(10), Mg1–O1 1.944(2), Mg1–O2 1.9439(18), Mg1–O3 2.010(2), Mg2–Cl2 2.3057(10), Mg2–Cl3 2.3084(12), Mg2–O1 1.9770(17), Mg2–O2 1.976(2), O1–C1 1.424(3), O2–C16 1.431(3), C1–C2 1.547(4), C16–C17 1.540(3); Cl1–Mg1–O1 124.66(7), Cl1–Mg1–O2 123.87(6), Cl1–Mg1–O3 106.95(6), O1–Mg1–O2 84.54(8), O1–Mg1–O3 107.78(8), O2–Mg1–O3 106.55(8), Cl2–Mg2–Cl3 115.94(4), Cl2–Mg2–O1 115.28(6), Cl2–Mg2–O2 113.18(7), Cl3–Mg2–O1 111.60(7), Cl3–Mg2–O2 113.69(7), O1–Mg2–O2 82.82(7), Mg1–O1–Mg2 96.08(8), Mg1–

$O2-Mg2$ 96.10(8), $O1-C1-C2$ 106.82(19), $O1-C1-C4$ 110.1(2), $O1-C1-C10$ 107.3(2), $C2-C1-C4$ 108.3(2), $C2-C1-C10$ 113.7(2), $C4-C1-C10$ 110.50(19), $O2-C16-C17$ 106.5(2), $O2-C16-C19$ 107.6(2), $O2-C16-C25$ 110.1(2), $C17-C16-C19$ 113.8(2), $C17-C16-C25$ 108.2(2), $C19-C16-C25$ 110.6(2).

The “magnesium-only” constitution of **44** contrasts with the mixed-metal nature of its precursor **41**, and paradoxically, to the best of our knowledge represents the first example of a structurally defined intermediate of the nucleophilic addition of a zincate to the carbonyl group of a ketone. Furthermore, its structure also highlights the important role of the inorganic salt ($MgCl_2$) in this reaction (present in both the anionic and cationic moieties of **44**), which acting as a strong Lewis acid provides a solvation anchor for the substrate and structural support for the newly generated alkoxide groups.

Confirmation of the successful alkylation of **43** was also provided by 1H and $^{13}C\{^1H\}$ NMR analysis of a d_8 -THF solution of **44**. The most diagnostic resonances of the 1H NMR spectrum were a triplet and quartet at δ 0.74 and 2.46 ppm respectively, belonging to the CH_2 and CH_3 protons of the ethyl group, which appear considerably downfield compared to those observed for the magnesium penta(ethyl)-dizincate **41** (δ -0.21 and 1.09 ppm for the CH_2 and CH_3 protons respectively). This remarkable change in the resonance is consistent with the transfer of the ethyl group from the zincate to the carbonyl carbon of the ketone. In addition, the $^{13}C\{^1H\}$ NMR spectrum reveals a substantial change in the chemical shift of the quaternary carbon that has experienced the nucleophilic addition, appearing considerably more shielded (δ 80.9 ppm) than the carbonyl carbon of benzophenone (δ 195.9 ppm), as would be expected due to the change in its hybridisation from sp^2 to sp^3 .

As mentioned above, despite the alkylation of **43** being performed with mixed magnesium-zinc species **41**, the isolated product from the reaction is the magnesium-magnesiato **44**, which implies that other zinc containing organometallic species must be formed during the reaction. In an attempt to confirm the fate of zinc in the stoichiometric alkylation reaction of **43** by **41**, the reaction was performed in d_8 -THF and monitored by 1H NMR spectroscopy at $0^\circ C$ (**Figure 5.2**). After 2 hours all of the benzophenone had been consumed, generating **44** as the major species (highlighted in blue, **Figure 5.2(b)**), along with a small amount of the reduction alkoxide “ $Mg-OC(H)Ph_2$ ” and ethene, resulting from competing β -hydride elimination. The most indicative resonances for this minor product were a small multiplet at δ

5.91 ppm for the hydride which has added across the ketone, along with some minor aromatic resonances (highlighted in red, **Figure 5.2(b)**). Analysis of the relative integration of these two species revealed a ratio of alkylation : reduction of 89:11. The high chemoselectivity of this reaction is similar to that previously reported by Ishihara for the reaction of EtMgCl and benzophenone in the presence of catalytic amounts of ZnCl₂ (in terms of the ratio of secondary and tertiary alcohols formed).^[137]

As well as the two alkoxide species, the ¹H NMR spectrum also revealed the presence of two resonances, a quartet and a triplet at δ 0.02 and 1.12 ppm respectively, consistent with the presence of an ethyl containing organometallic species (highlighted in green, **Figure 5.2(b)**). Comparison of the integration of these resonances with those of the ethyl group which has added across the C=O group of benzophenone revealed a ratio of ~4:1. These resonances were shifted slightly downfield compared to those of **41** (δ -0.21 and 1.09 ppm), suggesting the formation of neutral “Zn-Et” species with less carbanionic character. Furthermore, a comparison of these chemical shifts with those observed for ZnEt₂ in the same deuterated solvent (δ 0.04 and 1.12 ppm) suggested that the formation of **44** occurs with the formation of two equivalents of ZnEt₂, or a closely related species (vide infra).

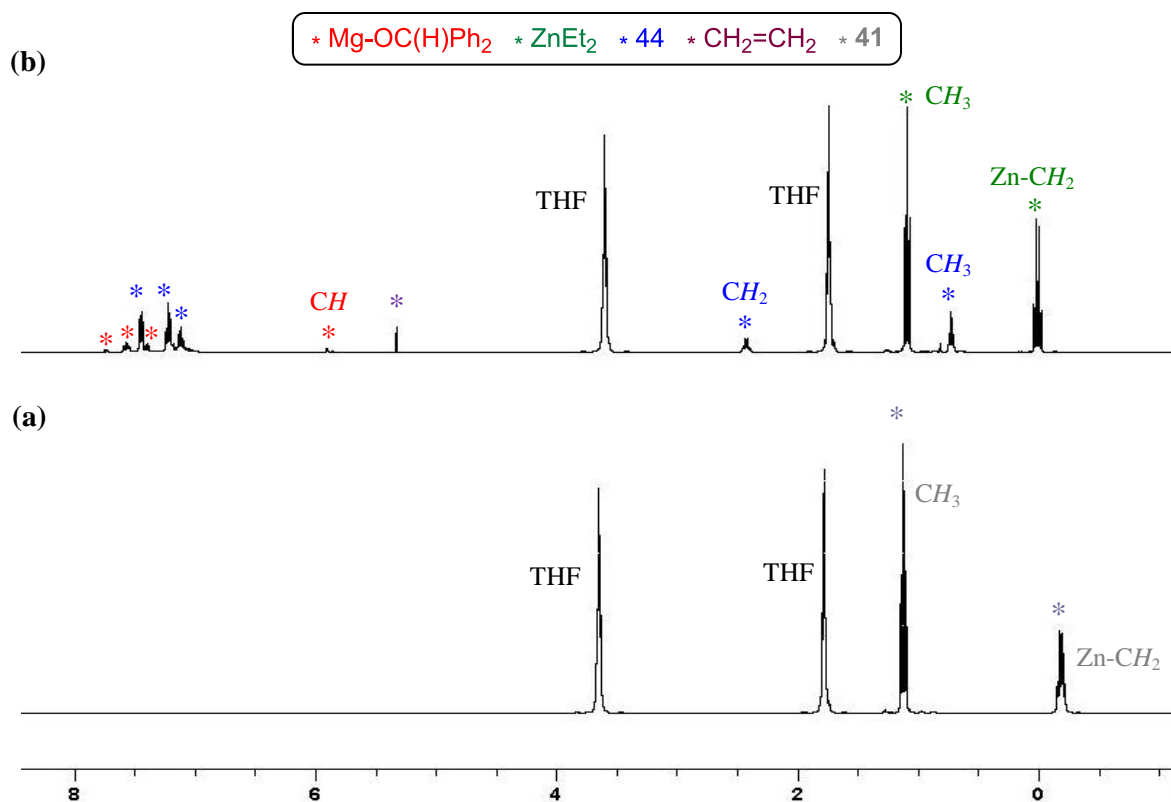


Figure 5.2: ¹H NMR spectra for d₈-THF solutions of (a) [$\{\text{Mg}_2\text{Cl}_3(\text{THF})_6\}^+\{\text{Zn}_2\text{Et}_5\}^-$] (**41**) and (b) equimolar amounts of **41** and benzophenone (**43**) after 2 hours at 0°C.

Contrasting with the high levels of selectivity displayed by [$\text{Mg}_2\text{Cl}_3(\text{THF})_6$] $^+\{\text{Zn}_2\text{Et}_5\}^-$ (**41**) in the alkylation of benzophenone (**43**), which led to the formation of the desired tertiary alcohol $\text{Ph}_2\text{C}(\text{OH})\text{Et}$ (**45**) in a yield of 90% after aqueous work-up, previous reports have shown that if **43** is reacted with EtMgCl then the major species obtained from the reaction is the reduction product $\text{Ph}_2\text{CH}(\text{OH})$ (**46**) (71%), formed through β -hydride elimination, along with only a small amount of the **45** (25%).^[137] Furthermore, the corresponding organozinc reagent (ZnEt_2) displays no reactivity (alkylation or reduction) towards the ketone, consistent with the low kinetic reactivity of the Zn-C bonds in this neutral organozinc species. As alluded to in **Chapter 4.5**, DOSY studies revealed that in solution the penta(ethyl)-dizinc anion of **41** $\{\text{Zn}_2\text{Et}_5\}^-$ exists in a complex equilibrium with smaller aggregates such as $\{\text{ZnEt}_3\}^-$ and ZnEt_2 . As a result, it is not possible to determine unequivocally which “Zn-Et” species performs the alkylation of benzophenone, although it would be expected that the triethylzincate anion $\{\text{ZnEt}_3\}^-$ would be more nucleophilic than $\{\text{Zn}_2\text{Et}_5\}^-$ where the negative charge is shared between two metal centres.

The enhanced levels of reactivity and selectivity displayed by **41** in the alkylation of benzophenone, compared with the results obtained when using the relevant homometallic reagents, EtMgCl and ZnEt_2 , can be attributed to the synergic cooperation of both magnesium and zinc in this bimetallic system. Although, conventional organozinc reagents are softer nucleophiles, and therefore less likely to undergo β -hydride elimination than RMgX ,^[159] they are also reluctant to react with non-activated ketones due to their low kinetic reactivity.^[26b] In the case of **41**, the formation of an ethylzincate anion $\{\text{Zn}_2\text{Et}_5\}^-$ overcomes this kinetic hurdle, allowing the selective transfer of the Et group to benzophenone. The magnesium cation $\{\text{Mg}_2\text{Cl}_3(\text{THF})_6\}^+$ also plays an important role in this reaction, acting as a strong Lewis acid (stronger than neutral MgCl_2), anchoring the ketone and activating the carbonyl group towards the nucleophilic attack by the zincate anion. These results are in agreement with theoretical studies by Uchiyama and Nakamura which have reported a similar increased reactivity in nucleophilic addition reactions of lithium trialkylzincates towards aldehydes, where the cooperative activation of the ketone by lithium is coupled with the enhanced nucleophilicity of the trialkylzincate fragment.^[25b]

Interestingly, along with the formation of **44**, the reaction of **41** with benzophenone proceeded with the generation of two equivalents of ZnEt_2 (**Figure 5.2(b)**), which coupled with the homometallic constitution of **44** provides new insights into how Zn could be recycled in a

catalytic process (similar to the one proposed by Ishihara using ZnCl_2 as a catalyst). It is also noteworthy that when the alkylation of benzophenone (**43**) was studied using a solution of **41** prepared *in situ* via the metathesis reaction of EtMgCl with ZnCl_2 (in a ratio of 5:2), analysis of the crude reaction mixture by ^1H NMR spectroscopy indicates the formation of **44** and the reduction alkoxide “ Mg-OC(H)Ph_2 ” in a ratio of 95:5, along with two equivalents of ZnEt_2 and excess THF due to the presence of $[(\text{THF})_4\text{MgCl}_2]$ (**Figure 5.3**). Surprisingly, unlike ZnEt_2 which is extremely volatile *in vacuo*, the “ ZnEt_2 ” species formed in this reaction can still be observed when an aliquot of the reaction mixture is analysed by NMR spectroscopy (after the volatiles have been removed *in vacuo*). This suggests that the “ ZnEt_2 ” fragment must be interacting with another species in solution, which significantly decreases its volatility. One possible scenario is that ZnEt_2 interacts with some of the MgCl_2 present in solution. To investigate this further, equimolar amounts of ZnEt_2 and MgCl_2 were mixed in THF and analysed by ^1H NMR spectroscopy, displaying a quartet and triplet at δ 0.00 and 1.08 ppm respectively, which were consistent with those for the “ ZnEt_2 ” species observed in the reactions of **41** and benzophenone (δ 0.01 and 1.10 ppm) (**Figure 5.2(b)** and **Figure 5.3**).

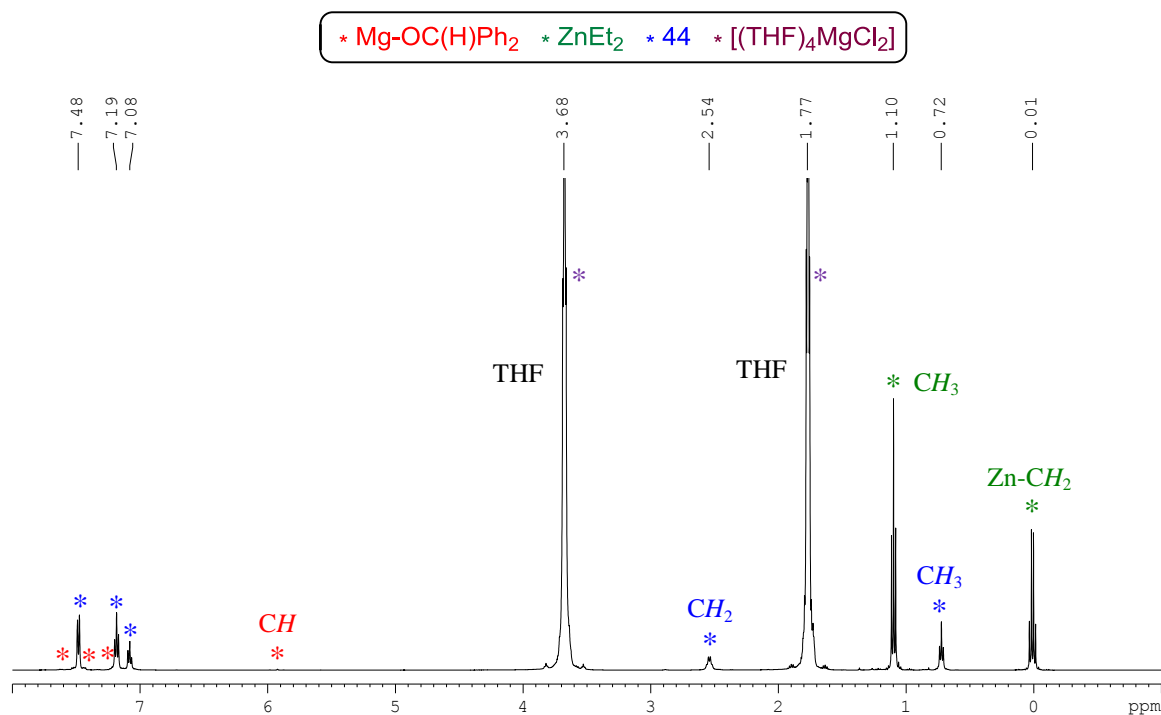


Figure 5.3: ^1H NMR spectrum in d_8 -THF of the crude organometallic species formed in the reaction of **41** (prepared via metathesis of 5 EtMgCl + 2 ZnCl_2) with **43** after 2 hours at 0°C .

Further support of this association between ZnEt_2 and MgCl_2 was provided when a ^1H DOSY study of this mixture was compared with the data obtained for a THF solution of ZnEt_2

(Figure 5.4 - see Appendix for full DOSY data). The results confirm that an interaction between MgCl_2 and ZnEt_2 must exist in THF solutions, as a substantial size increase is observed for the “Zn-Et” species (average volume increases from $136 \text{ cm}^3 \text{ mol}^{-1}$ for ZnEt_2 to $175 \text{ cm}^3 \text{ mol}^{-1}$ for $\text{ZnEt}_2 \cdot \text{MgCl}_2$). A comparison of the diffusion coefficients (D) of the relevant “Zn-Et” species with those obtained for the internal standards showed that whereas ZnEt_2 displays a larger D value ($1.86(3) \times 10^{-9} \text{ m}^2 \text{ s}^{-1}$), and therefore will be smaller in size, than PhN ($1.51(3) \times 10^{-9} \text{ m}^2 \text{ s}^{-1}$) (Figure 5.4(a)), for $\text{ZnEt}_2 \cdot \text{MgCl}_2$ the D value observed ($1.28(4) \times 10^{-9} \text{ m}^2 \text{ s}^{-1}$) is similar to that of PhN ($1.28(2) \times 10^{-9} \text{ m}^2 \text{ s}^{-1}$), indicating that both species have a similar sizes (Figure 5.4(b)).

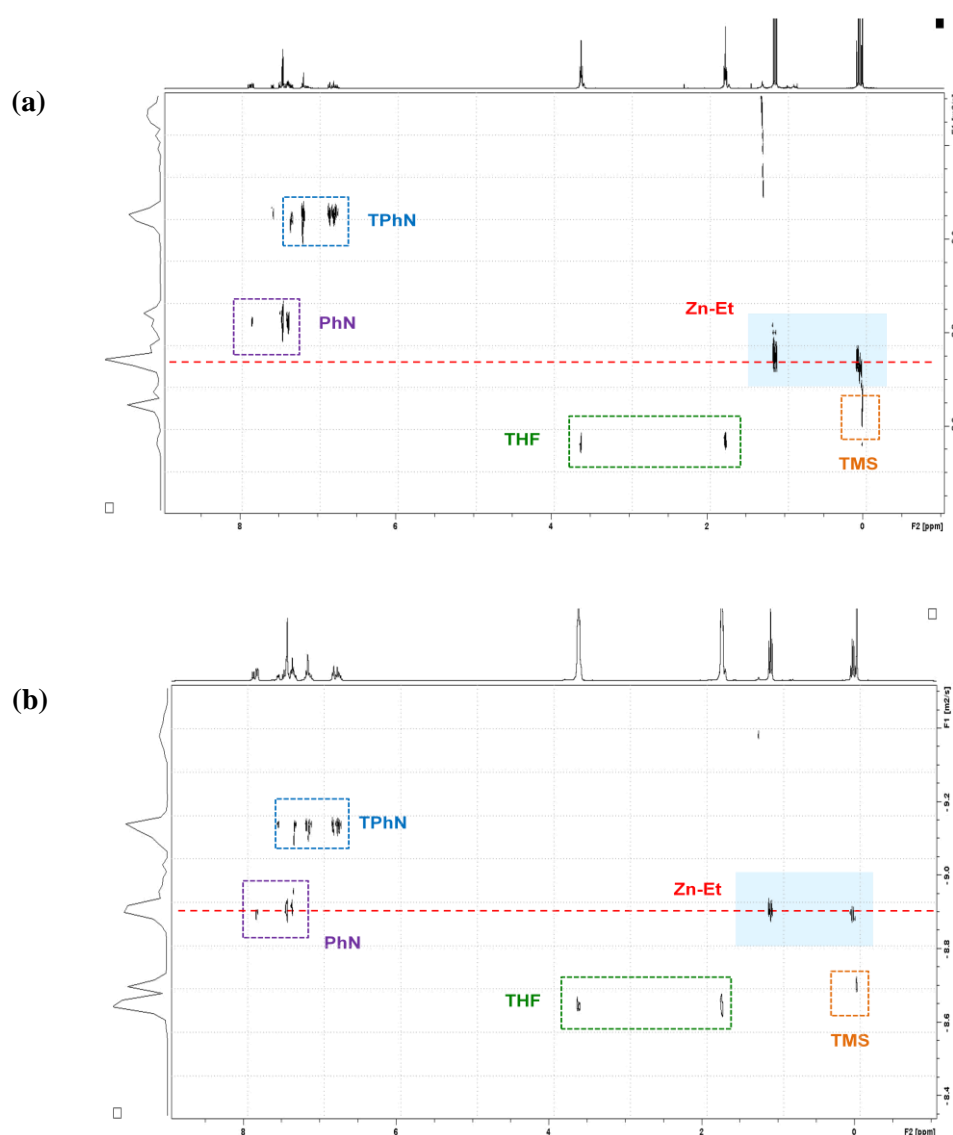
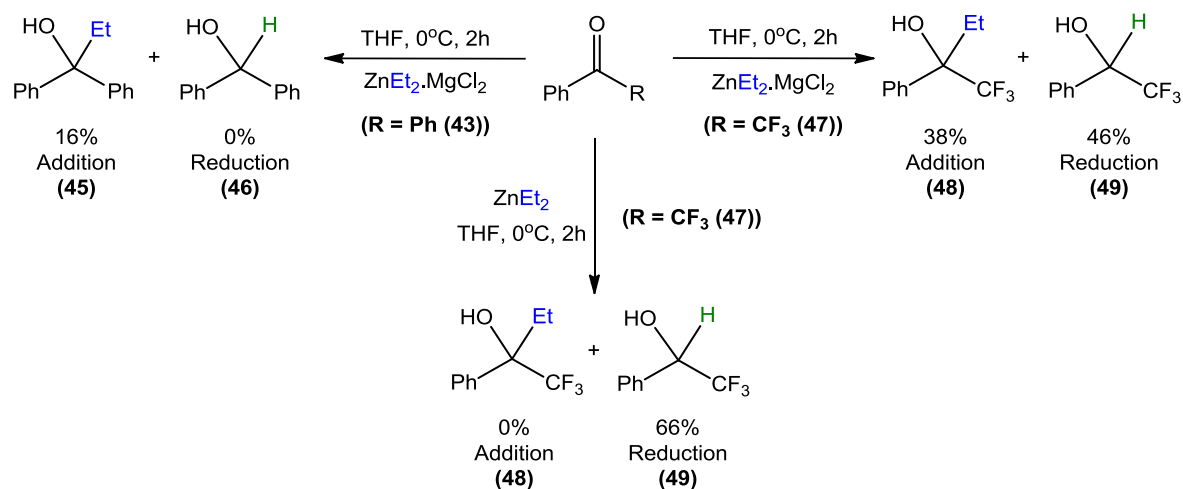


Figure 5.4: ^1H DOSY NMR spectra of (a) ZnEt_2 in d_8 -THF solution and (b) $\text{ZnEt}_2 \cdot \text{MgCl}_2$ in d_8 -THF solution, run at 25°C in the presence of internal standards (TPhN, PhN, TMS).

Thus, these DOSY studies revealed that a clear interaction between ZnEt_2 and MgCl_2 exists in solution. As already mentioned, Knochel has recently reported that the addition of stoichiometric amounts of MgCl_2 to organozinc reagents can significantly improve the reactivity of RZnCl and R_2Zn towards carbonyl compounds.^[123] In contrast, the 1:1 mixture of ZnEt_2 and MgCl_2 in THF reacted very slowly with benzophenone (16% conversion to the alkylation product over 20 hours). Slightly improved reactivity was observed with the more activated ketone 2,2,2-trifluoroacetophenone (**47**), which showed a conversion of 38% alkylation $\text{Ph}(\text{CF}_3)\text{C}(\text{OH})\text{Et}$ (**48**) and 46% reduction $\text{Ph}(\text{CF}_3)\text{CH}(\text{OH})$ (**49**), which contrasts with the complete lack of alkylation observed when homometallic ZnEt_2 is employed, where the secondary alcohol (**49**) is obtained in a 66% yield (**Scheme 5.3**). Thus, adding to previous findings discussed within this report, these results further emphasise the significant effect that MgCl_2 (or other inorganic salts such as LiCl), often present in solution due to the use of *in situ* metathetical approaches, can have in organic transformations, interacting with both the organic substrate and the organometallic species present in solution.^[127]



Scheme 5.3: Reactions of $\text{ZnEt}_2 \cdot \text{MgCl}_2$ with **43** and **47**, and ZnEt_2 with **47** in THF at 0°C, followed by aqueous work-up.

5.2 Investigating the catalytic activity of $[\{\text{Mg}_2\text{Cl}_3(\text{THF})_6\}^+\{\text{Zn}_2\text{Et}_5\}^-]$ (**41**) in alkylation reactions of benzophenone by EtMgCl

To investigate if Mg-Zn hybrid **41** could act as a catalyst for the alkylation of **43** by EtMgCl , the reaction of 0.9 equivalents of EtMgCl with **43** in the presence of 10 mol% of **41** was performed in d_8 -THF at 0°C and analysed by ^1H NMR spectroscopy after 2 hours (**Figure**

5.5(c)). The spectrum showed that that all of the ketone had been consumed, with the major product being the alkylated species **44** (90% yield) and a small amount of the reduction product (10%). The spectrum closely resembles that of the stoichiometric reaction of **41** and **43** (**Figure 5.5(b)**), although in this case the resonances corresponding to “ZnEt₂.MgCl₂” are significantly smaller as smaller amounts of ZnEt₂ are generated in this reaction due to substoichiometric amounts of **41** being employed. The high conversion observed for the alkylation product **44** shows that the competing background reaction of EtMgCl with **43** under these conditions is overridden by the co-complexation of the Grignard reagent with the *in situ* generated ZnEt₂, recycling the active species **41**. Furthermore, mirroring the conditions employed by Ishihara in the ZnCl₂ catalysed alkylation, the reaction of 1.3 equivalents of EtMgCl with benzophenone in the presence of ZnCl₂ (10 mol%) in d₈-THF solution was performed (**Figure 5.5(d)**). The ¹H NMR spectrum after 2 hours at 0°C displayed an almost identical NMR spectrum to that obtained when **41** was used as the catalyst, with a similar ratio of products (84:16 alkylation : reduction).

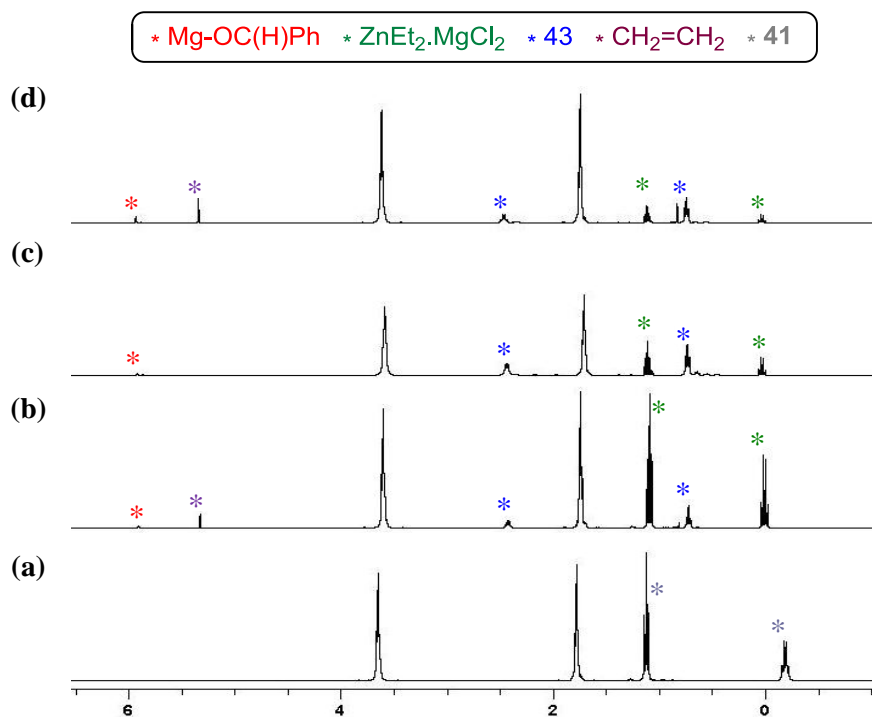
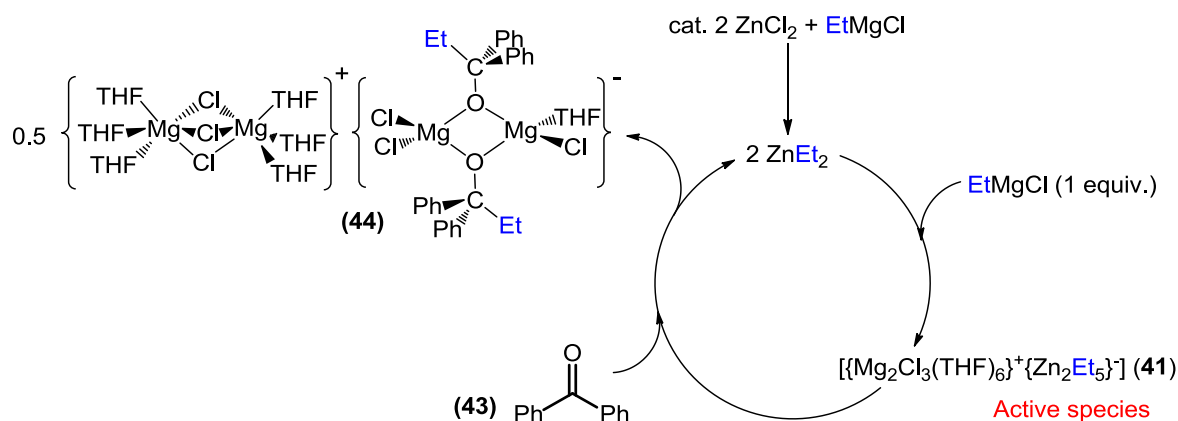


Figure 5.5: ¹H NMR spectra for d₈-THF solutions of (a) [$\{\text{Mg}_2\text{Cl}_3(\text{THF})_6\}^+\{\text{Zn}_2\text{Et}_5\}^-$] (**41**), (b) reaction of equimolar amounts of **41** with **43** after 2 hours at 0°C, (c) reaction of EtMgCl (0.9 eq, 1.15 M solution) and **41** (10 mol%) with **43** after 2 hours at 0°C, (d) reaction of EtMgCl (0.9 eq, 0.99 M solution) and ZnCl₂ (10 mol%) with **43** after 2 hours at 0°C.

Interestingly, these catalytic reactions are shown to be greatly affected by concentration. Thus, when **41** is employed as the catalyst, the reaction of EtMgCl (initial concentration of THF solution of EtMgCl 1.15 M) with benzophenone results in a ratio of alkylation : reduction of 9:1. Surprisingly, if the reaction is performed under more dilute conditions (initial concentration THF solution of EtMgCl 0.19 M) then the alkylation and reduction products are obtained in a ratio of approximately 1:1. Similar results are observed when ZnCl₂ is employed as the catalyst, with the alkylation and reduction products obtained in 84% and 16% yield respectively at high concentrations (initial concentration EtMgCl solution 0.99 M), but at lower concentrations a reversal in selectivity is observed, with only 30% of the alkylation product and 70% of the reduction product obtained (initial concentration EtMgCl solution 0.18 M). These results indicate that for the catalytic reactions concentration becomes a much more important factor, since under dilute conditions the large excess of EtMgCl present in solution can compete with the catalytic amounts of the zincate **41** to react with benzophenone, favouring β-hydride elimination, whereas when more concentrated solutions are employed the background reaction becomes less favoured.



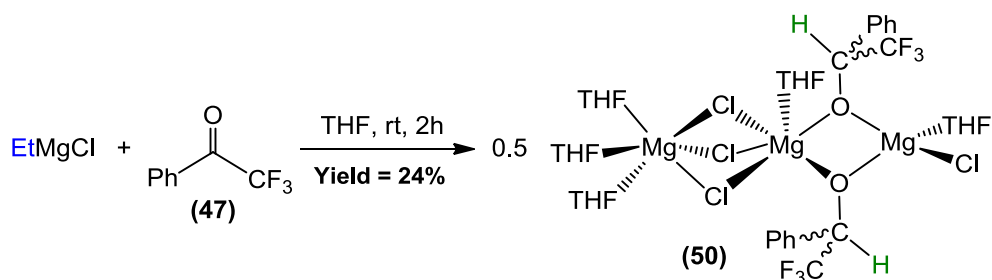
Scheme 5.4: Proposed catalytic cycle for the alkylation of benzophenone (**43**) by EtMgCl using catalytic ZnCl₂.

Based on these results, a catalytic cycle can be proposed where the active species $[\{\text{Mg}_2\text{Cl}_3(\text{THF})_6\}^+ \{\text{Zn}_2\text{Et}_5\}^-]$ (**41**) is generated *in situ* by reaction of catalytic ZnCl₂ with EtMgCl. This Mg-Zn hybrid can then react with the substrate to form the magnesium-magnesiato species **44** along with the re-generation of ZnEt₂ to continue the catalytic cycle (**Scheme 5.4**). Therefore, the success of this catalytic cycle is reliant on two key features, the first of which is that the alkylation of benzophenone by **41** (present in catalytic amounts)

proceeds more rapidly than the background reaction of EtMgCl with the substrate, which as described above is dependent on the concentration of the solution; and secondly, on the formation of the “magnesium-only” alkylated product $[\{\text{Mg}_2\text{Cl}_3(\text{THF})_6\}^+\{\text{Mg}_2(\text{OC}(\text{Et})\text{Ph}_2)_2\text{Cl}_3(\text{THF})\}^-]$ (**44**), which allows ZnEt_2 to be released to re-generate the active species **41**.

5.3 Insight into the constitution of the reduction products

One of the missing parts from this study of the alkylation reactions of ketones is the constitution of the alkoxide reduction product, resulting from the competing β -hydride elimination reaction. In an attempt provide further information of their constitution, EtMgCl was reacted with benzophenone at room temperature (conditions which favour reduction over alkylation, after aqueous work-up the secondary alcohol **46** is obtained in a 90% yield). Analysis of the crude reaction by ^1H NMR spectroscopy revealed that the alkoxide compound “Mg-OC(H)Ph $_2$ ” was the major product, although unfortunately crystals suitable for X-ray diffraction could not be obtained. However, when the same reaction was performed using 2,2,2-trifluoroacetophenone (**47**), colourless crystals of the reduction product $[\{(\text{THF})_5\text{Mg}_3\text{Cl}_4\{\text{OC}(\text{H})\text{Ph}(\text{CF}_3)\}_2\}]$ (**50**) were obtained in a 24% isolated yield (**Scheme 5.5**), which were characterised by X-ray crystallography and ^1H , $^{13}\text{C}\{^1\text{H}\}$ and $^{19}\text{F}\{^1\text{H}\}$ NMR spectroscopy.



Scheme 5.5: Reaction of EtMgCl with **47** to form $[\{(\text{THF})_5\text{Mg}_3\text{Cl}_4\{\text{OC}(\text{H})\text{Ph}(\text{CF}_3)\}_2\}]$ (**50**).

Contrasting with the SSIP structure of **44**, $[\{(\text{THF})_5\text{Mg}_3\text{Cl}_4\{\text{OC}(\text{H})\text{Ph}(\text{CF}_3)\}_2\}]$ (**50**) exhibits a CIP structure (**Figure 5.6**) containing three Mg centres, each of which is present in a different coordination environment. Mg1 bonds terminally to a chlorine atom and a molecule of THF, and is connected to Mg2 via two bridging $\{\text{OC}(\text{H})\text{Ph}(\text{CF}_3)\}^-$ alkoxide fragments, resulting from the addition of a hydride to the C=O bond of the ketone. Mg2 is also bonded to one molecule of THF, and completes its octahedral coordination by bonding to three Cl atoms

which bridge to Mg3, also found in a distorted octahedral geometry, bonding to three terminal THF molecules. This unusual combination of Mg centres connected either by bridging chlorine atoms or by alkoxide ligands, coupled with the different coordination geometries of the Mg atoms, must significantly contribute to the non-linearity of the Mg1-Mg2-Mg3 vector ($134.64(4)^\circ$) found in **50**. The trinuclear asymmetric structure of **41** contrasts with the previous example of a magnesium alkoxide reduction product reported by Henderson, resulting from the reaction of benzophenone with the alkylmagnesium amide $[\text{BuMgN}(\text{SiMe}_3)_2]$, resulting in the formation of $[\{(\text{Me}_3\text{Si})_2\text{NMg}(\mu\text{-OCHPh}_2)\cdot\text{Ph}_2\text{CO}\}_2]$ which exhibited a symmetric dimeric arrangement.^[158e]

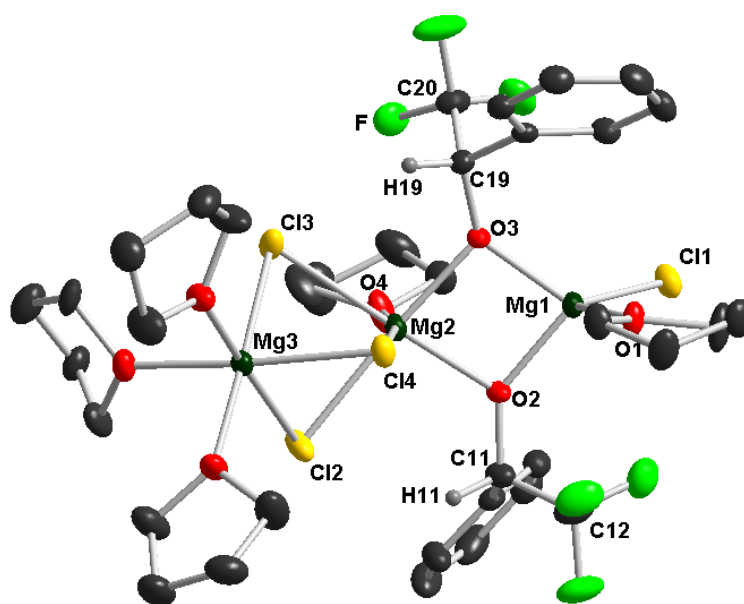


Figure 5.6: Molecular structure of $[\{(\text{THF})_5\text{Mg}_3\text{Cl}_4\{\text{OC}(\text{H})\text{Ph}(\text{CF}_3)\}_2]$ (**50**) with 40% probability ellipsoids. Hydrogen atoms and minor THF disorder component have been omitted for clarity. *Selected bond lengths (\AA) and angles ($^\circ$):* Mg1-O2 1.9187(17), Mg1-O3 1.9304(17), Mg2-Cl2 2.5404(10), Mg2-Cl3 2.5224(10), Mg2-Cl4 2.5915(9), Mg2-O2 2.0358(17), Mg2-O3 2.0404(16), Mg3-Cl2 2.4841(10), Mg3-Cl3 2.4684(10), Mg3-Cl4 2.4811(9) O2-C11 1.397(3), O3-C19 1.396(3), Mg1-O2-Mg2 $97.45(7)$, Mg1-O3-Mg2 $96.92(7)$, O1-Mg1-O2 $109.99(8)$, O2-Mg2-O3 $79.90(7)$.

Alternatively, **50** can be viewed as comprising of a neutral, symmetric dimer $[\{(\text{THF})\text{MgCl}(\text{OC}(\text{H})\text{Ph}(\text{CF}_3))\}_2]$, formed by the β -hydride elimination of EtMgCl with **47**, which co-complexes to a molecule of $[\text{MgCl}_2(\text{THF})_3]$, present in solution as a result of the Schlenk equilibrium on EtMgCl . This molecular structure contrasts with that of **44**, which

comprises an anionic, asymmetric dimer $\{\text{Mg}_2(\text{OC}(\text{Et})\text{Ph}_2)_2\text{Cl}_3(\text{THF})\}^-$, and cationic $\{\text{MgCl}(\text{THF})_3\}^+$ which co-complexes to $[\text{MgCl}_2(\text{THF})_3]$ (**Figure 5.7**). However, in both **44** and **50** the inorganic salt (MgCl_2) is incorporated into the structure of the organometallic species, providing further evidence of the important structural role that MgCl_2 plays in these processes by stabilising the final products of these alkylation/reduction reactions.

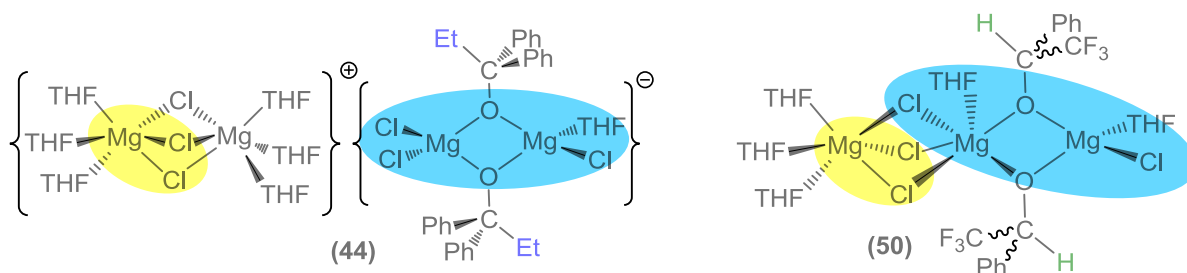


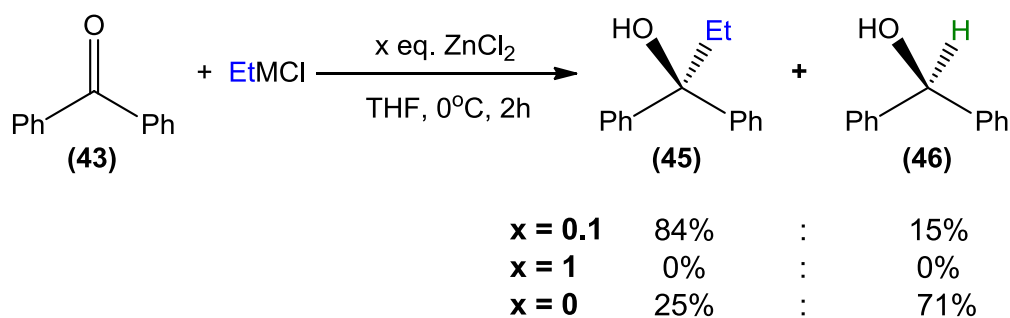
Figure 5.7: Comparison of the SSIP structure of **44** and the CIP structure of **50**.

Turning to the characterisation of **50** in solution, the ^1H NMR spectrum in d_8 -THF displayed three broad resonances in the aromatic region (δ 7.74, 7.32 and 7.29 ppm) for the phenyl groups of the alkoxide ligand, along with a further broad singlet at δ 5.41 ppm, corresponding to the hydride which has added across the carbonyl group. The resonance for this hydrogen would be expected to exist as a quartet as a result of coupling with the CF_3 group, but due to the poor resolution of the spectrum it appears as a broad singlet. The broadness of the resonances in the ^1H NMR spectrum can be attributed to the reduction of **47** generating a chiral centre in the alkoxide ligand (present as a racemic mixture) which results in the existence of two possible diastereoisomers (RR/SS and RS/SR), and the overlapping of the resonances of these closely related species.

The presence of two different diastereoisomers was also confirmed by the $^{19}\text{F}\{^1\text{H}\}$ NMR spectrum, which displayed two equivalent singlets at δ -77.19 and -77.40 ppm, which were shifted slightly upfield compared to the ketone (singlet at δ -74.28 ppm). The most characteristic resonance in the $^{13}\text{C}\{^1\text{H}\}$ NMR spectrum was a quartet at δ 75.4 ppm ($^2\text{J}_{\text{C-F}} = 31.9$ Hz) corresponding to the quaternary carbon which has experienced the hydride addition. The notable upfield shift for this carbon compared to the carbonyl carbon of the ketone (quartet at δ 181.2 ppm, $^2\text{J}_{\text{C-F}} = 35.2$ Hz) is again consistent with the change in hybridisation from sp^2 to sp^3 as a result of the hydride addition across the ketone.

5.4 Assessing the reactivity of 1st generation magnesium-zinc hybrid reagents in nucleophilic addition reactions: salt effects

Closely related to the alkyl-rich zincate [$\{\text{Mg}_2\text{Cl}_3(\text{THF})_6\}^+\{\text{Zn}_2\text{Et}_5\}^-$] (**41**) is the 1st generation magnesium-zinc hybrid species [$\{(\text{THF})_2\text{Mg}(\mu\text{-Cl})_3\text{ZnEt}\}_2$] (**38**). Contrasting with **41**, which is prepared via substoichiometric metathesis reaction of EtMgCl with ZnCl₂ (ratio of 3:1 or 5:2), **38** is prepared by the stoichiometric metathesis reaction, which results in the co-complexation of the two expected homometallic reagents, EtZnCl and MgCl₂, within the same molecular framework. As previously mentioned, the alkylation of benzophenone (**43**) by **41** followed by aqueous work-up yields the expected tertiary alcohol **45** in yields of 90-95%, with only a small amount of the reduction product **46** being formed. These yields are similar to those reported by Ishihara when catalytic amounts of ZnCl₂ (10 mol%) are employed to improve the selectivity of the alkylation of **43** by EtMgCl (**Scheme 5.6**).^[137] However, when the reaction of **43** with **38** is performed under identical conditions (2 hours, 0°C), no reaction (alkylation or reduction) is observed, even after extended reaction times (48 hours) and higher temperature (25°C) (**Scheme 5.6**). Thus, although the addition of ZnCl₂ inhibits the formation of secondary alcohol **46**, the new organometallic species present in solution is not nucleophilic enough to promote the alkylation of **43**.



Scheme 5.6: Comparison of the reactivity and selectivity of the alkylation of **43** by EtMgCl in the absence and presence of catalytic (10 mol%) and stoichiometric amounts of ZnCl₂.^[137]

This remarkable change in reactivity on adjusting the stoichiometry of ZnCl₂ employed in the initial metathesis reaction from 0.1 equivalents to 1 equivalent can be easily explained when the molecular structures of the relative Mg-Zn hybrid species is considered (**Figure 5.8**). Thus, under catalytic conditions ($x = 0.1$), the active species generated *in situ* will be theSSIP species [$\{\text{Mg}_2\text{Cl}_3(\text{THF})_6\}^+\{\text{Zn}_2\text{Et}_5\}^-$] (**41**), which will be activated towards the alkylation

reaction due to the combination of the alkyl rich $\{\text{Zn}_2\text{Et}_5\}^-$ anion, possessing an enhanced nucleophilic power, with the strongly Lewis acidic cation $\{\text{Mg}_2\text{Cl}_3(\text{THF})_6\}^+$, which can coordinate to the carbonyl group of the substrate and facilitate the nucleophilic addition. In contrast, the CIP structure of the halide-rich $[\{(\text{THF})_2\text{Mg}(\mu\text{-Cl})_3\text{ZnEt}\}_2]$ (**38**) will possess Zn-C bonds which are much less kinetically activated, displaying a reactivity similar to that observed for neutral organozinc reagents.

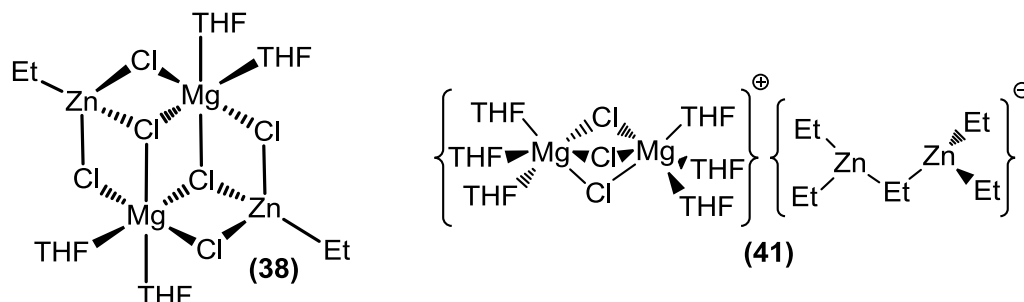
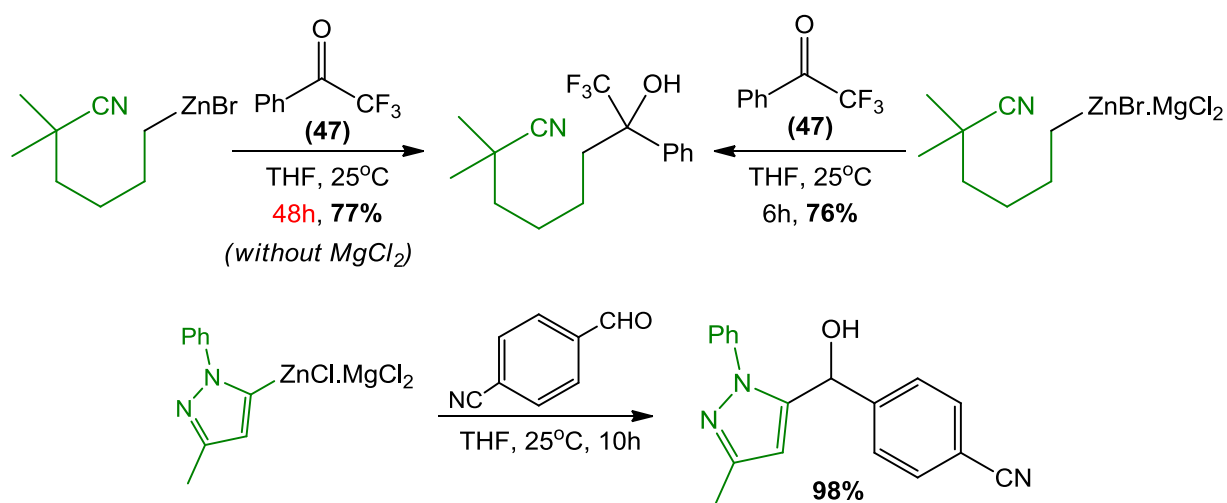


Figure 5.8: Comparison of the molecular structures of $[\{(\text{THF})_2\text{Mg}(\mu\text{-Cl})_3\text{ZnEt}\}_2]$ (**38**) and $[\{\text{Mg}_2\text{Cl}_3(\text{THF})_6\}^+\{\text{Zn}_2\text{Et}_5\}^-]$ (**41**), prepared via substoichiometric and stoichiometric metathesis reaction of EtMgCl with ZnCl_2 respectively.

The lack of alkylating ability displayed by **38** also contrasts with previous reports, where the addition of stoichiometric amounts of MgCl_2 greatly enhanced the reactivity of organozinc halides towards nucleophilic addition (**Scheme 5.7**).^[123] The active species proposed in these reactions was believed to be a mixed Mg-Zn hybrid species, containing the same “ RZnCl.MgCl_2 ” structural motif as is observed in **38**.



Scheme 5.7: Enhanced reactivity of “ RZnCl.MgCl_2 ” in nucleophilic addition to 2,2,2-trifluoroacetophenone (**47**) and 4-cyanobenzaldehyde.^[123]

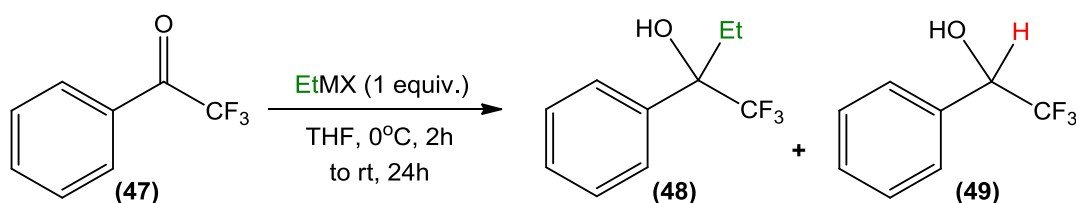
Thus, to further assess whether **38** could participate in this type of reaction, its reactivity towards the more activated ketone, 2,2,2-trifluoroacetophenone (**47**) was compared with other ethyl containing organometallic combinations (**Scheme 5.8, Table 5.1**). These reactions were performed in THF solution at 0°C for 2 hours, followed by a further 24 hours at room temperature. Following aqueous work-up, the conversion of **47** to the relevant addition and reduction products (**48** and **49**) was determined by analysis of the crude reaction mixture by GC-FID and ¹H NMR spectroscopy (in the presence of ferrocene as an internal standard).

Although **47** exhibits an enhanced electrophilicity of the carbonyl group towards nucleophilic addition, due to the presence of the highly electron withdrawing CF₃ group, in general, the chemoselective alkylation of trifluoromethyl ketones using classical homometallic reagents can be compromised by their greater tendency to undergo β-hydride elimination reactions.^[155, 160] Thus, the alkylation of **47** with homometallic reagents EtMgCl and [EtZnCl(TMEDA)] were ineffective, yielding the desired product **48** in only a 4% yield. Illustrating the marked difference in polarity and reactivity between organomagnesium and organozinc reagents, when EtMgCl was employed a large amount of the reduction product **49** (90%) was obtained, whereas reaction with [EtZnCl(TMEDA)] led mainly to the recovery of starting material **47** and only a 6% yield of **49** (**Table 5.1, Entry 1-2**).

The addition of LiCl to EtMgCl to form the corresponding turbo Grignard reagent (EtMgCl.LiCl) showed only a marginal improvement in selectivity with tertiary alcohol **48** obtained in a 19% yield (compared to 4% for EtMgCl), although the reduction product **49** is still the major product formed in a yield of 73% (**Table 5.1, Entry 3**). However, the analogous zinc modified turbo Grignard mixture (EtZnCl.LiCl) displayed both enhanced reactivity and selectivity (yield of 60% for **48, Table 5.1, Entry 4**) compared to that of the homometallic species [EtZnCl(TMEDA)].

Next, the reactivity of isolated crystals of **38** towards **47** was investigated, revealing the formation of only trace amounts of the desired product **48** (2%), along with 14% of the reduction product **49** and unreacted starting material **47** (84%) (**Table 5.1, Entry 5**). These results are comparable to those observed for the organozinc reagent [EtZnCl(TMEDA)] (**Table 5.1, Entry 2**). In contrast with the modest alkylating ability of **38**, Ishihara has previously shown that reaction of **47** with Grignard reagents in the presence of catalytic amounts of ZnCl₂ (30 mol%) results in the desired tertiary alcohols being obtained in high

yields (up to 78%),^[137] which as mentioned above can be rationalised by the different constitution of the magnesium-zinc hybrid species involved.



Scheme 5.8: Reaction of 2,2,2-trifluoroacetophenone (**47**) with different ethyl containing organometallic combinations.

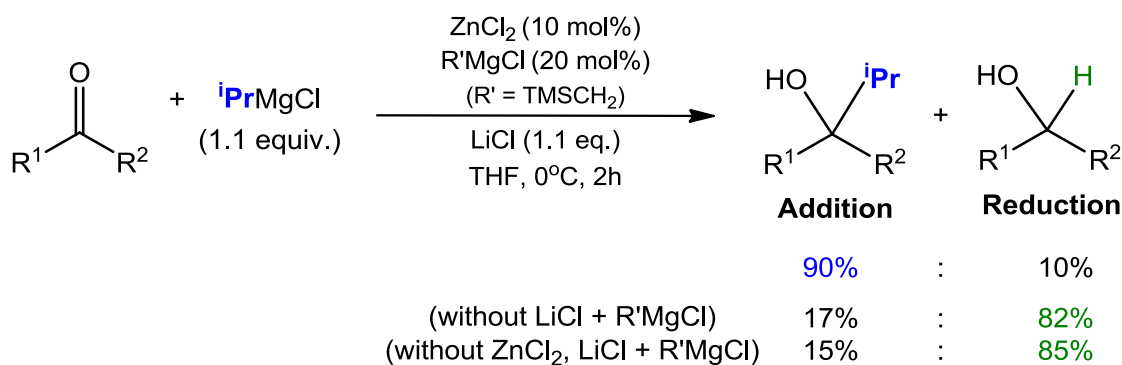
Entry	Reagent EtMX	47 (%)	48 (%)	49 (%)
1	EtMgCl	6	4	90
2	EtZnCl(TMEDA)	90	4	6
3	EtMgCl + LiCl	8	19	73
4	EtZnCl + LiCl	36	60	4
5	[{(THF) ₂ Mg(μ-Cl) ₃ ZnEt ₂ }] (38)	84	2	14
6	38 + LiCl	22	74	4
7	EtMgCl + LiCl + ZnCl ₂	24	72	4
8	38 + MgCl ₂	59	2	39

Table 5.1: Alkylation of **47** by [(THF)₂Mg(μ-Cl)₃ZnEt₂] (**38**) and other relevant organometallic combinations. Yields were determined by GC-FID analysis and ¹H NMR spectroscopy using ferrocene as an internal standard.

The poor conversion displayed by **38** contrasts even more with the high yields reported by Knochel and co-workers for the nucleophilic addition of several functionalised RZnX reagents to **47** (yields 60-87%) in the presence of MgCl₂ (**Scheme 5.7**).^[123] However, a closer look into these results revealed that the synthesis of the functionalised organozinc reagents is performed in the presence of one molar equivalent of LiCl, which is required to induce the oxidative insertion of zinc into the C-X bond of the relevant starting material.^[11] Thus, in order to further investigate the effect of LiCl in these alkylation reactions, the reaction of **38**

with **47** in the presence of one molar equivalent of LiCl was performed (**Table 5.1**, entry 6), which resulted in a substantial increase in the yield of the desired tertiary alcohol **48** (74% yield). Furthermore, generating the same reactive species *in situ* by combining equimolar amounts of EtMgCl, LiCl and ZnCl₂ resulted in a similar yield of **48** (**Table 5.1**, entry 7). Surprisingly, when MgCl₂, a stronger Lewis acid was used as an additive, Mg-Zn hybrid **38** failed to promote the alkylation of **47** (**Table 5.1**, entry 8).

Although the mechanistic implications of the presence of LiCl in these reactions can be considerably complex, the enhancement observed in the chemoselectivity of the reaction could be triggered by a new trimetallic reagent, where LiCl has been incorporated into the constitution of **38**. In this regard, a number of excellent reactivity,^[77, 79b, 161] structural,^[80a, 162] theoretical^[163] and spectroscopic^[80b, 163] studies have demonstrated that the addition of LiCl to single-metal organometallic reagents (such as RMgX or RLi) greatly affects their constitution and chemical properties through the formation of unique mixed-metal aggregates.^[127] Contrastingly, to the best of our knowledge the effect that LiCl may exert when added to bimetallic reagents, which could lead to the formation of trimetallic species, has not been explicitly studied, although the *in situ* formation of mixed Li/Mg/Zn reagents has been previously proposed. Thus, the trimetallic system of [Zn(TMP)₂.2LiCl.2MgCl₂] (prepared *in situ* by reaction of ZnCl₂ with two equivalents of to the turbo Hauser base [(TMP)MgCl.LiCl]) shows high levels of reactivity and selectivity in the direct zincation of sensitive aromatic substrates,^[79] which cannot be replicated in the absence of either MgCl₂ or LiCl.^[79c]



Scheme 5.9: Nucleophilic addition of ketones by RMgX (X = Br, I) catalysed by ZnCl₂ and TMSCH₂MgCl, and in the presence of stoichiometric amounts of LiCl.

Furthermore, in attempting to extend ZnCl_2 catalysed alkylation and arylation of ketones to both iodo and bromo containing Grignard reagents (RMgX , $\text{X} = \text{Br}, \text{I}$), Ishihara reported that the presence of a stoichiometric amount of LiCl was essential for promoting these addition reactions (**Scheme 5.9**), proposing trimetallic $[\text{R}_3\text{Zn}]^-\text{[Li]}^+\text{[MgX}_2\text{]}_m\text{[LiCl]}_n$ ($\text{X} = \text{Cl}, \text{Br}$ or I) as the active species.^[164] Providing some evidence of the effect which LiCl can have on these bimetallic systems, it was found that when LiCl is present in solution during the metathesis reaction of EtMgCl with ZnCl_2 , the formation of the magnesium halozincate $[\{\text{Mg}(\text{THF})_6\}^{2+}\{\text{Zn}_2\text{Cl}_6\}^{2-}]$ (**34**) is inhibited, giving rise to homogeneous solutions.

In an attempt to provide further information on the constitution of the reactive species present in solution in these different organometallic combinations, an aliquot of each of the solution mixtures was analysed by multinuclear (^1H , $^{13}\text{C}\{^1\text{H}\}$ and ^7Li) NMR spectroscopy (**Table 5.2**). In all cases the NMR spectra were run in d_8 -THF at room temperature, revealing the presence of only one set of ethyl resonances under these conditions. The most informative resonances were those of the M-CH_2 group, which are substantially different in **38** (δ 0.06 and 1.0 ppm in the ^1H and $^{13}\text{C}\{^1\text{H}\}$ NMR respectively, entry 1) compared to those of EtMgCl (δ -0.81 and -2.4 ppm, entry 2) or the turbo Grignard mixture $\text{EtMgCl}\cdot\text{LiCl}$ (δ -0.76 and -1.6 ppm, entry 4), demonstrating the difference in the environment of the ethyl group, which is bound to zinc in **38** and to magnesium in the other two cases.

Entry	Reagent EtMX	^1H NMR		$^{13}\text{C}\{^1\text{H}\}$ NMR		δ ^7Li
		δ CH_2	δ CH_3	δ CH_2	δ CH_3	
1	$[\{(\text{THF})_2\text{Mg}(\mu\text{-Cl})_3\text{ZnEt}\}_2]$ (38)	0.06	1.12	1.0	13.1	-
2	EtMgCl	-0.81	1.12	-2.4	14.0	-
3	$\text{EtZnCl}(\text{TMEDA})$	-0.02	1.15	-1.6	13.9	-
4	$\text{EtMgCl} + \text{LiCl}$	-0.76	1.15	-1.6	14.3	-1.56
5	$\text{EtZnCl} + \text{LiCl}$	0.01	1.10	1.5	13.4	-0.03
6	38 + LiCl	-0.01	1.09	1.6	13.4	0.02
7	$\text{EtMgCl} + \text{LiCl} + \text{ZnCl}_2$	-0.03	1.09	1.8	13.2	0.07
8	38 + MgCl_2	0.05	1.11	1.2	13.1	-

Table 5.2: Selected ^1H , $^{13}\text{C}\{^1\text{H}\}$ and ^7Li NMR data (ppm) for various ethyl containing organometallic combinations in d_8 -THF.

The addition of LiCl to **38** leads to a notable change in these chemical shifts from δ -0.01 and 1.6 ppm for **38** (entry 6) to δ 0.06 and 1.0 ppm (entry 1), but they are almost identical to those observed for the *in situ* mixture of EtMgCl, ZnCl₂ and LiCl (δ -0.03 and 1.8 ppm, entry 7). These resonances show that addition of LiCl to **38** and the *in situ* mixture of EtMgCl, ZnCl₂ and LiCl lead to the formation of the same organometallic species. This is consistent with the similar yields observed when these solutions were reacted with **47** (see **Table 5.1**, Entries 6-7), which coupled with the reactivity studies discussed above, hints at the possible formation of a trimetallic Li/Mg/Zn species in solution. Furthermore, comparison with the resonances of EtMgCl and EtMgCl.LiCl suggests that on addition of LiCl to **38** the ethyl group remains bound to zinc.

Attempts to isolate crystals of this putative trimetallic species by decreasing the temperature or adding non-polar solvents such as hexane led to the isolation of THF-solvated inorganic salts (LiCl, MgCl₂), as shown by X-ray crystallography and NMR spectroscopy. Highlighting the novelty of such species, a search of the Cambridge Crystallographic Data Base (CCDB) revealed that to date there have been no reported examples of structures combining all three of these metals in the same organometallic species. Thus, providing further insight into the constitution of trimetallic Li/Mg/Zn systems stands out as an important challenge in this area of organometallic chemistry. Understanding these complex systems is essential to improving their reactivity and developing new reagents. Future work in this area would focus on the isolation and characterisation of a trimetallic species from such organometallic mixtures, which could include the preparation of crystalline material suitable for X-ray diffraction, or DOSY studies, where a combination of ¹H and ⁷Li DOSY experiments could be used to establish if lithium and the ethyl groups are part of the same species in solution.

5.5 Conclusions

Investigating the reactivity of the alkyl-rich magnesium-zinc hybrid [$\{\text{Mg}_2\text{Cl}_3(\text{THF})_6\}^+\{\text{Zn}_2\text{Et}_5\}^-$] (**41**) with benzophenone (**43**) resulted in the isolation of the “magnesium-only” alkoxide complex [$\{\text{Mg}_2\text{Cl}_3(\text{THF})_6\}^+\{\text{Mg}_2(\text{OC}(\text{Et})\text{Ph}_2)_2\text{Cl}_3(\text{THF})\}^-$] (**44**), along with the formation of two equivalents of ZnEt₂ (detected by ¹H NMR monitoring of the reaction). These results provide valuable new insights into how Zn can be recycled in the catalytic process previously proposed by Ishihara for the ZnCl₂ catalysed alkylation of ketones. Furthermore, it has been shown that catalytic amounts of **41** can be employed instead

of ZnCl_2 , suggesting that the active species involved in these reaction could be a trialkylzincate or a penta(alkyl)-dizincate such as **41**.

These results also highlight the important role that inorganic salts, formed as co-products in metathesis reactions, can play in the final outcome of these alkylation reactions. In this case, the presence of Lewis acidic MgCl_2 not only activates the ketone towards nucleophilic addition by coordinating to the carbonyl group, but is also incorporated into the constitution of the alkylating reagent (**41**) as well as the alkylation and reduction products (**44** and **50**), providing structural support to the newly formed magnesium-alkoxide species.

New light has also been shed on the synergic partnership which exists between Mg and Zn in these systems. Thus, the formation of a Mg-Zn hybrid increases both the nucleophilicity of the anionic component and the electrophilicity of the cationic component of the organometallic reagent, enabling the chemoselective alkylation of ketones (and minimizes the formation of undesired products).

Contrastingly, this study has also shown that the first generation halide-rich magnesium-zinc hybrid [$\{(\text{THF})_2\text{Mg}(\mu\text{-Cl})_3\text{ZnEt}\}_2$] (**38**), obtained when equimolar amounts of ZnCl_2 and EtMgCl are combined in solution, displays a much lower alkylating power, unable to react with benzophenone even after prolonged reaction times. However, this species did show some reactivity towards the more activated ketone 2,2,2-trifluoroacetophenone (**47**). Assessing the reactivity of **38** along with a number of other ethyl containing organometallic mixtures towards **47**, it was established that greater conversions and levels of chemoselectivity were obtained when three metals, Li, Mg and Zn (accompanied by Cl and alkyl ligands) are present in solution, hinting at the existence of a trilateral multi-component partnership.

Collectively, these results provide important insights into the non-innocent role of inorganic salts on the structure and reactivity of organometallic reagents in organic reactions, and also raise awareness of the presence of these inorganic by-products when salt metathesis methodologies are employed to generate organometallic reagents.

Chapter 6: Applying magnesium-zinc hybrid chemistry to direct Zn-I exchange and Pd-catalysed Negishi cross-coupling reactions

Metal-halogen exchange is one of the most fundamental techniques for functionalising aromatic molecules, with organolithium reagents finding numerous applications in this type of reaction due to their high reactivity, allowing access to aryl and heteroaryl lithium compounds via direct lithium-halogen exchange.^[35] However, these methodologies require the use of very low temperatures (usually -78°C), display poor functional group tolerance, and more importantly are not compatible with transition metal catalysed cross-coupling reactions.^[156] One possible way around this problem is to perform the metathesis reaction of the resulting organolithium compound with a zinc salt to form more covalent organozinc species, which are key precursors in Negishi cross-coupling reactions.^[16] Thus, the formation of organozinc species via direct zinc-halogen exchange reactions is an extremely desirable prospect in synthetic chemistry. Unfortunately, due to the low polarity of neutral organozinc reagents, they are only able to react with aryl iodides in the presence of a catalyst,^[165] or when combined with a more polar organometallic reagent to form a zincate (see **Chapter 1.2.3** for discussion of lithium zincates in metal-halogen exchange).

Notwithstanding, as mentioned in **Chapter 1.2.3**, recent studies have shown that whereas Zn^iPr_2 fails to react with aryl iodides in THF, changing the solvent to a 1:10 mixture of $\text{Et}_2\text{O}/N$ -methylpyrrolidinone allows the desired arylzinc(alkyl) species ArZn^iPr to be formed in quantitative yields, while the addition of catalytic amounts of $\text{Li}(\text{acac})$ also allows the second ^iPr group to be activated towards Zn-I exchange.^[42] These studies also revealed that better results for the Zn-I exchange reactions were obtained when more bulky alkyl groups were present, with Zn^iPr_2 and Zn^sBu_2 displaying higher levels of reactivity than ZnMe_2 or ZnEt_2 . Furthermore, investigations into the Zn-I exchange reaction of Zn^iPr_2 with alkyl iodides, which are more reactive substrates than aryl iodides, revealed that the addition of magnesium salts increased the rate of the reaction by a factor of around 200.^[166] Encouraged by these results, the ability of $[\{\text{Mg}_2\text{Cl}_3(\text{THF})_6\}^+\{\text{Zn}^t\text{Bu}_3\}^-]$ (**40**) to promote direct Zn-I exchange reactions with aryl iodide substrates was investigated.

6.1 Investigating the reactivity of $[\{\text{Mg}_2\text{Cl}_3(\text{THF})_6\}^+\{\text{Zn}^t\text{Bu}_3\}^-]$ (**40**) in Zn-I exchange and Pd-catalysed Negishi cross-coupling Reactions

Initially, these studies began by probing the reactivity of **40** towards one equivalent of 4-iodotoluene (**51**), performing the reaction in THF at room temperature. A ^1H NMR spectrum of the crude reaction mixture after 1 hour suggested that **51** had successfully undergone metal-halogen exchange (**Figure 6.1**). To elaborate, the reaction mixture showed two doublets at δ 7.62 and 6.80 ppm, and a singlet at δ 2.18 ppm which can be assigned to the aromatic protons and the methyl group of a *p*-tolyl fragment respectively, along with a singlet at δ 0.98 ppm for the remaining *tert*-butyl groups, which is shifted marginally downfield compared to the major *tert*-butyl resonance of **40** (δ 0.89 ppm). Integration of these signals revealed a ratio of *p*-tolyl: ^tBu of \sim 1:2, which is consistent with the presence of a $\{\text{Zn}(p\text{-tolyl})^t\text{Bu}_2\}^-$ species.

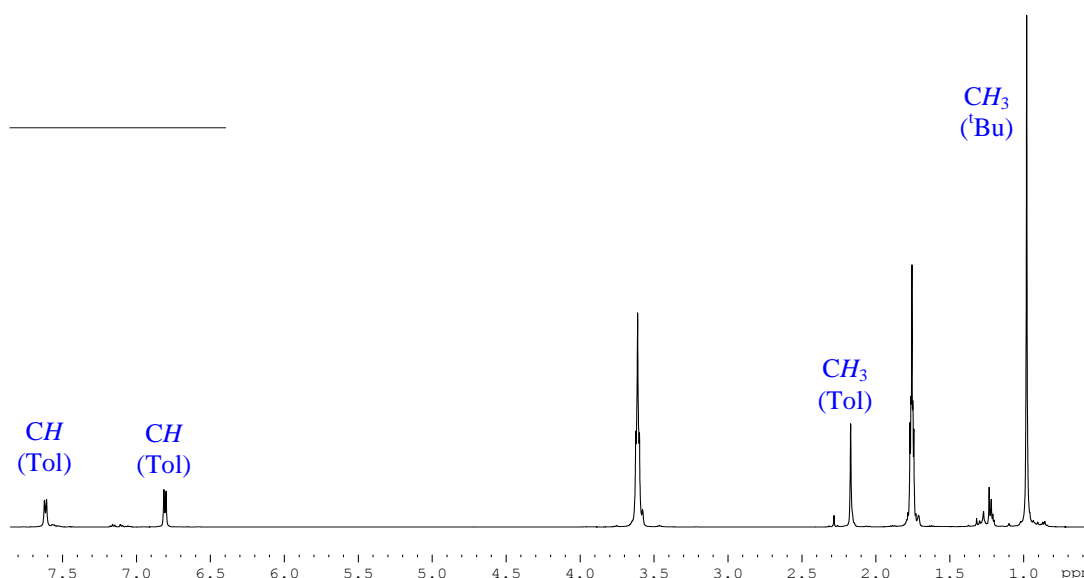


Figure 6.1: ^1H NMR spectrum in d_8 -THF of the crude product from the reaction between $[\{\text{Mg}_2\text{Cl}_3(\text{THF})_6\}^+\{\text{Zn}^t\text{Bu}_3\}^-]$ (**40**) and 4-iodotoluene (**51**) after 2 hours at room temperature.

To monitor this reaction more closely, isolated crystals of **40** were reacted with **51** in d_8 -THF solution, and the reaction followed by ^1H NMR spectroscopy. After 20 minutes (**Figure 6.2(b)**) the aromatic region displayed only one set of resonances (δ 7.56 and 6.76 ppm), along with a single resonance at δ 2.14 ppm for the methyl group, consistent with the quantitative Zn-I exchange of **51**. The aliphatic region displayed a singlet at δ 0.96 ppm for the remaining unreacted *tert*-butyl groups, with analysis of the integration of *p*-tolyl: ^tBu revealing a ratio of 1:2. A singlet at δ 1.89 ppm, corresponding to ^tBuI , provided further confirmation of the successful metal-halogen exchange of **51**.

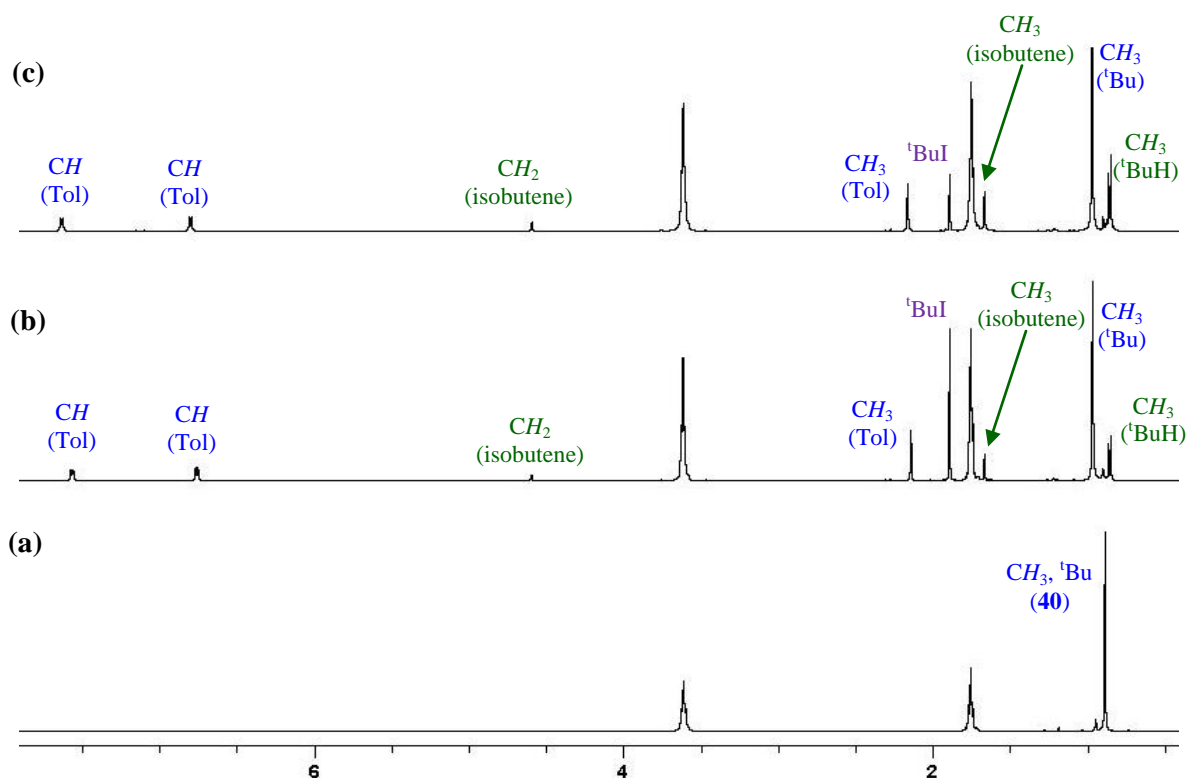
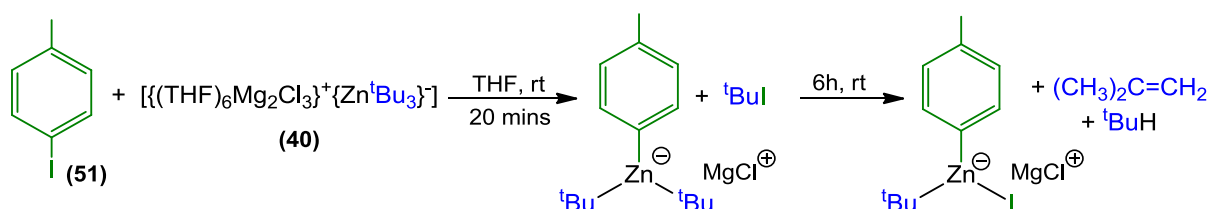


Figure 6.2: ^1H NMR spectra of the reaction of $[\{\text{Mg}_2\text{Cl}_3(\text{THF})_6\}^+\{\text{Zn}^t\text{Bu}_3\}^-]$ (**40**) with **51** in d_8 -THF (a) before addition of **51**, (b) 20 minutes after addition and (c) 6 hours after addition.

Interestingly, when the reaction was analysed again after 6 hours (**Figure 6.2(c)**) the intensity of the ^tBuI and $\text{Zn}-^t\text{Bu}$ resonances had decreased significantly, and two new singlets at δ 1.66 and 4.59 ppm had emerged, which were consistent with the formation of isobutene ($(\text{CH}_3)_2\text{C}=\text{CH}_2$), along with a doublet at δ 0.85 ppm which would indicate the presence of isobutane (^tBuH). These results suggest that following the initial formation of $\{\text{Zn}(p\text{-tolyl})^t\text{Bu}_2\}^-$ one of the remaining *tert*-butyl groups reacts with ^tBuI to form $\{\text{IZn}(p\text{-tolyl})^t\text{Bu}\}^-$, isobutene and isobutane (**Scheme 6.1**). The formation of these by-products can be detected even after 20 minutes (**Figure 6.2(b)**), demonstrating how rapidly ^tBuI reacts with $\text{Zn}-^t\text{Bu}$ groups. A similar side-reaction has also been reported for organolithium reagents, where metal-halogen exchange reactions performed with $^t\text{BuLi}$ often suffer from the side-reaction of ^tBuI with the organolithium reagent, reducing the yield of the metal-halogen exchange reaction. To overcome this limitation, two equivalents of the organolithium reagent are usually employed.^[36]



Scheme 6.1: Reaction of **40** with **51** to form putative intermediate $[\text{Zn}(p\text{-tolyl})(\text{tBu})_2]^-$, which undergoes subsequent reaction with tBuI to form $[\text{Zn}(p\text{-tolyl})(\text{tBu})(\text{I})]^-$, isobutane and isobutene.

Remarkably, even after this side reaction of the concomitantly formed tBuI , the organometallic intermediate still possesses one unreacted *tert*-butyl group. Encouraged by these results, and since **40** contains three *tert*-butyl groups, the reaction of **40** with three equivalents of **51** was next investigated, using identical conditions to those described above. Thus, monitoring the reaction in d_8 -THF by ^1H NMR spectroscopy revealed that after 30 minutes 83% of **51** had been consumed (**Figure 6.3**), as evidenced by the presence of two new doublets at δ 7.71 and 6.87 ppm and a singlet at 2.21 ppm, which can be assigned to the new Zn-Ar organometallic species, along with some unreacted **51** (δ 7.53 (d), 6.92 (d) and 2.24 (s) ppm), tBuI (singlet at δ 1.91 ppm) and some remaining Zn- tBu groups (δ 1.04 (s) ppm).

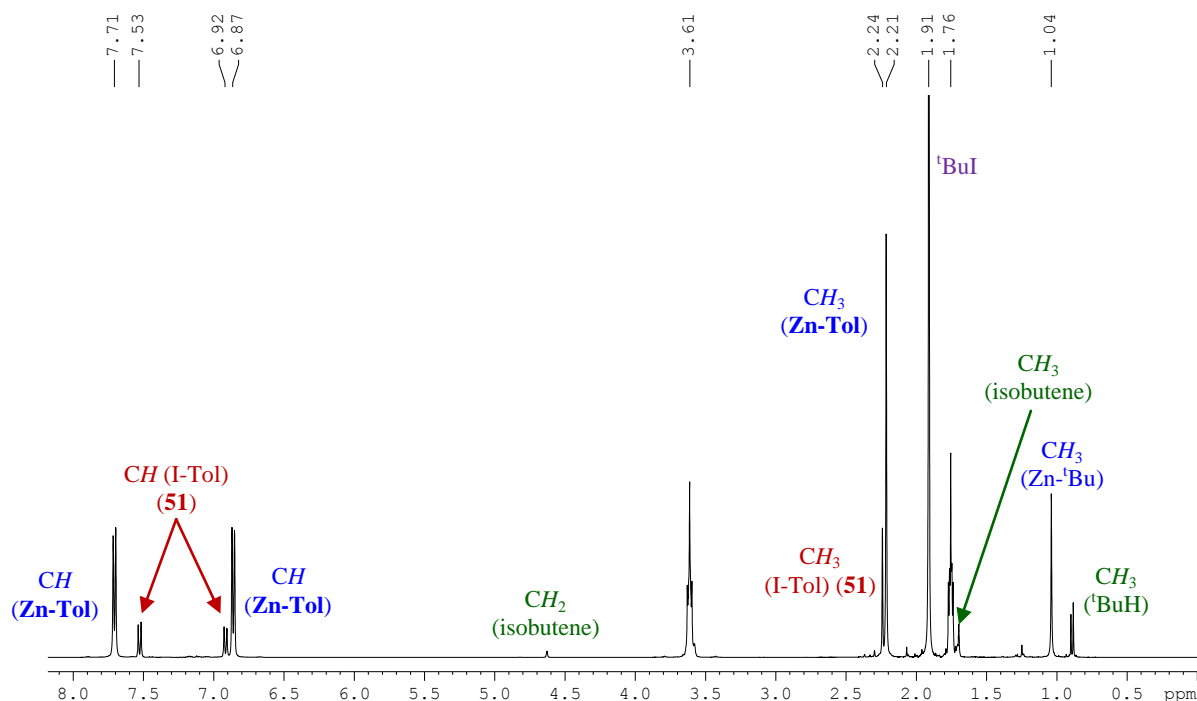
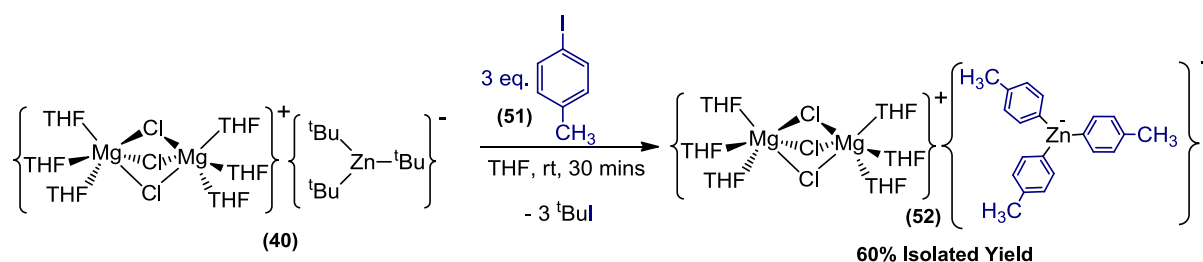


Figure 6.3: Reaction of $\left[\left\{ \text{Mg}_2\text{Cl}_3(\text{THF})_6 \right\}^+ \left\{ \text{Zn}^{\ominus}(\text{tBu})_3 \right\}^- \right]$ (**40**) with 3 equivalents of **51** in d_8 -THF, monitored by ^1H NMR after 30 minutes at room temperature.

Following the reaction over the next 4 hours showed only a marginal increase in the yield of Zn-I exchange is observed (to 85%), with the remaining unreacted Zn-^tBu groups being consumed by reaction with ^tBuI, forming isobutane and isobutene (traces of these by-products can already be observed after 30 minutes). Interestingly, although any unreacted *tert*-butyl groups readily undergo reaction with ^tBuI, the newly generated organometallic species containing *para*-tolyl groups remains intact even after 4 hours at room temperature, highlighting the greater stability of Zn-Ar bonds compared to Zn-^tBu bonds.

Performing the reaction of **51** (three equivalents) with **40** on a larger scale (2 mmol) afforded a pale yellow solution that was allowed to stir at room temperature for 30 minutes before being placed in the freezer (-30°C). After 24 hours colourless crystals of $[\{\text{Mg}_2\text{Cl}_3(\text{THF})_6\}^+\{\text{Zn}(p\text{-Tol})_3\}^-]$ (**52**) (*p*-Tol = 4-Me-C₆H₄) were deposited in a 60% yield (**Scheme 6.2**), as determined by X-ray crystallography and ¹H and ¹³C{¹H} NMR spectroscopy.



Scheme 6.2: Reaction of **40** with three molar equivalents of **51** to form $[\{\text{Mg}_2\text{Cl}_3(\text{THF})_6\}^+\{\text{Zn}(p\text{-Tol})_3\}^-]$ (**52**).

The molecular structure of **52** (**Figure 6.4**) is very similar to that of the precursor Mg-Zn hybrid **40** displaying a SSIP structure which contains the same $\{\text{Mg}_2\text{Cl}_3(\text{THF})_6\}^+$ cation, and the anionic fragment comprises of a zinc centre σ -bonded to three *para*-tolyl groups in a trigonal planar geometry. Providing confirmation that the Zn-I exchange reaction has occurred with the activation of all three *tert*-butyl groups attached to zinc in the Mg-Zn hybrid **40**, the structural elucidation of **52** demonstrates that this exchange process has taken place with an excellent atom economy. Furthermore, to the best of our knowledge, **52** constitutes the first example of an organometallic intermediate of direct Zn-halogen exchange to be structurally characterised. Previously, Uchiyama and Sakamoto have reported the application of lithium tri- and tetra-alkylzincates in Zn-halogen exchange reactions with a wide range of aryl halide substrates.^[24, 38-39] However, in these examples the zincate is reacted with equimolar amounts of the aryl halide substrate, resulting in only one of the alkyl ligands of

the zincate being consumed in the initial Zn-halogen exchange reaction. Therefore, the quenching step of the reaction will require an excess of the electrophile to be employed, as the remaining alkyl ligands on the zincate can also be transferred. Furthermore, the activation of the *tert*-butyl groups in **40** is in sharp contrast with the total lack of reactivity observed when Zn^tBu_2 is combined with 4-iodotoluene, emphasising that this Zn-I exchange reaction constitutes a new example of synergic synthesis.

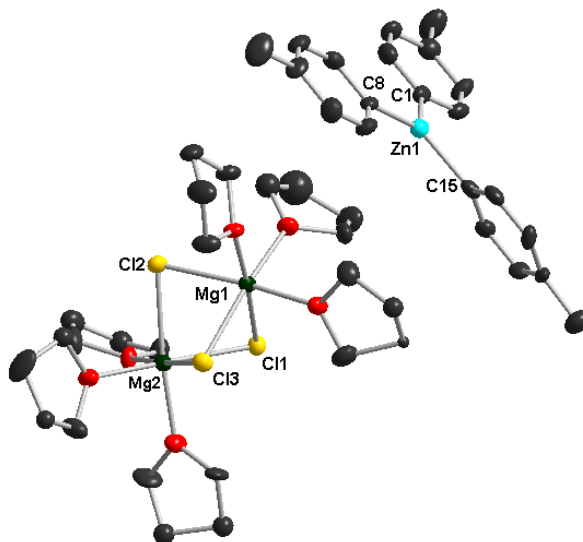


Figure 6.4: Molecular structure of $[\{\text{Mg}_2\text{Cl}_3(\text{THF})_6\}^+\{\text{Zn}(p\text{-Tol})_3\}^-]$ (**52**) with 50% probability ellipsoids. Hydrogen atoms and minor THF disorder components have been omitted for clarity. *Selected bond distances* (\AA) *and bond angles* ($^\circ$): Zn-C1 2.004(6), Zn-C8 2.005(6), Zn-C15 2.039(5), Mg1-C11 2.503(2), Mg1-C12 2.483(2), Mg1-C13 2.5253(19), Mg2-C11 2.5206(19), Mg2-C12 2.487(2), Mg2-C13 2.502(2), C1-Zn-C8 122.2(2), C1-Zn-C15 119.0(3), C8-Zn-C15 118.8(3).

Analysis of **52** by ^1H and $^{13}\text{C}\{^1\text{H}\}$ NMR spectroscopy confirmed that it is the same organometallic species generated when the reaction between **40** and **51** (3 equiv.) is performed in d_8 -THF. Thus, the ^1H NMR spectrum of **52** displayed two doublets at δ 7.67 and 6.87 ppm and a singlet at 2.21 ppm that can be assigned to the aromatic and the methyl protons of the *para*-tolyl ligand respectively. In addition, two multiplets were observed at δ 3.61 and 1.77 ppm corresponding to free THF, whose integration displayed a ratio of THF to Ar of 2:1, as observed in the molecular structure (**Table 6.1**). The most informative resonance of the $^{13}\text{C}\{^1\text{H}\}$ NMR spectrum is that at δ 162.8 ppm for the Zn- C_{ipso} , which has experienced the Zn-I exchange, exhibiting a large downfield shift compared to that of I- C_{ipso} in **51** (δ 91.1 ppm) (**Table 6.1**). Interestingly, whereas the NMR spectra of **40** displayed several resonances

for the *tert*-butyl group (as a result of a complex equilibrium between **40** and its homometallic constituents, Zn^tBu_2 and $^t\text{BuMgCl}$ - vide supra), in **52** there is only one set of resonances for the *para*-tolyl fragment, suggesting that **52** does not undergo a similar equilibrium with its monometallic components.

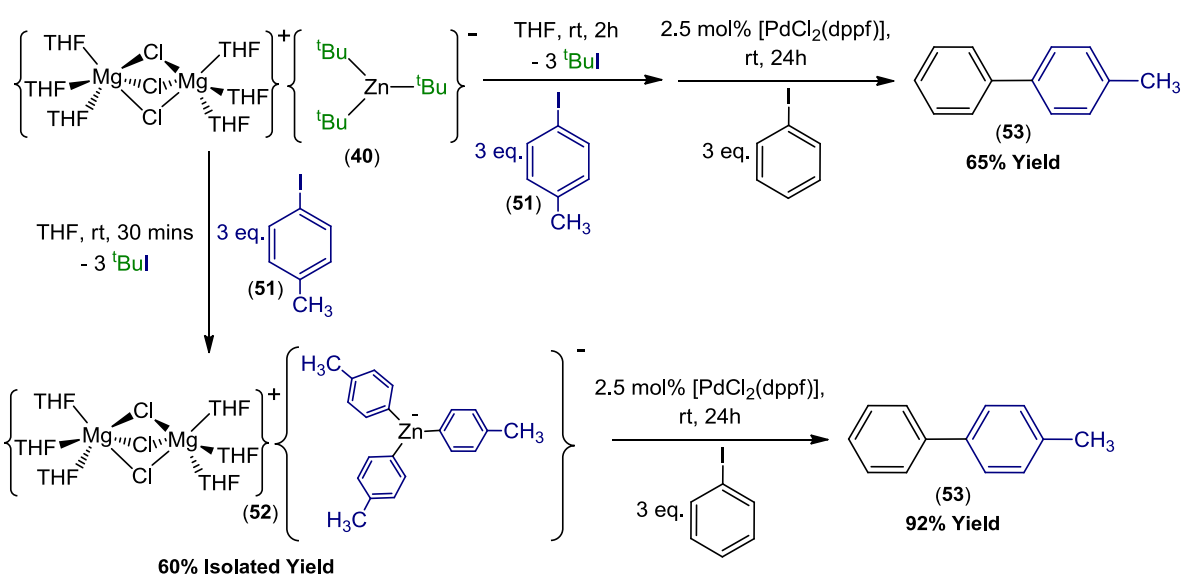
δ (ppm)	^1H (52)	^1H (51)	$^{13}\text{C}\{^1\text{H}\}$ (52)	$^{13}\text{C}\{^1\text{H}\}$ (51)
Tol (C_{ipso})	-	-	162.8	91.1
Tol (CH_{ortho})	7.67	7.54	141.3	138.4
Tol (CH_{meta})	6.87	6.93	127.5	132.3
Tol (C_{para})	-	-	133.0	138.6
Tol (CH_3)	2.21	2.25	22.0	21.3
THF	1.77, 3.61	-	26.6, 68.5	-

Table 6.1: Comparison of the ^1H and $^{13}\text{C}\{^1\text{H}\}$ chemical shifts (ppm) of **52** and **51** in d_8 -THF.

Taking into account the exceptional ability of organozinc compounds to facilitate transmetallation reactions with transition metal complexes,^[156] and the presence of three $\text{Zn-C}_{\text{aryl}}$ bonds within its anionic zincate structure, **52** could potentially be an excellent precursor for Negishi cross-coupling reactions. Thus, to investigate this important synthetic application, isolated crystals of **52** were reacted with three molar equivalents of iodobenzene in the presence of a palladium catalyst $[\text{PdCl}_2(\text{dppf})]$ ($\text{dppf} = 1,1'$ -bis(diphenylphosphino)ferrocene)^[167] for 24 hours at room temperature. This reaction proved to be extremely promising, yielding the expected cross-coupled product, 4-methylbiphenyl (**53**), in an isolated yield of 93% (**Scheme 6.3**). This reaction could also be performed by reacting the magnesium trialkylzincate **40** with three equivalents of **51** *in situ*, with subsequent Negishi cross-coupling affording the asymmetric bis(aryl) species **53** in a 65% yield (**Scheme 6.3**).

Building connections between organic and inorganic synthesis, these preliminary studies show that Mg-Zn hybrid **40** can readily perform direct Zn-I exchange reactions with simple aryl iodide molecules such as 4-iodotoluene (**51**) under mild conditions (room temperature, stoichiometric amounts of reagent and short reaction times of 2 hours). These studies reveal that all three alkyl groups on the *tert*-butyl precursor **40** are activated towards reaction with **51**, affording the magnesium tris(aryl)zincate **52**, demonstrating that the reaction takes place with the bonus of an excellent atom economy. By structurally defining this intermediate **52**,

the reaction has also been confirmed as a genuine example of a direct Zn-I exchange reaction. Furthermore, it has also been established that **52** can be used as a precursor in Pd-catalysed Negishi cross-coupling reactions, which further expands the synthetic potential of these bimetallic species.

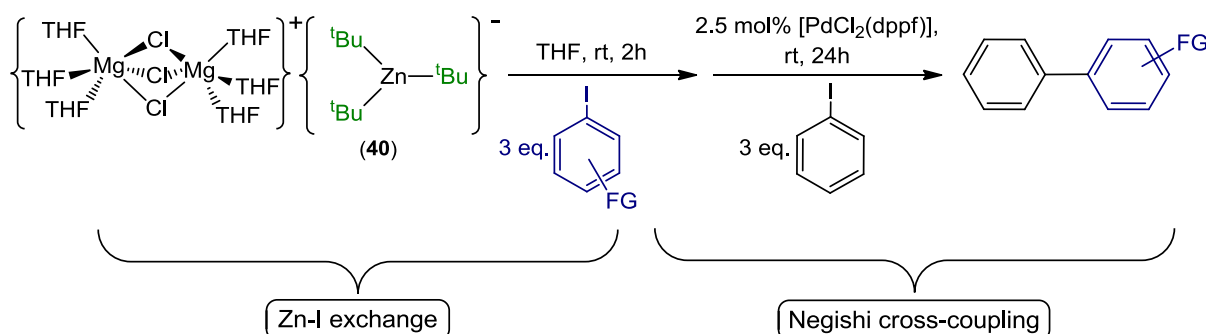


Scheme 6.3: Negishi cross-coupling reaction of $[\{\text{Mg}_2\text{Cl}_3(\text{THF})_6\}^+\{\text{Zn}(p\text{-Tol})_3\}^-]$ (**52**) with iodobenzene to form 4-methylbiphenyl (**53**), using isolated crystals of **52**, and **52** prepared *in situ* from reaction of **40** with three molar equivalents of **51**.

6.2 Expanding the scope of Zn-I exchange and Negishi cross-coupling reactions of $[\{\text{Mg}_2\text{Cl}_3(\text{THF})_6\}^+\{\text{Zn}^t\text{Bu}_3\}^-]$ (**40**) to 2-Iodotoluene and 3-Iodotoluene

To investigate the scope of this methodology, the reactivity of **40** with other aryl iodide substrates was studied (**Scheme 6.4**). Firstly, in order to assess the effect of the ring substitution on the aromatic substrate the reactivity of **40** towards 3-iodotoluene (**54**) and 2-iodotoluene (**55**) was investigated. The reactions of **54** and **55** (three equivalents) with **40** were initially performed in d_8 -THF and followed by ^1H NMR spectroscopy. After 2 hours the Zn-I exchange had proceeded in a yield of 87% for **54**, whereas for *ortho*-substituted **55** the yield was slightly lower (75%) (**Table 6.2**). Thus, although the three *tert*-butyl groups of **40** must still be active towards the exchange, the presence of the methyl group *ortho* to the C-I bond in **55** must have a detrimental effect on the reaction, probably due to a combination of steric and electronic effects. In this regard, a recent kinetic study by Knochel and Mayr has

shown that in Mg-Br exchange reactions for functionalised aryl bromide substrates with $^i\text{PrMgCl}\cdot\text{LiCl}$, the rate of the Mg-Br exchange reactions for 3- and 4-bromotoluene were almost two times faster than that observed for 2-bromotoluene.^[168]



Scheme 6.4: General mechanism for the Zn-I exchange reaction of functionalised aryl iodide substrates with **40**, followed by Pd catalysed Negishi cross-coupling with iodobenzene.

From these kinetic studies, it was also demonstrated that the presence of electron donating groups results in a decrease in the rate of the reaction. Thus, bromotoluene, which possesses a weakly electron donating Me group through a positive inductive effect (+I), displays a reduced rate of reactivity than unsubstituted bromobenzene, with a stronger deactivation experienced for 2-bromotoluene due to the proximity of the functional group to the C-Br bond. However, the authors suggest that steric shielding may also play a role in the decreased reactivity of the *ortho*-substituted species. A similar situation could be taking place in the Zn-I exchange reactions of **40**, which would explain the different reactivities observed for the iodotoluene substrates, with *ortho*-substituted **55** displaying reduced yields (**Table 6.2**).

Regarding the second step of this methodology, which involves a Negishi cross-coupling reaction of the aryl zincate species with iodobenzene (**Scheme 6.4**), it was found that **54** displayed an identical yield to that observed for **51** (65%), suggesting that substituents at the *meta* and *para* position have little effect on the overall yield of the coupling process. A reduced yield (60%) was found for **55**, which can be explained by the reduced rate of the initial Zn-I exchange, although the influence of steric factors due to the presence of the methyl group adjacent to the site of reactivity cannot be discarded. The relatively moderate yields obtained for these cross-coupling reactions (60-65%) can be attributed to the conversions observed in the Zn-I exchange reactions (75-87%). As a result of the incomplete reaction of **40** with the iodotoluene substrates, the subsequent cross-coupling reactions led to

the formation of some of the homocoupled species, dimethyl-biphenyl, formed by cross-coupling of the arylzincate intermediate with some of the unreacted iodotoluene substrate present in solution.

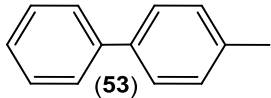
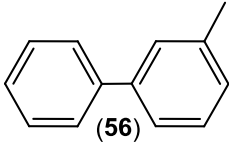
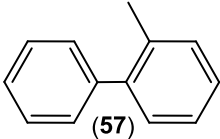
Substrate	% Zn-I Exchange after 2h ^[a]	Product	Isolated Yield
4-Iodotoluene (51)	85		65%
3-Iodotoluene (54)	87		65%
2-Iodotoluene (55)	75		60%

Table 6.2: Comparison of the isolated yields of the relevant products from Zn-I exchange of iodotoluene substrates (3 eq.) with **40**, followed by Pd catalysed Negishi cross-coupling with iodobenzene. ^[a] Determined by ¹H NMR spectroscopy.

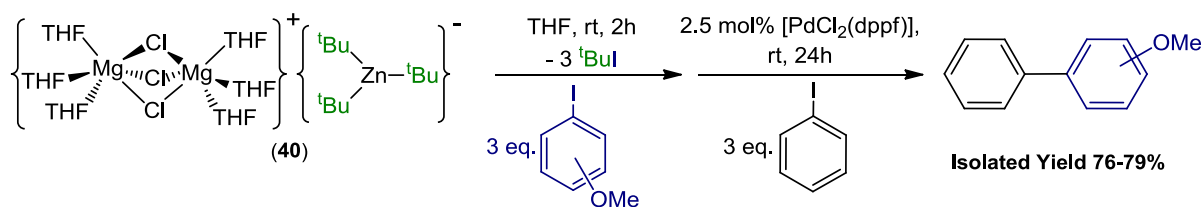
6.3 Investigating Zn-I Exchange and Negishi cross-coupling reactions of **40** with iodoanisole substrates

Studies then turned to the effects of altering the functional group present on the aryl iodide substrate, initially looking at the methoxy substituted 2-, 3- and 4-iodoanisole substrates (**58-60**). Based on the findings of the reactivity of **40** with iodotoluene, and taking steric effects into consideration, it may be expected that 2-iodoanisole (**58**) would display lower levels of reactivity than 3-iodoanisole (**59**) or 4-iodoanisole (**60**). Contrastingly, the previously mentioned kinetic studies of Mayr reported that Mg-Br exchange by ⁱPrMgCl.LiCl is accelerated by the presence of inductively electron withdrawing groups, with the magnitude of these rate enhancing effects decreasing in the order *ortho* >> *meta* > *para*.^[168] Thus, the rate of Mg-Br exchange for MeO substituted aryl bromides is greater than that of the Me substituted species, as a result of the slight activation of the C-Br bond by the inductively electron withdrawing MeO substituent (compared to the electron donating Me group), with the *ortho*-substituted aryl bromide displaying the greatest activation.

In order to assess the electronic and steric effects in our systems, the reaction of **40** with **58** (3 eq.) in d_8 -THF was monitored by ^1H NMR spectroscopy. The spectra revealed that the extent of Zn-I exchange after 15 minutes was 79%, increasing to 86% after 2 hours (**Scheme 6.5**, **Table 6.3**), as shown by the presence of four new aromatic resonances (δ 7.46 (d), 6.84 (t), 6.64 (t) and 6.53 (d) ppm) and a singlet at δ 3.70 ppm for the methoxy group which are significantly shifted from those of **58** (δ 7.70 (d), 7.25 (t), 6.84 (d), 6.64 (t) and 3.77 (s) ppm). After this time there was no further increase in the extent of Zn-I exchange, with the remaining unreacted Zn- ^tBu groups being consumed by ^tBuI . Interestingly, the yield of Zn-I exchange obtained is an improvement of the 75% yield obtained for 2-iodotoluene (**55**) under the same reaction conditions, suggesting a similar trend to that reported in the kinetic studies for Mg-Br exchange reactions.^[168]

Turning to the reactivity of **59** and **60** with **40**, analysis of the organometallic species present after 2 hours at room temperature by ^1H NMR spectroscopy revealed the extent of Zn-I exchange was 86% and 88% for **59** and **60** respectively (**Scheme 6.5**, **Table 6.3**). Thus, the crude product from the reaction between **40** and **59** displayed four aromatic resonances at δ 7.16 (d), 7.13 (d), 7.02 (t) and 6.59 (dd), along with a singlet at 3.70 ppm, which were significantly shifted from those of the unreacted substrate (δ 7.27 (dd), 7.25 (dt), 6.99 (t), 6.88 (ddd) and 3.75 (s) ppm). Similarly, the reaction between **40** and **60** displayed two doublets δ 7.46 and 6.71, along with a singlet at 3.69 ppm, and traces of the unreacted substrate (δ 7.53 (d), 6.71 (d) and 3.74 (s) ppm). Thus, mirroring the reactivity of the *ortho*-substituted substrate, 3- and 4-iodoanisole display enhanced reactivity compared to the corresponding iodotoluene substrates (**Scheme 6.5**, **Table 6.3**).

Kinetic studies for Mg-Br exchange reactions with $^i\text{PrMgCl}\cdot\text{LiCl}$ show that **58** should display an enhanced rate of Zn-I exchange (reaction of 2-bromoanisole with $^i\text{PrMgCl}\cdot\text{LiCl}$ proceeds 4 times faster than that of 4-bromoanisole)^[168] due to the proximity of the OMe group to the reactive C-X bond in the substrate which maximizes the inductive effect. However, **40** displays similar conversions for the Zn-I exchange for the three substrates (86-88%), suggesting that steric factors are playing a role in these reactions, counterbalancing the activating inductive effect (-I) of the OMe group.



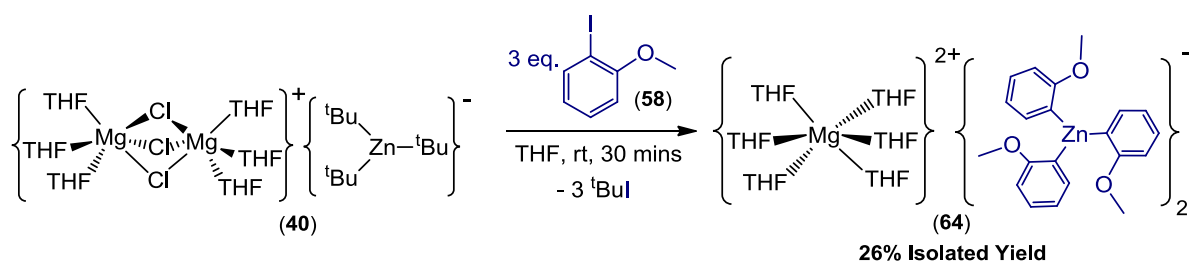
Scheme 6.5: Reaction of **40** with three molar equivalents of 2-/3-/4-iodoanisole (**58-60**), followed by Negishi cross-coupling with iodobenzene.

Substrate	% Zn-I Exchange after 2h ^[a]	Product	Isolated Yield
2-Iodoanisole (58)	86		76% (R = OMe) (61)
2-Iodotoluene (55)	75		60% (R = Me) (58)
3-Iodoanisole (59)	86		76% (R = OMe) (62)
3-Iodotoluene (54)	87		65% (R = Me) (57)
4-Iodoanisole (60)	88		79% (R = OMe) (63)
4-Iodotoluene (51)	85		65% (R = Me) (53)

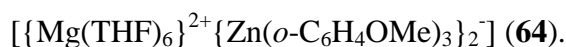
Table 6.3: Comparison of the isolated yields of the relevant products from Zn-I exchange of iodotoluene/iodoanisole substrates (3 eq.) with **40**, followed by Pd catalysed Negishi cross-coupling with iodobenzene. ^[a] Determined by ¹H NMR spectroscopy.

Further comparison of the reactivity of the three different iodoanisole substrates with **40** was provided by carrying out Negishi cross-coupling reactions. Using identical conditions to those employed for the iodotoluene substrates (and therefore allowing direct comparison of the effects of the different functional groups) cross-coupling reactions were performed for each of the substrates **58-60** with iodobenzene, and the products purified by column chromatography (**Scheme 6.5**, **Table 6.3**). The isolated yields of the final methoxybiphenyl products (76-79%) are greater than those obtained for the corresponding iodotoluene substrates (60-65%), consistent with the enhanced levels of Zn-I exchanges displayed by these substrates, which minimizes the competitive homocoupling process.

As previously mentioned, the yields determined for the initial Zn-I exchange reaction and the final isolated yields obtained for Negishi cross-coupling reactions confirm that all three *tert*-butyl groups of the magnesium zincate **40** can be activated towards Zn-I exchange for all of the iodoanisole substrates **58-60**. In order to get a better understanding of the organometallic species involved in these reactions, the reaction of three equivalents of 2-iodoanisole (**58**) with the magnesium trialkylzincate **40** was performed. After stirring for 30 minutes at room temperature hexane was added, and the solution left to stand overnight at room temperature, affording a crop of colourless crystals of the Mg-Zn hybrid species $[\{\text{Mg}(\text{THF})_6\}^{2+}\{\text{Zn}(\text{o-C}_6\text{H}_4\text{OMe})_3\}_2]^-$ (**64**) in an isolated yield of 29% (**Scheme 6.6**), which were analysed by X-ray crystallography and NMR spectroscopy.



Scheme 6.6: Reaction of **40** with three molar equivalents of **58** to form



The molecular structure of **64** (**Figure 6.5**) displayed a SSIP motif, comprising of an octahedral magnesium di-cation solvated by six molecules of THF, and two anionic fragments which each consist of a trigonal planar zinc centre (average angle around Zn 119.7°) bonded to three *ortho*-zincated molecules of anisole, confirming this reaction as another example of direct Zn-I exchange. The three Zn-C bonds (2.075(5), 2.061(10) and 2.083(10) Å) are marginally longer than the Zn-C bonds of the related magnesium tris(*p*-tolyl)zincate **52** (2.039(5), 2.004(6) and 2.005(6) Å), which could be attributed to the steric hindrance of the adjacent methoxy groups in **64**. Remarkably, no interaction between the methoxy groups and the magnesium cation is observed. Thus, the molecular structure of **64** confirms the activation of all three *tert*-butyl “arms” of **40**, and demonstrates another example of high atom economy using this magnesium-zinc hybrid reagent.

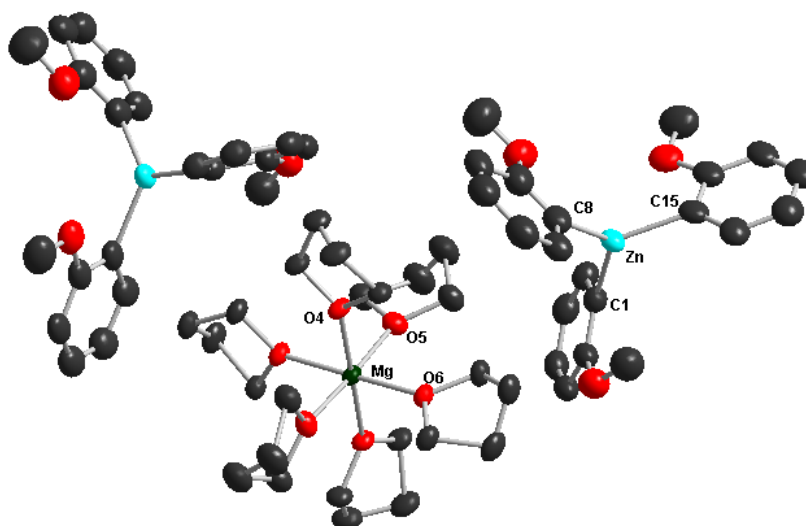


Figure 6.5: Molecular structure of $[\{\text{Mg}(\text{THF})_6\}^{2+}\{\text{Zn}(o\text{-C}_6\text{H}_4\text{OMe})_3\}_2]^-$ (**64**) with 30% probability ellipsoids. Hydrogen atoms and minor THF disorder components have been omitted for clarity. Selected bond distances (Å) and bond angles ($^\circ$): Zn-C1 2.075(5), Zn-C8 2.061(10), Zn-C15 2.083(10), Mg-O4 2.093(6), Mg-O5 2.062(6), Mg-O6 2.078(6), C1-Zn-C8 122.5(4), C1-Zn-C15 117.7(4), C8-Zn-C15 119.0(4), O4-Mg-O5 89.4(2), O4-Mg-O6 89.4(2), O5-Mg-O6 91.8(2), O4-Mg-O6A 178.9(2), O4A-Mg-O6 178.9(2), O5-Mg-O5A 177.2(4).

The ^1H NMR spectrum of **64** displayed four aromatic resonances (δ 7.48 (d), 6.93 (t), 6.71 (t) and 6.60 (d) ppm) and a singlet at 3.70 ppm for the methoxy group, consistent with those observed when the reaction of **40** with three equivalents of **58** is monitored by ^1H NMR spectroscopy in d_8 -THF, confirming that this is the same organometallic product. The most diagnostic resonance of the $^{13}\text{C}\{^1\text{H}\}$ NMR spectrum was that corresponding to the *ortho*-carbon bonded to zinc, which appears at δ 150.4 ppm, shifted significantly downfield from that observed for the *ortho*-carbon of the substrate **58**, which bonds to iodine (δ 86.7 ppm).

6.4 Investigating Zn-I exchange and Negishi Cross-coupling reactions of **40** with iodobenzonitrile substrates

In general, aromatic substrates which possess strongly electron withdrawing groups such as nitriles and carboxylates are more activated towards metal-halogen exchange reactions.^[168] However, the efficiency of these reactions can be compromised by the high electrophilicity of these groups, which when reacted with polar organolithium or Grignard reagents can readily undergo nucleophilic addition reactions.^[18, 99b] This problem can be overcome by using the

turbo Grignard reagent $^i\text{PrMgCl}\cdot\text{LiCl}$, which can react selectively with bromobenzonitrile substrates at 0°C .^[79d, 152b, 168-169] Bearing these precedents in mind, the reaction of **40** with 2-, 3- and 4-iodobenzonitrile (**65-67**) was investigated, allowing the compatibility of this Mg-Zn hybrid with more sensitive functional groups to be assessed.

Thus, previous kinetic studies suggest that the presence of this strongly electron withdrawing nitrile group should provide even greater activation of the substrates than that observed for the iodoanisole substrates (where enhanced reactivity was due to the relatively weak inductive electron withdrawing effect of the OMe group). Furthermore, given the magnitude of these rate enhancing effects decreases in the order *ortho* \gg *meta* $>$ *para*, it could be expected that 2-iodobenzonitrile (**65**) will display the highest rate of Zn-I exchange.^[168-169] Initially, the reactivity of **40** with the three different substrates was performed at room temperature in d_8 -THF and monitored by NMR spectroscopy. Analysis of reaction with 3-iodobenzonitrile (**66**) after 15 minutes indicated that Zn-I exchange had proceeded in a yield of 86%, improving to 93% after 2 hours, with no indication of any side reactions at the CN group. The aromatic region displayed four resonances for the zincated product (δ 8.04 (s), 8.03 (d), 7.33 (d) and 7.19 (t) ppm), along with traces of unreacted substrate **66** (δ 8.09 (s), 7.98 (d), 7.69 (d) and 7.25 (t) ppm) (**Table 6.4**) and the formation of ^tBuI (δ 1.91 ppm). A similarly high yield was also observed for the reaction of 4-iodobenzonitrile (**67**) with **40** (74% after 15 minutes, improving to 85% after 2 hours), with the new zincated species displaying two doublets at δ 7.91 and 7.32 ppm, and two further doublets for the unreacted substrate **67** (at δ 7.89 and 7.44 ppm) (**Table 6.4**).

	δ ^1H (ppm)
3-Iodobenzonitrile (66)	8.09 (s), 7.98 (d) 7.69 (d), 7.25 (t)
40 + 3 eq. 3-Iodobenzonitrile (66)	8.04 (s), 8.03 (d) 7.33 (d), 7.19 (t)
4-Iodobenzonitrile (67)	7.89 (d), 7.44 (d)
40 + 3 eq. 4-Iodobenzonitrile (67)	7.91 (d), 7.32 (d)
2-Iodobenzonitrile (65)	7.99 (d), 7.70 (d) 7.51 (t), 7.34 (t)
40 + 3 eq. 2-Iodobenzonitrile (65)	7.78 (d), 7.44 (d) 7.24 (t), 7.06 (t) (species 1)
	8.07 (d), 7.45 (d) 7.32 (t), 7.07 (t) (species 2)

Table 6.4: Comparison of ^1H NMR resonances (ppm) in d_8 -THF of the substrates (**65-67**) and the organozincate species formed through Zn-I exchange with **40**.

Contrasting with these relatively straightforward NMR spectra and the high yields observed for the Zn-I exchange of **66** and **67** with **40**, the reaction with 2-iodobenzonitrile (**65**) displayed a much more complex series of ^1H NMR spectra. After 15 minutes (**Figure 6.6(b)** and **Figure 6.7(a)**) four new aromatic resonances had emerged (δ 7.78 (d), 7.44 (d) 7.24 (t) and 7.06 (t) ppm), consistent with the formation of a new Ar-Zn species, along with a significant amount of unreacted substrate (δ 7.99 (d), 7.70 (d) 7.51 (t) and 7.34 (t) ppm) (**Table 6.4**). Analysis of the integration of these resonances indicated that the Zn-I exchange had proceeded in a yield of only 53% after 15 minutes, a significantly lower conversion to those observed for **66** or **67** (83% and 74% respectively). Furthermore, the aliphatic region displayed a single resonance at δ 0.98 ppm, which integrated to nine protons, consistent with the presence of one remaining *tert*-butyl group bound to zinc. This resonance is shifted slightly downfield compared to the major *tert*-butyl resonance of **40** (δ 0.89 ppm), which suggests that the $\{\text{Zn}^t\text{Bu}_3\}^-$ anion of **40** is no longer present in solution.

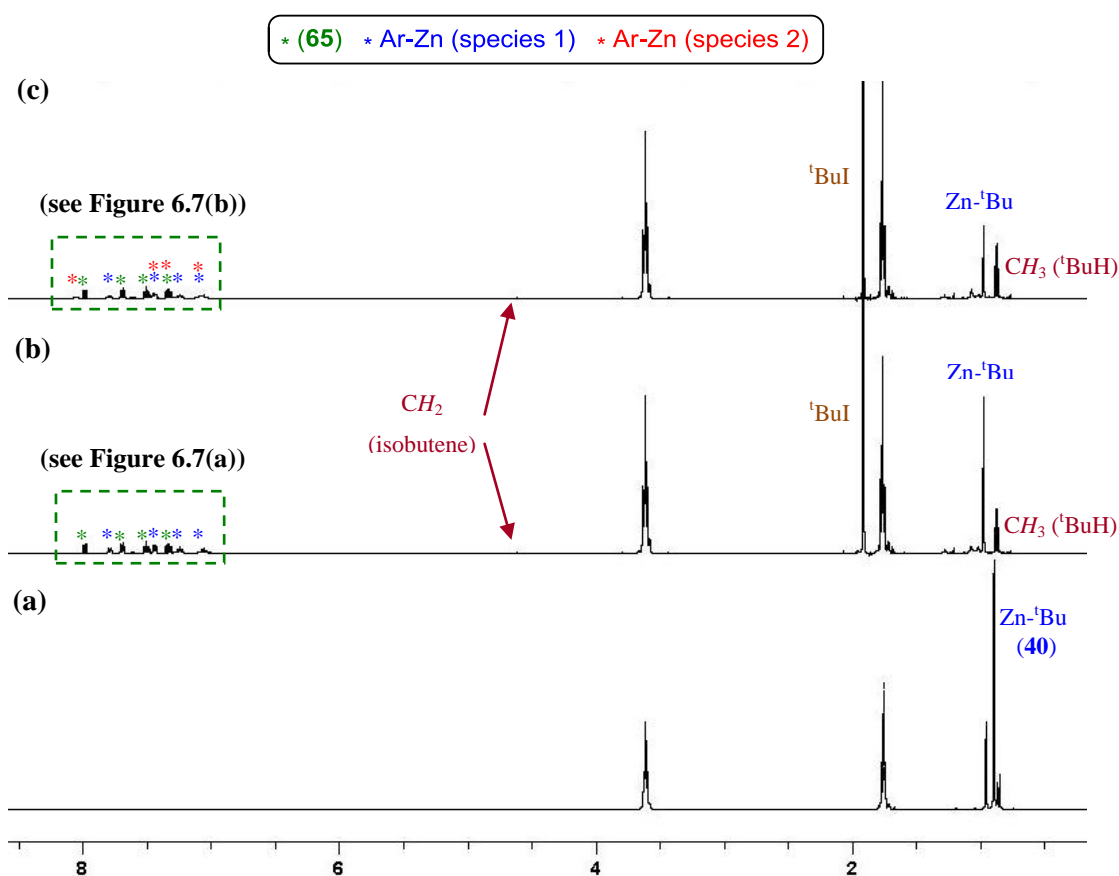


Figure 6.6: ^1H NMR spectra for the reaction of **40** with three equivalents of **65** (a) before the addition of Ar-I, (b) 15 minutes after addition and (c) 2 hours after addition.

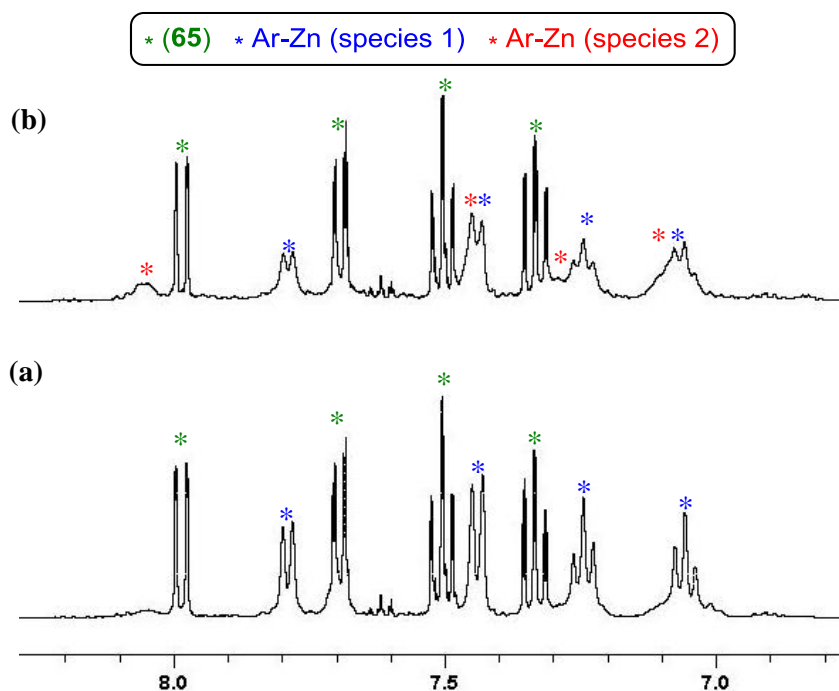


Figure 6.7: Expanded aromatic region of the ^1H NMR spectra for the reaction of **40** with three equivalents of **65** in d_8 -THF (a) 15 minutes after addition and (b) 2 hours after addition.

Even more surprisingly, after 2 hours (**Figure 6.6(c)** and **Figure 6.7(b)**) the moiety of the resonances of the Ar-Zn species (**species 1**) had decreased, and a new set of aromatic resonances (**species 2**) had begun to emerge (δ 8.07 (d), 7.45 (d) 7.32 (t) and 7.07 (t) ppm) (ratio of **species 1** species to **species 2** ~2:1) (**Table 6.4**). Combining the integration of both of these Ar-Zn species with those of the unreacted substrate **65** indicated that the extent of Zn-I exchange after 2 hours had not significantly increased compared to the conversion after 15 minutes (55% vs. 53%), although the moiety of the remaining *tert*-butyl ligand (δ 0.98 ppm), which previously integrated to nine protons had decreased to five.

Further monitoring of the reaction revealed no further conversion of the substrate **65**, even after 20 hours, although the ratio of **species 1** to **species 2** had changed to ~1:3 after 9 hours and ~1:10 after 20 hours (**Figure 6.8**). In addition, the remaining *tert*-butyl resonances had disappeared completely, along with a decrease in the amount of ^tBuI present in solution, as shown by the integration of the singlet at δ 1.91 ppm, and the emergence of resonances at δ 4.61, 1.68 and 0.87 ppm, consistent with the formation of isobutene and isobutane respectively, which suggests that the remaining *tert*-butyl group bonded to zinc has reacted with ^tBuI .

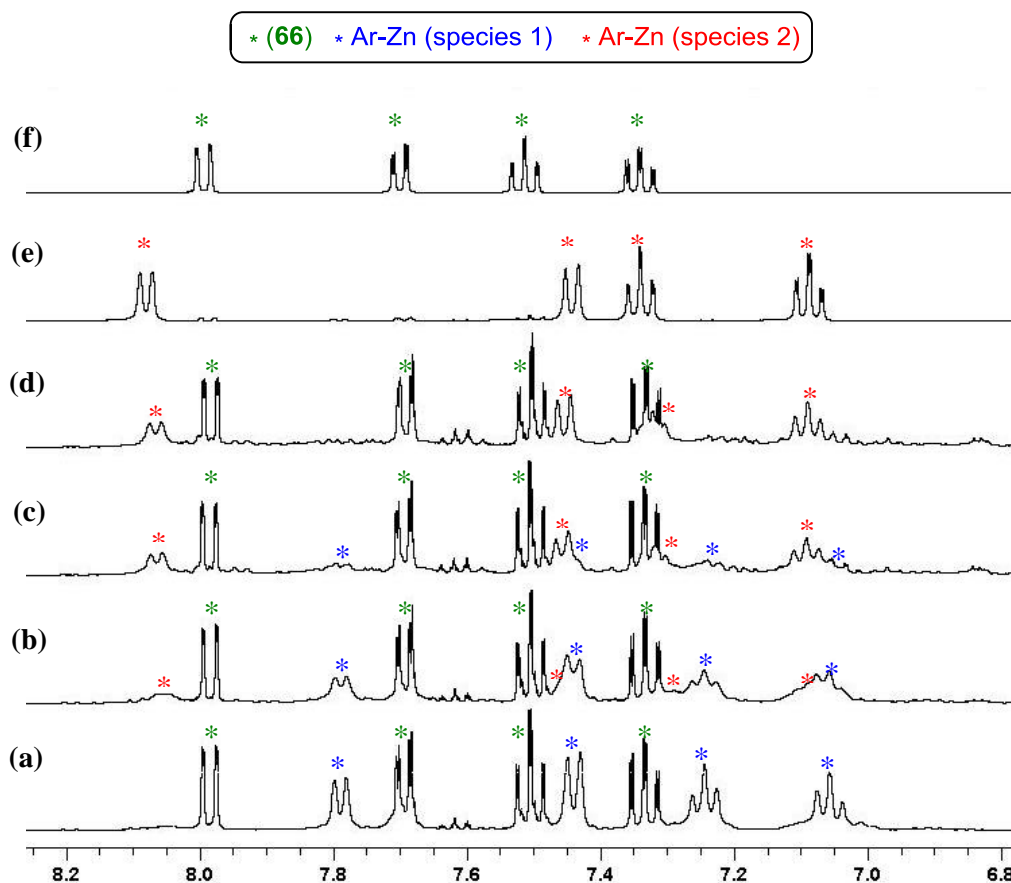


Figure 6.8: Aromatic region of the ^1H NMR spectra for the reaction of **40** with three equivalents of **65** (a) 15 minutes after addition, (b) 2 hours after addition, (c) 9 hours after addition, (d) 20 hours after addition, (e) $[(\text{THF})_4\text{MgCl}\{\text{NC-}o\text{-C}_6\text{H}_4\}\text{ZnI}(o\text{-C}_6\text{H}_4\text{CN})(\text{THF})]$ (**68**) (vide infra) and (f) 2-Iodobenzonitrile (**65**) in d_8 -THF.

Thus, in contrast with the reactivities observed for 3-iodobenzonitrile (**66**) and 4-iodobenzonitrile (**67**), monitoring the reaction of **40** with **65** by ^1H NMR spectroscopy suggests that only two of the *tert*-butyl ligands of **40** are activated towards Zn-I exchange with **65**, with the remaining *tert*-butyl group being consumed over time by reaction with ^tBuI . This reduced reactivity is an unexpected result given that the previously mentioned kinetic studies into Mg-Br exchange suggest that 2-bromobenzonitrile is much more activated than 3- or 4-bromobenzonitrile.^[168-169] In an attempt to shed some light on the reasons behind these results, **40** was reacted with three equivalents **65** in THF for 4 hours at room temperature, and following addition of hexane the dark red solution transferred to the freezer. After several days a crop of colourless cubic crystals were obtained of the magnesium-zincate species $[(\text{THF})_4\text{MgCl}\{\text{NC-}o\text{-C}_6\text{H}_4\}\text{ZnI}(o\text{-C}_6\text{H}_4\text{CN})(\text{THF})]$ (**68**) in an isolated yield of 8% (although analysis of the filtrate solution suggested that **68** was the major species present).

Contrasting with theSSIP structures previously described for the products of Zn-I exchange $[\{\text{Mg}_2\text{Cl}_3(\text{THF})_6\}^+\{\text{Zn}(p\text{-Tol})_3\}^-]$ (**52**) and $[\{\text{Mg}(\text{THF})_6\}^{2+}\{\text{Zn}(o\text{-C}_6\text{H}_4\text{OMe})_3\}_2^-]$ (**64**), **68** exhibits a CIP structure (**Figure 6.9**). Both metals are connected by an *ortho*-metallated $\{o\text{-C}_6\text{H}_4\text{-CN}\}^-$ fragment, which binds through the *ortho*-carbon to zinc forming a strong σ -bond (Zn-C12 2.008(3) Å) and through the nitrogen of the nitrile group to magnesium (Mg-N2 2.232(3) Å). Magnesium completes its distorted octahedral geometry by bonding to a Cl atom (in a *trans* disposition to the N atom, N2-Mg-Cl1 176.88(8) $^\circ$) and four molecules of THF, whereas distorted tetrahedral zinc binds to another $\{o\text{-C}_6\text{H}_4\text{-CN}\}^-$ unit (Zn-C5 2.013(3) Å), a molecule of THF and a terminal iodine atom (Zn-I1 2.6981(4) Å).

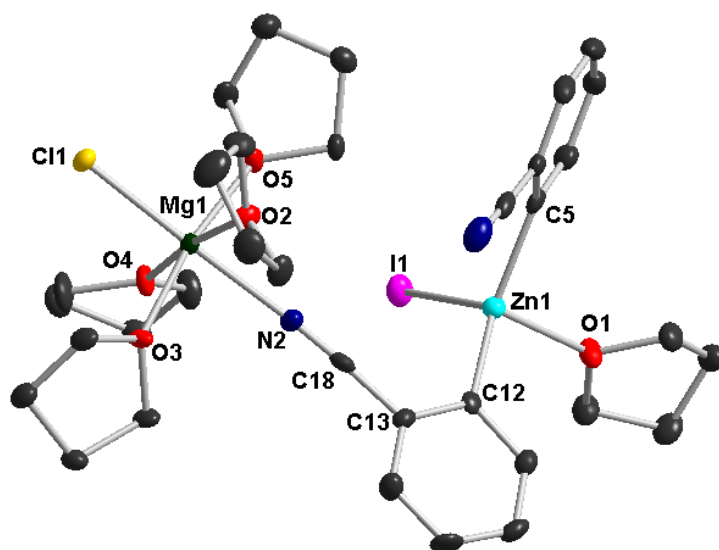


Figure 6.9: Molecular structure of $[(\text{THF})_4\text{MgCl}\{\text{NC-}o\text{-C}_6\text{H}_4\}\text{ZnI}(o\text{-C}_6\text{H}_4\text{CN})(\text{THF})]$ (**68**) with 50% probability ellipsoids. Hydrogen atoms have been omitted for clarity. *Selected bond distances* (Å) *and bond angles* ($^\circ$): Zn-I1 2.6981(4), Zn-C12 2.008(3), Zn-C5 2.013(3), Zn-O1 2.182(2), Cl1-Mg 2.3777(13), Mg-N2 2.232(3), C12-Zn-C5 135.57(13), C12-Zn-O1 97.82(11), C5-Zn-O1 98.82(11), C12-Zn-I1 113.59(8), C5-Zn-I1 105.60(10), O1-Zn-I1 95.05(6), N2-Mg-Cl1 176.88(8), N2-C18-C13 177.0(3), C18-N2-Mg 172.7(3).

The bidentate coordination mode of the $\{o\text{-C}_6\text{H}_4\text{-CN}\}^-$ fragment in **68** is similar to that observed in the related sodium zincate species $[(\text{TMEDA})_2\text{Na}\{2\text{-Zn}(\text{tBu})_2\text{-1-NC-C}_{10}\text{H}_6\}]$, resulting from the AMMZn of 1-cyanonaphthalene by the sodium zincate **3**,^[64] where the $\{\text{Zn}(\text{tBu})_2(o\text{-CN-C}_{10}\text{H}_6)\}^-$ anion bonds through the nitrile group to cationic $\{\text{Na}(\text{TMEDA})_2\}^+$ (**Figure 6.10**).

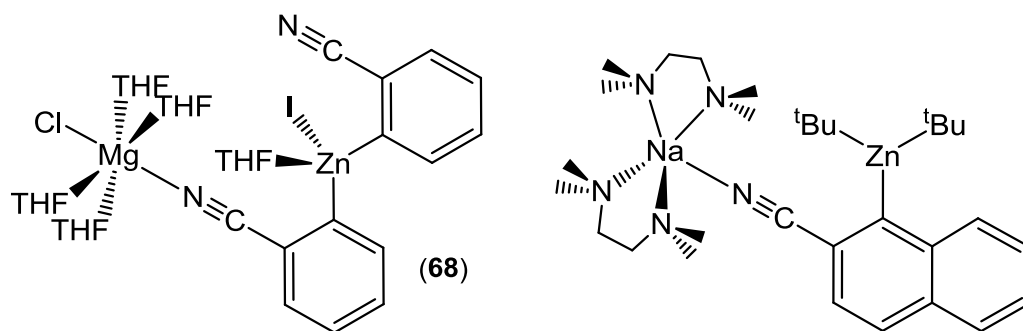
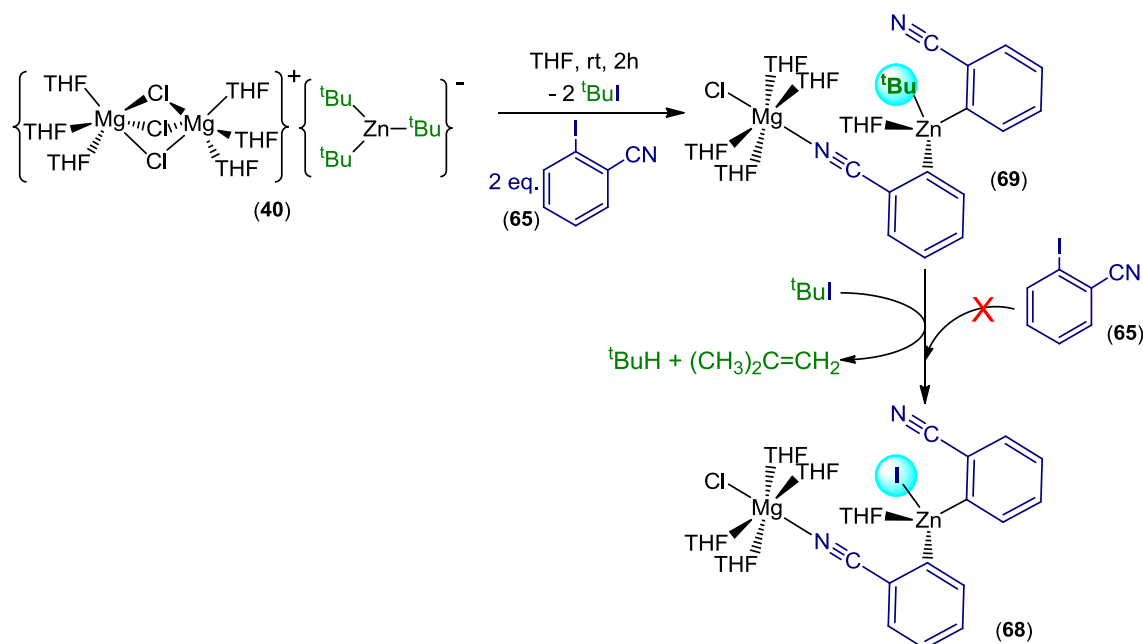


Figure 6.10: Comparison of the CIP structures of **68** and $[(\text{TMEDA})_2\text{Na}\{2\text{-Zn}(\text{tBu})_2\text{-1-NC-C}_{10}\text{H}_6\}]$.

Remarkably, the ^1H NMR spectrum of **68** in d_8 -THF displayed only one set of aromatic resonances (δ 8.08 (d), 7.44 (d) 7.34 (t) and 7.09 (t) ppm) (**Figure 6.8(e)**), suggesting that in solution the CIP structure may be breaking into a $\{\text{MgCl}(\text{THF})_4\}^+$ cation and a $\{\text{Zn}(\textit{o}\text{-CN-C}_6\text{H}_4)_2\text{I}(\text{THF})\}^-$ anion, or alternatively, the $\{\text{MgCl}(\text{THF})_4\}^+$ fragment, which coordinates to one of the nitrile groups in the molecular structure of **68** may be rapidly exchanging between each of the molecules of *ortho*-zincated benzonitrile in solution. Notwithstanding, analysis of these aromatic resonances revealed that **68** is the second organometallic species formed in the reaction of **40** with three equivalents of **65**, which is initially observed after 2 hours (**Figure 6.8(b)**), and becomes the major species after 20 hours (**Figure 6.8(d)**). Thus, these results strongly suggest that in the reaction of **40** with three equivalents of **65** only two *tert*-butyl groups of the $\{\text{Zn}^{\text{tBu}}_3\}^-$ anion are activated towards Zn-I exchange. This could lead to the formation of a magnesium bis(aryl)-*tert*-butylzincate $[(\text{THF})_4\text{MgCl}\{\text{NC-}\textit{o}\text{-C}_6\text{H}_4\}\text{Zn}^{\text{tBu}}(\textit{o}\text{-C}_6\text{H}_4\text{CN})(\text{THF})]$ (**69**), which may adopt a similar structural motif to that of **68** (**Scheme 6.7**). Over time, the remaining *tert*-butyl group of **69** will react preferentially with the $^{\text{tBu}}$ I generated by the Zn-I exchange reaction, instead of the remaining unreacted 2-iodobenzonitrile (**65**), forming the final magnesium-zincate species **68**, along with isobutene and isobutane (**Scheme 6.7**).

A plausible explanation for the lack of activation of the third *tert*-butyl group in **69** to undergo Zn-I exchange with **65** could be the fact that CIP Mg-Zn hybrid species are involved in this reaction. To elaborate, a recent theoretical study into Zn-I exchange reactions of lithium trialkylzincates (LiZnR_3) revealed that in the most energetically favoured pathway the first step of the reaction is coordination of the substrate through the iodine atom to lithium. This coordination of the substrate activates the C-I bond, facilitating the Zn-I exchange.^[29] A similar mechanism could also be taking place for magnesium-zincate **40**, where the organic

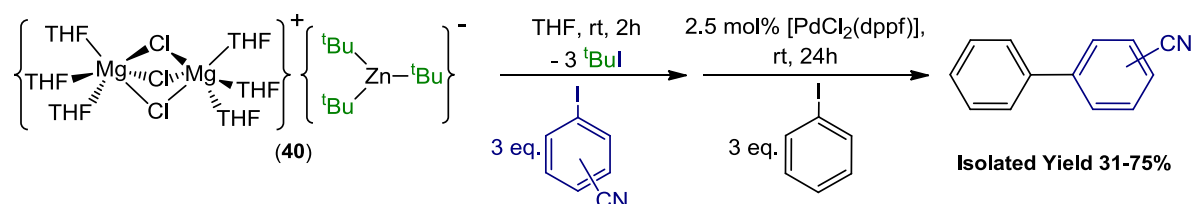
substrate will initially coordinate to the cationic Mg centre, allowing anionic $\{\text{Zn}^t\text{Bu}_3\}^-$ to react with the activated C-I bond. Assuming that the Zn-I exchange reactions of the three *tert*-butyl groups in **40** occurs in a sequential manner, after the successful reaction of two of the *tert*-butyl groups, formation of a CIP species such as **69** may hinder the coordination of the third molecule of substrate to magnesium, or if the substrate is able to coordinate, the less flexible CIP structure may prevent the approach of the remaining *tert*-butyl ligand close enough to the C-I bond for the reaction to occur.



Scheme 6.7: Proposed reaction of **40** with three molar equivalents of **65**, to form the putative intermediate **69**, which undergoes subsequent reaction with $t\text{BuI}$ to form **68**.

The reduced reactivity displayed by **40** towards 2-iodobenzonitrile (**65**) was mirrored by the isolated yields which were obtained when the Negishi cross-coupling reactions of **65-67** with iodobenzene were performed under the same conditions employed for the iodotoluene and iodoanisole substrates (**Scheme 6.8, Table 6.5**). Thus, whereas the cross-coupling reactions of 3- and 4-iodobenzonitrile (**66** and **67** respectively) yielded 3-cyanobiphenyl (**71**) and 4-cyanobiphenyl (**72**) in yields of 75% and 71% respectively, when the same cross-coupling reaction was performed with 3 equivalents of 2-iodobenzonitrile (**65**), the expected product, 2-cyanobiphenyl (**70**), was obtained in a yield of only 31%. This dramatic difference in yield is easily explained by the low yield of Zn-I exchange obtained for **65** (55% after 2 hours) compared to **66** and **67** (90% and 85% respectively) (**Table 6.5**). Therefore, the substantial

amount of **65** which remains unreacted in solution will greatly affect the final yield of the Negishi cross-coupling reaction.



Scheme 6.8: Reaction of **40** with three molar equivalents of 2-/3-/4-iodobenzonitrile (**65-67**), followed by Negishi cross-coupling with iodobenzene.

Substrate	% Zn-I Exchange after 2h ^[a]	Product	Isolated Yield
2-Iodobenzonitrile (65)	55		31% (R = CN) (70)
2-Iodoanisole (58)	86		76% (R = OMe) (61)
2-Iodotoluene (55)	75		60% (R = Me) (58)
3-Iodobenzonitrile (66)	93		75% (R = CN) (71)
3-Iodoanisole (59)	86		76% (R = OMe) (62)
3-Iodotoluene (54)	87		65% (R = Me) (57)
4-Iodobenzonitrile (67)	86		71% (R = CN) (72)
4-Iodoanisole (60)	88		79% (R = OMe) (63)
4-Iodotoluene (51)	85		65% (R = Me) (53)

Table 6.5: Comparison of the isolated yields of the relevant products from Zn-I exchange of functionalised aryl iodide substrates (3 eq.) with **40**, followed by Pd catalysed Negishi cross-coupling with iodobenzene. ^[a] Determined by ¹H NMR spectroscopy.

Since as previously mentioned the presence of unreacted aryl iodide substrate from the Zn-I exchange reaction can have a detrimental effect on the cross-coupling reaction, leading to the formation of the homocoupled product, the reaction of **40** with two equivalents of **65** was performed in an attempt to improve the isolated yield of 2-cyanobiphenyl (**70**). In order to first determine the extent of the Zn-I exchange, the reaction of **40** with two equivalents of **65** in d₈-THF was followed by ¹H NMR spectroscopy. After 15 minutes (**Figure 6.11(a)**) Zn-I

exchange had proceeded in a yield of 83%, forming the putative intermediate $[(\text{THF})_4\text{MgCl}\{\text{NC-}o\text{-C}_6\text{H}_4\}\text{Zn}^{\text{tBu}}(o\text{-C}_6\text{H}_4\text{CN})(\text{THF})]$ (**69**). After 2 hours the yield had improved to 86% (**Figure 6.11(b)**), with four new aromatic resonances corresponding to **68** beginning to appear, and those of **69** decreasing with **68** becoming the major species present after 6 hours (**Figure 6.11(c)**).

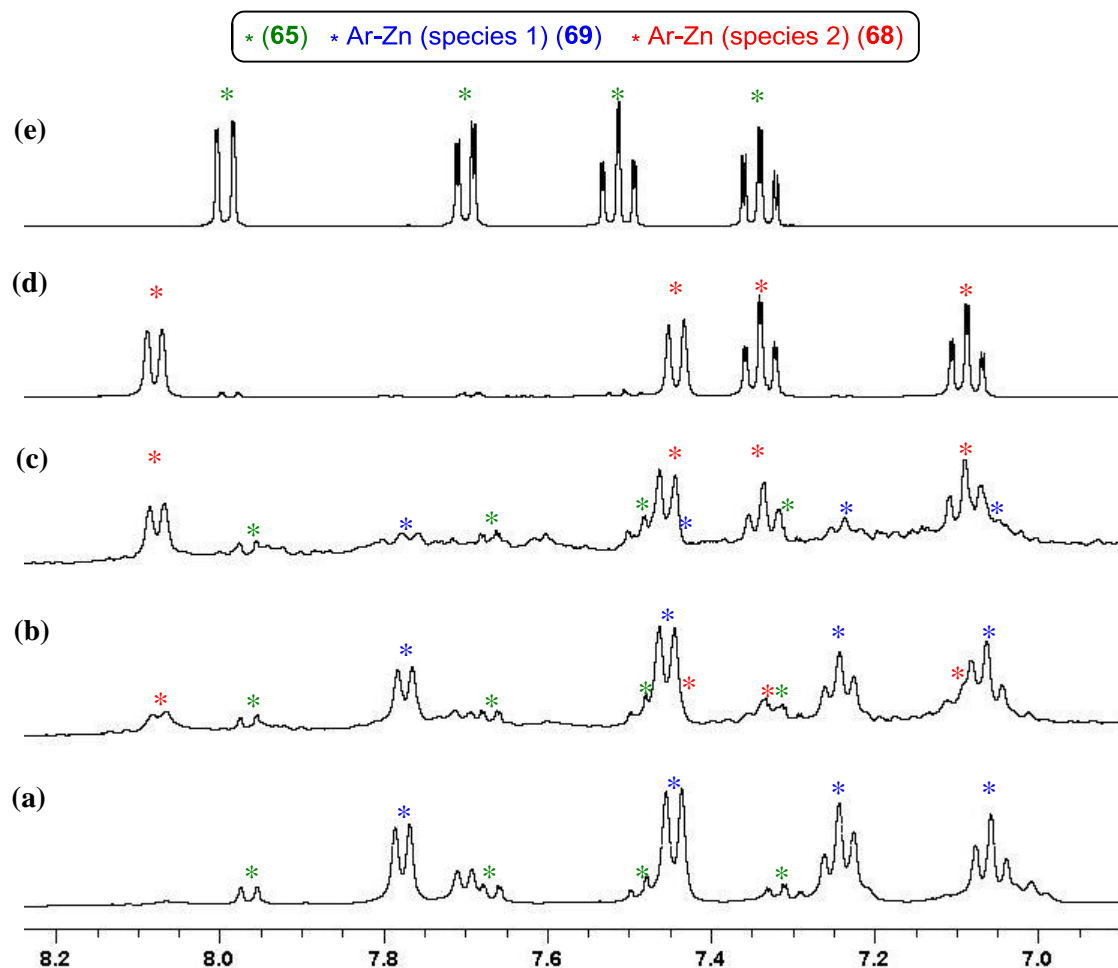
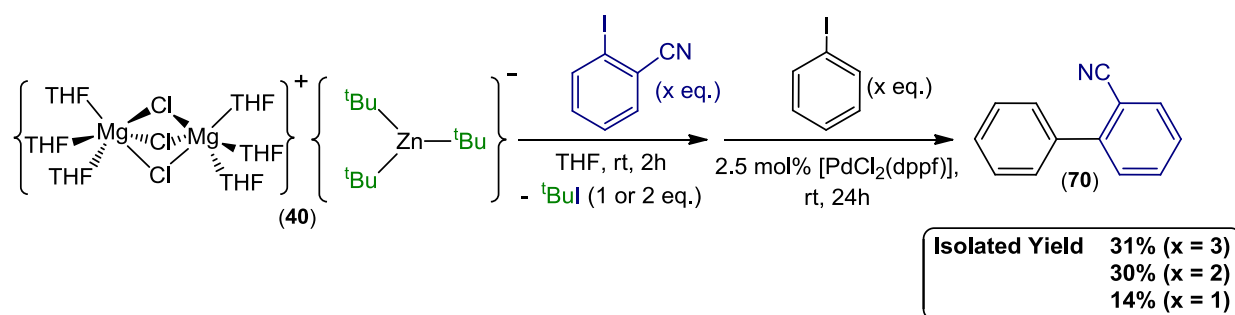


Figure 6.11: Aromatic region of the ^1H NMR spectra for the reaction of **40** with two equivalents of **65** (a) 15 minutes after addition, (b) 2 hours after addition, (c) 6 hours after addition, (d) **68** and (e) **65** in d_8 -THF.

Based on the improved yield for Zn-I exchange when **40** is reacted with only two equivalents of **65**, it would be expected that by applying the same Negishi cross-coupling protocol to this system as described previously, the isolated yield of 2-cyanobiphenyl (**70**) would be significantly higher than that obtained when three equivalents of **65** are employed (31%). Surprisingly, the cross-coupling reaction resulted in the isolation of **70** in an almost identical yield of 30%. Furthermore, when **40** was reacted with only one equivalent of **65** the

subsequent cross-coupling reaction led to the isolation of **70** in a modest 14% yield, half that of the reaction with two and three equivalents of **65** (Scheme 6.9).



Scheme 6.9: Reaction of **40** with 2-iodobenzonitrile (**65**) (1-3 equivalents), followed by Negishi cross-coupling with iodobenzene to form 2-cyanobiphenyl (**70**).

The similar yields obtained for **70** when two or three equivalents of **65** are employed not only provide further confirmation that only two of the *tert*-butyl groups of **40** can react with **65**, but also show that in this case excess **65** present in solution is not the cause of the low yields obtained for the cross-coupling reactions. This suggests that 2-iodobenzonitrile (**65**) not only shows a decreased reactivity towards **40** in the Zn-I exchange step, but also gives rise to a less reactive organozincate intermediate to participate in the Negishi cross-coupling step. In this regard, previous studies into Negishi cross-coupling reactions have revealed that the presence of strongly electron withdrawing groups on the aryl-zinc species can significantly decrease the rate of cross-coupling reactions, due to their deactivating effect on the transmetalation step.^[170] This negative effect of the nitrile group on the cross-coupling reactions appears to be less prominent for 3- and 4-iodobenzonitrile (**66** and **67**), as the yields observed for the relevant bis(aryl) species are comparable to those of the related iodoanisole substrates under the conditions employed. However, the molecular structure of the different types of Mg-Zn hybrids involved in these reactions could also be playing an important role, with the formation of CIP structures such as **68** perhaps affecting both the Zn-I exchange and transmetalation reactions.

These results would suggest that in order to overcome the lower yields of this cross-coupling reaction some of the reaction conditions, such as catalyst loading, reaction temperature or using a different catalyst altogether, may have to be altered. Recently, it has been reported that the challenging Negishi cross-coupling of benzylic pyridines can be achieved by the addition of a Lewis acid to the reaction (Sc(OTf)₃, BF₃·OEt₂).^[171] Thus, a similar Lewis acid

promoted cross-coupling protocol could be employed for the reaction between **40** and **65**. Furthermore, coordination of the Lewis acid to the iodobenzonitrile molecules may also activate the substrate towards Zn-I exchange with all three *tert*-butyl groups present in **40**, resulting in a further enhancement of the cross-coupling yields.

To sum up, a new methodology to prepare asymmetric bis(aryl) compounds by sequential direct Zn-I exchange, promoted by Mg-Zn hybrid **40**, followed by a Pd-catalysed Negishi cross-coupling reaction has been developed, which allows the synthesis of these important molecules in yields ranging from 31-79%. Comparison of the yields obtained for the Zn-I exchange and Negishi cross-coupling reactions in **Table 6.5** also provides an insight into the effect of the different functional groups (-Me, -OMe, -CN) and substitution pattern (*ortho*, *meta*, *para*) of the aromatic substrates in this system.

In general the presence of the electron donating Me group results in lower yields for the Zn-I exchange reaction (75-87%) compared to the inductively electron withdrawing OMe group (86-88%) and the strongly electron withdrawing CN group (86-93%), with the exception to this rule being 2-iodobenzonitrile (**65**), which as previously discussed displays surprisingly low yields for the Zn-I exchange when three equivalents of the substrate are reacted with **40** (55%). Interestingly, despite the significantly greater electron withdrawing ability of nitrile groups compared to methoxy groups, the yields of Zn-I exchange reactions for these substrates are comparable (excluding **65**), where previous studies would suggest that the nitrile substituted aryl halides should display greater reactivity.^[168-170] Therefore, these results suggests that for these magnesium triorganozincate systems steric effects, which may include the formation of CIP species such as **68**, may be playing an important role in the outcome of these Zn-I exchange reaction.

The lower yields of Zn-I exchange obtained for the iodotoluene substrates also provide an explanation for the lower yields observed in the Negishi cross-coupling reactions (60-65%), with a notable amount of the homocoupled (dimethylbiphenyl) species being formed. Furthermore, the cross-coupling yields of the methoxy substituted substrates are found to be higher than the corresponding nitrile substituted substrates, which can be explained by the tendency of the more strongly electron withdrawing CN groups to inhibit transmetallation of the organozincate species with the Pd catalyst.^[170]

Comparison of the different substitution patterns reveals that in general the *ortho*-substituted aryl iodide substrates display marginally lower yields for Zn-I exchange (55-86%) and Negishi cross-coupling (31-76%) than both the *meta*- (Zn-I exchange 86-93%, cross-coupling 65-76%) and *para*- (Zn-I exchange 85-88%, cross-coupling 65-79%) substituted aromatic substrates, which again hints at the influence of steric effects in these systems.

6.5 Conclusions

Initial studies, which involved ^1H NMR monitoring and structural elucidation of key organometallic intermediates, into the reactivity of magnesium tri-*tert*-butylzincate $[\{\text{Mg}_2\text{Cl}_3(\text{THF})_6\}^+\{\text{Zn}^t\text{Bu}_3\}^-]$ (**40**) with aryl iodide substrates have established that contrasting with the complete lack of reactivity shown by Zn^tBu_2 , all three *tert*-butyl groups bonded to Zn are active towards Zn-I exchange. Thus, reaction of **40** with three equivalents of 4-iodotoluene (**51**) and 2-iodoanisole (**58**) resulted in the isolation of the magnesium tris(aryl)zincate species $[\{\text{Mg}_2\text{Cl}_3(\text{THF})_6\}^+\{\text{Zn}(p\text{-C}_6\text{H}_4\text{Me})_3\}^-]$ (**52**) and $[\{\text{Mg}(\text{THF})_6\}^{2+}\{\text{Zn}(o\text{-C}_6\text{H}_5\text{OMe})_3\}_2^-]$ (**64**). Furthermore, these highly atom economical Zn-I reactions were performed at ambient temperature without observing any side reactions with sensitive functional groups such as nitriles, and required only stoichiometric amounts of the zincate to be employed.

Monitoring the reactions of **40** with three equivalents of iodotoluene (2-Me (**55**), 3-Me (**54**) and 4-Me (**51**)), iodoanisole (2-OMe (**58**), 3-OMe (**59**) and 4-OMe (**60**)), and iodobenzonitrile (3-CN (**66**) and 4-CN (**67**)) substrates by ^1H NMR spectroscopy indicated that similar tris(aryl)zincates could be obtained from all of these reactions. Furthermore, these zincates could be employed in simple Pd catalysed Negishi cross-coupling reactions with iodobenzene, yielding the expected asymmetric bis(aryl) products in yields ranging from 60-79%. However, performing a similar Zn-I exchange with 2-iodobenzonitrile (**65**) resulted in the formation of the unexpected CIP magnesium bis(aryl)zincate $[(\text{THF})_4\text{MgCl}\{\text{NC-}o\text{-C}_6\text{H}_4\}\text{ZnI}(o\text{-C}_6\text{H}_4\text{CN})(\text{THF})]$ (**68**), where only two of the *tert*-butyl ligands of the zincate were able to perform Zn-I exchange with the substrate, and the remaining *tert*-butyl group was replaced by iodine following a side-reaction with ^tBuI . Furthermore, this bis(aryl)zincate **68** displayed substantially lower levels of reactivity in Negishi cross-coupling reactions than any of the other substrates studied to date, which could be attributed to the presence of the highly

electron withdrawing nitrile group adjacent to the Zn-C bond, inhibiting the transmetallation reaction of the zincate with the Pd catalyst.

Of the different functionalised aryl iodides studied to date for this methodology, it is the iodoanisole substrates which overall display the greatest reactivity, providing a good balance of inductive electron withdrawing ability to facilitate the Zn-I exchange, coupled with the mesomeric electron donating ability to ensure they readily undergo transmetallation with the Pd catalyst. This is somewhat counter intuitive, as it would be expected that the stronger electron withdrawing ability of a nitrile group should result in enhanced yields for the Zn-I exchange reactions. However, based on the molecular structures of the magnesium aryl-zincates observed so far, it would also appear that the poorer donor ability of the OMe groups compared to that of the CN groups may also be an important factor. Thus, the CIP structure $[(\text{THF})_4\text{MgCl}\{\text{NC-}o\text{-C}_6\text{H}_4\}\text{ZnI}(o\text{-C}_6\text{H}_4\text{CN})(\text{THF})]$ (**68**) obtained from the reaction of **40** with 2-iodobenzonitrile (**65**) contrasts the SSIP structure $[\{\text{Mg}(\text{THF})_6\}^{2+}\{\text{Zn}(o\text{-C}_6\text{H}_5\text{OMe})_3\}_2^-]$ (**58**) obtained from the reaction of **40** with 2-iodoanisole (**58**), which may provide further explanation for the lower than expected reactivity observed for the iodobenzonitrile substrates in Zn-I exchange.

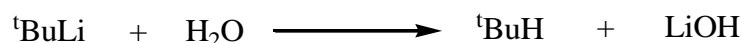
Future work in this area will focus on developing suitable reaction conditions to perform the cross-coupling reaction of 2-iodobenzonitrile in higher yields, as well as extending this Zn-I exchange/Negishi cross-coupling methodology to other aromatic and heteroaromatic halides.

Chapter 7: General experimental techniques & procedures

7.1 General experimental techniques

7.1.1 Schlenk techniques

Most of the organometallic species involved in this project were oxygen and moisture sensitive. Further still, some of these compounds, such as *tert*-butyllithium, were pyrophoric, as reaction with moisture leads to the formation of flammable hydrocarbons (**Scheme 7.1**)



Scheme 7.1: Reaction of ${}^t\text{BuLi}$ with water.

As a result, all reactions had to be carried out in a dry, inert atmosphere, using standard Schlenk techniques. This involved the use of a Schlenk line, and Schlenk glassware (**Figure 7.1**). Two of the most common pieces of apparatus used were the Schlenk tube, in which most of the reactions were carried out, and the Schlenk filter stick, which was used for the isolation of solid products, and the removal of insoluble impurities.

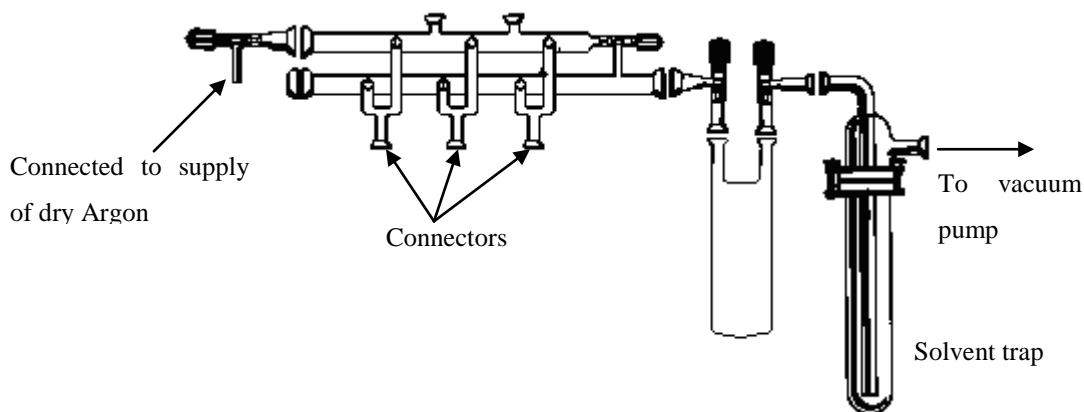


Figure 7.1(a): Standard Schlenk line.

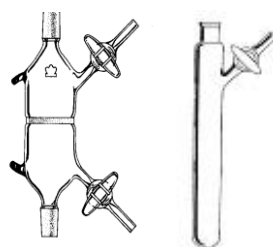


Figure 7.1(b): Standard Schlenk filter stick (left) and Schlenk tube (right).

The Schlenk line consists of an inert gas/vacuum double manifold, which contains two separate pathways; one connected to a vacuum pump, and the other to a supply of dry argon-gas. The Schlenk line contains separate connectors, which can be connected to the appropriate apparatus (usually a Schlenk tube). Each of these connectors has a two-way tap, which means that the apparatus can be subjected to either vacuum or to argon-gas. Oxygen is removed from the Schlenk tube by applying vacuum for a period of at least 10 minutes, allowing the apparatus to be evacuated, followed by re-filling with argon. This process is repeated three times as standard practice, to provide the dry, inert atmosphere required for reactions to be carried out. The addition of solvents and reagents to the apparatus was always carried out under a positive pressure of argon, so as to prevent any oxygen entering the system.

A liquid-nitrogen cooled trap was attached to the end of the Schlenk line, to condense any volatile substances, which could be potentially damaging, before they reach the vacuum pump. A pressure release bubbler is also incorporated into the line, which ensures that there is no build-up of pressure in the apparatus. Finally, all Schlenk glassware used contained ground-glass joints, which were lightly greased before being connected together, to seal the joints, and prevent the glass pieces from getting stuck together.

7.1.2 Glove box

Due to the oxygen and moisture sensitive nature of most of the compounds involved in this project, the manipulation of solid materials, which included the determination of weights of reactants and products, and the preparation of NMR samples, was carried out in a standard glove box (or dry box), which provides a sealed, inert atmosphere to work in (**Figure 7.2**).

The glove box comprises of two main chambers. The larger chamber, which contains a plastic window and two gloves, is the working area. This chamber is kept full of dry argon, and is where the manipulation of chemicals takes place. The second chamber is the port on the right hand side (**Figure 7.2**), which has an outer door and an inner door (connected to the main chamber), allowing the transfer of apparatus and chemicals into and out of the box. Items are placed in the port, which is then evacuated to remove oxygen and moisture, followed by the re-filling of the port with dry argon gas. As with the Schlenk line, this process is carried out three times as standard practice, to ensure that only negligible quantities of oxygen and moisture are present. After this, the inner door of the port can be opened, and the contents

transferred to the main chamber to be used. The gas in the glove box is constantly circulated over a catalyst and molecular sieve unit, which removes any oxygen or water which may be present in the system. The catalyst and sieve unit have to be regularly regenerated.

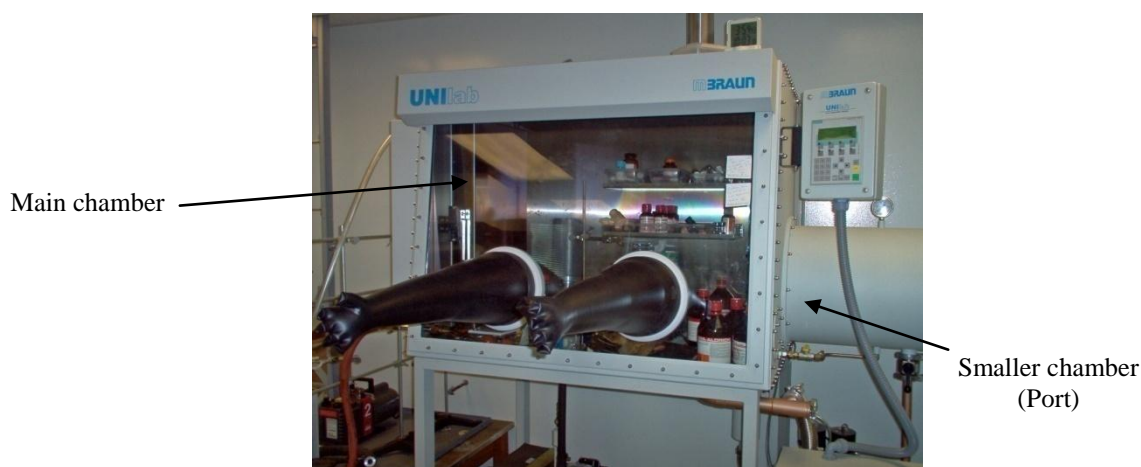


Figure 7.2: Standard glove box.

7.1.3 Solvent purification

As a result of the sensitivity of the reactants and products to oxygen and moisture, any solvents which were used had to first be dried and de-gassed. Solvents such as THF, hexane, toluene and diethyl ether were distilled over nitrogen, in the presence of sodium and benzophenone. The generation of the sodium benzophenone ketyl radical, which displays an intense blue colour, confirms that the solvents are dry and free from oxygen contaminant.^[172] Deuterated solvents, such as d_8 -THF and d_6 -benzene, which were purified on a smaller scale were dried over molecular sieves, and de-gassed using a standard freeze-pump-thaw procedure,^[172] then stored in the dry box.

7.1.4 Standardisation of organometallic reagents

The standardisation organolithium and Grignard reagents was performed using a 1 M solution of 2-butanol in *p*-xylene and *N*-phenyl-1-naphthylamine.^[173] The addition of the organometallic species to the indicator results in the formation of a bright yellow/orange solution, which on addition of 2-butanol results in the formation of colourless/cloudy solution, which indicates that the end-point has been reached. The standardisation of organozinc reagents was performed using I_2 and a THF solution of LiCl, with the end point determined when the addition of the organozinc reagent had turned the brown solution colourless.^[174]

7.1.5 Analytical Procedures

All ^1H NMR spectroscopic analysis were carried out a Bruker AVANCE-400 NMR spectrometer operating at 400.13 MHz under TopSpin (version 2.0, Bruker Biospin, Karlsruhe). The $^{13}\text{C}\{^1\text{H}\}$ NMR spectra were carried out on the same instrument, operating at 100.62 MHz, and all were proton decoupled. The ^7Li NMR spectra were recorded at 155.50 MHz. The $^{19}\text{F}\{^1\text{H}\}$ NMR spectra were recorded at 376.36 MHz. Abbreviations of NMR patterns are as follows: s (singlet), d (doublet), t (triplet), m (multiplet) and b (broad peak).

The X-ray crystallographic data were recorded on Nonius Kappa CCD diffractometers at 150K, and Oxford Diffraction (now Agilent Technologies) Xcalibur and Gemini diffractometers at 123K using $\text{MoK}\alpha$ and $\text{CuK}\alpha$ radiation ($\lambda = 0.71073$ and 1.54180 \AA , respectively). The structures were solved by direct methods and refined on all unique F^2 values.^[175]

7.2 Synthesis of common starting materials

7.2.1 Synthesis of Zn^tBu_2

Et_2O (60 mL) was added to solid ZnCl_2 (5.44 g, 40 mmol, dried *in vacuo* at 200°C for 2 days), and the resulting suspension cooled to 0°C , to which $^t\text{BuLi}$ (1.7 M in pentane, 47 mL, 40 mmol) was slowly added over a period of 30 minutes. The resulting suspension was then gradually warmed to room temperature and stirred for 3 hours. The precipitate was removed by filtration through celite, and the resulting colourless solution concentrated *in vacuo*. Purification was performed by vacuum sublimation, yielding Zn^tBu_2 as a white solid (typical isolated yield 5.3 g, 74%).

7.2.2 Synthesis of BuNa

A suspension of NaO^tBu (3.84 g, 40 mmol) in hexane (50 mL) was cooled to 0°C , to which was added $^n\text{BuLi}$ (1.6 M in hexane, 25 mL, 40 mmol) over a period of 20 minutes. The resulting suspension was stirred overnight at room temperature, and then filtered and washed with hexane (3 x 30 mL). The resulting white solid was dried *in vacuo* and isolated (typical yield 2.5 g, 75%).

7.2.3 Synthesis of [(THF)Li(TMP)Zn^tBu₂] (**1**)

Following the procedure outlined in the literature,^[50] a solution of hexane (10 mL) and TMP(H) (0.34 mL, 2 mmol) was added ^tBuLi (1.6 M in hexane, 1.25 mL, 2 mmol), and the resulting colourless solution was stirred for 1 hour at room temperature. A solution of ^tBu₂Zn (0.36 g, 2 mmol in 10 mL of hexane) was added via canula, followed by THF (0.18 mL, 2 mmol) to give a colourless solution. This solution could then be employed in the desired reaction, or placed in the freezer (-30°C) overnight, yielding **1** as colourless crystals. Analysis of the crystals by ¹H, ¹³C{¹H} and ⁷Li NMR spectroscopy was consistent with that reported in the literature.^[50]

7.2.4 Synthesis of [(TMEDA)Na(TMP)Zn^tBu₂] (**3**)

Following the procedure outlined in the literature,^[57] BuNa (0.36 g, 4 mmol) was suspended in hexane (20 mL), to which was added TMP(H) (0.68 mL, 4 mmol) and the resulting suspension was stirred for 1 hour at room temperature. In a second Schlenk tube freshly distilled ^tBu₂Zn (0.72 g, 4 mmol) was dissolved in hexane (20 mL), and this was added via cannula to the suspension of Na(TMP), followed by TMEDA (0.60 mL, 4 mmol). The reaction mixture was then gently heated to afford a pale yellow solution, which was allowed to cool to room temperature. Placing this solution in the freezer placed (-30°C) overnight affording a crop of pale yellow crystals of **3** (1.352 g, 74%). Analysis of the crystalline material by ¹H and ¹³C{¹H} spectroscopy was consistent with that reported in the literature.^[57]

7.3 Synthesis of Products

7.3.1 Synthesis of [(THF)Li(TMP){PhOSi(CH₃)₂CH₂}Zn^tBu] (**13**)

A hexane solution of **1** (2 mmol) was prepared as described above, to which was added trimethyl(phenoxy)silane (**12**) (0.36 mL, 2 mmol) and after stirring for 1 hour the solution was concentrated *in vacuo*, then placed in the freezer (-30°C) for 4 days, and large colourless crystals of **13** were obtained (0.518 g, yield 52%; NMR analysis of the filtrate indicated that metallation is almost quantitative).

^1H NMR (400.13 MHz, 298K, C_6D_6) δ 7.04 (2H, t, H_{meta}), 6.84 (1H, t, H_{para}), 6.84 (2H, d, H_{ortho}), 3.34 (4H, m, OCH_2 , THF), 1.83 (2H, m, H_γ , TMP), 1.68 (2H, m, H_β , TMP), 1.63 (9H, s, CH_3 , ^tBu), 1.45 (2H, m, H_β , TMP), 1.38 (6H, s, $\alpha\text{-CH}_3$, TMP), 1.19 (6H, s, $\alpha\text{-CH}_3$, TMP), 1.19 (4H, m, CH_2 , THF), 0.29 (6H, s, $\text{OSi}(\text{CH}_3)_2$), -0.59 (2H, s, OSiCH_2). **$^{13}\text{C}\{^1\text{H}\}$ NMR** (100.62 MHz, 298K, C_6D_6) δ 154.6 (C_{ipso}), 129.8 (C_{ortho}), 122.8 (C_{para}), 120.7 (C_{meta}), 68.3 (OCH_2 , THF), 52.8 (C_α , TMP), 39.9 (C_β , TMP), 36.1 ($\alpha\text{-CH}_3$, TMP), 35.0 (CH_3 , ^tBu), 33.3 ($\alpha\text{-CH}_3$, TMP), 25.0 (CH_2 , THF), 20.0 ($\text{C}(\text{CH}_3)_3$, ^tBu), 19.8 (C_γ , TMP), 2.6 ($\text{OSi}(\text{CH}_3)_2$), -3.9 (OSiCH_2). **^7Li NMR** (298K, $\text{d}^8\text{-THF}$, reference LiCl in D_2O at 0.00 ppm): δ 1.07.

7.3.2 Synthesis of [(TMEDA)Na(TMP){PhOSi(CH₃)₂CH₂}Zn^tBu] (14)

A hexane solution of **3** (2 mmol) was prepared as described above, to which trimethyl(phenoxy)silane (**12**) was added (0.36 mL, 2 mmol) and after stirring for 1 hour at room temperature the solution was concentrated *in vacuo*, then placed in the freezer (-78°C) for 4 days. Large colourless crystals of **14** were isolated (0.472 g, yield 42%; NMR analysis of the filtrate indicated that the reaction is almost quantitative).

^1H NMR (400.13 MHz, 298K, C_6D_6) δ 7.07 (2H, t, H_{meta}), 6.90 (2H, d, H_{ortho}), 6.85 (1H, t, H_{para}), 1.79 (12H, s, CH_3 , TMEDA), 1.74 (8H, s, CH_2 , TMEDA), 1.70 (9H, s, CH_3 , ^tBu), ~1.68-1.82 (6H, bm, H_γ , & H_β , TMP), 1.50 (6H, s, $\alpha\text{-CH}_3$, TMP), 1.16 (6H, s, $\alpha\text{-CH}_3$, TMP), , 0.31 (6H, s, $\text{OSi}(\text{CH}_3)_2$), -0.73 (2H, s, OSiCH_2). **$^{13}\text{C}\{^1\text{H}\}$ NMR** (100.62 MHz, 298K, C_6D_6) δ 155.3 (C_{ipso}), 129.5 (C_{ortho}), 122.6 (C_{para}), 121.9 (C_{meta}), 60.0 (CH_2 , TMEDA), 52.6 (C_α , TMP), 45.9 (CH_3 , TMEDA), 40.0 (C_β , TMP), 35.4 ($\alpha\text{-CH}_3$, TMP), 35.0 (CH_3 , ^tBu), 34.7 ($\alpha\text{-CH}_3$, TMP), 19.9 (C_γ , TMP), 19.5 ($\text{C}(\text{CH}_3)_3$, ^tBu), 2.7 ($\text{OSi}(\text{CH}_3)_2$), -3.3 (OSiCH_2).

7.3.3 Synthesis of [(PhOSiMe₃)Li(TMP){PhOSi(CH₃)₂CH₂}Zn^tBu] (16)

To a solution of hexane (10 mL) and TMP(H) (0.34 mL, 2 mmol) was added $^n\text{BuLi}$ (1.6 M in hexane, 1.25 mL, 2 mmol), and the resulting colourless solution was stirred for 1 hour at room temperature. A solution of $^t\text{Bu}_2\text{Zn}$ (0.36 g, 2 mmol in 10 mL of hexane) was added via canula, followed by trimethyl(phenoxy)silane (**12**) (0.36 mL, 2 mmol) and after stirring for 1 hour the solution was concentrated *in vacuo*, then placed in the freezer (-30°C) for 7 days. A batch of large colourless crystals were isolated (0.194 g, yield 16%). The isolated yield of **16** could be

improved (0.451g, 37%) when the reaction was performed with two molar equivalents of trimethyl(phenoxy)silane (0.72 mL, 4 mmol).

^1H NMR (400.13 MHz, 298K, C_6D_6) δ 7.10 (2H, t, H_{meta} (co-ord.)), 7.04 (2H, t, H_{meta} , (met.)), 6.89-6.84 (4H, m, H_{para} (met. & co-ord.) & H_{ortho} (co-ord.)), 6.74 (2H, d, H_{ortho} (met.)), 1.72 (2H, m, H_γ , TMP), 1.60 (2H, m, H_β , TMP), 1.53 (9H, s, CH_3 , ^tBu), 1.48 (2H, m, H_β , TMP), 1.25 (6H, s, $\alpha\text{-CH}_3$, TMP), 1.04 (6H, s, $\alpha\text{-CH}_3$, TMP), 0.22 (6H, s, $\text{OSi}(\text{CH}_3)_2$), 0.15 (9H, s, $\text{OSi}(\text{CH}_3)_3$), -0.68 (2H, s, OSiCH_2). **$^{13}\text{C}\{^1\text{H}\}$ NMR** (100.62 MHz, 298K, C_6D_6) δ 155.7 (C_{ipso} (co-ord.)), 153.7 (C_{ipso} (met.)), 130.2 (C_{ortho} (met.)), 129.8 (C_{ortho} (co-ord.)), 123.5 (C_{para} (met.)), 121.8 (C_{para} (co-ord.)), 120.4 (C_{meta} (co-ord.)), 119.9 (C_{meta} (met.)), 52.7 (C_α , TMP), 40.6 ($\alpha\text{-CH}_3$, TMP), 35.8 ($\alpha\text{-CH}_3$, TMP), 34.2 (CH_3 , ^tBu), 34.1 (C_β , TMP), 20.6 ($\text{C}(\text{CH}_3)_3$, ^tBu), 19.5 (C_γ , TMP), 2.2 ($\text{OSi}(\text{CH}_3)_2$), 0.2 ($\text{OSi}(\text{CH}_3)_3$), -4.2 (OSiCH_2). **^7Li NMR** (298K, d^8 -THF, reference LiCl in D_2O at 0.00 ppm): δ 1.89.

7.3.4 Synthesis of [(TMEDA)Na(μ -TMP)Zn{OC(^tBu)($\eta^5\text{-C}_5\text{H}_3$)Fe($\eta^5\text{-C}_5\text{H}_5$)}] (18)

To a hexane solution of **3** (2 mmol, prepared as described above) was added one molar equivalent of benzoylferrocene (0.580 g, 2 mmol). The resulting deep red suspension was stirred for 2 hours at room temperature, after which time the solvent was removed *in vacuo*, and toluene (5 mL) added to give a dark red solution. After 48 hours in the freezer (-30°C) a batch of orange, cubic crystals of **18** were obtained (0.172 g, 12%).

^1H NMR (400.13 MHz, 298K, C_6D_6) δ 8.19 (2H, doublet, CH_{ortho}), 7.36 (2H, triplet, CH_{meta}), 7.26 (1H, triplet, CH_{para}), 4.70 (1H, broad singlet, C_5H_3), 4.63 (1H, broad singlet, C_5H_3), 4.33 (1H, broad singlet, C_5H_3), 3.84 (5H, singlet, C_5H_5), 1.94 (12H, singlet, CH_3 , TMEDA), 1.79 (2H, m, $\gamma\text{-CH}_2$, TMP), 1.78 (4H, singlet, CH_2 , TMEDA), 1.52 (6H, singlet, $\alpha\text{-CH}_3$, TMP), 1.44 (6H, singlet, $\alpha\text{-CH}_3$, TMP), 1.39 (4H, m, $\beta\text{-CH}_2$, TMP), 1.07 (9H, singlet, $\text{C}(\text{CH}_3)_3$, ^tBu). **$^{13}\text{C}\{^1\text{H}\}$ NMR** (100.62 MHz, 298K, C_6D_6) δ 154.5 (C_{ipso}), 128.7 (C_{ortho}), 126.0 (C_{meta}), 124.9 (C_{para}), 111.8 (C-Zn , C_5H_3) 81.3 (C-O), 75.3 ($\text{OC-C}_5\text{H}_3$), 73.0 (C_5H_3), 70.8 (C_5H_3), 70.0 (C_5H_3), 68.0 (C_5H_5), 57.5 (CH_2 , TMEDA), 53.0 ($\alpha\text{-TMP}$), 46.6 (CH_3 , TMEDA), 41.2 ($\beta\text{-CH}_2$, TMP), 40.5 ($\text{C}(\text{CH}_3)_3$, ^tBu), 36.8 and 36.1 ($\alpha\text{-CH}_3$, TMP), 28.2 ($\text{C}(\text{CH}_3)_3$, ^tBu), 19.8 ($\gamma\text{-CH}_2$, TMP). **Elemental Analysis** calculated (%) for $\text{C}_{36}\text{H}_{56}\text{FeN}_3\text{NaOZn}$: C 62.57, H 8.18, N 6.08; found C 62.24, H 8.07, N 5.97.

N.B. A polymorph of **18** was also obtained from a second batch of crystals, but contained a molecule of the solvent of crystallisation [(TMEDA)Na(μ -TMP)Zn{OC(^tBu)(η^5 -C₅H₃)Fe(η^5 -C₅H₅)}].C₇H₈] (**18B**).

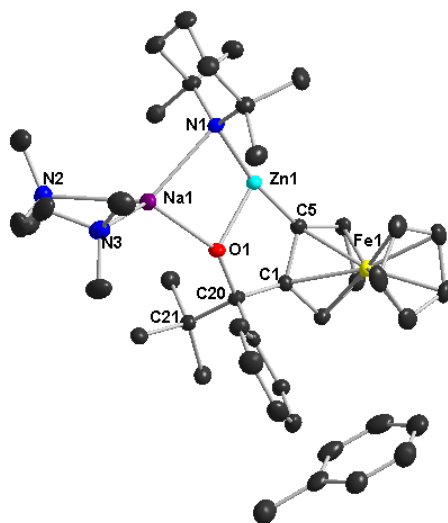


Figure 7.3: Molecular structure of [(TMEDA)Na(μ -TMP)Zn{OC(^tBu)(η^5 -C₅H₃)Fe(η^5 -C₅H₅)}].C₇H₈] (**18B**) with 50% probability ellipsoids. Hydrogen atoms and minor disordered component of TMEDA have been omitted for clarity.

7.3.5 Synthesis of [PhC(OH)(^tBu)(η^5 -C₅H₃I)Fe(η^5 -C₅H₅)] (**19**) and [4-^tBu-C₆H₄C(=O)(η^5 -C₅H₄)Fe(η^5 -C₅H₅)] (**21**)

Benzoylferrocene (0.290 g, 1 mmol) was dissolved in toluene (7 mL) and added via cannula to a second Schlenk tube containing isolated crystals of **3** (0.460 g, 1 mmol, prepared as described above). The resulting deep red solution was stirred for 2 hours at room temperature, after which time I₂ solution (1 M in THF, 3 mL, 3 mmol) was added, and the reaction stirred for a further 4 hours at room temperature. The reaction was then quenched with saturated Na₂S₂O₃ solution (5 mL) and saturated NH₄Cl solution (5 mL) and then extracted with EtOAc (3 x 15 mL). The combined organic extracts were dried over MgSO₄ and concentrated *in vacuo*. The crude residue was purified by column chromatography (eluent: hexane/diethyl ether, 1:0 – 9:1) affording **19** as an orange solid (0.1380 g, 29% - as a mixture with [PhC(OH)(^tBu)(η^5 -C₅H₃I)Fe(η^5 -C₅H₄I)] (**20**) in a ratio of 95:5, **19:20**) and **21** as a red solid (0.0845 g, 24%).

NMR data for 19: ¹H NMR (400.13 MHz, 298K, CDCl₃) δ 7.90 (2H, doublet, CH_{ortho}), 7.42 (2H, triplet, CH_{meta}), 7.33 (1H, triplet, CH_{para}), 4.45 (2H, m, C₅H₃), 4.30 (1H, triplet, C₅H₃),

3.74 (5H, singlet, C_5H_5), 2.63 (1H, singlet, OH), 0.97 (9H, singlet, $C(CH_3)_3$, tBu). $^{13}C\{^1H\}$ NMR (100.62 MHz, 298K, $CDCl_3$) δ 146.4 (C_{ipso}), 127.2 (C_{ortho} , C_{meta}), 126.6 (C_{para}), 89.9 (C-O), 81.1 (OC- C_{Cp^*}), 77.4 (C_5H_3), 71.7 (C_5H_5), 70.8 (C_5H_3), 69.2 (C_5H_3), 41.2 (C-I), 40.0 ($C(CH_3)_3$, tBu), 27.0 ($C(CH_3)_3$, tBu). Both the 1H and $^{13}C\{^1H\}$ NMR spectra showed trace impurities which were assigned to compound **20**. **Elemental analysis** calculated (%) for $C_{21}H_{22.95}FeI_{1.05}O$: C 52.49, H 4.91; found C 51.76, H 4.82. **GC-MS**: m/z 474.0 (M^+).

NMR data for 21: 1H NMR (400.13 MHz, 298K, $CDCl_3$) δ 7.88 (2H, doublet, CH_{ortho}), 7.49 (2H, doublet, CH_{meta}), 4.93 (2H, triplet, C_5H_4), 4.58 (2H, triplet, C_5H_4), 4.23 (5H, singlet, C_5H_5), 1.38 (9H, singlet, $C(CH_3)_3$, tBu). $^{13}C\{^1H\}$ NMR (100.62 MHz, 298K, $CDCl_3$) δ 198.7 (C-O), 155.1 (C_{ipso}), 137.0 (C_{para}), 128.2 (C_{ortho}), 125.2 (C_{meta}), 78.6 (C_5H_5), 72.3 (C_5H_4), 71.6 (C_5H_4), 70.2 (OC- C_{Cp^*}), 35.0 ($C(CH_3)_3$, tBu), 31.2 ($C(CH_3)_3$, tBu). **Elemental analysis** calculated (%) for $C_{21}H_{22}FeO$: C 72.85, H 6.40; found C 72.60, H 6.40. **GC-MS**: m/z 346.2 (M^+).

7.3.6 Synthesis of $[C_6H_5C(OH)^tBu(\eta^5-C_5H_3D)Fe(\eta^5-C_5H_5)]$ (**23**) and $[^tBu-C_6H_4CO(\eta^5-C_5H_4)Fe(\eta^5-C_5H_5)]$ (**21**)

Benzoylferrocene (0.290 g, 1 mmol) was dissolved in Toluene (7 mL) and added via cannula to a second Schlenk tube containing isolated crystals of **3** (0.460 g, 1 mmol, prepared as described above). The resulting deep red solution was stirred for 2 hours at room temperature, after which time D_2O (4 mL) was added. The product was then extracted with EtOAc (3 x 15 mL), the combined organic extracts were dried over $MgSO_4$ and concentrated *in vacuo*. The crude residue was purified by column chromatography (eluent: hexane/diethyl ether, 1:0 – 9:1) giving **23** as a yellow solid (0.119 g, 32%) and **21** as a red solid (0.0935 g, 27%).

NMR data for 23: 1H NMR (400.13 MHz, 298K, $CDCl_3$) δ 7.68 (2H, doublet, CH_{ortho}), 7.35 (2H, triplet, CH_{meta}), 7.27 (1H, triplet, CH_{para}), 4.33 (1H, m, C_5H_3D), 4.21 (1H, m, C_5H_3D), 4.17 (1H, m, C_5H_3D), 3.88 (5H, singlet, C_5H_5), 2.65 (1H, singlet, OH), 0.95 (9H, singlet, $C(CH_3)_3$, tBu). 2D NMR (61.41 MHz, 298K, $CHCl_3$) δ 4.53 (singlet, C_5H_3D). $^{13}C\{^1H\}$ NMR (100.62 MHz, 298K, $CDCl_3$) δ 146.0 (C_{ipso}), 127.3 (C_{ortho}), 126.8 (C_{meta}), 126.2 (C_{para}), 95.7 (C-O), 79.6 (OC- C_{Cp^*}), 69.7 (C_5H_3), 68.9 (C-D), 68.4 (C_5H_3), 68.3 (C_5H_5), 66.9 (C_5H_3), 39.0

(C(CH₃)₃, ^tBu), 26.5 (C(CH₃)₃, ^tBu). **Elemental analysis** calculated (%) for C₂₁H₂₃DFeO: C 72.21, H 7.21; found C 71.55, H 6.53. **GC-MS**: *m/z* 349.0 (M⁺).

7.3.7 Synthesis of [C₆H₅C(OH)^tBu(η⁵-C₅H₄)Fe(η⁵-C₅H₅)] (24) and [^tBu-C₆H₄CO(η⁵-C₅H₄)Fe(η⁵-C₅H₅)] (21)

Benzoylferrocene (0.290 g, 1 mmol) was dissolved in Toluene (7 mL) and added via cannula to a second Schlenk tube containing isolated crystals of **3** (0.460 g, 1 mmol, prepared as described above). The resulting deep red solution was stirred for 2 hours at room temperature, after which time TEMPO (0.468 g, 3 mmol) was added, and the reaction stirred for a further 20 hours at room temperature. The reaction was quenched with saturated NH₄Cl solution (5 mL) and then extracted with EtOAc (3 x 15 mL). The combined organic extracts were dried over MgSO₄ and concentrated *in vacuo*. The crude residue was purified by column chromatography (eluent: hexane/diethyl ether, 1:0 – 9:1) giving **24** as an orange solid (0.1185 g, 34%) and **21** as a red solid (0.1415 g, 41%).

NMR data for 24: ¹H NMR (400.13 MHz, 298K, CDCl₃) δ 7.67 (2H, doublet, CH_{ortho}), 7.35 (2H, triplet, CH_{meta}), 7.27 (1H, triplet, CH_{para}), 4.52 (1H, m, C₅H₄), 4.33 (1H, m, C₅H₄), 4.21 (1H, m, C₅H₄), 4.17 (1H, m, C₅H₄), 3.88 (5H, singlet, C₅H₅), 2.65 (1H, singlet, OH), 0.95 (9H, singlet, C(CH₃)₃, ^tBu). ¹³C{¹H} NMR (100.62 MHz, 298K, CDCl₃) δ 146.0 (C_{ipso}), 127.3 (C_{ortho}), 126.8 (C_{meta}), 126.2 (C_{para}), 95.8 (C-O), 79.6 (OC-C_{Cp}*), 69.8 (C₅H₄), 68.9 (C₅H₄), 68.5 (C₅H₄), 68.4 (C₅H₅), 67.0 (C₅H₄), 39.0 (C(CH₃)₃, ^tBu), 26.5 (C(CH₃)₃, ^tBu). **Elemental analysis** calculated (%) for C₂₁H₂₄FeO: C 72.42, H 6.94; found C 72.66, H 7.01. **GC-MS**: *m/z* 348.0 (M⁺).

7.3.8 Synthesis of [Li₄(*o*-C₆H₄OMe)₄(THF)₂] (25)

A solution of THF (10 mL) and anisole (0.54 mL, 5 mmol) was cooled to 0°C in an ice bath, then ^tBuLi (1.7 M in pentane, 2.9 mL, 5 mmol) was added to give a pale yellow solution, which was stirred at 0°C for 25 minutes. The solvent was removed *in vacuo* yielding a yellow oil, which was dissolved in hexane (10 mL). This solution was concentrated by removing some solvent under vacuum and placed in the freezer (-30°C). A crop of colourless crystals was deposited overnight (isolated yield 0.16 g, 22%; NMR analysis of the filtrate indicated the metallation is almost quantitative).

^1H NMR (400.13 MHz, 298K, C_6D_6) δ 8.18 (1H, d, CH_{meta}), 7.39 (1H, t, $\text{CH}_{\text{meta}^*}$), 7.26 (1H, t, CH_{para}), 6.78 (1H, d, $\text{CH}_{\text{ortho}^*}$), 3.41 (3H, s, $-\text{OCH}_3$), 3.10 (2H, s, $-\text{OCH}_2$, THF), 1.17 (2H, s, $-\text{CH}_2$, THF). ^{13}C $\{^1\text{H}\}$ NMR (100.62 MHz, 298K, C_6D_6) δ 169.9 (C_{ipso}), 159.2 (C_{ortho}), 142.3 (C_{meta}), 127.2 (C_{meta^*}), 121.8 (C_{para}), 106.4 ($\text{C}_{\text{ortho}^*}$), 67.2 ($-\text{OCH}_3$), 54.3 ($-\text{OCH}_2$, THF), 25.2 ($-\text{CH}_2$, THF). ^7Li NMR (298K, C_6D_6 , reference LiCl in D_2O at 0.00 ppm): δ 3.28

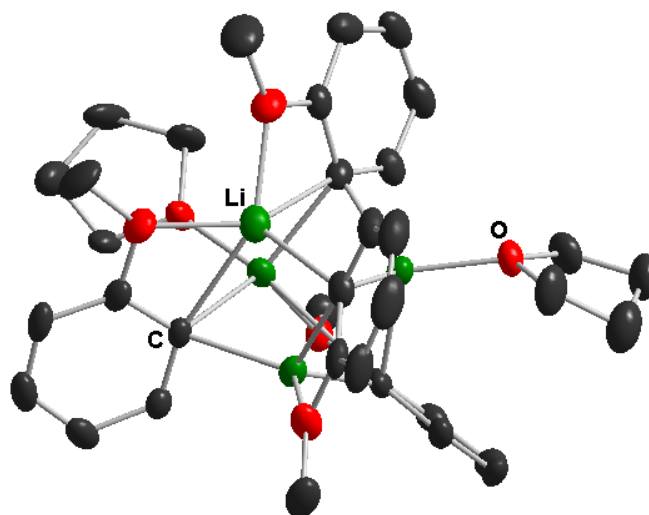


Figure 7.4: Molecular structure of $[(\text{THF})_2\text{Li}_4(o\text{-C}_6\text{H}_4\text{OMe})_4]$ (**25**) with 30% probability ellipsoids. Hydrogen atoms and minor disordered component of THF have been omitted for clarity.

7.3.9 Synthesis of $[(\text{THF})_2\text{Li}(o\text{-C}_6\text{H}_4\text{OMe})\text{ZnMe}_2]$ (**26**)

A solution of THF (10 mL) and anisole (0.54 mL, 5 mmol) was cooled to 0°C in an ice bath, $t\text{-BuLi}$ (1.7 M in pentane, 2.9 mL, 5 mmol) was added to give a yellow solution, which was stirred at 0°C for 25 minutes. Me_2Zn (2 M in toluene, 2.5 mL, 5 mmol) was added, and the solution slowly warmed to room temperature to give a very pale yellow solution, which was stirred for 15 minutes. The solvent was removed *in vacuo* to yield a yellow oil (**26**), which was analysed by ^1H , ^7Li and $^{13}\text{C}\{^1\text{H}\}$ NMR spectroscopy.

^1H NMR (400.13 MHz, 298K, C_6D_6) δ 8.26 (1H, d, CH_{meta}), 7.24 (1H, t, $\text{CH}_{\text{meta}^*}$), 7.17 (1H, t, CH_{para}), 6.78 (1H, d, $\text{CH}_{\text{ortho}^*}$), 3.44 (3H, s, OCH_3), 3.24 (8H, s, OCH_2 , THF), 1.21 (8H, s, CH_2 , THF), -0.17 (6H, s, $\text{Zn}(\text{CH}_3)_2$). $^{13}\text{C}\{^1\text{H}\}$ NMR (100.62 MHz, 298K, C_6D_6) δ 165.9 (C_{ipso}), 154.8 ($\text{Zn-C}_{\text{ortho}}$), 142.8 (C_{meta}), 126.7 (C_{meta^*}), 122.8 (C_{para}), 110.0 ($\text{C}_{\text{ortho}^*}$), 67.8

(OCH₂, THF), 56.0 (OCH₃), 24.8 (CH₂, THF), -8.6 (Zn(CH₃)₂). ⁷Li NMR (298K, C₆D₆, reference LiCl in D₂O at 0.00 ppm): δ 0.72

7.3.10 Synthesis of [(THF)₂Li₂Zn(*o*-C₆H₄OMe)₄] (27)

A solution of THF (10 mL) and anisole (0.54 mL, 5 mmol) was cooled to 0°C in an ice bath, then ^tBuLi (1.7 M in pentane, 2.9 mL, 5 mmol) was added to give a yellow solution, which was stirred at 0°C for 25 minutes. Me₂Zn (2 M in toluene, 5 mL, 5 mmol) was added, and the solution slowly warmed to room temperature to give a colourless solution, which was stirred for 15 minutes, then the solvent was removed *in vacuo*, to give a yellow oil (**26**). Hexane (5 mL) was then introduced, to give an oily white solid. The addition of toluene (5 mL) gave a white precipitate, and gently heating for a few minutes resulted in the formation of a yellow solution, which was placed in a Dewar of hot water, and after standing overnight yielded a white needle-like crystalline solid (**27**) (isolated yield 0.28 g, 9%; maximum possible yield = 25%).

¹H NMR (400.13 MHz, 298K, C₆D₆) δ 8.35 (3H, d, CH_{meta}), 7.20 (3H, t, CH_{meta}*), 7.10 (3H, t, CH_{para}), 6.73 (3H, d, CH_{ortho}*), 3.24 (3H, s, OCH₃), 3.16 (12H, t, OCH₂, THF), 1.23 (11H, m, CH₂, THF). ⁷Li NMR (298K, C₆D₆, reference LiCl in D₂O at 0.00 ppm): δ 0.96

7.3.11 Synthesis of [(TMEDA)Li(*o*-C₆H₄OMe)ZnMe₂] (28)

A solution of hexane (10 mL), TMEDA (0.75 mL, 5 mmol) and anisole (0.54 mL, 5 mmol), was cooled to 0°C in an ice bath. ^tBuLi (1.7M in pentane, 2.9 mL, 5 mmol) was then added to give a pale yellow solution, which was stirred at 0°C for 25 minutes, then Me₂Zn (2 M in toluene, 2.5 mL, 5 mmol) was added to afford a white precipitate. Toluene was introduced at this stage (2 mL) and the mixture was gently heated until all the solid had dissolved, affording a pale yellow solution. Allowing this solution to cool slowly to room temperature afforded a crop of colourless crystals (**28**) (1.03 g, 62%).

¹H NMR (400.13 MHz, 298K, C₆D₆) δ 8.27 (1H, d, CH_{meta}), 7.23-7.19 (2H, m, CH_{meta}* and CH_{para}), 6.77 (1H, d, CH_{ortho}*), 3.42 (3H, s, OCH₃), 1.65 (12H, s, CH₃, TMEDA), 1.62 (2H, s, CH₂, TMEDA), -0.14 (6H, s, Zn(CH₃)₂). ¹³C{¹H} NMR (100.62 MHz, 298K, C₆D₆) δ 166.0 (C_{ipso}), 155.1 (Zn-C_{ortho}), 142.9 (C_{meta}), 127.2 (C_{meta}*), 124.1 (C_{para}), 113.9 (C_{ortho}*), 59.5

(OCH₃), 56.0 (CH₂, TMEDA), 45.0 (CH₃, TMEDA), -9.2 (Zn(CH₃)₂). ⁷Li NMR (298K, C₆D₆, reference LiCl in D₂O at 0.00 ppm): δ 0.67

7.3.12 Synthesis of [(THF)₃Li(*o*-C₆H₄OMe)Zn^tBu₂] (29)

A solution of THF (4 mL) and anisole (0.22 mL, 2 mmol) was cooled to 0°C in an ice bath, then ^tBuLi (1.7 M in pentane, 1.2 mL, 2 mmol) was then added to give a yellow solution which was stirred at 0°C for 50 minutes. A solution of ^tBu₂Zn (0.36 g, 2 mmol in 10 mL THF) was added via canula, and the solution was slowly warmed to room temperature, and allowed to stir for 30 minutes. The solution was then placed in the freezer overnight. The solvent was removed *in vacuo* to yield a yellow oil (**29**), which was analysed by ¹H, ⁷Li and ¹³C{¹H} NMR spectroscopy.

¹H NMR (400.13 MHz, 298K, C₆D₆) δ 7.26 (1H, d, CH_{meta}), 7.14 (1H, t, CH_{meta}*), 6.80 (1H, t, CH_{para}), 6.74 (1H, d, CH_{ortho}*), 3.43 (3H, s, OCH₃), 3.13 (12H, t, OCH₂, THF), 1.58 (18H, s, CH₃, ^tBu), 1.38 (12H, m, CH₂, THF). ¹³C{¹H} NMR (100.62 MHz, 298K, C₆D₆) δ 167.0 (C_{ipso}), 147.8 (Zn-C_{ortho}), 140.9 (C_{meta}), 129.7 (C_{meta}*), 122.5 (C_{para}), 110.6 (C_{ortho}*), 68.3 (OCH₂, THF), 56.3 (OCH₃), 36.6 (CH₃, ^tBu), 25.4 (CH₂, THF), 24.2 (Zn-C, ^tBu). ⁷Li NMR (298K, C₆D₆, reference LiCl in D₂O at 0.00 ppm): δ -0.28.

7.3.13 Synthesis of [(PMDETA)Li(*o*-C₆H₄OMe)Zn^tBu₂] (30)

A solution of hexane (10 mL), PMDETA (0.42 mL, 2 mmol) and anisole (0.54 mL, 5 mmol), was cooled to 0°C in an ice bath, then ^tBuLi (1.7 M in pentane, 2.9 mL, 5 mmol) was added to give a pale yellow solution, which was stirred at 0°C for 25 minutes. A solution of ^tBu₂Zn (0.36 g, 2 mmol in 10 mL hexane) was added, to afford two layers, a yellow oil and a colourless solution. The reaction mixture was warmed slowly to room temperature and stirred for 1 hour. The solvent was then removed *in vacuo*, and toluene (3 mL) added. Gentle heating afforded an orange solution, which was left in a Dewar filled with hot water overnight, resulting in the formation of small cubic crystals of **30** (0.32 g, 34%).

¹H NMR (400.13 MHz, 298K, C₆D₆) δ 8.18 (1H, d, CH_{meta}), 7.19 (1H, t, CH_{para}), 7.06 (1H, t, CH_{meta}*), 6.21 (1H, d, CH_{ortho}*), 3.83 (3H, s, OCH₃), 1.81 (3H, s, CH₃, PMDETA), 1.75 (18H, s, CH₃, ^tBu), 1.65 (8H, m, CH₂, PMDETA), 1.63 (12H, s, CH₃, PMDETA). ¹³C{¹H} NMR

(100.62 MHz, 298K, C₆D₆) δ 163.4 (C_{ipso}), 157.3 (Zn-C_{ortho}), 140.6 (C_{meta}), 124.0 (C_{meta}*), 122.3 (C_{para}), 112.6 (C_{ortho}*), 57.0 (CH₂, PMDETA), 56.9 (OCH₃), 56.0 (CH₂, PMDETA), 45.3 (CH₃, PMDETA), 44.1 (CH₃, PMDETA), 37.1 (CH₃, ^tBu), 24.4 (Zn-C, ^tBu). ⁷Li NMR (298K, C₆D₆, reference LiCl in D₂O at 0.00 ppm): δ - 0.15.

7.3.14 Synthesis of [(THF)Li(TMP)ZnMe₂] (**32**)

Me₂Zn (2 M in toluene, 2 mL, 4 mmol) was added to a solution of Li(TMP) [prepared *in situ* by reaction of ⁿBuLi (1.6 M solution in hexane, 2.5 mL, 4 mmol) and TMP(H) (0.68 mL, 4 mmol)] to afford a white precipitate. After stirring for a further 15 minutes, THF (0.33 mL, 4 mmol) was added to give a yellow solution. This solution was concentrated by removing some solvent under vacuum and placed in the freezer (-30°C). A crop of colourless crystals of **32** were deposited overnight (0.12 g, 10%; NMR analysis of the filtrate showed the formation of **32** is almost quantitative).

¹H NMR (400.13 MHz, 298K, C₆D₆) δ 3.26 (4H, t, -OCH₂, THF), 1.91 (2H, bs, H _{γ} , TMP), 1.66 (4H, bs, H _{β} , TMP), 1.45 (7H, bs, α -CH₃, TMP), 1.21 (5H, m, -CH₂, THF), 1.10 (6H, bs, α -CH₃, TMP), -0.36 (6H, s, -Zn(CH₃)₂). ¹³C {¹H} NMR (100.62 MHz, 298K, C₆D₆) δ 68.78 (-OCH₂, THF), 55.12 (C _{α} , TMP), 41.44 (C _{β} , TMP), 36.25, 31.12 (CH₃, TMP), 25.27 (-CH₂, THF), 20.01 (C _{γ} , TMP), -6.88 (-Zn(CH₃)₂). ⁷Li NMR (298K, C₆D₆, reference LiCl in D₂O at 0.00 ppm): δ 1.53.

7.3.15 Synthesis of [(THF)₄Mg(μ -Cl)₂Zn(^tBu)(Cl)] (**34**)

A solution of *tert*-butylmagnesium chloride (1 M in THF, 2 mL, 2 mmol) in THF (10 mL) was cooled to 0°C, and zinc chloride (1 M in diethyl ether, 2 mL, 2 mmol) was added dropwise, resulting in the formation of a white precipitate. After stirring for 1 hour at 0°C, the solid [{Mg(THF)₆}²⁺{Zn₂Cl₆}²⁻] (**33**) was removed by filtration (average yield based on ZnCl₂ 0.49 g, 62%). The filtrate was concentrated *in vacuo* (to approx. 3 mL), and then hexane (2 mL) was added. The resulting colourless solution was then transferred to the freezer (-30°C) and after 48 hours a crop of colourless crystals (**34**) were isolated (average isolated yield 0.05 g, 5%; the isolated yield could be improved to ~95% by reacting ^tBuZnCl (2 mmol) with MgCl₂ (2 mmol) in THF).

^1H NMR (400.13 MHz, 298K, d_8 -THF) δ 3.63 (16H, m, OCH_2 , THF), 1.77 (16H, m, CH_2 , THF), 0.99 (9H, s, $\text{C}(\text{CH}_3)_3$). $^{13}\text{C}\{^1\text{H}\}$ NMR (100.62 MHz, 298K, d_8 -THF) δ 68.2 (OCH_2 , THF), 33.6 ($\text{C}(\text{CH}_3)_3$), 26.2 (CH_2 , THF), 21.9 ($\text{C}(\text{CH}_3)_3$)

7.3.16 Synthesis of $[(\text{THF})_2\text{Mg}(\mu\text{-Cl})_3\text{ZnR}]_2$ (36-39)

Synthesis of 36 (R = ^tBu): To a solution of $^t\text{BuMgCl}$ (5 mL of 1 M solution in THF 5 mmol) in toluene (45 mL) was added ZnCl_2 (0.680 g, 5 mmol), and the resulting suspension was stirred at room temperature for 20 hours. The solid was removed by filtration, then the filtrate slowly concentrated *in vacuo*, and left to stand at room temperature. After 24 hours a crop of colourless crystals of **36** was obtained (0.524 g, 26% yield).

^1H NMR (400.13 MHz, 298K, d_8 -THF) δ 3.62 (m, 13H, OCH_2 THF), 1.77 (m, 13H, CH_2 THF), 1.01 (t, 18H, $\text{C}(\text{CH}_3)_3$, $\text{Zn-}^t\text{Bu}$). $^{13}\text{C}\{^1\text{H}\}$ NMR (100.62 MHz, 298K, d_8 -THF) δ 68.48 (OCH_2 , THF), 33.74, ($\text{C}(\text{CH}_3)_3$, $\text{Zn-}^t\text{Bu}$), 26.60 (CH_2 , THF), 22.01 ($\text{C}(\text{CH}_3)_3$, $\text{Zn-}^t\text{Bu}$).

Synthesis of 37 (R = ^nBu): To a solution of $^n\text{BuMgCl}$ (1 mL of 2 M solution in THF 2 mmol) in THF (10 mL) was added ZnCl_2 (0.272 g, 2 mmol), and the resulting suspension was stirred at room temperature for 2 hours. The solvent was then concentrated *in vacuo* to approximately 2 mL, and toluene (30 mL) added. The resulting suspension was stirred for 1h at room temperature, then the solid removed by filtration. The filtrate was slowly concentrated *in vacuo*, and left to stand at room temperature. After 24 hours a crop of colourless crystals of **37** was obtained (0.197 g, 24% yield).

^1H NMR (400.13 MHz, 298K, d_8 -THF) δ 3.61 (m, 12H, OCH_2 THF), 1.75 (m, 12H, CH_2 THF), 1.48 (m, 4H, $\text{Zn-CH}_2\text{CH}_2\text{CH}_2\text{CH}_3$), 1.25 (m, 4H, $\text{Zn-CH}_2\text{CH}_2\text{CH}_2\text{CH}_3$), 0.82 (t, 9H, $\text{Zn-CH}_2\text{CH}_2\text{CH}_2\text{CH}_3$), 0.14 (t, 4H, $\text{Zn-CH}_2\text{CH}_2\text{CH}_2\text{CH}_3$). $^{13}\text{C}\{^1\text{H}\}$ NMR (100.62 MHz, 298K, d_8 -THF) δ 68.50 (OCH_2 , THF), 32.02 ($\text{Zn-CH}_2\text{CH}_2\text{CH}_2\text{CH}_3$), 30.12 ($\text{Zn-CH}_2\text{CH}_2\text{CH}_2\text{CH}_3$), 26.50 (CH_2 , THF), 14.64 ($\text{Zn-CH}_2\text{CH}_2\text{CH}_2\text{CH}_3$), 10.09 ($\text{Zn-CH}_2\text{CH}_2\text{CH}_2\text{CH}_3$).

Synthesis of 38 (R = Et): To a solution of EtMgCl (2 mL of 2 M solution in THF 4 mmol) in toluene (40 mL) was added ZnCl_2 (0.544 g, 4 mmol), and the resulting suspension was stirred at room temperature for 20 hours. The solid was removed by filtration, then the filtrate slowly

concentrated *in vacuo*, and left to stand at room temperature. After 24 hours a crop of colourless crystals of **38** was obtained (0.493 g, 33% yield).

$^1\text{H NMR}$ (400.13 MHz, 298K, d_8 -THF) δ 3.61 (m, 12H, OCH_2 THF), 1.76 (m, 12H, CH_2 THF), 1.12 (t, 6H, CH_3 , Zn-Et), 0.06 (q, 4H, CH_2 , Zn-Et). $^{13}\text{C}\{^1\text{H}\}$ NMR (100.62 MHz, 298K, d_8 -THF) δ 68.51 (OCH_2 , THF), 26.57 (CH_2 , THF), 13.11, (CH_3 , Zn-Et), 0.98 (CH_2 , Zn-Et).

Synthesis of 39 (R = *o*-C₆H₄OMe): To a solution of (*o*-MeO-C₆H₄MgCl (2 mL of 1 M solution in THF 2 mmol) in THF (10 mL) was added ZnCl₂ (0.272 g, 2 mmol), and the resulting suspension was stirred at room temperature for 2 hours. The solvent was then concentrated *in vacuo* to approximately 2 mL, and toluene (30 mL) added. The resulting suspension was stirred for 1 hour at room temperature, then the solid removed by filtration. The filtrate was slowly concentrated *in vacuo*, and left to stand at room temperature. After 24 hours a crop of colourless crystals of **39** were obtained (0.303 g, 34% yield).

$^1\text{H NMR}$ (400.13 MHz, 298K, d_8 -THF) δ 7.39 (d, 2H, CH_{meta}), 7.01 (t, 2H, CH_{para}), 6.73 (t, 2H, $\text{CH}_{\text{meta}^*}$), 6.66 (d, 2H, $\text{CH}_{\text{ortho}^*}$), 3.66 (s, 6H, OCH_3), 3.62 (m, 12H, OCH_2 THF), 1.75 (m, 13H, CH_2 THF). $^{13}\text{C}\{^1\text{H}\}$ NMR (100.62 MHz, 298K, d_8 -THF) δ 166.76 (C_{ipso}), 142.41 (C_{ortho}), 140.20 (C_{meta}), 127.92 (C_{meta^*}), 121.17 (C_{para}), 109.29 ($\text{C}_{\text{ortho}^*}$), 68.48 (OCH_2 , THF), 55.38 (OCH_3), 26.53 (CH_2 , THF).

7.3.17 Synthesis of $[\{\text{Mg}_2\text{Cl}_3(\text{THF})_6\}^+\{\text{Zn}^t\text{Bu}_3\}]$ (**40**)

Method 1: To a solution of *tert*-butylmagnesium chloride (3 mL of a 1 M solution in THF, 3 mmol) zinc chloride (0.136 g, 1 mmol) was added. The resulting colourless solution was stirred at room temperature stirred for 3 hours, then transferred to the freezer (-30°C). After 24 hours a crop of colourless crystals of $[(\text{THF})_4\text{MgCl}_2]$ were isolated (0.357 g, 0.9 mmol). The solvent was removed from the filtrate *in vacuo*, hexane (1 mL) and THF (1 mL) added, and the resulting solution returned to the freezer for 48 hours. A batch of colourless crystals of **40** were isolated (crystalline yield = 0.09 g, 11%).

Method 2: To a solution of *tert*-butylmagnesium chloride (1 M solution in THF, 4 mL, 4mmol) was added Zn^tBu₂ (0.72 g, 4 mmol in 20 mL THF) and MgCl₂ (0.360 g), and the resulting solution stirred for 2 hours at room temperature. The solvent was then removed *in*

vacuo, THF (4 mL) and hexane (3 mL) added, then placed in the freezer (-30°C) overnight, from which a batch of colourless crystals of **40** were obtained (typical crystalline yield = 2.05 g, 62%).

Method 3: Crystalline [(Et₂O)₂Mg^tBu₂] (0.870 g, 3 mmol) was dissolved in THF (20 mL) and ZnCl₂ (0.272g, 2 mmol) added. After stirring for 2 hours at room temperature the solution was concentrated *in vacuo*, and hexane (2 mL) added, and the resulting solution placed in the freezer for several days. A batch of colourless crystals of **40** were isolated (crystalline yield = 0.474 g, 29%).

¹H NMR (400.13 MHz, 298K, d₈-THF) δ 3.63 (24H, m, OCH₂, THF), 1.77 (24H, m, CH₂, THF), 0.97 (1.91H, s, C(CH₃)₃, ^tBu₂Zn), 0.91 (23.4 H, s, C(CH₃)₃, {Zn^tBu₃}⁻), 0.89 (0.59H, s, C(CH₃)₃, ^tBuMgCl), 0.87 (0.42H, s, C(CH₃)₃, ^tBuMgCl). ¹³C{¹H} NMR (100.62 MHz, 298K, d₈-THF) δ 68.5 (OCH₂, THF), 36.8 (C(CH₃)₃, {Zn^tBu₃}⁻), 35.9 (C(CH₃)₃, ^tBuMgCl), 35.2 (C(CH₃)₃, ^tBuMgCl), 33.1 (C(CH₃)₃, ^tBu₂Zn), 26.5 (CH₂, THF), 25.4 (C(CH₃)₃, ^tBu₂Zn), 24.2 (C(CH₃)₃, {Zn^tBu₃}⁻), 15.8 (C(CH₃)₃, ^tBuMgCl), 15.2 (C(CH₃)₃, ^tBuMgCl).

7.3.18 Synthesis of [{Mg₂Cl₃(THF)₆}⁺{Zn₂Et₅}⁻] (**41**)

To a solution of ethylmagnesium chloride (5 mL of a 2 M solution in THF, 10 mmol) in THF (2 mL) zinc chloride (0.544 g, 4 mmol) was added, giving a suspension, which was stirred for 3 hours at room temperature. The precipitate [(THF)₄MgCl₂] was then removed by filtration, and the filtrate concentrated *in vacuo* (to approx. 2 mL), hexane (1 mL) was added and then transferred to the freezer (-30°C). After 48 hours a crop of colourless crystals of [(THF)₄MgCl₂] and **41** was isolated. Compound **41** could also be prepared using an alternative co-complexation route by reacting EtMgCl (2.5 mL of a 2 M solution in THF, 5 mmol) with ZnEt₂ (5 mL of a 1 M solution in hexane, 5 mmol) using THF as a solvent (10 mL), which allowed the isolation of **41** (0.96 g, 21%, maximum possible yield 50%) in pure crystalline form. Better yields could be obtained when the reaction was carried out using a 1:2 ratio of EtMgCl/ZnEt₂ (1.96 g, 45%).

¹H NMR (400.13 MHz, 298K, d₈-THF) δ 3.64 (m, 24H, OCH₂ THF), 1.76 (m, 24H, CH₂ THF), 1.09 (t, 15H, CH₃, Zn-Et), -0.21 (q, 10H, CH₂, Zn-Et). ¹³C{¹H} NMR (100.62 MHz, 298K, d₈-THF) δ 68.47 (OCH₂, THF), 26.37 (CH₂, THF), 13.59, (CH₃, Zn-Et), 0.79 (CH₂, Zn-Et).

7.3.19 Synthesis of $[\{\text{Mg}_3(\text{OEt})_2\text{Br}_3(\text{THF})_6\}^+\{\text{Zn}_2\text{Et}_5\}^-]$ (**42**)

To a solution of ethylmagnesium bromide (2 mL of a 1 M solution in THF, 2 mmol) in THF (10 mL) diethylzinc (4 mL of a 1 M solution in hexanes, 4 mmol) was added dropwise. The resulting colourless solution was stirred for 1 hour at room temperature, concentrated *in vacuo* (to approx. 3 mL) and then transferred to the freezer (-30°C). After 24 hours a crop of colourless crystals of $[(\text{THF})_4\text{MgBr}_2]$ were isolated (0.14 g, 0.3 mmol). The solvent was removed from the filtrate *in vacuo*, hexane (1 mL) and THF (1 mL) added, and then returned to the freezer (-30°C). After 48 hours a crop of colourless crystals of **42** were isolated (0.17 g, 24 %).

^1H NMR (400.13 MHz, 298K, d_8 -THF) δ 3.81 (bs, 4H, OCH_2 , Zn-OEt), 3.61 (m, 24H, OCH_2 , THF), 1.77 (m, 24H, CH_2 , THF), 1.19 (m, 9H, CH_3 , Zn-OEt) 1.13 (t, 15H, CH_3 , Zn-Et), -0.19 (bs, 10H, CH_2 , Zn-Et). $^{13}\text{C}\{^1\text{H}\}$ NMR (100.62 MHz, 298K, d_8 -THF) δ 68.22 (OCH_2 , THF), 58.20 (OCH_2 , Zn-OEt), 26.32 (CH_2 , THF), 21.73 (CH_3 , Zn-OEt), 12.56, (CH_3 , Zn-Et), 1.93 (CH_2 , Zn-Et).

7.3.20 Synthesis of $[\{\text{Mg}_2\text{Cl}_3(\text{THF})_6\}^+\{\text{Mg}_2(\text{OC}(\text{Et})\text{Ph}_2)_2\text{Cl}_3(\text{THF})\}^-]$ (**44**)

Method 1: To a solution of ethylmagnesium chloride (2 M solution in THF, 1 mL, 2 mmol) in THF (5 mL) was added diethylzinc (2 mL of a 1 M solution in hexanes, 2 mmol). The resulting solution was stirred for one hour at room temperature, cooled to 0°C in an ice bath, and then benzophenone (**43**) (0.364 g, 2 mmol) was added, to give a pink solution which after stirring for one hour at 0°C turned light yellow. Approximately half of the solvent was removed *in vacuo* and hexane (2 mL) was then introduced. The resulting solution was transferred to a freezer (-30°C). After 24 hours a crop of colourless crystals of **44** was isolated (isolated yield = 0.286 g, 21%).

Method 2: Compound **44** could alternatively be prepared by reacting isolated crystals of **41** (0.863 g, 1 mmol) with benzophenone (**43**) (0.182 g, 1 mmol) in THF solution (3 mL). The reaction mixture was stirred for one hour at 0°C, affording a light yellow solution which on cooling deposited a crop of crystals of **44** (isolated yield = 0.284 g, 41%).

Method 3: To a solution of ethylmagnesium chloride (2 M solution in THF, 2 mL, 4 mmol) in THF (10 mL) was added zinc chloride (1 M solution in diethylether, 0.4 mL, 0.4 mmol). The resulting solution was stirred for one hour at room temperature, cooled to 0°C in an ice bath,

and then benzophenone (**43**) (0.728 g, 4 mmol) was added, to give a deep pink/red solution which after stirring for one hour at 0°C turned light yellow. Approximately half of the solvent was removed *in vacuo* and hexane (2 mL) was then introduced. The resulting solution was transferred to a freezer (-30°C). After 24 hours a crop of colourless crystals of **44** was isolated (typical isolated yield = 0.588 g, 23%).

¹H NMR (400.13 MHz, 298K, d₈-THF) δ 7.47 (d, 8H, *H*_{ortho}), 7.23 (t, 8H, *H*_{meta}), 7.13 (t, 4H, *H*_{para}), 3.61 (m, 28H, OCH₂ THF), 2.46 (q, 4H, CH₂, Zn-Et), 1.76 (m, 28H, CH₂ THF), 0.74 (q, 6H, CH₃, Zn-Et). ¹³C{¹H} NMR (100.62 MHz, 298K, d₈-THF) δ 149.77 (*C*_{ipso}), 128.96 (*C*_{ortho}), 128.31 (*C*_{meta}), 126.85 (*C*_{para}), 80.79 (C-O), 68.36 (OCH₂, THF), 37.17 (CH₂, Et), 26.39 (CH₂, THF), 10.96 (CH₃, Et).

7.3.21 Synthesis of [(THF)₅Mg₃Cl₄{OC(H)Ph(CF₃)₂}] (**50**)

To a solution of ethylmagnesium chloride (2 M solution in THF, 2 mL, 4 mmol) in THF (10 mL) was added 2,2,2-trifluoroacetophenone (**47**) (0.56 mL, 4 mmol), affording a pale yellow solution. After stirring for one hour at room temperature, the solvent was removed *in vacuo*. THF (8 mL) and hexane (1 mL) were then introduced. The resulting pale yellow solution was placed in a refrigerator (5°C). After 24 hours a crop of colourless crystals of **50** was obtained (0.459 g, 24%).

¹H NMR (400.13 MHz, 298K, d₈-THF) δ 7.74 (m (broad), 2H, *H*_{ortho}), 7.25-7.38 (m (broad), 3H, *H*_{meta} and *H*_{para}), 5.41 (m (broad), 1H, CH), 3.61 (m, 9H, OCH₂, THF), 1.77 (m, 9H, CH₂, THF). ¹³C{¹H} NMR (100.62 MHz, 298K, d₈-THF) δ 140.57 (*C*_{ipso}), 130.11 (*C*_{ortho}), 128.93 (*C*_{meta}), 128.78 (*C*_{para}), 75.43 (q, C-O, 31.9 Hz), 67.62 (OCH₂, THF), 25.42 (CH₂, THF) (due to the moderate solubility of **48** in d₈-THF the relevant resonance for the CF₃ group could not be detected). ¹⁹F{¹H} NMR (376.36 MHz, 298K, d₈-THF) δ -77.19 and -77.40 (CF₃).

7.3.22 General procedure for alkylation studies of 2,2,2-trifluoroacetophenone (**47**)

To a Schlenk tube was added 1 mmol of the required metal salt(s) (MX, where MX = LiCl (0.042 g), ZnCl₂ (0.136 g), MgCl₂ (0.095 g) or (TMEDA)ZnCl₂ (0.252 g)) along with THF (10 mL), and the resulting suspension was sonicated for 1 hour to give a solution. To this

solution was then added 1 mmol of the relevant organometallic species (RMX, where RMX = [(THF)₂Mg(μ-Cl)₂Zn(Et)(Cl)]₂ (**38**) (0.416 g), EtMgCl (0.5 mL of a 1M solution in THF) or EtLi (2 mL of a 0.5M solution in benzene/cyclohexane 90:10), and the resulting solution stirred for 1 hour at room temperature. The solution was then cooled to 0°C and 2,2,2-trifluoroacetophenone (**47**) (135 μL, 1 mmol) was then introduced. The reaction mixture was stirred for 2 hours at 0°C, then allowed to warm slowly to room temperature and stirred for a further 24 hours. The resulting solution was then quenched with a concentrated NH₄Cl solution, and the yields of the products and starting material were quantified by ¹H NMR spectroscopy and GC-FID chromatography of the crude reaction mixture, using ferrocene (0.093 g, 0.5 mmol) as an internal standard.

7.3.23 Synthesis of [$\{\text{Mg}_2\text{Cl}_3(\text{THF})_6\}^+\{\text{Zn}(p\text{-C}_6\text{H}_4\text{Me})_3\}^-$] (**52**)

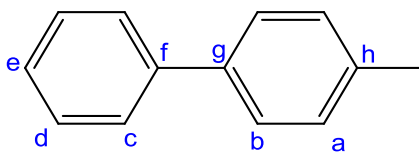
Compound **40** was generated *in situ* by adding Zn^tBu₂ (0.36 g, 2 mmol in 10 mL THF) to a solution of *tert*-butylmagnesium chloride (1 M solution in THF, 2 mL, 2mmol), and the resulting solution stirred for 1 hour at room temperature. 4-iodotoluene (1.308g, 6 mmol) was then introduced and the resulting yellow solution stirred for 30 minutes at room temperature. The volatiles (including ^tBuI) were then removed *in vacuo*, then THF (20 mL) was added and the solution stirred at room temperature for one hour. The solution was concentrated *in vacuo*, and then transferred to the freezer for 48 hours. A batch of colourless crystals of **52** were isolated (average crystalline yield = 0.994 g, 60%).

¹H NMR (400.13 MHz, 298K, d₈-THF) δ 7.67 (6H, d, CH_{ortho}), 6.87 (6H, d, CH_{meta}), 3.61 (24H, m, OCH₂, THF), 2.21 (9H, s, CH₃), 1.77 (24H, m, OCH₂, THF). ¹³C{¹H} NMR (100.62 MHz, 298K, d₈-THF) δ 162.8 (Zn-C_{ipso}), 141.3 (C_{ortho}), 133.0 (C_{para}), 127.5 (C_{meta}), 68.5 (OCH₂, THF), 26.6 (CH₂, THF), 22.0 (CH₃).

7.3.24 Cross-coupling reaction of **52** with iodobenzene

Isolated crystals of **52** (2.779 g, 3 mmol) (prepared as described above) were dissolved in THF (10 mL), to which was added a solution of [PdCl₂(dppf)₂] (0.054 g, 2.5 mol%) and Iodobenzene (0.34 mL, 3 mmol) in THF (10 mL), affording a yellow suspension, which was stirred at room temperature for 24 hours. The reaction was quenched with saturated NH₄Cl, extracted with Et₂O (3 x 15 mL) and dried over MgSO₄. The solvent was removed *in vacuo*,

and the crude product purified by column chromatography (SiO₂, hexane). The product, 4-methylbiphenyl (**53**) (0.464 g, 92%) was obtained as a white solid.



¹H NMR (400.13 MHz, 298K, CDCl₃) δ 7.58 (2H, d, H_c), 7.50 (2H, d, H_b), 7.43 (2H, t, H_d), 7.33 (1H, t, H_e), 7.26 (2H, d, H_a), 2.41 (3H, s, CH₃). ¹³C{¹H} NMR (100.62 MHz, 298K, CDCl₃) δ 141.2 (C_f), 138.4 (C_g), 136.9 (C_h), 129.5 (C_a), 128.7 (C_d), 126.9 (C_b and C_c), 126.8 (C_e), 21.0 (CH₃).

7.3.25 General procedure for monitoring Zn-I exchange reactions of **40** with functionalised aryl iodide substrates in d₈-THF

Isolated crystals of **40** (0.103 g, 0.125 mmol, prepared as described in **Chapter 7.3.17**) were placed in an NMR tube and dissolved in d₈-THF (0.5 mL). The sample was then analysed by ¹H NMR spectroscopy to confirm the purity of the zincate. To the NMR tube was then added x equivalents (x = 1-3) of the relevant aryl iodide substrate (0.125-0.375 mmol). Analysis of the reaction was then performed ¹H NMR spectroscopy as quickly as possible after the addition of the substrate (after approximately 15-30 minutes), and again 2 hours after addition, and at any required time interval thereafter. The extent of Zn-I exchange was determined by the relative integration of the aromatic resonances of the unreacted substrate with those of the Zn-Ar species.

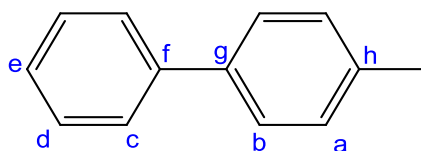
7.3.26 General procedure for Zn-I exchange reactions of **40** with functionalised aryl iodide substrates followed by Negishi cross-coupling with iodobenzene

To a THF solution of **40** (1.1 mmol, prepared either by metathesis reaction of 3.3 eq. of ^tBuMgCl with ZnCl₂, or co-complexation of 1.1 eq. ^tBuMgCl and 1.1 eq. Zn^tBu₂ – see **Chapter 7.3.17**) was added x equivalents (x = 1,2 or 3) of the relevant aryl iodide substrate (1-3 mmol). The reaction was stirred for 30 minutes at room temperature, followed by the removal of the solvent and volatiles *in vacuo*. THF (5 mL) was then added, and the reaction stirred for a further 2 hours at room temperature, followed by the addition of [PdCl₂(dppf)₂] (0.054 g, 2.5 mol%) and iodobenzene (0.12-0.34 mL, 1-3 mmol), and the reaction mixture

stirred for a further 24 hours at room temperature. The reaction was quenched with saturated NH_4Cl , extracted with Et_2O (3 x 15 mL) and dried over MgSO_4 . The solvent was removed *in vacuo*, and the crude product purified by column chromatography (SiO_2 , hexane/ Et_2O). For isolated product yields and NMR data see below.

(a) 4-methylbiphenyl (53)

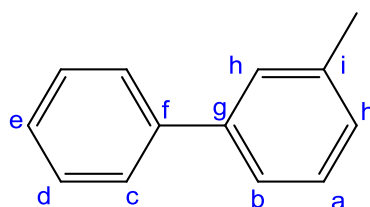
Reaction performed with 3 equivalents of 4-iodotoluene (**51**) (0.654 g, 3 mmol) resulted in the isolation of the desired product (**53**) as a white solid (0.3985 g). Analysis by GC-MS and NMR spectroscopy indicated the presence of some of the homo-coupled species 4,4'-dimethylbiphenyl, which could not be separated from the desired product by column chromatography. The purity of the sample was determined by GC-MS to be 82%, giving the final isolated yield of **53** (0.3298 g, 65% yield).



$^1\text{H NMR}$ (400.13 MHz, 298K, CDCl_3) δ 7.58 (2H, d, H_c), 7.50 (2H, d, H_b), 7.43 (2H, t, H_d), 7.33 (1H, t, H_e), 7.26 (2H, d, H_a), 2.41 (3H, s, CH_3). $^{13}\text{C}\{^1\text{H}\}$ NMR (100.62 MHz, 298K, CDCl_3) δ 141.2 (C_f), 138.4 (C_g), 136.9 (C_h), 129.5 (C_a), 128.7 (C_d), 126.9 (C_b and C_c), 126.8 (C_e), 21.0 (CH_3).

(b) 3-methylbiphenyl (56)

Reaction performed with 3 equivalents of 3-iodotoluene (**54**) (0.39 mL, 3 mmol) resulted in the isolation of the desired product (**56**) as a colourless liquid (0.3600 g). Analysis by GC-MS and NMR spectroscopy indicated the presence of a small amount of the homo-coupled species 3,3'-dimethylbiphenyl, which could not be separated from the desired product by column chromatography. The purity of the sample was determined by GC-MS to be 91%, giving the final isolated yield of 3-methylbiphenyl (**56**) (0.3276 g, 65% yield).

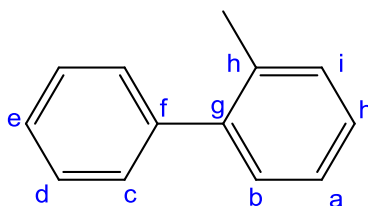


$^1\text{H NMR}$ (400.13 MHz, 298K, CDCl_3) δ 7.60 (2H, d, H_c), 7.44 (4H, m, H_d , H_b and H_h), 7.35 (2H, m, H_a , H_e), 7.18 (1H, d, H_j), 2.44 (3H, s, CH_3). $^{13}\text{C}\{^1\text{H}\}$ NMR (100.62 MHz, 298K,

CDCl_3) δ 141.4 (C_f), 141.2 (C_g), 138.3 (C_i), 128.7 (C_d), 128.6 (C_e), 128.0 (C_h and C_j), 127.2 (C_c and C_a), 124.3 (C_b) 21.5 (CH_3).

(c) 2-methylbiphenyl (**57**)

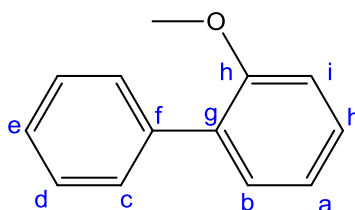
Reaction performed with 3 equivalents of 2-iodotoluene (**55**) (0.39 mL, 3 mmol) resulted in the isolation of the desired product (**57**) as a pale orange liquid (0.3258 g). Analysis by GC-MS and NMR spectroscopy indicated the presence of a small amount of the homo-coupled species 2,2'-dimethylbiphenyl, which could not be separated from the desired product by column chromatography. The purity of the sample was determined by GC-MS to be 93%, giving the final isolated yield of 2-methylbiphenyl (**57**) (0.3030 g, 60% yield).



$^1\text{H NMR}$ (400.13 MHz, 298K, CDCl_3) δ 7.58 (2H, d, H_c), 7.50 (2H, d, H_b), 7.43 (2H, t, H_d), 7.33 (1H, t, H_e), 2.30 (3H, s, CH_3). $^{13}\text{C}\{^1\text{H}\}$ NMR (100.62 MHz, 298K, CDCl_3) δ 142.0 (C_g), 141.9 (C_f), 135.4 (C_h), 130.3 (C_i), 129.8 (C_j), 129.2 (C_d), 128.1 (C_c), 127.3 (C_e), 126.8 (C_b), 125.8 (C_a) 20.3 (CH_3).

(d) 2-methoxybiphenyl (**61**)

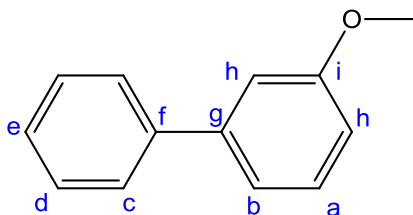
Reaction performed with 3 equivalents of 2-iodoanisole (**58**) (0.36 mL, 3 mmol) resulted in the isolation of the desired product (**61**) as an orange liquid (0.4226 g, 76%).



$^1\text{H NMR}$ (400.13 MHz, 298K, CDCl_3) δ 7.54 (2H, d, H_c), 7.42 (2H, t, H_d), 7.33 (3H, m, H_j , H_b , H_e), 7.05 (1H, t, H_a), 7.00 (1H, d, H_i), 2.83 (3H, s, OCH_3). $^{13}\text{C}\{^1\text{H}\}$ NMR (100.62 MHz, 298K, CDCl_3) δ 156.5 (C_h), 138.5 (C_f), 130.8 (C_g), 130.9 (C_j), 129.5 (C_c), 128.6 (C_b), 128.0 (C_d), 126.9 (C_e), 120.8 (C_a), 111.2 (C_i), 55.6 (OCH_3).

(e) 3-methoxybiphenyl (62)

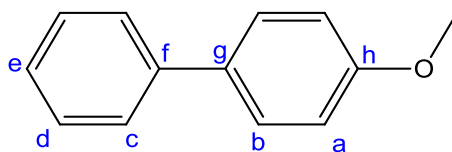
Reaction performed with 3 equivalents of 3-iodoanisole (**59**) (0.702 g, 3 mmol) resulted in the isolation of the desired product (**62**) as a colourless liquid (0.4225 g, 76%).



$^1\text{H NMR}$ (400.13 MHz, 298K, CDCl_3) δ 7.61 (2H, d, H_c), 7.45 (2H, t, H_d), 7.37 (2H, m, H_a and H_e), 7.20 (1H, d, H_b), 7.14 (1H, d, H_h), 6.92 (1H, dd, H_j), 3.88 (3H, s, OCH_3). $^{13}\text{C}\{^1\text{H}\}$ NMR (100.62 MHz, 298K, CDCl_3) δ 159.9 (C_i), 142.8 (C_g), 141.1 (C_f), 129.7 (C_a), 128.7 (C_d), 127.4 (C_e), 127.2 (C_c), 119.7 (C_b), 112.9 (C_h), 112.7 (C_j), 55.3 (OCH_3).

(f) 4-methoxybiphenyl (63)

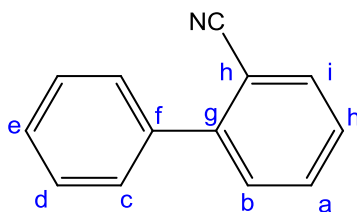
Reaction performed with 3 equivalents of 4-iodoanisole (**60**) (0.654 g, 3 mmol) resulted in the isolation of the desired product (**63**) as a white solid (0.4340 g, 79%).



$^1\text{H NMR}$ (400.13 MHz, 298K, CDCl_3) δ 7.56 (2H, d, H_c), 7.54 (2H, d, H_a), 7.43 (2H, t, H_d), 7.31 (1H, t, H_e), 6.99 (2H, d, H_b), 3.89 (3H, s, OCH_3). $^{13}\text{C}\{^1\text{H}\}$ NMR (100.62 MHz, 298K, CDCl_3) δ 159.1 (C_h), 140.8 (C_f), 133.8 (C_g), 128.7 (C_c), 128.1 (C_a), 126.7 (C_d), 126.6 (C_e), 114.2 (C_b), 55.3 (OCH_3).

(g) 2-cyanobiphenyl (70)

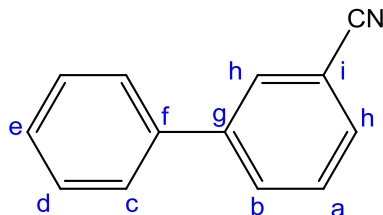
Reaction performed with 3 equivalents of 2-iodobenzonitrile (**65**) (0.687 g, 3 mmol) resulted in the isolation of the desired product (**70**) as a pale yellow oil (0.1667 g, 31%). When 2 equivalents of **65** (0.458 g, 2 mmol) were employed, **70** was obtained an isolated yield of 30% (0.1067 g). When 1 equivalent of **65** (0.229 g, 1 mmol) was employed, **70** was obtained in an isolated yield of 14% (0.0248 g).



^1H NMR (400.13 MHz, 298K, CDCl_3) δ 7.79 (1H, d, H_i), 7.66 (1H, t, H_a), 7.57 (2H, d, H_d), 7.55 (1H, d, H_b), 7.51 (2H, d, H_c), 7.48 (1H, t, H_e), 7.46 (1H, t, H_h). ^{13}C $\{^1\text{H}\}$ NMR (100.62 MHz, 298K, CDCl_3) δ 145.5 (C_g), 138.1 (C_f), 133.8 (C_i), 132.8 (C_a), 130.0 (C_b), 128.7 (C_c , C_d , C_e), 127.5 (C_j), 118.7 (CN), 111.3 (C_h).

(h) 3-cyanobiphenyl (71)

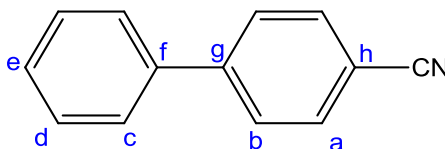
Reaction performed with 3 equivalents of 3-iodobenzonitrile (**66**) (0.687 g, 3 mmol) resulted in the isolation of the desired product (**71**) as a colourless liquid (0.4034 g, 75%).



^1H NMR (400.13 MHz, 298K, CDCl_3) δ 7.88 (1H, t, H_h), 7.82 (1H, dt, H_j), 7.64 (1H, dt, H_b), 7.58 (1H, t, H_a), 7.56 (2H, d, H_c), 7.49 (2H, t, H_d), 7.43 (1H, t, H_e). $^{13}\text{C}\{^1\text{H}\}$ NMR (100.62 MHz, 298K, CDCl_3) δ 142.5 (C_g), 138.9 (C_f), 131.5 (C_j), 130.7 (C_h), 130.6 (C_b), 129.6 (C_a), 129.1 (C_d), 128.4 (C_e), 127.1 (C_c), 118.8 (CN), 112.9 (C_i)

(i) 4-cyanobiphenyl (72)

Reaction performed with 3 equivalents of 4-iodobenzonitrile (**67**) (0.687 g, 3 mmol) resulted in the isolation of the desired product (**72**) as a white solid (0.3806 g, 71%).



^1H NMR (400.13 MHz, 298K, CDCl_3) δ 7.73 (2H, d, H_a), 7.71 (2H, d, H_b), 7.60 (2H, d, H_c), 7.50 (2H, d, H_d), 7.44 (1H, t, H_e). $^{13}\text{C}\{^1\text{H}\}$ NMR (100.62 MHz, 298K, CDCl_3) δ 145.7 (C_g), 139.2 (C_f), 132.6 (C_a), 129.1 (C_d), 128.6 (C_e), 127.7 (C_b), 127.2 (C_c), 118.9 (CN), 110.9 (C_h).

7.3.27 Synthesis of $[\{\text{Zn}(o\text{-C}_6\text{H}_4\text{OMe})_3\}_2\{\text{Mg}(\text{THF})_6\}^{2+}]$ (**64**)

Compound **40** was generated *in situ* by adding Zn^tBu_2 (0.18 g, 1 mmol in 5 mL THF) to a solution of *tert*-butylmagnesium chloride (1 M solution in THF, 1 mL, 1 mmol), which was stirred for 1 hour at room temperature. 2-iodoanisole (**58**) (0.39 mL, 3 mmol) was then introduced and the resulting pale yellow solution stirred for 30 minutes at room temperature.

The volatiles (including ¹BuI) were then removed *in vacuo*, then THF (6 mL) was added and the resulting solution left to stand at room temperature overnight. A batch of colourless crystals of **64** were isolated (typical crystalline yield = 0.360 g, 29%).

¹H NMR (400.13 MHz, 298K, d₈-THF) δ 7.49 (6H, d, CH_{meta}), 6.93 (6H, t, CH_{para}), 6.71 (6H, t, CH_{meta*}), 6.60 (6H, t, CH_{ortho*}), 3.70 (18H, s, OCH₃), 3.62 (24H, m, OCH₂, THF), 1.77 (24H, m, OCH₂, THF). ¹³C{¹H} NMR (100.62 MHz, 298K, d₈-THF) δ 167.5 (MeO-C_{ipso}), 150.4 (Zn-C_{ortho}), 140.2 (C_{meta}), 126.6 (C_{para}), 121.2 (C_{meta}), 10.3 (C_{ortho*}) 68.5 (OCH₂, THF), 55.4 (OCH₃), 26.6 (CH₂, THF).

7.3.28 Synthesis of [(THF)₄MgCl{N≡C-C₆H₄}ZnI(C₆H₄CN)(THF)] (**68**)

Compound **40** was generated *in situ* by adding Zn¹Bu₂ (0.18 g, 1 mmol in 5 mL THF) to a solution of *tert*-butylmagnesium chloride (1 M solution in THF, 1 mL, 1 mmol), and the resulting solution stirred for 1 hour at room temperature. To this was added 2-iodobenzonitrile (**65**) (0.687 g, 3 mmol) and the resulting deep red solution stirred for 24 hours at room temperature. The solvent and volatiles were removed *in vacuo*, THF (4 mL) added and the resulting red solution placed in the freezer (-30°C) for several days, from which a crop of colourless crystals of **68** (0.062 g, 8% yield) were obtained.

¹H NMR (400.13 MHz, 298K, d₈-THF) δ 8.08 (2H, d, CH_{meta}), 7.44 (2H, d, CH_{ortho*}), 7.34 (2H, t, CH_{para}), 7.09 (2H, t, CH_{meta*}), 3.62 (30H, m, OCH₂, THF), 1.77 (30H, m, OCH₂, THF). ¹³C{¹H} NMR (100.62 MHz, 298K, d₈-THF) δ 172.4 (Zn-C_{ipso}), 141.6 (C_{meta}), 132.1 (C_{ortho*}), 131.0 (C_{para}), 125.9 (C_{meta*}), 124.7 (C_{ipso}) 120.6 (C-Zn), 68.5 (OCH₂, THF), 26.6 (CH₂, THF).

Chapter 8: Overview, conclusions and outlook

Recent pioneering work from around the world has recognized the potential of mixed-metal reagents in synthetic chemistry, revealing a number of advantages over conventional monometallic reagents (e.g. RLi, RMgX, ZnR₂) such as improved levels of reactivity, selectivity and functional group tolerance, and often resulting in examples of unprecedented chemoselectivity. These bimetallic reagents usually combine two metals of different polarity, for example zinc with a more polar metal such as Li or Mg. Within the context of zincate chemistry, and using a structurally focussed inorganic approach, this PhD programme was designed with the main objective of advancing the understanding of how these mixed-metal reagents operate in organic synthesis (in particular in deprotonative metallation, metal-halogen exchange and nucleophilic addition reactions) as well as exposing some of the origins of their unique chemical behaviour. To reach this target, a combination of different analytical techniques have been employed, including X-ray crystallography (*solid-state*), multinuclear NMR spectroscopy (*solution chemistry*) and DFT calculations (*gas phase*). For studies of the solution phase (probably the most important of the three phases, as it is the one where the reactions take place) NMR reaction monitoring techniques have been employed along with diffusion-ordered NMR spectroscopy studies (DOSY).

Within the context of deprotonation chemistry, previous studies in the area of AMMZn have identified the alkali metal TMP-zincates [(THF)Li(TMP)Zn^tBu₂] (**1**) and [(TMEDA)Na(TMP)Zn^tBu₂] (**3**) as versatile and highly regioselective reagents for performing the direct zincation of aromatic molecules. Building on these previous studies, two new synthetic applications of these bimetallic reagents has been reported. Prior to this work, all the examples of AMMZn have been confined to aromatic (sp²) carbons. By investigating the reactions of **1** and **3** with the aromatic molecule trimethyl(phenoxy)silane (**12**), the concept of AMMZn has been extended to lateral metallation, providing the first example of a selective α -zincation of **12**. Conventional group I organometallic reagents fail to deprotonate this substrate instead affording complicated mixtures of products, including substitution products resulting from the Si-O bond cleavage, while organozinc reagents are inert towards this substrate. However when the bimetallic bases **1** or **3** are employed, the selective removal of one of the α -protons of the silane is accomplished at ambient temperature, leaving the Si-O intact, constituting the first example of direct lateral zincation (D/Zn) using these bimetallic

bases. In order to shed some light on the mechanism involved in this intriguing deprotonation, the reaction of “un-cocomplexed” mixtures of Li(TMP) and $t\text{Bu}_2\text{Zn}$ with **12** was also investigated revealing that initially, a mixed-metal complex where the silane acts as a donor must be generated.

The applications of (TMP)dialkyl zincate **3** in the area of metallocene functionalisation have also been investigated, using benzoylferrocene (**17**) as a case study. These investigations show that at room temperature two different reactivity pathways are available for the bimetallic reagent: (i) remote 1,6-nucleophilic addition of a *tert*-butyl group to the phenyl ring of **17** and (ii) simultaneous α -deprotonation of the substituted cyclopentadienyl ring of the metallocene and 1,2-addition of a *tert*-butyl anion to the electrophilic carbonyl group of the ketone. The latter involves an unprecedented two-fold activation of the *tert*-butyl groups of bimetallic base **3**, where the two alkyl groups display strikingly different reactivities (deprotonation vs. alkylation) towards the substrate, which is in sharp contrast to the lack of reaction observed when **17** is treated with homometallic Zn^tBu_2 .

Overall these findings highlight some of the complexity of these organometallic species and the mechanisms involved in the reactions of alkali metal zincates as well as unveiling new reactivity patterns for molecules **12** and **17** which are not available to any significant extent using more conventional monometallic systems. Thus, there is a great scope for these alkali metal zincates to act as bases towards other functionalised aromatic substrates which could combine strong directing groups such as CN or CONR_2 with OSiMe_3 groups, in order to assess if $Dt\text{Zn}$ can prevail over $D\text{oM}$, or if the combination of those functional groups may direct the zincation towards an alternative site. Similarly, the extension of these metallation studies to other molecules combining relatively acidic hydrogen atoms (therefore susceptible towards C-H deprotonation) with an electrophilic benzoyl fragment (which can undergo 1,2- or 1,6-addition reactions) would also be interesting in order to assess the metallating power of these bimetallic reagents against their ability to promote remote nucleophilic additions.

In order to shed new light on the mechanisms involved for these TMP-zincates in $D\text{oM}$ reactions, the reaction of **1** with anisole (a classical substrate in $D\text{oM}$ chemistry) was investigated. Due to the heteroleptic nature of these zincates there has been a significant amount of debate as to whether these reagents act as alkyl or amido bases. Definitive structural elucidations of metallated intermediates show that for the vast majority of the

aromatic substrates studied these zincates react overall as alkyl bases. Contrastingly, a number of theoretical (DFT) studies have reported that a possible two-step mechanism could be taking place, where the substrate is initially deprotonated by the amido ligand (due to the greater kinetic reactivity of the Zn-N bonds) affording a reaction intermediate which could then react with concomitantly generated TMP(H) giving rise to final metallated species and ^tBuH. In an attempt to further investigate this two-step mechanism, the proposed intermediate species were prepared via a co-complexation approach, generating the new lithium dialkyl(aryl) zincates [(THF)₂Li(*o*-C₆H₄OMe)ZnMe₂] (**26**) and [(THF)₃Li(*o*-C₆H₄OMe)Zn^tBu₂] (**29**).

Mimicking the second step of this proposed two-step mechanism, the reactivity of compounds **26** and **29** towards TMP(H) was then studied, providing the first tangible experimental evidence that lithium TMP-zincate **1** operates via a two step mechanism for the AMMZn of anisole. These reactivity studies also revealed the important role of the alkyl groups in dialkyl(TMP)zincates [(THF)Li(TMP)(R)Zn(R)], which far from being just mere spectators, play a crucial role in the final success of the metallation, by reacting with the concomitant TMP(H) released in the first step of the reaction and therefore precluding the reversibility of the metallation. In addition the importance of the Lewis donor ability of the solvent employed in the reaction is also assessed showing that the use of a polar solvent such as THF diminishes the yield of the final metallated product [(THF)Li(TMP)(*o*-C₆H₄OMe)Zn^tBu] (**2**) since in the second step of the reaction TMP(H) can also react with the *ortho*-metallated anisole ligand in **29**. Thus, by providing a greater understanding of the mechanisms involved in the AMMZn of aromatic molecules by TMP-dialkyl zincates, this study may contribute to further advances in this area, helping to rationalise the unusual regioselectivities and conversions observed when bimetallic base **1** and **3** are employed.

Moving away from alkali metal zincates, a number of recent reports have demonstrated the influential role that inorganic salts can play in the reactivity of organometallic reagents. Thus in the second part of this report, by isolating and structurally defining key organometallic intermediates of salt metathesis reactions involving equimolar amounts of several Grignard reagents with ZnCl₂, the hidden complexity of this widely used methodology for preparing organozinc reagents was exposed, resulting in the formation of mixed-metal magnesium zinc species (Mg-Zn hybrids). Furthermore, a DFT computational study of these reactions reveals that the formation of these hybrid species is energetically more favoured than the expected homometallic products of this metathesis reaction (MgCl₂ and RZnCl), supporting the view

that mixed-metal compounds of this type may be involved in or even responsible for reactivities previously attributed to conventional monometallic organozinc species.

In addition, by performing the reactions of RMgCl ($\text{R} = \text{}^t\text{Bu}, \text{Et}$) with substoichiometric amounts of ZnCl_2 (ratio of 3:1), mimicking the conditions employed in ZnCl_2 catalysed reactions of Grignard reagents, the alkyl-rich magnesium zinc hybrids $[\{\text{Mg}_2\text{Cl}_3(\text{THF})_6\}^+\{\text{Zn}^t\text{Bu}_3\}^-]$ (**40**) and $[\{\text{Mg}_2\text{Cl}_3(\text{THF})_6\}^+\{\text{Zn}_2\text{Et}_5\}^-]$ (**41**) have been isolated and structurally defined. DOSY NMR studies of **41** have revealed its intricate constitution in THF solutions, which appears to be in a temperature-dependent equilibrium with a related triethylzincate species and charge-neutral $\text{ZnEt}_2 \cdot (\text{THF})_x$ ($x = 0-2$). These results call for a future systematic study of the metathesis reactions between high polarity organometallics with other low polarity inorganic salts (e.g. AlCl_3 , MnCl_2 or FeCl_3) as a new methodology for preparing new bimetallic compounds. Results emerging from these studies can have important implications in synthesis, in particular in catalysis since mixed Li-Fe and Mg-Fe compounds have been previously proposed as the reactive intermediates involved in iron-catalysed cross coupling reactions, while potential applications of mixed Mg-Al compounds in rechargeable batteries have also been recently reported.

Having prepared several Mg-Zn hybrid reagents, their application the nucleophilic alkylation of ketones was investigated. Thus, despite several organic studies on the preparation of tertiary alcohols by reacting Grignard reagents with ketones in the presence of zinc salts, the true constitution of the organometallic species involved in these reactions remained unclear. By investigating the organometallic species involved prior to aqueous workup, it has been demonstrated that magnesium penta(ethyl) zincate **41** is the active species responsible for carrying out these alkylation reactions (both stoichiometrically and catalytically in the presence of an excess of EtMgCl). Furthermore, structural elucidation of the alkylation product $[\{(\text{THF})_6\text{Mg}_2\text{Cl}_3\}^+\{\text{Mg}_2(\text{OC}(\text{Et})\text{Ph}_2)_2\text{Cl}_3(\text{THF})\}^-]$ (**44**) along with ^1H NMR monitoring of these reactions has provided valuable clues into how zinc can be recycled in these catalytic processes. The success of this methodology can be described in terms of the combined Lewis acid-Lewis base activation, where the cationic $\{(\text{THF})_6\text{Mg}_2\text{Cl}_3\}^+$ moiety acts as a Lewis acid (activating the substrate) whereas the alkylating species is the zincate anion $\{\text{Zn}_2\text{Et}_5\}^-$ which is a much more powerful nucleophile than charge-neutral ZnEt_2 (Lewis base activation). Building on these initial findings, a more detailed study should be directed towards the development of new catalytic systems to enable chemoselective alkylation of a

wide range of organic molecules containing C=O and C=N bonds which should lead to the formation of alkoxide and amide ligands which will preferentially bond to the high polarity metal, allowing the low polarity catalyst to be recycled.

Also, by assessing the alkylation reactions of several equimolar organometallic combinations towards 2,2,2-trifluoroacetophenone, greater conversions and levels of chemoselectivity have been accomplished when the three metals Li, Zn and Mg (accompanied by Cl and alkyl ligands) are present in the reaction mixture, hinting at the existence of a trilateral-multicomponent-partnership which adds further level of intrigue to these reactions. These findings provide important insights into the non-innocent role of inorganic salts on the structure and reactivity of organometallic reagents in organic reactions, and should raise awareness of the presence of these inorganic by-products when salt metathesis methodologies are employed to generate organometallic reagents. Therefore further investigations should be directed towards shedding new light on the complicated role that LiCl can play when added to bimetallic compounds, which can modify both the structure and reactivity of these mixed-metal species. Thus, the isolation and characterisation of these species in the solid-state and/or in solution remains as a key goal in this area of mixed-metal chemistry.

Extending the applications of these Mg-Zn hybrid reagents, the reactivity of magnesium *tert*-butyl zincate **40** in metal-halogen exchange reactions, one of the most powerful synthetic tools for the functionalisation of aromatic molecules, was investigated. Initial studies revealed that the three *tert*-butyl groups in **40** are active towards reaction with 4-iodotoluene, allowing the preparation of tris(aryl) zincate **52**, the structure of which was determined by X-ray crystallography, representing the first intermediate of a Zn-I exchange reaction to be structurally defined. The direct zincation of 4-iodotoluene can be easily accomplished under mild conditions and with the bonus of a high atom economy, contrasting with the lack of reactivity displayed by conventional monometallic organozinc reagents. Furthermore, it was established that the resulting aryl zincate **52** can be employed as a precursor in Negishi cross-coupling reactions using [PdCl₂(dppf)] as a catalyst, which expands even more the synthetic potential of this bimetallic approach. This methodology can also be further extended to other functionalised aromatic molecules, being compatible at room temperature with functional groups such OMe or CN. Further investigations of the application of this mixed magnesium-zinc approach to metal-halogen exchange/Negishi cross-coupling reactions to other aromatic and heteroaromatic substrates are currently underway in our laboratory. These studies will

include not only the assessment of the substrate scope of this method but also the optimisation of the conditions employed in the cross-coupling reaction. Thus different catalytic systems based on Pd, Ni or Fe will be probed along with the use of inorganic salts such as LiCl or MgCl₂ which, as recent reports have shown, can have a beneficial effect in this C-C bond formation processes.

In summary, new insights into the cooperative effects between zinc and more polar metals (Li, Na or Mg) have been disclosed. Revealing new synthetic applications, key organometallic intermediates, mechanistic studies and unprecedented structural motifs, the work presented in this thesis has demonstrated that new and synthetically useful synergic chemistry can be obtained by these bimetallic reagents, which extends beyond the scope of classical monometallic systems (**Figure 8.1**). Given that numerous areas of mixed-metal chemistry have not yet been explored, a systematic approach covering most of the metals of the periodic table (main group, transition metal, lanthanide) will be vital to determine the full scope of mixed-metal (hybrid) chemistry, and the different applications, and limitations of particular metal-metal partnerships.

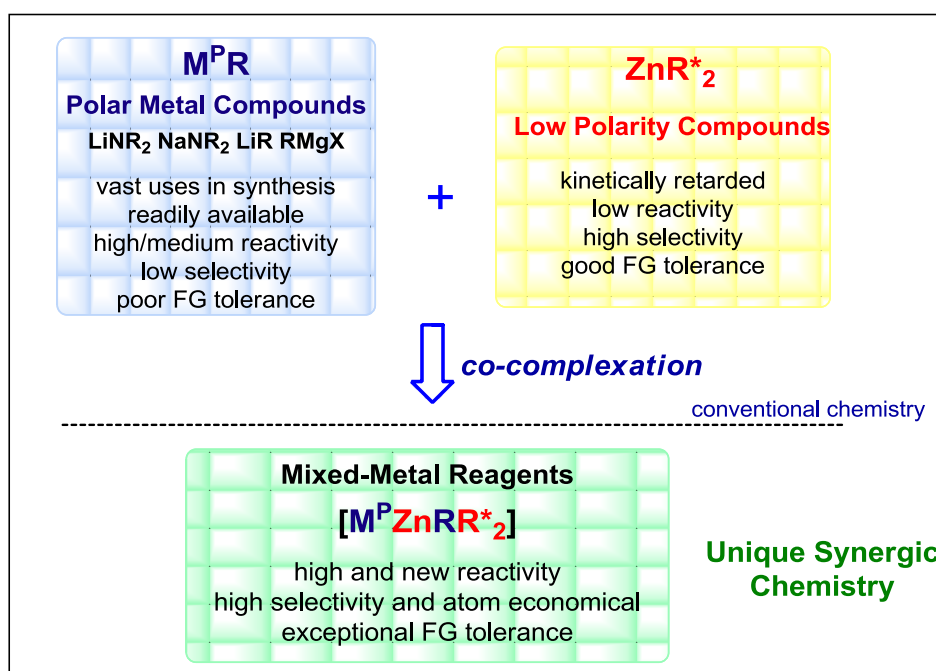


Figure 8.1

Bibliography

- [1] E. Frankland, *Justus Liebigs Ann. Chem.* **1849**, 71, 171.
- [2] P. Knochel, P. Jones, F. Langer, in *Organozinc Reagents: A Practical Approach* (Eds.: P. Knochel, P. Jones), Oxford University Press, Oxford, **1999**, pp. 1.
- [3] R. E. Mulvey, *Organometallics* **2006**, 25, 1060.
- [4] W. B. Jensen, *J. Chem. Ed.* **2003**, 80, 952.
- [5] H. Yamamoto, in *Organometallics in Synthesis*, 2nd ed. (Ed.: M. Schlosser), John Wiley & Sons, Chichester, **2002**, pp. 579.
- [6] Z. Rappoport, I. Marek, in *The Chemistry of Organozinc Reagents*, Wiley, Chichester, **2006**.
- [7] R. F. Jackson, in *Organozinc Reagents: A Practical Approach* (Eds.: P. Knochel, P. Jones), Oxford University Press, Oxford, **1999**, pp. 37.
- [8] R. D. Smith, H. E. Simmons, *Org. Synth.* **1947**, 41, 72.
- [9] (a) R. D. Rieke, P. M. Hudnall, S. J. Uhm, *J. Chem. Soc. Chem. Commun.* **1973**, 269; (b) R. D. Rieke, S. J. Uhm, *Synthesis* **1975**, 7, 452.
- [10] P. Knochel, M. C. P. Yeh, S. C. Berk, J. Talbert, *J. Org. Chem.* **1988**, 53, 2390.
- [11] (a) A. Krasovskiy, V. Malakhov, A. Gavryushin, P. Knochel, *Angew. Chem. Int. Ed.* **2006**, 45, 6040; (b) H. Ren, G. Dunet, P. Mayer, P. Knochel, *J. Am. Chem. Soc.* **2007**, 129, 5376; (c) N. Boudet, S. Sase, P. Sinha, C-Y. Liu, A. Krasovskiy, P. Knochel, *J. Am. Chem. Soc.* **2007**, 129, 12358; (d) J. E. Fleckenstein, K. Koszinowski, *Organometallics* **2011**, 30, 5018.
- [12] A. Furstner, in *Organozinc Reagents: A Practical Approach* (Eds.: P. Knochel, P. Jones), Oxford University Press, Oxford, **1999**, pp. 287.
- [13] A. Furstner, G. Kollegger, H. Weidmann, *J. Organomet. Chem.* **1991**, 414, 295.
- [14] P. Knochel, P. Jones, F. Langer, in *Organozinc Reagents: A Practical Approach* (Eds.: P. Knochel, P. Jones), Oxford University Press, Oxford, **1999**, pp. 77.
- [15] (a) E. Negishi, A. King, O. Okukado, *J. Org. Chem.* **1978**, 42, 1821; (b) A. King, E. Negishi, F. J. Villani Jr., A. Silveria Jr., *J. Org. Chem.* **1978**, 43, 358; (c) E. Negishi, S. Gagneur, *Handbook of Organopalladium Chemistry for Organic Synthesis, Vol. 1*, Wiley, New York, **2002**.
- [16] E. Negishi, in *Organozinc Reagents: A Practical Approach* (Eds.: P. Knochel, P. Jones), Oxford University Press, Oxford, **1999**, pp. 213.
- [17] T. Thaler, B. Haag, A. Gavryushin, K. Schober, E. Hartmann, R. M. Gschwind, H. Zipse, P. Mayer, P. Knochel, *Nature Chem.* **2010**, 2, 125.
- [18] J. Clayden, *Organolithiums: Selectivity for Synthesis*, Permagon, Oxford, **2002**.
- [19] J. A. Wanklyn, *Justus Liebigs Ann. Chem.* **1858**, 107, 125.
- [20] D. T. Hurd, *J. Org. Chem.* **1948**, 13, 711.
- [21] E. Weiss, R. Wolfrum, *Chem. Ber.* **1968**, 101, 35.
- [22] G. Wittig, F. J. Meyer, G. Lange, *Justus Liebigs Ann. Chem.* **1951**, 571, 167.
- [23] (a) R. E. Mulvey, *Acc. Chem. Res.* **2009**, 42, 743; (b) R. E. Mulvey, F. Mongin, M. Uchiyama, Y. Kondo, *Angew. Chem. Int. Ed.* **2007**, 46, 3802.
- [24] (a) M. Uchiyama, M. Kameda, O. Mishima, N. Yokoyama, M. Koike, Y. Kondo, T. Sakamoto, *J. Am. Chem. Soc.* **1998**, 120, 4934; (b) M. Uchiyama, M. Koike, M. Kameda, Y. Kondo, T. Sakamoto, *J. Am. Chem. Soc.* **1996**, 118, 8733; (c) M. Uchiyama, T. Furuyama, M. Kobayashi, Y. Matsumoto, K. Tanaka, *J. Am. Chem. Soc.* **2006**, 128, 8404; (d) T. Furuyama, M. Yonehara, S. Arimoto, M. Kobayashi, Y. Matsumoto, M. Uchiyama, *Chem. Eur. J.* **2008**, 14, 10348.

- [25] (a) M. Uchiyama, S. Furumoto, M. Saito, Y. Kondo, T. Sakamoto, *J. Am. Chem. Soc.* **1997**, *119*, 11425; (b) M. Uchiyama, S. Nakamura, T. Ohwada, M. Nakamura, E. Nakamura, *J. Am. Chem. Soc.* **2004**, *126*, 10897.
- [26] (a) A. E. H. Wheatley, *New J. Chem.* **2004**, *28*, 435; (b) D. R. Armstrong, C. Dougan, D. V. Graham, E. Hevia, A. R. Kennedy, *Organometallics* **2008**, *27*, 6063.
- [27] S. Merkel, D. Stern, J. Henn, D. Stalke, *Angew. Chem. Int. Ed.* **2009**, *48*, 6350.
- [28] T. Harada, A. Oku, in *Organozinc Reagents: A Practical Approach* (Eds.: P. Knochel, P. Jones), Oxford University Press, Oxford, **1999**, pp. 101.
- [29] S. Nakamura, C-Y. Liu, A. Muranaka, M. Uchiyama, *Chem. Eur. J.* **2009**, *15*, 5686.
- [30] (a) R. A. Watson, R. A. Kjonaas, *Tet. Lett.* **1986**, *27*, 1437; (b) W. Tuckmantel, K. Oshima, H. Nozaki, *Chem. Ber.* **1986**, *119*, 1881.
- [31] H. G. Richey Jr., *Grignard Reagents: New Developments*, John Wiley & Sons Ltd, Chichester, **2000**.
- [32] M. Isobe, S. Kondo, N. Nagasawa, T. Goto, *Chem. Lett.* **1977**, 679.
- [33] (a) R. A. Kjonaas, R. K. Hoffer, *J. Org. Chem.* **1988**, *53*, 4133; (b) W. Tuckmantel, K. Oshima, N. Hozaki, *Chem. Ber.* **1986**, *119*, 1581.
- [34] C. A. Musser, H. G. Richey Jr., *J. Org. Chem.* **2000**, *65*, 7750.
- [35] J. Clayden, in *Organolithiums: Selectivity in Synthesis*, Permagon, Oxford, **2002**, pp. 111.
- [36] D. Seyferth, *Organometallics* **2001**, *20*, 2940.
- [37] (a) T. Harada, T. Katsuhira, K. Hattori, A. Oku, *J. Org. Chem.* **1993**, *58*, 2958; (b) T. Harada, T. Katsuhira, D. Hara, Y. Kotani, K. Maejima, R. Kaji, A. Oku, *J. Org. Chem.* **1993**, *58*, 4897.
- [38] Y. Kondo, N. Takazawa, C. Yamazaki, T. Sakamoto, *J. Org. Chem.* **1994**, *59*, 4717.
- [39] Y. Kondo, M. Fujinami, M. Uchiyama, T. Sakamoto, *J. Chem. Soc. Perkin Trans. 1* **1997**, 799.
- [40] N. T. T. Chau, M. Meyer, S. Komagawa, F. Chevallier, Y. Fort, M. Uchiyama, F. Mongin, P. C. Gros, *Chem. Eur. J.* **2010**, *16*, 12425.
- [41] W. Clegg, S. H. Dale, A. M. Drummond, E. Hevia, G. W. Honeyman, R. E. Mulvey, *J. Am. Chem. Soc.* **2006**, *128*, 7434.
- [42] F. F. Kneisel, M. Dochnahl, P. Knochel, *Angew. Chem. Int. Ed.* **2004**, *43*, 1017.
- [43] J. Clayden, in *Organolithiums: Selectivity for Synthesis*, Permagon, Oxford, **2002**, pp. 30.
- [44] V. Snieckus, *Chem. Rev.* **1990**, *90*, 879.
- [45] E. Anctil, V. Snieckus, in *Metal-Catalyzed Cross-Coupling Reactions* (Eds.: F. Diederich, F. de Meijere), Wiley-VCH, Weinheim, **2004**, pp. 761.
- [46] C. J. Upton, P. Beak, *J. Org. Chem.* **1975**, *40*, 1094.
- [47] Y. Kondo, M. Shilai, M. Uchiyama, T. Sakamoto, *J. Am. Chem. Soc.* **1999**, *121*, 3539.
- [48] T. Imahori, M. Uchiyama, T. Sakamoto, Y. Kondo, *Chem. Commun.* **2001**, 2450.
- [49] M. Uchiyama, T. Miyoshi, Y. Kajihara, T. Sakamoto, Y. Otani, T. Ohwada, Y. Kondo, *J. Am. Chem. Soc.* **2002**, *124*, 8514.
- [50] W. Clegg, S. H. Dale, E. Hevia, G. Honeyman, R. E. Mulvey, *Angew. Chem. Int. Ed.* **2006**, *45*, 2370.
- [51] C. G. Hartung, V. Snieckus, in *Modern Arene Chemistry* (Ed.: D. Astruc), Wiley-VCH, New York, **2002**, pp. 330.
- [52] H. Gilman, R. L. Bebb, *J. Am. Chem. Soc.* **1939**, *61*, 109.
- [53] W. Bauer, P. V. R. Schleyer, *J. Am. Chem. Soc.* **1989**, *111*, 7191.
- [54] M. Stratakis, *J. Org. Chem.* **1997**, *62*, 3024.
- [55] R. A. Rennels, A. J. Maliakal, D. B. Collum, *J. Am. Chem. Soc.* **1998**, *120*, 421.

- [56] (a) F. P. Doyle, J. H. C. Nayler, G. N. Rolinson, *Vol. US pat. 2 951 839*, USA, **1960**; (b) F. Totter, P. Rittmeyer, in *Organometallics in Synthesis*, 1st ed. (Ed.: M. Schlosser), John Wiley & Sons, Chichester, **1994**, pp. 167.
- [57] P. C. Andrikopoulos, D. R. Armstrong, H. R. L. Barley, W. Clegg, S. H. Dale, E. Hevia, G. W. Honeyman, A. R. Kennedy, R. E. Mulvey, *J. Am. Chem. Soc.* **2005**, *127*, 6184.
- [58] K. Shen, Y. Fu, J.-N. Li, L. Liu, Q.-X. Guo, *Tetrahedron* **2007**, *63*, 1568.
- [59] M. D. Rausch, D. J. Ciappenelli, *J. Organomet. Chem.* **1967**, *10*, 127.
- [60] E. Erdik, in *Organozinc Reagents in Organic Synthesis*, CRC Press, New York, **1996**.
- [61] D. R. Armstrong, W. Clegg, S. H. Dale, D. V. Graham, E. Hevia, L. M. Hogg, G. W. Honeyman, A. R. Kennedy, R. E. Mulvey, *Chem. Commun.* **2007**, 598.
- [62] D. R. Armstrong, J. Garcia-Alvarez, D. V. Graham, G. W. Honeyman, E. Hevia, R. E. Mulvey, *Chem. Eur. J.* **2009**, *15*, 3800.
- [63] D. R. Armstrong, W. Clegg, S. H. Dale, E. Hevia, L. M. Hogg, G. W. Honeyman, R. E. Mulvey, *Angew. Chem. Int. Ed.* **2006**, *45*, 3775.
- [64] W. Clegg, S. H. Dale, E. Hevia, L. M. Hogg, G. W. Honeyman, R. E. Mulvey, C. T. O'Hara, L. Russo, *Angew. Chem. Int. Ed.* **2008**, *47*, 731.
- [65] (a) W. Clegg, S. H. Dale, R. W. Harrington, E. Hevia, G. W. Honeyman, R. E. Mulvey, *Angew. Chem. Int. Ed.* **2006**, *45*, 2374; (b) L. Balloch, A. R. Kennedy, R. E. Mulvey, T. Rantanen, S. D. Robertson, V. Snieckus, *Organometallics* **2011**, *30*, 145.
- [66] W. Clegg, S. H. Dale, E. Hevia, L. M. Hogg, G. W. Honeyman, R. E. Mulvey, C. T. O'Hara, *Angew. Chem. Int. Ed.* **2006**, *45*, 6548.
- [67] L. Balloch, A. R. Kennedy, J. Klett, R. E. Mulvey, C. T. O'Hara, *Chem. Commun.* **2010**, *46*, 2319.
- [68] B. Conway, E. Hevia, A. R. Kennedy, R. E. Mulvey, *Chem. Commun.* **2007**, 2864.
- [69] A. R. Kennedy, J. Klett, R. E. Mulvey, D. S. Wright, *Science* **2009**, *326*, 706.
- [70] (a) R. B. Bates, L. M. Kroposki, D. E. Potter, *J. Org. Chem.* **1972**, *37*, 560; (b) J. Clayden, S. A. Yasin, *New. J. Chem.* **2002**, *26*, 191; (c) A. Maercker, *Angew. Chem. Int. Ed.* **1987**, *26*, 972; (d) J. Clayden, in *Organolithiums: Selectivity for Synthesis*, Permagon, Oxford, **2002**, pp. 1.
- [71] A. Streitwieser, D. W. Boerth, *J. Am. Chem. Soc.* **1978**, *100*, 755.
- [72] A. Seggio, F. Chevallier, M. Vaultier, F. Mongin, *J. Org. Chem.* **2007**, *72*, 6602.
- [73] (a) A. Seggio, M.-I. Lannou, F. Chevallier, D. Nobuto, M. Uchiyama, S. Golhen, T. Roisnel, F. Mongin, *Chem. Eur. J.* **2007**, *13*, 9982; (b) J.-M. L'Helgoual'ch, A. Seggio, F. Chevallier, M. Yonehara, E. Jeanneau, M. Uchiyama, F. Mongin, *J. Org. Chem.* **2008**, *73*, 177.
- [74] K. Snegaroff, S. Komagawa, F. Chevallier, P. C. Gros, S. Golhen, T. Roisnel, M. Uchiyama, F. Mongin, *Chem. Eur. J.* **2010**, *16*, 8191.
- [75] D. Li, I. Keresztes, R. Hopson, P. G. Williard, *Acc. Chem. Res.* **2009**, *42*, 270.
- [76] P. Garcia-Alvarez, R. E. Mulvey, J. A. Parkinson, *Angew. Chem. Int. Ed.* **2011**, *50*, 9668.
- [77] (a) A. Krasovskiy, V. Krasovskaya, P. Knochel, *Angew. Chem. Int. Ed.* **2006**, *45*, 2958; (b) G. C. Clososki, C. J. Rohbonger, P. Knochel, *Angew. Chem. Int. Ed.* **2007**, *46*, 7681.
- [78] M. Mosrin, P. Knochel, *Org. Lett.* **2009**, *11*, 1837.
- [79] (a) C. J. Rohbonger, S. H. Wunderlich, G. C. Clososki, P. Knochel, *Eur. J. Org. Chem.* **2009**, 1781; (b) S. H. Wunderlich, C. J. Rohbonger, A. Unsinn, P. Knochel, *Org. Process Res. Dev.* **2010**, *14*, 339; (c) S. H. Wunderlich, P. Knochel, *Angew. Chem. Int. Ed.* **2007**, *46*, 7685; (d) Z. Dong, G. C. Clososki, S. H. Wunderlich, A. Unsinn, J. Li, P. Knochel, *Chem. Eur. J.* **2009**, *15*, 457.

- [80] (a) P. García-Álvarez, D. V. Graham, E. Hevia, A. R. Kennedy, J. Klett, R. E. Mulvey, C. T. O'Hara, S. Weatherstone, *Angew. Chem. Int. Ed.* **2008**, *47*, 8079; (b) D. R. Armstrong, P. García-Álvarez, A. R. Kennedy, R. E. Mulvey, J. A. Parkinson, *Angew. Chem. Int. Ed.* **2010**, *122*, 3253.
- [81] C. D. Broadus, *J. Org. Chem.* **1970**, *35*, 10.
- [82] J. Clayden, N. Greaves, S. Warren, P. Wothers, in *Organic Chemistry*, Oxford, New York, **2001**, pp. 1290.
- [83] T. Tatic, H. Ott, D. Stalke, *Eur. J. Inorg. Chem.* **2008**, 3765.
- [84] S. Corbelin, N. P. Lorenzen, J. Kopf, E. Weiss, *J. Organomet. Chem.* **1991**, *415*, 293.
- [85] D. J. Peterson, *J. Organomet. Chem.* **1967**, *9*, 373.
- [86] (a) R. West, G. A. Gornowicz, *J. Organomet. Chem.* **1971**, *28*, 25; (b) G. A. Gornowicz, R. West, *J. Am. Chem. Soc.* **1968**, *90*, 4478.
- [87] T. F. Bates, R. D. Thomas, *J. Organomet. Chem.* **1989**, 359, 285.
- [88] T. F. Bates, S. A. Dandekar, J. L. Longlet, K. A. Wood, R. D. Thomas, *J. Organomet. Chem.* **2000**, 595, 87.
- [89] E. Hevia, G. W. Honeyman, A. R. Kennedy, R. E. Mulvey, *J. Am. Chem. Soc.* **2005**, *127*, 13106.
- [90] J. J. Crawford, B. J. Fleming, A. R. Kennedy, J. Klett, C. T. O'Hara, S. A. Orr, *Chem. Commun.* **2011**, *47*, 3772.
- [91] H. R. L. Barley, W. Clegg, S. H. Dale, E. Hevia, G. W. Honeyman, A. R. Kennedy, R. E. Mulvey, *Angew. Chem. Int. Ed.* **2005**, *44*, 6018.
- [92] W. Clegg, K. W. Henderson, A. R. Kennedy, R. E. Mulvey, C. T. O'Hara, R. B. Rowlings, D. M. Tooke, *Angew. Chem. Int. Ed.* **2001**, *40*, 3902.
- [93] A. H. Stoll, P. Mayer, P. Knochel, *Organometallics* **2007**, *26*, 6694.
- [94] G. Dayaker, A. Sreeshailam, F. Chevallier, T. Roisnel, P. R. Krishna, F. Mongin, *Chem. Commun.* **2010**, *46*, 2862.
- [95] A. Sreeshailam, G. Dayaker, F. Chevallier, T. Roisnel, P. R. Krishna, F. Mongin, *Eur. J. Org. Chem.* **2011**, 3715.
- [96] (a) I. R. Butler, W. R. Cullen, J. Trotter, *Acta. Crystallogr. Sect C, Cryst. Struct. Commun.* **1988**, *44*, 1666; (b) J. C. Barnes, W. Bell, C. Glidewell, R. A. Howie, *J. Organomet. Chem.* **1990**, 385, 369.
- [97] N. Seidel, K. Jacob, P. Zanello, M. Fontani, *J. Organomet. Chem.* **2001**, 620, 243.
- [98] (a) I. J. Blackmore, A. N. Boa, E. J. Murray, M. Dennis, S. Woodward, *Tetrahedron Lett.* **1999**, *40*, 6671; (b) A. N. French, S. Bissmire, T. Wirth, *Chem. Soc. Rev.* **2004**, *33*, 354.
- [99] (a) G. A. Olah, A.-H Wu, O. Farooq, *Synthesis* **1991**, 1179; (b) T. Holm, I. Crossland, in *Grignard Reagents: New developments* (Ed.: H. G. R. Jr.), John Wiley and Sons Ltd, Chichester, **2000**, pp. 1.
- [100] (a) H. Yamataka, N. Fujimura, Y. Kawafuji, T. Hanafusa, *J. Am. Chem. Soc.* **1987**, *109*, 4305; (b) T. Holm, I. Crossland, *Acta. Chem. Scand.* **1971**, *25*, 59.
- [101] (a) W. Adam, C. R. Saha-Möller, P. A. Ganeshpure, *Chem. Rev.* **2001**, *101*, 3499; (b) T. Vogler, A. Studer, *Synthesis* **2008**, 1979; (c) L. De Luca, G. Giacomelli, S. Masala, A. Porcheddu, *J. Org. Chem.* **2003**, *68*, 4999; (d) W. Peng, K. Ashida, T. Hirabaru, L. J. Ma, T. Inokuchi, *Tetrahedron* **2010**, *66*, 9714.
- [102] M. Uchiyama, Y. Matsumoto, D. Nobuto, T. Furuyama, K. Yamaguchi, K. Morokuma, *J. Am. Chem. Soc.* **2006**, *128*, 8748.
- [103] D. Nobuto, M. Uchiyama, *J. Org. Chem.* **2008**, *73*, 1117.
- [104] Y. Kondo, J. V. Morey, J. C. Morgan, H. Naka, D. Nobuto, P. R. Raithby, M. Uchiyama, A. E. H. Wheatley, *J. Am. Chem. Soc.* **2007**, *129*, 12734.

- [105] M. Uchiyama, Y. Matsumoto, S. Usui, Y. Hashimoto, K. Morokuma, *Angew. Chem. Int. Ed.* **2007**, *46*, 926.
- [106] S. Harder, J. Boersma, L. Bransma, *J. Organomet. Chem.* **1988**, *339*, 7.
- [107] D. V. Graham, E. Hevia, A. R. Kennedy, R. E. Mulvey, *Organometallics* **2006**, *25*, 3297.
- [108] C. A. Ogle, B. K. Huckabee, H. C. Johnson IV, P. F. Sims, S. D. Winslow, A. A. Pinkerton, *Organometallics* **1993**, *12*, 1960.
- [109] B. Conway, E. Hevia, J. Garcia-Alvarez, D. V. Graham, A. R. Kennedy, R. E. Mulvey, *Chem. Commun.* **2007**, 5241.
- [110] T. Chivers, D. J. Eisler, C. Fedorchuk, G. Schatte, H. M. Tuononen, R. T. Boere, *Inorg. Chem.* **2006**, *45*, 2119.
- [111] H. O. Frohlich, B. Kosan, B. Undeutsch, *J. Organomet. Chem.* **1994**, *472*, 1.
- [112] E. Rijnberg, J. T. B. H. Jastrzebski, J. Boersma, H. Kooijman, N. Veldam, A. L. Spek, G. v. Koten, *Organometallics* **1997**, *16*, 2239.
- [113] R. Wyrwa, H. O. Frohlich, H. Gorls, *Organometallics* **1996**, *15*, 2833.
- [114] H. O. Frohlich, B. Kosan, B. Muller, W. Hiller, *J. Organomet. Chem.* **1992**, *441*, 177.
- [115] A. J. Edwards, A. Fallaize, P. R. Raithby, M.-A. Rennie, A. Steiner, K. L. Verhorevoort, D. S. Wright, *J. Chem. Soc. Dalton Trans.* **1996**, 133.
- [116] T. A. Mobley, S. Berger, *Angew. Chem. Int. Ed.* **1999**, *38*, 3070.
- [117] D. R. Armstrong, V. L. Blair, W. Clegg, S. H. Dale, J. Garcia-Alvarez, G. W. Honeyman, E. Hevia, R. E. Mulvey, L. Russo, *J. Am. Chem. Soc.* **2010**, *132*, 9480.
- [118] (a) S. Yamabe, S. Yamazaki, in *The Chemistry of Organomagnesium Compounds* (Eds.: Z. Rappoport, I. Marek), Wiley, Chichester, **2008**, pp. 369; (b) P. Knochel, A. Gavryushin, K. Brade, in *The Chemistry of Organomagnesium Compounds* (Eds.: Z. Rappoport, I. Marek), Wiley, Chichester, **2008**, pp. 511.
- [119] Z. Rappoport, I. Marek, in *The Chemistry of Organomagnesium Compounds*, Wiley, Chichester, **2008**.
- [120] V. Bonnet, F. Mongin, F. Trécourt, G. Quéguiner, *J. Chem. Soc. Perkin Trans. 1* **2000**, 4245.
- [121] J. Boersma, in *Comprehensive Organometallic Chemistry*, Vol. 2, Pergamon, New York, **1982**, p. 832.
- [122] (a) J. G. Kim, P. J. Walsh, *Angew. Chem. Int. Ed.* **2006**, *45*, 4175; (b) L. Salvi, J. G. Kim, P. J. Walsh, *J. Am. Chem. Soc.* **2009**, *131*, 12483.
- [123] A. Metzger, S. Bernhardt, G. Manolikakes, P. Knochel, *Angew. Chem. Int. Ed.* **2010**, *49*, 4665.
- [124] A. W. Buesking, T. D. Baguley, J. A. Ellman, *Org. Lett.* **2011**, *13*, 964.
- [125] L. Jin, C. Liu, J. Liu, F. Hu, Y. Lan, A. S. Batsanov, J. A. K. Howard, T. B. Marder, A. Lei, *J. Am. Chem. Soc.* **2009**, *131*, 16656.
- [126] A. Krasovskiy, P. Knochel, *Angew. Chem. Int. Ed.* **2004**, *43*, 3333.
- [127] E. Hevia, R. E. Mulvey, *Angew. Chem. Int. Ed.* **2011**, *50*, 6448.
- [128] J. Lewinski, M. Dranka, W. Bury, W. Sliwinski, I. Justyniak, J. Lipkowski, *J. Am. Chem. Soc.* **2007**, *129*, 3096.
- [129] M. D. McCall, E. Hevia, P. Garcia-Alvarez, *Unpublished result*.
- [130] S. Sakamoto, T. Imamoto, K. Yamaguchi, *Org. Lett.* **2001**, *3*, 1793.
- [131] P. C. Andrews, C. L. Raston, B. W. Skelton, A. H. White, *Organometallics* **1998**, *17*, 779.
- [132] (a) M. Bolte, S. Scholz, W. Lerner, *Private Communication* **2002**; (b) S. Parsons, S. Pace, N. Buschmann, P. Bailey, P. Wood, *Private Communication* **2004**; (c) K. Handlir, J. Holecek, L. Benes, *Collect. Czech. Chem. Commun.* **1985**, *50*, 2422; (d) H. Qichen, Q. Yanlong, Z. Junming, T. Youqi, *Chin. J. Struct. Chem.* **1987**, *6*, 43.

- [133] (a) R. E. Mulvey, *Chem. Commun.* **2001**, 1049; (b) E. Hevia, A. R. Kennedy, R. E. Mulvey, S. Weatherstone, *Angew. Chem. Int. Ed.* **2004**, *43*, 1709; (c) N. D. R. Barnett, W. Clegg, A. R. Kennedy, R. E. Mulvey, S. Weatherstone, *Chem. Commun.* **2005**, 375.
- [134] J. Toney, G. D. Stucky, *J. Organomet. Chem.* **1971**, *28*, 5.
- [135] J. Campora, P. Palma, C. M. Perez, A. Rodriguez-Delgado, E. Alvarez, E. Gutierrez-Puebla, *Organometallics* **2010**, *29*, 2960.
- [136] J. F. G. A. Jansen, B. L. Feringa, *Chem. Commun.* **1989**, 741.
- [137] M. Hatano, S. Suzuki, K. Ishihara, *J. Am. Chem. Soc.* **2006**, *128*, 9998.
- [138] R. A. Kjonaas, E. J. Vawter, *J. Org. Chem.* **1986**, *51*, 3993.
- [139] K. Murakami, H. Yorimitsu, K. Oshima, *J. Org. Chem.* **2009**, *74*, 1415.
- [140] (a) E. Rijnberg, J. T. B. H. Jastrzebski, J. Boersma, H. Kooijman, A. L. Spek, G. V. Koten, *J. Organomet. Chem.* **1997**, *541*, 181; (b) M. Krieger, G. Geiseler, K. Harms, J. Merle, W. Massa, K. Dehnicke, *Z. Anorg. Allg. Chem.* **1998**, *624*, 1387; (c) M. Ruben, D. Walther, R. Knake, H. Goris, R. Beckert, *Eur. J. Inorg. Chem.* **2000**, 1055; (d) W. Clegg, D. R. Harbron, B. P. Straughan, *Acta. Crystallogr. Sect C, Cryst. Struct. Commun.* **1991**, *47*, 267; (e) W. Clegg, I. R. Little, B. P. Straughan, *Inorg. Chem.* **1988**, *27*, 1916.
- [141] C. Studte, B. Breit, *Angew. Chem. Int. Ed.* **2008**, *47*, 5451.
- [142] G. J. Brand, C. Studte, B. Breit, *Org. Process Res. dev.* **2009**, *11*, 4668.
- [143] (a) S. R. Boss, M. P. Coles, R. Haigh, P. B. Hitchcock, R. Snaith, A. E. H. Wheatley, *Angew. Chem. Int. Ed.* **2003**, *42*, 5593; (b) S. R. Boss, M. P. Coles, V. Eyre-Brook, F. Garcia, R. Haigh, P. B. Hitchcock, M. McPartlin, J. V. Morey, H. Naka, P. R. Raithby, H. A. Sparkes, C. W. Tate, A. E. H. Wheatley, *Dalton Trans.* **2006**, 5574.
- [144] (a) P. C. Andrews, P. C. Junk, I. Nuzhnaya, L. Spiccia, N. Vanderhoek, *J. Organomet. Chem.* **2006**, *691*, 3426; (b) J. K. Vohs, L. E. Downs, M. E. Barfield, K. Latibeaudiere, G. H. Robinson, *J. Organomet. Chem.* **2003**, 666, 7.
- [145] E. Alvarez, A. Grirane, I. Resa, D. del Rio, A. Rodriguez, E. Carmona, *Angew. Chem. Int. Ed.* **2007**, *46*, 1296.
- [146] R. Kerssebaum, G. Salnikov, in *DOSY and Diffusion by NMR, a Tutorial for TopSpin 2.0*, Bruker Biospin GmbH, Rheinstetten, Germany, **2002**, pp. 14.
- [147] E. O. Stejskal, J. E. Tanner, *J. Chem. Phys.* **1965**, *42*, 288.
- [148] K. F. Morris, C. S. Johnson, *J. Am. Chem. Soc.* **1992**, *114*, 3139.
- [149] (a) D. Li, C. Sun, P. G. Williard, *J. Am. Chem. Soc.* **2008**, *130*, 11726; (b) D. Li, R. Hopson, W. Li, J. Liu, P. G. Williard, *Org. Lett.* **2008**, *10*, 909; (c) G. Kagan, W. Li, R. Hopson, P. G. Williard, *Org. Lett.* **2009**, *11*, 4818; (d) D. Li, G. Kagan, R. Hopson, P. G. Williard, *J. Am. Chem. Soc.* **2009**, *131*, 5627.
- [150] (a) S. E. Denmark, J. Fu, *Chem. Rev.* **2003**, *103*, 2763; (b) P. Knochel, A. Krasovisky, I. Sapountiz, in *Handbook of Functionalized Organometallics* (Ed.: P. Knochel), Wiley-VCH, New York, **2005**, pp. 109; (c) M. Hatano, S. Suzuki, K. Ishihara, *Synlett* **2010**, 321; (d) L. Pu, H. B. Yu, *Chem. Rev.* **2001**, *101*, 757; (e) H. Li, P. Walsh, *J. Am. Chem. Soc.* **2005**, *127*, 8355.
- [151] T. Imamoto, N. Takiyama, K. Nakamura, T. Hatajima, Y. Kamiya, *J. Am. Chem. Soc.* **1989**, *111*, 4392.
- [152] (a) E. C. Ashby, S. A. Noding, *J. Org. Chem.* **1979**, *44*, 4371; (b) A. Krasovskiy, P. Knochel, *Angew. Chem. Int. Ed.* **2004**, *43*, 3333.
- [153] (a) B. Scheiper, M. Bonnekessel, H. Krause, A. Furstner, *J. Org. Chem.* **2004**, *69*, 3943; (b) A. Furstner, H. Krause, C. W. Lehmann, *Angew. Chem. Int. Ed.* **2006**, *45*, 440.

- [154] (a) A. Krasovskiy, F. Kopp, P. Knochel, *Angew. Chem. Int. Ed.* **2006**, *45*, 497; (b) A. Metzger, A. Gavryushin, P. Knochel, *Synlett* **2009**, 1433.
- [155] K. Yearick, C. Wolf, *Org. Lett.* **2008**, *10*, 3915.
- [156] P. Knochel, P. Jones, F. Langer, in *Organozinc Reagents: A Practical Approach* (Eds.: P. Knochel, P. Jones), Oxford University Press, Oxford, **1999**, pp. 179.
- [157] (a) H. Kutzke, H. Klapper, R. B. Hammond, K. J. Roberts, *Acta. Crystallogr. Sect B, Struct. Sci.* **2000**, *56*, 486; (b) J. Moncol, P. Coppens, *Private Communication* **2004**; (c) J. Bernstein, A. Ellern, J.-O. Henck, *Private Communication* **2002**.
- [158] (a) P. T. Moseley, H. M. M. Shearer, *Chem. Commun.* **1968**, 279; (b) C. A. Zechmann, T. J. Boyle, M. A. Rodriguez, R. A. Kemp, *Inorg. Chim. Acta* **2001**, *319*, 137; (c) J. F. Allan, K. W. Henderson, A. R. Kennedy, *Chem. Commun.* **1999**, 1325; (d) P. L. Arnold, I. J. Casely, Z. R. Turner, R. Bellabarba, R. B. Tooze, *Dalton Trans.* **2009**, 7236; (e) K. W. Henderson, J. F. Allan, A. R. Kennedy, *Chem. Commun.* **1997**, 1149.
- [159] P. Knochel, P. Jones, *Organozinc Reagents: A Practical Approach*, Oxford University Press, Oxford, **1999**.
- [160] S. Sasaki, T. Yamauchi, H. Kubo, M. Kanai, A. Ishiib, K. Higashiyama, *Tet. Lett.* **2005**, *46*, 1497.
- [161] (a) A. C. Hoepker, L. Gupta, Y. Ma, M. F. Faggin, D. B. Colum, *J. Am. Chem. Soc.* **2011**, *133*, 7135; (b) Y. Ma, A. C. Hoepker, L. Gupta, M. F. Faggin, D. B. Colum, *J. Am. Chem. Soc.* **2010**, *132*, 15610; (c) L. Gupta, A. C. Hoepker, K. J. Singh, D. B. Colum, *J. Org. Chem.* **2009**, *74*, 2231.
- [162] D. Stern, N. Finkelmeier, D. Stalke, *Chem. Commun.* **2011**, 47, 2113.
- [163] B. Lecachey, H. Oulyadi, P. Lameiras, A. Harrison-Marchland, H. Gerard, J. Maddaluno, *J. Org. Chem.* **2010**, *75*, 5976.
- [164] (a) M. Hatano, O. Ito, S. Suzuki, K. Ishihara, *J. Org. Chem.* **2010**, *75*, 5008; (b) M. Hatano, O. Ito, S. Suzuki, K. Ishihara, *Chem. Commun.* **2010**, 46, 2674.
- [165] H. Fillon, C. Gosmini, J. Perichon, *J. Am. Chem. Soc.* **2003**, *125*, 3867.
- [166] L. Micouin, P. Knochel, *Synlett* **1997**, 327.
- [167] (a) G. Cahiez, F. Lepifre, P. Ramiandrasoa, *Synthesis* **1999**, 2138; (b) E. Riguet, M. Alami, G. Cahiez, *J. Organomet. Chem.* **2001**, *624*, 376; (c) V. L. Blair, W. Clegg, B. Conway, E. Hevia, A. R. Kennedy, J. Klett, R. E. Mulvey, L. Russo, *Chem. Eur. J.* **2008**, *14*, 65.
- [168] L. Shi, Y. Chu, P. Knochel, H. Mayr, *J. Org. Chem.* **2009**, *74*, 2760.
- [169] L. Shi, Y. Chu, P. Knochel, H. Mayr, *Angew. Chem. Int. Ed.* **2008**, *47*, 202.
- [170] Z. Dong, G. Manolikakes, L. Shi, P. Knochel, H. Mayr, *Chem. Eur. J.* **2010**, *16*, 248.
- [171] S. Duez, A. K. Steib, S. M. Manolikakes, P. Knochel, *Angew. Chem. Int. Ed.* **2011**, *50*, 7686.
- [172] W. L. F. Armarego, D. D. Perrin, *Purification of Laboratory Chemicals*, 4th ed., Butterworth-Heinemann, Oxford, **1996**.
- [173] D. E. Bergbreiter, E. Pendergrass, *J. Org. Chem.* **1980**, *46*, 219.
- [174] A. Krasovskiy, P. Knochel, *Synthesis* **2006**, *5*, 890.
- [175] G. M. Sheldrick, *Acta Crystallogr. Sect. A* **2008**, *64*, 112.